Electrochemical Determination of Dissolved and Particulate Iron in Mine-waters

Liadi Kolapo Mudashiru

Newcastle University

A thesis submitted to the University of Newcastle Upon Tyne
In partial fulfilment of the requirements of the degree of
Doctor of Philosophy

October 2008

Declaration

The work contained in this thesis was carried out in the School of Chemistry at Newcastle University, during the period between September 2005 and October 2008 and is original except where acknowledged with reference.

Dedication

To my late parents:

Mr. Atanda Kolapo Mudashiru

&

Mrs. Mariam Ajogbe Mudashiru

Acknowledgements

I would like to express my profound and deepest sense of gratitude to my supervisors Dr. B.R.Horrocks and Prof. A.C.Aplin for their inspiration, motivation, guidance, advice, encouragements, patience, invaluable support (morally and financially) and constructive criticism throughout this research work and for painstakingly proofreading the entire thesis. I am particularly indebted to Dr. Horrocks who rekindled my interest and enthusiasm in electrochemistry through his unflinching passion for the subject and his discipline, thoroughness and eyes for details has made me a better chemist, scientist and researcher.

I am grateful to Ms. Jane Davis and Mr. Patrick Orme, both of the HERO research group at Newcastle University for taking me on sampling trips to the studied sites and for helping me to acclimatise to the rainy British weather and the freezingly cold sampling sites. My thanks also go to Dr. Adam Jarvis, also of the HERO group for providing me with background sites information including sites images used in this thesis. The data used for the analytical validation of the voltammetric technique was with permission from the HERO research group and some of these data have been collected under the auspices of the CoSTaR facility, which is funded by an EU-FP6 Access to Research Infrastructure grant, co-ordinated by Prof. Paul Younger at Newcastle University.

I sincerely thank Drs. Andy Brown, Andrew Scott and Mr. John Harrington of the Electron Microscopy and Spectroscopy Centre (LEMAS) at Leeds University for the microscopic characterisation studies and for their comments and suggestions in writing this chapter for my thesis. I also thank Dr. Kath Liddle at Newcastle University for the XRD analysis. I thank the entire technical and administrative staff in the School of Chemistry especially Mrs. Isobel Lamb, Mrs. Janny Rolf, Mrs. Josee Charbonneau (late) and Mrs. Margaret Douglas for their kindness, generosity and for always smiling at me.

Special thanks to my colleagues and the entire Chemical Nanoscience research group, past and present; (Drs. David Fulton, Andrew Pike, Stela Pruneanu, Liqin Dong, Chao Yimin, Norah O'Farrell and Miss Jennifer Hannant) for their friendships, motivation, great research environment and cordiality. I specially thank Prof. Andrew Houlton for his leadership of the group and support throughout my time with the group. I must specially mention Dr. Miguel A.Galindo, Mr. Timothy Hawkins and Mr. Said Al-Said for their comments, suggestions and for being there for me when I needed help during my writing-up of this thesis.

I gratefully acknowledged financial assistance and grants awarded to me during my PhD from the following funding bodies and organisations; Newcastle University, School of Chemistry, the Royal Society of Chemistry (RSC), Society for Chemical Industry (SCI) for the AJ Banks and Messel Awards, RSC-Electrochemistry Group, European Association of Geochemistry (EAGE), Goldschmidt 2008 Travel Award Program funded by NSF, EAG, GS, MAC, GSJ and GBC, the Leche Trust, the British Association for the Advancement of Science, the African Educational Trust (AET) and Churches' Commission for International Students (CCIS) for the Mountbatten Memorial Award.

I am extremely grateful to the following people for their generous assistance and kind support when I first arrived in Britain and have made my academic pursuit successful: Dr. Brian Blandford (Mansion House, London), Mr. Simon Alan-Wright (Camden, London) and Mr. & Mrs. Ajiginni (London).

Last but not the least; I thank all my friends and reviewers from India, Canada and USA for their encouragements, support and for painstakingly proofreading this thesis. I specially thank my beautiful, darling, angelic and my heart desire- Katie Ridley for making me happy and smile all the time during my writing-up and for proofreading part of the thesis. I thank Prof. Dermot Roddy (Science City Professor of Energy), SWAN Institute at Newcastle University for giving me a job in his research group, which catalysed my timely completion of this thesis. Finally, special thanks to my entire family for their encouragements, unconditional love, support and patience for allowing me to pursue my academic ambitions-I love you all.

Abstract

A voltammetric procedure for the determination of dissolved and colloidal iron in mine-waters has been developed. Whilst mine-waters are of course enriched in iron, we are remarkably ignorant of the physical state and chemical speciation of the iron. This is a problem since the physical and chemical state of iron is central to understanding a range of processes relevant to mine-water geochemistry and remediation. Examples include hydrolysis of dissolved Fe (III) to release protons, the adsorption of trace metals onto iron colloids and the bioavailability of iron within wetlands designed to remediate acidic waters.

In this work, we have developed differential pulse voltammetry (DPV) as a rapid and robust method of determining the concentration of truly dissolved and colloidal iron in 0.45 μm filtered waters from a series of mine-water discharges and remediation sites in NE, England. Mine-water samples were collected from CoSTaR sites: these are abandoned mine sites in the UK, designated by the UK Coal Authority for remediation research and routine monitoring of water quality. The sites comprise of six full-scale bioreactors receiving a wide range of mine-waters with pH ranging from 3 to 5 and concentrations of < 0.45 μm iron between 30 and 800 mg L^{-1} across the sites.

Monthly samples were collected over the period March 2006 to April 2007. The samples were analysed directly using differential pulse voltammetry (DPV) at gold electrode. The results show that our analysis provides data for total dissolved iron of comparable analytical quality to the established mine-water analysis techniques based on inductively couple plasma spectroscopy (ICP-OES). The good agreement between the iron concentrations measured in acidified samples electrochemically and by ICP-OES validates the accuracy of DPV as an analytical method for iron.

Colloidal and particulate iron was also determined since DPV measures only dissolved iron, particulate (>0.45 μm) and/or colloidal (<0.45 μm) iron can then be estimated as the difference between the voltammetric responses of natural samples and samples in which the solid phase iron has been dissolved by the addition of HCl.

The percentage dissolved iron ranged from 60-90% (in most cases) in unfiltered samples, while the percentage of colloidal iron varied widely across the sites; from 25-45% in unfiltered samples and 50—75% and 38-85% for dissolved and colloidal iron in the 0.45 μm filtered samples.

The ratio of Fe (II) to Fe (III) in the dissolved fraction was determined using ultramicroelectrodes (UME) method. Iron ratio varied widely for the three sites studied. However, in general, the ratio is 1:1 for the surface influent waters, 1:3 for the sub-surface waters (underground water-Shilbottle site) and 3: 1 for most of the effluent samples. Results suggest that in general, the influent waters are more oxidised and the effluent more reduced.

Finally, characterisation of solid phase iron was done using a wide range of spectroscopic techniques. Atomic Force Microscopy (AFM) shows that iron colloids range from nm to μm for lower pH mine waters; at higher pH, particles mainly aggregates on the μm to mm scale. FT-IR, XRD, TEM and EDX show that the most common colloidal phase is poorly crystalline Fe oxyhydroxides, however certain unusual crystalline phases, e.g., Schwertmannite were found.

Table of Contents

Abbreviations

CV	Cyclic Voltammetry
DPV	Differential Pulse Voltammetry
ICP-OES	Inductively Coupled Plasma-Optical Emission Spectroscopy
AAS	Atomic Absorption Spectrometry
HR-TEM	High Resolution Transmission Electron Microscopy
XRD	X-ray Diffraction
FTIR	Fourier Transform Infrared Spectroscopy
HR-SEM	High Resolution Scanning Electron Microscopy
STEM	Scanning Tunnelling Electron Microscopy
SECM	Scanning Electrochemical Microscopy
EDX	Electron Diffraction X-ray
AFM	Atomic Force Microscopy
CoSTaR	Coal Mine Sites Targeted for Remediation Research.
EU-WFD	European Union Water Framework Directive
HERO	Hydrogeological Engineering Research Outreach
SB	Shilbottle
BC	Bowden Close
QH	Quaking Houses
WS	Whittle Site
AS	Acomb Site
RAPS	Reducing Alkalinity Producing System
SRB	Sulphate-Reducing Bacteria
PRB	Permeable Reactive Barrier
EU-FP	European Union Water Framework Programme
min	Minutes
s	Seconds
L	Litres
h	Hours
mg	Milligrams
UME	Ultramicroelectrodes
DNA	Deoxyribonucleic acid

SCE	Saturated Calomel Electrode
CCD	Charge Coupled Device
FEG	Field Emission Gun
GIF	Gatan Imaging Filter
EELS	Electron Energy Loss Spectroscopy
AMD	Acid Mine Drainage
DME	Dropping Mercury Electrode
HDME	Hanging Dropping Mercury Electrode
SAM	Self Assembly Monolayer
EIS	Electrochemical Impedance Spectroscopy
EN	Electrochemical Noise
CL: AIRE	Contaminated Land: Application in Real Environment
VIP	Voltammetric In-situ Profiling
TNT	Trinitrotoluene
HDPE	High Density Polyethelene
EC	Electrical Conductivity
DO	Dissolved Oxygen
TDS	Total Dissolved Solid
DS	Dissolved Solid
ORP	Oxidation Reduction Potential
Eh	Redox Potential
EA	Environment Agency
ICDD	International Centre for Diffraction Data
ED	Electron Diffraction
COD	Chemical Oxygen Demand
NRA	National Rivers Authority
CA	The Coal Authority
DEFRA	Department of Environment, Food and Rural Affairs
CDENT	County Durham Environment Trust
BSR	Bacterial Sulphate Reduction
SSSI	Site of Special Scientific Interest
T	Temperature
K	Conductivity

List of Figures

List of tables

Chapter 1

INTRODUCTION TO MINE-WATER POLLUTION

This introductory chapter discusses and overviews the history and background of polluted mine-waters. The chapter reviews mine-water pollution under the following headings: chemistry of mine-water formation, environmental impacts of polluted mine-waters, traditional mine-water remediation techniques, advances and current trends in mine-water remediation, present challenges in mine-water remediation, social-economic impacts of mine-water pollution and UK mine-water pollution in the context of the European Union-Water Framework Directive (EU-WFD). The chapter ends by providing an overview of the studied sites (CoSTaR sites), summary of the main aims and objectives of this research work and the broader impacts and significance of this research work.

1.1: Introduction

Mine-water pollution is a major cause of surface and ground water pollution in former mining districts throughout the world [1, 2, 3]. The international mining industry acknowledges that the mitigation of impacts associated with acidic and /or metalliferous mine drainage waters are amongst the most significant environmental challenges facing the industry [12, 13, 14, 15]. One of the key characteristics of the global mining sector from the mid-20th century onwards has been the dramatic expansion of surface mining, which currently accounts for about 80% of global mineral production [12]. As surface mining necessarily involves large scale excavation of overburden (in contrast to deep mining, which delves beneath it), it is not surprising that more than 70% of all the material excavated in modern mining operations world-wide is waste, and more than 99% of all mine waste rock is being generated by surface mines [16]. Acidic discharge from underground mines usually lasts much longer than from surface mines [17] and surface mining generally removes 90% or more of the coal (which often contains the highest sulphide content and acid-producing potential), thereby leaving little in the backfill for continued reaction and acid generation [18].

Mine-water pollution is caused by the oxidation and dissolution of sulphide minerals exposed during mining, this process is catalysed by bacteria activities [4. 5]. The aftermath of coal and sulphide minerals ore mining are widespread and well documented [1, 2, 3, 4]: unless measures are taken to address this trend, mine-water pollution with all its detrimental effects can ensue. Contamination of rivers by ochreous discharges remains a common sight in the former coal and metal mining areas around the world [3, 4]. Uncontrolled pollution discharges from operating and abandoned mines pose significant environmental hazard to groundwater table and freshwater resources worldwide [2, 3]. The acidity and dissolved metals contamination associated with the weathering of sulphide minerals poses an immediate threat to groundwaters that interact with mine workings and to surface waters that receive contaminated discharges. Current estimates reveal that 11% of the global sulphate flux from the continents to the oceans arises from mining activities alone [1, 2].

Quantifying weathering processes and the subsequent transport of elements to the ocean is a fundamental aim of geochemistry and the mining community [3]. The process that plays a significant role in the environmentally damaging phenomenon known as acid mine drainage (AMD) is the reaction of FeS_2 (pyrite) with water and dissolved molecular oxygen to form sulphate and iron oxyhydroxides [4]. During mining processes, pyritic minerals in ore bodies oxidise, resulting in the pollution of mine-water with high concentrations of sulphuric acid and/or metal sulphates [9]. Examples of these processes leading to the generation of abundant quantities of sulphuric acid, generally known as acid mine drainage (AMD) are represented by these chemical equations [8]:

$$2FeS_2 + 7O_2 + 2H_2O \text{ -----} \rightarrow \ 2FeSO_4 + 2H_2SO_4 \quad \text{-------} (1)$$

$$4FeS_2 + 15O_2 + 10H_2O \text{-------} \rightarrow 4FeOOH + 8H_2SO_4 \text{ -------} (2)$$

The growth of autotrophic iron-oxidising bacteria is essential for the formation of AMD under low pH conditions typical of weathered pyrite found in many hard-rock mining sites [7]. Thus, it is generally accepted that the AMD is caused by the oxidation of pyrite by biologically produced ferric iron using O_2 [7].

Pyrite weathering produces acidity and dissolved iron loads, while calcite and to a lesser extent, alumino-silicate minerals provide neutralising capacity that helps maintain circumneutral pH [5]. The acid-base balance of a mine-water discharge is therefore determined by the intrinsic rates and relative abundance and the weathering rate of the respective minerals that produce and consume acidity dictates whether a mine water discharge will be acidic or alkaline [5]. Neutralisation of acid mine-water is achieved by dosing with slaked lime ($Ca(OH)_2$) after which it is separated of suspended metal hydroxides like $Fe(OH)_3$, MnO_2 and others before discharge into the watercourse[10]. However, the discharge of acidic or neutralised acid water. from mining sources contributes to the salinity of surface water [11]. Consequently. because metal ion solubility generally decreases with increasing pH. acidic waters are associated with greater risk from environmental degradation. The oxidative precipitation of iron can then form ochreous deposits in surfaces of water channels [5]. In pyrite, both iron and sulphur are in reduced forms (Fe^{2+} and S^{2-}) respectively [8]. Other transition elements such as cobalt, nickel and copper may partially replace iron and arsenic can replace sulphur in this mineral to some extent [8]. The longevity of the contamination source in mine-water pollution is determined by the lifetime of the source minerals, in particular, the lifetime of pyrite dissolutions dictates how long acidity release will persist [5, 6].

1.2: Mine-Water Pollution in the UK

Mining was once one of the important economic activities in the UK. Britain has one of the longest mining histories in the world. The 18^{th} and 19^{th} centuries saw Britain emerge as the vanguard of the industrial revolution. This era brought considerable prosperity to the country, but not without its price-the pollution and contamination of land. Since 1979, 203 mine sites have been closed and there are only 28 pits now in operation in the whole of the country [19]. There are now 211 significant discharges from abandoned coal mines [20]. Of these about 100 are "significant discharges" affecting almost 200 km of watercourses [21] and about 1.5% of UK rivers by length are already affected by mine-water pollution [22].

Since the late 1970's many coal mines within the United Kingdom have become uneconomic and as a consequence of this economic instability, over 75% of UK mines have been decommissioned [23]. The consequent abandonment of these mine sites and associated operations has resulted in rapid increase in underground rebound within the affected areas [24]. Mine-waters are a major cause of pollution in the UK particularly in Wales, and the north and west of England. The North East of England has a long history of mining dated back to 1811 when the first pit was sunk at Haswell County Durham [25, 26]. Mine-water pollution is the biggest factor affecting water quality in the North East of England [27, 28]. The legacy of the mining era remains as polluted watercourses and large areas of contaminated land and today cleaning up these sites in a sustainable manner is of increasing concern [26].

There are over 900 former deep mines in the UK [26]. Although, virtually all Durham and Northumberland coalfields have been closed and great steps have been taken to reclaim/remediate old mine sites, evidence of their existence can still be seen in the presence of spoil heaps, old adits and mine-water pollution of water resources [29, 30]. The mining industry has changed dramatically in the UK in recent years, as prior to 1999; there was no legal requirement for mine owners to clean up pollution from closure. Perhaps, the most historic events in the history of mining in Britain was the nationalisation of the industry in 1947, during which coal mines previously under private ownership were taken into government control [30] and the privatisation of the industry in 1995. Groundwater from hundreds of former mine sites now threatens the rivers, farmlands, bridges and homes [31].

1.3: Chemistry of mine-water formation

Mine-water pollution has become a major concern because of the environmental impacts of groundwater table recovery and acidic discharge on surface water [32]. Since many of the mines involve sulphide minerals, the production of acid mine drainage is a common problem from abandoned mine sites [34]. The chemistry of mine-water formation is complex and largely controlled by the geology and geochemistry of the parent rocks, oxidation of pyrite is the major determinant [20].

Iron disulphide (FeS_2), or pyrite is the most important mineral associated with acidic mine-water generation [35]. Pyrite breakdown is influenced by a number of factors including variation in its morphology, crystallinity, particle size and reactivity [36, 37. 38]. During coal mining, a significant amount of pyrite (FeS_2) is exposed to air, water and chemosynthetic bacteria [38]. During this period, pyrite is oxidised and the chemosynthetic bacteria utilize the energy obtained from converting reduced iron and sulphur to oxidised iron and sulphate:

$$2FeS_2 + 2H_2O + 7O_2 \text{ --------} \rightarrow 2FeSO_4 + 2H_2SO_4$$

$$2FeSO_4 + 9O_2 + 2H^+ \text{ ----------} \rightarrow 2Fe(SO_4)_3 + 2H_2O$$

$$2Fe(SO_4)_3 + 6H_2O \text{ ----------} \rightarrow 2Fe(OH)_3 + 3H_2SO_4$$

The generalised chemical reactions describing the oxidation of pyrite in the presence of water and oxygen leading to the formation of acidity and sulphate are well known [39].

$$FeS_2(s) + 7/2O_2 + H_2O \text{ --------} \rightarrow Fe^{2+} + 2SO_4^{2-} + 2H^+ \text{ ---------- (1)}$$

$$Fe^{2+} + 1/4O_2 + H^+ \text{ --------} \rightarrow Fe^{3+} + 1/2H_2O \text{ ---------- (2)}$$

$$Fe^{3+} + 3H_2O \text{ ----------} \rightarrow Fe(OH)_3(s) \textbf{ (ochre)} + 3H^+ \text{ ---------- (3)}$$

$$FeS_2(s) + 14Fe^{3+} + 8H_2O \text{ --------} \rightarrow 15Fe^{2+} + 2SO_4^{2-} + 16H^+ \text{ ---------- (4)}$$

Acidity and ferric iron are produced during oxidative weathering of pyrites ($FeS_2(s)$), by either (equation 1) or Fe^{3+} (equation 4) above. The overall rate limiting step for these processes has been shown by Singer and Stumm [39] to be the oxidation of ferrous iron.

Natural attenuation of acidity is provided by weathering of calcite and alumino-silicate minerals associated with the surrounding rocks. The relative rates of these weathering reactions determine whether a mine-water discharge will be net acidic or net alkaline. Thus, the rates of weathering reactions that produce and consume acidity determine the acid-base balance of a mine-water discharge. The acidity and alkalinity for a natural water is defined by the standard zero point which is the acidimetric titration endpoint for carbonic acid. This endpoint corresponds to a pH of 5.6 at atmospheric $pCO_2(g)$ [38]. This classification of mine-water as "acidic" or "alkaline" corresponds to pH ranges below and above 5.6 respectively. These acidic discharges are associated with soluble metals contamination, while neutral or alkaline water discharges are associated with ochre formation due to low solubility of iron (III) oxyhydroxide minerals in this pH range. Generation of alkalinity is associated with microbial sulphate reduction [52] and the process is illustrated by the equation below, in which CH_2O represents the carbon sources utilised by sulphate reducing bacteria (SRB) [53].

$$SO_4^{2-} + 2CH_2O \dashrightarrow H_2S + 2HCO_3^-$$

Generally, as with any groundwater, mine-water pollutions are usually classified according to their major-ion chemistry by using standard geochemical plotting techniques [40]. Although sulphate is usually the dominant anion in polluted mine-water discharges, where biotically mediated oxidation of ferrous iron resulted in precipitation of amorphous ferric hydroxide (ochre), substantial quantities of common metals that could be found in mine-waters are Fe, Al, Zn, Mn, [30] alongside lesser quantities of silicate depending on the associated surrounding parent rocks.

1.4: Mine-water pollution and environmental impacts in the UK

One of the most damaging legacies of mining activities and mine closure has been serious environmental contamination. Since the closure of most of the deep mines in this country in the early 1990's, there has been a steady increase in the discharges of mine-water from abandoned mines and the production of environmentally degrading ocherous waters into surface waters [41].

As a consequence, in the past two decades, there has been increasing public awareness of the potential environmental hazards arising from mining activities, in particular mine-water. Acidic mine-water has been shown to be a multi-factor pollutant due to its complexity and it is therefore difficult to predict and quantify/qualify its overall impact, especially in riverine systems [38].

Mine-water pollution has become a major concern because of the environmental impacts on groundwater table recovery and acidic discharges on surface waters. Pollution from mining activities is one of the main sources of chemical threats to water quality [22]. Mine-waters are a major source of pollution in the UK-particularly in Wales, and the North and West of England [42]. Recent estimates suggest that 7% of rivers and 13% of groundwater in the UK are at the risk of failing the EU water legislation -Water Framework Directive (WFD) targets because of pollution from mining [43]. In addition, latest estimates suggest that there are more than 600 km rivers in the UK, and more than 3000 km in Europe as a whole, that are degraded by abandoned mine drainage [30, 44].

Mine-waters are often characterized by their bright red colour, due to the presence of iron. Other pollutants include zinc, lead, cadmium, manganese and copper [46, 47]. These heavy metals are released as a result of the oxidation of sulphide minerals, particularly pyrite (FeS_2), which are closely associated with coal seams and mineral veins [38]. Aluminium is a particularly ecotoxic metal and is associated with a wide range of human ailments including neurological and bone diseases and may trigger the onset of Alzheimer's diseases. Aluminium contamination of natural waters is therefore a great concern to environmental regulators.

Mine effluent is often acidic and has the potential to cause severe damage to the water courses it enters. Mine closure and water rebound has seen this problem escalate in recent years. Direct public expenditure on mine-water remediation in the UK currently exceeds £8M per annum, and is likely to grow at least £0.25M per annum over the next decade or so [29]. It is generally known that metal ion solubility is pH dependent-solubility decrease with increasing pH, therefore acidic waters are associated with greater risk from dissolved metal loads while alkaline waters are

associated with environmental degradation due to the precipitation of iron as ocherous deposits in surface water channels.

Summary of pollutants associated with mine-waters:

1. Low pH [e.g., 32, 35, 44].
2. Elevated metal concentrations e.g., iron, manganese, aluminium, copper, nickel and zinc [e.g., 35, 48].
3. High inorganic concentrations, e.g., chloride, sodium and particularly sulphate [e.g., 29, 33, 34].
4. High salinity and turbidity [e.g., 38].
5. High chemical oxygen demand (COD) and low dissolved oxygen (DO) concentrations [e.g. 28, 30, 33].
6. Sedimentation processes [e.g., 1, 22, 30].

Summary of impacts associated with mine-water pollution:

1. Pollution of groundwaters, freshwaters and surface water courses [e.g., 46].
2. Metal toxicity, particularly, iron, zinc, manganese, copper, and sometimes lead and silver [e.g., 38].
3. Change in water physico-chemical conditions, e.g., oxygen, temperature, salinity, turbidity and alkalinity [e.g., 21, 24, 38].
4. Acidity-change in pH leading to acidification [e.g., 20, 25, 26].
5. Contamination and degradation of rivers, streams, oceans through discharge into aquifers [e.g., 24].
6. Ecological damage and damage to terrestrial and aquatic ecosystems thus, affecting fish breeding [e.g., 47].
7. Degradation of water quality and biological status of recipient watercourses [e.g., 42, 46].
8. Threat and causing of flooding, thus, damaging water [e.g., 49] and properties and stain deposits of ferric hydroxide, a highly distinctive rust-coloured sludge, on rocks and stream beds. [e.g., 47].
9. Polluted mine-water drastically alters the appearance and ecology of watercourse and wetland wildlife sites [e.g., 19].

1.5: Traditional mine-water remediation techniques

Environmental pollution has become unacceptable to the technological societies due to the increased awareness of pollution effects, tighter controls and stringent regulations on the discharge of potential pollutants and toxic materials. Pollution from mining activities is one of the main sources of chemical threats to water quality. Technologies to treat this problem are currently advancing owing to new developments in the use and application of fundamental science to solve environmental issues. The treatment of polluted mine-waters is a major problem in the mining industry because it is a very complicated, complex and long term process (cost intensive). In particular, the life cycle of contaminant and measurements of speciation of iron species in mine-water discharges is critical when choosing treatment technology or selecting approaches to handling mine-water pollution. A wide range of treatment technologies have been developed over the last decades which can be generally classified as active or passive remediation technology. There are three principal options for mine-water remediation [30]. These are:

(a). Monitored natural attenuation; which is based on natural processes. Though it takes a long time, it is by far the best option due to low cost, sustainability and it is environmentally friendly. However, the choice of this method depends heavily on the concentrations of the pollutants in the mine-water. Previous studies [e.g., 30, 48] have identified a number of factors which affect the natural attenuation rates of mine-water pollution. These factors include the rainfall profiles, water flow rate among others.

(b). Prevention/minimisation of pollutant release processes; the choice of this option depends on individual case study and the geochemistry of the site and also on the concentration of the pollutants.

(c). Mine-water treatment by either active or passive means or a combination of both.

Until the 1990s, the only 'proven technologies' for abating mine-water pollution were what is now called 'active treatment' [30]. which involves the application of industrial reagents and external power sources (for stirring, pumping, heating etc) by means of

conventional unit processes common to many chemical and environmental engineering plants [30]. Active treatment is simply a process of chemically dosing mine-water. Passive treatment (wetland) is rapidly becoming the technology of choice for the long term treatment of mine-water in Britain where certain criteria are met, e.g., enough land space for the construction of wetlands [26, 29, 30]. Compost-based systems can cope with a wide range of influent pH and a broader cocktail of contaminant metals than aerobic reed-beds [48]. Contaminant removal processes in most compost wetlands are predominantly microbial [e.g., 62, 81]. Bacterial sulphate reduction generally governs both the raising of pH and the removal of those metals that form sulphides at ambient temperatures and pressures (Fe^{2+}, Zn^{2+}, Cu^{2+}, etc). The most common formulation of the treatment pathway presumed to be occurring in compost wetlands is represented by equations 1 and 2 [62].

$$2CH_2O + SO_4^{2-} \text{----------} \rightarrow H_2S + 2HCO_3^- \qquad (1)$$

$$HCO_3^- + H^+ \text{---------} \rightarrow H_2O + CO_2 \qquad (2)$$

The reaction of bicarbonate with protons present in the water (equation 2), yields a rise in pH (at least as long as the CO_2 is able to vent to the atmosphere). This rise in pH fosters the precipitation of hydroxide minerals, which can help remove metals that do not form sulphides at ambient temperatures and pressures (e.g., Al^{3+} and Fe^{3+}). Laboratory investigations at Newcastle University (2000-2001) funded by Northumbria Water Ltd has demonstrated that ochre ($Fe(OH)_3$ / FeO.OH) is capable of removing very high concentration of phosphate in polluted mine-water [30].

At the end of 2001, 14 mine-water treatment systems were in operation and some 30 more at various stages of development in England, Scotland and Wales [26]. Six types of passive systems are now being used in the UK (and each of these technologies is appropriate for a different kind of mine-water) for mine-water treatment namely [26, 27, 30, 48]:

- Aerobic, surface flow wetlands (reed-beds) [e.g., 78]
- Anaerobic, compost wetlands with significant surface flow [e.g., 40, 46, 79]
- Mixed compost/limestone systems, with predominantly subsurface flow (so-called Reducing and Alkalinity Producing Systems (RAPS) [e.g., 46, 80]

- Subsurface reactive barriers to treat acidic, metalliferous ground waters [e.g., 30]
- Roughing filters for treating ferruginous mine waters where land availability is limited [e.g., 32, 35]
- Closed-system limestone dissolution systems for zinc removal from alkaline waters.

1.6: Advances and current trends in mine-water remediation

Traditional active treatment processes such as reverse osmosis or the addition of chemicals are often not very efficient and not cost effective [72]. In some cases, the use of such processes is not even feasible [69]. Therefore alternative methods have to be considered. One of the alternative methods is the bioremediation process in which sulphate-reducing bacteria (SRB) are used to decontaminate mine pollution in a wetland system. The sulphate reducing bacteria are able to eliminate metals such as iron, zinc, copper and others and neutralise the water and lower sulphate concentrations [52, 54, 58]. In this process, SRB reduce metal sulphates to insoluble metal sulphides as part of their metabolic activity. These sulphides precipitate, removing the metals from the water. In addition, a number of species of SRB are also able to reduce some radioactive and dangerous metals, e.g., reduction of uranium (VI) (soluble) to uranium (IV) (insoluble). It is important to add that anaerobic wetlands have been found to be most appropriate for mine-water pollution with net alkalinity to neutralise metal acidity [82], while aerobic wetlands are recommended for use where mine pollution has net acidity [83]. This is because generally, SRB do not grow well at pH below 5.5 and prefer higher levels of alkalinity, with pH 6.6 being optimal [84]. Therefore, a treatment such as constructed wetland should include a process step in which the pH of the mine drainage is first raised [85]. The basic equations for SRB-mediated sulphate reduction are represented below [86, 87, 88].

$$2CH_2O + SO_4^{2-} \longrightarrow H_2S + 2HCO_3^- \quad (1)$$

$$M^{2+} + H_2S \longrightarrow MS\,(s) + 2H^+ \quad (2)$$

Where CH_2O (equation 1) represents a carbon source and M is a typical dissolved divalent metal cation in mine-water drainage and MS is the solid precipitate. The hydrogen sulphide quickly reacts with any dissolved divalent cation in the water (e.g.. Zn, Cd, Ni) (equation 2), which results in the precipitation of relatively insoluble metal sulphides. Thus the overall action of the SRB is to raise alkalinity and buffer the solution. The constructed wetland technology for the treatment of mine drainage became common in the USA in the 1980s and by 1989, there were at least 300 constructed wetlands in operation across the US at mining facilities [88] and well over 1000 by the end of the twentieth century [82].

The fundamental aim of treatment of mine-water is to remove iron, sulphate and heavy metals from waters and to increase alkalinity [44]. However, the situation is complex due to the variable oxidation states of iron and compositional changes in the pyrite concentration over time. Therefore it is necessary to complement the traditional remediation techniques (mainly active and passive treatments) to understand and identify the relevant biogeochemical processes that regulate the fate of pollutants and the cycling of essential elements in polluted mine-waters. Of particular interest in mine-water are the speciation of dissolved Fe and S species and the nature and interplay of the host of redox transformations involving these species.

In the UK, prior to the 1990's, mine-water remediation was aimed at regeneration of the sites through re-vegetation; there has been a change of paradigm and focus in the last decade. Efforts are now directed at total and long-term control. A wide range of treatment technologies have been developed in the last decades [26, 34, 40, 54, 56]. These may be classified as "active" or "passive". Active systems employ forced aeration and/or addition of chemical reagents (chemical dosing) to cause iron to oxidise and precipitate rapidly as orange hydrated iron oxide (ochre) sediments in lagoons. Passive systems are usually constructed wetlands, which filter residual ochre overflowing from the lagoons. They are aesthetically pleasing and inexpensive to construct, operate and maintain compared to active systems [40, 56, 57].

Passive treatment technology for mine wastes was introduced to the UK during the 1990s' principally by adopting the U.S. Bureau of Mines experiences [62]. Passive treatment systems are now widely used because of the cost associated with active

treatment systems. Under passive systems, mine-water treatment systems are designed to fit sustainably into the local environment and to operate in perpetuity with the minimum of maintenance [40]. Their designs are subject to full regional government planning criteria, in particular with regard to efficient technology, public acceptance and enhancement of the environment. New developments need to take account of all of these criteria and are normally undertaken in collaboration with a consulting company, relevant land owners, the planning authorities and the Environment Agency [54, 55, 56]. Because of the variability of the numerous criteria involved every new system has novel aspects. Research is therefore required to understand the details of their operation.

Electrochemical techniques have been widely used in environmental analysis, especially for the determination of heavy metals and their speciation, other redox active analytes, e.g., oxygen and sulphur can also be determined [58, 59, 60]. The last ten years have seen a dramatic increase in the use and utility of electrochemical techniques in environmental analysis [58]. Robust electrochemical analyses provide understanding of the dynamics and mechanisms of pyrite dissolution and compositional changes in the pyrite concentration with time can be monitored by using in-situ electrochemical analysis. Since the 1970s, when the first in-situ measurements of oxygen in the ocean were reported, the development of electrochemical sensors for in-situ measurements in aquatic systems has significantly intensified [61].

Application of electrochemical sensors (amperometric, potentiometric and voltammetric) for in-situ analysis has been reported by Taillefert and co-workers [62]. Voltammetric techniques are attractive to measure chemical species in-situ because they can detect several analytes in the same potential scan; they have lower detection limits, and generally do not suffer from matrix interference problems of the kind that affect atomic spectroscopy [61, 62]. Although on-site measurements of voltammetric studies of Pb, and Cd have been reported [62], reports of in-situ measurements using voltammetric sensors are still uncommon, tests in the laboratory are promising [63, 64, 65, 66, 67].

1.7: Challenges in mine-water remediation

Dealing with high concentrations of sulphates and metals is one of the major problems connected with the closure of many base metal and coal mines [76]. Large volumes of acidic water from the mines, waste rock piles and tailings can be generated as presented in some of the sites studied in this research work. Usually, this acidic discharge can not be disposed off until it has been treated in some way as it poses a direct threat to drinking water, agriculture, vegetation, wildlife and waterways. One of the key challenges during the closure and reclamation of mines is the prevention and management of pollution arising from the mines. Although, iron disulphide (FeS_2), or pyrite is the most important mineral associated with acidic mine-water generation, the breakdown of pyrite is influenced by a number of factors such as crystalline structure, particle size and reactivity [36, 37, 40] revealed that "vestigial" and "juvenile" rocks are the two components responsible for the long-term generation of acidity of mine-water. The acidity arising from the latter is due to the continual pyrite oxidation within the mined system. Treatment of this could take up to many hundred years or centuries until the supply of pyrite (the main source) is finally exhausted [51]. So, in terms of cost etc, this is a very long period of pollution management. Often, the need for long-term active treatment of mine-water can be minimised or eliminated by effective closure designs that use combinations of passive systems for managing acid mine drainage (AMD).

It is generally known that metal ion solubility is pH dependent. However, the solubility of aluminium is particularly highly pH sensitive, thus at pH 4.5, little aluminium remains soluble and therefore precipitates.

As a consequence, the treatment of aluminium contaminated waters are complex because, these aluminium precipitates can be wind-blown onto adjoining land, downstream and watercourses due to the low density of the aluminium hydroxide/hydrophosphate precipitates [52, 53]. In addition, aluminium hydroxide precipitation is an acidity-generating process in itself as shown in this well known equation:

$$Al^{3+}(aq) + 3H_2O \text{ -------} \rightarrow Al(OH)_3(s) + 3H^+$$

As a consequence, as more solid $Al(OH)_3$ precipitates, the pH drops and Al^{3+} becomes more soluble, thus creating an aluminium cycle.

The long-term water quality of mine-water discharges particularly the matured mine-water discharges (after the "first flush") can be predicted from the geological features of the site [47]. However, predicting and quantifying the overall effects is an onerous task and usually difficult. So, in general, the lifetime of the source minerals determine the longevity of the contaminant source in mine-water pollution [e.g., 40]. In particular, the lifetime of pyrite dissolution dictates how long acidity release will persist.

1.8: UK Mine-water pollution in the context of European Union Water Framework Directive (EU-WFD)

Worldwide well-publicised instances of aquatic pollution due to mining accidents have prompted re-evaluation of environmental policies related to mining in North America, Europe and Australia [86]. While the protection of ground and surface waters from most forms of industrial pollution has long been subject to legislative protection, mine-water pollution has been less regulated. This led to the formation of the Europe-wide mine-water legal and policy framework known as the EU-WFD.

The achievement of the European Union-Water Framework Directive (EU-WFD) goals by the UK government is significantly undermined by the legacy of the coal and metal mining era, since pollution from abandoned mines constitutes one of the major causes of surface and ground water contamination in many catchments, especially in Wales, and the north and west of England. Due to economic instability, over 75% of the UK mines have been closed or decommissioned since 1970's as many coal mines within the UK became uneconomical [30]. The abandonment of these mines and associated operations subsequently resulted in a rapid increase in groundwater rebound within the affected areas. As a consequence, Britain's mining regions including the North East of England have faced a serious pollution crisis since late 1970's.

In the UK, iron, manganese, aluminium and sulphate (generating mine-water acidity) are the most prolific contaminants. In addition, as most mines in the UK extracted coal rather than metalliferous minerals, the main metal of concern is iron. As a consequence, Fe is the most common metal found in polluted mine-water discharges and plays a crucial role in determining the fate, interactions, biogeochemical cycle and the behaviours of redox species in the mine-water environment. In 1997, the report "Undermining Our Future" by the shadow Environmental Protection Minister, Michael Meacher revealed that pollution from rising mine-water threatens more than 211 sites in Britain-consisting of 110 sites in Scotland, 36 sites in Yorkshire, 25 sites in North West and 21 sites in Wales. In 1994, the Environment Agency estimated that there are about 100 "significant discharges" affecting almost 200 km of water courses (about 1.5% of UK rivers by length) in its report "Abandoned Mines and the Water Environment.

After diffuse agricultural pollution, mining poses the most widespread pollution threat to status objectives in England and Wales [26, 30, 76]. In 2004, The Environment Agency's (EA) initial characterisation of water bodies in England and Wales for the Water Framework Directive (WFD) indicated that mine-water pollution is one of the most significant causes of water bodies being at risk of their WFD environmental objectives [76]. Across the EU (based on fifteen Member States), it has been suggested that the total length of watercourses polluted by mine drainage is in excess of 5000 km [65, 66, 68]. In the UK, the Environment Agency (EA) assessment estimated that 26 out of 356 groundwater bodies (7.3% but 14% by land surface area) and 226 out of 5868 surface water bodies (3.9%, but 7% by river length) are "at risk" due to mine-water pollution [76].

1.9: An overview of the CoSTaR sites studied in this thesis

Mine-water pollution is a serious problem in areas of extensive surface and underground coal mining, such as the North East region, where pyrite and other metal sulphides are found within the coal and associated rocks. In the North East of England, particularly in County Durham, since the closure of the last pits in 1993, mine-water pollution has been rising, contaminating drinking water supplies, the aquifer and the underground reservoir in the east Durham area. Since then, mine-water pollutions due to abandoned mine sites have been reported in other locations across the region [26, 27, 28]. These sites include Shilbottle and Whittle in Northumberland County, Acomb in Hexham, Quaking Houses and Bowden Close in county Durham and St. Helen Auckland in Bishop Auckland. This led to the establishment of the CoSTaR sites in 2002 by the Hydro- geological Engineering Research Outreach (HERO) Group at Newcastle University, the Coal Authority, Durham and Northumberland Councils and CL:AIRE (Contaminated Land: Application In Real Environment). CoSTaR consists of the six sites that comprise the Coal mine Site for Targeted Remediation Research (CoSTaR) facility in the northeast, England (figure.1).

Coal Mine Sites Targeted for Remediation Research (CoSTaR) sites are the UK abandoned mine sites identified, designed and established by Coal Authority for remediation research and for routine monitoring of mine-water quality. All sites are within 45 minutes drive of Newcastle University and comprise six full-scale bioreactors, including a Permeable Reactive Barrier (PRB), a compost wetland, a reducing and alkalinity producing system (RAPS) and four varieties of aerobic wetlands (receiving a range of acidic and alkaline mine-waters with peroxide pre-dosing in one case). The similarities between these sites are that they are all abandoned mine sites with significant metal pollution, particularly iron and are established to remediate watercourses contaminated by colliery spoil leachates.

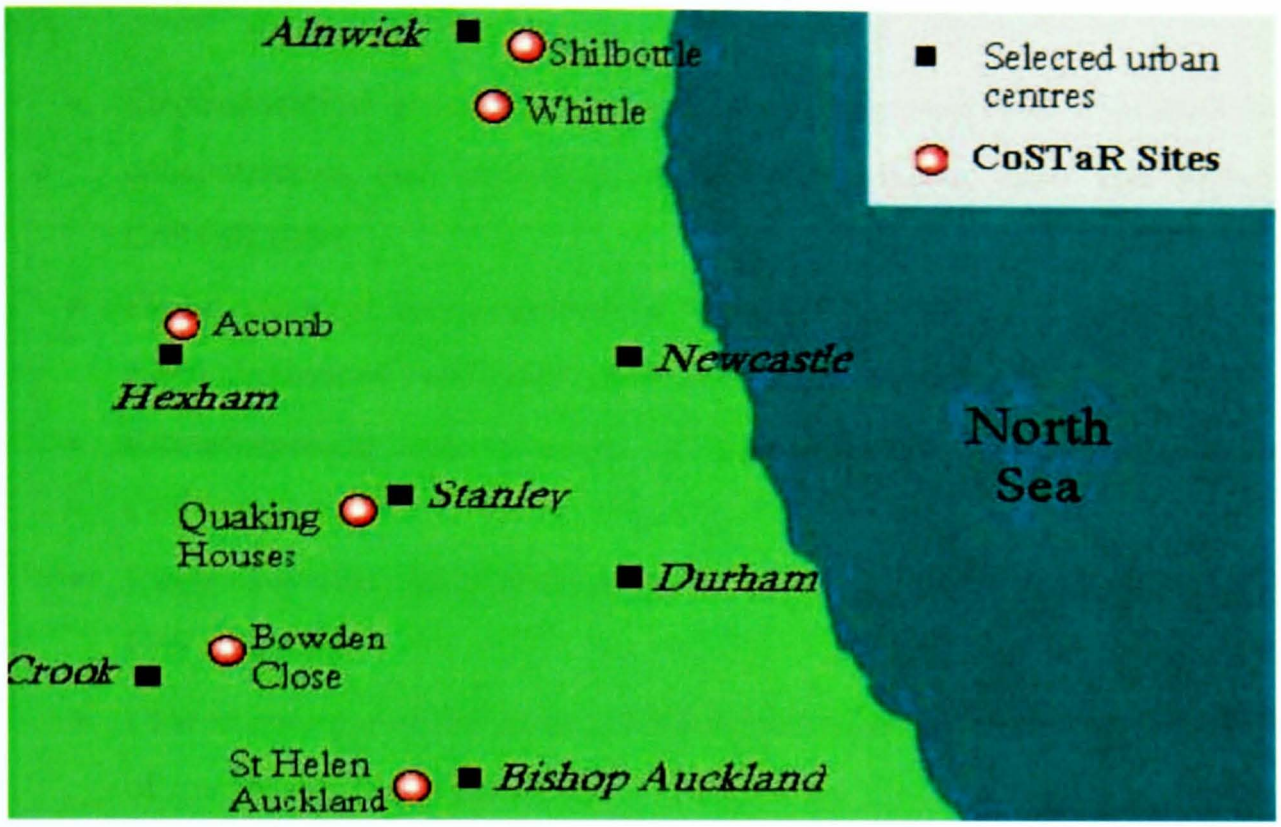

Figure 1.1: Map showing an overview of the CoSTaR sites and locations of the studied areas-Courtesy of HERO Research Group at Newcastle University.

1.9.1: Research aims and objectives

In-situ monitoring of the dynamics, mechanisms, and compositional changes in the concentrations of iron species namely Fe(II) and Fe(III), with time is critical to understanding and implementation of any successful remediation strategy. One of the novel monitoring techniques is in-situ electrochemical measurements which offer the possibility of providing results in real-time. The particular application of interest in this research project is the study and investigation of mine-water remediation in compost-based wetlands. Hopefully, it would lead to better and more effective management of polluted mine-waters and in better understanding of the mine-water systems so as to help in the choice and implementation of sustainable and cost-effective remediation strategies.

Summary of research aims and objectives are:

- Electrochemical measurements of temporal and seasonal variability in the concentrations and speciation of dissolved/soluble total iron across the CoSTaR sites.
- Electrochemical measurements of temporal and seasonal variability in the concentrations of Fe(II) and Fe(III) across the CoSTaR sites.
- Electrochemical determination of colloidal/solid phase iron across the CoSTaR sites.
- Electrochemical determination of the ratio of Fe(II) to Fe(III) across the CoSTaR sites.
- Characterisation of the observed solid phase/colloidal iron using a wide range of spectroscopic and microscopic techniques.

1.9.2: Broader impacts and significance of research

Mine-water pollution is a major cause of surface and ground water pollution in former mining districts throughout the world [5, 7, 8]. In many parts of Europe, mine-water pollution constitutes the greatest potential barrier to achieving "good status" water bodies, a key requirement of the EU-Water Framework Directorate. For example, one of our study sites (Shilbottle Mine, Northumberland) emits one of the most polluted coal spoil heap leachates in the UK, discharging large volumes of iron- (and other metal) rich, low pH waters into a major regional river system close to a major abstraction point. This significantly increases the cost of water purification and treatment.

Thus, across the CoSTaR sites, as with other mine-waters, the physical and chemical state of iron is central to understanding a range of processes relevant to mine-water geochemistry and remediation. Examples include the hydrolysis of dissolved Fe(III) to release protons, the adsorption of trace metals onto iron colloids and the bioavailability of iron within wetlands designed to remediate acidic mine waters.

Key biogeochemical issues include the physicochemical state of the iron, e.g. its redox state and its division between particulate (including colloidal) and truly dissolved.

Conventional techniques to differentiate (a) Fe(II)/Fe(III) and (b) solid phase vs. truly dissolved iron have hitherto been lab-based, time-consuming and unsuited to continuous monitoring. My work demonstrates, for the first time, the potential of voltammetric methods to monitor dissolved and colloidal iron in polluted mine-waters in-situ. I have shown that a substantial proportion of < 0.45 μm iron is in fact solid phase, and have combined the novel analytical work with state of the art imaging techniques (AFM, XRD, HR-TEM, HR-SEM, STEM and EDX) to demonstrate the nature of the iron-rich colloids, and their mineralogy.

Although we have yet to conduct a field trial, the robust, reliable and accurate voltammetric techniques described here have huge potential for obtaining the kind of real-time data which are rarely gathered but which are critical to both environmental monitoring and understanding temporal variations in biogeochemical cycles.

1.9.3: References

[1]. Nordstrom, D.K. and Southham, G. *American Mineralogical Society*. **1997**. 35. 361-390.

[2]. Berner, E.K. and Berner, R.A. G. *Environmental Science and Technology*, **1996**. 29, 2169-2175.

[3]. Hill, D.M. and Aplin, C.A. *Limnology Oceanography*, **2001**, 46, 331-344.

[4]. Banwart, S.A. *Tsinghua Science and Technology*. **2000**, 5. 310-313.

[5]. Usher, C.R., Cleveland (JR), C.A., Strongin, D.R. and Schoonen, M.A. *Environmental Science and Technology*, **2004**, 38, 5604-5606.

[6]. Younger, P.L. *Contaminant Hydrology*, **2000a**, 44, 47-69.

[7]. Bilgin, A.Z., Silverstein, J. and Hernandez, M. *Environmental Science and Technology*, **2005**, 39, 7826-7832.

[8]. Murad, E. and Rojik, P. 3rd *Australian New Zealand Soils Conference, 5-9 December, University of Sydney, Australia*, **2004**.

[9]. Jones, G.A., Harris, R.C. and Greig, J.D. *Report 136/1/89 to Water Research Commission by Steffen, Robertson and Kirsten (Pretoria) Inc.*, **1988**, 1-8.

[10]. Hlabela, P., Maree, J. and Bruinsma, D. *Mine Water and the Environment*, **2007**, 26, 14-22.

[11]. Verhoef, L.H. *Groundwater*, **1982**, 141-147.

[12]. Younger, PL. and Robins, N.S. *Mine Water Hydrogeology and Geochemistry*. *Geochemical Society*, London, **2002**. Special Publication 198. 404pp.

[13]. ICOLD/UNEP. International Commission on Large Dams (ICOLD) Bulletin 12.1. *Jointly published by ICOLD and the United Nations Environment Programme (UNEP) Division of Technology, Industry and Economics (DTIE)*, **2001**. ICOLD, Paris, 144pp.

[14]. UNEP. Results of the survey for the years 1980-1996. *Prepared by Mining Journal Research Services for the United Nations Environment Programme*, **1996**, Paris, 130pp.

[15]. UNEP. Assessment Mission Report. *United Nations Environment Programme, Office for the Co-ordination of Humanitarian Affairs*, **2000**, Geneva, 60pp.

[16]. Younger, P.L., Banwart, S.A. and Hedin, R.S. Mine Water: Hydrology, Pollution, Remediation. *Kluwer Academic Publishers, Dordrecht (ISBN-1-4020-0137-1)*, **2002**, 464pp.

[17]. Wood, S.C., Younger, P.L. and Robins, N.S. *Engineering Geology*, **1999**, 32, 69-79.

[18]. Demchak, J., Skousen, J. and McDonald, M. *American Association for Surface Mining and Reclamation*, **1997**, 656-668.

[19]. Chapman, C.S. and Van Den Berg, C.M.G. *Environment Science and Technology*, **2005**, 39, 2769-2776.

[20]. Banks, D. and Younger, P.L. *Hydrogeology*, **1996**, 4, 55-68.

[21]. Environmental Agency. Abandoned Mines and the Water Environment, *Environment Agency Report*, **1994**.

[22]. National Rivers Authority (NRA). *Report of the National Rivers Authority, Northumbria and Yorkshire regions*, Leeds, **1994**, 54pp.

[23]. DETR. *The Government's Response to the Coalfield Taskforce Reports*, **1998**.

[24]. Henton, M.P. *Quality of Groundwater*, **1981**, 111-116.

[25]. Bank, D., Younger, P.L., Arnesen, R.T., Iversen, E.R. and Banks, S.B. *Environmental Geology*, **1997**, 32, 157-174.

[26]. Banks, S.B. *Chartered Institute of Water and Environmental Management*, **2003**, 17, 117-122.

[27]. Younger, P.L. *Institute of Water and Environmental Management*, **1993**, 7, 521-531.

[28]. Younger, P.L. *Mineral Planning*, **1994**, 4, 6-8.

[29]. Younger, P.L. *Contaminant Hydrology*, **2002**, 44, 47-69.

[30]. Piramid Consortium. *European Commission 5th Framework RTD Project no EVK1-CT-199-000021*, **2003**, 166PP.

[31]. Younger, P.L. *Mineral Planning*, **1995b**, 65, 38-41.

[32]. Younger, P.L. *Science of the Environment*, **2000a**, 115-119.

[33]. Younger, P.L. *Applied Geochemistry*, **2000b**, 15, 1383-1397.

[34]. Younger, P.L. *Transaction of the Institute of Mining and Metallurgy Section a-Mining Technology*, **2001**, 109, A210-A218.

[35]. Younger, P.L. *Applied Geochemistry*, **2000c**, 15, 1383-1397.

[36]. Riley, C.V. *Water Ecology*, **1960**, 60, 106-121.

[37]. Barnes, H.L. and Romberger, S.B. *Water Pollution Control*, **1968**, 40, 371-384.

[38]. Gray, N.F. *Environmental Geology*, **1997**, 30, 62-71.

[39]. Singer, P.C. and Stumm, W. *Science (New York)*, **1970**. 167. 1121-1123.

[40]. Younger, P.L. *Society for Environmental Geochemistry*. **1997**.

[41]. Younger, P.L. *Quarterly Journal of Engineering Geology*, **1995**, 34, 1262-1268.

[42]. Younger, P.L. *Chartered Institute of Water and Environmental Management*, **1997a**, 189pp.

[43]. Younger, P.L., Coulton, R.H. and Froggatt, E.C. *Science of the Environment*, **2004**, 338, 137-154.

[44]. Strumberg, B. and Banwart, S. *Applied Geochemistry*, **1999**, 14, 116-121.

[45]. NRA, Report of the National Rivers Authority, *Water Quality Series*, **1994**, No.14. HMSO, 44pp.

[46]. Younger, P.L. *The Science of the Total Environment*, **1997a**, 194, 457-466.

[47]. Younger, P.L. *The Science of the Total Environment*, **2001**, 265, 309-326.

[48]. Younger, P.L. and Nuttall, C.A. *Water Research*, **2000**, 34, 1262-1268.

[49]. Schmolke, C.MR. *Land Reclamation*, **1998**, 517-523.

[50]. Butler, I.B. and Rickard, D. *Geochemica et Cosmochimica Acta*, **2000**, 64, 2665-2672.

[51]. Stromberg, B. and Banwart, S. *Applied Geochemistry*, **1994**, 9, 583-595.

[52]. Fabian, D., Aplin, C. and Younger, P.L. *Unpublished report*, **2006**.

[53]. Fabian, D., Jarvis, A.P. and Younger, P.L. *CL: AIRE Research Report: TDP5*, May **2006**.

[54]. CL: AIRE Case Study Bulletin. Shilbottle Colliery Remediation Scheme: *The UK's First Large-Scale Permeable Reactive Barrier for Mine Spoil Leachate Remediation*, autumn, **2002**.

[55]. CL: AIRE Case Study Bulletin. *Mine Water Treatment at Wheal Jane Tin Mine. Cornwall*, March, CSB4, **2004**.

[56]. CL: AIRE Case Study Bulletin. Coal Mine Site for Targeted Remediation Research: *The CoSTaR Initiative*, CB3, March, **2006**.

[57]. Whitehead, P.G. and Prior, H. *Science of the Total Environment*, **2005**, 338, 15-21.

[58]. Brendel, P.J. and Luther III, G.W. *Environmental Science and Technology*, **1995**, 29, 751-1013-1016.

[59]. Luther III, G.W. *Geomicrobiology*, **2005**, 22, 195-203.

[60]. Luther III, G.W., Brendel, P.J., Lewis, B.L., Sundby, B., Lefrancois, L., Silverberg, N. and Nuzzio, D.B. *Limnology and Oceanography*, **1998**, 43, 325-333.

[61]. Taillefert, M., Rozan, T.F., Glazer, B.T., Herszage, J., Trouwborst, R.E. and Luther, G.W. *American Chemical Society, Washington D.C.*, **2002**, 811, 247-264.

[62]. Taillefert, M., Bono, A.B. and Luther III, G.W. *Environmental Science and Technology*, **2000a**, 34, 2169-2177.

[63]. Richard, D., Oldroyd, A. and Cramp, A. *Estuaries*, **1999**, 22, 693-701.

[64[. Richard, D. *Geochimica et Cosmochimica Acta*, **1997**, 61, 115-134.

[65]. Richard, D. and Luther III, G.W. *Geochimica et Cosmochimica Acta*, **1998**, 61, 135-147.

[66]. Rozan, T.F., Taillefert, M., Trouwborst, R.E., Glazer, B.T., Ma, S., Herszage, J., Valdes, L.M., Price, K.S. and Luther III, G.W. *Limnology Oceanography*, **2002**. 47. 1346-1354.

[67]. Rozan, T.F., Theberge, S.M. and Luther III, G.W. *Analytical Chimica Acta*. **2000**,415, 175-184.

[68]. Taillefert, M., Luther III, G.W. and Nuzzio, D.B. *Electroanalysis*, **2000b**. 12. 401-412.

[69]. Pizeta, I., Billion, G., Fischer, J. and Wartel, M. *Electroanalysis*, **2003**, 15. 1389-1396.

[70]. Luther III, G.W., Theberge, S.M., Rickard, D. and Oldroyd, A. *Environmental Science and Technology*, **1996**, 30, 671-679.

[71]. Luther III, G.W. *Geochemical Society*, **2002**, 113, 14-19.

[72]. Luther III, G.W., Shellenbarger, P.A. and Brendel, P.J. Geochimica *Cosmochimica Acta*, **1996**, 60, 951-960.

[73]. Ibanez, J.G. *Chemical Education*, **1995**, 72, 1050-1052.

[74]. Banwart, S., Destouni, G. and Mahistrom, M. *International Association of Hydrological Sciences*. **1998**.

[75]. Dollhope, M.E., Nealson, K.H., Simon, D.M. and Luther III, G.W. *Marine Chemistry*, **2000**, 70, 171-180.

[75]. Hedin, R.S., Nairn, R.W. and Kleinmann, R.L.P. *U.S. Bureau of Mines Information Circular 9387*, **1994**, 35pp.

[76]. Gandy, C.J., Smith, J.W.N. and Jarvis, A.P. *Science of the Total Environment*, **2007**, 373, 435-446.

[77]. Environment Agency: www.environment-agency.gov.uk. Retrieved on 18th September, 2008.

[78]. Laine, D.M. *Chartered Institute of Water and Environmental Management.* **1997**, 83-103.

[79]. Edwards, P.J., Bolton, C.P., Ranson, C.M. and Smith, A.C. *Chartered Institute of Water and Environmental Management*, **1997**, 17-32.

[80]. Kepler, D.A. and McCleary, E.C. *Proceedings of the International Land Reclamation and Mine Drainage*, **1994**, 1, 195-204.

[81]. Walton-Day, K. *Society of Economic Geologists*, **1999**, 6, 215-228.

[82]. Skousen, J. *American Society for Agronomy, and the American Association for Surface Mining and Reclamation*, **1998**.

[83]. Mattes, A. *Nature Works Remediation Corporation Progress report for Environment Canada*, **2002**.

[84]. Govind, R., Yong, W. and Tabak, H. Allemans (eds), *Battellee Press, Columbus*, **1999**, OH. 37pp.

[85]. Mattes, A., Gould, W. and Duncan, B. *ESSA conference, Banff, Alberta*, October **2002**.

[86]. Kleinman, R. and Grits, M. Reddy, K. and Smith, W. (eds), *Magnolia Publishing*, **1987**, 225pp.

[87]. Huntsman, B., Solch, J. and Potter, D. *Geological Society*, **1978**, 91st Annual Meeting, Ottawa, ON.

[88]. Kadlec, R. and Knight, R. *Lewis Publishers, Boca Raton, FL*, **1996**.

[89]. Watzlaf, G., Schroeder, K. and Kairies, C. *Proceedings of 17 Annual Meeting, ASSMR, Tampa, FL*, June **2000**.

[90]. Higgins, J. *Environmental Science Health*, **2000**, A35, 1309-1334.

[91]. Higgins, J., Hurd, S. and Weil, C. *Proceedings of 4th International Conference on Ecol.Eng. Oslo, Norway*, June **1999**.

[92]. Hard, B., Friednich, S. and Babel, W. *Microbiology Research*, **1997**, 152, 65-73.

[93]. Grits, M. and Kleinmann, R. *Proceedings of National Symposium on Mining, Hydrology, Sedimentology and Reclamation, University of Kentucky*, **1986**, 165-171.

[94]. Fortin, D., Goulet, R. and Roy, M. *Geomicrobiology*, **2000**, 17, 221-235.

[95]. Brown, M., Barley, B. and Wood, W. *IWA Publishing*, **2002**, London, UK.

Chapter 2

ELECTROCHEMICAL TECHNIQUES AND TECHNOLOGIES

This chapter provides an overview of the development and advances in the use of electrochemical technologies and applications to environmental monitoring. The chapter covers sections on electrochemical sensors, ultramicroelectrodes technology (UMEs), trends and advances in electrochemical technologies. applications of electrochemical technologies in environmental analysis and challenges in the use of electrochemical technologies for in-situ monitoring.

2.1: Introduction: An overview of electrochemical sensors

The development of chemical sensors is currently one of the most active areas of analytical research [20, 81]. Electrochemical sensors represent an important subclass of chemical sensors with wide applications in the fields of clinical, industrial, environmental and agricultural analyses [105, 106]. It is an interdisciplinary area of research with possibilities in a number of directions including electrochemical biosensors, gas sensors, etc. Generally speaking, virtually all areas of professional science, human endeavours and engineering have been permeated by this fast-growing branch of science and technology called sensors. This field of research generates thousands of new publications every year [105, 106]. In broader terms, there are generally two divisions of sensors; physical and chemical/biochemical sensors with broad applications in industry, medical and environment. This overview will provide an overview of chemical sensors with emphasis on electrochemical sensors technology.

Electrochemical detection is usually performed by controlling the potential of the working electrode at a fixed value and monitoring the current as a function of time. The current response thus generated reflects the concentrations profiles of these compounds as they pass through the detector. The periodic or continuous measurements of activities of chemical species and their variation with time is an extremely important area of application of electrochemical sensors.

Electrochemical sensors have been widely used in such applications as critical care, safety, industrial hygiene, process controls, product quality controls, human comfort controls, emission monitoring, automotive, clinical diagnostics, home safety alarms, biomedical applications, environmental sensing and monitoring and more recently in security and defence for the detection and prevention of terrorist activities [12, 27]. The basis of electrochemical sensors is on the interaction of the analyte with the recognition layer which produces an electrical signal from which analytical information is obtained. Based on the devices, most electrochemical devices, sensors and technologies fall broadly into two major categories depending on the nature of the electrical signal: potentiometric or amperometric methods [28, 29, 30]. Amperometric sensors is the detection of electroactive species involved in the chemical or biological recognition process whilst in potentiometric sensors; the analytical information is obtained by converting the recognition process into a potential signal, which is proportional to the concentration of the electroactive species [32, 33].

As a class of sensors, electrochemical sensors probably constitute the largest group of chemical sensors and one of the broadest and oldest types. The oldest electrochemical sensors date back to the 1950s when they were first used for oxygen monitoring [82]. These sensors consist of potentiometric, voltammetric, electrochemical sensors and electrochemical gas sensors. All voltammetric techniques are based on potential control; that is, a measure of the current response as a function of applied potential. A wide variety of electrochemical sensors have been developed to study the environment [22, 24, 26]. These sensors ranged from amperometric to potentiometric sensors that can measure a single species to voltammetric sensors that can measure several species during the same scan [23, 24]. Electrochemical sensors are highly attractive because of high speed of analysis, capability of analysing extremely small volumes without significantly causing any sample perturbation and they allow steady-state measurements which is critical to getting redox state out. The development of enzyme biosensors and DNA detection methods in the last few years has led to significant growth in the field of electrochemical biosensors [19]. A wide range of electrochemical sensors exist for medical diagnosis (e.g. for the detection of the end point of kidney dialysis, blood pH, drug levels among others [35, 97].

Electrochemical biosensors hold a leading position among bioprobes currently available and has the advantage of the highly specificity of biological recognition processes in the development of highly selective biosensing devices [103]. Electrochemical sensors have a wide range of applications and can be applied to solid, liquid or gaseous analytes but are most commonly used for liquid and gaseous analytes [19, 26].

Although, the expanding and increasing fields of applications of electrochemical technologies/sensors are inexhaustible, few of these applications are summarised below (adapted from [11]).

1. Environmental control sensors, e.g., for monitoring pollutants and waste water control etc.

2. Biotechnology, e.g., bioprocesses (as in bioreactors).

3. Corrosion electroplating (for monitoring corrosion processes).

4. Food industry (for monitoring pH etc).

5. Swimming pool (for the detection of chlorine level).

6. Chemical process applications.

7. Biochemical and pharmacological analysis.

8. Aquatic systems, particularly in limnology and oceanography.

2.2: Ultramicroelectrodes (UMEs) technologies

Miniaturisation is a growing trend in the field of analytical chemistry [11, 81]. The past three decades have seen enormous advances in electrochemical techniques and one of the most recent advances has been the advent and the development of ultramicroelectrodes. Ultramicroelectrodes (UME) also known as microelectrodes consist of a class of electrodes at micro and nano scale called microelectrodes and nanoelectrodes; they are typically of 1-25 μm in diameter compared with conventional macroelectrodes (several mm in radius) [73, 74]. The miniaturisation of working electrodes not only has obvious practical advantages, but also opens some fundamentally new possibilities [20, 25, 105]. Potentiometric microelectrodes are suitable for in-vivo real-time clinical monitoring of blood electrolytes, intracellular studies, in-situ environmental surveillance or industrial process control [27]. In general, ultramicroelectrodes can be classified into two groups; single microelectrodes and composite microelectrodes [20]. There are different geometries; single microelectrodes such as ring, sphere, disc, cylinder etc while composite microelectrodes can be array or ensemble electrodes depending on whether the electrode surface has a uniform array or random (ensemble). Microelectrodes offer many fundamental characteristics and practical analytical advantages including high mass transport, steady state currents, high faradaic-to-capacitative current ratio or signal-to-noise ratio, low ohmic drop, independency from hydrodynamics etc [36]. Therefore, instruments with UMEs provide superior diffusion behaviour and improved measurement sensitivity compared to macroelectrode based analytical instruments [93, 100]. They routinely give current responses in the nano and pico ampere range and because relatively small current can passes compared to macroelectrodes, two electrode cells are often used.

For many decades, (DME/HDME)-dropping mercury electrodes and hanging drop mercury electrodes were the favoured choice of electrode for electroanalytical research due to their high reproducibility, renewable and smooth surface [82]. However, because of the toxicity of mercury and the green chemistry revolution, the desire for alternative and environmentally friendly electrodes became increasingly intensified. The search for this alternative led to the use of environmentally benign carbon electrodes and other solid electrodes; gold and platinum [96].

The importance of microlectrodes first attracted the attention of the electrochemical community in the early 1980s. However, the benefits of microelectrodes was only recognised on a massive scale when the developments in microelectronic technologies made it possible to reliably measure very low currents to construct microstructures [81, 85]. In addition to being chemically inert, they can be chemically modified to suit a specific purpose and can be miniaturized [92, 93]. The capabilities of chemically modifying these electrodes have been widely used and exploited in the self assembly monolayer (SAMs) researches where electrodes fabrications are crucial and fundamental in the understanding of biological activities and phenomena [103]. It is the miniaturisation capabilities of solid electrodes that led to this new increasingly expanding area of electrochemistry at microelectrodes and nanoelectrodes.

Microelectrodes offer better signal/noise ratio when compared to macroelectrodes with larger surfaces due to the fact that the capacity of the double layer and the capacitance current decrease proportion [81] to the surface area, while faradaic current decreases is proportional to the radius. In addition to the efficient mass transport, attainment of steady state current, independency of the natural convention effects and high sensitivity, they are suitable for contact in low ionic strength natural water environments [84, 85]. Usually the natural environments are of low conductivity media with low current, under this condition, microelectrodes are suitable for minimising the resistance between a working electrode and reference electrode.

The advantageous characteristics and properties of ultramicroelectrodes have opened new possibilities in the research fields of electrochemistry, biotechnology, medicine and environmental sciences, with wide range of applications [97, 98, 99]. For example, microelectrodes are highly attractive in chemical sensor research and scanning electrochemical microscopy (SECM) due to their numerous advantages over macroelectrodes [19]. Application of microelectrode capabilities have been well documented with increased application in the field of heavy metals analyses in aquatic systems for in-situ and on-line monitoring and in medicine as in microanalysis for neuroanalysis [1, 9, 70].

Recently Brendel and Luther, Xie and co-workers, to name a few, developed a solid state voltammetric gold amalgam microelectrode for the measurement of dissolved oxygen, sulphur, iron and manganese in porewaters of marine and freshwater sediments and for trace metals measurements in water respectively. In 2002, Pizeta and co-workers developed Au and Ag microelectrodes for in-situ measurements of manganese, iron, iodine and sulphur [82].

2.3: Trends and recent advances in electrochemical technologies

The study of electrochemistry and microelectrodes has taken the research in electrochemistry to new heights with broad range of applications in different field of endeavours. The past two decades have seen enormous advances in electrochemical techniques and technologies. These advances include the development of modified or ultramicroelectrodes, the design of highly selective chemical or biological recognition layers, of molecular devices or sensor arrays, and developments in the areas of microfabrication, computerised instrumentation and flow detectors [35, 36, 37]. Relevant to this research work, is the review and evaluation of currently reported field of analytical technologies. The next few sections in this chapter will therefore focus on the most important advances and recently reported devices which hold great promise for the application of electrochemical techniques and technologies in environmental monitoring and analysis. Some of these advances in the application of electrochemical devices in environmental monitoring technologies are reported.

2.4: Applications of electrochemical technologies in environmental analysis

Due to significant technological advances during the 1980s and early 1990s which have facilitated the environmental applications of electrochemical devices, electrochemical sensors are now playing an increasing role in environmental monitoring [54, 55, 56]. The last decade has seen an increase in the investigation and research involving the applications of electrochemical techniques for environmental pollution abatement [72, 73, 74]. This section surveys important advances in electrochemical sensor technology applications in environmental applications and future prospects. For many years, several electrochemical devices, such as pH or oxygen electrodes have been used routinely in environmental analyses [92, 93] and

recent advances in electrochemical sensor technology will certainly expand the scope of these devices towards a range of organic and inorganic contaminants and will facilitate their role in field analyses.

There is now a considerable demand for innovative analytical methodologies due to stricter environmental control, effective process monitoring and the greener chemistry revolution. In recent years, there has been a growing interest in finding innovative, alternative and greener solutions for the efficient removal, treatment and monitoring of contaminants from water, soil and air [21]. Applications of electrochemical technologies and sensors in environmental treatment have been reported, including clean synthesis, monitoring of process efficiency and pollutants, removal of contaminants, recycling of process streams, water sterilization, clean energy conversion, and the efficient storage and utilization of electrical energy [21, 27]. The expanding field of environmental electrochemistry has witnessed many developments and has demonstrated many successful applications and this is evident by the growing number of literature in this area [105, 106]. Wang and co-workers have reported extensively in many of their published articles, the applications of electrochemical technologies and sensor in environmental monitoring towards achieving greener chemistry [5, 7, 8, 10, 11, 12].

The past three decades have seen an increase in the implementation of more stringent environmental legislations in the industrialised nations to combat the size and diversity of environmental hazards resulting from the past and present industrial processes. Notable among these legislations to prevent pollution and environmental damage are The Environmental Protection Act (1989) in the UK, Clean Air (1990) and Water (1987) Acts in the US and the Water Framework Directive (WFD) Act (2005) in the European Union [12, 34]. Increasingly, electrochemical technologies are making important contributions to the solution of pollution control and recycling problems with applications in water, wastewater, waste and soils treatment [7, 26,]. Compared to other alternative technologies, electrochemical technologies offer specific advantages relative to other technologies for different environmental remediation schemes. Electrochemical technologies are characterised by versatility (ability to simultaneously measure more than one species), energy efficiency (minimal power requirements; operate at low temperature with minimum power loss),

amenability to automation (suited for facilitating data acquisition, process automation and control), environmental compatibility (environmentally friendly as the process uses a clean reagent-the electron), cost effectiveness (low-cost instrumentation; equipment operations are generally simple and inexpensive). portability and flexibility (minimal space; they are easily deployed and small size), high sensitivity (low limit of detection), selectivity, wide linear range and ability to provide immediate feedback [12].

Although electrochemical sensor technology is still limited in scope of application and can not solve all environmental monitoring needs, however, a wide range of electrochemical sensor technology have been applied in the last decade for monitoring a wide range of inorganic and organic pollutants in the environment and recent developments in the field of biosensor technology hold more great promising future in environmental characterisation and monitoring [19, 20]. Examples of these electrochemical sensors and biosensors for environmental analysis are provided in the table below (adapted from [12].

Table 2.1: Examples of electrochemical sensor technology and biosensors for environmental analysis (adapted from [12])

Analyte	Recognition	Process	Transduction Element
Benzene	Modulated microbial activity	Whole cell	Amperometry
Cyanide	Enzyme inhibition	Tyrosinase	Amperomery
Hydrazines	Electrocatalysis	Ruthenium catalyst	Amperometry
Lead	Ion recognition	Macrocyclic ionophore	Potentiometry
Mercury	Preconcentration	Crown ether	Voltammetry
Nickel	Preconcentration	Dimethylglyoxine	Voltammetry
Nitrite	Preconcentration	Aliguat 336 ion exchanger	Voltammetry
Nitrosamines	Electrocatalysis	Ruthenium catalyst	Amperometry
Peroxides	Biocatalysis	Peroxidase	Amperometry
Pesticides	Enzyme inhibition	Acetylcholinesterase choline oxidase	Amperometry
Phenol	Biocatalysis	Tyrosinase	Amperometry
Sulfite	Biocatalysis	Sulfite oxidase	Amperometry
Uranium	Preconcentration	Nafion	Voltammetry

2.5: Why electrochemical technologies are well suited for in-situ analysis?

Traditionally, routine analyses are performed on samples collected and transported to central laboratories. The desire for in-situ analysis was driven by the need for rapid, continuous and real-time measurements and remote monitoring of environmental pollution. The new electrochemical technologies have moved beyond the laboratory environment to the field [78]. In-situ analytical technique implies on-site analysis, that is, measurements carried out on-site with little or no perturbation to the samples [102]. Very close to the in-situ analysis are the online measurements. In this method, analysis is carried out on board ship and because the sample is not handled or exposed to the atmosphere, these measurements are considered close to in-situ analysis, though not truly in-situ measurements [85]. Electrochemical technologies are particularly very attractive for in-situ, on-site monitoring and for providing real-time and remote monitoring of priority pollutants as well as addressing and meeting other environmental needs [7, 17, 19]. For example, Wang and co-workers and Tercier and Buffle, in independent research work, have reported the use of remote electrochemical sensors for the measurements of trace metals (Cu, Pb, Hg, Se) in natural waters [24, 74].

The development of electrochemical sensors for in-situ measurements has significantly intensified since the first in-situ measurements of oxygen in the oceans were reported in the 1970's [85, 86, 87]. In-situ measurements are important in natural water environment where parameters such as oxygen abundance and redox potential vary considerably with time and depth which make samples preservation very difficult. The use of in-situ measurements to study the natural environment is important due to oxygen contamination when samples are exposed to the atmosphere and to avoid contamination of samples due to sampling and handling. For the assessment and better understanding of electroactive pollutants in natural environments, reliable and robust analytical techniques with low detection limits are required. High speed of analysis, simplicity, high sensitivity, low power, small size, low-cost and capability of detecting extremely small volume without significantly causing any sample perturbation are some of the attributes that make electrochemical technologies highly attractive for in-situ environmental monitoring [62, 63, 64].

In addition, the periodic and continuous measurements of activities of chemical species and their variations with time is an extremely important area of application of electrochemical sensor technologies.

Compared to conventional analytical methods such as Atomic Absorption Spectrometry (AAS) and Inductively Coupled Plasma (ICP) used for routine analyses in central laboratories which are too expensive and time consuming, in-situ and on-line measurements offer several advantages, including elimination of artefacts due to sample handling (e.g., storage, pre-treatment and transportation) [62]. Electrochemical technologies are now finding increasing use in aquatic systems, particularly in limnology and oceanography where in-situ analysis is important to minimise sample contamination mainly oxygen contamination where samples are exposed to the atmosphere. For examples, Brendel and Luther, Taillefert and co-workers recently reported in-situ measurements of O_2, using amperometric sensors and pH, CO_2, H_2S and trace metals using potentiometric sensors [84, 85]. Wang and co-workers recently developed a wide range of potentiometric sensors for in-situ measurements of trace concentration of copper in the marine environments using potentiometric stripping with gold microelectrode [16].

Voltammetric techniques have become increasingly popular methods for in-situ measurements of chemical species because they can measure several species within the same potential scan range and low detection limit, in the order of 10^{-3} to 10^{-8} M and up to 10^{-12} M in a very few favourable cases [82, 88, 89]. Although, literatures on voltammetric sensors for in-situ analysis are still relatively scarce, some of recent advancements in this research area are reported here. For example in 2000, Taillefer and co-workers reported in-situ measurements of H_2S, O_2 and trace metals using in-situ voltammetric sensors; the authors also reported online voltammetric measurements of H_2S and trace metals [35]. Voltammetric in-situ profiling (VIP) system is now commercially available for in-situ measurements and Mn profiles in the water column of lake have been determined using square wave voltammetry [63]. Luther and co-workers have reported the use of Au/Hg voltammetric microelectrodes for the in-situ measurement of O_2 profiles with similar profiles as obtained in the use of a Clarke microelectrode [93].

The development of voltammetric technologies is on the increase, and in 2003, Wang and Thongngamdee reported the development of remote voltammetric sensors for monitoring silver and TNT in natural water environments but these devices are not yet tested in the field [94].

2.6: Present challenges in in-situ electrochemical technologies

Like any analytical techniques, despite major advances in electrochemical technologies, there are still many limitations and challenges related to the achievement of highly stable and reliable monitoring. However, the increasing wide use and application of these technologies has resulted in greater awareness of difficulties associated with a correct interpretation of the measurements [101, 102, 103]. On the other hand, using modern instrumentation, it is often possible to obtain qualitative diagnostic and mechanistic information as well as quantitative data from the same experiment. Achievements of highly stable, long-term stability (of both the recognition and transduction elements) and reliable monitoring are many of challenges confronting in-situ electrochemical measurements [19, 20, 26]. However, the real challenges for the future use are those of good electrode materials, miniaturisation and of measurements in as close to real-time as possible [12, 78]. Although, accurate results can be obtained from monitoring of an industrial process where sample matrix are usually known, however, results are unlikely to be accurate in the analysis of environmental samples in the field where sample matrix are usually unknown [56, 58].

Some of the major challenges in in-situ environmental technologies are summarised below as identified by Wang [74, 94].

1. Matrix effects.
2. In-situ calibration.
3. Related baseline drift.
4. Reversibility.

Luther and Brendel identified the following challenges hindering the successful application of in-situ electrochemical technologies [98].

1. Miniaturisation of electrochemical sensors.
2. The on-line use of electroanalytical techniques.
3. Reduction of their response time
4. Automation e.g., solving problems such as periodic calibration, electrode fouling and being sufficiently robust.

Taillefer and co-workers [35] identified the following limitations:

1. Electrode characteristics determine the number of species that can be detected which may be limited.
2. Possibility of ion interference.
3. The limit of detection may be high.
4. The response may be operationally defined.

However, perhaps, the biggest challenge and limitation to the widespread use of in-situ electrochemical measurements and monitoring is the poisoning of electrode surfaces known as "electrode fouling" due to the adsorption of organic matter which could degrade and interfere with the voltammetric signals. Although, in the laboratories, electrode surfaces could be regenerated through cleaning or polishing, this is time consuming and possibly be avoided for continuous or regular monitoring. Research towards addressing the fouling and degrading of electrochemical sensors during use and the development of remote electrodes for unattended operations are on-going like the use of disposable and single use electrodes which are employed for short period of time during which adsorption problems are negligible [78, 79, 80]. Other methods are modification or covering of electrode surface with a specially designed membrane and reduction of contact time of the analyte with the electrode surface [103]. Research towards developing modified electrode surfaces for in-situ measurements has intensified [78, 79]. Numerous current research activities in electrochemical techniques are concerned with investigating sensors for gases such as O_2, CO_2, SO_x, NO_x, H_2, Cl_2 and multi-sensor systems for simultaneous monitoring of several priority contaminants [23, 24, 53]. In spite of all these limitations and challenges, the future of electrochemical technologies for in-situ analyses is very promising.

2.7: References

[1]. Buffle, J., Horvai, G., Eds. In Situ Monitoring of Aquatic Systems: Chemical Analysis and Speciation; Wiley, New York, **2001**.

[2]. Wang, J. Analytical Electrochemistry, 2nd ed.; Wiley, New York, **2000**.

[3]. Brett, C.M. A, Brett, A.M.O. Electrochemistry: Principles. Methods and Applications, Oxford University Press: Oxford, **1993**, 427pp.

[4]. Bakker, E., Buhlmann, P., Prestch, E. *Electroanalysis*, **1999**, 11. 915-933.

[5]. Wang, J. *Trends Anal.Chem.* **1997**, 16, 84-88.

[6]. Tercier, M.L., Buffle, J., Graziottin, F.A. *Electroanalysis*, **1998**, 10, 355-363.

[7]. Wang, J., Larson, D., Foster, N., Armalis, S., Lu, J., Rongrong, X., Olsen, K., Zirino, *Anal. Chem.* **1995**, 67 1481-1485.

[8]. Wang, J., Foster, N., Armalis, S., Larson, D., Zirino, A., Olsen, K. *Anal. Chim. Acta* **1995**, 310, 223-231.

[9]. Tercier, M.L., Buffle, J. *Electroanalysis*, **1993**, 5, 187-2000.

[10]. Wang, J., Zadeii, J. *J. Electroroanal. Chem.* **1988**, 246, 297-305.

[11]. Wang, J. *Acc. Chem. Res.* **2002**, 35, 811-816.

[12]. Wang, J. Electrochemical Sensors for Environmental Monitoring: A Review of Recent Technology, U.S. Environmental Protection Agency, Solicitation No: LV-94-012.

[13]. Wang, J. *Electroanalysis*, **1991**, 3, 255.

[14[. Florence, T.M. *Analyst*, **1986**, 111, 489.

[15]. Zirino, A., Lieberman, S., Clavell, C. *Environ. Sci. Technol.*, **1992**, 12, 73.

[16]. Wang, J., Sediadji, R., Chen, L., Morton, S. *Electroanalysis*, **1992**, 4, 161.

[17]. Tercier, M., Buffle, J., Zirino, A., De Vitre, R. *Anal. Chem. Acta.*, **1990**, 237, 429.

[18]. Bodewig, F., Valenta, P., Nurnberg, H. *Anal. Chem.*, **1982**, 311, 187.

[19]. Jiri, J., Mira, J. *Anal. Chem.*, **1998**, 70, 179R-208R.

[20]. Xie, X., Stuben, D., Berner, Z., Albers, J., Hintsche, R., Jantzen, E. *Sensors and Actuators*, **2004**, 97, 168-173.

[21]. Carlos, A. M., Sergio, F. *Chem. Soc. Re.*, **2006**, 35, 1324-1340.

[22]. Rajeshwar, K., Ibanez, J.G., Swain, G.M. *J. Appl. Electrochem.*, **1994**, 24, 1077-1091.

[23]. Tercier, M.L., Parthasarathy, N., Buffle, J. *Electroanalysis*, **1995**, 7, 55-63.

[24]. Tercier, M.L., Buffle, J. *Anal.Chem.*, **1996**, 68, 3670-3678.

[25]. Bohni, H., Suter, T. and Assi, F. *Surface and Coating Technology*, **2000**, 130, 80-86.

[26]. Walsh, F.C. *Pure Appl. Chem.*, **2001**, 73, 1819-1837.

[27]. Alkire, R.C. and Braatz, R.D. *J. Amer.Inst.Chem.Engineers*, **2004** 50, 2000-2007.

[28]. Brett, C.M.A. *Appl. Chem.*, **2001**, 73, 1967-1977.

[29]. Brett, C.M.A. and Brett, A.M.O. *Electroanalysis*. Oxford University Press, Oxford, **1998**.

[30]. Compton, R.G. Eklund, J.C. and Marken, F. *Electroanalysis*, **1997**. 9. 509.

[31]. Brett, C.A. Brett, A.M.O., Matysik, F.M., Matysik, S. and Kumbhat, S. *Talenta*, **1996**, 43, 2015.

[32]. Fisher, A.C. Electrode Dynamics. *Oxford Chemistry Primers*, Oxford University Press, Oxford, **1996**.

[33]. Brett, C.M.A., Brett, A.M.O. and Mitoseriu, L.C. *Electroanalysis*, **1995**, 7. 225.

[34]. Nikolelis, D.P., Krull, U.J., Wang, J. and Mascini, M. Eds. Biosensors for Direct Monitoring of Environmental Pollutants in the Field, NATO ASI Series 2/38, Kluwer, Dordrecht, **1997**.

[35]. Taillefert, M., Luther III, G.W. and Nuzzio, D.B. *Electroanalysis*, **2000**, 12, 401.

[36]. Compton, R.G. and Sanders, G.H.W. Electrode Potentials, *Oxford Chemistry Primers*, Oxford University Press, Oxford, **1996**.

[37]. Xie, X., Stueben, D. and Berner, Z. *Analytical Letters*, **2005**, 38: 14, 2281-2300.

[38]. Achterberg, E.P. and Brungardt, C. *Anal. Chim. Acta*.**1999**, 400, 381-397.

[39]. Belmont, C. Tercier, M.L., Buffle, J., Fiaccabrino, C.C. and Koudelka-Hep, M. *Anal. Chim. Acta*.**1996**, 329, 203-214.

[40]. Belmont-Hebert, C., Tercier, M.L. Buffle, J., Fiaccabrino, G.C., Rooiji, N.F. and Koudelka-Hep, M. *Anal.Chem*.**1998**, 70, 2949-2956.

[41]. Bond, M.A. *Analyst* **1994**, 119: R1-R20.

[42]. Brainina, K.Z., Malakhova, N.A. and Stojko, N.Y. *Anal. Chem.* **2000**. 368. 307-325.

[43]. Brett, C.M.A. *Electroanalysis* **1999**, 11, 1013-1016.

[44]. Buffle, J. and Horvai, H. John Wiley & Sons **2000**, Chichester.

[45]. Buffle, J., Tercier, M.L., Parthasarathy, N. and Wilkinson. K.J. *Chimia* **1997a**. 51, 690-693.

[46]. Buffle, J., Wilkinson, K.J., Tercier, M.L. and Parthasarathy. N. *Analytical di Chimica* **1976**, 87, 67-83.

[47]. Cassidy, J., Ghoroghchian, J., Sarfarazi, F.. Smith, J.J. and Pons, S. *Electrochim. Acta*. **1986**, 31, 629-638.

[48]. Ciszkowska, M. and Osteryoung, J.G. *Anal. Chem.* **1995**, 67. 1125-1131.

[49]. Daniele, S., Baldo, M.A. and Bragato, C. *J. Braz.Chem.Soc*. **2002**, 13, 425-432.

[50]. Daniele, S., Bragato, C., Baldo, M.A., Wang, J. and LU, J. ***Analyst 2000***, 125, 731-735.

[51]. Emons, H., Baade, A. and Schoning, M.J. *Electroanal.* **2000**, 12, 1171-1175.

[52]. Feeney. R. and Kounaves, S.P. *Talenta*, **2002**. 58. 23-31.

[53]. Fleischmann, M., Pons, S.. Rolison. D. and Schmidt. P.P. Datatech Science. **1987**. Morganton, NC.

[54]. Florence. T.M. *Analyst* **1986**. 111. 489-503.

[55]. Forster. R.J. *Chemical Society Review* **1994**. 289-297.

[56]. Hart, J.P. and Wring, S.A. *Trend in Anal. Chem.* **1997**, 16, 89-103.

[57]. Heinz, J. *Angew. Chem. Inst.Ed. Engl.* **1993**, 32, 1268-1288.

[58]. Herdan, J., Feeney, R. and Kounaves, S.P. *Environ.Sci.Technol.* **1998**, 32, 131-136.

[59]. Hill, S.J. *Chem. Soc. Review* **1997**, 26, 291-298.

[60]. Howell, J.O. and Wightman, M. *Anal. Chem.* **1984**, 56, 524-529.

[61]. Howell, K.A., Achterberg, E.P., Braungardt, C.B., Tappin, A.D., Worsfold, P.J. and Turner, D.R. *Trend Anal. Chem.* **2003**, 22, 828-835.

[62]. Mart, L. *Talenta* **1982**, 29, 1035-1040.

[63]. Millero, F. and Pierrot, D. International School on Marine Chemistry, 3rd ed. Palermo, Italy. Meeting Data Sept. **2000**, 193-220.

[64]. Montenegro, M.I., Queiros, M.A. and Daschbach, J.L. NATO ASI Series, Kluwer Academic Publishers **1991**, Dordrecht, 3-16.

[65]. Moore, J.W. and Ramamoorthy, S. Springer-Verlag **1984**, New York.

[66]. Nurnberg, H.W. *Sci. Tot. Environ.* **1984**, 37, 9-34.

[67]. Palchetti, I., Marrazza, G.I. and Maschini, M. *Anal. Lett.* **2001**, 34, 813-824.

[68]. Pons, S. and Fleischmann, M. *Anal. Chem.* **1987**, 59, 1391-1399.

[69]. Schultze, J.W. and Bressel, A. *Electrochimica Acta* **2001**, 47, 3-21.

[70]. Tercier-Waeber, M.L. and Buffle, J. *Environ.Sci.Technolo.* **2000**, 34, 4018-4024.

[71]. Tercier-Waeber, M.L., Buffle, J., Confalonieri, F., Riccardi. G.. Sina, A.. Graziottin, F., Fiaccabrino, G.C. and Koudelka-Hep, M.K. Meas. Sci. Technolo. **1999**, 10, 1202-1213.

[72]. Vitre, R.R.D. Tercier, M.L. and Buffle, J. Laboratory Techniques in Electrochemical Chemistry **1991**; Kinsinger, P.T. and Heineman, W.R.. eds.. Marcel Dekker, New York, 719-738.

[73]. Wang, J. Analytical Electrochemistry 2000, 2nd ed. John Wiley & Sons, New York.

[74]. Wang, J. LRA 2000b, 12, 178-182.

[75]. Wightman, R.M. *Anal. Chem.* **1981a**, 53. 1125A-1134A.

[76]. Wightman, R.M. *Science* **1988**, 240, 415-420.

[77]. Wightman, R.M. and Wipf, D.O. *Electroanalytical Chemistry* **1989**, Bard, A.J.. ed.; Marccel Dekker, New York, vol. 15.

[78]. Whelan, A. and Regan, F. J.*Environ.Monit. 2006*, 8, 880-886.

[79]. Wynne, K.J., Swain, G.W., Fox, R.B., Bullock, S. and Uilk, J. *Biofouling*, **2000**, 16, 277.

[80]. Sreenivasan, P.K. and Chorny, R.C. *Biofouling*, **2005**, 21, 141.

[81]. Holme. E.R.. Nedved, B.T.. Phillips, N.. Deangelis, K.L.. Hadfield. M.G. and Smith, C.M. *Biofouling*. **2000**, 15. 95.

[82]. Pizeta. I.. Billion. G., Fischer. J.C. and Wartel. M. *Electroanalysis*. **2003**. 15 (17). 1389-1396.

[83]. Kouvanes. S.P. and Deng. W. *Anal. Chem*. **1993**. 65. 375.

[84]. Luther III, G.W, Reimers, C.E., Nuzzio, D.B. and Lovalvo, D. **Environ.** *Sci.Technol.* **1999**, 33, 4352.

[85]. Wang, J. and LU, Lu, J. *Electrochem. Commun.* **2000**, 2, 390.

[86]. Brendel, P.J. and Luther III, GW. *Environ.Sci.Technol.* **1995**, 29, 751.

[87]. Theberg, S.M. and Luther III, G.W. *Aquat.Geochem. 1997*, 3, 191.

[88]. Xu, S., Dexter, S.C. and Luther III, G.W. *Corrosion*, **1998**, 54, 814.

[89]. Luther III, G.W., Brendel, P.J., Lewis, B.L., Sundby, B., Lefrancois, L., Silvergerg, N. and Nuzzio, D.B. *Limnol. Oceanorgr.* **1998**, 43, 325.

[90]. Rozan, T.F., Theberge, S.M. and Luther III, .W. *Anal. Chim. Acta* **2000**, 415, 175.

[91]. Taillefer, M., Luther III, G.W. and Nuzzio, D.B. *Electroanalysis*, **2000**, 12, 401-412.

[92]. Wang, J. and Greene, B. *Wat.Res.* **1983**, 17, 1635.

[93]. Hitchman, M.L. Measurement of Dissolved Oxygen, a *Wiley-Interscience publication*, **1978**.

[94]. Skoog, D.A. and Leary, J.J. Principles of Instrumental Analysis, 4th ed., Saunders College Publishing, **1992**.

[95]. Ibanez, J.G., Sigh, M.M., Szafran, Z. and Pike, R.M. *J.Chem. Educ.*, **1998**, 75(5), 634-635.

[96]. Ibanez, J.G., Takimoto, M.M., Vasquez, R.C., Basak, S., Myung, N., Rajeshwar, K.J. *J.Chem. Educ.*, **1995**, 72, 1050-1052.

[97]. Rajeshwar, K.J., Ibanez, J.G., Swain, G.J. *Appl.Electrochem.*, **1994**, 24, 1077-1091.

[98]. Luther III, G.W. J.*Geomicrobiology*, **2005**, 22, 195-203.

[99]. Luther III, GW. *Geochim Cosmochin Acta*, **1987**, 51, 3193-3199.

[100]. Morgan, J.J. *Geochim Cosmochim Acta*, **2005**, 69, 35-48.

[101]. Stumm, W. and Morgan, J.J. **1996**. Aquatic Chemistry, 3rd edition. New York, John Wiley. 1022p.

[102]. Tercier, M.L. and Buffle, J. Electroanalysis, 1993, 5, 187-200.

[103]. Luther III, G.W. *Geochemical Society*, **2002**, 113, 14-19.

[104]. Aslanoglu, M., Isaac, C.J., Houlton, A. and Horrocks, B.R. *Analyst*, **2000**, 125, 1791-1798.

[105]. Chapman, C.S. and Van Den Berg, C.M. *Environ.Sci.Technol.*, **2005**, 39, 2769-2776.

[106]. Stetter, J.R., Penrose, R. and Yao, Sheng. *J. Electrochemical Society*, **2003**, 150 (2), S11-S16.

[107]. Editorial of the 53rd Annual Meeting of ISE jointly organise with the GDCh-Fachgruppe Angewandte Elecktrochemie. *Electrochimica Acta*, **2003**, 48, 2851-2852.

[108]. Wang, J., Larson, D., Foster, N., Armalls, S., Lu, J. and Rongrong, X. *Anal. Chem.*, **1995**, 67, 1481-1485.

[109]. Gerger, I. and Haubner, R. *Diamond and Related Materials*, **2005**, 14, 369-374.

[110]. Bakker, E. and Pretsch, E. *Trends in Analytical Chemistry*, **2005**, 24 (3), 1999-207.

[111]. Bakker, E. *Anal. Chem.*, **2004**, 76 (12), 3285-3298.

[112]. Bond, M.A. *Analyst*, **1994**, 119, R1-R20.

[113]. Brendel, P.J. and Luther III, G.W. *Environ.Sci.Technol.*, **1995**, 29, 751-761.

[114]. Brown, R.J.C. and Milton, M.J.T. *Trends in Analytical Chemistry*, **2005**, 24 (3), 266-274.

[115]. Taillefer, M., Bono, A.B. and Luther III, G.W. *Environ.Sci.Technol.*, **2000a**, 34, 2169-2177.

Chapter 3

EXPERIMENTAL PROTOCOLS

Brief descriptions of the techniques and methods together with instruments types used in this research are discussed in this chapter. Electrochemical measurement were performed on a wide range of analytical aqueous solutions containing iron species in laboratory experiments and on environmental samples taken from abandoned mine sites. Characterisation of colloidal and particulate matters and iron-containing nanoparticles was made using a number of spectroscopic methods, probe and electron microscopy. Sampling protocols, sample treatments together and the voltammetric and spectroscopic methods used in the research work are also described in this chapter.

3.1: Reagents and Chemicals

All the reagents used were of analytical reagent grade (AnalaR) and were purchased from Sigma-Aldrich Chemicals (Gillingham, UK). All electroanalytical calibration measurements were made with 0.1M KCl or 0.1M Na_2SO_4 solutions in water as background electrolytes. Water used for preparation of electrolyte solutions in calibration experiments and cleaning of the electrodes was purified using a milli-(Q) Plus filter - NANOpure RO, Model D11931 (Barnstead International, Dubuque, Iowa, USA) and had a nominal resistivity of 18.2 MΩ cm.

3.2: Field/On-site Analyses

The chemical compositions of both influents and effluents from the sites have been routinely monitored over a three year period and pH, oxidation-reduction potential (ORP/E_h), temperature and electrical conductivity measurements were performed on-site with a Camlab 6T Ultrameter (Myron L. Company, Karlsbad, USA). On-site determination of alkalinity (expressed as mg L^{-1} of $CaCO_3$) was carried out by titration with 1.6N sulphuric acid to an end-point at pH 4.5 using a Hach ALDT test kit (Hach Company, Loveland, USA). Bromocresol green-methyl red indicator powder was used to identify this end-point.

3.3: Washing of sampling bottles

Sampling bottles were soaked in 10% v/v conc. KNO_3 overnight in acid bath. and rinsed thoroughly (thrice) with tap water, followed by thorough rinse with nanopure water (thrice). The bottles were then allowed to dry in air.

3.4: Collection, storage and treatments of samples

Monthly samples were taken over a three year period from six abandoned mine sites in the NE England which together comprise the CoSTaR (Coal Mine Sites for Targeted Remediation Research) facility for the investigation of passive mine water treatment technologies. CoSTaR sites have been fully described in section 1.9-an overview of CoSTaR sites in the introductory chapter. Polyethylene sample bottles (125 mL) were cleaned in 10% v/v conc. HNO_3 overnight and then rinsed thoroughly with water (x3). The bottles were then allowed to dry in air. Samples for laboratory analysis were collected in pre-washed polyethylene bottles that had been pre-acidified with concentrated hydrochloric acid and some bottles unacidified depending on the type of analysis. The sampling protocols followed those used by the HERO-group to ensure comparability of the data. 125 mL mine-water samples were collected at each location and refrigerated at 4 ^oC before analysis. Efforts were made to ensure that all samples were analyzed within 72 hours of sampling to prevent sample deterioration and degradation. Fluxing of electrochemical cell with nitrogen gas ensured that oxygen does not interfere with the measurements. In order to investigate the occurrence of total iron, particulate iron, colloidal iron and dissolved iron. four types of samples were taken at each sampling point: (a) an unacidified sample; (b) an unfiltered sample which was acidified by the addition of 1 mL concentrated HCl; (c) a sample filtered through 0.45 μm cellulose nitrate membrane and (d) a 0.45 μm filtered sample which was acidified.

Acidified samples

Sample bottles for total [Fe] analyses were acidified by addition of 1 mL conc. HCl or, in some cases 1.25 mL conc. HNO_3 before collection of a 125 mL mine-water

sample. This procedure inhibits oxidation of Fe^{2+} and hydrolysis of Fe^{3+} during transport and storage. Iron-containing oxyhydroxides dissolve under these conditions and all the iron in the sample is in solution. No difference in the analytical data was observed between acidification with HCl and HNO_3.

Filtered samples

Some samples were filtered with 0.45 μm cellulose nitrate membranes (Whatman International Ltd, Maidstone, England) to remove micrometre-sized solid-phase material.

3.5: Nanopure water

Ultrapure water was generated using milli-(Q) Plusfilter apparatus- NANOpure Diamond Life Science (UV/UF), Barnstead Diamond RO, Model D11931 ultrapure water system by Barnstead International, 2555 Kerper Boulevard Dubuque, IOWA 52001, USA. Tap water was passed through a 0.2 μm filter, kept at 4 °C and resistivity of 18.2 MΩ cm.

3.6: Electrode Polishing

Electrodes were cleaned by using alumina polishing dissolved in nanopure water. This is made by dissolving a tip of spatula of deagglomerated gamma Alumina powder of size 0.05 μm in nanopure water on a porous neoprene self-adhesive pad of 200 mm diameter. Electrode polish is ensured by random and uniform rubbing of electrode across the adhesive pad in the form of figure 8. This continues for about 3 min. The Deagglomerated Gamma Alumina was Buehler Micropolish by Buehler, 41, Waukegan Road, Lake Bluff, Il, 60044, USA while the Porous Neoprene (self-adhesive-OP-Chem) was by Struers A/S, Pederstrupvej 84, 2750 Ballerup, Denmark. The electrode was rinsed with nanopure water and then dipped in absolute alcohol (99%) and sonicated for 2 min using Transonic T310 by CAMLAB Serving Science, CamLab Limited, Nuffield Road, Cambridge, CB4 1TH, UK. The sonicated electrode is then rinsed with nanopure water and then dried using air-gun BOSCH PHG2 by Robert Bosch Gmbh, D-70745 Leinfelden Echterdingen, Germany.

Different adhesive pad and alcohol solution for sonication were used for different metal electrode, so as to prevent any mixture of electrode nanoparticles of different electrode at the electrode surface. Glassy carbon electrodes were electrochemically cleaned by cycling at -0.1 V to +1.3 V in the presence of 0.5 M conc. H_2SO_4. And finally, electrodes were dipped into the samples for at least 2 min prior to analysis and samples run several times (up to 6 times) before measurements taken. These measures were taken to allow the instrument/electrode to settle and stabilize in the cell. The electrochemical cell was fluxed with nitrogen gas to remove any oxygen contaminations that may interfere with the analysis. The success of this cleaning process was checked by recording a blank voltammogram.

3.7: Voltammetric Methods

Voltammetric techniques, mainly cyclic voltammetric (CV) and differential pulse voltammetric (DPV) were used for all the electrochemical measurements. CV and DPV measurements were performed in a standard glass three-electrode cell containing 10 mL of sample solution. The cell consisted of a gold working electrode of 2 mm diameter, platinum counter electrode and saturated calomel (SCE) reference electrode (Sycopel Scientific Ltd., Washington, UK). The electrodes were dipped in the sample for at least 2 min prior to analysis and the electrochemical cell purged with nitrogen gas to remove any oxygen that may interfere with the analysis. At least triplicate scans were performed on each sample to verify the consistency of the measurements.

Voltammetric techniques are based on electron transfer between electrodes and the reactant molecules (electroactive species) usually in a solution phase [4, 5]. Voltammetric methods have some advantages over other analytical techniques, such as atomic absorption spectrometry (AAS), because they allow the determination of electroactive elements in different oxidation states, e.g., it is possible to distinguish Fe(II) from Fe(III). Voltammetric methods depend on the transport of materials to the surface of electrodes where reactions take place. Whilst mass transport of materials to the electrode surface occurs principally via three processes; diffusion, convection and migration, diffusion is the dominant mechanism in unstirred solutions of moderate or high ionic strength. The rate of diffusion is governed by the concentration gradient and Fick`s first law of diffusion [1].

3.7.1: Cyclic Voltammetry (CV)

Cyclic Voltammetry were used to investigate the Fe speciation and to understand the voltammetric responses. CV is the most widely used voltammetric technique for acquiring information about electrochemical reactions by rapid location of redox potentials of the electroactive species. The technique provides considerable information on the thermodynamics of redox processes, reaction mechanisms, kinetics of heterogeneous electron-transfer reactions and on coupled chemical reactions or adsorption processes. The technique involves application of a triangular potential wavefunction to stationary working electrode. During the potential sweep, the potentiostat measures the current resulting from the applied potential. The corresponding plot of current versus potential is known as voltammogram. This current-potential plot/curve is then used for the identification and measurement of the concentration of each species. For freely diffusing species, the measured peak current is proportional to square-root of scan rate and the current is proportional to the concentration of the electroactive species (analyte). The formal [1] potential for a reversible couple is the potential midway between the anodic and cathodic peak potentials.

In CV, typically the potentiostat applies a linear ramp of the potential to the working electrode, then reverses the scan, returning to the initial potential (figure 3.1). Typical cyclic voltammetric potential waveform is shown in figure 3.2.

---

[1] The formal potential can be used as an approximation to the standard potential in which the ratio of activity coefficients is negligible.

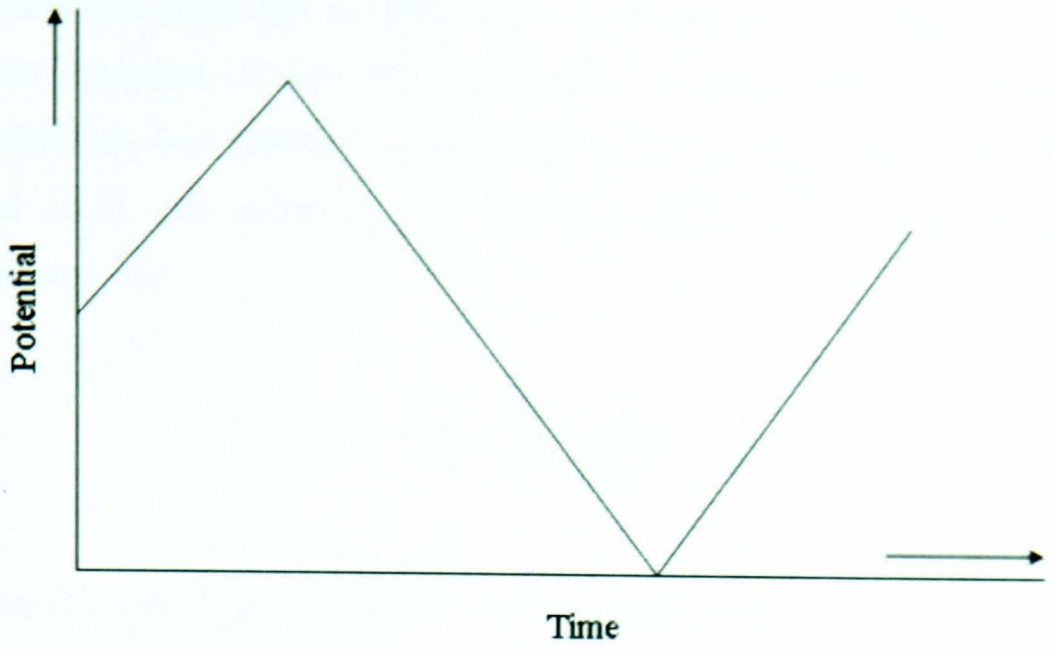

Figure 3.1: Schematic of principle of one cyclic voltammetric (CV) cycle.

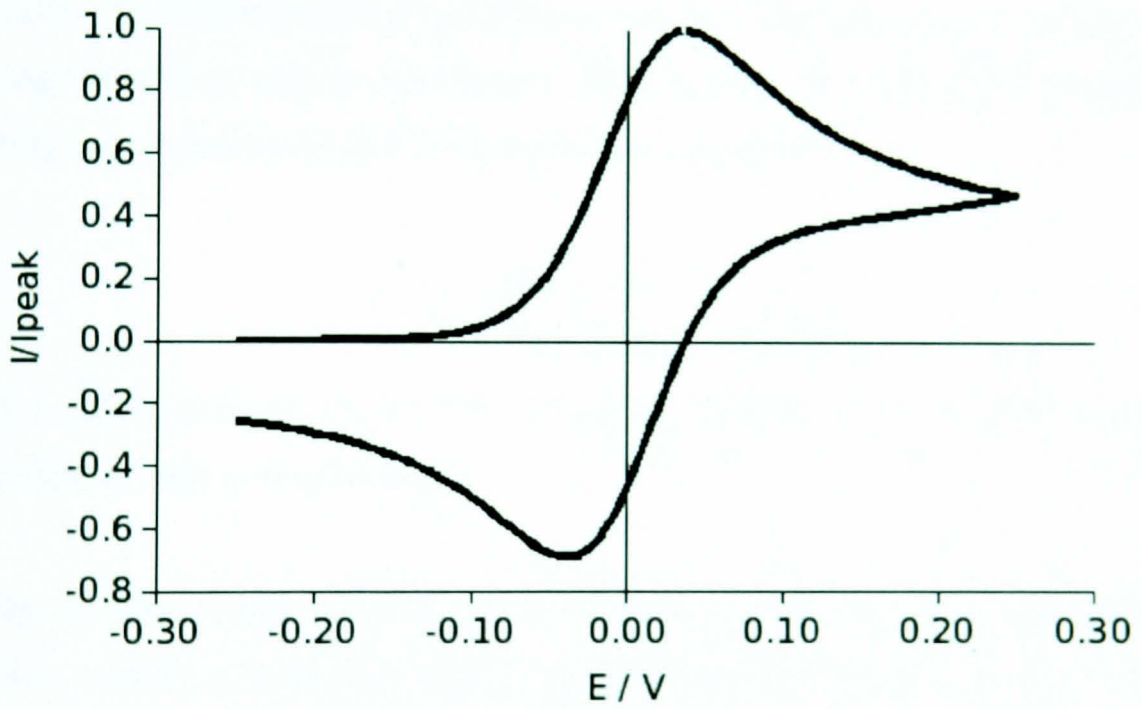

Figure 3.2: Shows a reversible CV of a freely-diffusing species with a formal potential of 0 V. The shape of the CV is determined by a combination of the concentration gradient at the electrode surface (via the diffusion equation) and the concentration ratio of oxidised: reduced forms at the electrode surface (via the Nernst equation).

If the electron transfer (ET) at the electrode/solution interface is not the rate limiting step (the case for most of the measurements reported in later chapters), the shape of a

cyclic voltammogram can be understood on the basis of the Nernst equation and the diffusion equation. Under the assumption of rapid ET. the solution at the electrode/electrolyte interface is in local equilibrium and the concentrations of the reduced (red) and oxidised (ox) forms of the redox couple are related by thermodynamics:

$$E^o = E^{O'} + \frac{RT}{nF} \ln \frac{[ox]}{[red]} \qquad (1)$$

Equation (1) is the Nernst equation for the redox reaction:

$$ox + ne^- = red \qquad (2)$$

$E^{o'}$ is called the formal potential and differs from the standard potential (E^o) by a term involving the ratio of activity coefficients which have been omitted from equation (1) in writing concentrations [ox] & [red] rather than activities.

$$E = E^{O'} + \frac{RT}{nF} \ln \frac{\gamma_{ox}}{\gamma_{red}} \qquad (3)$$

Except in high-precision work, this is usually assumed to be a small correction. independent of bulk concentrations.

Consider the case drawn in fig 3.2 where only reduced species are present in the bulk (no initial current at potentials $<<E^o$). As the electrode potential, E, increases, the reduced form is depleted at the electrode surface and a concentration gradient develops. Reduced species diffuse from bulk solution towards the electrode at a rate determined by Fick's first law:

$$j = -D \frac{\delta[red]}{\delta x} \approx \frac{D}{L} \left([red]_{surf} - [red]_{bulk} \right) \quad (4)$$

where j is the flux in mol m^{-2} s^{-1} of material, D is the diffusion coefficient m^2 s^{-1} and L is the thickness of the diffusion layer – depletion of red at the electrode increases L and also the concentration difference between the bulk solution and the electrode

surface. This gradient reaches a maximum value at the peak in the CV. The concentration of red at the electrode surface tends to zero and the current now declines because further consumption of red increases the diffusion layer thickness. L. When the scan is reversed, a similar peak occurs due to reduction of ox produced in the forward sweep. The formal potential is obtained from the mean of the anodic and cathodic peak potentials.

In the case where ET is not rapid, the concentrations of red and ox at the electrode surface must be related to the potential via the Butler-Volmer equation coupled to the diffusion equation. The overall shape of the voltammogram is similar, but it is different quantitatively and the peak potentials depend on scan rate. For the work in this thesis, considerations of electrode kinetics were of secondary importance. Although the Fe(III)/Fe(II) couple is known to have fairly sluggish ET kinetics (especially at carbon electrodes), low scan rates and metal electrodes were employed. Further, owing to the complexity of the samples, there was no quantitative use of the standard or formal potentials which can be obtained from CV; these were merely used to identify different redox couples. Finally, since the diffusion equation is linear, the peak currents are proportional to concentrations whether or not the assumption of rapid ET applies. Also used was the fact that the peak current is proportional to $D^{1/2}$- small species tend to have larger diffusion coefficients.

Instrumentation/Equipment

Two different types of electrochemical workstations (both giving similar results) were used for the CV analyses. One was the analytical electrochemical workstation; Model AEW2-10 by Sycopel Scientific Limited (Washington, UK) with sensitivity of 0.1 nA. The cell consisted of a gold working electrode, a platinum counter electrode and a saturated calomel reference electrode (SCE). The scan rate of 100 mV s^{-1} was used for all the measurements and analyses involving microelectrodes whilst 10 mV s^{-1} scan rate was used for all the ultramicroelectrodes (UME) cyclic voltammetry measurements. The three electrodes (connected to an electrochemical workstation) were immersed in the electrolytes/samples, properly connected and scanned from -200 mV to +800 mV potential.

The resulting voltammogram was processed by the PC (under Windows environment) attached to the electrochemical workstation which measures the current as a function of applied voltage. The second analytical workstation was an electrochemical Analyser/Workstation CH1760B, Model 700B Series by CH Instruments, Inc., USA with sensitivity of up to picoamperes. The instrument is controlled by an external laptop under Windows environment. The working, counter and reference electrodes and the analytical conditions were as described above.

3.7.2: Differential Pulse Voltammetry (DPV)

Differential pulse voltammetry was used as the main analytical tool for the monitoring of iron speciation at the CoSTaR sites in this research work because of its superior detection limit compared to cyclic voltammetry. The quantitative application of DPV to analysis is based on measurements of the peak current, which is proportional to concentration of the electroactive species in the sample. As with all pulse techniques, the basis of DPV is the difference in the rate of the decay of the charging and the faradaic currents following a potential step. For a reversible reaction, the faradaic current is proportional to the inverse of the square root of the time after a potential pulse. In contrast, the charging current decays exponentially; it is therefore possible to choose times for which the charging current is negligible, but the faradaic current is still measurable. This allows for the discrimination of the faradaic current relevant to the analysis from the charging current (figure 3.3).

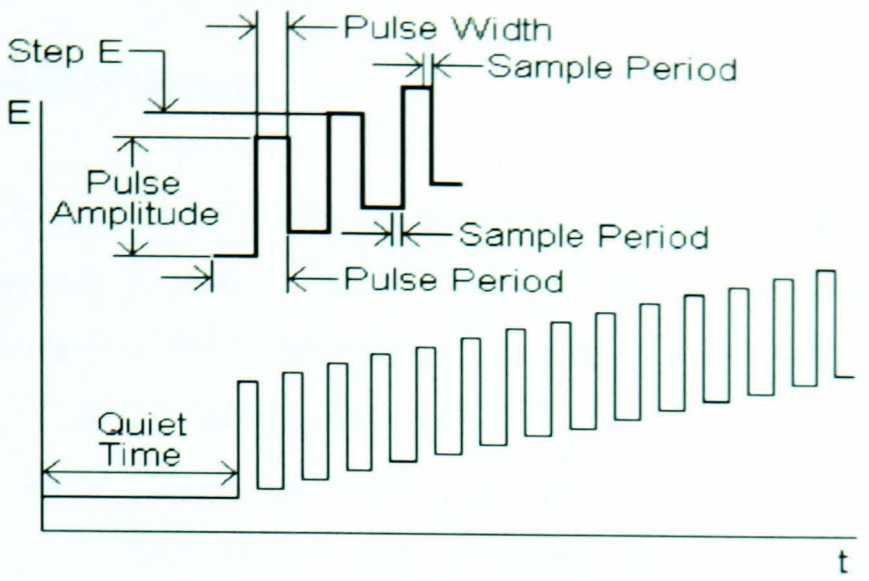

Figure 3.3: Typical diagrams of current sampling in differential pulse voltammetry (DPV) in the potential staircase leading to discrimination between the faradaic and the charging current [25].

The DPV technique further suppresses the contribution of the charging current to the current signal by recording a differential current response. DPV measures the difference between two currents sampled immediately prior to the application of the pulse and at the end of the pulse in the potential increment in the form of a stair-case. The difference between the two sampled currents is then plotted as a function of the stair-case potential, giving a peak-shaped response. The peak current is proportional to the concentration of the electroactive species in the electrochemical cell. This elimination of the charging current increases the signal to noise ratio and makes DPV suitable for quantitative analysis with lower detection limit. In favourable circumstances, the DPV technique has a detection limit of the order of 10^{-8} M.

A useful characteristic of DPV is its ability to distinguish between a reversible and irreversible redox processes by showing symmetrical peaks for reversible reactions while irreversible reactions show asymmetrical peaks and the peak current is proportional to the concentration for reversible reactions.

Instrumentation/Equipment

All DPV measurements were performed on an electroanalytical workstation (EG & G Princeton Applied Research Potentiostat/Galvanostat Model 263A and M270 Research Software: Echem. Software 4.11) connected to a PC under MS-DOS environment. The instrument parameters of 75 mV as pulse height, pulse width of 50 ms, and scan increment of 2 mV with scan rate of 10 mV s^{-1} were used in all the measurements. Triplicate scans were performed on each sample to allow the electrodes to settle and stabilize in the cell and ensure consistent responses. The scan range for all the samples was from +0.8 V to -1.2 V. Schematic of the analytical determination of iron fractions is presented in figure 3.4.

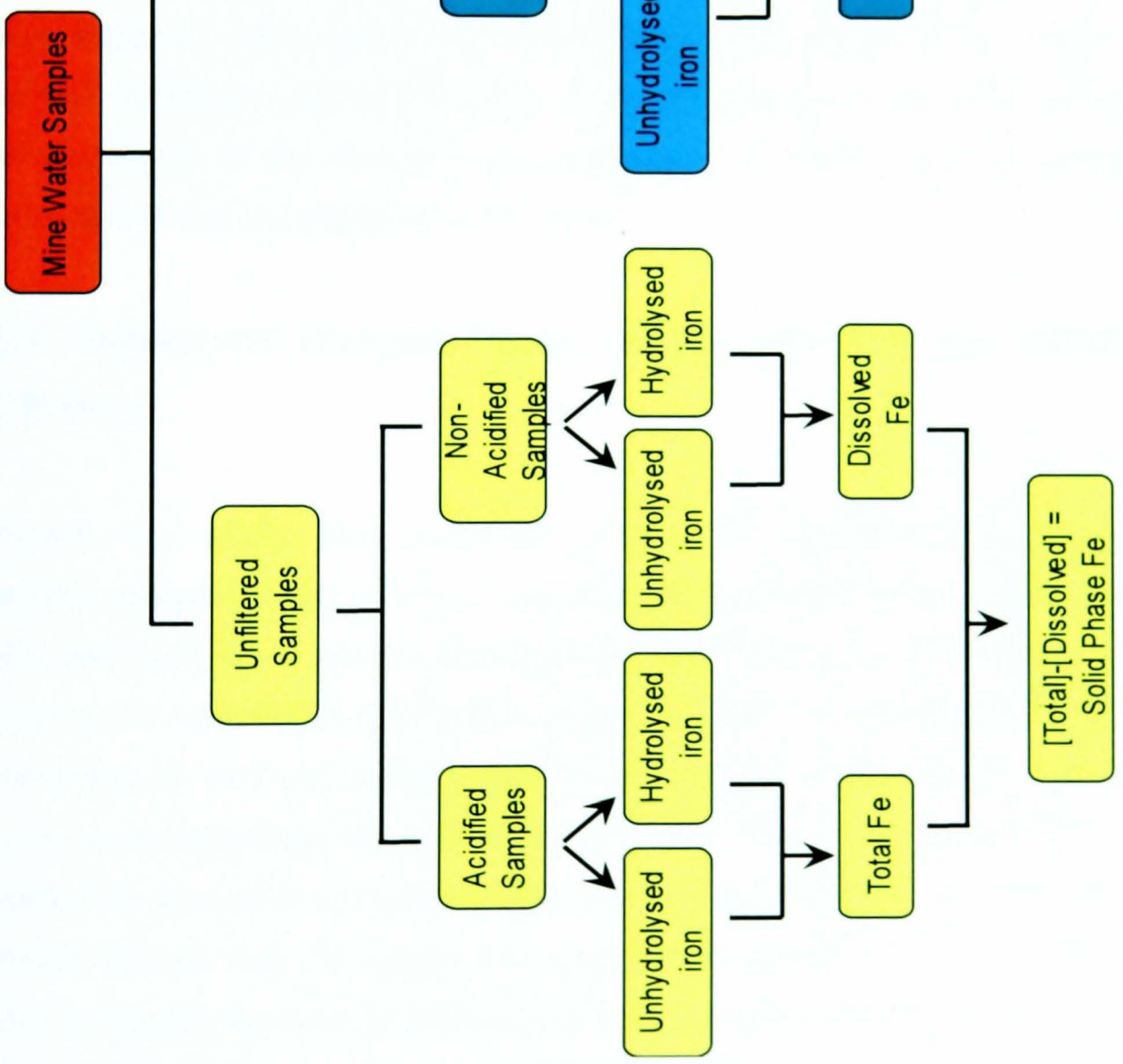

Figure 3.4: Schematic of the analytical steps employed in the determination of iron speciation and fractions; total, dissolved, solid and colloidal together with the hydrolysed and unhydrolysed iron concentrations in the environmental samples.

3.8: Spectroscopic and Microscopic Techniques

A number of spectroscopic and microscopic methods have been used for the study and characterisation of the colloidal iron particles and nanoparticles in the mine water samples. These techniques include the inductively coupled plasma-optical emission spectrometry (ICP-OES) used by the HERO group for the quantitative measurement of total iron concentrations, which provides a means to validate the electrochemical method. Microscopy methods, such as atomic force microscopy (AFM), scanning electron microscopy (SEM) and scanning transmission electron microscopy (STEM) are good for solid surface and particle characterisation, while spectroscopic and diffraction techniques such as Fourier Transform infrared spectroscopy (FTIR), energy dispersive x-ray analysis (EDX) and x-ray diffraction (XRD) are useful for structural elucidation and identification of molecular species. This section gives a brief description of the principles and instrumentation for the spectroscopic and microscopic techniques employed in this work.

3.8.1: Inductively Coupled Plasma-Optical Emission Spectrometry (ICP-OES)

ICP-OES is a widely used analytical technique for routine determination and elemental analysis; it can also be a sensitive trace analytical method. Plasma is a highly energized gas in which a significant fraction of the atoms have been ionized and there is a substantial concentration of free electrons. The ionized gas in ICP is derived from an inert gas, usually argon. In such a plasma, most complex chemical species are broken down and exist as atoms or ions. The atoms in the plasma are identified by absorption or emission spectroscopy. The sensitivity and generality of ICP-OES derives from the narrow line width of atomic spectra which enables the analyst to identify the atoms of interest in complex mixtures where the broad bands of molecular spectroscopy would make analysis impossible.

An ICP source consists of a flowing stream of argon gas ionised by an applied radio frequency (RF) field, typically oscillating at 27.1 MHz. This field is inductively coupled to the ionised gas by a water-cooled coil surrounding a quartz torch that

supports and confines the plasma. Liquid samples are nebulised and injected into the argon which also serves to transport the sample into the plasma. A typical temperature in the plasma (figure 3.5) is 6800 K compared to 3300 K for the traditional flames and furnaces used in atomic absorption spectrophotometry (AAS). The plasma therefore causes the sample aerosols to desolvate, vaporize and atomise before undergoing excitation and/or ionization within the ICP chamber. The excited atoms or ions then emit their characteristic wavelengths which are analysed by a spectrograph. Quantitative information is obtained using calibration plots of emission intensity versus concentration. Standard solutions with known concentrations of the elements of interest are prepared and the intensity of the characteristic emissions of each element is measured. ICP-OES has high sensitivity with low detection limits, typically in the μg L^{-1} range. It is also capable of simultaneous multielement analysis and because of the high temperatures, can suffer fewer matrix interferences compared to flame spectrometers. A schematic layout of the main components of an ICP is shown in figure 3.5.

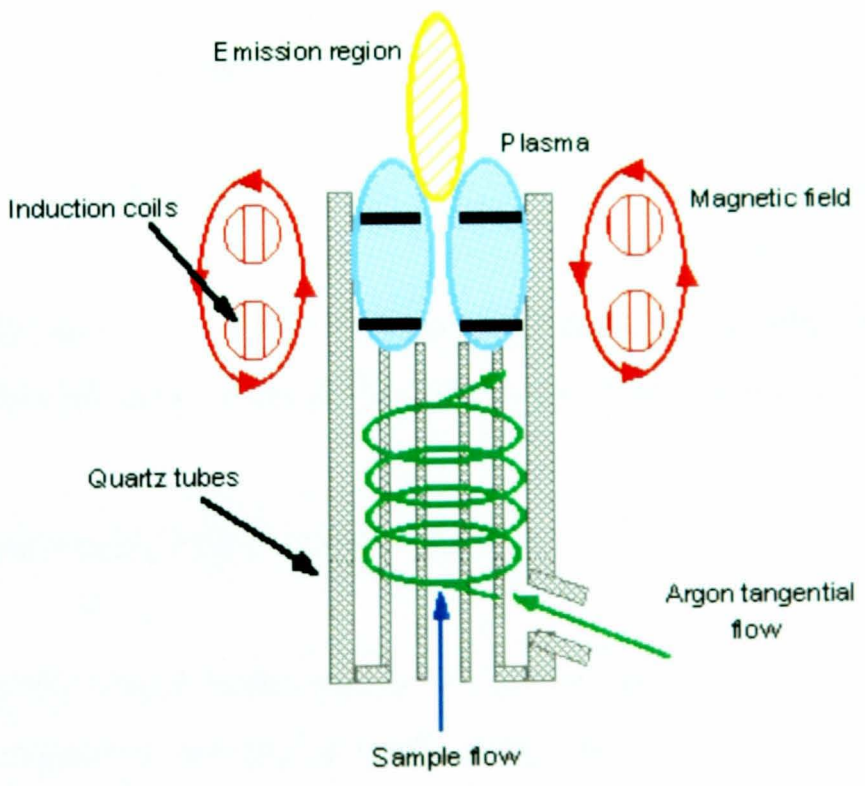

Figure 3.5: Schematic features of the key components of an inductively coupled plasma (ICP) system [24].

Instrumentation/Equipment

In this work, a Vista-MPX ICP-OES with charge coupled device (CCD) (Varian Incorporated, Australia) was used for all the ICP analyses, including those carried out by the HERO research group who provided access to this data for comparison with and validation of our electrochemical technique. Typical concentric glass nebuliser and plasma torch of an ICP-OES, similar to the one used in this research is shown in figure 3.6.

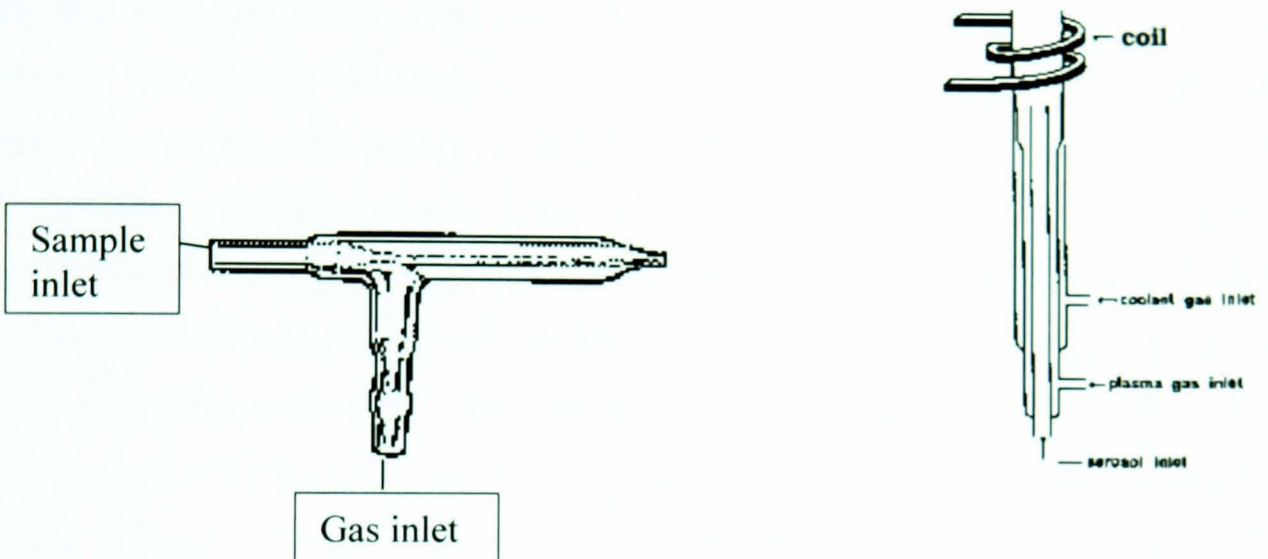

Nebuliser Plasma torch

Figure 3.6: Diagrams of the concentric glass nebuliser and plasma torch of an ICP-OE, similar to the one used for the ICP-OES analysis in this research [25].

3.8.2: Atomic Force Microscopy (AFM)

AFM is one of the major scanning probe microscopies; it is used as an imaging technique for measuring and manipulating matter at the nanoscale level. AFM has become a standard technique for high resolution imaging of the topography of the surfaces by providing nanoscopic surface features. The technique employs a force sensor comprising a sharp tip attached to a cantilever and reveals information about the vertical height of the sample surface through the displacement of the probe required to maintain a given force in a feedback loop.

AFM can also determine some mechanical characteristics of the sample material itself, tip/sample forces and, in favourable cases produces 10 nm crystal lattices images. AFM can be operated in a number of modes, depending on the application and type of information required. In general, there are two possible standard imaging modes; static or contact mode and a variety of dynamic or non-contact modes (e.g., Tapping mode AFM).

The attractive or repulsive forces between the tip and the sample determine the appropriate mode of operation. Samples of soft or loosely-bound material produce artefacts in contact mode images because the force exerted by the tip may disturb or displace the object being imaged. Tapping mode ™ , also called intermittent contact mode, has become the method of choice for routine imaging of such samples; in this experiment, the tip is subjected to an oscillatory driving force and the amplitude and phase of the tip motion are recorded as the tip is rastered across the surface. Height information is obtained, via the feedback loop, from the amplitude of the tip as it 'taps' the surface. The phase signal reflects aspects of the tip/surface interaction such as the relative hardness of objects or tip-sample interaction force. The technique can image samples in both air and liquids and can achieve up to 0.1 nm (in the vertical direction) and 10 nm (in the lateral direction) image resolution, in favourable circumstances.

Sample preparation and instrumentation/equipment

Samples for AFM analyses were prepared by applying a few drops of mine-water to mica slides and allowing them to dry overnight. The slides were covered to prevent deposition of atmospheric particles and dust. The mica was then mounted on the sample holder of the AFM for analysis.

AFM analyses were performed on the Nanoscope III/Multimode, MMAFM-2, Series 1425EX, Atomic Force Microscope in tapping mode™. Tapping mode was used because of the loosely-bound nature of the material on the mica. The reduction of lateral and vertical tip/sample forces eliminates many artefacts due to sample movement and deformation during imaging. Measurements of height and width were determined by recording changes in the oscillation amplitude of the tip as it scanned

across the mica surface. The nominal tip radius of curvature is 8-10 nm. The AFM was by Digital Instruments (VEECCO Instruments Ltd.), 112 Robinhill Road, Santa Barbara, CA93117, USA. The dried mica containing the sample is then carefully loaded on the AFM with the aid of thong. The sample is placed below the cantilever with focussed microscope. The AFM mode parameter is then set to tapping mode. Schematic representation of the components of an AFM is shown in figure 3.7.

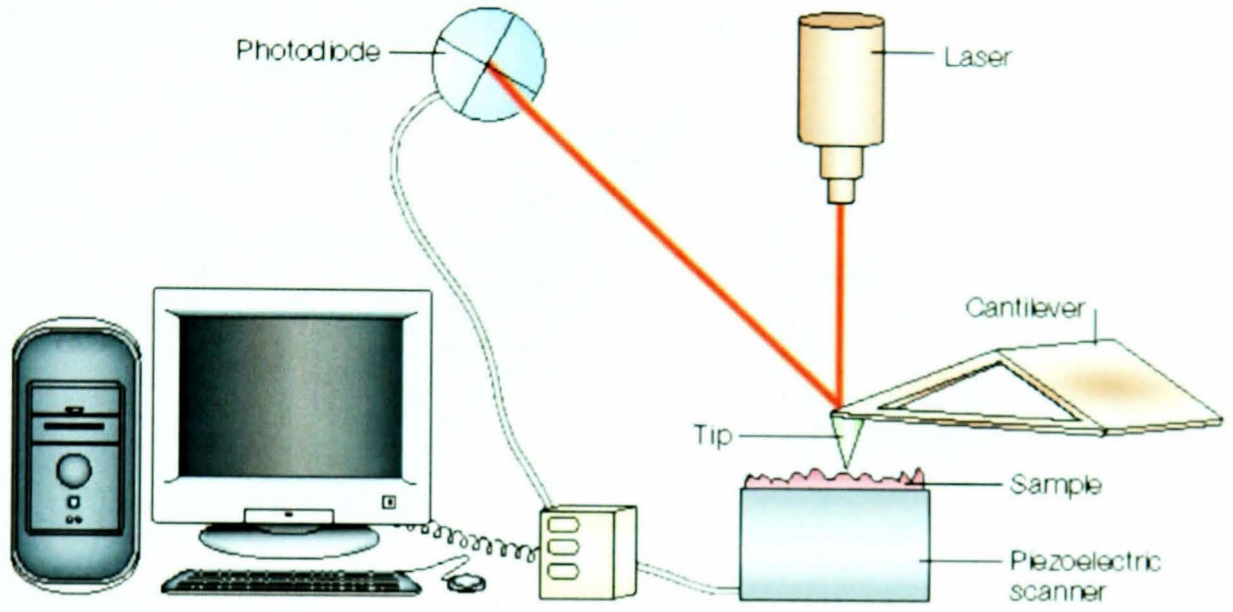

Schematic representation of the components of an atomic force microscope (AFM).

Figure 3.7: Schematic representation of typical components of an atomic force microscope (AFM), adapted from [36].

3.8.3: Fourier Transform Infrared Spectroscopy (FTIR)

Infrared spectroscopy is a widely used technique for the recognition of molecular functional groups with wide applications in organic, inorganic chemistry and solid state sciences. FTIR is an analytical technique for collecting infrared spectra by performing a complex Fourier transform of the IR light that passed through an interferometer and the resulting signal is collected as spectrum. The interferometer (figure 3.8) produces a time-varying light intensity at the sample. The light transmitted through (or in some experiments reflected) the sample is detected and a

Fourier analysis of the frequency components in this signal is made. Because the signal of the sample contains a superposition of all the relevant frequencies; there is no need to measure sequentially the absorption at each frequency as in a non-FT instrument. This advantage increases the speed of FT instruments and, through signal averaging procedures, allows superior signal-to-noise ratios to be achieved. Other advantages of FT instruments exist and are discussed in specialist texts [11].

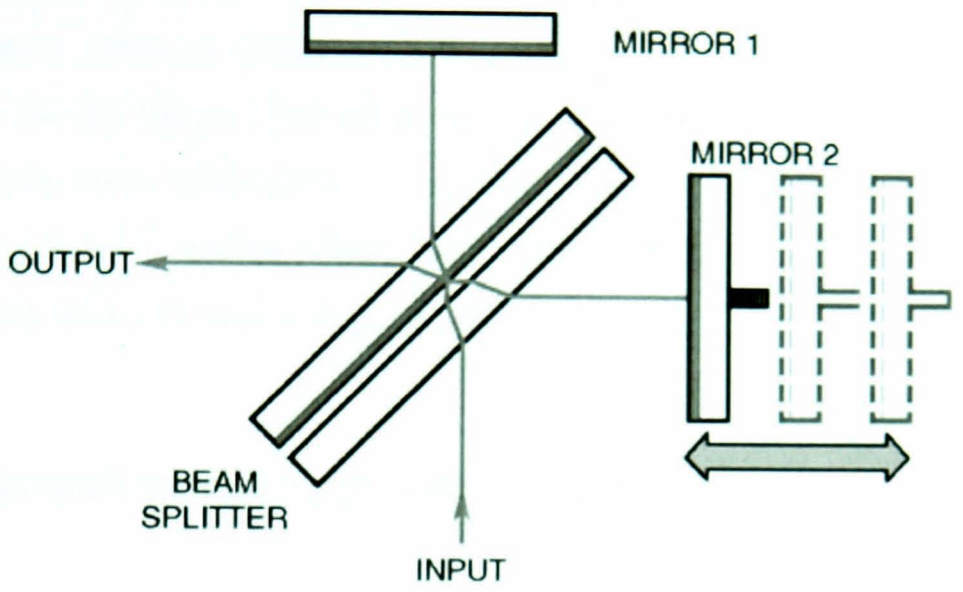

Figure 3.8: A schematic of a generic Michelson interferometer, similar to the one used in the FTIR instrument used in this research work [27].

For a molecule to be IR active, its vibrational mode must be associated with changes in its permanent dipole. IR spectroscopy is based on the fact that molecules have specific frequencies that are characteristics of individual functional group, and these vibrations are quantised. For frequencies in the chemically-relevant part of the IR spectrum, the majority of molecules are in the ground state: most of the IR bands observed correspond to the excitation of the first excited states; the corresponding fundamental frequencies depend on the stiffness of the chemical bonds involved (k) and the mass of the atoms. These frequencies can often be assigned to particular chemical functional groups and correlation table summarising the range of observed fundamentals for a variety of functional groups are widely available. However, peaks at low frequencies, i.e., wavenumbers in the region 900-1300 cm^{-1} are often hard to assign because numerous functional groups have normal modes in this region.

Nevertheless, FTIR instruments routinely achieve resolution <1 cm^{-1} and this region of the spectrum can be highly characteristic of particular compounds even if individual peak assignments are impossible-it is often referred to as the fingerprint region.

The spectra reported in this thesis were obtained in the normal transmission geometry which is the simplest, from an experimental point of view. A clean silicon plate was used to support a solid powder and the absorbances reported were calculated using the spectrometer software (Merlin ^{TM}) to compute $\log_{10} Io/I$ where *Io* is the intensity spectrum for the silicon plate alone and *I* that with the plate and sample in the beam. The spectra were analysed by comparing the observed peak wavenumbers with spectra of known related compounds. The fingerprint region (900-1300 cm^{-1}) is particularly useful for compound identification.

Sample preparation and instrumentation/equipment

Samples for FTIR were prepared by filtering mine waters through a 0.45 μm size cellulose nitrate filter paper and the sediment allowed to dry in open air on (100) oriented silicon chips 1 x 1 cm^2 . A small quantity of solid/ground powder sample (few milligrams) of the sample was then placed on the sample plate using spatula. A metallic rod was then screwed to squash the sample before analysis. Sample plates were cleaned and dried using industrial methylated spirit (I.M.S) and wiped with medical wipes by Kimberly-Clark Ltd, Surrey, UK. A one minute wait is normally observed after drying the sample plate with I.M.S, before loading the sample on the plate; this is to allow the solvent to evaporate.

All FTIR analyses were made on Varian 800, FTS 800, Excalibur series by Varian Australia Pty Ltd connected to a PC. Normal backgrounds together with the Si (100) background analyses were recorded. Samples were analysed in the wavelength range 4000-750 cm^{-1}, typically under the following conditions: resolution 2 cm^{-1}, scan time of 2 min and background scan of 16 times and the absorbance spectrum collected for each analysis. Triplicate analysis of each sample was employed.

3.8.4: X-ray Diffraction (XRD)

X-ray diffraction is a widely used technique by mineralogists. metallurgist and mineral scientists for the structural characterisation of crystalline materials. The arrangement of atoms within a crystal is inferred from maps of the electron density within the crystal. XRD is able to characterise different crystals with the same chemical compositions but different structures. In its determination of structures of materials, emphasis is on the geometrical arrangement and symmetry of the arrangement of atoms and distribution of electrons in the crystals rather than the energy levels. XRD (figure 3.9) involves the scattering of monochromatic X-rays from a single crystal which produces a diffraction pattern which can be related to the density of the electrons in the crystal by various methods. Identification is achieved by comparing the X-ray diffraction pattern or "diffractogram" obtained from unknown samples with an internationally recognised database containing more than 70,000 phases. One of the major limitations of XRD technique is that samples must have high degree of crystallinity and be in powder form because some of the crystallites will always be oriented so as to satisfy the Bragg condition of 2θ deviation principle.

It should be added that single crystal XRD gives atomic structure for single crystals while powder XRD gives only some of the information. Powder XRD was used for this study, thus, the need for complementary structural characterisation techniques like spectroscopic and microscopic methods used in this study. For example the Bragg condition is exact for infinite crystals-these would give infinitely thin spikes on the XRD pattern while Scherrer equation relates the actual, finite width of the peaks to the size of the crystal because the destructive interference of scattered waves which nearly, but not quite, satisfy the Bragg condition is incomplete in finite-sized crystals. Thus, for a given angle θ, depending on the electron wavelength and the crystal lattice spacing (according to Bragg's law), a crystalline specimen will diffract the electron beam strongly through well-defined directions.

$$n\lambda = 2d\sin\theta \qquad \text{(Bragg's law)}$$

Where:

n= integer, λ= electron wavelength, d= crystal lattice spacing between atomic planes and θ= angle of incidence and also of reflection.

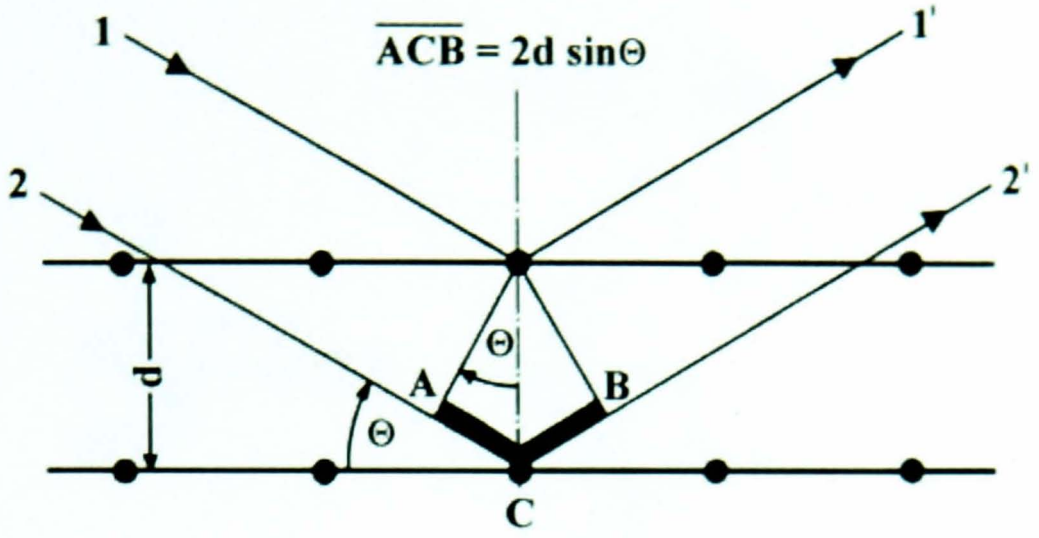

Figure 3.9: Diagram of Bragg's law showing the major Bragg parameters; (d)-crystal lattice spacing between atomic planes and (2θ)-angles of incidence and reflection [28].

The mean crystalline dimension (crystallite size) is then estimated using Scherrer equation after correction for instrumental broadening.

Scherrer equation:

$$d = K\lambda / (\beta \cos\theta)$$

where d is the diameter of the crystallite, K is a constant which is about 0.9. β is the breadth of the peak in the diffraction pattern at an angle, θ. λ is the wavelength of the X-rays.

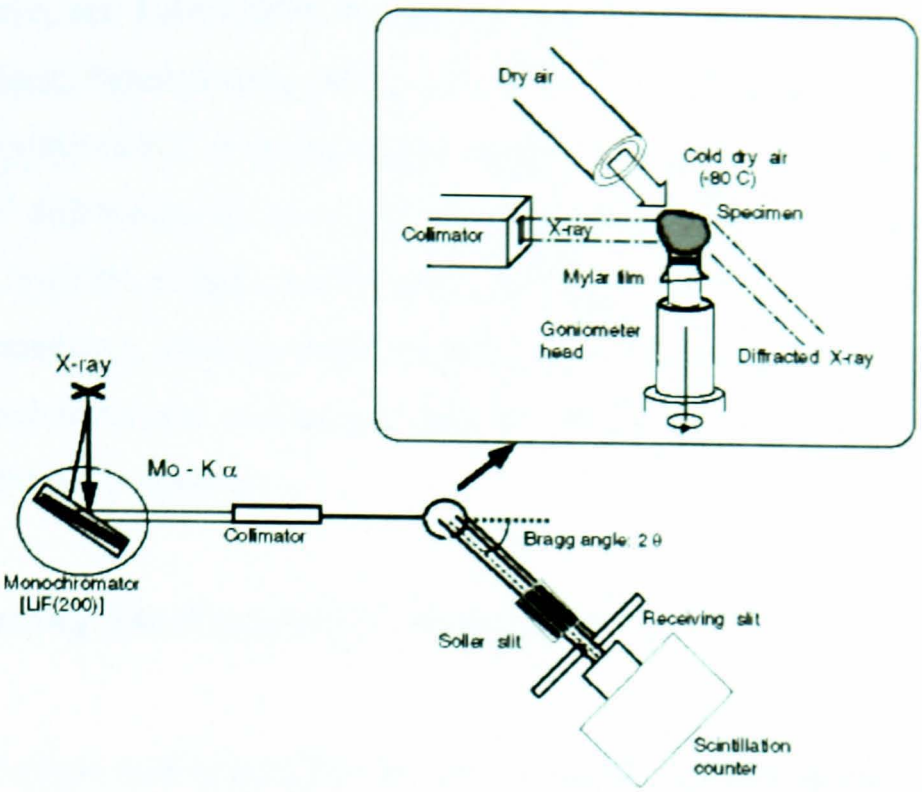

Figure 3.10: Schematic layout of the major components of the X-ray diffraction (XRD) measurement system, adapted from [29].

Sample preparation and instrumentation/equipment

Samples were prepared for XRD analysis by spreading approximately 25 mg of the powered samples on a zero background slide. Powdered samples were made by crushing with mortar and pestle the solid materials obtained after filtering mine-water samples through 0.45 μm filter paper and dried. All XRD analyses were made using a PANanalytical X'Pert Pro diffractometer, fitted with an X'Celerator. The scan range was 5-70- degree, programmed to a normal step size of 0.033 deg 2-theta and time per step of 100 s. The scan was carried out in "continuous" mode, rather than "step scan" and took 2 h 12 min per run (five times the normal scan time), giving a speed of ~0.9 degrees per min. Each sample was analysed twice; one at normal scan time for 30 min and the second for five times the normal scan time and run for 2 h 12 min. The long accumulation times were necessary because of the poorly crystalline and highly amorphous nature of the samples. However, successive scans at five times the normal scan time showed no difference in structural information and details which shows that the samples were not damaged by the X-ray beam in anyway. The radiation source was Cu K1-alpha: wavelength=1.54059 angstroms. Phase identification was carried out by means of the X'Pert accompanying software program High Score Plus and the

ICDD database, set 1-49 (1999) by the International Centre for Diffraction Data, Newtown Square, Pennsylvania 19073-3273, USA. The attachment of X'Celerator to the X'Pert has the effect of giving a good quality pattern in a fraction of the time of the traditional diffractometer. A secondary monochromator would normally eliminate fluorescence from the sample, resulting in a good peak; background ratio for samples containing transition metals (as in this work) and rare earths. However, for the present work, the monochromator was unavailable, so, the background scatter is high where there is significant Fe content.

3.8.5: Scanning Electron Microscopy (SEM)

SEM is a technique widely used for surface studies of materials, particle morphology, topographic characterisation/contrast of surface materials, shape and particle size. The most common type of image produced by SEM is by detecting secondary electrons. The SEM produces images by detecting low energy secondary electrons which are scattered from the surface of the sample due to excitation by the primary electron beam. It can produce images that are good representation of the 3D structure of the sample. The SEM requires the sample to be pumped down under high vacuum so that the electron beam is not scattered before it interacts with the sample and the electromagnetic lenses. In SEM, characteristic X-rays are produced when the samples are bombarded by the electron beam. Standard SEM uses a tungsten filament as an electron source with typical magnifications in the range 20-20,000 times. A recent development in electron sources are thermally assisted field emission gun (FEG)-tips. A FEG-SEM is capable of generating high resolution images of greater than 100,000 magnifications at low accelerator voltages (kV). High magnifications obviously give more details and low kV gives more surface details and prevents particle aggregation which makes characterization more difficult. This high resolving power capability of FEGSEM enables particles as small as 5-20 nm in length to be resolved and characterized. It should be noted that SEM works best with conductive samples where the electrons do not accumulate on the sample.

The relationship between electron wavelength and momentum or energy is given by de Broglie expression:

$$\lambda = h/p = h/(2m_e eV)^{1/2}$$

Where: λ= electron wavelength, h= Planck constant (6.634×10^{-34} J s) and p= linear momentum = $(2m_e eV)^{1/2}$.

As a consequence of this relationship (de Broglie equation above), electron microscopes can have higher resolution than optical ones and their resolution gets better as the voltage is increased and as such, high voltages lead to high electron speed, high momentum, short wavelength and better resolution.

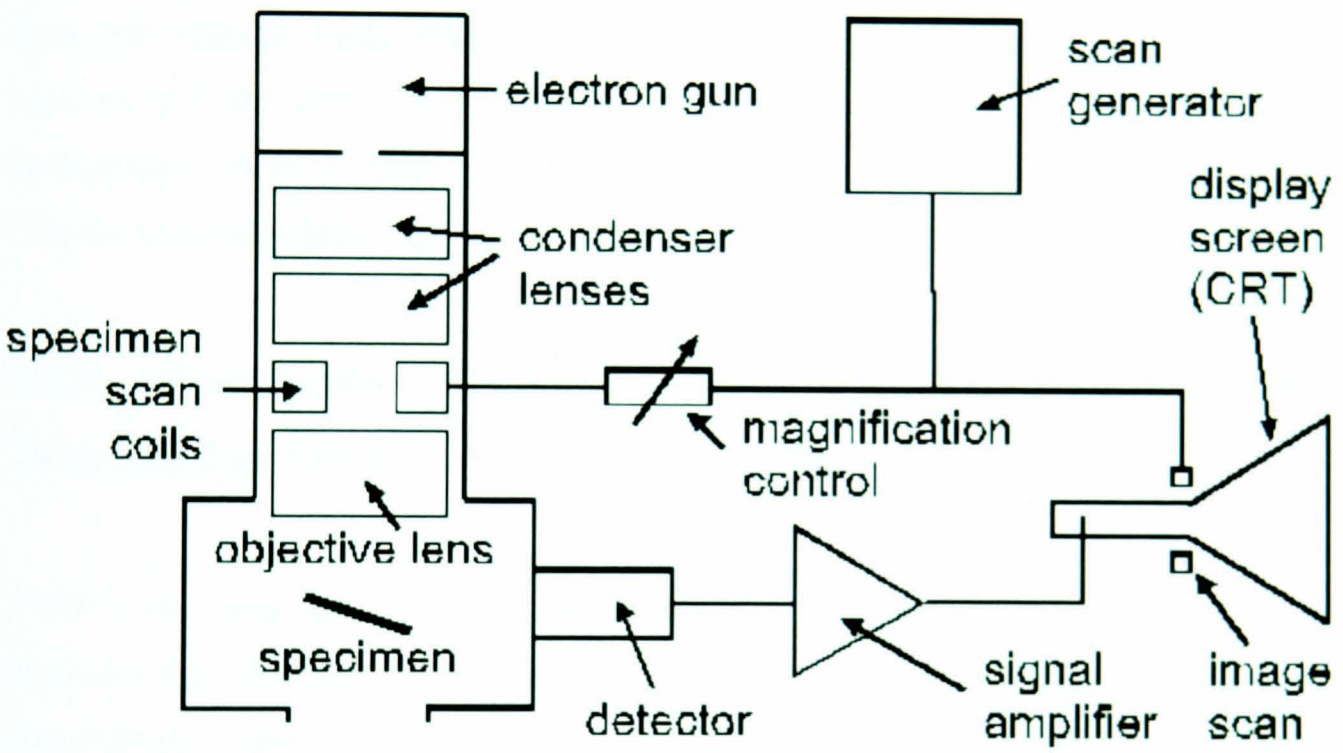

Figure 3.11: Schematic drawing of a scanning electron microscope (SEM) with secondary electron forming the image on the CRT display screen [30].

Sample preparation and Instrumentation/Equipment

Small quantity (few mg) of samples were placed on carbon conductive pads and mounted on a standard aluminium SEM stub and blown with compressed air (to remove any loose dust) using a clean Air Dust by Kenair, Swindon, UK. This was then coated with 3 nm of Pt/Pd metallic coating (80% to 20% respectively) using an Agar High Resolution Sputter Coater. This metallic coating is to make the samples conductive under the electron beam.

This was then followed by analysis by loading samples into the specimen chamber of a LEO 1530 Gemini SEM column, fitted with Field Emission Gun source which was used for all the SEM analyses. Like all SEMs, the Gemini column consists of electron magnetic lenses. The 3 nm Pt/Pd sputter coated samples were then viewed with the FEG-SEM operating at an accelerating voltage of 3 kV and using a solid state detector at the pole piece of the objective lens (as so called in-lens detectors) to generate images with good surface details. The gas used to vent the chamber when changing samples is high purity nitrogen in order to prevent water vapour forming and contaminating the column. SEM images were collected for each sample at 10,000, 25,000, 50,000, 100,000 and 250,000 times magnifications and were recorded at a slow line integrated scan rate and at a 3 mm working distance. The slow scan rate is used so that the detail in the higher magnification images is enhanced while the background noise is reduced. All electronic units are housed in the microscope console and controlled by an attached PC.

3.8.6: Transmission Electron Microscopy (TEM) & Scanning Transmission Electron Microscopy (STEM)

TEM is an imaging technique that allows for the visualisation of the projected structure both external and internal of a thin sample rather than just the surface morphology obtained by SEM. It involves emission of high voltage electron beam by a cathode. TEM works at high resolution because of the accelerating voltage applied to the incident electron beam~197 kV and is notable for producing images of the internal structure of a sample with resolutions down to 0.1 nm as the electron beam is transmitted through the sample. The TEM can produce images with magnifications of above 250,000 times the size of the material. Because of its high resolution, TEM has the ability to determine the positions of atoms within materials and has become very attractive in nanotechnology research and development. It has also found wide applications in all branches of science and technology where the study of the internal structure of materials or samples down to the atomic level is desired.

The only disadvantage of TEM relates to the higher beam energies required to achieve short electron wavelengths. In addition, the samples must be thin enough for the electrons to pass through.

STEM is the combination of SEM and TEM techniques. This principle is based on the fact that sample in a TEM is sufficiently transparent for electrons to be transmitted through the sample; these can be collected with a suitably placed detector. STEM technique provides both images and quantitative data, thus, making it possible for mass determination and mass/elemental mapping of structures to be determined simultaneously. In STEM, detailed structural and chemical information is simultaneously obtained by focussing the electron beam using the objective lens onto an atomic scale sample and by collecting all scattered electrons by a variety of detectors placed behind the sample. STEM images are therefore a collection of individual scattering experiment. The TEM used for this work was fitted with STEM (figure 3.12) capability as described in the above section.

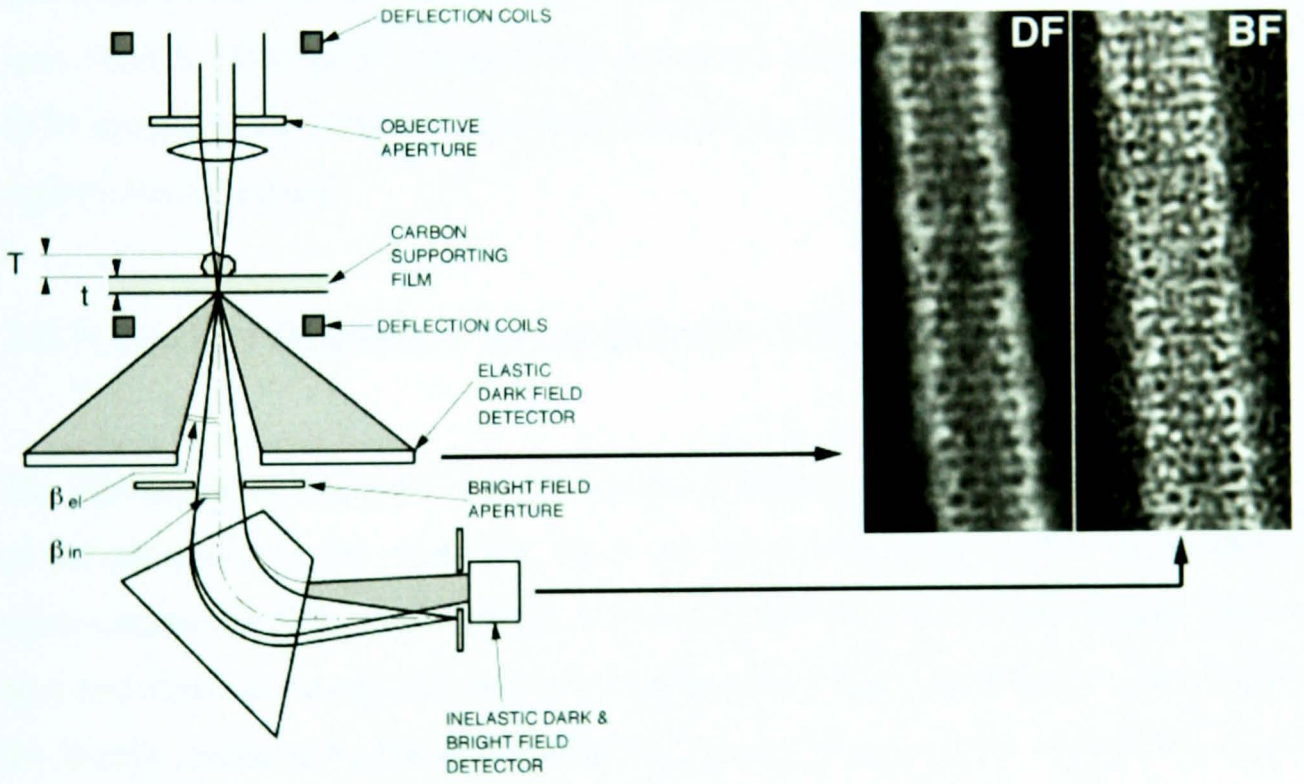

Figure 3.12: Schematic diagram of a STEM showing the lens, aperture and deflection systems. Elastically scattered electrons are collected by a ring and provide the elastic dark field (DF) or bright field (BF) signal [31].

Sample preparation and instrumentation/equipment

The drop-casting technique was used for sample preparation. This is done by dissolving a few milligrams of samples in an organic solvent-ethanol (~1 mL), then sonicated for 2 min (to mix the solvent and the sample properly).

This was followed by depositing a drop of this mixture on the TEM grid of 3 mm diameter. The TEM is composed of a 400 mesh Cu support grid (3 mm in diameter) with a 30 nm thick amorphous carbon film laid across it. The carbon film is electron transparent and contains many holes (<100 μm in diameter), thus enabling particle support on the film to be imaged in transmission. The films are standard holey carbon support films purchased from Agar Scientific Ltd.

High-resolution TEM analyses were then carried out on the thin specimens and carefully examined using a Philips CM200 FEG-SEM, operated at 197 keV. The HR-TEM is equipped with scanning STEM capability. and fitted with an Oxford Instruments ultra thin window energy dispersive X-ray (EDX) spectrophotometer and a Gatan (GIF 200) imaging filter used for digital imaging but with electron energy loss spectroscopy (EELS) capability. All images were digitally recorded using slow scan 1024 x 1024 CCD cameras and processed using Digital Micrograph (Gatan). TEM images of the samples were then collected at both the bright field and dark field regions among others.

3.8.7: Energy Dispersive X-ray Detector (EDX)

The interaction of electrons with the sample produces X-rays which are characteristic of the elements in the materials. Most of the new generation FEG-TEM electron microscopes are fitted with special microanalytical systems which analyse these X-rays and allow the composition to be determined and spatially mapped. The energy of the X-rays produced by the electrons bombardment of the sample is determined by the elemental composition which is done by EDX (figure 3.13). Compositional analysis of a sample can be obtained by analysing the x-rays produced by the electron-sample interaction. This enables detailed maps of elemental distribution to be produced from multi-phase materials by the acquired spectra showing distinctive peaks for elements present with the peak height indicating the element concentration.

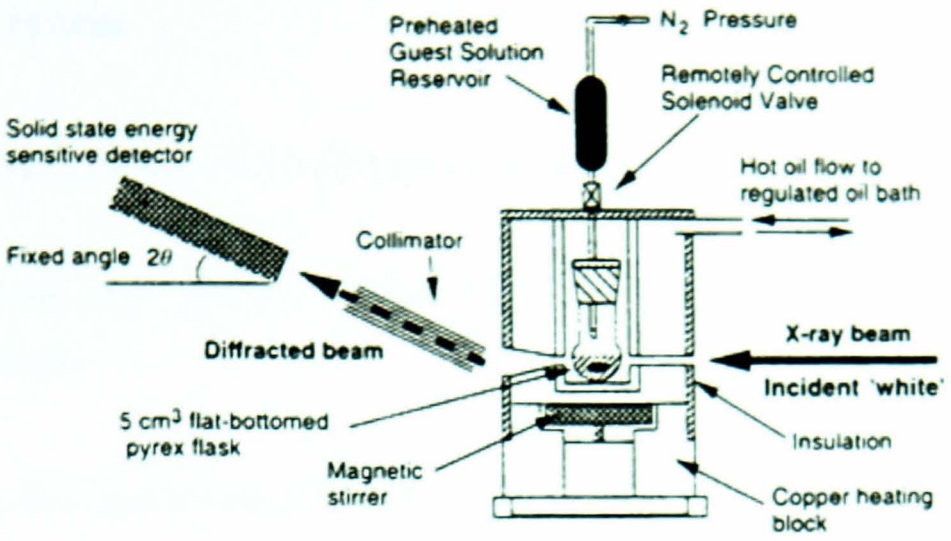

Figure 3.13: Schematic layout of the atomic process responsible for the energy dispersive X-ray detector (EDX) analysis [32].

In this research work, elemental analysis was done by EDX (Energy Dispersive X-ray Analysis). The EDX does the elemental composition analysis by measuring the characteristic X-rays generated when the electron beam impinges on the sample. The X-ray diffraction patterns of selected area electron diffraction (ED) patterns were recorded to relate to the TEM sample crystallography to that observed by the X-ray diffraction. As already mentioned, the TEM used for this work is fitted with energy dispersive x-ray analysis systems which allow elements in the samples to be analysed.

3.8.8: References

[1]. Greenfield, S., Jones, I.L.I. and Berry, C.T. *Analyst*, **1964**, 713-720.

[2]. Koirtyohann, S.R., Jones, J.S., Jester, C.T. and Yates, D.A. *Spectrochim. Acta.* **1981**, 36B, 49-59.

[3]. Browner, R.F. and Boorn, A.W. *Anal. Chem.*, **1984**, 56, 786A-798A.

[4]. Dickenson, G.W. and Fassel, V.A. *Anal. Chem.*, **1969**, 41. 1021-1024.

[5]. Deemer, D.R. *Applied Spectroscopy*, **1979**, 33, 584-586.

[6]. Ramsey, M.H. and Thompson, M. *Analyst*, **1985**, 110, 519-530.

[7]. Cornell, R.M. and Schwertmann, U. *Wiley-VCH*, **2003**. 664pp.

[8]. Philips Electron Optics, *Instrument Manual*, **1990**, ISBN number 90-907755-3

[9]. Charles, B.S. and Kenneth, J.F. *Perkin Elmer*, **1999**, 58pp.

[10]. Atkins, P.W. *Physical Chemistry*, 6th edition, **1998**, 1014pp.

[11]. Banwell, C.N. and McCash, E.M. *Fundamentals of Molecular Spectroscopy*, 4th edition, **1993**, 308pp.

[12]. Brett, C.M.A. and Oliveira Brett, A.M. Electrochemistry: Principles, methods and applications, *Oxford University Press*, Oxford, **1993**.

[13]. Compton, R.G. and Sanders, G.H.W. Electrode Potentials, *Oxford University Press*, Oxford, **1995**.

[14]. Brett, C.M.A. and Oliveira Brett, A.M. Electroanalysis, *Oxford University Press*, Oxford, **1998**.

[15]. Fisher, A.C. Electrode Dynamics, *Oxford University Press*, Oxford, **1996**.

[16]. Kissinger, P.T. and Heineman, W.R. *J. Chem. Educ.*, **1963**, 60, 702.

[17]. Van Benschoten, J.J., Lewis, J.Y., Heineman, W.R., Rosten, D.A. and Kissinger. P.T. *J. Chem. Educ.*, **1983**, 60, 772.

[18]. Mabbott, G.M. *J.Chem. Educ.*, **1983**, 60, 697.

[19]. Ogren, P.J. and Jones, T.P. *J. Chem. Educ.*, **1996**, 73, 1115-1116.

[20]. Mowry, S. and Ogren, P.J. *J. Chem. Educ.*, **1999**, 76, 970.

[21]. Weinberger, P. *Philosophical Magazine Letters*, **2006**, 86, 405-410.

[22]. Petterson, A.L. *Physical Review*, **1939**, 56, 978-982.

[23]. Nelson, F., Randall, H.M. and Dennison, D.M. *Physical Review*, **1939**, 56, 160.

[24]. http://elchem.kaist.ac.kr/vt/chem-ed/spec/atomic/emission/icp.htm , retrieved on October 30, **2008**.

[25]. www.autolab.com/appl.files/electrochem.html, retrieved on September 30, **2008**.

[26]. www.electrochem.org, retrieved on September 30, **2008**.

[27]. www.minerals.cr.usgs.gov/icpms/intro.html, retrieved on September 30, **2008**.

[28]. Charles, B.S. and Kenneth, J.F. *Perkin Elmer*, **1999**, 12-78.

[29]. www.geobacter.org/.../images/jpg/AFM diagram.jpg, retrieved on September 30, **2008**.

[30]. www.trace.en.org/fa/rpm/indexx.php, retrieved on September 30, **2008**.

[31]. www.fkf.mpge.de/.../x-rays/x-rays.html, retrieved on September 30, **2008**.

[32]. www.odp.tamu.edu/.../164_SR/chap-02/ch2-f7.html Retrieved on September 30, **2008**.

[33]. www.lasers.phys.ualberta.ca/-egerton/SEM/sem.html Retrieved on September 30, **2008**.

[34]. www.mih.unibas/.../chapter4/chapter4.html, retrieved on September 30, **2008**.

[35]. Evans, J.S.O., Price, S.J., Wong, H.V. and O'Hare, D.J. *J. American Chemical Society*, **1998**, 120, 10837pp.

[35]. www.cee.vt.edu/.../teach/smprimer/icp.html, retrieved on September 30, **2008**.

[37]. www.svvt.edu/.../experimental/electron.html, retrieved on September 30, **2008**.

[38]. www.acept.asu.edu/PIN/rdg/elmicr/elmicr.html, retrieved on September 30, **2008**.

[39]. www.newport.com/-images/2402.gif, retrieved on September 30, **2008**.

[40]. www.tkk.fi/yksikot/paperi/laitteet.html, retrieved on September 30, **2008**.

Chapter 4

VOLTAMMETRIC METHODS

This chapter describes in detail the voltammetric methods-differential pulse voltammetry (DPV) and cyclic voltammetric (CV) techniques that have been used for the analysis and quantification of iron speciation in polluted mine-water studied in this thesis. Method validation was done by comparing the voltammetric data with the established mine-water analytical techniques based on atomic spectroscopy-inductively coupled plasma-optical emission spectroscopy (ICP-OES) used by the HERO research group at Newcastle University who have carried out extensive research on the studied sites.

4.1: Introduction

Acidic, metalliferous pollution arising from abandoned mine workings and spoil heaps is a major environmental threat to substantial lengths of river courses worldwide [1, 2]. Iron is a key contaminant in mine-waters, occurring in concentrations up to 0.1 mol dm^{-3} as a result of a series of well-known acidification reactions ultimately related to the oxidation of pyrite (FeS_2) by oxygenated waters penetrating spoil heaps and mine voids. The relevant redox chemistry may be summarised as follows in equations 1-4: [3].

$$FeS_2(s) + \frac{7}{2}O_2 + H_2O \rightarrow Fe^{2+} + 2SO_4^{2-} + 2H^+ \quad (1)$$

$$Fe^{2+} + \frac{1}{4}O_2 + H^+ \rightarrow Fe^{3+} + \frac{1}{2}H_2O \quad (2)$$

$$FeS_2(s) + 14Fe^{3+} + 8H_2O \rightarrow 15Fe^{2+} + 2SO_4^{2-} + 16H^+ \quad (3)$$

$$Fe^{3+} + 3H_2O \rightarrow Fe(OH)_3(s)\{ochre\} + 3H^+ \quad (4)$$

The direct reaction of dioxygen with pyrite (equation 1) is slow, but iron-oxidizing bacteria can accelerate the oxidation of the Fe^{2+} and facilitate the oxidation of pyrite by Fe^{3+} (equation 3), which is rapid and produces a low pH [3]. Mixing of acidic,

iron-rich waters with oxygenated, higher pH surface waters results in a series of hydrolysis and oxidation reactions leading to the precipitation of yellow Fe(III) oxyhydroxides called ochre. Although not inherently toxic, the presence of iron in mine-waters causes major environmental degradation in surface waters due to the deposition of iron oxides and oxyhydroxides on sub-aqueous plants and river beds. The abundance of iron in mine-affected waters is generally measured by spectroscopic methods such as AAS or ICP-OES. Either total iron may be determined. or the waters are filtered at 0.45 μm or 0.2 μm in order to differentiate solid phase and "dissolved" iron. These conventional data have two main limitations: they give no idea of the redox state or speciation of iron and do not differentiate colloidal iron (i.e., sub 0.45 μm or 0.2 μm particles) from truly dissolved iron. Ultrafiltration has been used to fractionate colloidal and "dissolved" (<1 kDa) metal species and suggests that much of the iron in the sub 0.45 μm filtrate from both uncontaminated and mine-affected water courses is in fact colloidal [4, 5, 6, 7, 8, 9]. The environmental significance of colloidal iron is that it (a) strongly absorbs trace metals [10] (b) is prone to flocculation [11] and (c) may be less bioavailable than truly dissolved iron [12].

Whilst ultrafiltration has given important insights into the occurrence of colloidal metal oxides in aqueous systems, it is a time-consuming procedure and is unsuited to continuous monitoring of metal species in situ. A voltammetric experiment distinguishes solid-phase particles from soluble Fe species based on the greater diffusional mass transport rate of the latter. The electrochemical approach has advantages because it is rapid and there is no need to choose a filter with an arbitrary molecular mass cut-off. There have been many voltammetric studies of iron in natural waters, especially in oceanography and limnology [e.g., 20, 21, 22, 24 & 25]. However these mainly deal with trace analysis of Fe which presents different analytical challenges compared to the high concentrations typically observed in mine-affected waters. Some voltammetric studies of dissolved iron relevant to acid mine-water discharges have been reported, however their focus has mainly been on electrochemical remediation [45] or fundamental studies of bacterial iron respiration related to mine-water remediation [46].

This studies show how voltammetric techniques can be employed to make accurate and precise measurements, not only of total iron ([Fe]total), but also dissolved ([Fe]aq) and solid-phase iron ([Fe]sol) . It further shows that voltammetric techniques are sensitive to aspects of iron speciation, including the presence of hydrolysed versus unhydrolysed Fe ([Fe]hyd, [Fe]unh), and that they can be used to monitor the ratio of Fe(II) and Fe(III) redox states. The detailed interpretation of the biogeochemical significance of these analytical and speciation data for iron are presented in chapters 5-9, on a site -by -site basis.

4.2: Results and Discussion

The voltammograms of Fe(II) and Fe(III) in aqueous calibration solutions, as well as the mine-water samples, show at least three peaks (figi.4.1). It is well known that the speciation of Fe aquo ions is complex: extensive hydrolysis of Fe(III), leading eventually to precipitation of oxyhydroxides, occurs unless the solution is strongly acidic. Most physicochemical studies of Fe(aq) voltammetry are carried out in strong acid solutions to suppress the hydrolysis [44]. However, the pHs observed in our samples varies substantially from 2.85 to 7.90. Therefore the effect of the hydrolytic reactions on the voltammetry that were observed in the mine-water samples is briefly discussed before describing the analytical results. Finally, the results show how a comparison of acidified and unacidified samples enables a simple determination of the amount of solid phase Fe present in the samples and that, by filtering samples before acidification, and therefore the determination of Fe present in nanoparticulate form.

4.3: Speciation of Fe(III) and Fe(II) - voltammetric studies

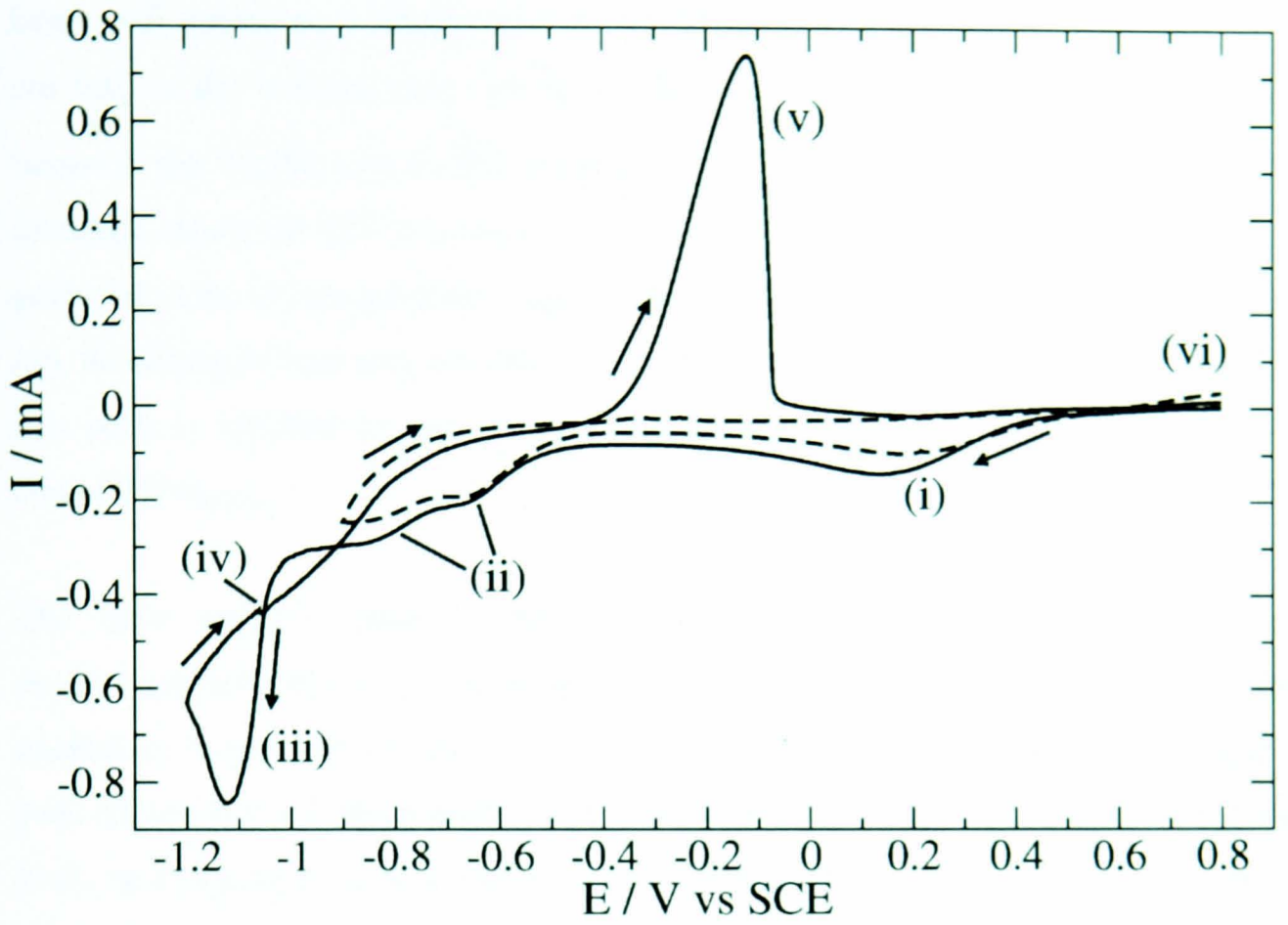

Figure 4.1: Two cyclic voltammograms of 5 mM $FeCl_3$ in 0.1M KCl and degassed with nitrogen gas. The scan rate was 0.1 V s^{-1}, the reference electrode was a saturated calomel electrode with gold and platinum as working and counter electrodes respectively. Various peaks of interest are labelled (i)-(v) and their assignments are discussed in the text.

The standard potential for the electrode reaction,

$$Fe(H_2O)_6^{3+} + e^- \Leftrightarrow Fe(H_2O)_6^{2+}$$

is +0.77 V vs SHE, or about +0.53 V vs SCE. However, $[Fe(H_2O)_6]^{3+}$ is acidic and the pK_as for the first two deprotonation steps are 2.19 and 5.67 [42]. There may therefore be significant amounts of $[Fe(H_2O)_5OH]^{2+}$ and $[Fe(H_2O)_4(OH)_2]^{+}$in the mine-water samples. Since the pK_a for $Fe(H_2O)_6^{2+}$ is 9.5, [31] Fe(II) species in the mine-waters will mostly be unhydrolysed.

In our voltammetric experiments, the reduction of $[Fe(H_2O)_6]^{3+}$ and its conjugate bases will appear as a single wave (or peak) because the proton transfers to oxygen are fast on the voltammetric timescale. However, because of the difference in pK_a between the Fe(III) and Fe(II) oxidation states, the wave will shift in a negative direction when the pH increases - as observed. Therefore the most positive peak potential in the voltammograms was assigned to the reduction of the Fe(III) hexaaquo ion, its conjugate base and any other species in rapid equilibrium with it. In figure 4.1, this peak is labelled (i) and the concentration of the species contributing to it is denoted $[Fe]_{unh}$.

The most negative peak is labelled (iii) in figure 4.1: it is clearly due to electrodeposition of Fe by reduction of Fe(II). This is evident from the presence of a nucleation loop in the CV (figure 4.1iv) and the presence of a characteristic stripping peak (figure 4.1v). If the potential scan is reversed before peak (iii) (figure 4.1, dashed line), no stripping peak is observed, which confirms that peak (figure 4.1iii) is due to electrodeposition of Fe. This leaves the question of the assignment of the peaks (figure 4.1ii) at intermediate potentials. In the concentration range 1-10 mM, the formation of significant quantities of dinuclear and multinuclear Fe species is known [33, 34, 35, 36, 37]. The Fe aqua dimer ($[Fe_2(OH)_2(H_2O)_8]^{4+}$ or $[Fe_2O(H_2O)_{10}]^{4+}$ is kinetically stable in mildly acidic solutions (pH $\approx$ 2) and in the presence of excess $[Fe(H_2O)_6]^{3+}$ and $[Fe(H_2O)_5OH]^{2+}$ [37, 38, 39]. The break-up of the aqua dimer into monomeric Fe species has been shown to follow a rate law, rate = ($0.4\ s^{-1}+3.1\ M^{-1}\ s^{-1}[H^+]$) [dimer] [41, 42]. This rate is sufficiently slow for the reduction of the aqua dimer to appear as a separate wave in the voltammetric experiments. Therefore assign the voltammetric waves (ii) at intermediate potentials to the reduction of the aqua dimer and possibly also higher nuclearity species and/or complexes with sulphate. The concentration of the species contributing to the peak (ii) is denoted $[Fe]_{hyd}$ below. Finally, although the Fe aqua dimer is thought to be thermodynamically unstable with respect to FeOOH(s) and monomeric Fe species [40], the slow kinetics of the system mean the use of thermodynamic arguments based on, e.g., E_h-pH diagrams, to predict the actual composition of mine-water samples must be applied with caution.

4.4: Voltammetric analysis of dissolved Fe in mine-waters

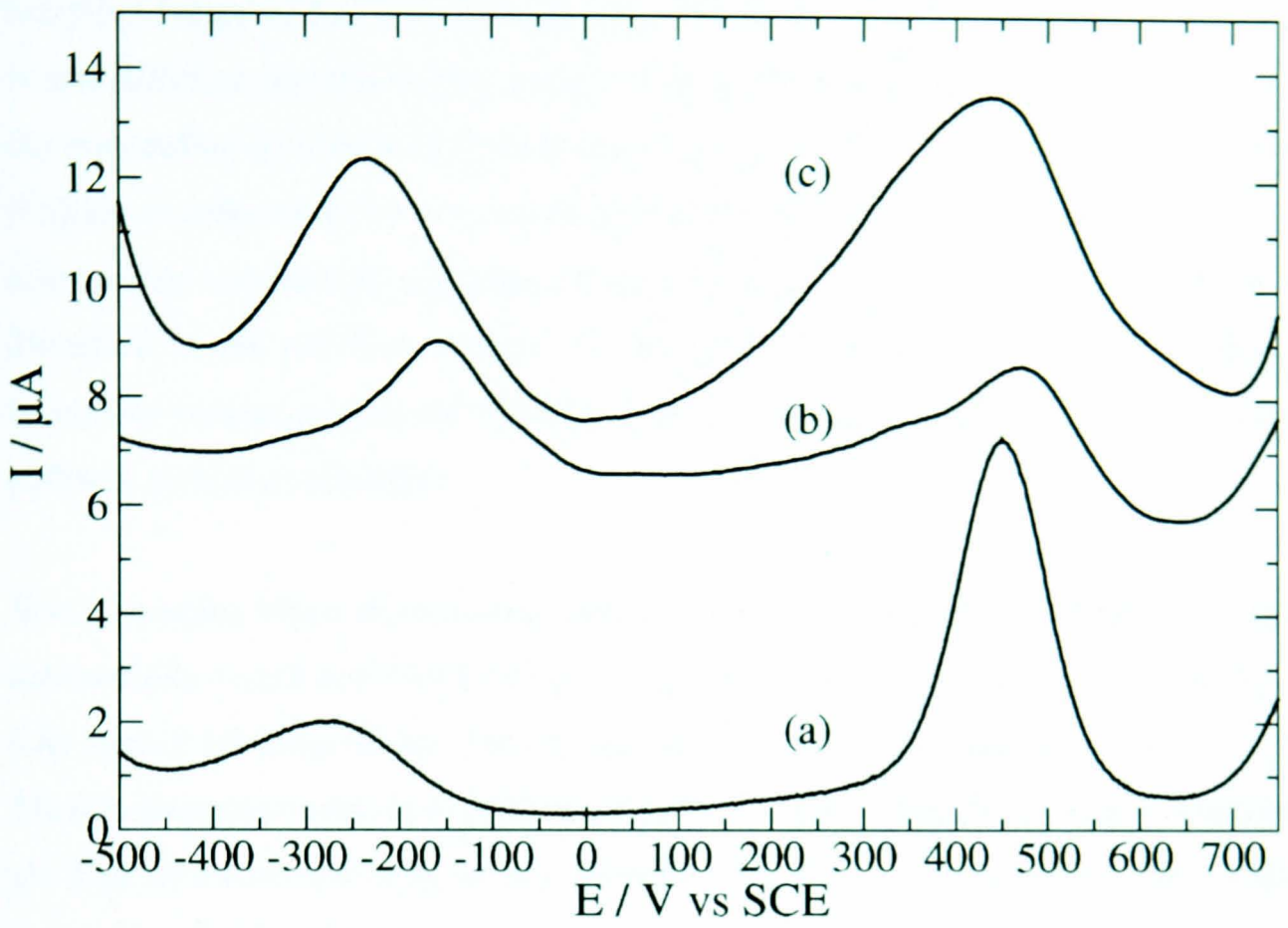

Figure 4.2: Differential pulse voltammograms of unfiltered mine-water samples taken from: (a) RAPS 2 inlet, Bowden Close site, Co Durham, pH 4.52 and [Fe]total= 29.59 mg L^{-1}; (b) Lagoon 2 Inlet, Acomb site, Hexham, pH 6.43 and [Fe]total= 33.46 mg L^{-1}; (c) Lagoon 1, Shilbottle site, Northumberland, pH 3.10 and [Fe]total= 61.54 mg L^{-1}. DPV parameters: pulse width = 50 ms; pulse height = 75 mV and step height = 2 mV. Scanning from right to left, the working electrode was a 2 mm diameter Pt disc and an SCE reference electrode was used and degassed. Vertical offset was 20,000.

Figure 4.2 shows representative differential pulse voltammograms (DPVs) over the potential range corresponding to the peaks due to unhydrolysed ([Fe]unh; $E^{\theta} \approx 0.45$ V) and hydrolysed Fe species ([Fe]hyd; $E^{\theta} \approx -0.2$ to -0.3 V) in mine-water samples from a selection of sampling points across the CoSTaR sites examined in this study. The DPVs are substantially simpler in appearance than the cyclic voltammograms, even of laboratory calibration solutions (figure 4.1). The DPVs are therefore less informative about details of speciation, but are preferable for analytical determinations.

Nevertheless, it is clear from the peak currents, potentials and even wave-shapes that the concentration and speciation of dissolved Fe varies substantially between sampling locations and CoSTaR sites. The pH at the various sampling points and sites is also different and this causes a shift in the voltammetric peak potentials because of the protonation equilibria of Fe(II/III) aquo ions and the extent of hydrolysis of Fe(III). [Fe]unh as determined by a voltammetric method includes not only $[Fe(H_2O)_6]^{3+}$, but also species obtained by rapid proton transfer equilibria such as $[Fe(H_2O)_5OH]^{2+}$. As discussed in the previous section, the fraction of dissolved Fe we denote [Fe]hyd comprises species such as the Fe aquo dimer and perhaps, higher oligomers along the pathway towards FeOOH(s).

Water samples taken at inlet and outlet locations at different CoSTaR sites varied substantially in pH and *Eh* (Table 4.1). The pH of inlet samples ranged form 2.85 to 6.81 across all sites, while that of samples from outlet ranged from 3.33 to 7.90. Though there is overlap in the pH ranges of sites, outlet samples generally had higher pH than their corresponding influent samples. The *Eh* of outlet samples were typically lower than the *Eh* of inlet samples: the observed trend is probably due to the aerobic environment of the influent and the anaerobic nature of the wetlands. Two exceptions to the general trend were found at the Quaking Houses and Whittle sites. Solid-phases such as FeOOH are expected to be thermodynamically stable at nearly all the measured *Eh* and pH values, nevertheless substantial dissolved Fe was found (figure 4.2) and clearly the samples are out of equilibrium in this respect.

Table 4.1: Representative pH and *Eh* measurements of the inlet (polluted) and outlet (treated) waters at several CoSTaR sites showing the increase in pH and decrease in Eh upon treatment of the mine-waters.

Site	Inlet pH	Outlet pH	Inlet E_h/ mV	Outlet E_h/ mV
Bowden Close	4.33	6.90	220	170
Shilbottle	2.85	3.33	550	470
Quaking Houses	6.26	6.55	30	60
Whittle	6.81	7.90	-120	-50
Acomb	5.51	7.07	260	210

[Fe] in all the samples studied in this research is much larger than voltammetric detection limits and several orders of magnitude greater than [Fe] measured in marine environments see [e.g., 43]. However, the analytical challenge is to develop a simple method to quantify dissolved and colloidal Fe species that is capable of being applied on-site. In addition, owing to the large datasets (multiple sampling locations and sites, long-term pollution monitoring) the method should be simple to calibrate and involve the minimum of data processing. At the values of [Fe]total found in mine-water, there is significant deprotonation of Fe(III) aquo ions and these species are determined by the peak at ca. 0.45V vs SCE. For simplicity fraction is denoted [Fe]unh and refer to it as unhydrolysed. A significant fraction is likely to be present as dimers or higher oligomers (peak at ca. -0.3V vs SCE) and this was denoted as [Fe]hyd and refer to it as hydrolysed Fe. The simplest calibration of the voltammetric responses that yields reliable [Fe]total is based on measurement of the peak currents due to [Fe]unh and [Fe]hyd. Because $Fe^{2+}(aq)$ and $Fe^{3+}(aq)$ hydrolyse to different extents, calibration solutions prepared with a constant [Fe]total, but varying Fe(II)/Fe(III) ratios produce a range of values of [Fe]unh and [Fe]hyd. Over the range of conditions of pH and [Fe]total that was encountered, a simple linear calibration sufficed:

$$I_{peak}(i)/\mu A = 8.8(1)\{[Fe]_{unh} / mmoldm^{-3}\} + 1.81(1) \quad (5)$$

$$I_{peak}(ii)/\mu A = 9.9(9)\{[Fe]_{hdy.} / mmoldm^{-3}\} + 0.49(1) \quad (6)$$

The total dissolved Fe was obtained by adding the concentrations of hydrolysed and unhydrolysed Fe: [Fe]total = [Fe]unh + [Fe]hyd. The voltammetric data was checked by comparison of [Fe]total with ICP-OES data with which satisfactory agreement was obtained, as discussed below.

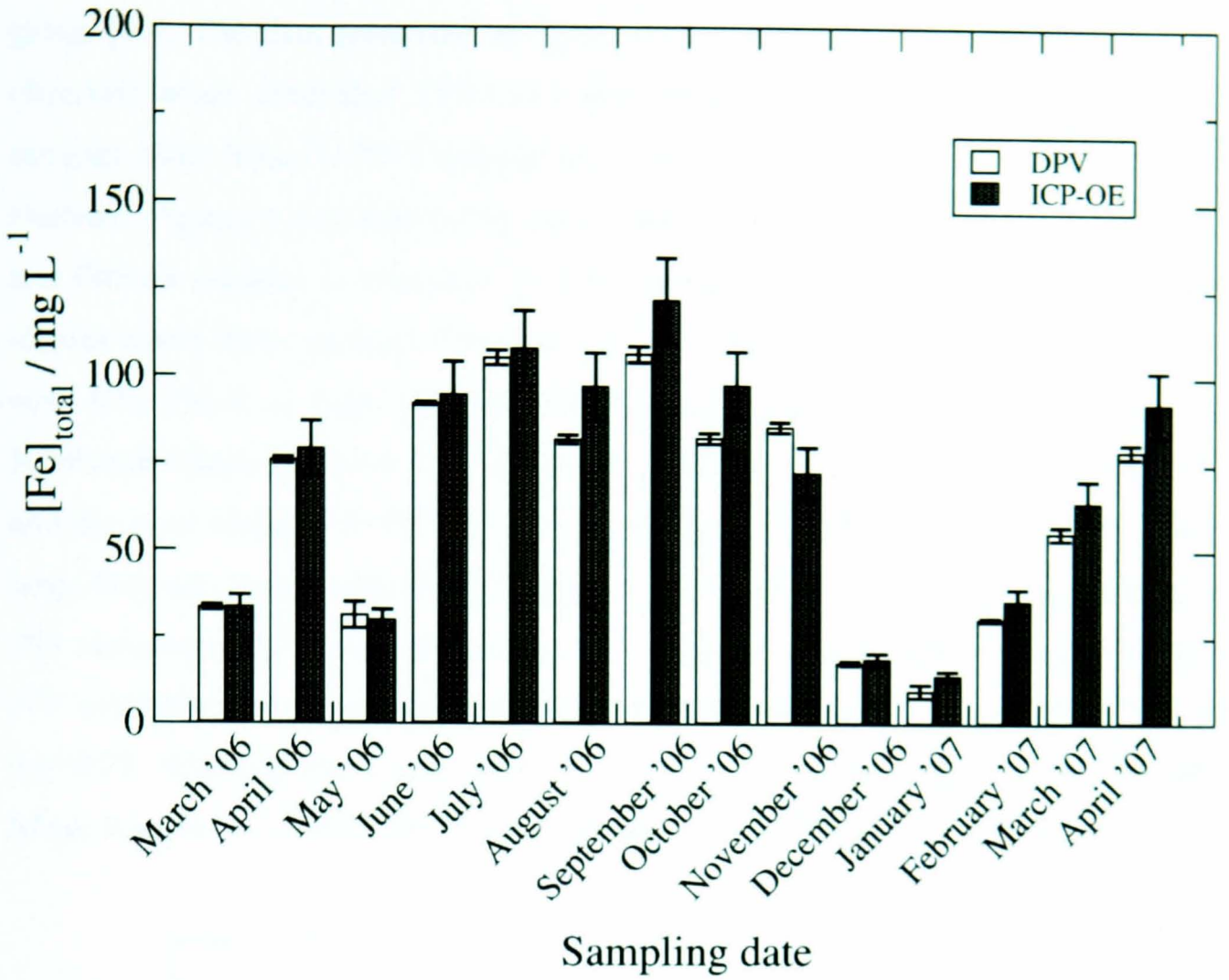

Figure 4.3: Comparison of Total Fe/mg L^{-1} measured by DPV and ICP for the aquifer/surface mine-water samples taken from the RAPS 2 influent at the Bowden Close site. The electrochemical total Fe concentrations were obtained by adding the concentrations of hydrolysed and non-hydrolysed Fe determined by differential pulse voltammetry. The ICP-OES (Inductively Coupled Plasma-Optical Emission) values were taken from the HERO database and are known to have an uncertainty of 5-10% (Personal Communication, 2007). The error bars on the DPV data are 95% confidence intervals: these uncertainties are discussed in the text. In both cases (Voltammetry and ICP methods), the samples were acidified with 1% v/v HCl to remove solid Fe oxyhydroxides.

Figure 4.3 shows how the DPV measurements of total dissolved Fe compared with the ICP-OES method used previously by the HERO group.[47] Polluted mine-water samples were acidified on-site to 1% v/v (conc. HCl / mine-water) to dissolve solid phase Fe and to ensure that all Fe species are in soluble forms in the samples. The two methods agree within the 10% uncertainties associated with the ICP data of the HERO

group [49]. The data presented in figure 4.3 is representative of the general trend observed when compared DPV and ICP-OES. This dataset was obtained from samples taken from RAPS 2 influent into a settlement lagoon at Bowden Close, Co. Durham. Figures 4.4(a) and 4.4(b) show comparisons of [Fe]total for both unfiltered and filtered samples as measured by DPV and ICP-OES for the portion of the full dataset where there are both ICP-OES and DPV measurements. Most of the outliers, especially those at high [Fe]total derive from one particular site, at Shilbottle, Northumberland. The most concentrated samples correspond to about 0.1 M (by ICP) and the most dilute to 2×10^{-5} M (by ICP). Overall, the DPV statistical errors are not large-they are mainly related to changes in the shape of voltammograms. A total of 298 measurements of total samples and 95 measurements for filtered samples where ICP available were compared. Unfiltered rsq=0.67 but 0.94 for log10 data. Filtered rsq=0.75, 0.92 for log10 data stdev of % error ≈18 after remove >50% outliers. Mean % error = -3.7 and 0.61 %. The full dataset is close to 1000 samples.

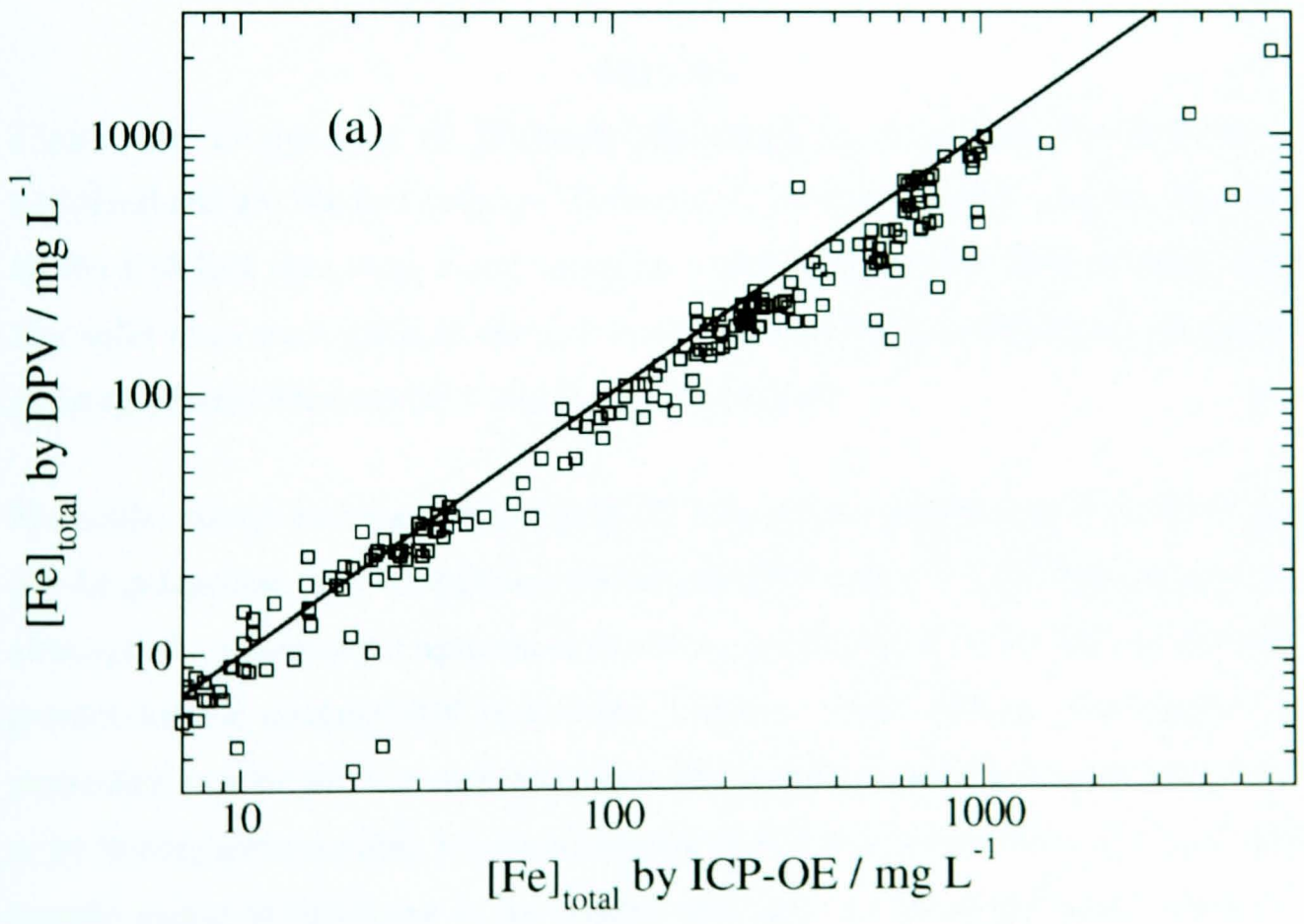

Fig. (4a)

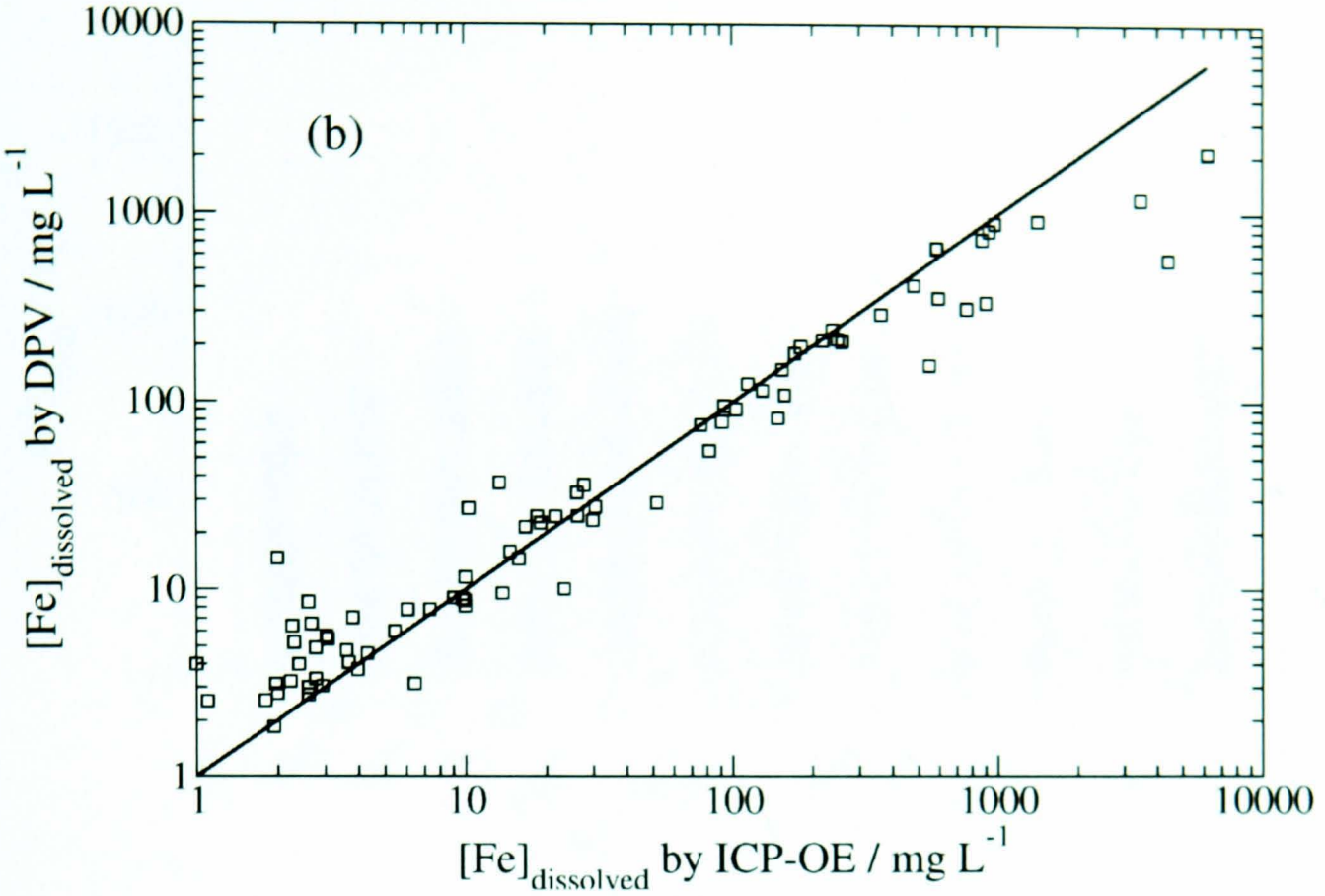

Fig. (4b).

Figure 4.4: Comparison of [Fe]total determined by DPV and ICP-OES for (a) unfiltered and (b) filtered samples. The datasets shown comprise samples taken from all the CoSTaR sites over a full season of monitoring (March 2006 to April 2007). The solid lines are a guide to the eye; measurements lying on this line correspond to exact agreement between DPV and ICP-OES analyses.

Shilbottle, shows extremely high [Fe]total because the pollution at this site is mine soil-heap leachate. The correlation between the DPV and ICP-OES data remains good, although the quantitative agreement is not as good (figure 4. 5). The agreement is poorest for the underground mine-water samples, which contain more organic and particulate matter that may decrease the voltammetric signals by complexation of Fe or by fouling the electrode. It is an advantage of ICP in a purely analytical context that organic matter is destroyed in the plasma and does not affect [Fe]total, however Fe complexed to organic ligands may have a significant role in the geochemistry of acid mine drainage.

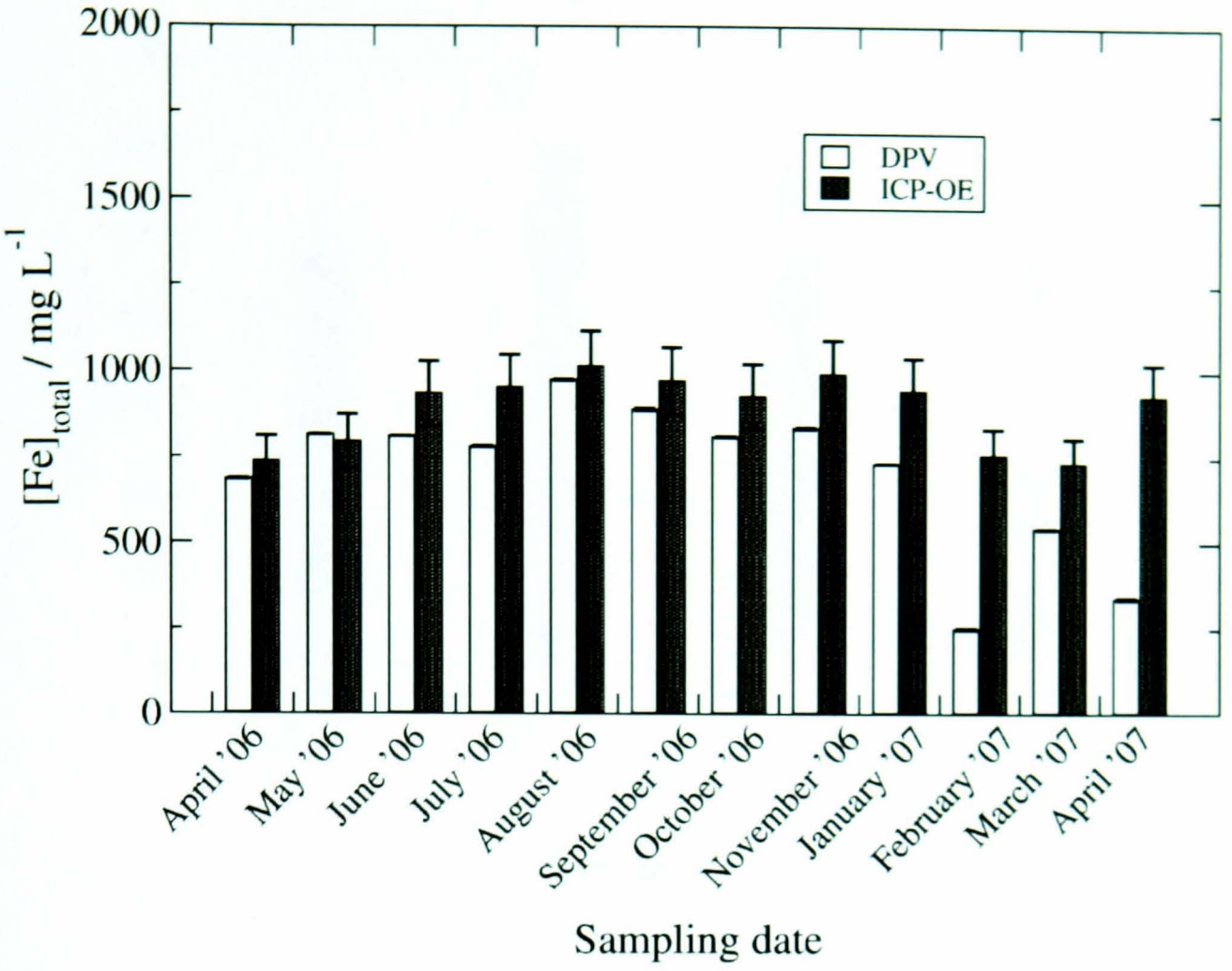

Figure 4.5: Comparison of total Fe / mg L^{-1} measured by DPV and ICP-OES for the underground mine-water samples taken at sampling location B1L at the Shilbottle site.

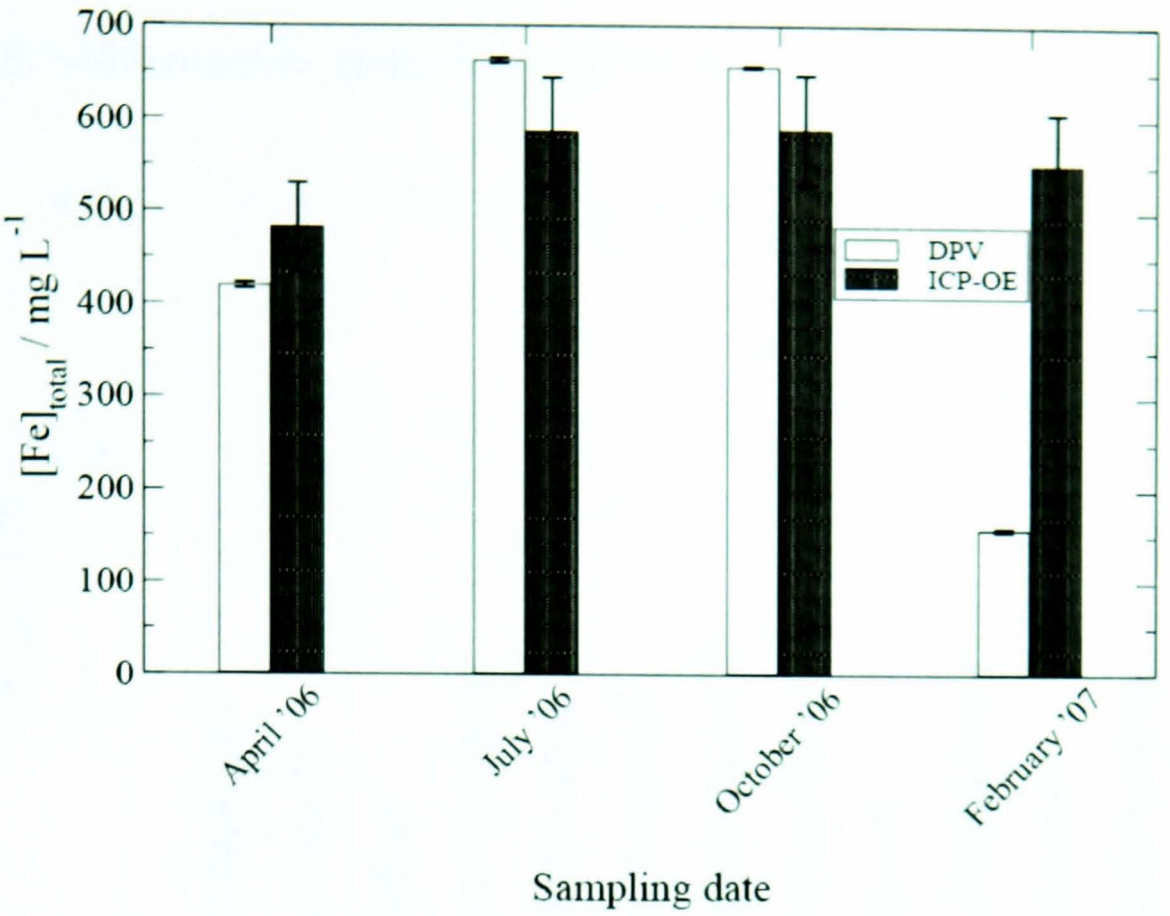

Figure 4.6: Comparison of Filtered Fe / mg L^{-1} measured by DPV and ICP for underground mine-water samples taken at sampling location B2L at Shilbottle site. All samples were filtered with Whatman Cellulose Nitrate Membrane Filters of 0.45 μm and then acidified using 1% v/v HCl.

Figure 4.6 shows that filtration of these underground mine-water samples before analysis improves the agreement between ICP and DPV methods a little. However, Fe bound to organic ligands is not expected to be removed by filtration and would contribute to the ICP measurement after decomposition of organic matter in the plasma. However, during the winter (February, 2007), a large deviation was observed when the mine-water was frozen. In this case, the samples may have changed upon thawing in the laboratory.

4.5: Voltammetric analysis of solid phase Fe species in mine-waters

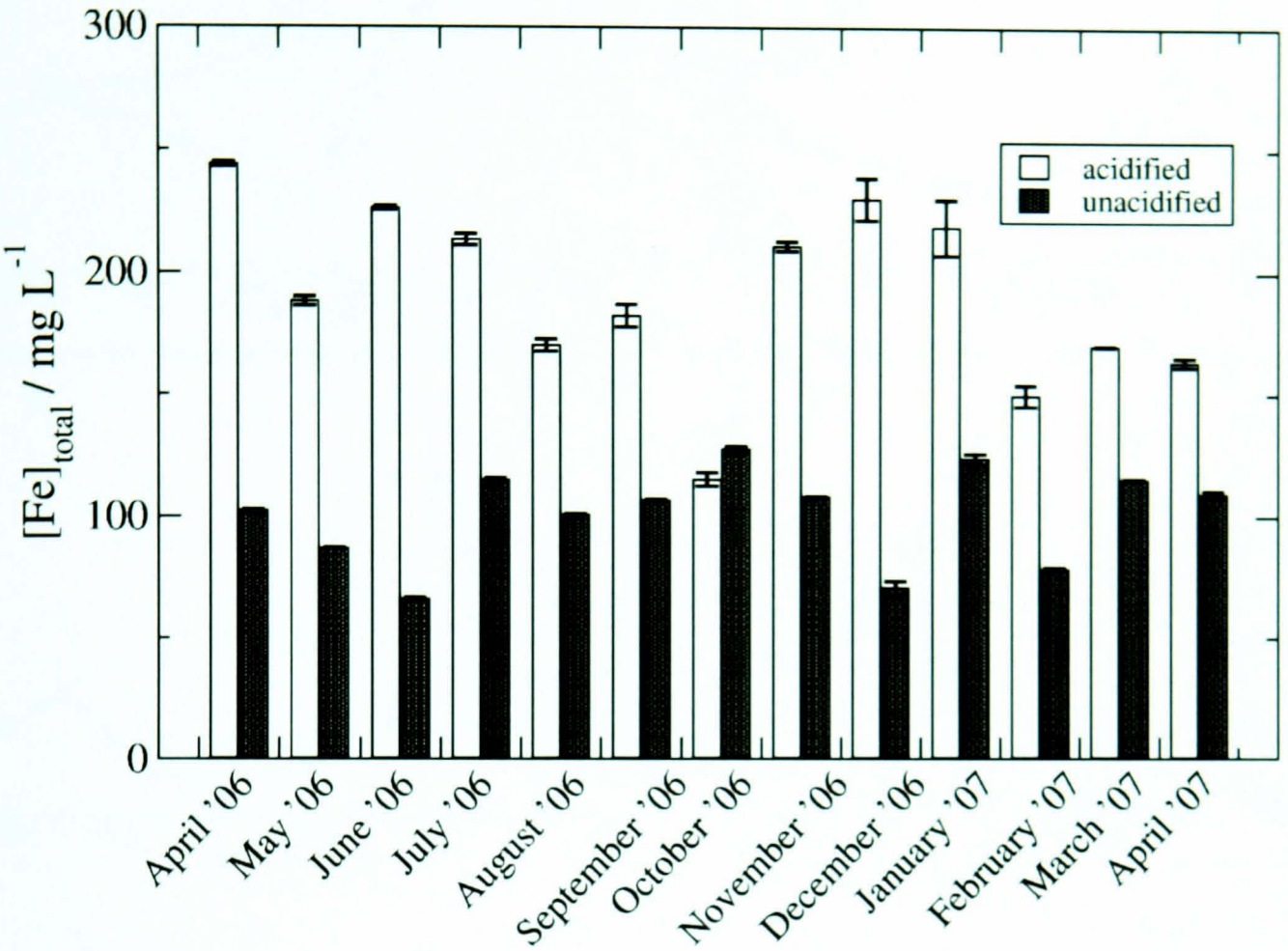

Figure 4.7: Comparison of Fe / mg L^{-1} concentrations measured from the acidified and unacidified samples.

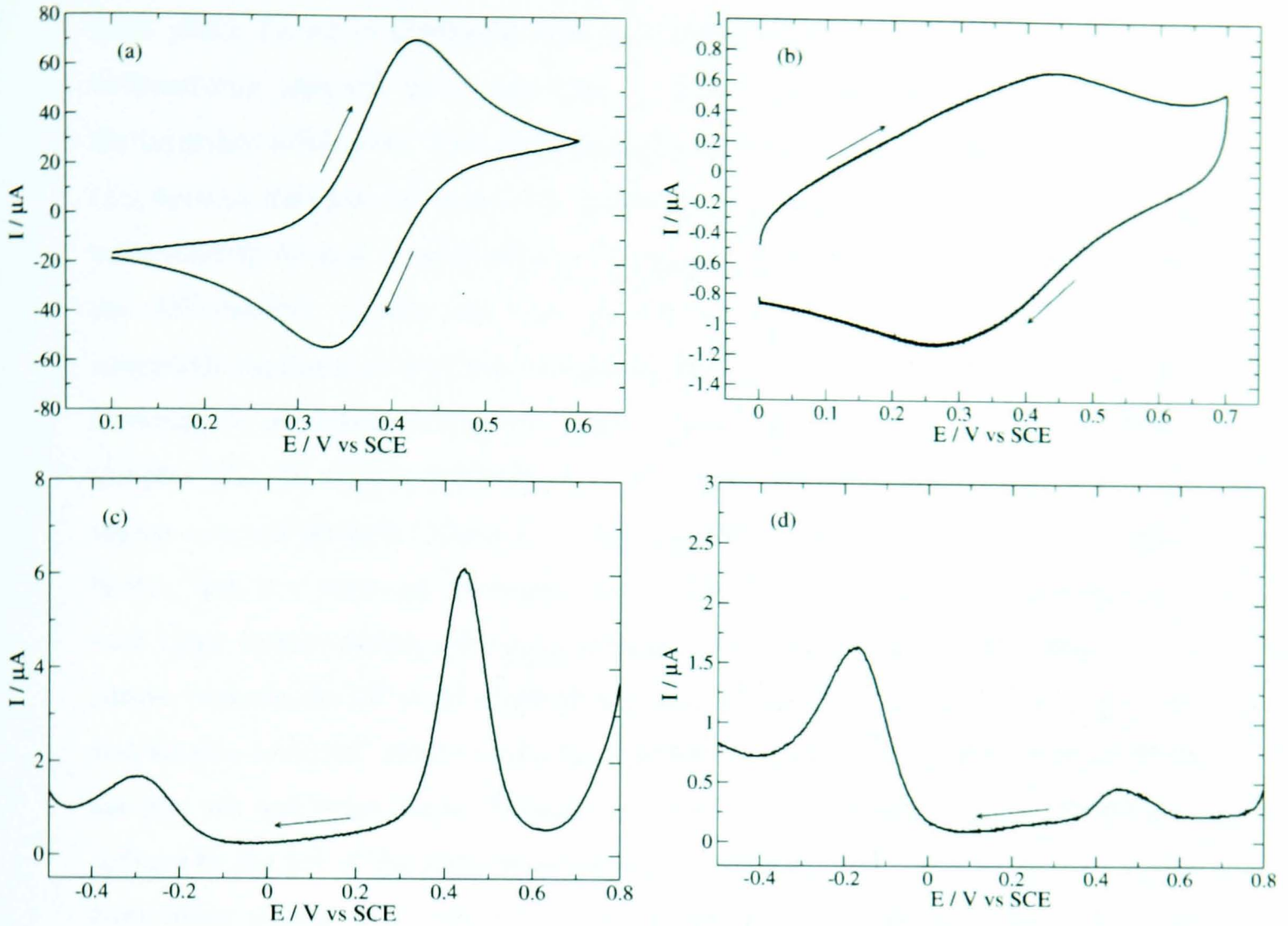

Figure 4.8: Representative cyclic and differential pulse voltammograms of unfiltered mine-water samples with and without acidification. All these samples were taken from the RAPS2 inlet of the Bowden Close site: (a) CV of acidified sample; (b) CV of unacidified sample; (c) DPV of acidified sample and (d) DPV of unacidified sample. CV parameters: scan rate = 0.1 V s^{-1}; DPV parameters: pulse width = 50 ms; pulse height = 75 mV and step height = 2 mV. The working electrode was a 2 mm diameter Pt disc and an SCE reference electrode was used.

Figures 4.7 and 4.8 show that acidification of samples changes the voltammetric peak currents for hydrolysed and unhydrolysed Fe; these values increase and approach the values determined by ICP-OES and the difference is due to dissolution of solid-phase Fe in acidified samples. Filtered samples also gave increased values on acidification and based on these measurements, up to 30% of the solid phase Fe consists of particles less than 0.45 µm depending on the sampling locations and sites. For example, underground/borehole mine-water samples show the presence of increased

solid phase Fe when compared with the aquifer/surface mine-water samples. The voltammetric method does not have a sharp particle size cut-off. instead it distinguishes solid phase and freely-diffusing Fe based on their diffusion coefficient (D), because the peak currents in CV and DPV are proportional to $D^{1/2}$. In practice the voltammetric method is equivalent to filtration with an extremely fine filter, because the voltammetric signals for even 10 nm Fe-containing particles are orders of magnitude smaller than the peak currents for the relevant concentrations of soluble Fe. Comparison of figures 4.8(a) and 4.8(b) shows that CVs of acidified mine-water samples have the normal voltammetric wave shape for pure laboratory reagents in the region denoted [Fe]unh, whilst CVs for unacidified mine-water samples are rather broad. This is a result of the additional complexity of Fe speciation in mine-water with large concentrations of organic ligands and other dispersed solid phases. In a similar manner, the DPVs of acidified and unacidified samples as shown in figures 8c and 8d also revealed 'sharp' peaks for acidified samples whilst peaks for unacidified samples are somewhat broad. Though the overall characteristics of the peaks are also defined by the pH of the mine-water samples concerned. For example, an unacidified mine-water sample with a pH of 3-5 would normally show sharp and symmetric peaks for both CV and DPV whilst mine-water samples with pH of 5 upward would normally show broad and asymmetric peaks for both CV and DPV.

These effects are harder to quantify and cannot be accounted for by a simple linear calibration such as equations (5) and (6). This is the major source of the outlying points in figures 4.4(a) and 4.4(b).

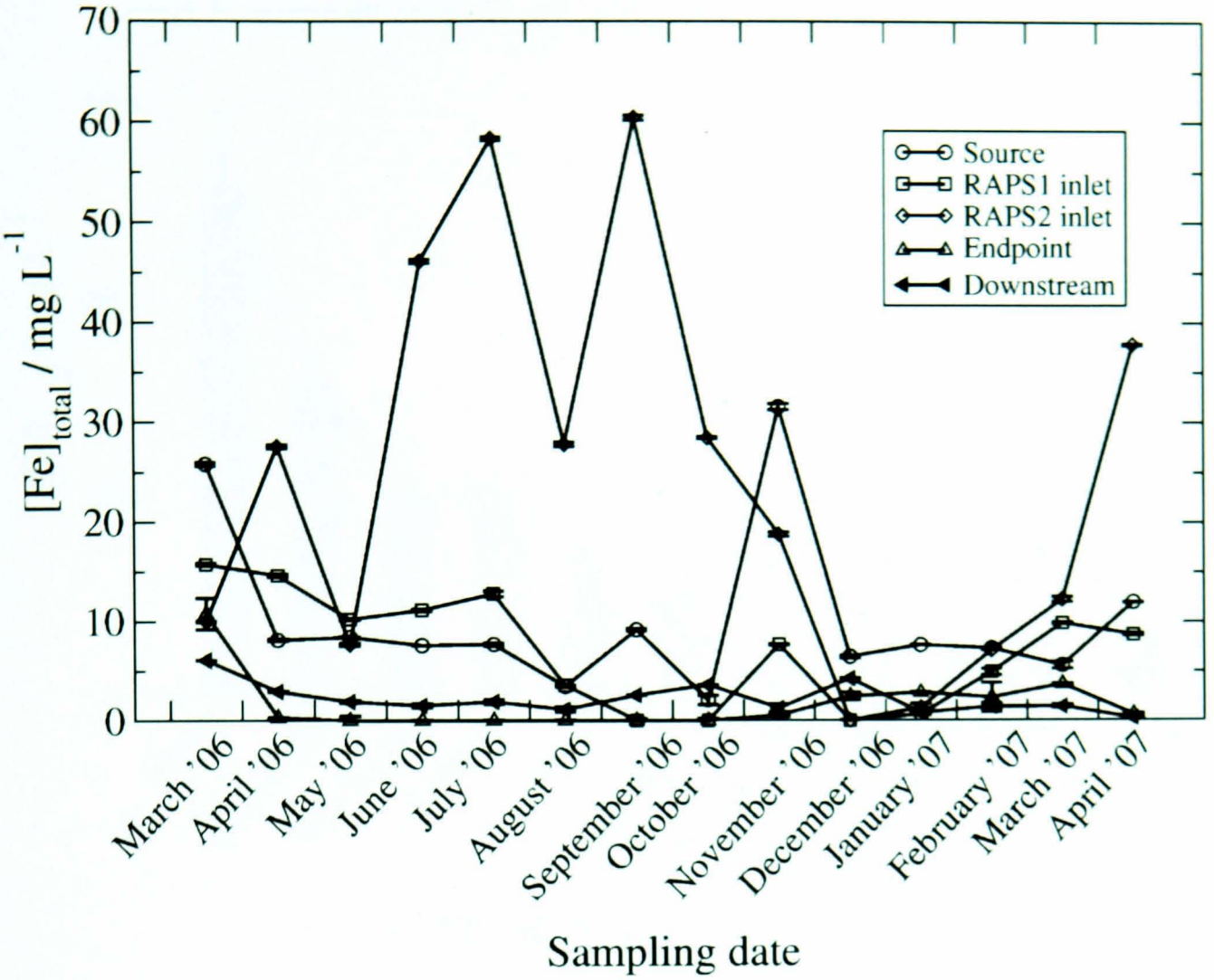

Figure 4. 9: Variation in solid/colloidal phase Fe / mg L^{-1} as determined by DPV using the procedure of figure 4.8 at different sampling points at the Bowden Close site. Monthly samples were obtained over a period of 14 months, sufficient to observe the seasonal trends.

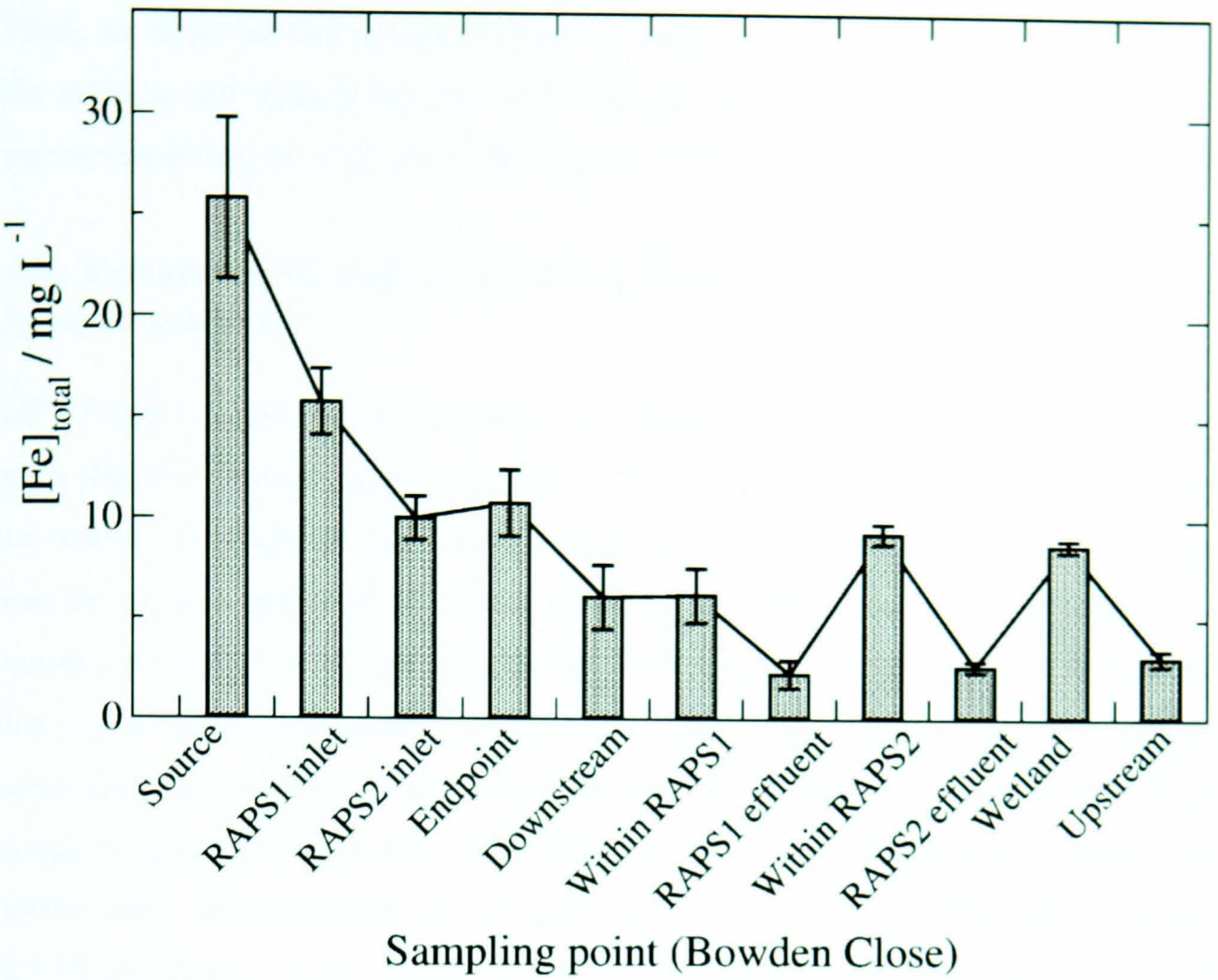

Figure 4.10: Variation in solid/colloidal phase Fe / mg L^{-1} across a mine-water remediation site as measured by DPV using the procedure of figure 4.8 .The graph shows the trend in solid phase Fe for October, 2006 at different sampling locations across the Bowden Close site.

Finally, the studies show how the simple DPV analysis can be used to track variations in solid-phase Fe at the CoSTaR sites as part of the long-term monitoring programme for mine-water remediation. Figures 4.9 and 4.10 show quantification of solid phase/colloidal Fe at Bowden Close and the variations in the amount of determined solid phase Fe is due to the sampling locations. For example, there are more solid phase/colloidal Fe in the source samples due to the presence of more dissolved organic and particulate matters in these sampling point whilst, end point and downstream samples show low dissolved organic and particulate matters in the samples after the mine-water has been treated, thus, the reduced values of solid phase/colloidal Fe observed at these sampling locations. The seasonal variation in the measured/observed values of solid phase/colloidal Fe across this site could also be attributed to the rainfall/flow rate profile across the site.

Thus, we observed that during rainfall, the water flow rate increases, which increases the dilution and reduces the dissolved organic and particulate matters in the samples and thus reducing the measured solid phase/colloidal Fe during this period.

4.6: Voltammetric determination of the oxidation states of Fe species in mine-waters

DPV is not suited to the determination of oxidation states because the same symmetric peak shape is observed irrespective of scan direction and therefore it does not depend on whether the bulk solution contains Fe(II) or Fe(III). In principle, a CV experiment can be used to determine the ratio of oxidised/reduced species because the initial current at the start of the sweep depends on the composition of the bulk solution and the scan direction. However, analysis of this current requires a calculation of the time-dependent wave-shape; steady-state voltammetry provides the same information in a much simpler voltammogram. The diffusion-limited anodic (cathodic) currents in a steady-state voltammogram are proportional to the bulk concentrations of reduced (oxidised) forms of the redox couple. In the mine-waters there are at least two dissolved Fe species and therefore multiple diffusion-limited currents are expected, which complicates the analysis. Figure 4.11 shows a near steady-state microelectrode voltammogram, typical of those observed in mine-waters.

On the negative-going scan, a wave is observed at about +0.1 V and a second, larger wave at about -0.5 V. Based on the same arguments used to interpret the DPV, we assign the two waves to the reduction of unhydrolysed Fe at +0.1V and the reduction of the hydrolysed Fe at -0.5 V. Therefore the limiting anodic current at potentials >0.1 V was taken to be proportional to [Fe(II)]unh and the limiting cathodic current as proportional to [Fe(III)]unh.

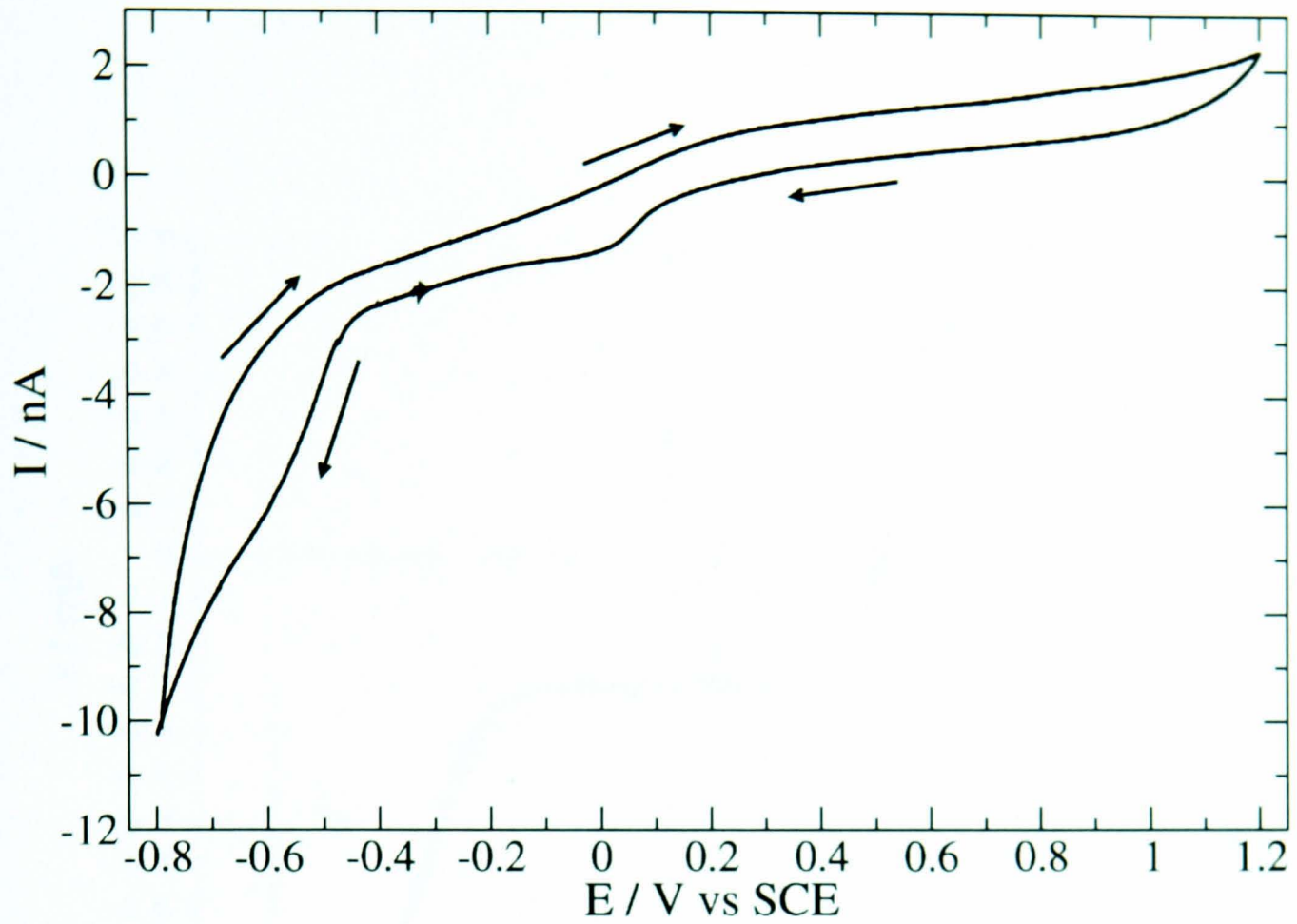

Figure 4.11: Typical microelectrode voltammogram of unfiltered, unacidified mine-water. The electrode was a 50 μm radius Pt inlaid disc, the reference electrode was an SCE and the scan rate was 10 mV s^{-1}.

However this interpretation does require an assumption about the wave at -0.5 V, namely that this is entirely due to reduction of [Fe(III)]hyd, otherwise it is not possible to assign the current between +0.1 V and -0.5 V entirely due to reduction of [Fe(III)]unh. This assumption is reasonable given the known chemistry of Fe aquo ions: the pKa of $Fe(H_2O)_6^{2+}$ is 9.5, which is higher than the pH of any of the samples (Table 4.1), so hydrolysed Fe(II) is unlikely to be present. There are no data on Fe(II)/Fe(III) ratios comparable to the ICP-OES determinations of [Fe]total against which the UME data can be compared. However, it is possible to study the variation of the Fe(II)/Fe(III) ratio at different sampling locations and show that the gross features of the data are in line with expectations based on geochemical knowledge of the site.

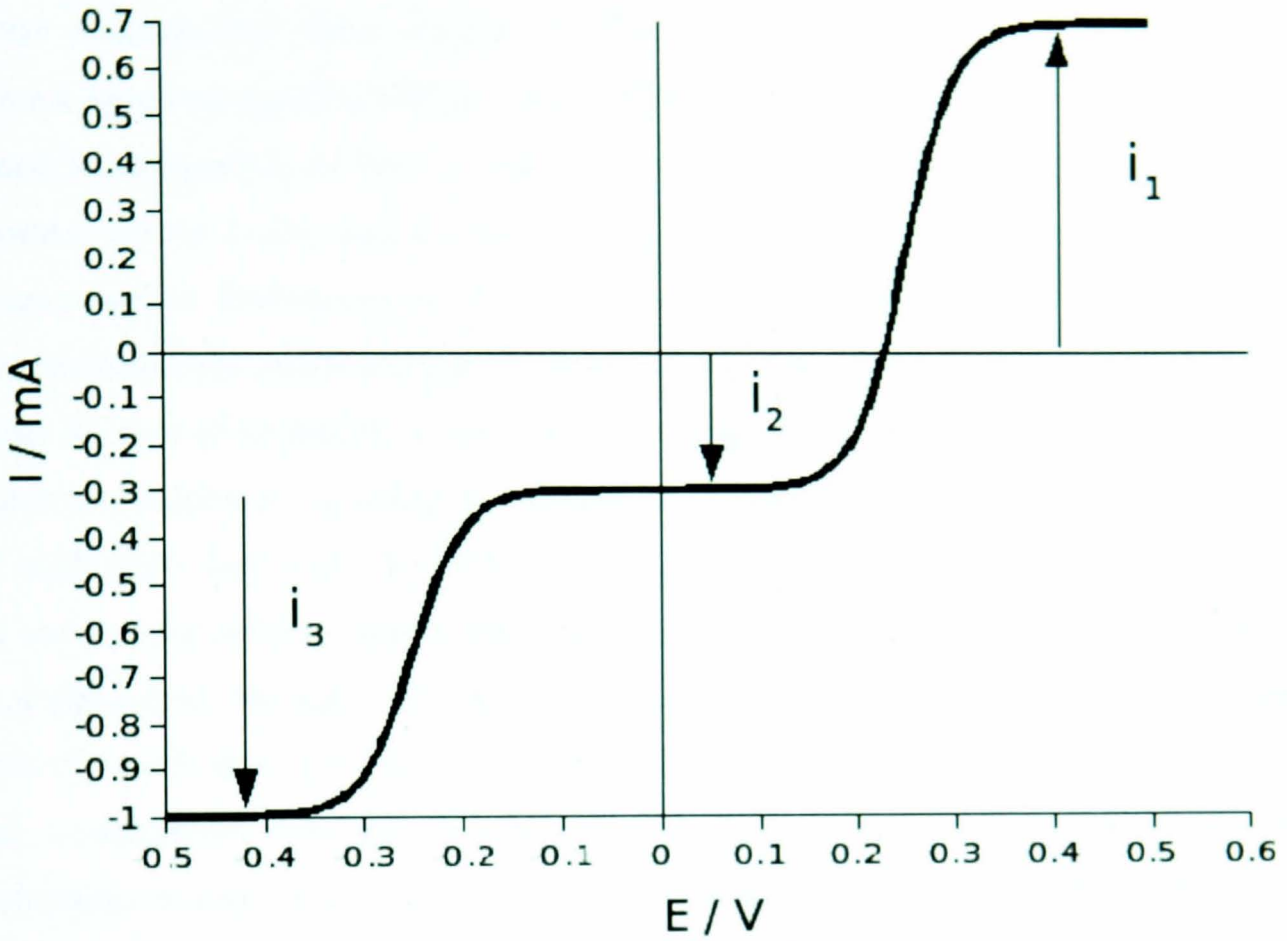

Figure 4.12: Shows a schematic steady-state voltammogram at an ultramicroelectrode (UME) for the Fe(III)/Fe(II) system. Three limiting currents can be identified; i_1 and i_2 correspond to the oxidation and reduction of unhydrolysed Fe respectively; i_3 corresponds to the reduction of hydrolysed Fe species.

This assignment is justified by the known values of pKa for Fe(II) and Fe(III) which are 9.5 and 2.19. Clearly, Fe(II) has little tendency to hydrolyse at the pHs encountered in our samples (acidic-neutral). This is why i_3 can be assigned entirely to the reduction of hydrolysed Fe(III) and, importantly, the current, i_2, can therefore be assigned to reduction of unhydrolysed Fe(III) rather than a mixture of that and the oxidation of hydrolysed Fe(III).

4.7: Conclusions

After addition of acid to samples taken from mine-water remediation sites, differential pulse voltammetry yields results for [Fe]total shows substantial agreement with atomic spectroscopy (ICP-OES) - the standard analytical method in this application. Detailed comparison of both methods (ICP vs. electrochemical) over a period of 14 months, across 6 sites and a total of 59 sampling locations shows that the total Fe concentrations determined by ICP are systematically higher than those measured electrochemically at locations in the most polluted site (Shilbottle) at which there is a large fraction of suspended solids and organic matter. Nevertheless, it was possible to determine soluble Fe by differential pulse voltammetry in many untreated (no addition of acid) mine-waters and, by difference, the solid phase Fe. Atomic force microscopy of some of the solid material remaining after drying filtered samples shows that there is a significant amount of Fe-containing colloidal particles with size of order a few tens of nanometres (see chapter 10) for details. This fraction of the solid-phase Fe is not conveniently removed, except by ultrafiltration methods, and therefore the voltammetric experiment offers practical advantages for its quantitation. The simple electrochemical method reported here has enabled the speciation of dissolved Fe and the quanfitation of solid phase/colloidal Fe in the polluted mine-water samples across the CoSTaR sites and the observation of trends in both soluble and solid phase Fe over a period of 14 months. This dataset (59 sampling locations across 6 sites) provides a valuable resource for the understanding of the factors controlling the efficiency of mine-water remediation in these systems.

4.8: References

[1]. Younger, P.L. *Science of the Total Environment*, **1997**, 194, 457-466.

[2]. Younger, P.L., Banwart, S. A. and Hedin, R. S. Mine Water: Hydrology. Pollution, Remediation, Kluwer Academic Publishes, The Netherlands, **2002**.

[3]. Appelo, C. A. J. and Postma, D. Geochemistry, groundwater and pollution, 2nd edition, Balkema, A. A. Leiden, **2006,** pp450-452.

[4]. Mayer, T. D. and Jarrell, W. M. *Environmental Quality,* **1995**, 24, 1117-1124.

[5]. Kimball, B. A., Callender, E and Axtmann, E. V. *Applied Geochemistry*, **1995**, 10, 285-306.

[6]. Ross, J.M. and Sherrell, R.M. *Limnology and Oceanography,* **1999**, 44, 1019-1034.

[7]. Schemel, L.E., Kimball, B.A. and Bencala, K.E. *Applied Geochemistry*, **2000**, 15, 1003-1018.

[8]. Hill, D.M. and Aplin, A.C. *Limnology and Oceanography*, **2001**, 46, 331-344.

[9]. Allard, T., Menguy, N., Salomon, J., Calligaro, T., Weber, T., Calas, G. and Benedetti, M.F. *Geochim. Et Cosmochim. Acta*, **2004**, 68, 3079-3094.

[10]. Pokrovsky, O.S. and Schott, J. *Chemical Geology,* **2002**, 190, 141-179.

[11]. Sholkovitz, E.R. and Copland, D. *Geochim. Cosmochim. Acta*, **1981**, 45, 181-189.

[12]. Deein, G., Thimdee, W. and Matsunaga, K. *Marine Freshwater Research*, **2002**, 53, 43-47.

[13]. Benner, S.G., Blowes, D.W.,Gould, W. D., Herbert Jr, R. B. and C. J. Ptacek, C. *Environmental Science and Technology*, **1999**, 33, 2793-2799.

[14]. Hallberg, K. B. and. Johnson, D. B. Proceedings of a National Conference Held at the University of Newcastle Upon Tyne, 11-13 November, **2002**.

[15]. Benner, S. G., Blowes, D.W. and Ptacek, C. J.*Ground Water Monitoring and Remediation*, **1997**, 17, 99-107.

[16]. Younger, P.L., Curtis, T. P., Jarvis, A. and R. Pennel, R. *Chartered Institute of Water and Environmental Management*, **1997**, 11, 200-208.

[17]. Younger, P.L. *Geoscience in South-west England*, **2002**, 10, 255-266.

[18]. Younger, P.L. *Contaminant Hydrology*, **2000**, 44, 47-69.

[19]. Banks, D.P. and Younger, P.L. *Hydrogeology*, **1996**, 4, 55-68.

[20]. Rickard, D. and Luther III, G.W. *Geochimica et Cosmochimica Acta*, **1997**, 61, 135-147.

[21]. Luther III, G.W., Theberge, S.M., Rickard, D. and Oldroyd, A. *Environmental Science and Technology*, **1996**, 30, 671-679.

[22]. Butler, I.B. and Rickard, D. *Geochimica et Cosmochimica Acta*, **1997**, 64, 2665-2672.

[23]. Banks, D.P., Younger, P.L., Arnesen, R.T., Iversen, E.R. and Banks, S.B. *Environmental Geology*, **1997**, 32,157-174.

[24]. Banks, S.B. *Chartered Institute of Water and Environmental Management*, **2003**, 17,117-122.

[25]. Luther III, G.W., Nuzzio, D.B., Taillefert, M., Glazer, B.T., Kraiya, C., Waite, T., Tsang, J., Janzen, C. and Drusche, G. *Am. Chem. Soc.*, **2005**, 229. U152-U156.

[26]. Younger, P.L. *Engineering Geology*, **1995**, 28, S101-S113.

[27]. Younger, P.L. *Institute of Mining and Metallurgy*, **109**, A210-A218.

[28]. Younger, P.L. *Science of the Total Environment*, **265**, 309-326.

[29]. Younger, P.L. *Applied Geochemistry*, **2000**, 15, 1383-1397.

[30]. Younger, P.L. *Science of the Total Environment*, **2001**, 265, 309-326.

[31]. Baes, C.F. and Mesmer, R.E. The Hydrolysis of Cations, Krieger, Florida, **1998**, 226-8.

[32]. Baes, C.F. and Mesmer, R.E. The Hydrolysis of Cations, Krieger, Florida, **1999**, 235-7.

[33]. Sylva, R.N. *Pure. Appl. Chem.*, **1972**, 22, 115.

[34]. Flynn, C.M. *Chemical Review*, **1984**, 84, 31.

[35]. Cornell, R.M., Giovanoli, R. and Schneider, W. *Chem. Tech. Biotechnology.*, **1989**, 46, 115.

[36]. Schneider, W. *Chimica*, **1988**, 42, 9.

[37]. Schneider, W. and Schwyn, B. The hydrolysis of iron in synthetic, biological and aquatic media, in Aquatic Surface Chemistry, ed. W. Stumm., Wiley, New York, **1987**, 167pp.

[38]. Richens, D.T. *Science of the Total Environment*, **1999**, 372-376.

[39]. Feitknecht, W. and Michaelis, M. *Chim. Acta*, **1962**, 45, 212.

[40]. Biedermann, G. and Schindler, P.W. *Acta Chem. Scand.*, **1957**, 11, 731.

[41]. Sommer, B.A. and Margerum, D.W. Inorg. Chem., **1970,** 9, 2517.

[42]. Lutz, B. and Wendt, H. Ber. Bunsenges. Phys. Chem., **1970**, 74, 372.

[43]. Aldrich, A.P. and van den Berg, C.M.G. *Electroanalysis*, **1998**, 10, 369-373.

[44]. Hromadova, M. and Fawcett, W.R. *Phys. Chem.* A, **2001,** 105, 104-111.

[45]. Bilgin, A.A., Silverstein, J. and Hernandez, M. *Environ. Sci. Technol.*, **2005**, 39, 7826-7832.

[46]. Hatfield, T.L. and Pierce, D.T. *Appl. Electrochem.*, **1998**, 28, 397-403.

[47]. Jarvis, A.P., Moustafa, M., Orme, P.H.A. and P.L. Younger, *Environmental Pollution*, **2006**, 143, 261-268.

[48]. APHA, **1998**. Standard Methods for the Examination of Water and Wastewater, 20th Edition. American Public Health Association. American Water Works Association and the Water Environment Federation, Washington DC.

[49]. Personal communication, **2007**. Patrick Orme and Jane Davis, Hydrogeochemical Engineering Research and Outreach Group, Institute for Research on Environment and Sustainability, Devonshire
Building, University of Newcastle, Newcastle upon Tyne NE1 7RU, UK

[50]. Wigginton, N.S., Haus, K.L. and Hochella Jr.M.F. *Environmental Monitoring*, **2007**, 9, 1306-1316.

[51]. Richard, D., Oldroyd, A. and Cramp, A. *Estuaries*, **1999**, 22, 693-701.

Chapter 5

QUAKING HOUSES SITE, DURHAM

This chapter presents background information and oxidative dissolution of pyritiferous acidic leachate problems associated with Quaking Houses site before dealing with the results acquired from both on-site measurements of pH, *Eh*, alkalinity, conductivity, temperature and laboratory electrochemical analysis. The observed temporal, variations and trends of these parameters together with geochemical implications and significance of these results are also discussed.

5.1: Site History, Problems and Treatment Regime

Quaking Houses in County Durham was a coal mining industry village in the 19th century with a number of pits opened and closed in the vicinity over the next 200 years. This village of a former coal mine site which operated under the name Morrison Busty Colliery was closed in 1974. The problem of watercourse contamination by colliery spoil leachates at Quaking Houses began in 1980 during road construction through the 35 hectares colliery spoil heap. This led to infiltration of water and air into the spoil and caused the oxidation of sulphide minerals, producing significant water pollution by generating iron-rich, depressed pH and acidic waters in the process, which are subsequently discharged directly into nearby Stanley Burn-a third order tributary of River Wear [1, 2]. The streambed was discoloured and the habitat of many aquatic organisms was destroyed [3]. This drainage from this acidic spoil heap contains elevated concentrations of metal contaminations such as iron, aluminium, manganese and zinc [1, 2].

A full-scale constructed wetland was constructed in 1997 following the success of laboratory and pilot scale trial by the HERO research group at Newcastle University. Figure 5.1 shows a schematic diagram of the site. The wetland consisted of a 30: 40: 30 mix of cow, horse manure and municipal composted waste as substrate, up to the 0.3-0.5m depth with limestone berm situated close to the system effluent to boost the alkalinity of the existing waters [1, 2, 3]. The total surface area of the substrate covered an extensive area of up to 440 m^2. The overall aims and objectives of the constructed wetland was to reduce metal concentrations by precipitating for example, iron as iron oxide (ochres) and aluminium as aluminium hydroxide, and to increase

the pH and overall quality of water discharge into Stanley Burn to support aquatic organisms and habitat. Based on the monitoring of the quality of discharge from this site by the HERO group at Newcastle University, the wetland has successfully treated metal contamination arising from the colliery spoil heap. For this research work, monthly samples have been taken from this site after the wetland was refurbished in 2005.

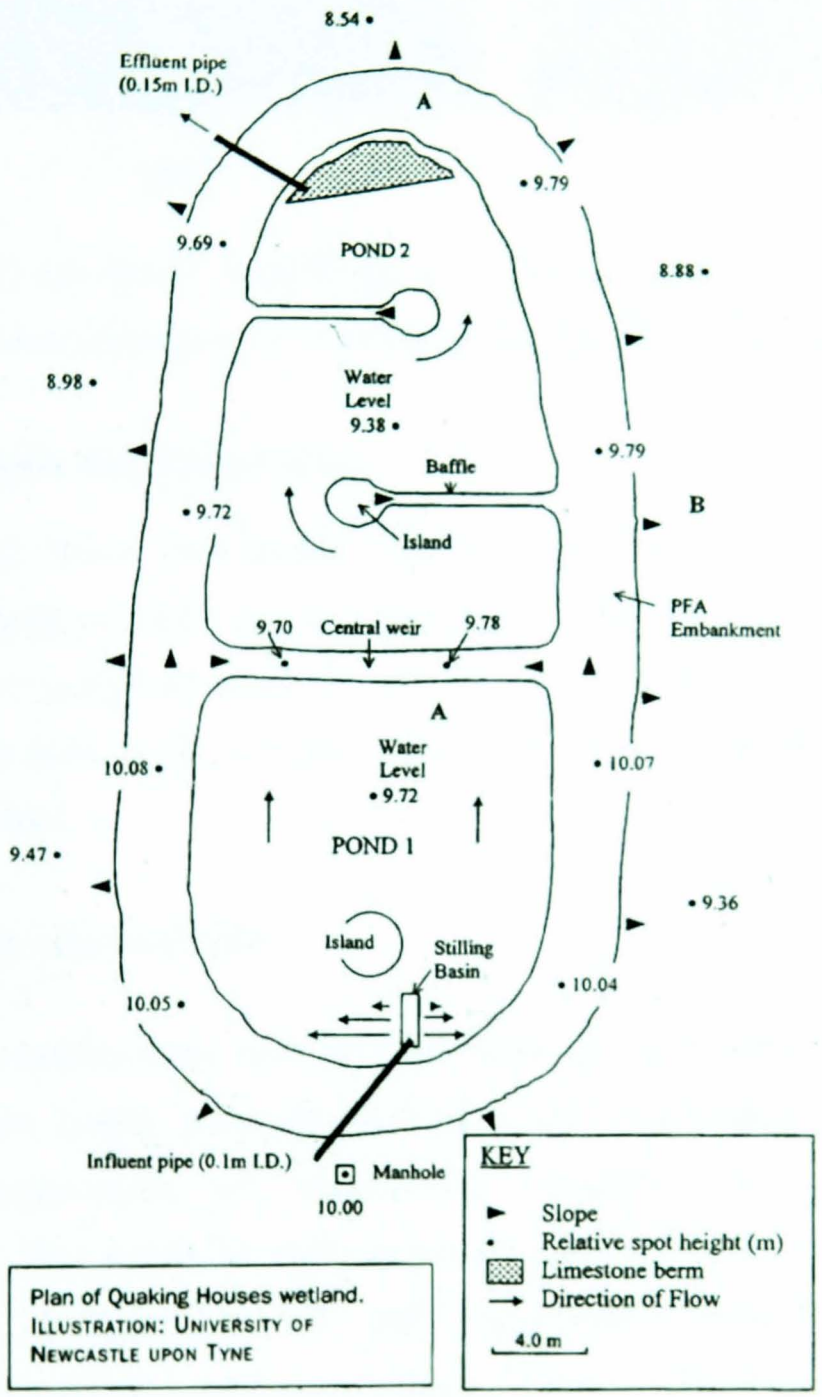

Figure 5.1: Schematic of constructed wetland system, showing water inlet, settlement ponds (1 & 2) and the outlet at Quaking Houses treatment site, County Durham- Courtesy of HERO research Group at Newcastle University.

Samples were taken from March-October, 2006. Figure 5.2 (a & b) shows the panoramic view of the site before and after refurbishment.

(a) **(b)**

Figure 5.2: (a) before refurbishment and (b) after refurbishment-both pictures represent views from pond 1 as shown in the site schematic (figure 5.1).

5.2: Results and Discussion

Differential Pulse Voltammetry method have been used to measure total iron, dissolved and colloidal iron concentrations at this site as described in the previous chapter on analytical methods. Results of the monitoring of the water quality parameters such as pH, temperature, *Eh*, conductivity and alkalinity for this site are also presented.

5.2.1: On-site analysis

Monthly samples were collected from this site from March-October 2006, during which water quality parameters/indicators were measured on-site. These parameters include temperature, pH, conductivity, oxidation reduction potential (*Eh*) and alkalinity. The trends of each measured parameter over the sampling period are presented in figures 5.3-5.7 while relationships between these geochemically important parameters are shown in figures 5.8-5.12. The results presented in tables 5.1 and 5.2 show the monthly and mean of these measured parameters together with the concentrations of iron fractions measured using voltammetric method.

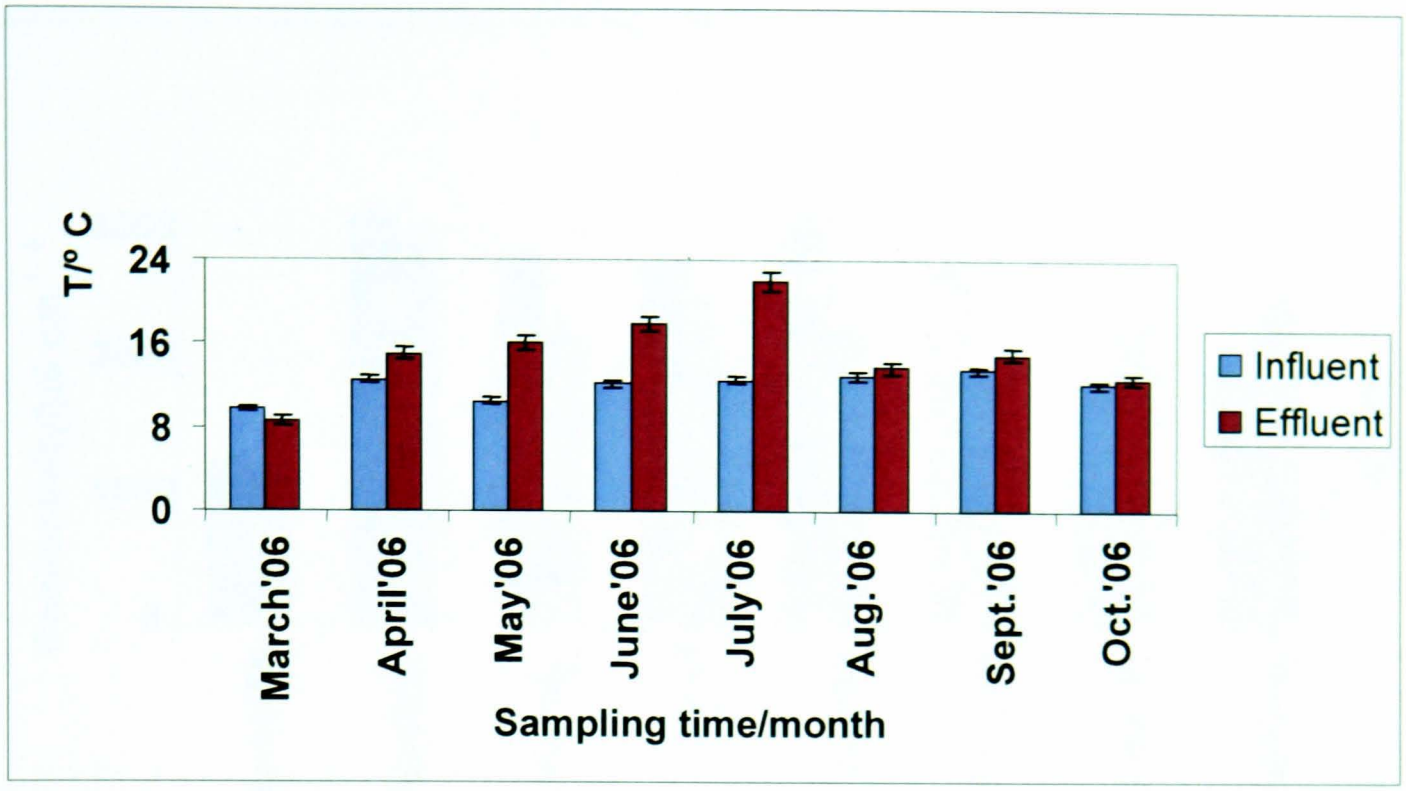

Figure 5.3: Shows temporal trend of temperature profile for the influent and outlet samples taken March-October 2006 at Quaking Houses treatment system site.

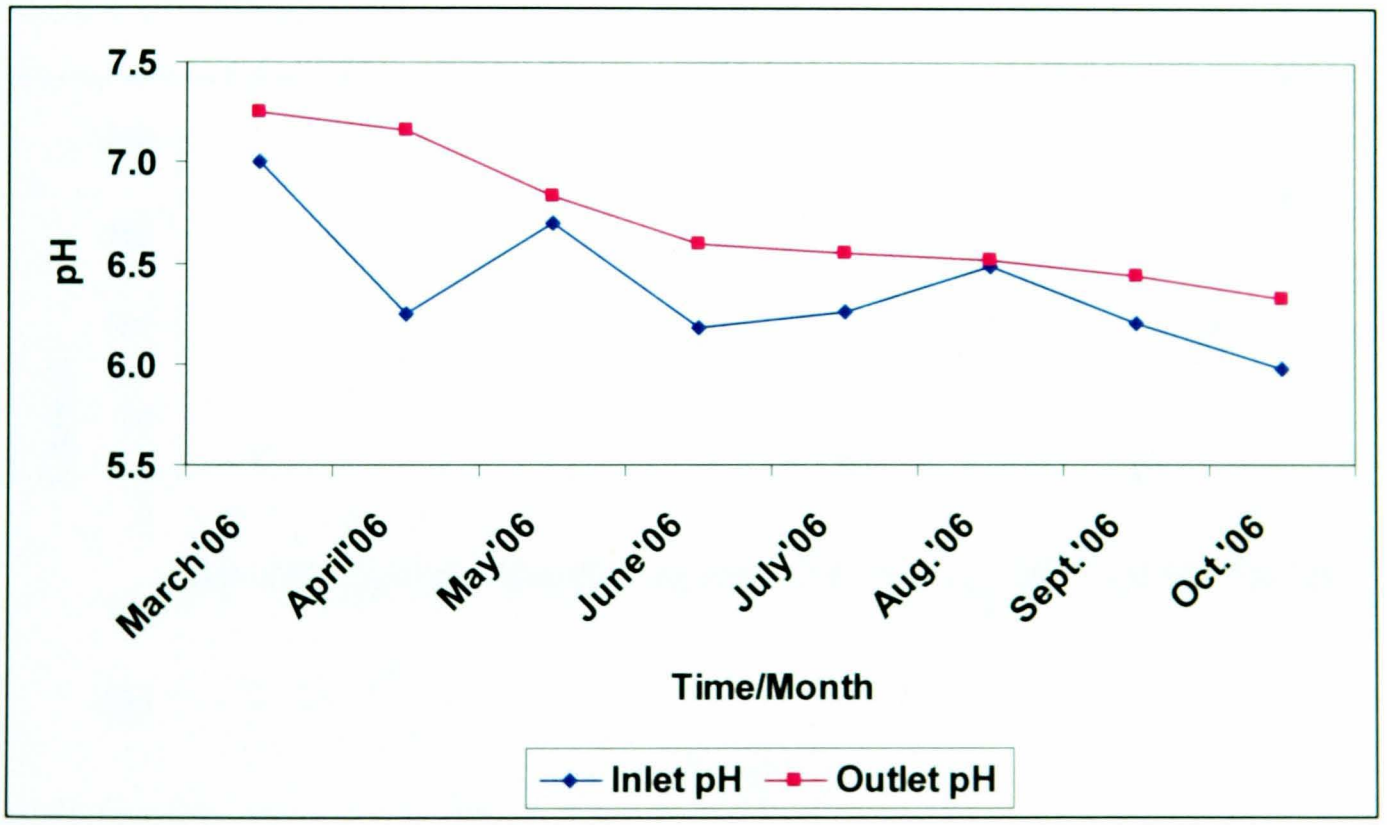

Figure 5.4: Graph showing temporal trend of measured pH over time for the influent and outlet samples taken March-October, 2006 at Quaking Houses treatment system site.

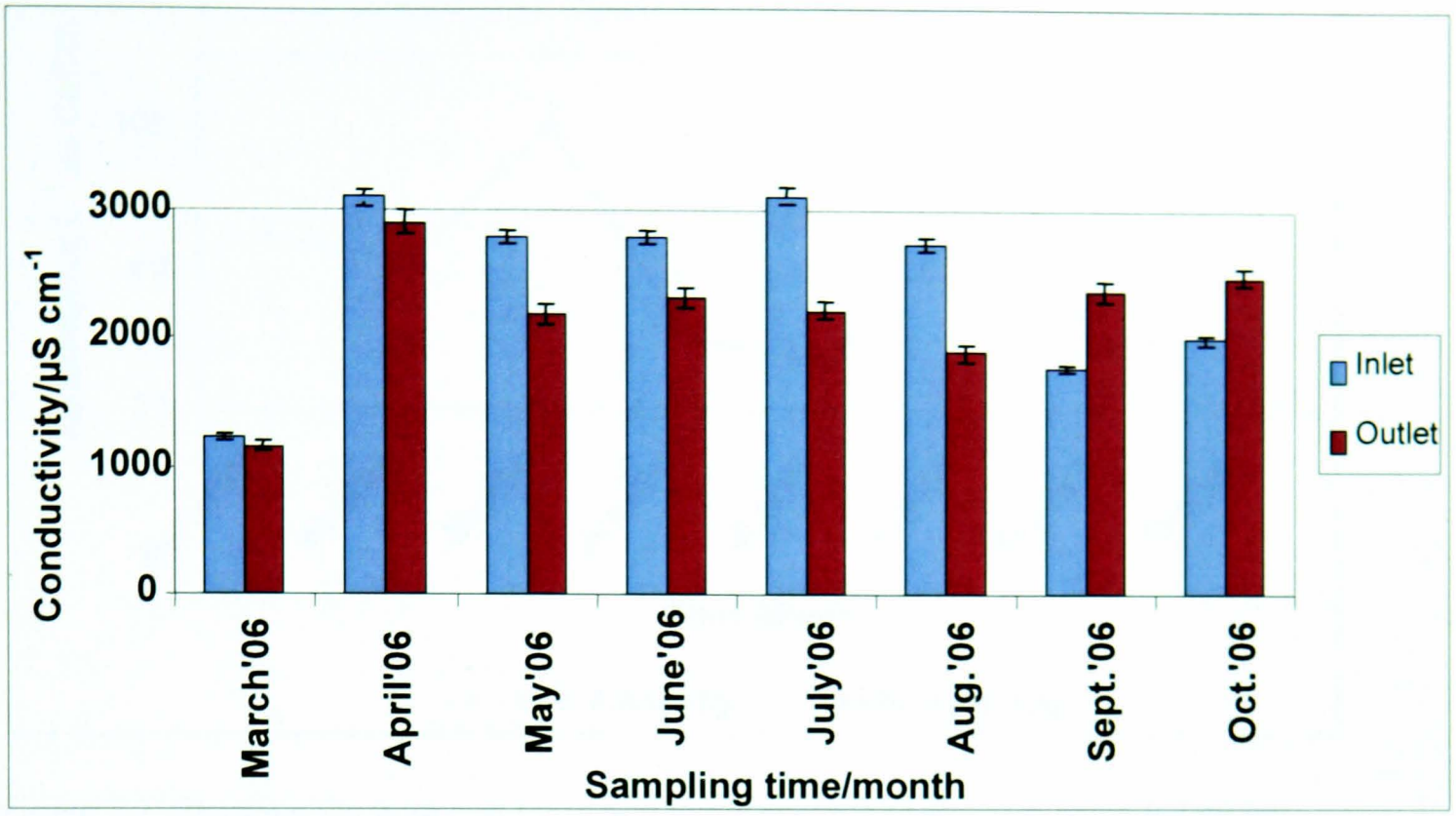

Figure 5.5: Shows the measured conductivity temporal trend for the influent and outlet samples taken March-October, 2006 at Quaking Houses treatment system site.

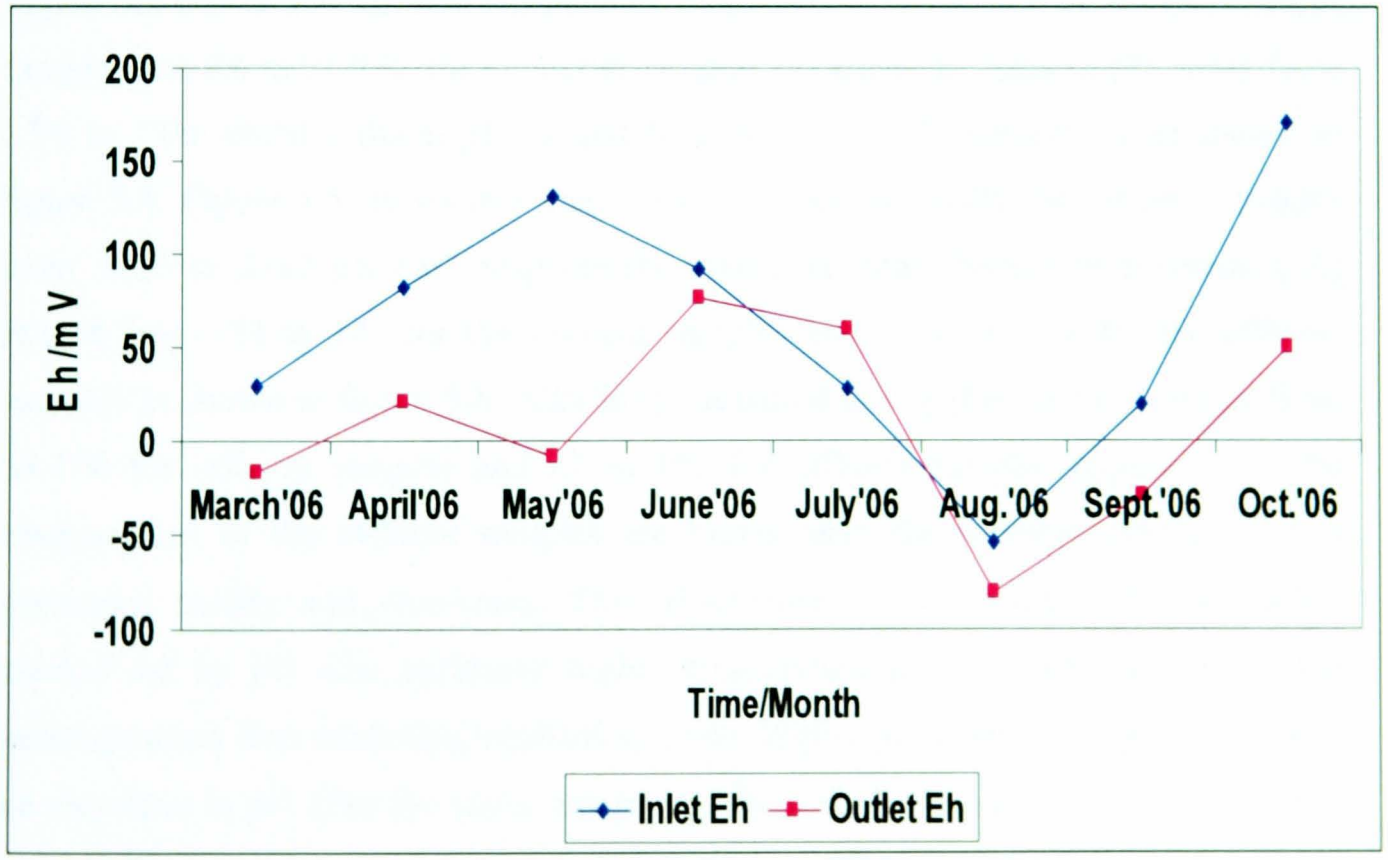

Figure 5.6: Measured *Eh* as a function of time (monthly sampling) from March - October 2006 for inlet and outlet water samples at Quaking Houses treatment system site.

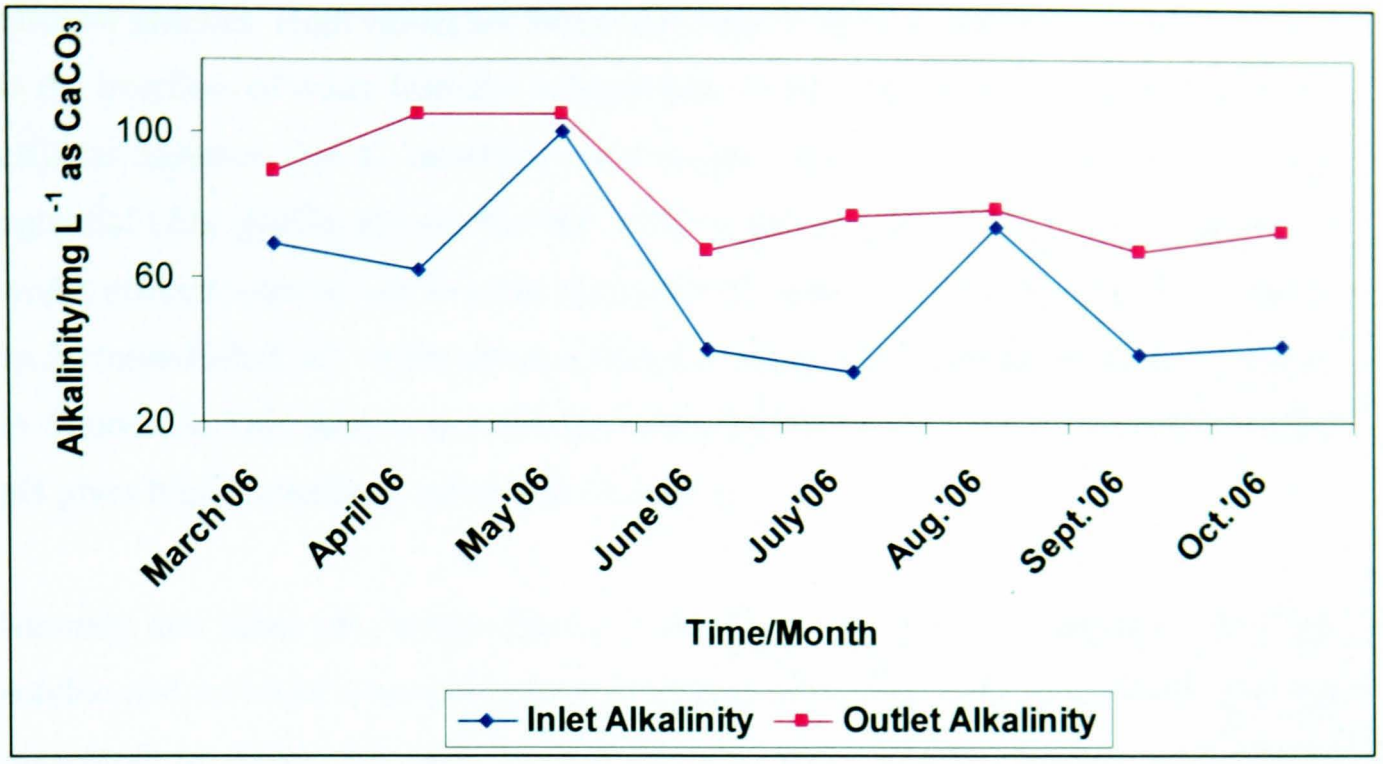

Figure 5.7: Showing the temporal trend and variation in the measured inlet and outlet alkalinity at Quaking Houses treatment system site, over the sampling period (March-October 2006).

Figure 5.3 shows that influent temperature ranged from 9.7 to 13.5 °C for the influent samples and 8.6 to 21.9 °C for the outlet samples respectively. Influent pH varies from 5.98 to 7.00 whilst effluent pH ranged from 6.33 to 7.25 respectively as shown in figure 5.4. Figure 5.5 shows that conductivity ranged markedly for influent samples from 1226 to 3112 μS cm^{-1} respectively whilst oxidation reduction potential (*Eh*) ranged from -54 to 171 for the influent samples and -9 to 76 mV for the effluent samples as shown in figure 5.6. Alkalinity measured as mg [$CaCO_3$] L^{-1} ranged from 34-100 for influent samples and 67 to 105 for effluent samples (figure 5.7). The temperatures of the effluent samples are higher than the influent samples due to decreased acidity and vice-versa. This observation is consistent with the studies carried out by [4] who attributed higher temperature in the outlet samples to the heterogeneous iron oxidation mechanism under higher pH conditions [4, 5]. There is an elevation in pH after the water has passed through the wetland system which was essentially designed to increase the pH of the effluent water which shows the effectiveness of the wetland system at this site. Since conductivity can give a rough measure of the level of dissolved ions in water bodies, higher values of conductivity for the influent samples compared to the effluent (except for September and October) indicates that there are more dissolved ions in the influent samples compared to the

effluent samples. High values for September and October could probably be attributed to the overflow of water from the influent pipe to the wetland and subsequently to the effluent samples due to excessive rain during these months. Oxidation reduction potential (*Eh*) profile shows that the influent samples are in oxidised environment whilst effluent samples are in more reduced environment. Trend in alkalinity revealed an increased alkalinity of the effluent samples compared to influent samples as shown in figure 5.8. This pattern is consistent with the pH profile which shows that higher pH gives higher alkalinity value and vice-versa.

Monthly and mean pH, temperature, conductivity, *Eh*, alkalinity together with total, soluble and colloidal iron and percentage dissolved and percentage colloidal iron are presented in tables 5.1 and 5.2 for influent and effluent samples respectively. Relationships between these on-site measured parameters, particularly pH as it is central to the extent of iron dissolution geochemistry and other interactions between these parameters are presented in figures 5.8-5-12.

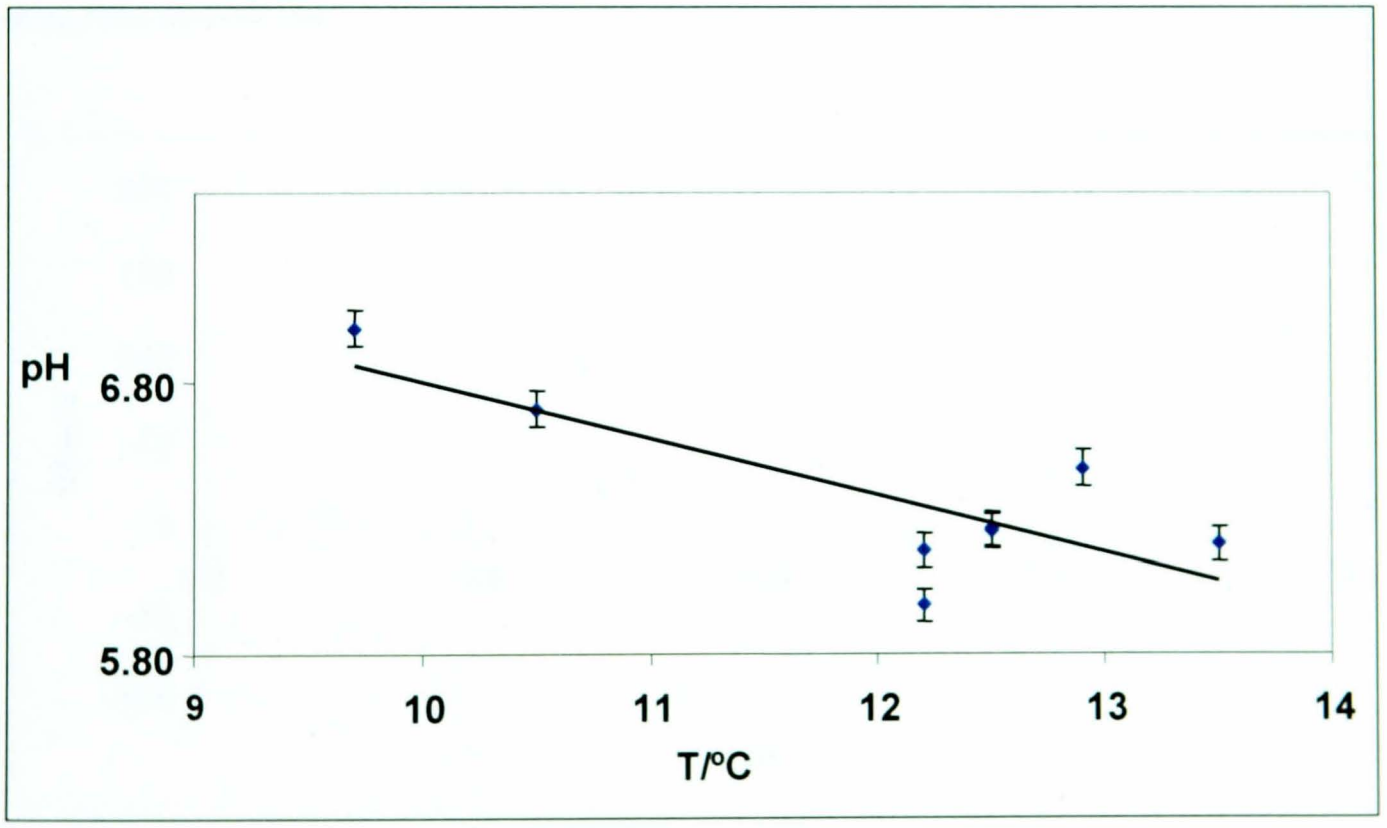

Figure 5.8: Shows the relationship between pH and temperature over time (monthly sampling) for the influent samples taken from March-October 2006 at Quaking Houses treatment system site. The least square regression equation is: T= -0.21* pH + 8.88 and R^2=0.64.

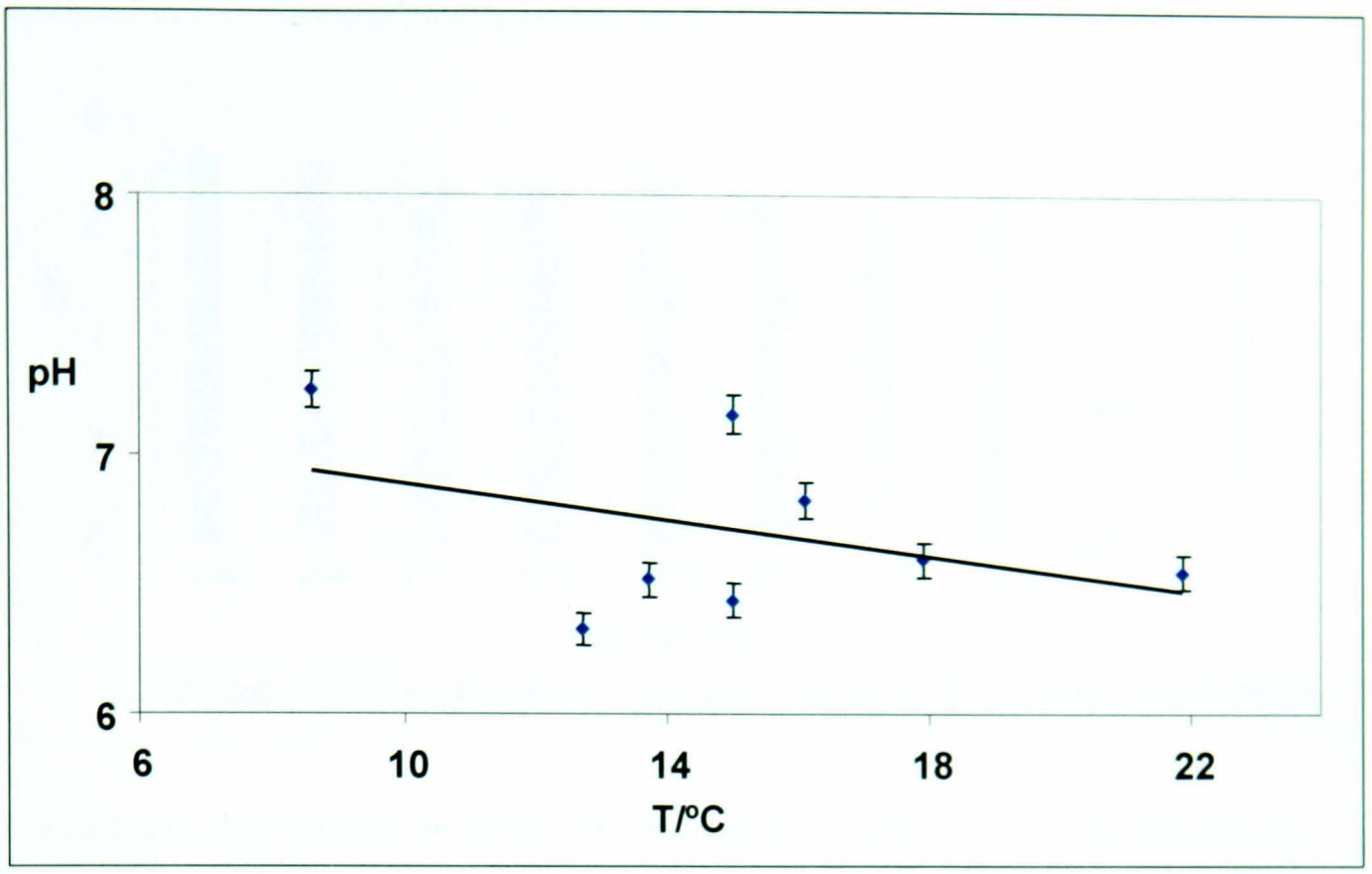

Figure 5.9: Shows the relationship between pH and temperature over time (monthly sampling) for the outlet samples taken from March-October 2006 at Quaking Houses treatment system site.

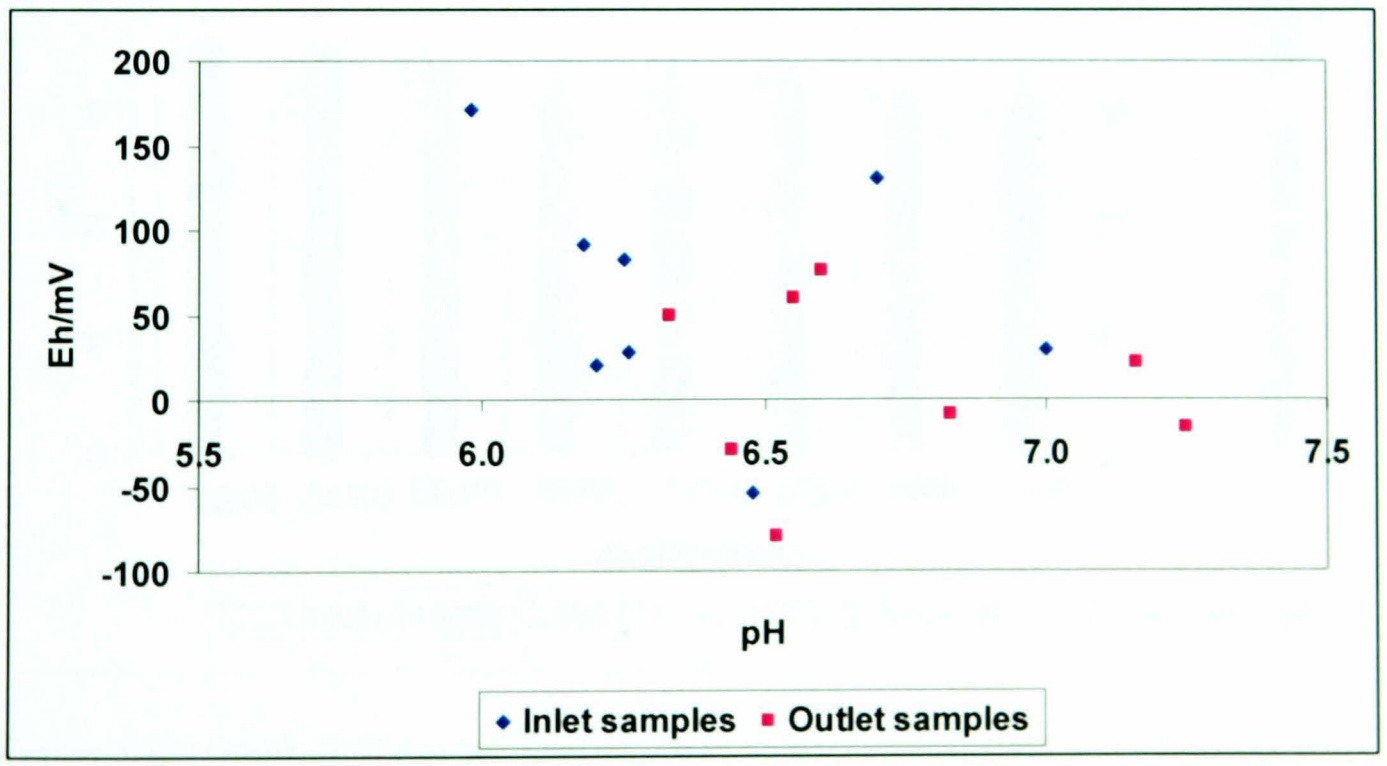

Figure 5.10: Measured *Eh* as a function of pH for inlet and outlet samples taken from March-October 2006 Quaking Houses treatment system site. The least square regression equation is: pH= - Eh* 66.20 + 484.67 and R^2=0.09.

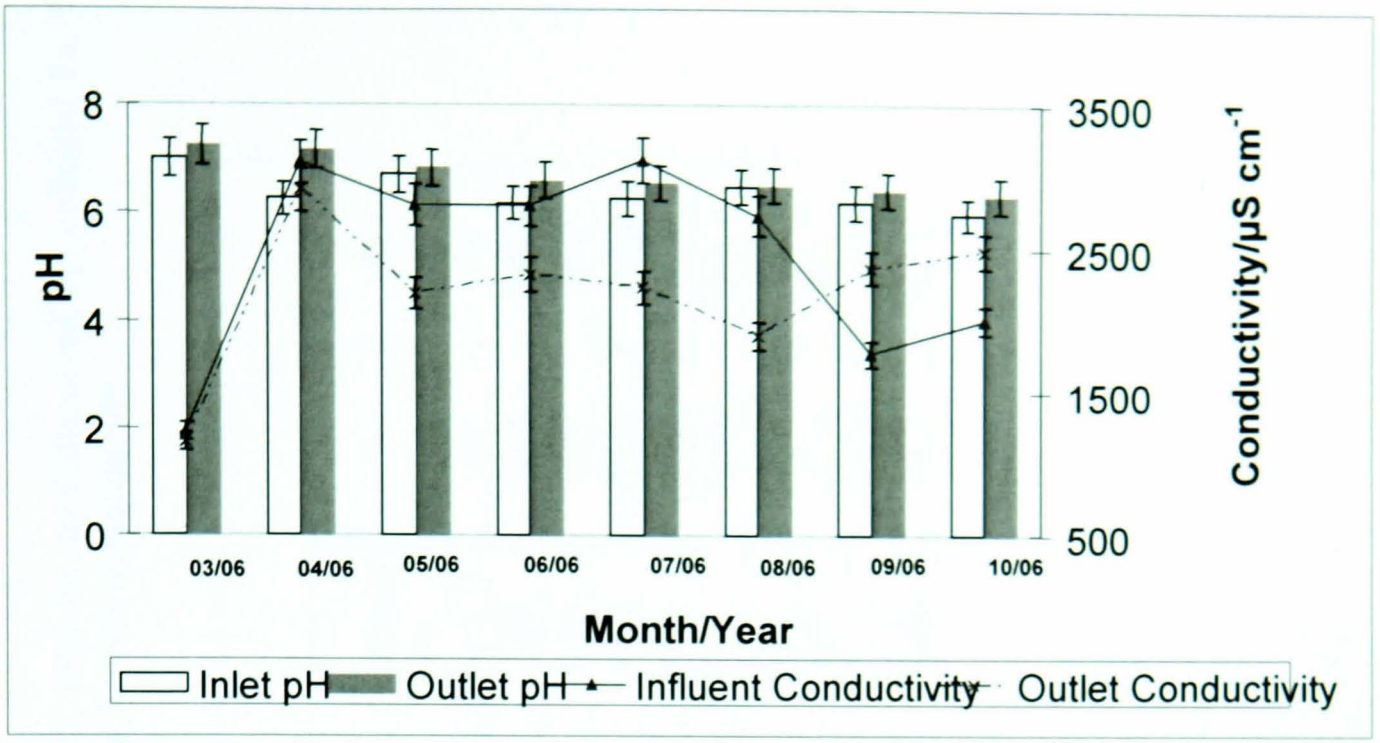

Figure 5.11: Plot showing the temporal relationship between pH and conductivity for the inlet and outlet samples taken March-October, 2006 at Quaking Houses treatment system site.

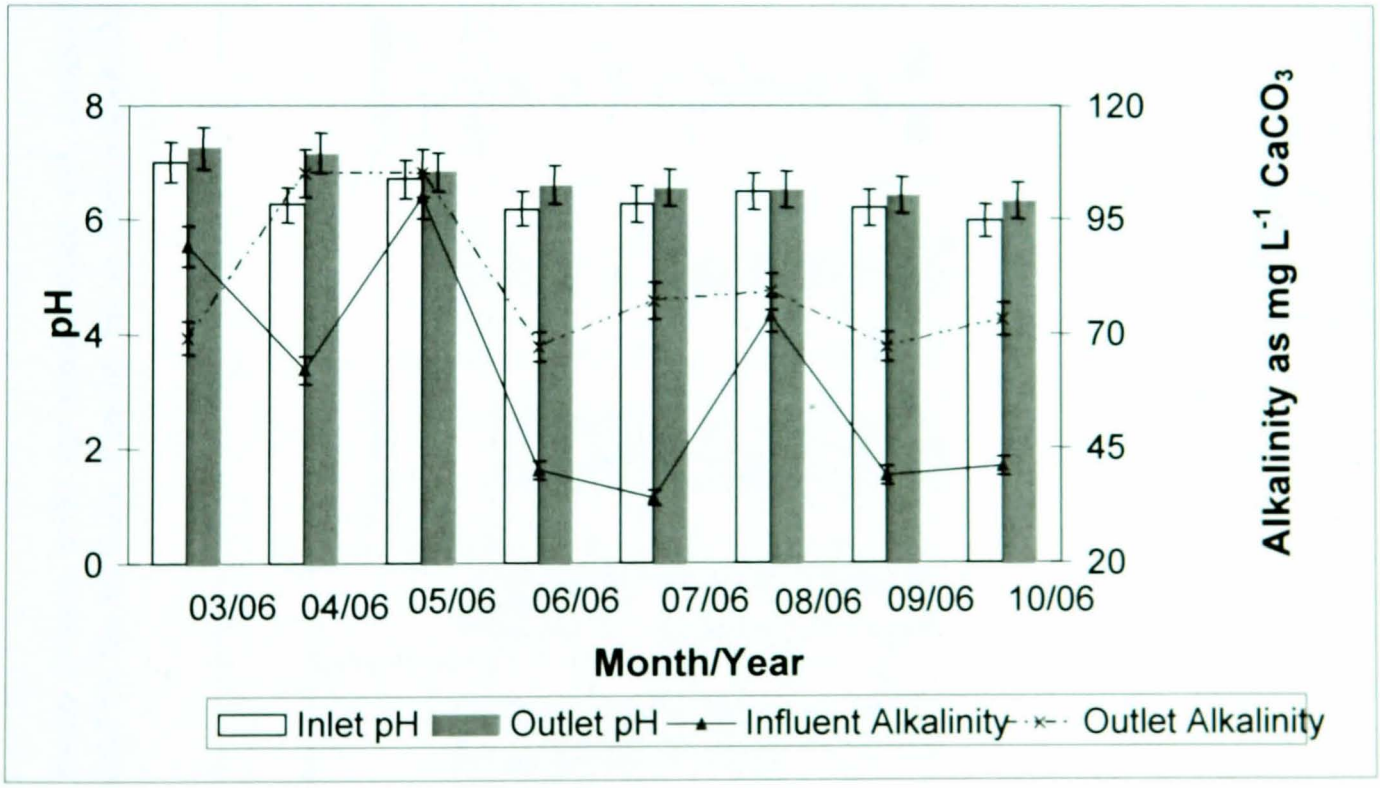

Figure 5.12: Graph showing the temporal relationship between pH and alkalinity for the inlet and outlet samples taken March-October 2006 at Quaking Houses treatment site.

Table 5.1: Monthly and mean (where n=8) for temperature, pH, conductivity (k), *Eh*, alkalinity, total Fe, total dissolved Fe, colloidal Fe, % dissolved Fe, and % colloidal Fe for influent samples taken from March-October, 2006 at Quaking Houses treatment site.

	influent									
Months	T/°C	pH	K (µs cm^{1})	(*Eh*)/mV	Alkalinity (mg L^{-1} CaCO3)	Total Fe (mg L^{-1})	Soluble Fe (mg L^{-1})	Colloidal Fe (mg L^{-1})	% Dissolved Fe	% Colloidal Fe
March'06	9.70	7.00	1226	29	69	9.12	5.62	3.50	61.6	38.4
April'06	12.5	6.25	3098	82	62	9.72	5.22	4.50	53.7	46.3
May'06	10.5	6.70	2800	131	100	11.45	6.58	4.87	57.5	42.5
June'06	12.2	6.18	2798	91	40	11.60	7.56	4.04	65.2	34.8
July'06	12.5	6.26	3112	28	34	14.35	7.74	6.61	53.9	46.1
Aug.'06	12.9	6.48	2731	-54	74	14.70	7.89	6.81	53.7	46.3
Sept.'06	13.5	6.20	1772	20	39	13.34	5.68	7.66	42.6	57.4
Oct.'06	12.2	5.98	2007	171	41	11.57	6.45	5.12	55.8	44.3
Mean	**12.0**	**6.38**	**2443**	**62.25**	**57.38**	**11.98**	**6.59**	**5.39**	**55.5**	**44.5**

Table 5.2: Monthly and mean (where n=8) for temperature, pH, conductivity (k), *Eh*, alkalinity, total Fe, total dissolved Fe, colloidal Fe, % dissolved Fe, and % colloidal Fe for effluent samples taken from March-October, 2006 at Quaking Houses treatment site.

	Effluent									
Months	T/°C	pH	k ($\mu s\ cm^{-1}$)	(*Eh*)/mV)	Alkalinity ($mg\ L^{-1}$ CaCO3)	Total Fe ($mg\ L^{-1}$)	Soluble Fe ($mg\ L^{-1}$)	Colloidal Fe ($mg\ L^{-1}$)	% Dissolved	% Colloidal
March'06	8.60	7.25	1154	-17	89	8.56	4.70	3.86	54.9	45.2
April'06	15.00	7.16	2904	21	105	4.33	4.33	0.00	100	0.00
May'06	16.10	6.83	2191	-9	105	3.14	3.14	0.00	100	0.00
June'06	17.90	6.60	2318	76	67	5.57	3.35	2.22	60.1	39.9
July'06	21.90	6.55	2229	60	77	4.15	2.90	1.25	69.9	30.1
Aug.'06	13.70	6.52	1894	-80	79	4.53	1.87	2.66	41.3	58.7
Sept.'06	15.00	6.44	2373	-29	67	6.09	2.04	4.05	33.5	66.5
Oct.'06	12.70	6.33	2489	50	73	3.23	3.23	0.00	100	0.00
Mean	**15.1**	**6.71**	**2194**	**9**	**82.8**	**4.95**	**3.20**	**1.76**	**70.0**	**30.0**

Relationship between water pHs and temperatures of influent and effluents samples as shown in figures 5.8 and 5.9 respectively show that in general, water temperatures increase with decreasing water pHs and vice-versa with few exceptions. The pH and water temperature profile show inverse relationships for both inlet and outlet samples. While inlet samples show reasonable correlation (R^2=0.64), there is no correlation in the outlet samples (R^2=0.16). These observed trends showed that at lower pH, more materials are more dissolved particularly iron for which solubility increases with decreasing pH. The lack of correlation in the outlet samples is unexpected but similar analyses of pH and temperature at common sampling stations have not been reported, so, it is unknown whether this is a common phenomena or a unique result of the Quaking Houses treatment system water chemistry. However, inverse relationship between pH and water temperature at the effluent of a treatment system has been reported by Hedin [4]. In addition, these increasing water temperatures with decreasing pHs may be due to more soluble materials at lower pH and vice-versa.

The *Eh*-pH profile across as the site (figure 5.10) shows an irregular pattern but in general, influent samples are in a more oxidising environment whilst effluent samples are in more reducing environment. Lack of correlation (R^2= 0.9 and 0.01) between the *Eh*-pH profile for both inlet and outlet samples respectively is rather surprising as one would generally expect that elevated pH will accompany lower *Eh* and reduction on iron concentration [5]. However, this unusual trends is in accord with previous works on this site by Younger et al. [6, 7], who observed lack of correlation between Eh-pH for circumneutral pH water systems. Thus, *Eh*-pH trends show no correlation probably due to reduced acidity and circumneutral nature of this site. Thus, one would expect to find a change from Fe^{2+} to Fe^{3+} or vice-versa depending on the shift in the pH or *Eh* of the environment. Measurements of *Eh* in nature is also difficult due to the fact that some of the reactions that determine the redox potential of a natural settings are slow and the measured *Eh* values are usually lower than the equilibrium values [8].

Generally, conductivity for influent samples is higher than their corresponding effluent samples as shown in figure 5.5. However, the pH-conductivity profile shows an irregular pattern (figure 5.11) which may be attributed to variation in the dissolved sulphates or other ions in the water sample.

The pH-alkalinity profile presented in figure 5.12 reveals that as would be expected, alkalinity is higher in samples with high pHs and that effluent samples have higher alkalinity than influent samples. This trend in pH-alkalinity profile is in accord with the fact that increased pH and net water alkalinity are common features of passive remediation systems like Quaking Houses treatment system [4, 6, 7].

Tables 5.1 and 5.2 show monthly and mean pH, temperature, conductivity, *Eh*, alkalinity, together with total iron, soluble and colloidal and percentage dissolved and colloidal iron for both influent and effluent samples respectively. On comparing the two tables, we observed that the mean influent pH is 6.38 and the mean effluent pH is 6.71; this indicates that the Quaking Houses site is no longer acidic and the treatment regime has proved to be effectively over the years. In fact, this site is the least acidic of all the sites studied in this thesis.

5.2.2: Voltammetric results

Temporal changes in mean total concentrations for unhydrolysed and hydrolysed iron (mg L^{-1}) for the inlet and outlet samples are presented in figures 5.13 and 5.14 respectively whilst figure 5.15 shows the variation in the hydrolysed and unhydrolysed iron concentrations for the sampling period (March-October, 2006) under review. Mean concentrations of total dissolved and colloidal iron at various sampling points are presented in figure 5.16 whilst figure 5.17 shows the profile of total dissolved iron concentrations. Concentrations of dissolved iron in filtered samples (0.45 μm) are presented in figure 5.18 whilst figure 5.19 shows the percentage dissolved and colloidal iron at various sampling points.

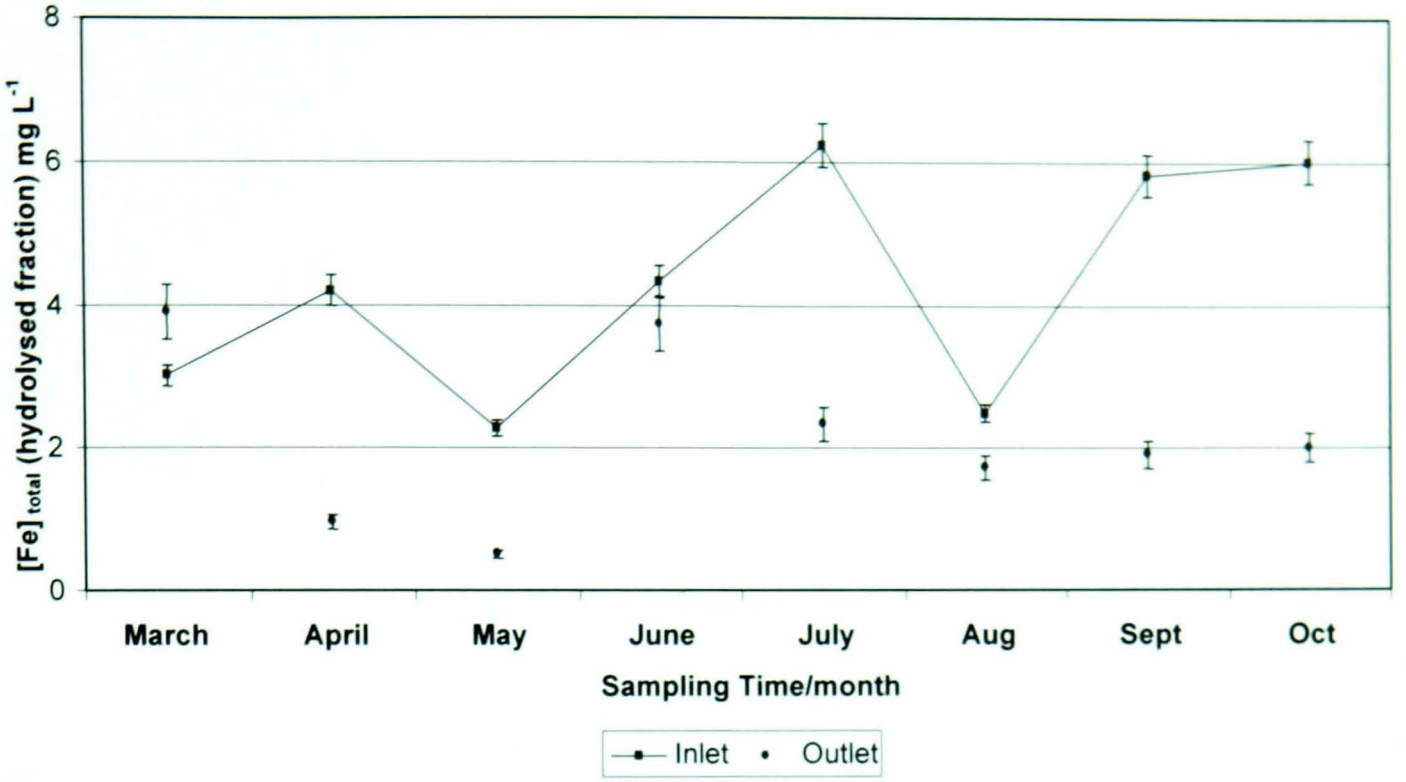

Figure 5.13: Mean total hydrolyzed iron concentrations (mg L^{-1}) for samples collected March-October 2006 at Quaking Houses treatment site. Error bars denote standard error of the mean, where n=4.

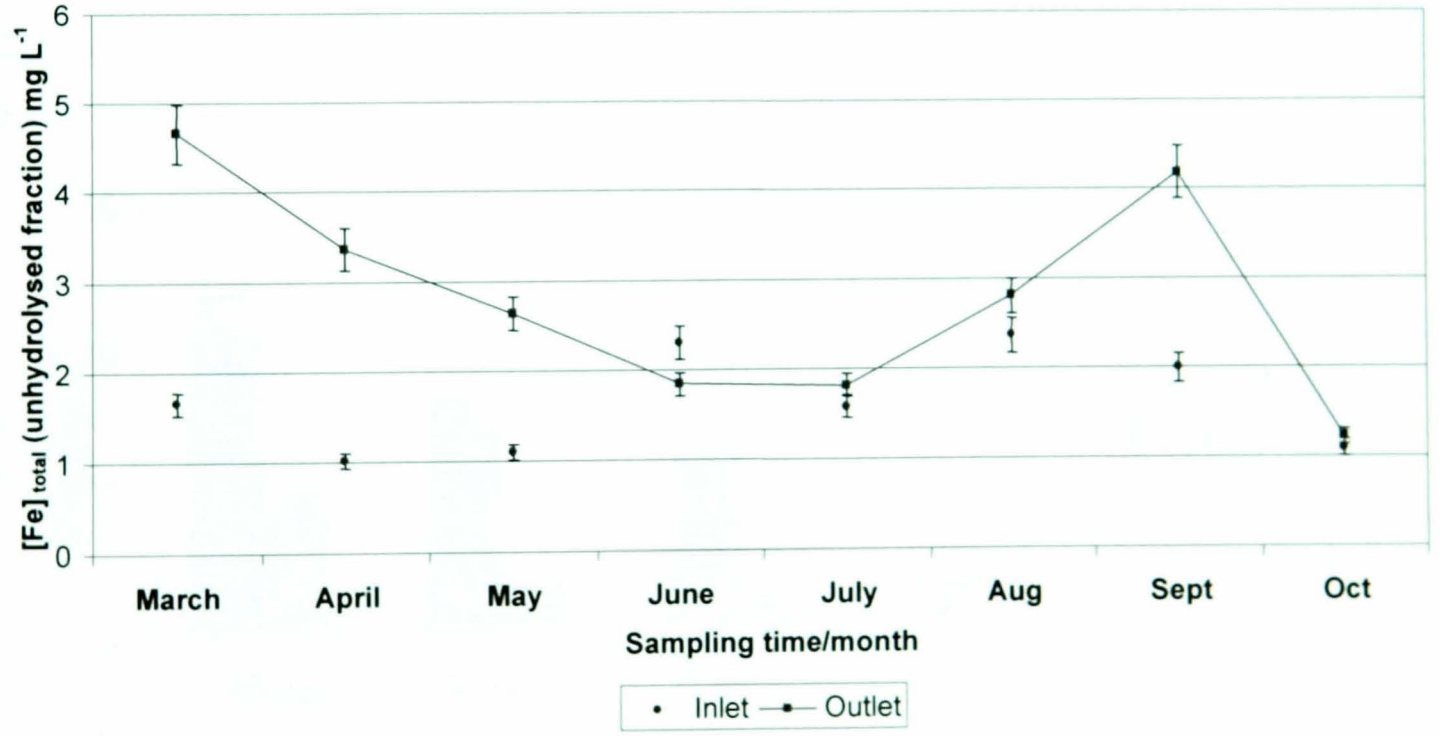

Figure 5.14: Mean total unhydrolysed iron concentrations (mg L^{-1}) for samples collected March-October 2006 at Quaking Houses treatment site. Error bars denote standard error of the mean, where n=4.

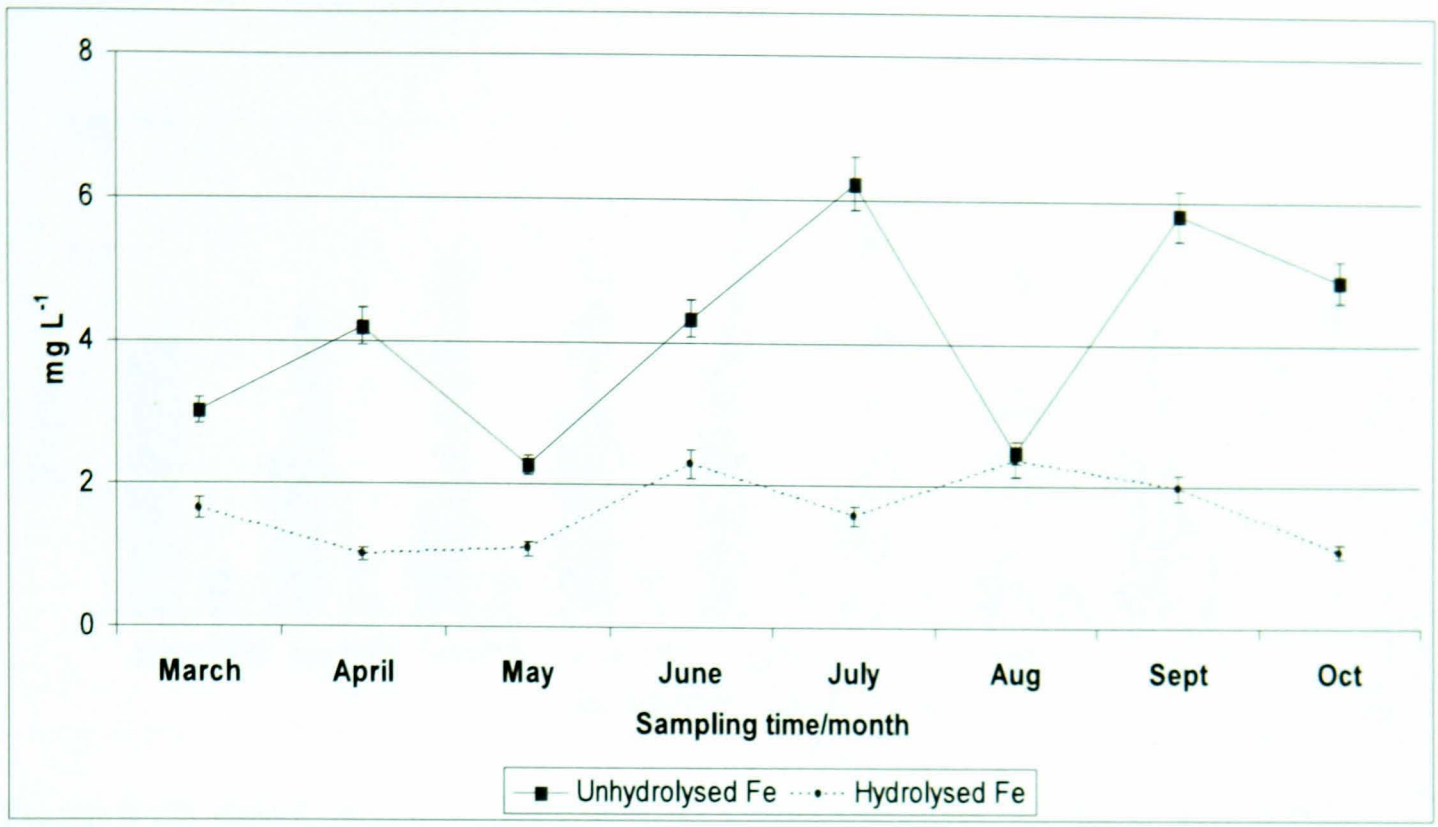

Figure 5.15: Mean total hydrolyzed and unhydrolysed iron concentrations (mg L^{-1}) for samples collected March-October 2006 at Quaking Houses treatment site. Error bars denote standard error of the mean, where n=4.

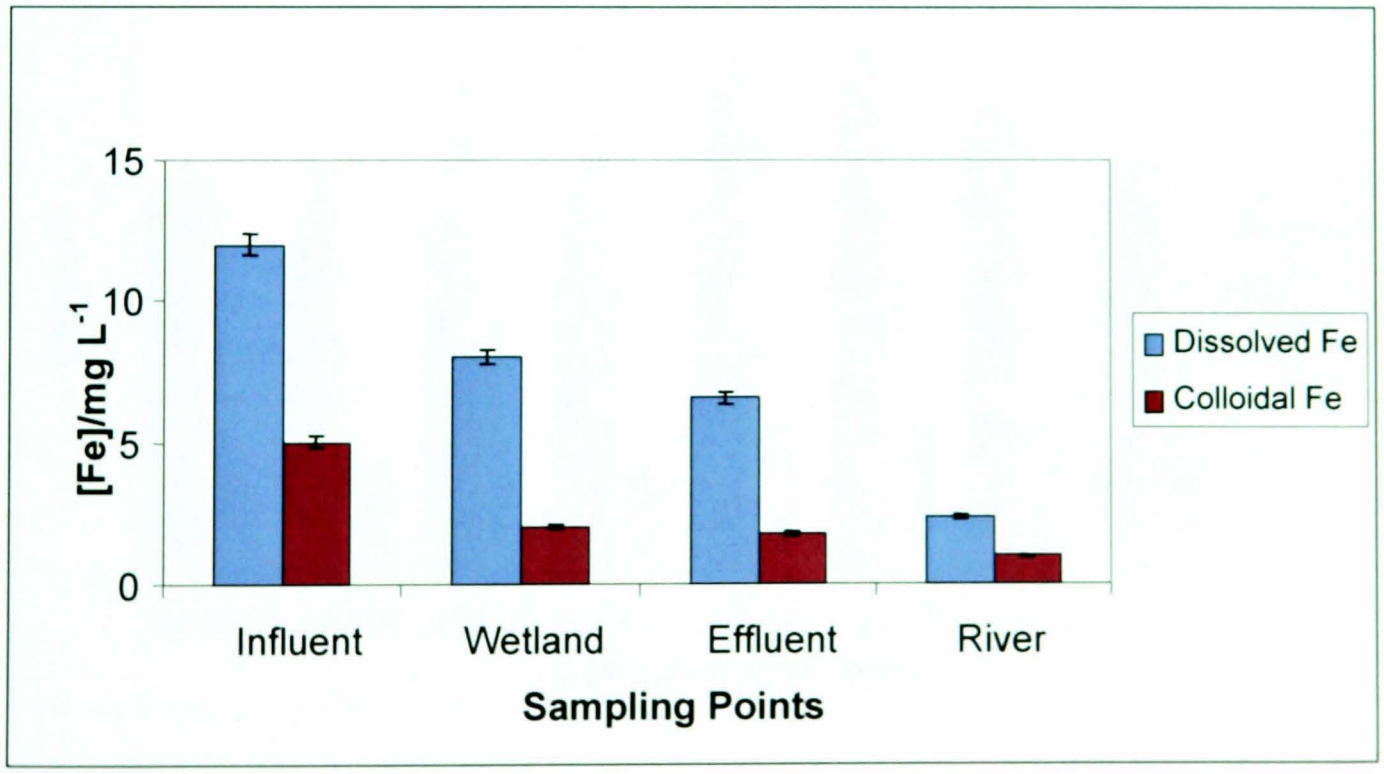

Figure 5.16: Mean concentrations of total dissolved and colloidal iron concentrations for samples taken March-October 2006 across various sampling points at Quaking Houses treatment site.

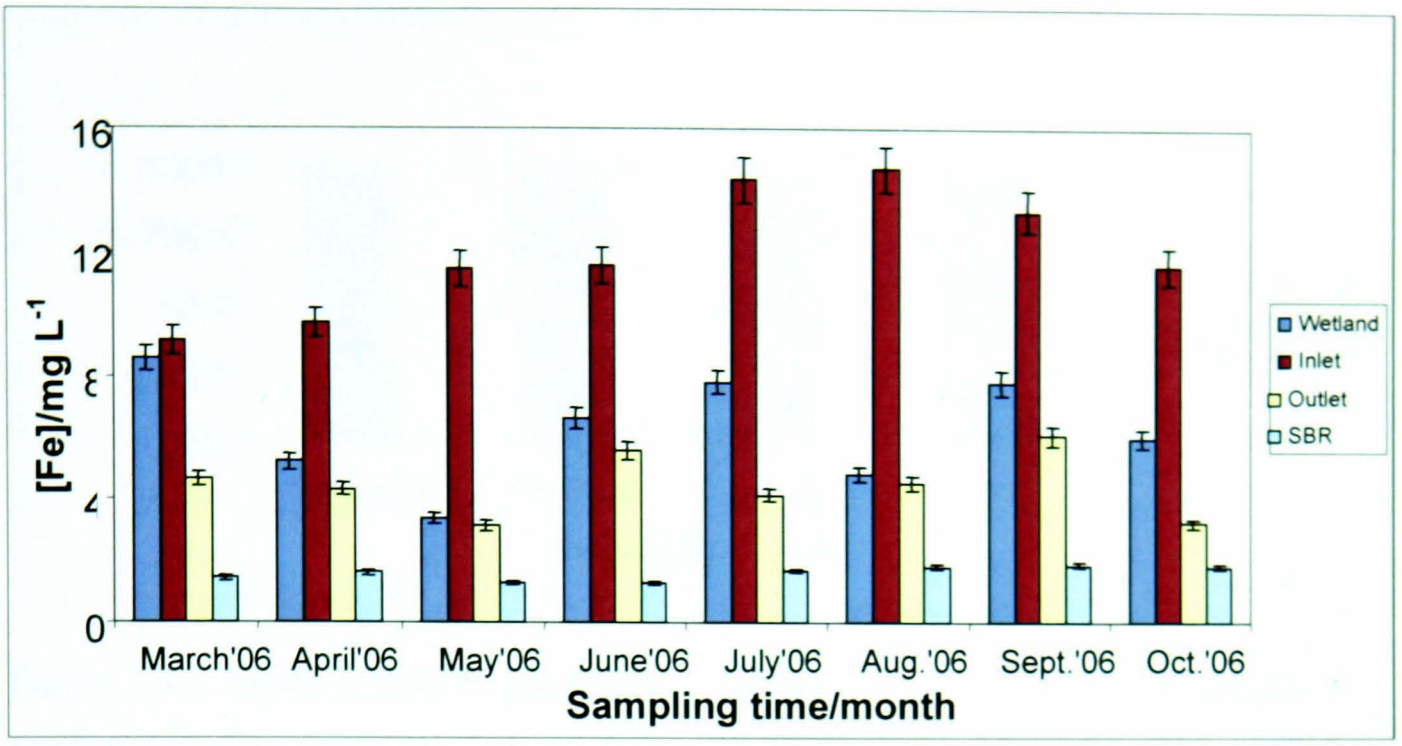

Figure 5.17: Graph showing temporal trend of total iron concentrations profile for samples taken March-October 2006 at various sampling points at Quaking Houses treatment site.

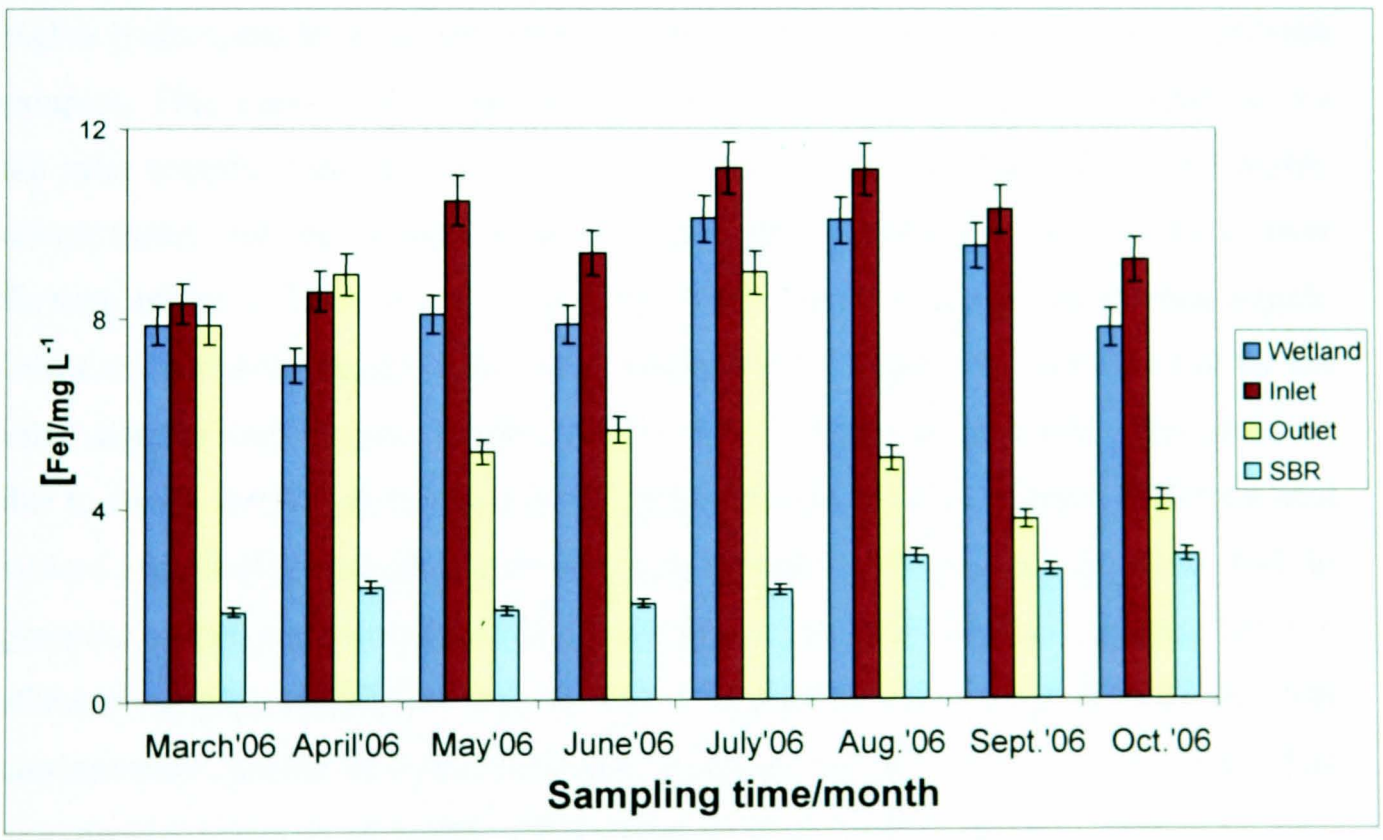

Figure 5.18: Graph showing temporal trend of filtered iron concentrations profile for samples taken March-October 2006 at various sampling points at Quaking Houses treatment site.

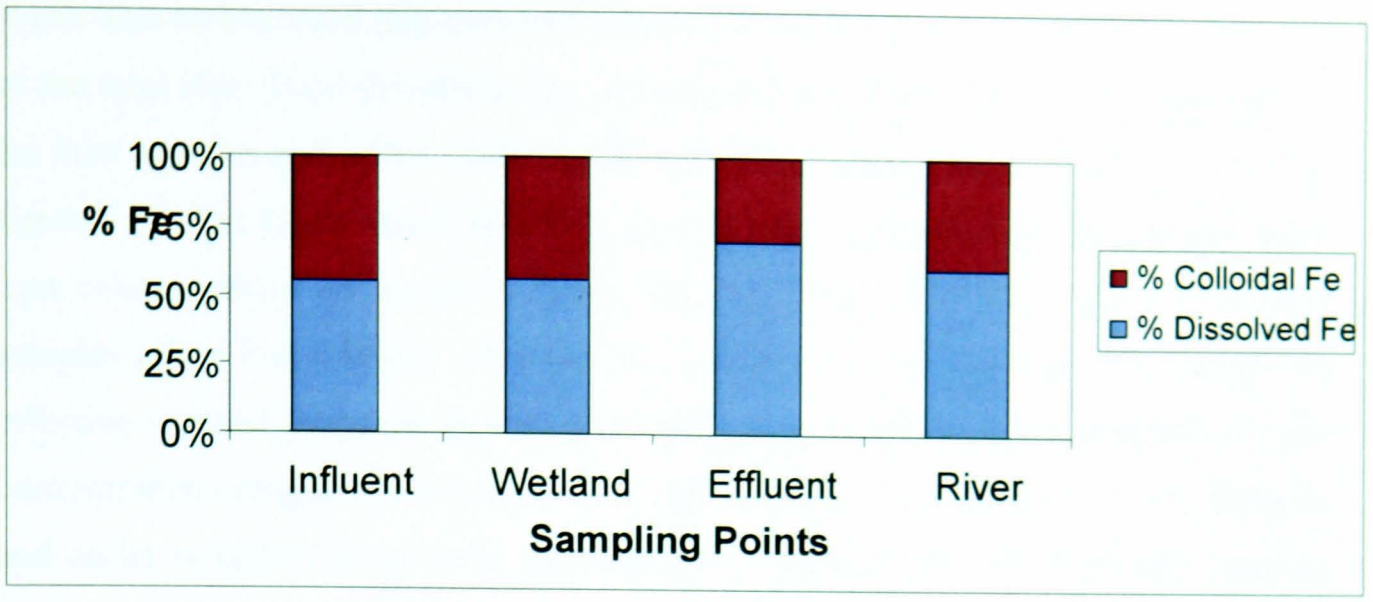

Figure 5.19: Mean profile of percentage dissolved and colloidal iron measured at various sampling points for samples taken March-October 2006 at Quaking Houses treatment site, where n=8.

An irregular pattern was observed in the hydrolysed iron concentrations which show higher hydrolysed iron concentrations for the inlet samples compared to the effluent samples. This trend is not surprising as one would expect higher concentrations for the inlet samples than the outlet samples as can be seen in figure 5.13. The higher concentration for the effluent sample in the month of March could be due to over flowing of the influent water to the outlet water due to blockage during this month. Iron concentrations appear stable and comparable for September and October for the inlet samples and August-October for the outlet samples respectively. This could be due to steady rainfall pattern and in the consistency of the effectiveness of the wetland system. Similarly, unhydrolysed iron concentrations follow similar trend and in general, higher concentrations are observed for the inlet samples compared to the effluent samples except for June as shown in figure 5.14. Comparison of the total concentration profile of hydrolysed and unhydrolysed iron (figure 5.15) shows that unhydrolysed iron is of higher concentrations than hydrolysed iron. However, they both follow similar pattern of variations.

Mean total dissolved and colloidal iron concentrations show a gradual and steady reduction in concentrations from the inlet samples to the river samples-figure 5.16. This trend is not surprising as one would expect reduction in iron concentrations as a measure of effectiveness of the wetland system.

It can also be observed that colloidal iron concentration also account for about a half of the total iron. Total dissolved iron concentrations ranged from 9.12 to 14.7 mg L^{-1} for inlet samples and 3.14 to 6.09 mg L^{-1} for outlet samples respectively as shown in figure 5.17. The figure shows that there is progressive reduction in the total dissolved iron concentrations as we move from the inlet to the end point and to the river samples where it discharges. This trend is not surprising as would be expected for an effective wetland treatment system as in this case. Similarly, filtered dissolved iron concentrations ranged from 8.32 to 11.16 mg L^{-1} and 3.75 to 8.94 mg L^{-1} for influent and outlet samples respectively as presented in figure 5.18. Although this trend is similar to the one observed for the total dissolved iron profile, however, the concentrations are lower than the total iron concentrations and would be expected. The average percentage iron concentrations for dissolved and colloidal iron (figure 5.19) shows that almost half of the total iron is made up of colloidal iron and similar trend was observed in the wetland. However, there is a significant reduction in the colloidal iron fraction for the effluent samples which accounts for almost a quarter of the total fraction. The trend changed when the water has been discharged into local stream to almost 1: 1.

Monthly total iron concentration for influent (table 5.1) shows that iron concentration is relatively stable and ranged from 9.12 to 14.7 mg L^{-1} and mean of 12.0 mg L^{-1}. Conversely, although there is wide variation in the monthly total iron concentrations for the effluent samples (table 5.2), which ranged from 3.14 to 8.56 mg L^{-1}, however, the mean of 4.95 mg L^{-1} shows that influent iron concentration has been reduced by half. Comparison of soluble and colloidal iron fractions shows that about half of the total iron exists in colloidal form for the influent samples (table 5.1), and about a third of the total iron in the colloidal fraction form in the effluent samples (table 5.2). This result suggest that about 20% of the solid phase iron oxy-hydroxide has been physically trapped or removed through the wetland system in this site. Few cases of 100 percent in dissolved iron (table 5.2) are due to the fact that the concentrations of colloidal iron are below the detection limit during these months.

5.2.3: Relationships between iron concentrations and the various measured parameters that controls iron geochemistry; *Eh*, pH and alkalinity

To have an understanding and appreciation of the potential effects of water quality monitoring parameters such as pH, temperature, oxidation reduction potential (*Eh*), conductivity and alkalinity on the concentrations of dissolved and colloidal iron, these relationships are represented graphically and are presented in figures 5.22 to 5.26 for both inlet and outlet samples for comparison and for each parameter. Although, relationships between iron concentrations and these parameters are yet to be well understood and have never been established in any previous known literature, attempts will be made to see if there is any significant correlation and any trends and patterns. Thus, data presented here are for ease of presentation and it may be difficult to make any generalised statement regarding the relationships between these parameters and variations in iron concentrations.

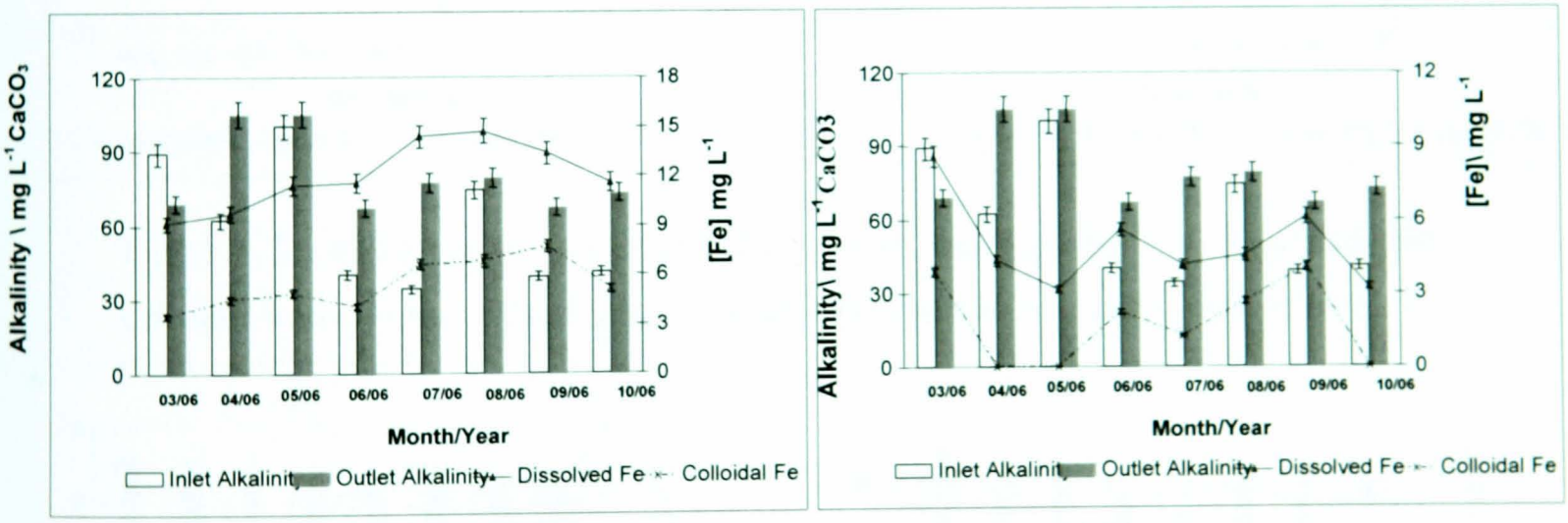

Figure 5.20: Shows alkalinity together with variations in dissolved and colloidal iron concentrations for inlet and outlet samples taken March-October 2006 at Quaking Houses treatment site.

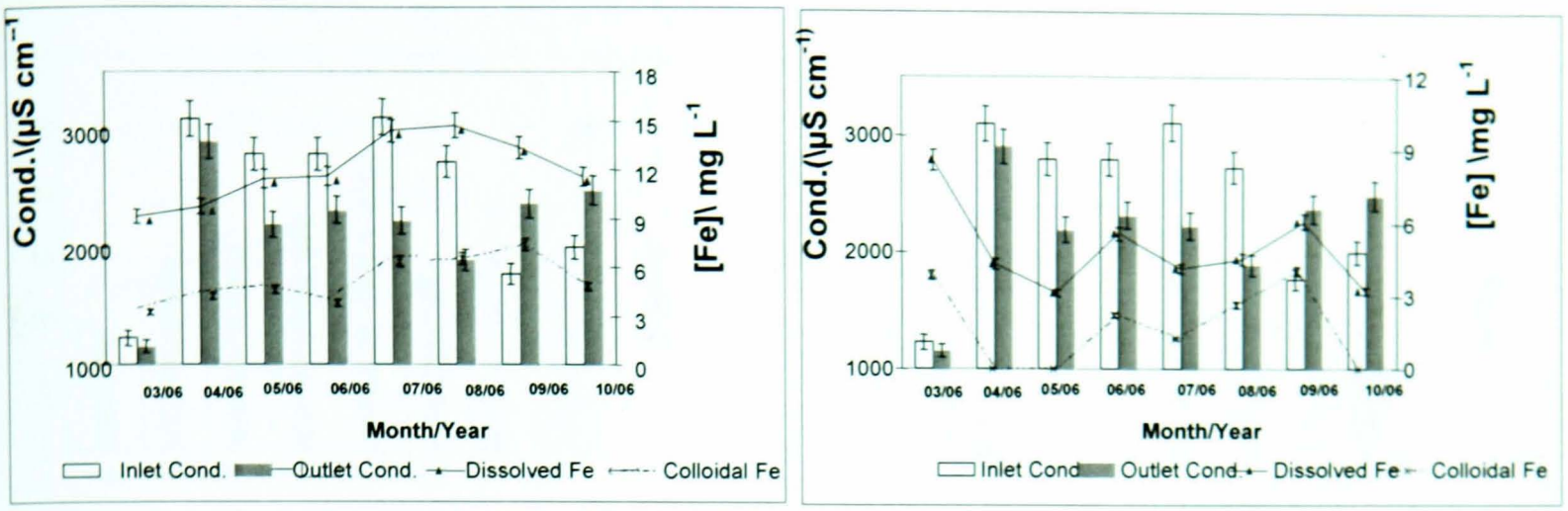

Figure 5.21: Shows conductivity together with variations in dissolved and colloidal iron concentrations for inlet and outlet samples taken at Quaking Houses site.

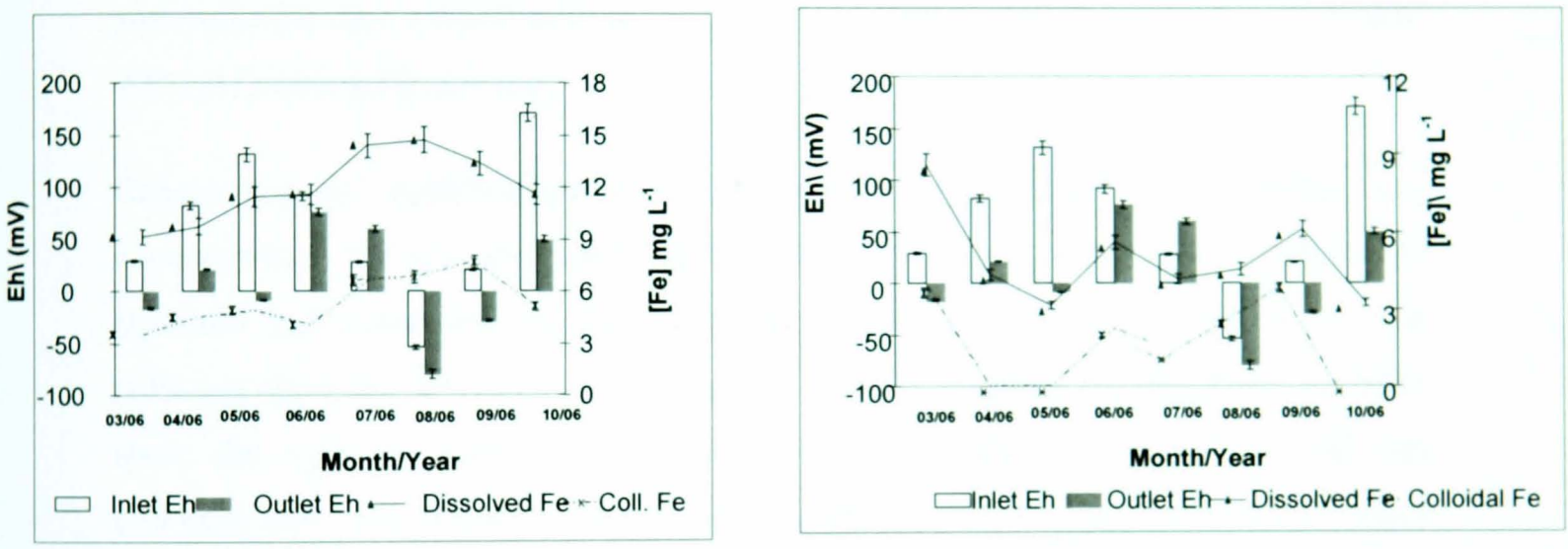

Figure 5.22: Shows redox potential (Eh) together with variations in dissolved and colloidal iron concentrations for inlet and effluent samples at Quaking Houses site.

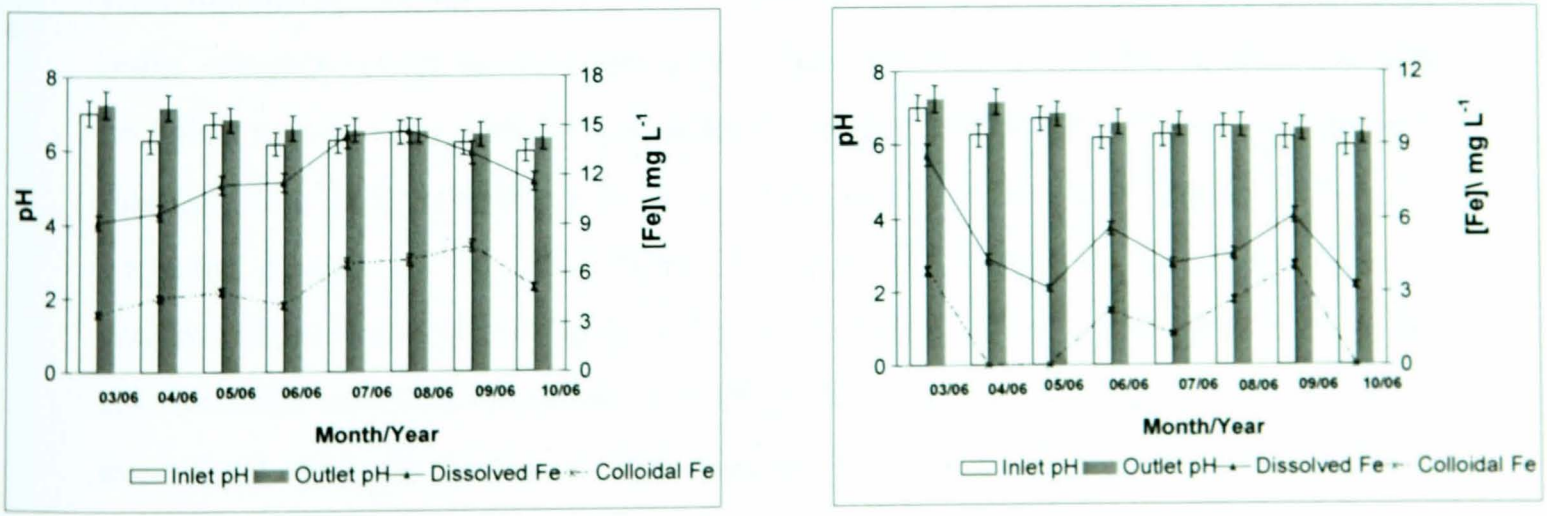

Figure 5.23: Graph showing pH together with temporal variations in dissolved and colloidal iron concentrations for inlet and outlet samples taken at Quaking Houses site.

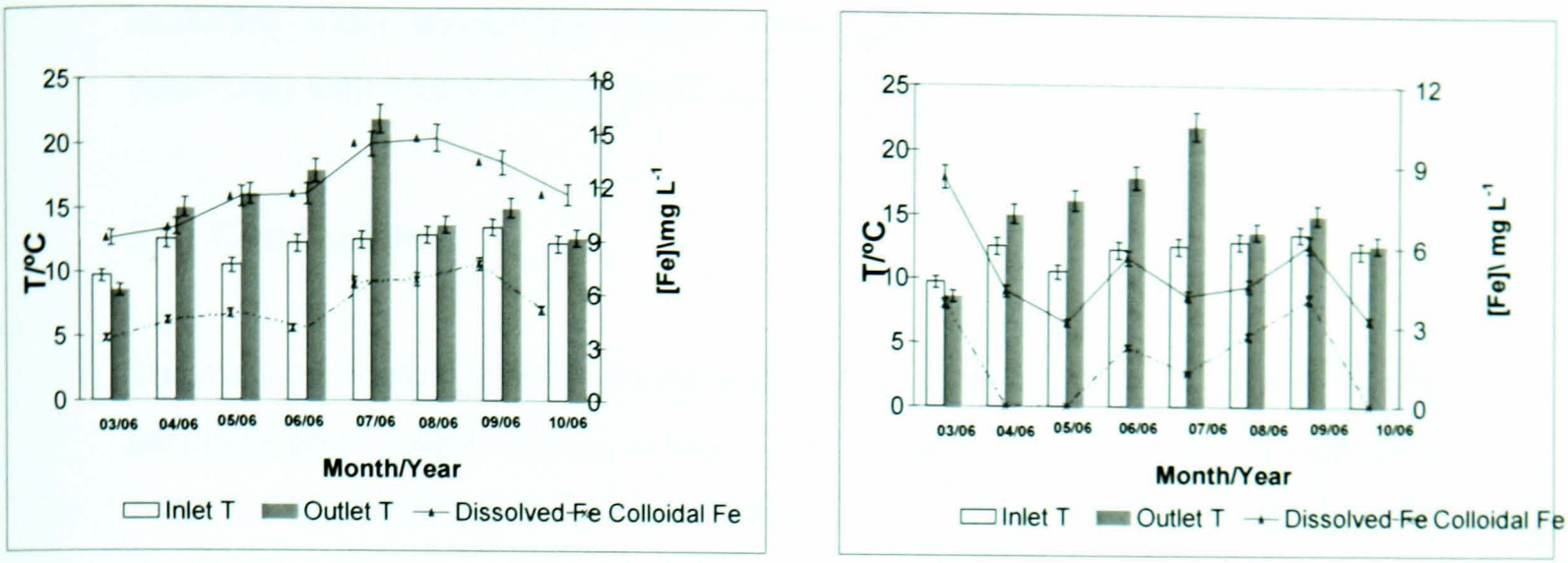

Figure 5.24: Graph showing temperature trend together with variations in dissolved and colloidal iron concentrations for inlet and outlet samples taken March-October 2006 at Quaking Houses site.

Comparison of relationships between alkalinity, dissolved and colloidal iron concentrations for inlet and outlet samples (figure 5.20) shows that both dissolved and colloidal iron concentrations follow similar pattern of increasing concentration with reducing alkalinity with few exceptions (for influent samples) whilst effluent samples show the opposite trend, that is, reduced concentrations in both dissolved and colloidal iron concentrations with some exceptions. With these observed irregular pattern/trends in these relationships, one can not be too certain to make a generalised statement. Dissolved and colloidal iron concentrations show increasing concentrations with increasing conductivity for inlet samples as shown in figure 5.21. However, outlet samples reveal the opposite trend. This observation can be explained in that probably iron is more dissolved in influent samples than in the effluent samples and this may also have something to do with the water pH at each sampling point. An irregular pattern in the relationship between *Eh*, dissolved and colloidal iron concentrations was observed in fig.5.22, but in general, there is reduction in dissolved and colloidal iron concentrations at both positive and negative potentials with some exceptions, for both inlet and outlet samples. In most cases, dissolved and colloidal iron concentrations increase with reducing pH for both inlet and outlet samples as presented in figure 5.23. This trend is not surprising and it shows that although, the pH for both inlet and outlet samples are quite close and near neutral, iron is still relatively more dissolved in inlet samples, compared to outlet samples.

For inlet samples, dissolved and colloidal iron show increasing concentrations with increasing water temperature whilst outlet samples show an irregular pattern of behaviours with wide variations as shown in figure 5. 24.

5.3: Conclusions

The measured water quality parameters such as pH, temperature, *Eh*, conductivity and alkalinity give a rough estimate of the level of contamination (inlet) and the quality of water (outlet) discharged into the Stanley Burn (stream) which is important for monitoring purposes. In fact, elevated pH of the outlet water suggests that the wetland increases the alkalinity of the water as it passes through and this is not surprising considering that the wetland was constructed with substrates to increase water alkalinity by addition of limestone. In fact, the pH of the water discharged to the Stanley Burn is suitable for sustaining aquatic life and other water ecosystems.

Whilst there are clear correlations between some of the water quality parameters with the measured concentrations of total, soluble and colloidal iron, for example, pH versus iron concentrations, the relationship between others varied widely.

The proportion of hydrolysed iron is greater than the unhydrolysed iron which suggests that probably most iron on this site exist as Fe (III). To the best of our knowledge, this is the first time this has been established and reported.

Reduction in total iron concentration shows the effectiveness of the constructed wetland in removing iron. In fact, there is evidence of iron hydroxide precipitation on the surface of the wetland substrate with black deposits of iron monosulphide below the surface. This observation is consistent with the liberation of hydrogen sulphide gas from the substrate, with the identity of the gas being confirmed by occasional faint odours.

The proportion of colloidal iron makes up significant amount of total iron in the inlet water with a mean average of 44.5% over the sampling period and 30% mean average for the outlet samples. This shows that about 55.5% of iron actually exists in dissolved form for the inlet samples and about 70% for the outlet respectively. This has very significant geochemical implications for remediation strategies.

Overall, the treatment regime for this site is very effective for iron removal through trapping and precipitation.

5.4: References

[1]. Jarvis, A.P. & Younger, P.L. *Chemistry and Ecology*, **1997**, 13, 249-270.

[2]. CL: AIRE Case Study Bulletin CSB4 (November **2002**). A Constructed Wetland to Treat Acid Mine Drainage from Colliery Spoils at Quaking Houses, County Durham.

[3]. CL: AIRE Case Study Bulletin CSB4 (March **2006**). Coal Mine Sites for Targeted Remediation Research: The CoSTaR initiative.

[4]. Jarvis, A.P. & Younger, P.L. *Journal of the Chartered Institute for Water and Environmental Management*, **1999**, 13 (5), 313-318.

[5]. Younger, P.L., Curtis, T.P., Jarvis, A.P. & Pennell, R. *Journal of the Chartered Institute for Water and Environmental Management*, **1997**, 11, 200-2008.

[6]. Younger, P.L. *International Mine Water Association, Johannesburg*, **1998**

[7]. Jarvis, A.P. Design, Construction and Performance of Passive Systems for the Treatment of Mine and Spoil Heap Drainage, **2000**, PhD Thesis, Newcastle University.

[8.]. Kemp, P. and Griffiths, J. Quaking Houses-Arts, Science and the Community: a collaborative approach to water pollution, **1999**, Jon Carpenter Publishing, Charlbury.

[9]. Hedin, R.S. *Mine Water Environment*, **2000**, 7, 230-241.

[10]. Krauskopf, K.B. Introduction to Geochemistry, *McGraw-Hill Inc.*, **1979**, 617pp.

[11]. Younger, P.L. *Mine Water Environment*, **2000**, 2, 84-97.

[12]. Younger, P.L., Barnwat, S.A. and Hedin, R.S. Mine Water: Hydrology, Pollution, Remediation. *Kluwer*, **2000**, Dordrecht, 442pp.

[13]. Harrison, R., Scott, W.B. and Smith, T. *Quarterly Journal of Engineering Geology*, **1989**, 22, 355-358.

[14]. Edward, P.J., Bolton, C.P., Ranson, C.M. and Smith, A.C. *Chartered Institute of Water and Environmental Management*, **1997**, 17-32.

[15]. Hamilton, Q.U.I., Lamb, H.M., Hallett, C. and Proctor, J.A. *Chartered Institute of Water and Environmental Management*, **1997**, 33-56.

[16]. Jarvis, A.P. and Younger, P.L. *Chartered Institute of Water and Environmental Management*, **1999**, 13, 313-318.

[17]. Jarvis, A.P. and Younger, P.L. *South African Journal of Science*, **2000**, 14, 23-28.

[18]. National River Authority. Report of the National Rivers Authority, *Water Quality Series NO 14*, **1994**, London, HMSO, 46pp.

[19]. Nuttal, C.A. and Younger, P.L. *Water Research*, **2000**, 34, 1262-1268.

[20]. Tarutis, W.J., Stark, L.R. and Williams F.M. *Ecological Engineering*, **1999**, 12, 353-372.

[21]. Younger, P.L. *Quarterly Journal of Engineering Geology*, **1995**, 28, S101-s113.

[22]. Younger, P.L. *Science of the Total Environment*, **1997a**, 194, 457-466.

[23]. Younger, P.L. *Chartered Institute of Water and Environmental Management*, **1997b**, 189pp.

[24]. Younger, P.L. *Chartered Institute of Water and Environmental Management*, **1997c**, 65-81.

Chapter 6

BOWDEN CLOSE SITE, DURHAM

This chapter deals with Bowden Close site. The chapter starts with an overview of the background information and the problem of spoil heap discharges at this site, discusses the results obtained with conclusions.

6.1: Site History, Background, Problems and Treatment Regime

Bowden close is the site of a former coke-works and colliery which was abandoned in the 1960s. After the closure, the site was inherited by Durham County Council who carried out restoration work in 1970s which consisted of demolition of buildings, sealing and burial of mine entrances, reshaping of spoil heaps and re-profiling and vegetation through the application of topsoil over made ground. This resulted in creating a popular golf course in a pleasant rural setting. The restoration and reclamation works were carried out according to the best practice of the period which did not address the issues of subsurface pollution nor were attempts made to either intercept or reduce subsurface flow through heaps or made ground. However, by the end of 1990s, Durham County Council were re-evaluating the Bowden Close site on the two separate aspects of groundwater contamination and associated pollution seepages to the surface environment. Consequently, during 1998/99, highly acidic (pH 3-4; [4], metalliferous (high concentrations of metals, in particular Fe, Al and Mn [1]), waters began to emanate from various spring-like features and land drains within the site, causing severe contamination of the local water course- Willington Burn [7, 8]. As a result, a series of studies were conducted at the Bowden Close site in the 1990s, revealing the nature of the acidic drainage [1,2], assessing the ecological damage to the receiving watercourse [3,4] and identifying three distinct, perennial discharges of acidic mine drainage at this site [5].

Subsequently, a pilot passive treatment system was constructed to treat these acidic leachates using subsurface flow biogeochemical reactors containing a mixture of compost and limestone and operated from 1999 to 2001-when further site work was suspended due to outbreak of the Foot and Mouth Disease which restricted countryside access. The pilot system comprises of a single reducing and alkalinity-

producing system (RAPS) unit with an area of 120 m^2 followed by a small aerobic pond. The design and performance of this system has been described in detail by Younger [5, 6, 7]. Following the success and encouraging performance of this pilot scheme, a full scale treatment system was constructed and commissioned in early 2004 [6]. The passive treatment system concept at Bowden Close site is based on the principles of reducing and alkalinity-producing systems (RAPS).

The so-called '<u>R</u>educing and <u>A</u>lkalinity <u>P</u>roducing <u>S</u>ystem (RAPS)' improves water quality by the combined action of bacterial sulphate reduction and calcite dissolution. In a RAPS-type passive treatment system, polluted leachate is forced to flow downwards through a mixed compost limestone gravel bed (figure 6.1). Detailed descriptions of the geochemical reactions occurring in figure 6.1 have been fully described by many authors [e.g., 5, 6, 7].

RAPS unit functioning:

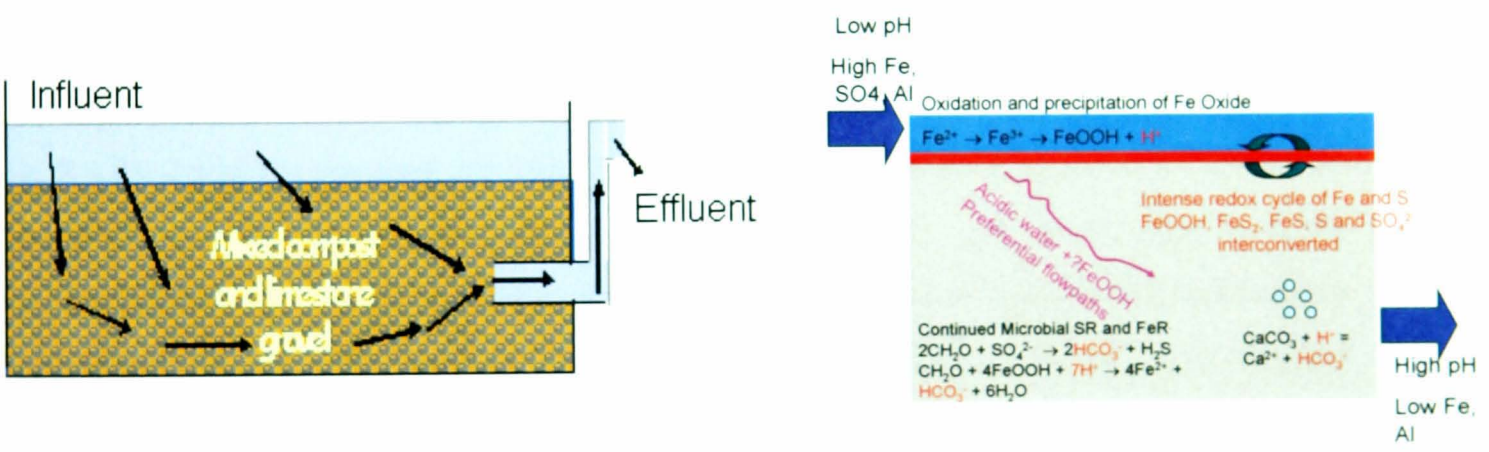

Figure 6.1: Schematic cross-section through a typical RAPS unit which is usually sized to allow 14 hours retention time. In the RAPS, there is a downward flow of polluted mine drainage through a compost layer (0.5m thick) and a limestone gravel bed -adapted from [7].

The treatment processes occurring in a RAPS unit as shown in figure 6.1 are thought to consist of the following stages [9, 10]:

1. Bacterial sulphate reduction, which generates alkalinity, raises pH and traps Fe as a sulphide within the compost layer.

2. Limestone dissolution, which further elevates the pH and generates more alkalinity.
3. Oxidation and hydrolysis of iron, manganese and aluminium to form hydroxides (both within the RAPS unit itself, and in the small aerobic pond which is installed downstream of the RAPS unit).

The treatment system at Bowden Close site consists of two subsurface flow RAPS units and an aerobic polishing reed-bed wetland. The layout of the system is summarised in figure 6.2 below. RAPS lagoon number one (RAPS 1) receives discharge from an old mine access drift and seasonal leachate from a small drill-cutting spoil. RAPS 2 received acidic leachates and the perennial aluminium rich discharge from a point source, associated with spoil toe drainage from a perched water table within the soil [10]. The substrate for both RAPS is a mixture of horse manure plus straw and limestone pebble, designed to improve water quality by the combination of microbial iron and sulphate-reduction and limestone dissolution. In addition, RAPS 1 is fitted with an HDPE membrane artificial liner while RAPS 2 is unlined but has been excavated into low permeability glacial till. The areas of RAPS 1, RAPS 2 and the reedbed are 1511 m^2, 1124 m^2 and 990 m^2 respectively. There are three discharges, discharges 1 and 2 are treated in RAPS 1 while the third and the most polluted discharge feeds into RAPS 2. The effluent of both RAPS units drain into a polishing aerobic wetland planted with *Typha latifolia* before being discharged into a small local stream (Willington Burn).

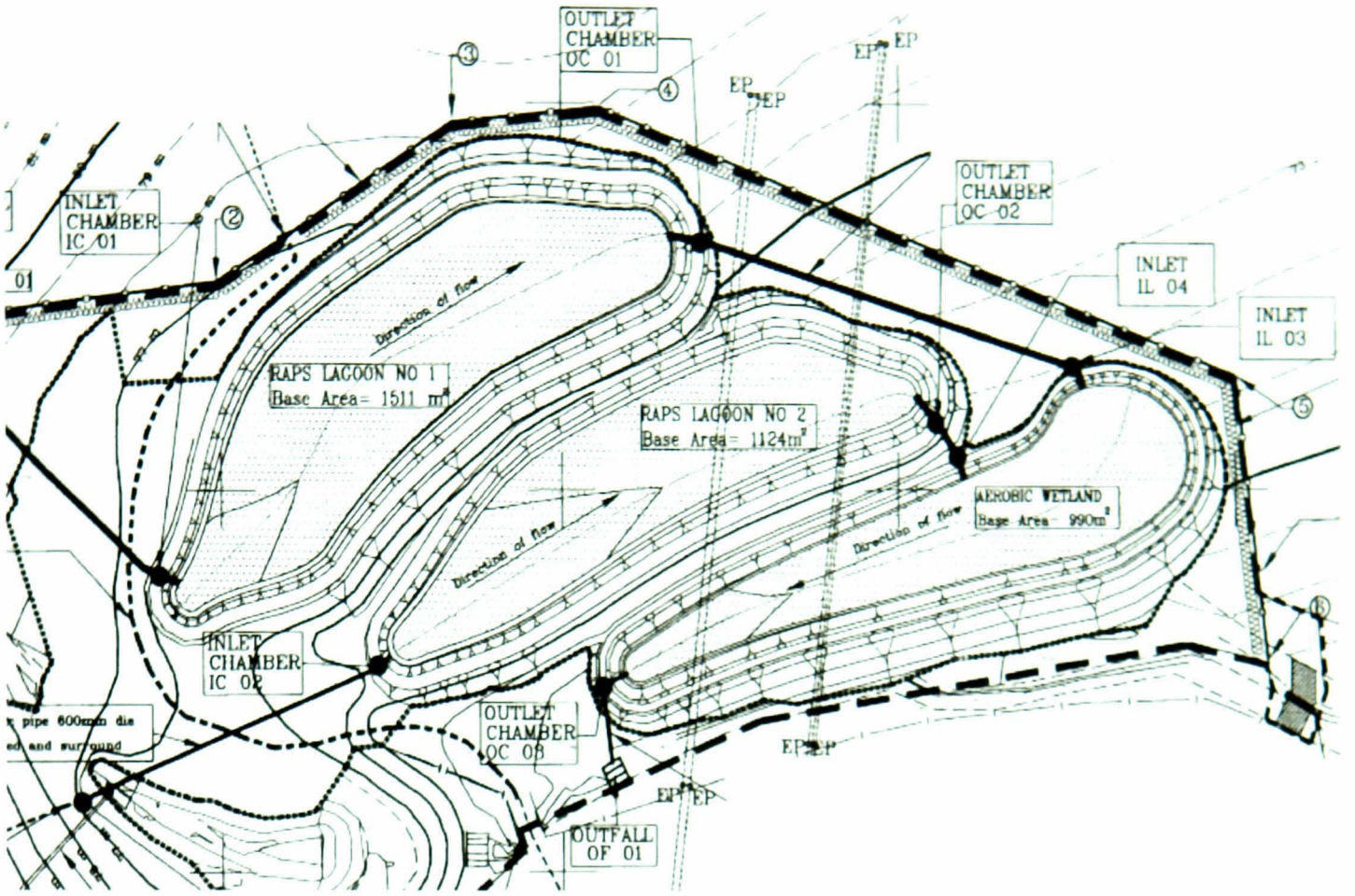

Figure 6.2: Layout of the passive treatment system at Bowden Close. The two RAPS units receive different mine water discharges. Both RAPS units feed the aerobic wetland in the lower part of that discharge into the local stream (Willington Burn)- Courtesy of the HERO research Group at Newcastle University.

Figure 6.3: Showing RAPS 1 unit, fitted with HDPE artificial liner and aluminium hydroxide precipitation at Bowden Close site. The RAPS receives discharge from an old mine access drift and seasonal leachate.

6.2: Results and Discussion

Monthly monitoring of water quality by measurement of on-site parameters; pH, *Eh*, temperature, alkalinity and conductivity obtained from Bowden Close site are presented and discussed in this section. Also presented and discussed are the voltammetric results showing dissolved and colloidal iron concentrations across the site.

6.2.1: On-site results

Monthly samples were collected from five different sampling points namely: RAPS 1 inlet, RAPS 2 inlet, RAPS 1 outlet, RAPS 2 outlet and wetland outlet (endpoint) between March 2006-April 2007 at the Bowden Close site. During sample collection, water quality parameters including temperature, pH, *Eh*, electrical conductivity (E.C) and alkalinity were measured in on-site (table 6.1) including various electrochemically determined iron fractions; total, dissolved, solid phase and colloidal iron (Table 6.3). Table 6.2 shows the mean chemical characteristics of the water quality at the sampling stations over 14 months sampling period. Temporal and season trends and relationships between the measured geochemically significant on-site parameters that are likely to affect iron concentrations in each RAPS are presented in figures 6.4 to 6.13. These geochemically significant parameters include pH, *Eh* and alkalinity.

These three parameters are geochemically important due to the significant roles they play in determining the fate of iron geochemistry within the mine-water systems. For examples, water pH is a good and useful indicator of the chemical balance in water, presents the balance between H^+ and OH^- and describes the acidity or alkalinity of water. The importance and influence of pH in controlling the redox processes in natural environments have been highlighted by several authors [e.g., 15, 16]. Water alkalinity describes how well water recovers from acidic punch, expressed as mg L^{-1} of $CaCO_3$ because $CaCO_3$ is a good acid neutraliser. So, water with low alkalinity has low capacity to neutralise or buffer incoming acids, thus susceptible to acidic pollution. In addition, sufficient alkalinity in water protects aquatic life against rapid

changes in pH. Water redox potential (*Eh*) is geochemically important as it provides information about general oxidising or reducing characteristics of water environment.

RAPS 1 treatment system at Bowden Close site.

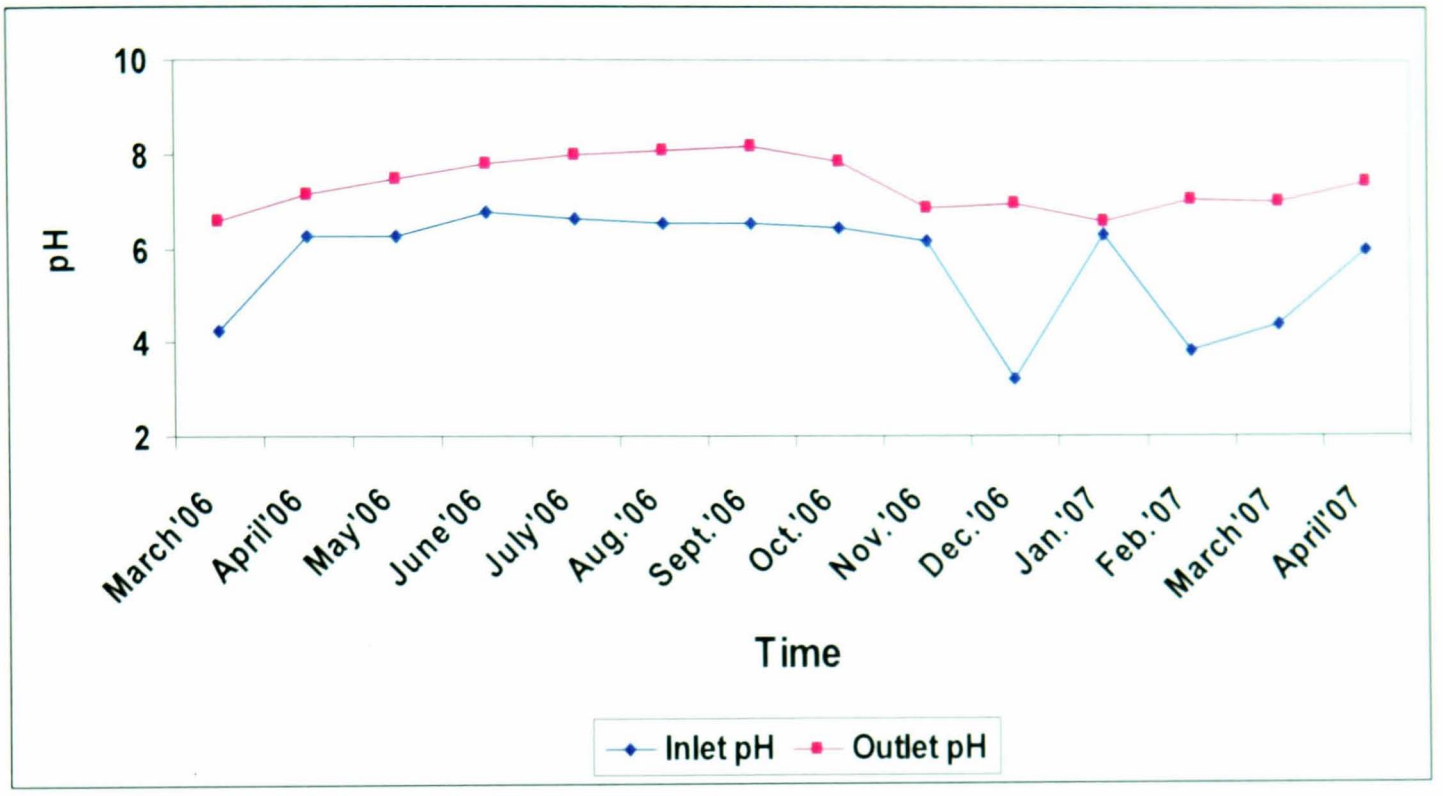

Figure 6.4: Showing the temporal trend and variation in the measured inlet and outlet pH at RAPS 1 treatment system at Bowden Close site, over the sampling period (March 2006-April 2007).

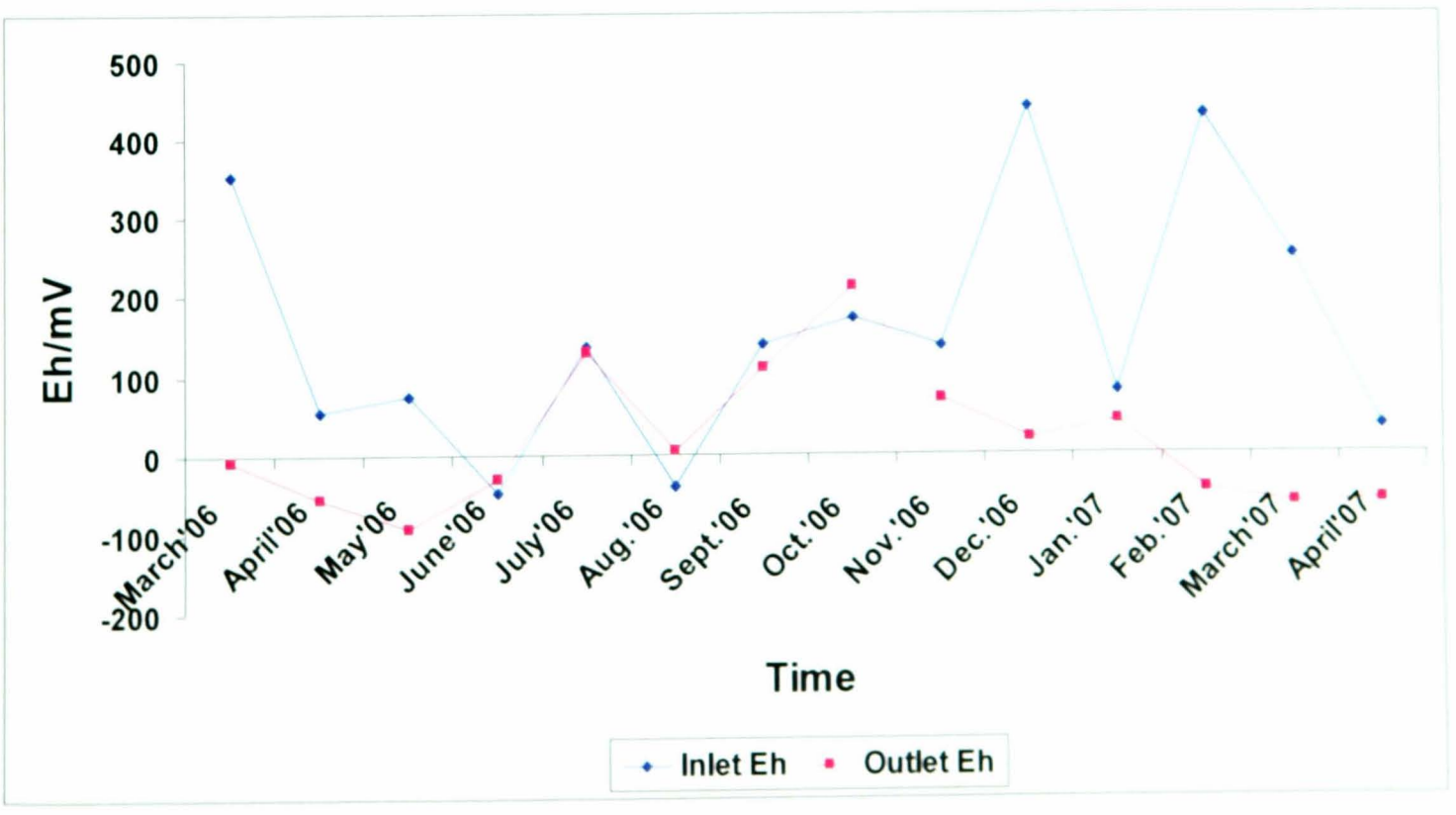

Figure 6.5: Measured *Eh* as a function of time (monthly sampling) from March 2006-April 2007 at RAPS 1 for inlet and outlet water samples at Bowden Close site.

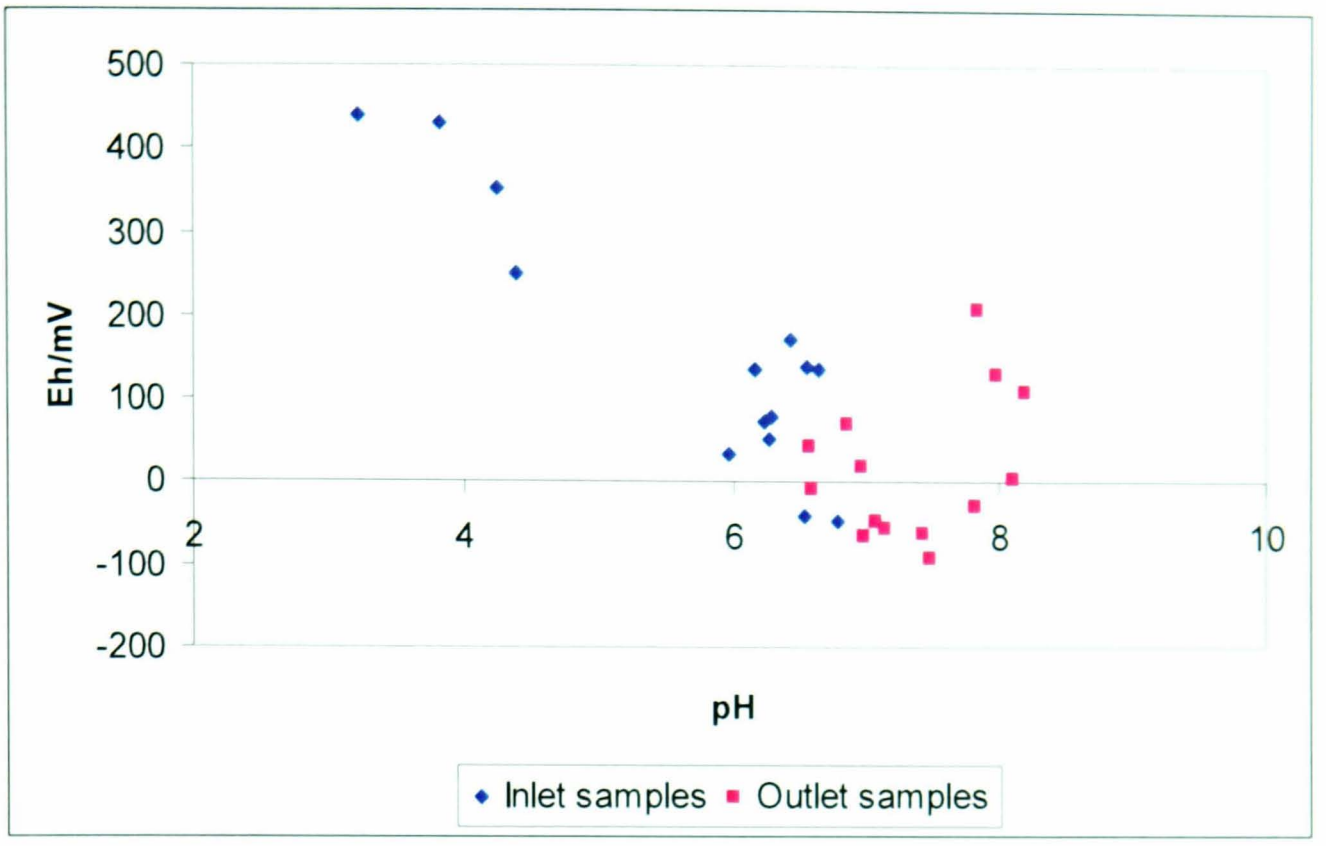

Figure 6.6: Measured *Eh* as a function of pH for inlet and outlet samples taken from March 2006-April 2007 at RAPS 1 treatment system at Bowden Close site. The least square regression equation is: *Eh*=-118.63* pH + 832.28 and R^2=0.82.

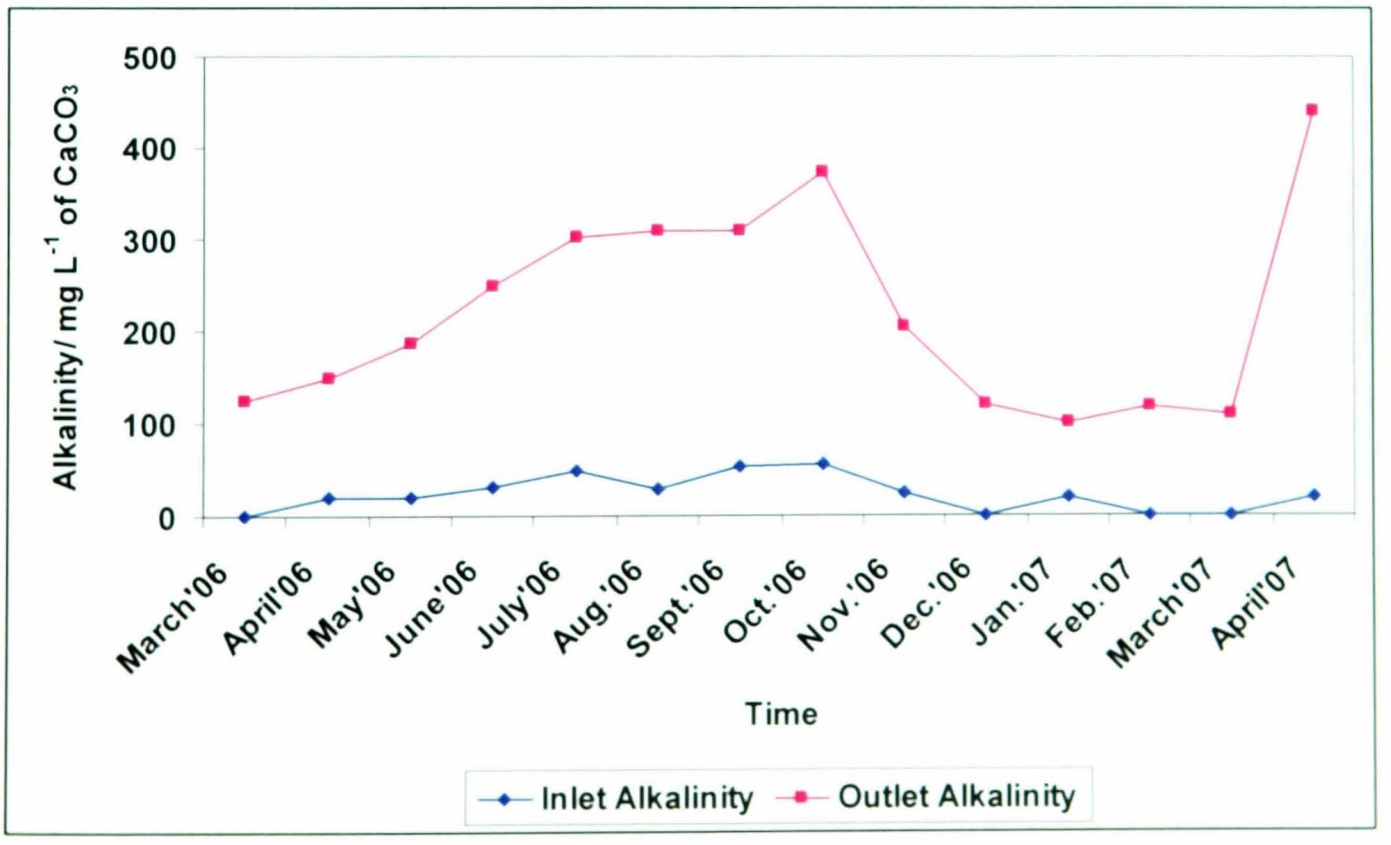

Figure 6.7: Showing the temporal trend and variation in the measured inlet and outlet alkalinity at RAPS 1 treatment system at Bowden Close site, over the sampling period (March 2006-April 2007).

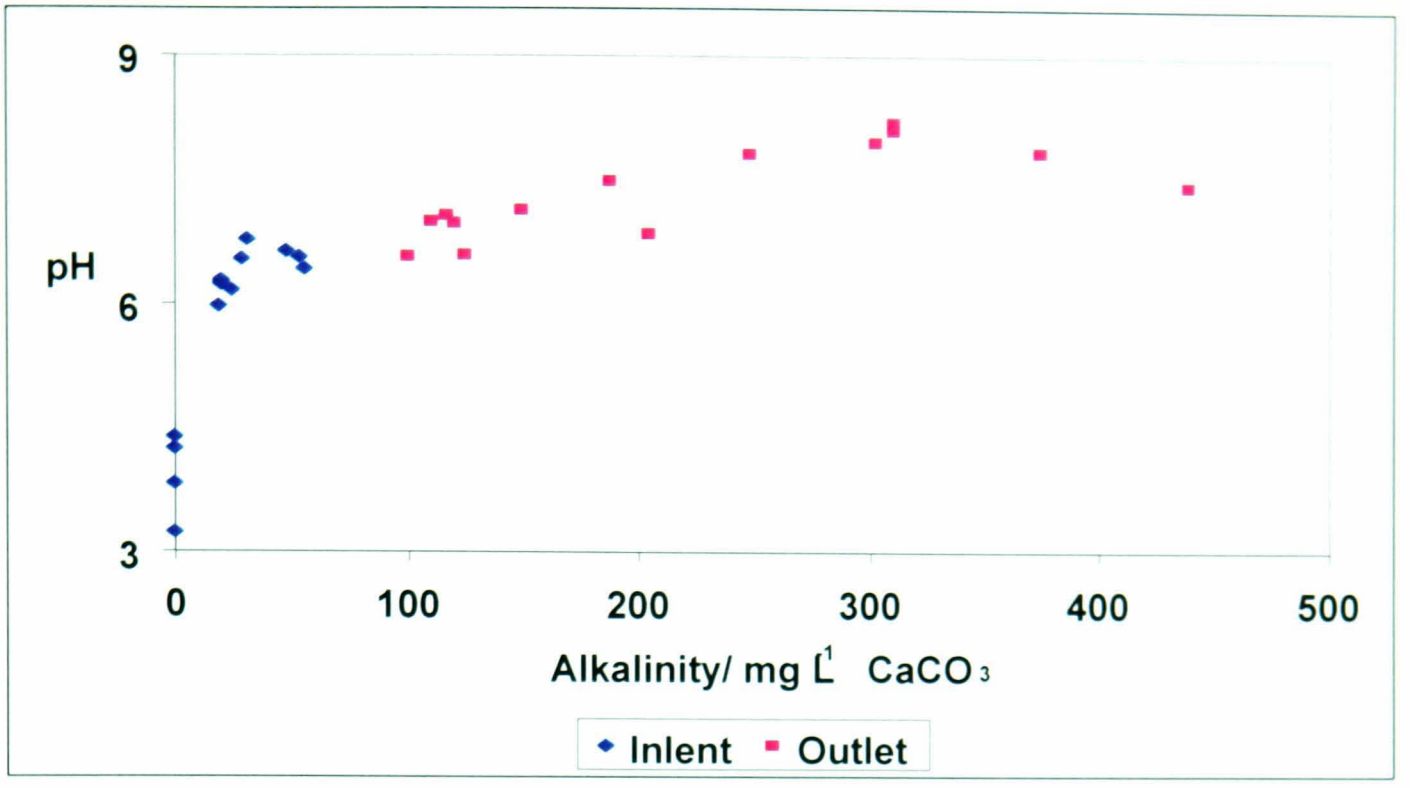

Figure 6.8: Showing the relationship between pH and alkalinity for inlet and outlet samples taken from March 2006-April 2007 at RAPS 1 treatment system at Bowden Close site. The least square regression equation is: pH= 0.05*Alkalinity + 4.54 and R^2=0.65.

RAPS 2 treatment system at Bowden Close site.

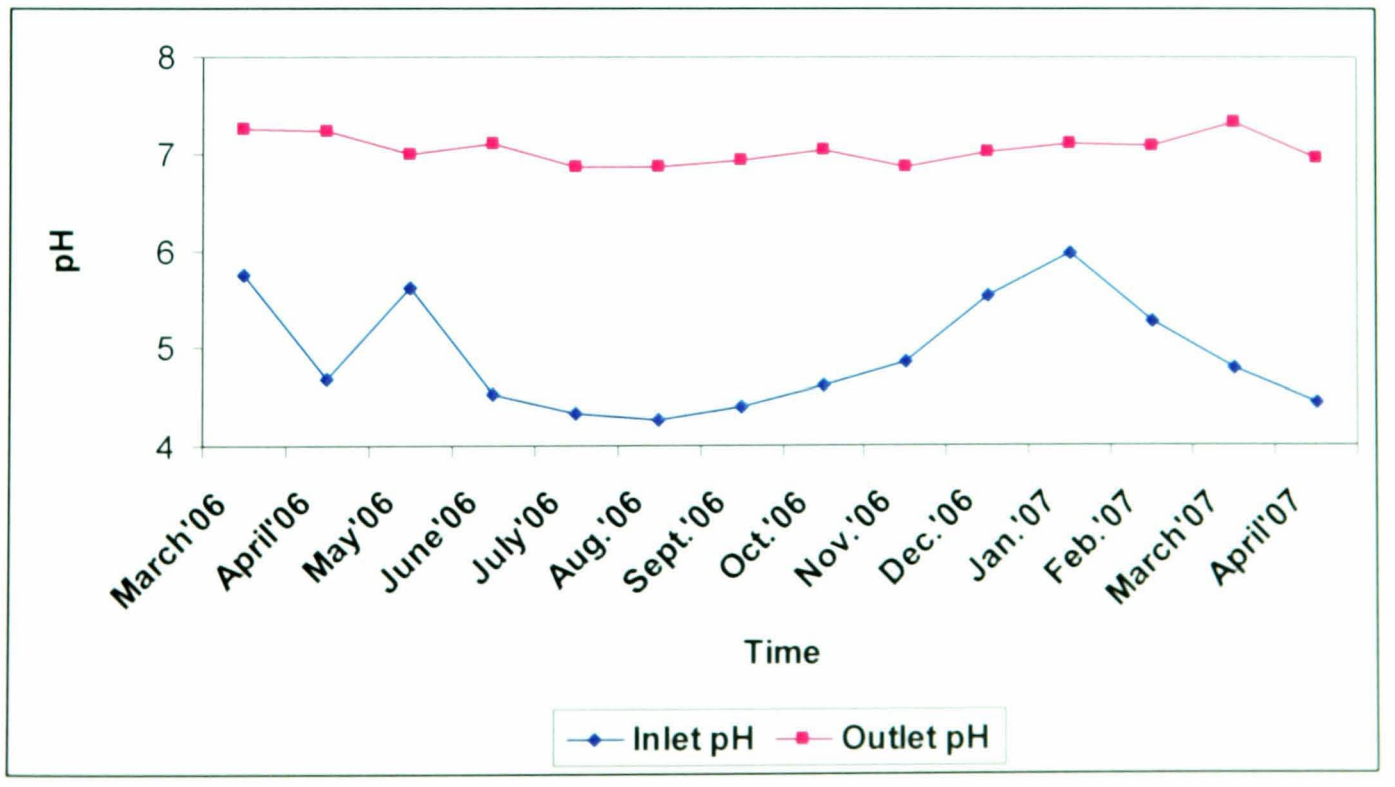

Figure 6.9: Showing the temporal trend and variation in the measured inlet and outlet pH at RAPS 2 treatment system at Bowden Close site, over the sampling period (March 2006-April 2007).

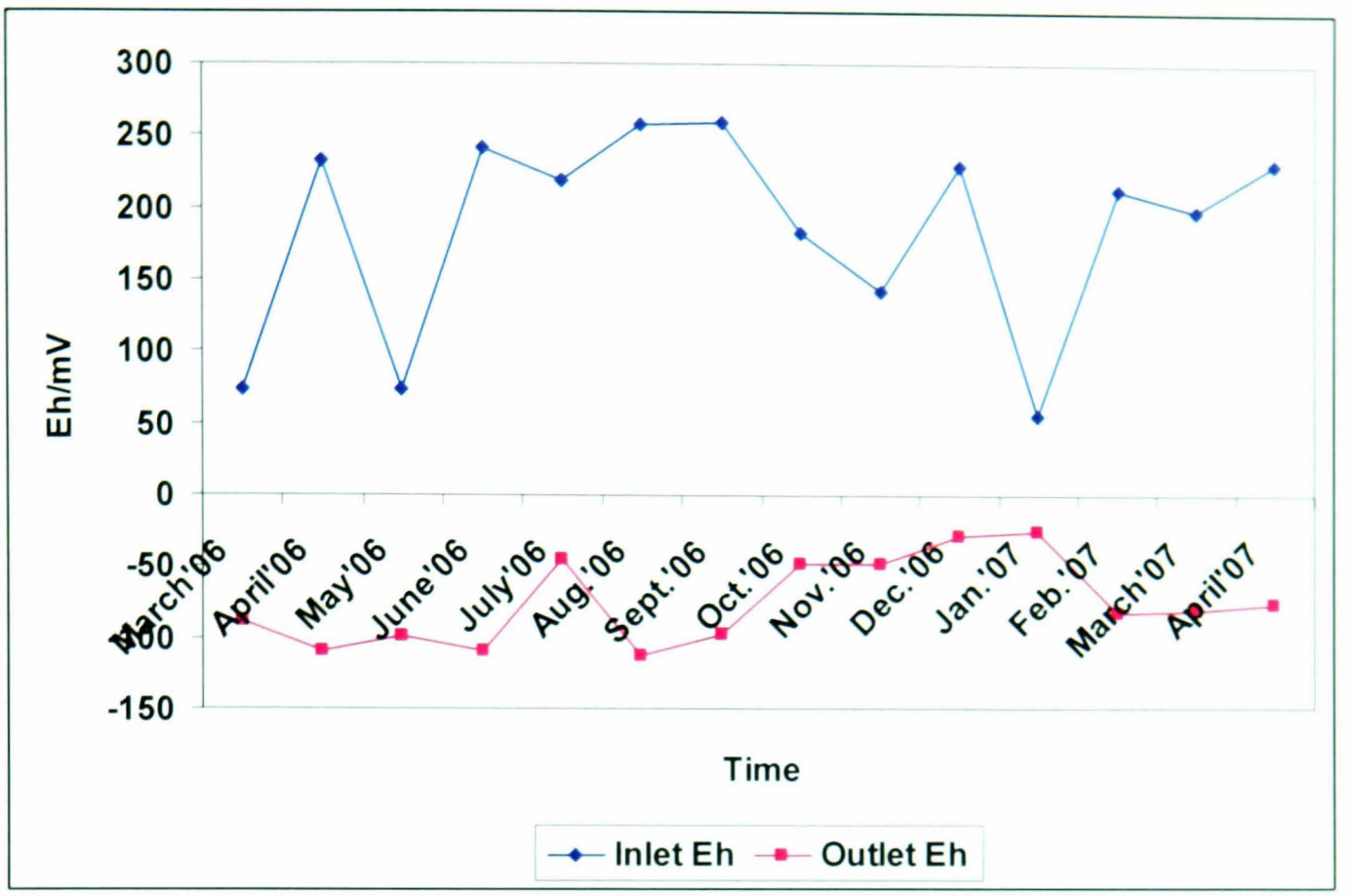

Figure 6.10: Measured *Eh* as a function of time (monthly sampling) from March 2006-April 2006 at RAPS 2 for inlet and outlet water samples at Bowden Close site.

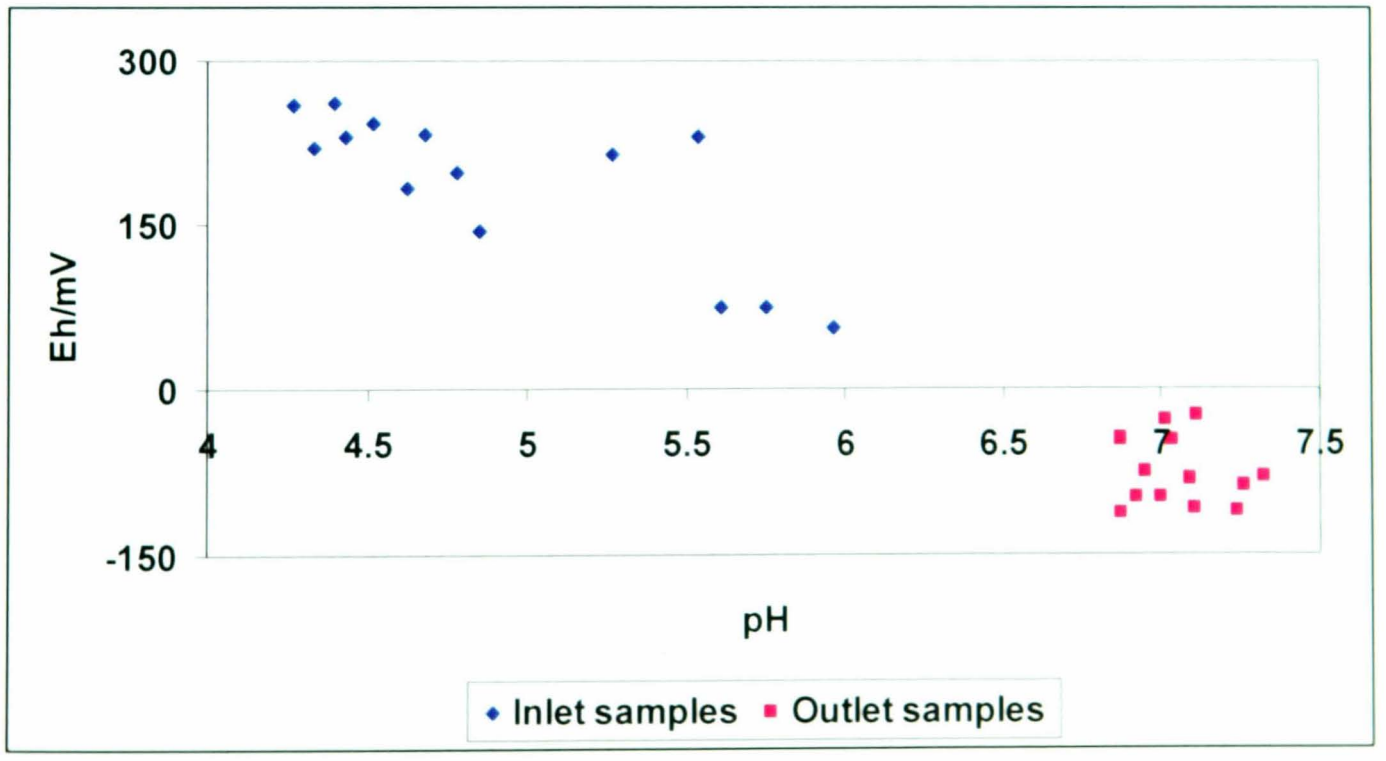

Figure 6.11: Measured Eh as a function of pH for inlet and outlet samples taken from March 2006-April 2007 at RAPS 2 treatment system at Bowden Close site. The least square regression equation is: Eh=-98.41* pH + 671.56 and R^2=0.64.

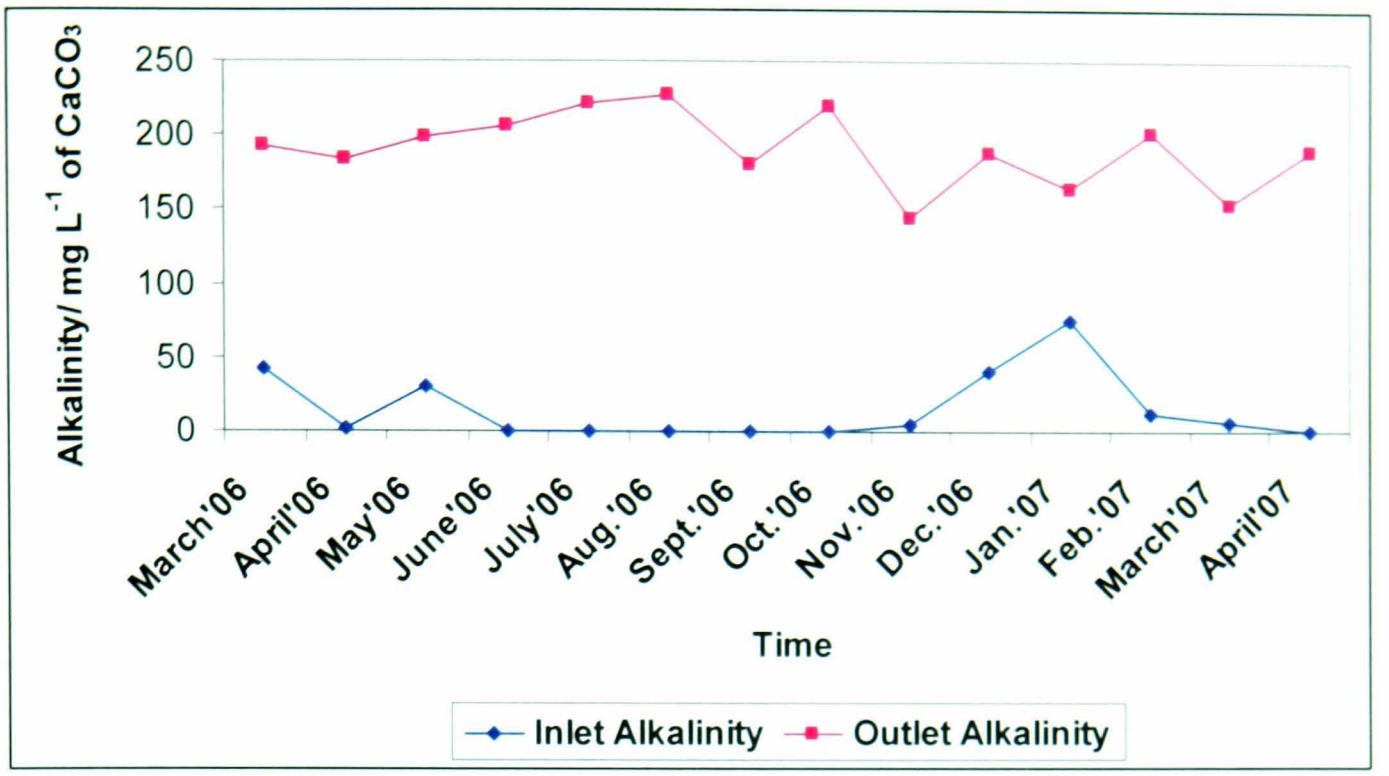

Figure 6.12: Showing the temporal trend and variation in the measured inlet and outlet alkalinity at RAPS 2 treatment system at Bowden Close site, over the sampling period (March 2006-April 2007).

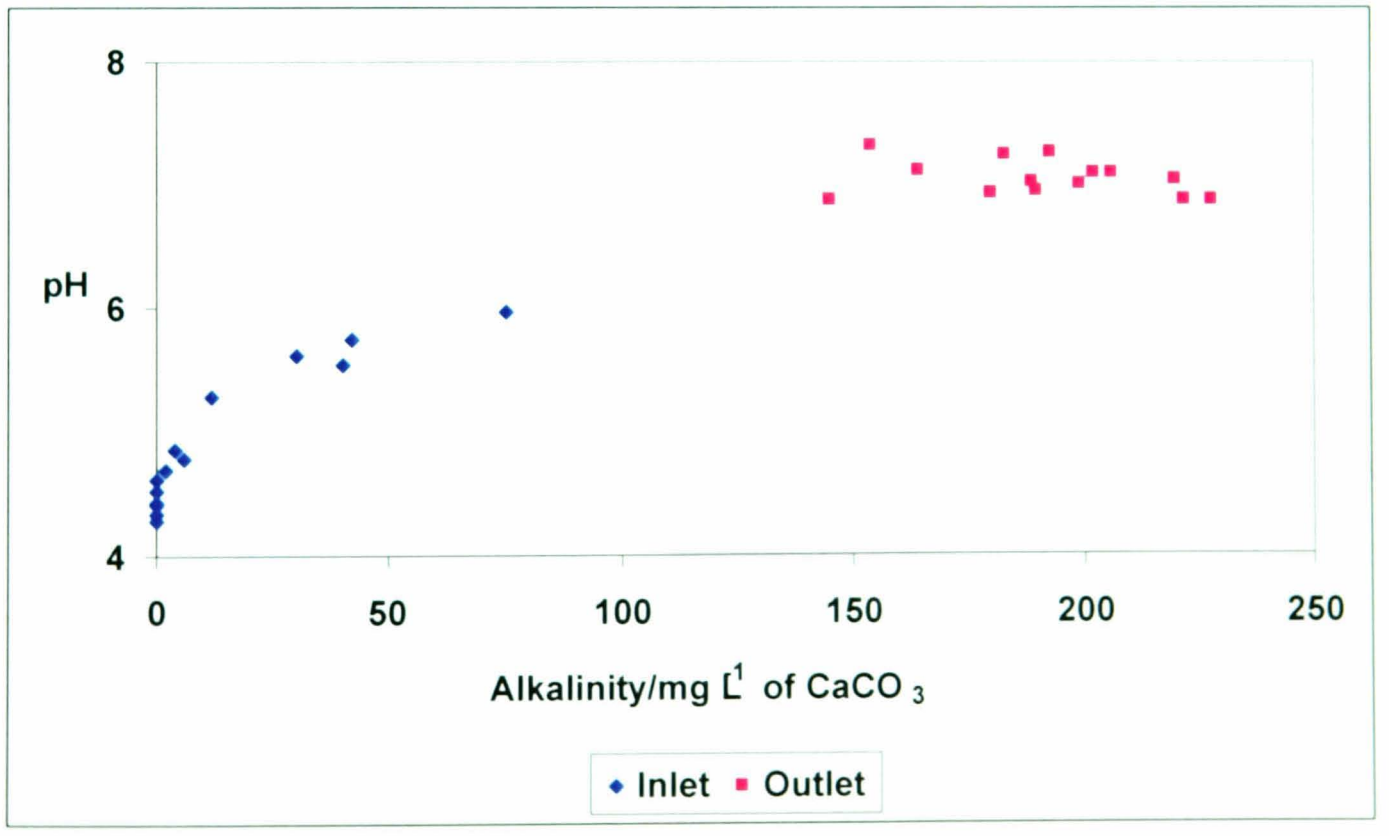

Figure 6.13: Showing the relationship between pH and alkalinity for inlet and outlet samples taken from March 2006-April 2007 at RAPS 2 treatment system at Bowden Close site. The least square regression equation is: pH=0.02*Alkalinity + 4.58 and R^2=0.84.

Table 6.1: Water quality parameters determined at various sampling points at Bowden Close treatment system from March 2006-April 2007.

Dates	Sample	pH	*K* (μS cm^{-1})	Alkalinity mg L^{-1} $CaCO_3$)	*Eh*/mV	T/°C
	Source Point	NA	NA	NA	NA	NA
30-Marchl'06	RAPS1 inlet	4.25	628	0	352	7.10
	RAPS2 inlet	5.75	768	42	73	7.50
	RAPS1 effluent	6.60	797	125	-7	7.50
	RAPS2 effluent	7.26	1066	193	-89	7.90
	End point	7.14	717	17	-55	8.80
	Source Point	NA	NA	NA	NA	NA
25-April'06	RAPS1 inlet	6.27	795	20	53	10.4
	RAPS2 inlet	4.68	1704	2	233	9.5
	RAPS1 effluent	7.14	964	149	-56	10.5
	RAPS2 effluent	7.24	1771	183	-110	12.0
	End point	6.83	1433	48	4	13.6
	Source Point	NA	NA	NA	NA	NA
18-May'06	RAPS1 inlet	6.24	749	20	73	9.50
	RAPS2 inlet	5.61	950	30	73	9.50
	RAPS1 effluent	7.49	864	187	-92	12.3
	RAPS2 effluent	7.00	1623	199	-99	13.4
	End point	6.85	968	45	-8	16.0
	Source Point	NA	NA	NA	NA	NA
19-June'06	RAPS1 inlet	6.79	778	31	-47	10.5
	RAPS2 inlet	4.52	2009	0	242	10.1
	RAPS1 effluent	7.81	966	248	-30	15.3
	End point	7.14	1734	144	-24	18.6
10-July'06	RAPS1 inlet	6.64	819	48	136	11.5
	RAPS2 inlet	4.33	2278	0	219	10.2
	RAPS1 effluent	7.97	961	302	130	15.1
	RAPS2 effluent	6.87	2434	222	-45	18.8
	End point	6.90	2152	156	165	17.5
	Source Point	NA	NA	NA	NA	NA
14-Aug.'06	RAPS1 inlet	6.54	1016	29	-40	13.3
	RAPS2 inlet	4.27	2327	0	258	10.2
	RAPS1 effluent	8.10	1016	310	4	14.1
	RAPS2 effluent	6.87	2625	228	-112	16.4
	End point	7.30	2299	186	-36	14.0

Table 6.1 continued

Dates	Sample	pH	*K* (µS cm^{-1})	Alkalinity mg L^{-1} $CaCO_3$)	*Eh*/mV	*T*/°C
	RAPS2 inlet	4.40	2526	0	260	10.4
	RAPS1 effluent	8.19	1022	310	108	15.9
	RAPS2 effluent	6.92	2582	180	-98	16.8
	End point	7.49	2421	150	-38	15.6
	Source Point	NA	NA	NA	NA	NA
17-Oct.'06	RAPS1 inlet	6.43	984	56	172	12.2
	RAPS2 inlet	4.62	2287	0	183	10.2
	RAPS1 effluent	7.84	1083	374	210	12.1
	RAPS2 effluent	7.03	2230	220	-48	13.0
	End point	7.40	1966	166	1	12.4
14-Nov.'06	RAPS1 inlet	6.16	957	25	136	11.1
	RAPS1 effluent	6.86	1053	204	69	7.40
	End point	7.01	1361	103	21	6.80
	Source Point	NA	NA	NA	NA	NA
11-Dec.'06	RAPS1 inlet	3.23	1033	0	439	8.80
	RAPS2 inlet	5.54	835	40	230	9.10
	RAPS1 effluent	6.97	888	120	19	5.70
	RAPS2 effluent	7.01	1055	189	-29	7.10
	End point	7.02	772	51	-18	6.70
	Source Point	NA	NA	NA	NA	NA
4-Jan.'07	RAPS1 inlet	6.29	380	20	80	5.80
	RAPS2 inlet	5.96	622	75	55	6.80
	RAPS1 effluent	6.57	866	100	42	5.80
	RAPS2 effluent	7.11	1108	164	-25	7.30
	End point	6.66	606	46	5	4.90
	Source Point	NA	NA	NA	NA	NA
20-Feb.'07	RAPS1 inlet	3.82	879	0	431	7.80
	RAPS2 inlet	5.27	1094	12	213	8.40
	RAPS1 effluent	7.07	925	117	-46	5.50
	RAPS2 effluent	7.09	1294	202	-82	6.60
	End point	6.56	959	45	15	7.30
	Source Point	NA	NA	NA	NA	NA
13-March'07	RAPS1 inlet	4.40	820	0	251	8.10
	End point	5.91	1261	20	84	7.70
24-April'07	RAPS1 inlet	5.97	844	19	35	8.80
	RAPS2 inlet	4.43	2040	0	231	9.70
	RAPS1 effluent	7.43	1483	439	-61	10.1
	RAPS2 effluent	6.95	2158	190	-76	11.5
	End point	6.83	1846	113	-4	13.9

Table 6.2: Mean water quality parameters determined at various sampling points across Bowden Close treatment site from March 2006-April 2007(where n=14).

Sample	pH	*K* ($\mu S\ cm^{-1}$)	Alkalinity mg L^{-1} $CaCO_3$)	*Eh*(mV)	*T*/°C
Source Point	NA	NA	NA	NA	NA
RAPS1 inlet	5.80	852.0	24.8	142.9	10.1
RAPS2 inlet	4.87	1696	13.0	195.2	9.45
RAPS1 effluent	7.42	1005	228	17.9	10.5
RAPS2 effluent	7.03	1851	191	-74.0	12.1
End point	6.92	1521	97.9	12.9	11.9

* NA- not applicable (sample not taken), BC-Bowden Close.

Table 6.3: Proportion of various Iron fractions determined electrochemically at various points at Bowden Close system from March 2006-April 2007. All measurements are in mg L^{-1}.

Dates	Sampling points	Total Fe	Dissolved Fe	Solid Phase Fe	Colloidal Fe
		mg L^{-1}	mg L^{-1}	mg L^{-1}	mg L^{-1}
	Source Point	36.3	29.6	3.86	2.81
30-Marchl'06	RAPS1 inlet	26.3	20.4	4.17	1.75
	Within RAPS1	20.8	11.9	7.41	1.52
	RAPS2 inlet	33.4	27.2	4.19	2.03
	Within RAPS2	27.8	16.2	9.05	2.56
	RAPS1 effluent	4.89	3.23	1.44	0.22
	RAPS2 effluent	15.1	8.55	4.95	1.64
	Within Wetland	19.3	8.70	6.87	3.69
	End point	19.6	8.13	6.67	4.76
	Upstream river	4.98	1.08	2.31	1.59
	Downstream river	9.34	3.10	4.36	1.88
	Source Point	34.5	23.1	10.4	1.06
25-April'06	RAPS1 inlet	24.6	14.6	6.36	3.64
	Within RAPS1	24.4	13.1	8.45	2.81
	RAPS2 inlet	75.8	58.4	13.1	4.30
	Within RAPS2	35.0	19.2	9.63	6.11
	RAPS1 effluent	3.99	0.89	1.51	1.57
	RAPS2 effluent	8.55	2.06	4.03	2.46
	Within Wetland	29.5	8.53	14.2	6.74
	End point	5.64	1.30	2.85	1.49
	Upstream river	3.07	1.07	1.71	0.29
	Downstream river	3.93	0.93	2.03	0.97
	Source Point	13.0	8.40	3.15	1.42
18-May'06	RAPS1 inlet	14.2	10.4	2.54	1.25
	Within RAPS1	16.4	6.32	8.27	1.82
	RAPS2 inlet	31.3	25.7	3.40	2.22
	Within RAPS2	35.8	16.0	12.3	7.56
	RAPS1 effluent	3.09	1.24	1.73	0.12
	RAPS2 effluent	4.68	1.31	2.71	0.66
	Within Wetland	33.9	12.3	14.6	7.06
	End point	18.6	4.67	10.6	3.33
	Upstream river	0.90	0.90	0.00	0.00
	Downstream river	1.91	1.46	0.45	0.00
	Source Point	14.2	9.57	3.22	1.45
19-June'06	RAPS1 inlet	19.6	14.1	3.82	1.64

Table 6.3 continued.

Dates	Sampling points	Total Fe	Dissolved Fe	Solid Phase Fe	Colloidal Fe
	Within RAPS1	18.9	9.18	7.04	2.68
	RAPS2 inlet	92.2	74.1	11.6	6.49
	Within RAPS2	59.3	39.1	14.7	5.56
	RAPS1 effluent	4.6	1.26	2.36	0.94
	RAPS2 effluent	8.18	3.54	3.35	1.29
	Within Wetland	9.93	0.72	4.94	4.27
	End point	1.30	0.19	0.74	0.37
	Upstream river	0.75	0.57	0.18	0.00
	Downstream river	1.50	0.00	1.44	0.06
	Source Point	14.4	11.68	1.61	1.15
10-July'06	RAPS1 inlet	21.2	15.31	3.33	2.59
	Within RAPS1	19.9	7.76	9.26	2.88
	RAPS2 inlet	105	69.9	19.8	15.6
	Within RAPS2	46.3	8.07	23.7	14.5
	RAPS1 effluent	7.89	1.86	3.81	2.22
	RAPS2 effluent	12.0	5.18	4.27	2.58
	Within Wetland	11.6	1.01	8.48	2.09
	End point	1.10	0.00	0.83	0.27
	Upstream river	0.53	0.53	0.00	0.00
	Downstream river	1.88	0.57	0.94	0.37
	Source Point	12.9	8.44	3.58	0.85
14-Aug.'06	RAPS1 inlet	8.08	6.57	1.39	0.12
	Within RAPS1	7.04	0.98	4.92	1.14
	RAPS2 inlet	98.1	72.8	17.7	7.58
	Within RAPS2	88.5	40.1	36.5	12.0
	RAPS1 effluent	7.23	1.35	3.54	2.34
	RAPS2 effluent	14.9	5.65	4.48	4.82
	Within Wetland	16.2	3.15	7.82	5.18
	End point	1.12	0.00	0.74	0.38
	Upstream river	0.68	0.68	0.00	0.00
	Downstream river	1.10	1.10	0.00	0.00
	Source Point	17.4	9.18	4.64	3.70
14-Sept.'06	RAPS1 inlet	6.12	3.52	1.55	1.05
	Within RAPS1	3.73	1.21	1.19	1.33
	RAPS2 inlet	117	70.44	29.5	16.6
	Within RAPS2	85.2	38.0	39.1	8.11
	RAPS1 effluent	1.99	0.44	0.16	1.39
	RAPS2 effluent	11.1	5.39	3.59	2.12
	Within Wetland	17.2	3.55	9.65	4.01
	End point	1.11	0.00	0.37	0.74

Table 6.3 continued.

Dates	Sampling points	Total Fe	Dissolved Fe	Solid Phase Fe	Colloidal Fe
	Upstream river	2.60	1.60	1.00	0.00
	Downstream river	2.55	0.00	1.06	1.49
	Source Point	11.3	7.08	2.66	1.56
17-Oct.'06	RAPS1 inlet	6.53	2.88	2.25	1.40
	Within RAPS1	4.10	0.20	3.35	0.55
	RAPS2 inlet	98.5	82.5	9.15	6.87
	Within RAPS2	40.5	15.1	17.7	7.71
	RAPS1 effluent	4.73	1.51	2.16	1.06
	RAPS2 effluent	8.96	2.11	4.81	2.04
	Within Wetland	8.37	2.89	3.88	1.60
	End point	1.44	0.00	0.64	0.80
	Upstream river	3.77	0.57	1.60	1.60
	Downstream river	3.61	0.29	2.16	1.16
	Source Point	39.7	31.6	4.42	3.67
14-Nov.'06	RAPS1 inlet	12.6	7.69	3.09	1.83
	Within RAPS1	13.9	3.15	6.33	4.44
	RAPS2 inlet	85.8	65.9	12.4	7.53
	Within RAPS2	41.9	12.8	20.4	8.67
	RAPS1 effluent	5.79	1.67	2.63	1.49
	RAPS2 effluent	6.97	1.48	3.54	1.95
	Within Wetland	17.8	4.17	10.2	3.41
	End point	2.67	0.25	1.25	1.17
	Upstream river	1.64	0.00	0.86	0.78
	Downstream river	1.26	0.00	0.27	0.99
	Source Point	13.4	6.47	3.65	3.30
11-Dec.'06	RAPS1 inlet	24.4	19.7	3.25	1.51
	Within RAPS1	14.0	5.95	6.59	1.46
	RAPS2 inlet	17.7	12.0	3.28	2.40
	Within RAPS2	30.0	9.24	14.1	6.73
	RAPS1 effluent	2.86	0.22	1.39	1.25
	RAPS2 effluent	3.45	0.67	1.82	0.96
	Within Wetland	26.4	11.7	9.76	4.99
	End point	6.20	2.45	2.64	1.11
	Upstream river	3.10	0.28	1.41	1.41
	Downstream river	4.26	1.06	1.60	1.60
	Source Point	14.7	8.34	4.31	2.08
4-Jan.'07	RAPS1 inlet	5.13	3.53	0.68	0.92
	Within RAPS1	11.12	4.40	4.45	2.27
	RAPS2 inlet	13.6	7.74	3.71	2.13
	Within RAPS2	5.92	0.76	3.63	1.53

Table 6.3 continued.

Dates	Sampling points	Total Fe	Dissolved Fe	Solid Phase Fe	Colloidal Fe
	RAPS1 effluent	4.08	1.16	2.13	0.79
	RAPS2 effluent	1.78	0.85	0.63	0.30
	Within Wetland	21.7	6.29	11.4	4.05
	End point	9.75	2.83	4.77	2.15
	Upstream river	1.99	0.58	0.98	0.43
	Downstream river	3.08	0.78	1.44	0.86
	Source Point	13.7	8.73	2.75	2.24
20-Feb.'07	RAPS1 inlet	23.1	14.3	5.92	2.94
	Within RAPS1	17.8	6.75	7.38	3.65
	RAPS2 inlet	35.4	24.5	6.44	4.43
	Within RAPS2	11.8	3.81	5.32	2.66
	RAPS1 effluent	3.82	0.94	1.79	1.09
	RAPS2 effluent	2.41	0.32	0.63	1.46
	Within Wetland	12.7	2.02	7.48	3.15
	End point	11.8	2.33	5.95	3.49
	Upstream river	2.20	0.96	1.24	0.00
	Downstream river	3.25	1.39	0.59	1.27
	Source Point	11.0	6.59	3.22	1.22
13-March'07	RAPS1 inlet	25.6	19.8	4.33	1.46
	Within RAPS1	23.4	6.03	14.3	3.08
	RAPS2 inlet	65.4	36.4	16.8	12.2
	Within RAPS2	42.1	12.2	21.7	8.27
	RAPS1 effluent	3.43	0.20	1.79	1.44
	RAPS2 effluent	1.34	0.00	0.51	0.83
	Within Wetland	18.1	4.80	11.63	1.71
	End point	9.6	3.67	4.63	1.29
	Upstream river	1.39	0.49	0.14	0.76
	Downstream river	3.18	1.41	0.23	1.54
	Source Point	17.8	12.0	3.69	2.19
24-April'07	RAPS1 inlet	29.7	20.5	6.08	3.13
	Within RAPS1	31.4	18.1	8.63	4.73
	RAPS2 inlet	91.1	73.9	10.4	6.85
	Within RAPS2	7.45	1.75	4.23	1.47
	RAPS1 effluent	3.75	0.72	1.02	2.01
	RAPS2 effluent	3.33	0.67	0.89	1.77
	Within Wetland	9.19	3.31	3.36	2.52
	End point	2.54	0.60	0.00	1.94
	Upstream river	1.35	0.24	0.29	0.82
	Downstream river	3.24	1.22	0.00	2.02

Figure 6.4 shows that outlet water pH from RAPS 1 treatment system is consistently higher than the pH of the inlet water whilst the outlet water pH appeared stable at circumneutral pH of 7, inlet water pH varied widely between 3 and 6. This trend in inlet and outlet water pHs is not surprising and it shows that water acidity has been reduced as it passes through the RAPS system. Similarly, pH profile of RAPS 2 treatment system follows the same trend as that of RAPS 1 where outlet pHs appeared stable and consistently higher than the inlet pHs over the sampling period (figure 6.6). Whilst the inlet pHs varied from 4.27 in August 2006 to 5.96 in January 2007, reflecting water quality variations, outlet pHs are mostly greater than 7, showing that the water quality has improved through neutralisation of acidity by the RAPS system. The pH of influent samples (table 6.1) varied widely because of varying level of oxidation and dissolution of sulphide minerals e.g., pyrites (Fe_2S) and the concentration of dissolved metals. In general, influent water pH is controlled by the degree of acidity generated during the oxidation and dissolution of pyrite, where reaction with oxygen and water results in the release of ferrous iron and proton acidity [13] as shown in these equations:

$$2FeS_2 + 7O_2 + 2H_2O \dashrightarrow 2Fe^{2+} + 4SO_4^{2-} + 4H^+ \quad (1)$$

Oxidation of ferrous iron produced in equation (1) results in the formation of ferric ion (Fe^{3+}) which may generate eight times as much proton acidity (H^+) as equation (1) under the right conditions. Ferric ion directly oxidizes iron pyrite (Fe_2S) in the presence of water (equation 2).

$$FeS_2 + 14Fe^{3+} + 8H_2O \dashrightarrow 15Fe^{2+} + 2SO_4^{2-} + 16H^+ \quad (2)$$

The reaction in equation 2 is faster at low pH where the solubility of ferric iron is greatest [13]. Whereas, effluent pH was more stable and probably controlled by the geological formation and concentration of dissolved carbon dioxide confined in the aquifer.

RAPS 1 Eh profile as shown in figure 6.5 indicates that the *Eh* for effluent samples is significantly lower than that of the influent samples. Influent *Eh* varies from -40 to 539 mV, whereas, effluent Eh ranged from -7 to 210 mV. This observation reveals the oxidising characteristics of the environment of the influent samples and the reduced environment that characterised the effluent samples. Lower influent *Ehs* for the months of June and August (-47 and -40 mV respectively) could be attributed to elevated water pH (6.79 and 6.54 respectively-figure 6.4 & table 6.1) during these

months. Effluent water *Eh* also appeared stable for February-April 2007 sampling period due to similar pH. Relationship between the observed temporal trends and variability of *Eh*-pH and the implication for the control iron geochemistry at this site is fully discussed in section 6.2.2. In general, acidic mine-water has higher *Eh* due to the dissolution of pyrite mineral leading to the generation of proton [18]. The temporal *Eh* of the inlet and outlet samples for RAPS 2 treatment shows similar trend (figure 6.10) for the same reasons stated above. In RAPS 2, the inlet *Eh* appeared to vary very widely, ranged from 55 to 260 mV whereas, the outlet Eh appeared to be stable and varies from -112 to -25 mV. However in general, in a complex water bodies like mine-water systems, apart from pyrite oxidation and dissolution that can lead to proton generation, depressed pH and high *Eh* values, in addition, *Eh* and pH values are also influenced by the combined effects of the carbon dioxide system, the boric acid system and various organic acids with the water body [17] and the particular controlling reactions are difficult to identify to know the effects on the ability of the environment to maintain its *Eh* and pH in the presence of foreign materials [17].

Electrical conductivity profile shows that effluent conductivity is higher (1500 $\mu s\ cm^{-1}$) than the RAPS 1 inlet (800 $\mu s\ cm^{-1}$) but lower than the RAPS 2 inlet (1700 $\mu s\ cm^{-1}$) (table 6.1). Since electrical conductivity is related to the concentration of dissolved solid (DS) in the water, it can provide an estimate of the total dissolved solid (TDS) concentration in water. These materials (natural and anthropogenic) are mainly inorganic solutes with a small amount of organic materials, depending on the water type. In addition, sulphate and specific conductivity measurements have traditionally been used as indicators of mine-water contamination in surface and ground water [14]. Thus, table 6.1 shows that RAPS 2 has more total dissolved solids (TDS) and is more contaminated than RAPS1 and that effluent samples have less sulphate, total dissolve solid and contamination than RAPS 2 but higher than RAPS 1.

Measured *Eh* as a function of pH for both the inlet and outlet samples respectively at RAPS 1 treatment system shows that *Eh* values increases with decreasing pH and vice-versa (figure 6.3). The *Eh*-pH profile shows a rather complex trend (showing a strong linear correlation for the influent samples with R^2=0.82) but no correlation for the effluent samples with (R^2=0.13). In RAPS 2 treatment system, the *Eh*-pH profile

follows a similar trend to that observed in RAPS 1 though with a weak linear correlation for the inlet samples with R^2=0.64 and no correlation for the outlet samples with R^2=0.04 (figure 6.8). The weak correlation observed in RAPS 2 compared to RAPS 1 could be attributed to the poor water quality of RAPS 2 and it is more polluted than RAPS 1. However, in general, *Eh* tends to increase with increasing pH (with few exceptions) which shows that influent samples are in oxidised environment whilst effluent samples are in reduced environment. This observation is consistent with the fact that high *Eh* and low pH in the influent samples are probably controlled by the degree of acidity (H^+) generated during the oxidation and dissolution of pyrite. *Eh*-pH of effluent samples is poorly correlated probably due to reduced acidity of the effluent samples. Thus, we would expect to find a change from Fe^{2+} to Fe^{3+} or vice-versa depending on the shift in the pH or *Eh* of the environment.

Alkalinity trend for RAPS 1 treatment system shows very low alkalinity for the influent samples which varied from 0 to 56 mg L^{-1} of $CaCO_3$ whilst effluent samples show high degree of alkalinity which ranged from 100 to 439 mg L^{-1} of $CaCO_3$ (figure 4.7). This increased alkalinity of the effluent water samples show that the acidity of the influent samples has been neutralised as the water passes through the treatment system. In fact, influent alkalinity appeared stable over the sampling period which follows the pH trends observed during the same period. Sharp decreased in alkalinity observed in the effluent samples between December 2006 and March 2007 (120, 100, 117 and 110 mg L^{-1} of $CaCO_3$ respectively) is quite surprising and this observation could be attributed to a number of factors including sulphate and iron reduction leading to elevated pH. In addition, reduced rainfall event over the same period which could affect water flow rate through the RAPS system and affect water residence time in the RAPS and also the dilution from the rainfall. Secondly, reduced bacterial activities within the compost layer which would normally raise pH and generate alkalinity. Thirdly, reduced rate of limestone dissolution within the RAPS system which should further elevates the pH and generate more alkalinity. Although, rainfall data are not available to support this fact, however, previous studies on this site by Younger et al. [4, 5] have shown that there is a correlation between rainfall profile and water pH and water alkalinity.

The sudden jump in alkalinity from 110 mg L^{-1} of $CaCO_3$ in March 2007 to 439 mg L^{-1} of $CaCO_3$ in April 2007 could be due to water dilution through rainfall event which lead to elevated pH and increased alkalinity. Similarly, the temporal trend in alkalinity profile for RAPS 2 shows similar trend to that of RAPS 1, however at reduced values (particularly for the inlet samples) which reflect the poor and acidic nature of the inlet samples in this RAPS (figure 6.12). In fact, alkalinity for June 2006-November 2006 and April 2007 were 0 mg L^{-1} of $CaCO_3$ in these months which shows the acidic nature of this water during these months. The corresponding pHs measured during these months were also the lowest over the sampling period under discussion. However, alkalinity for the outlet samples showed marked increases varying from 154-222 mg L^{-1} of $CaCO_3$ which reflects elevated pHs of the outlet samples and also alkalinity. The trends observed in both inlet and outlet alkalinity could be attributed to the earlier explanation provided for the observed alkalinity trend in RAPS 1 treatment system.

The pH-alkalinity profile for RAPS 1 treatment system shows that alkalinity increases with increasing pH (figure 6.8). The correlation between pH and alkalinity for the inlet and outlet samples are very similar with R^2= 0.65 and 0.56 for both inlet and outlet samples respectively (fig. 6.8). In most cases, outlet samples attained pH > 7 with increasing alkalinity. This indicates that acidity has been neutralised and the outlet water has become net alkaline. Furthermore, previous work by [6] shows that alkalinity generation could be associated with sulphate removal due to microbial activities of the sulphate reducing bacterial (SRB), thus giving a rather complex and variable behaviour. As stated in the above paragraph, pH-alkalinity relationship is determined by complex biogeochemical processes of iron and sulphate reductions, coupled with pH elevation and $CaCO_3$ dissolution. Similar pH-alkalinity trend was observed in RAPS 2 treatment system (figure 6.13) for the same reasons as above. However, whilst pH-alkalinity for the inlet samples are strongly correlated with R^2=0.84, outlet pH-alkalinity profile show no correlation with R^2=0.10. Lack of correlation in the outlet samples is quite surprising as one would expect the outlet samples with elevated pH to show more correlation and this unexpected trend could only be attributed to the rather complex geochemistry occurring in the system as explained earlier.

6.2.2: Relationships between iron concentrations and the various measured parameters that controls iron geochemistry; *Eh*, pH and alkalinity

The purpose of this section is to establish whether there is any correlation or relationship between the measured geochemically significant water quality parameters (mainly pH, *Eh* and alkalinity) and electrochemically determined total iron concentrations that could help explain changes in equilibrium chemistry in the RAPS (1 & 2) systems and the final end point (particularly iron geochemistry which is the main focus of this research work) determined at the Bowden Close site. These relationships are presented figures 6.14 to 6.22. This section is aimed at establishing an understanding of the key processes in iron oxidation and reduction in the RAPS systems and the interactions between physical and geochemical mechanisms which underlie the passive treatment technology. The section focuses on identifying significant correlations and seasonal changes between electrochemically measured total iron concentrations influenced by changes in key geochemical parameters.

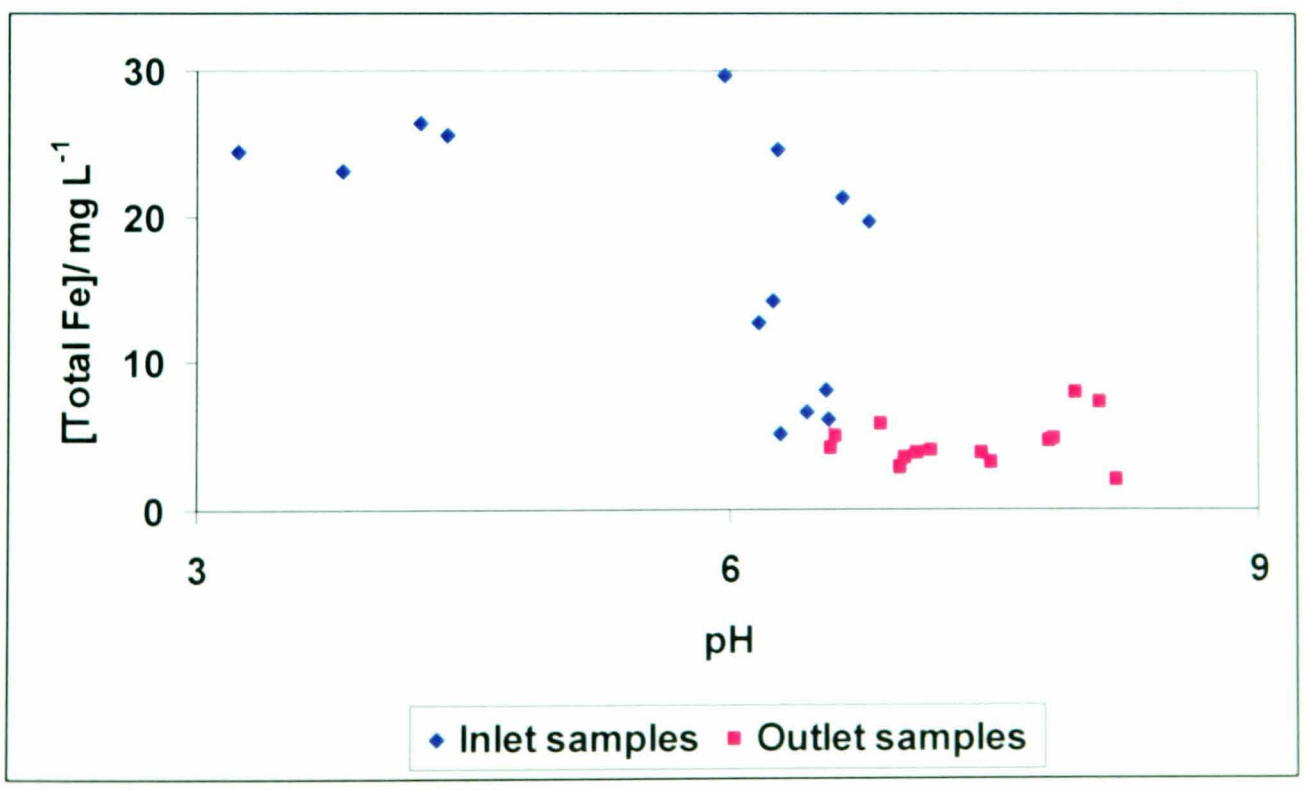

Figure 6.14: Total iron concentration as a function of pH for inlet and outlet samples taken from March 2006-April 2007 at RAPS 1 treatment system at Bowden Close site. The least square regression equation is: pH= -4.00* Fe + 40.4 and R^2=0.31.

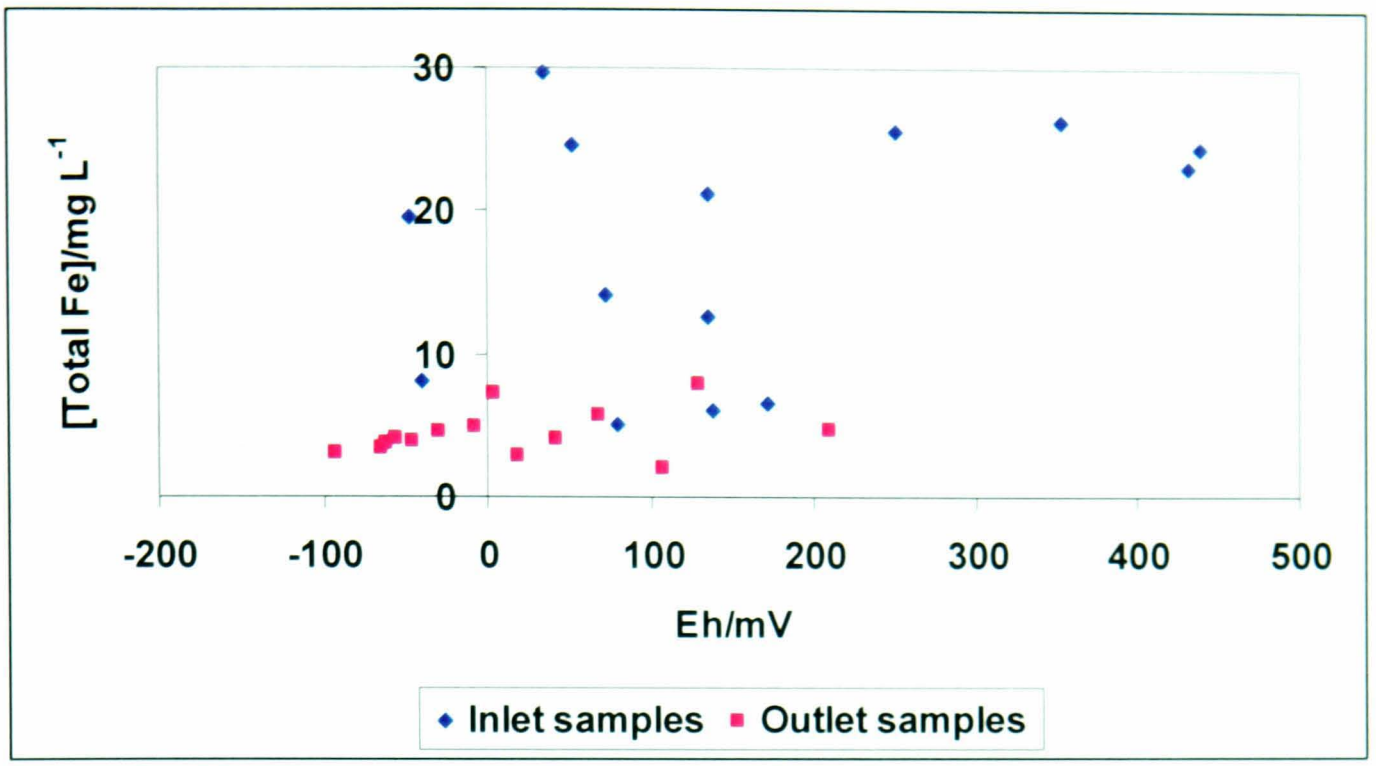

Figure 6.15: Total iron concentration as a function of redox potential (*Eh*) for inlet and outlet samples taken from March 2006-April 2007 at RAPS 1 treatment system at Bowden Close site.

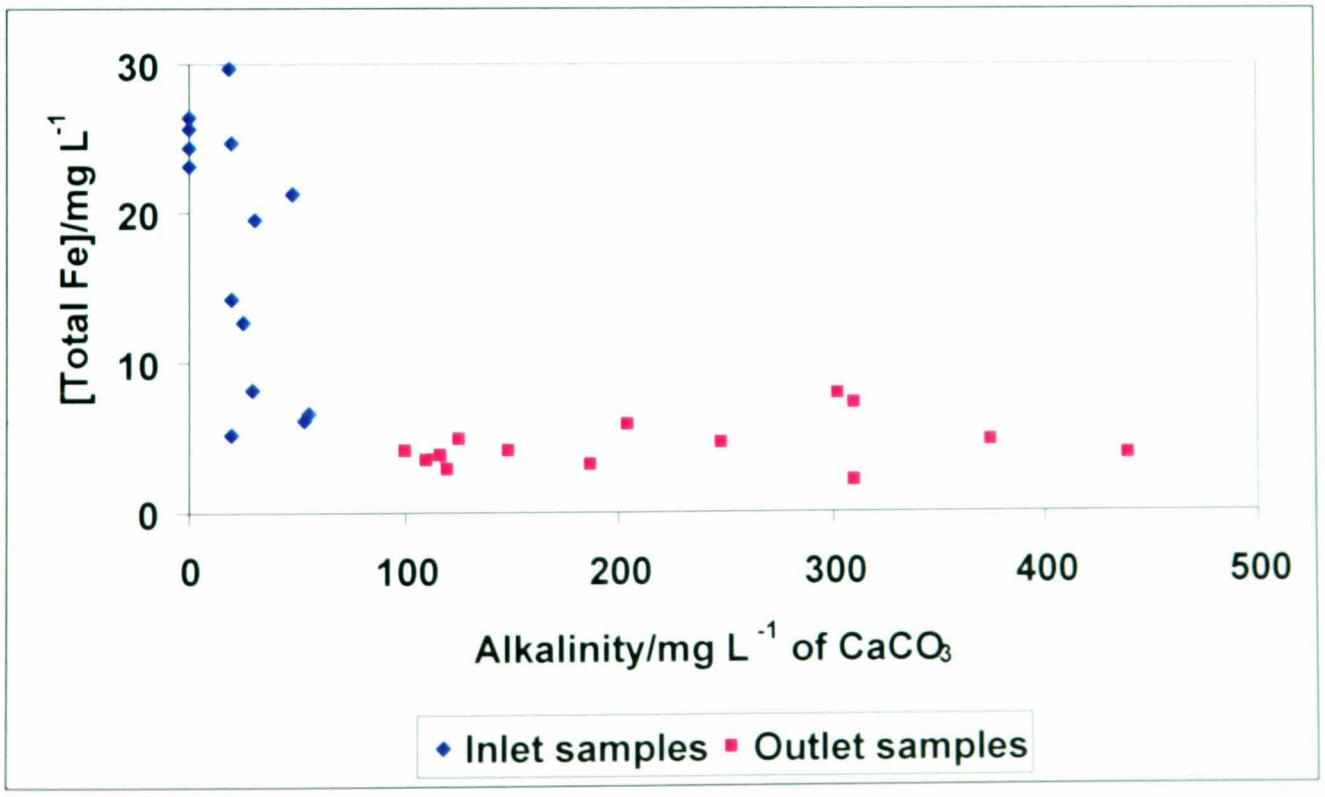

Figure 6.16: Total iron concentration as a function of alkalinity measured as mg L^{-1} of $CaCO_3$ for inlet and outlet samples taken from March 2006-April 2007 at RAPS 1 treatment system at Bowden Close site.

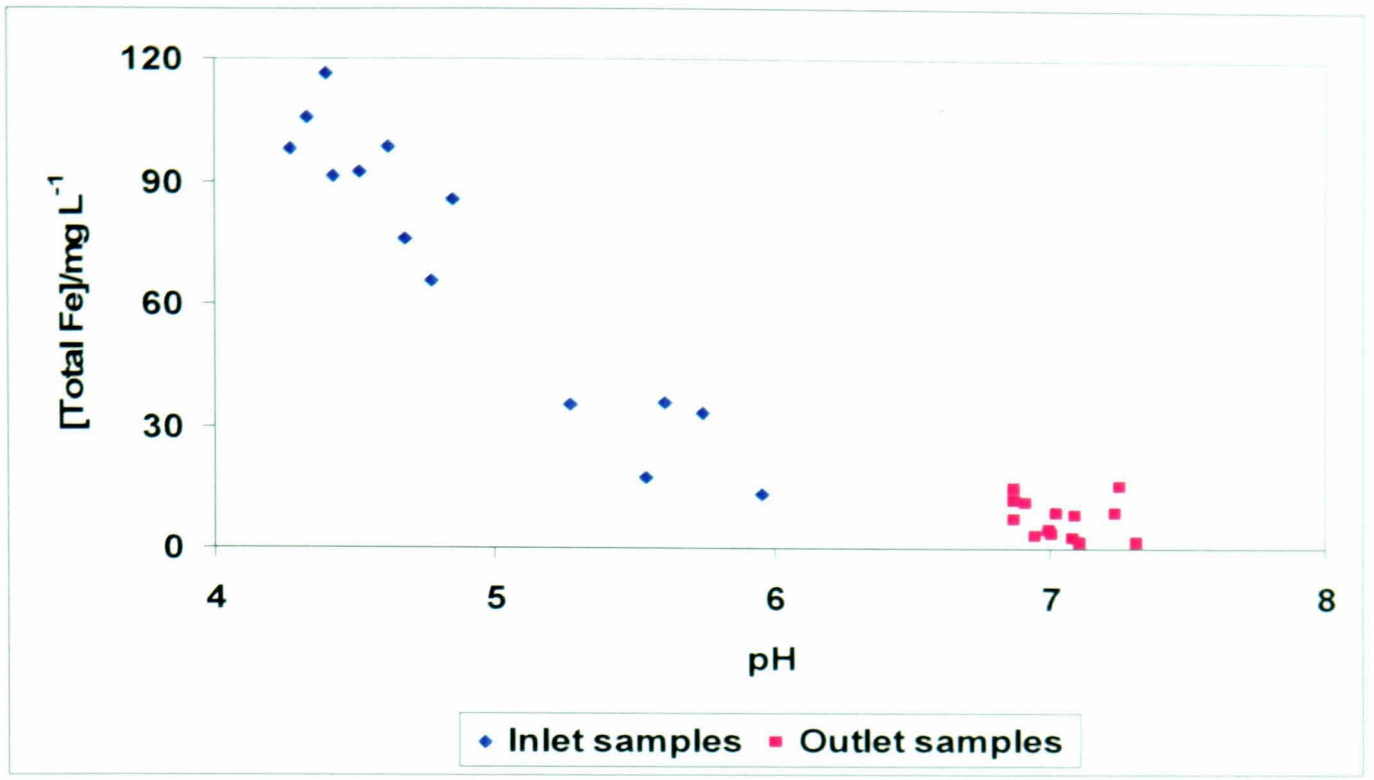

Figure 6.17: Total iron concentration as a function of pH for inlet and outlet samples taken from March 2006-April 2007 at RAPS 2 treatment system at Bowden Close site.

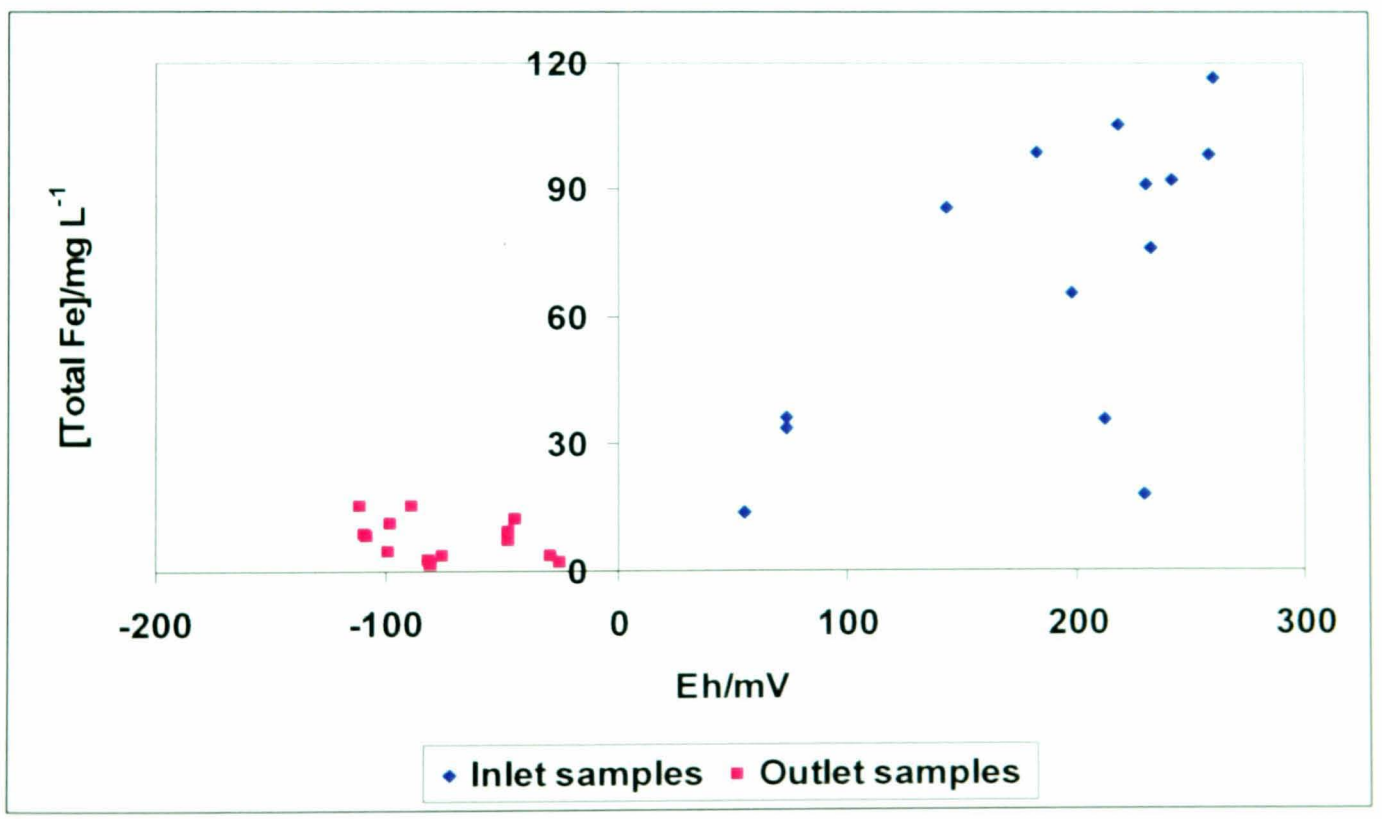

Figure 6.18: Total iron concentration as a function of redox potential (Eh) for inlet and outlet samples taken from March 2006-April 2007 at RAPS 2 treatment system at Bowden Close site.

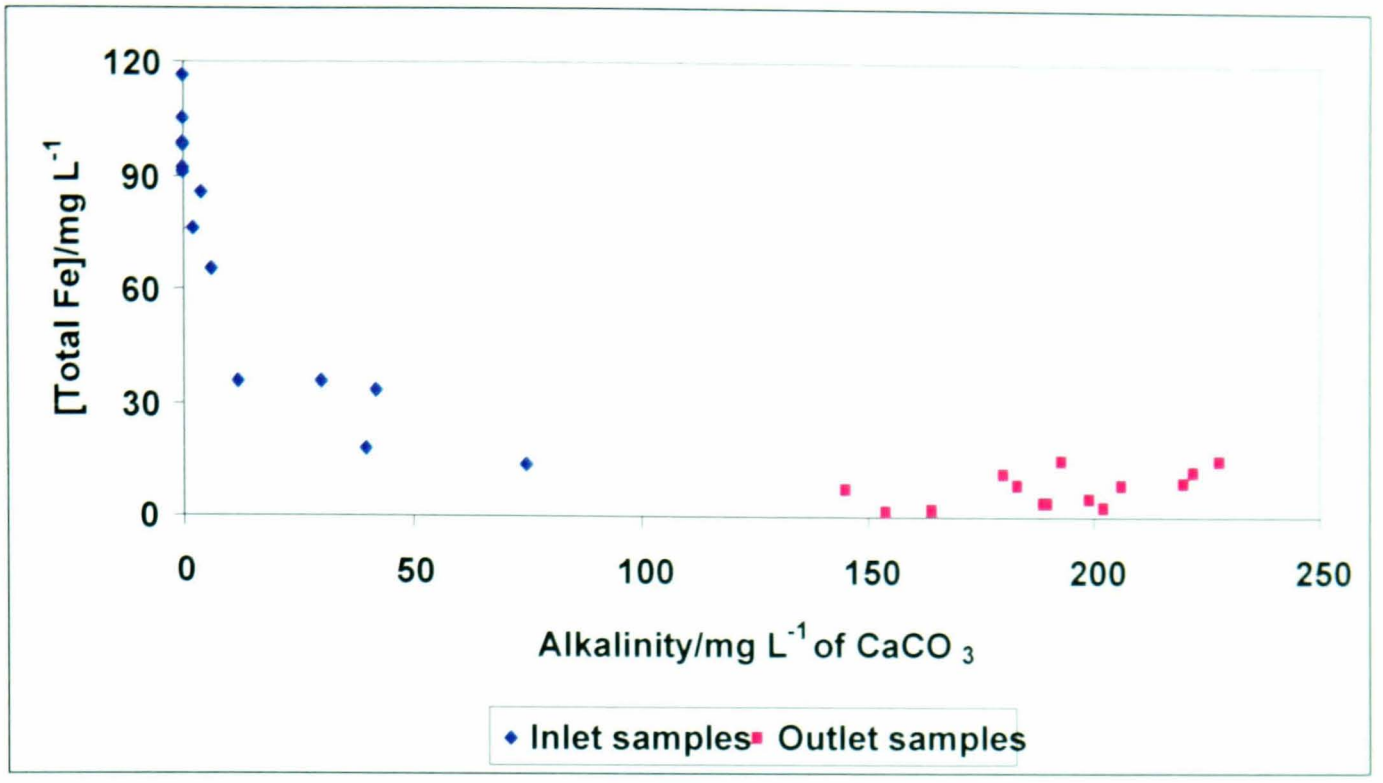

Figure 6.19: Total iron concentration as a function of alkalinity measured as mg L^{-1} of $CaCO_3$ for inlet and outlet samples taken from March 2006-April 2007 at RAPS 2 treatment system at Bowden Close site.

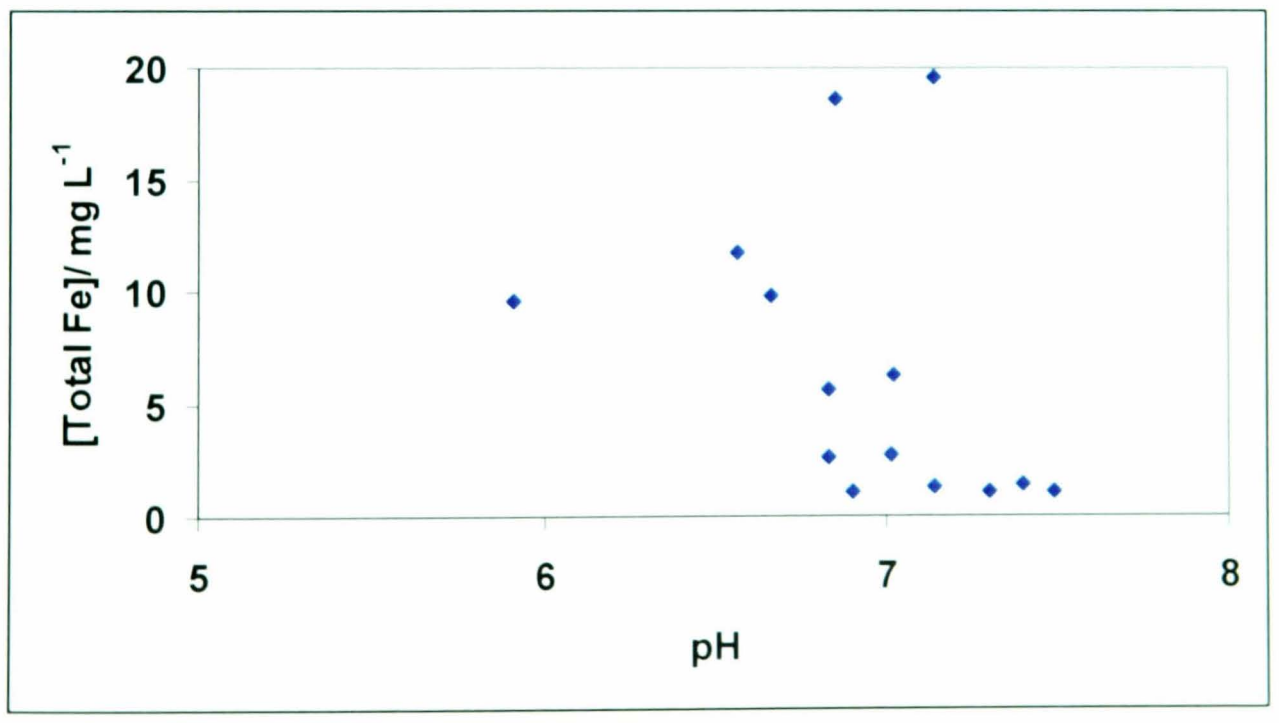

Figure 6.20: Total iron concentration as a function of pH for wetland outlet (final end point) samples taken from March 2006-April 2007 at Bowden Close site. .

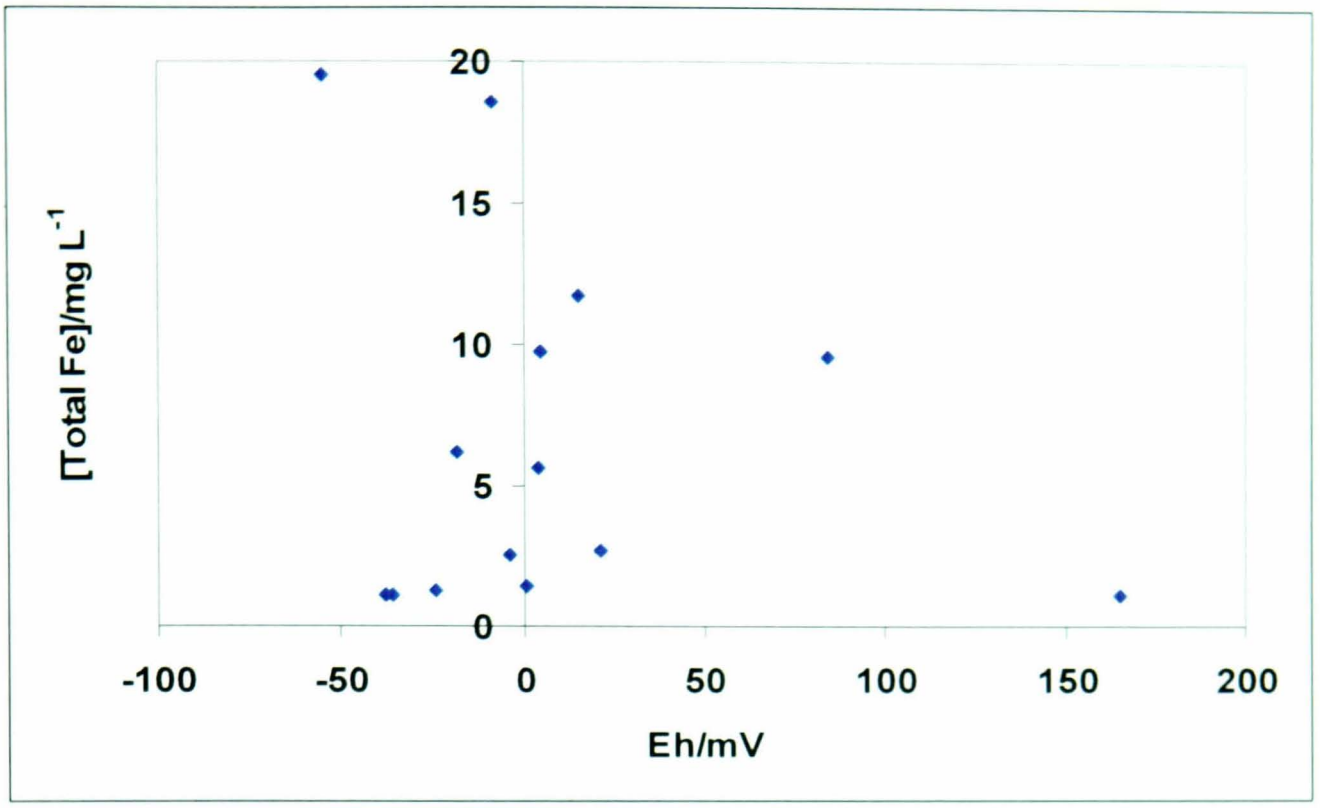

Figure 6.21: Total iron concentration as a function of redox potential (*Eh*/mV) for wetland outlet (final end point) samples taken from March 2006-April 2007 at Bowden Close site.

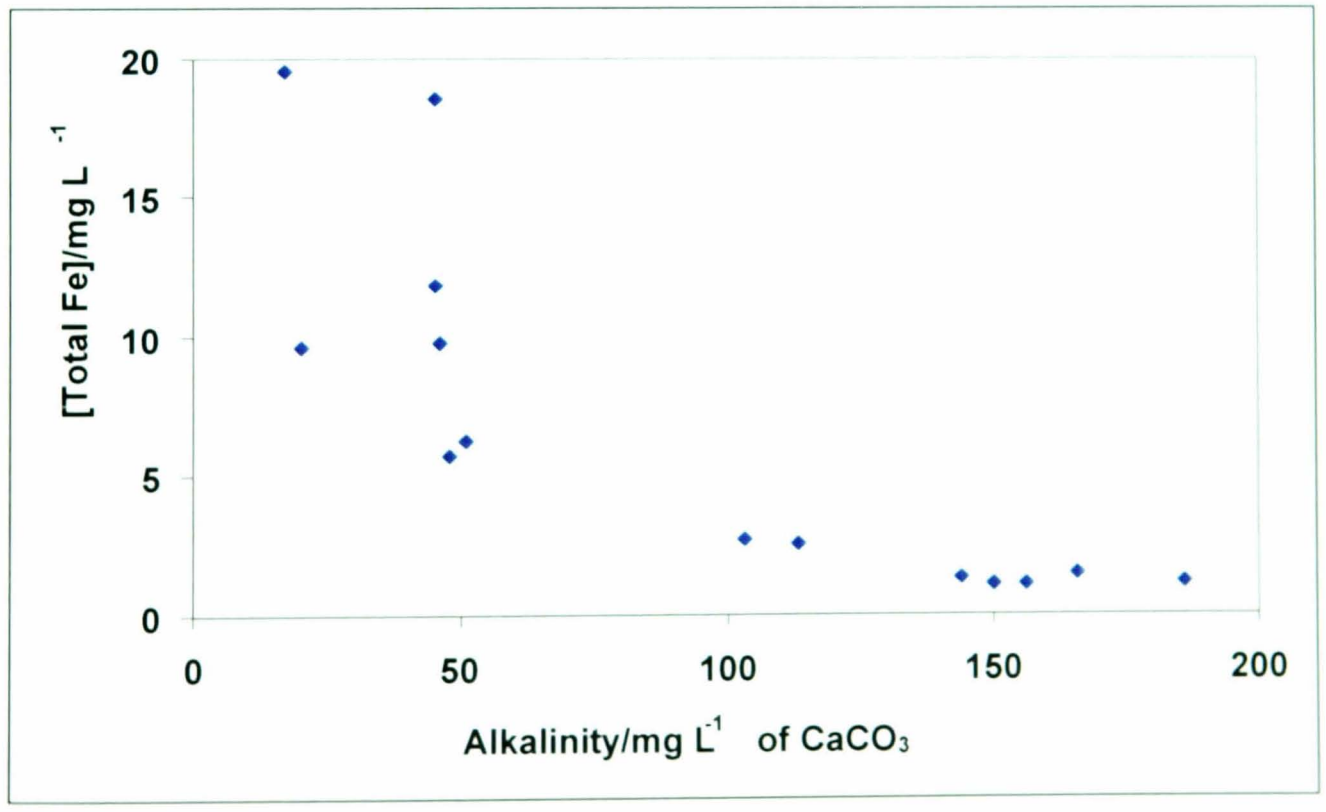

Figure 6.22: Total iron concentration as a function of alkalinity measured as mg L^{-1} of $CaCO_3$ for wetland outlet (final end point) samples taken from March 2006-April 2007 at RAPS 2 treatment system at Bowden Close site.

Measured total iron concentrations as a function of pH for inlet and outlet RAPS 1 samples showed very poor correlation for the inlet samples (R^2=0.31) and no correlation for the outlet samples (R^2=0.01) respectively (figure 6.14) which is quite surprising. However on the contrary, RAPS 2 treatment system shows very strong correlation for the total iron concentrations as a measured of pH for the inlet samples (R^2=0.90) but no correlation for the outlet samples (R^2=0.06) respectively (figure 6.17). The poor correlation observed in the inlet RAPS 1 treatment system could be attributed to the fact that the water pH (from 3.23-6.79) and measured iron concentrations (5.12 to 29.74 mg L^{-1}) varied widely over the sampling period whilst lack of any correlation with the outlet RAPS 1 treatment system could be due to the elevated pH of the outlet samples (> 7) in most cases with substantially reduced iron concentrations between 1.99 and 7.89 mg L^{-1}. The observed strong correlation observed in the inlet RAPS 2 treatment system is not surprising as water emanating from this sampling point is more polluted with reduced but less varied pH (4.27-5.75) than in RAPS 1. Similarly, iron concentrations in RAPS 2 inlet is significantly higher (between 13.5 to 116.54 mg L^{-1}) than in RAPS 1 as would be expected due to the level of contamination and extent of iron dissolution at reduced pH [5]. Lack of correlation between iron concentrations and water pH for the RAPS 2 outlet samples could be due to similar reasons as earlier explained and water pH and iron concentrations followed similar trends as observed in RAPS 1 outlet samples. That is, reduced iron concentrations at elevated pH for the outlet samples. In general, we observed that as water flowed through the treatment systems (RAPS 1 & 2), the pH rose while iron concentrations fell. Figure 6.20 shows that there is no correlation (R^2=0.14) between measured total iron concentrations and the water pH for the wetland outlet (the final end point), and this observation could be attributed to the reasons provided above. This observation is consistent with previous studies on this site and by many other authors [e.g., 2, 5, 8, 9].

It is clear from figure 6.15 that there is no correlation between water *Eh* and the measured total iron concentrations for both inlet and outlet RAPS 1 treatment system (R^2=0.13 and 0.10) respectively while RAPS 2 treatment system shows a weak correlation for the inlet samples (R^2=0.40) but no correlation for the effluent samples (R^2=0.14) respectively (figure 6.18). This complex observation is quite surprising however, in both cases (RAPS 1 & 2), we observed positive *Eh* for higher iron

concentrations for the inlet samples and negative *Eh* values for reduced iron concentrations observed in the outlet samples with few exceptions. For examples, corresponding *Eh* values for all inlet samples for RAPS 1 are positive except for June and August 2006 (-47 and -40 mV) respectively. Similar trend is observed in the results presented in figure 6.21 showing lack of correlation (R^2=0.04) for the measured total iron concentrations as a function of Eh. This observation of reduced *Eh* accompanied by total iron concentration reduction is in accordance with general fundamental geochemical principles and controlling parameters that have been published by many authors [e.g. 17, 19, 20]. The aforementioned similarity of the trend in *Eh* and total iron concentration profiles indicate that the controlling influence of *Eh* and pH is very significant in determining the iron chemistry. These complex influences include redox transformations associated with oxidation and reduction of iron and sulphur (genesis of alkalinity) and overall iron precipitation. Previous studies have reported high degree of variability in the extent to which RAPS treatment systems is remediated by wetland ecosystems [19, 20, 21].

Previous studies have shown that major remediative processes including iron geochemistry within the RAPS systems are microbially driven [21, 22] and many dissolved trace elements including iron have been found to exhibit strong relationship with flow conditions [22], suggesting predominantly diffuse nature of these elements [23]. For example, it has been observed that sulphate-reducing zones are characterised with low concentrations of dissolved iron (through iron disulfide precipitation) [16] and both aerobic and anaerobic bacteria can proliferate around areas of high dissolved iron concentrations [15, 16]. The possible seasonal variations in the performance of RAPS could be attributed to the fact that, it is difficult to predict the thermodynamically most stable form of an element such as iron, as a function of potential (*Eh*) and pH and its relative stability of its predominant form under a range of environmental conditions [17, 23]. Moreover, redox potentials (*Eh*) in natural environments are difficult to predict because some of the reactions that determine *Eh* are slow and the measurements may not give the true equilibrium potentials differences, this is particularly true for reactions involving oxygen-containing environment with rather complicated mechanism and which generally give *Eh* values lower than equilibrium values [17].

This limits of measured *Eh* values means that redox potential measurements in natural environments can only provide qualitative or semi-quantitative information [17]. Nevertheless, the general observation (with few exceptions) from total iron concentrations as a function of *Eh* is that elevated pH and reduced *Eh* environment lead to reduction in total iron concentrations.

The plots of total iron concentrations against measured alkalinity as mg L^{-1} of $CaCO_3$ presented in figures 6.15, 6.19 and 6.22 respectively show mixed correlation between total iron concentrations as a function of alkalinity. While figure 6.16; inlet RAPS 1 treatment system shows rather weak correlation (R^2=0.40), RAPS 2 inlet (figure 6.19) shows strong positive relationship (R^2=0.74) and the wetland outlet (the final system outlet) shows a good correlation (R^2=0.67) for measured total iron concentrations as a function of alkalinity (figure 6.22) respectively. However, there is no correlation (R^2=014 & 0.26) in the outlet of both RAPS (1 & 2) with respect to measured total iron concentrations as a function of alkalinity (figures 6.16 & 6.19). In general, total iron concentrations decreases with increasing alkalinity and vice-versa, thus, the strongest correlation observed in the RAPS 2 inlet treatments system, where water quality is poorest and pH is lowest. The weak correlation observed in the RAPS 1 inlet treatment could be attributed to a number of factors including the rate of dissolution of limestone/calcite that controls alkalinity and the rate of iron precipitation. Lack of correlation in the outlet of both RAPS is probably due to the fact that at elevated pH, the rate of iron precipitation becomes variables and depends on a number of geochemical parameters. This observation is consistent with studies by Hedin [19], attributing water alkalinity to the rate of iron oxidation and hydrolysis. In general, as water flows through the RAPS treatment system, water pH will rise while concentrations of alkalinity and iron will fall. The observed decreased in alkalinity is due to the neutralisation of acidity produced by iron oxidation and hydrolysis:

$$Fe^{2+} + 2HCO_3^- + 1/4O_2 \dashrightarrow FeOOH\,(s) + 3/2H_2O + 2CO_2.$$

Increased pH is a common feature of passive treatment systems such as RAPS with net alkaline water which is attributed to exsolution of CO_2 as shown in the equation above [23, 24]. This implies that acidity has been neutralised and the effluent water has become net alkaline.

Furthermore, oxidation of iron takes place much more completely in alkaline medium than in acid medium. Thus, larger amounts of dissolved iron are commonly present in slightly acidic waters than in the faintly alkaline waters [23]. Previous work by [6] shows that alkalinity generation could also be associated with removal of sulphate, that is, with microbial sulphate reduction, thus, giving a rather complex and variable behaviour.

6.2.3: Hydrolysed and unhydrolysed iron results

Iron concentrations were determined in laboratory by differential pulse voltammetry (DPV) and these results are presented here. Mean concentrations of both hydrolysed and unhydrolysed iron for influent and effluent samples are presented in figures 6.23 and 6.24 respectively. Temporal and seasonal variations in concentration profile of hydrolysed and unhydrolysed iron are shown in figure 6.25.

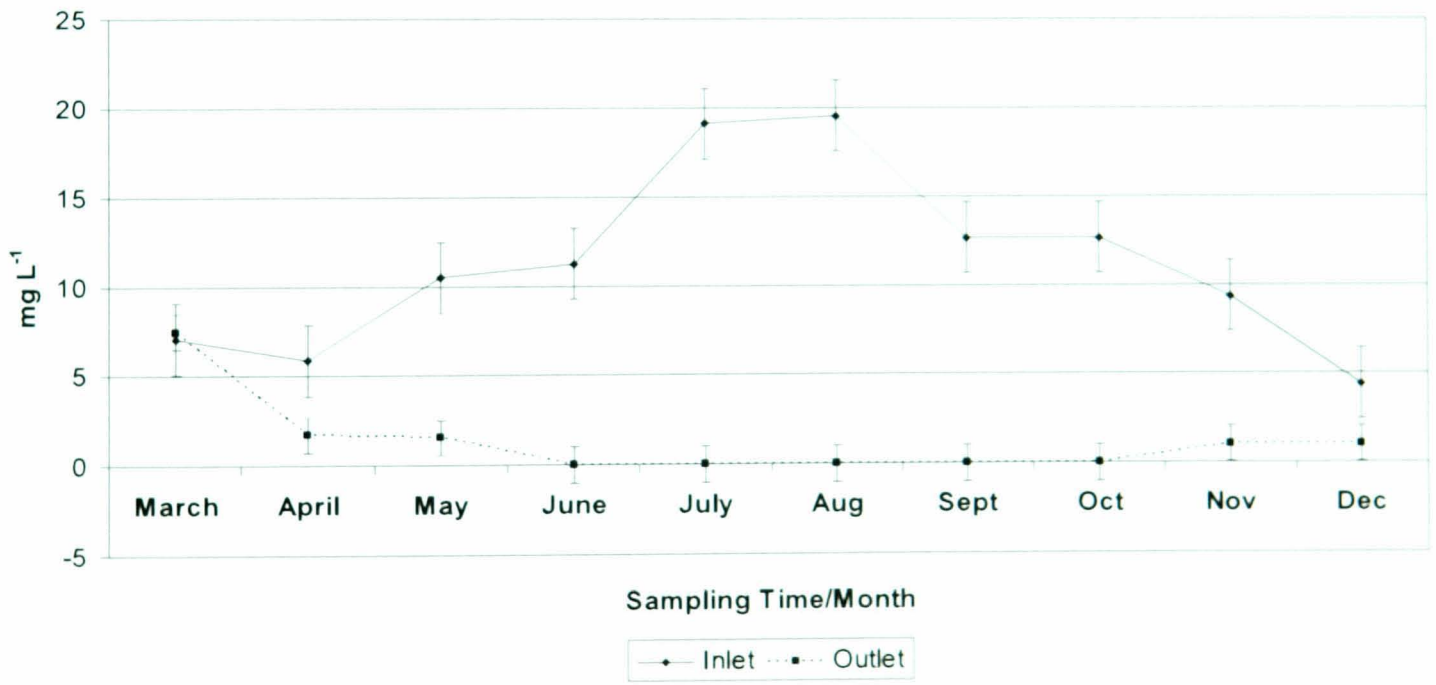

Figure 6.23: Mean total unhydrolysed iron concentrations (mg L^{-1}) for samples collected between March-December 2006 at Bowden Close site. Error bars denote standard error of the mean (where n=4).

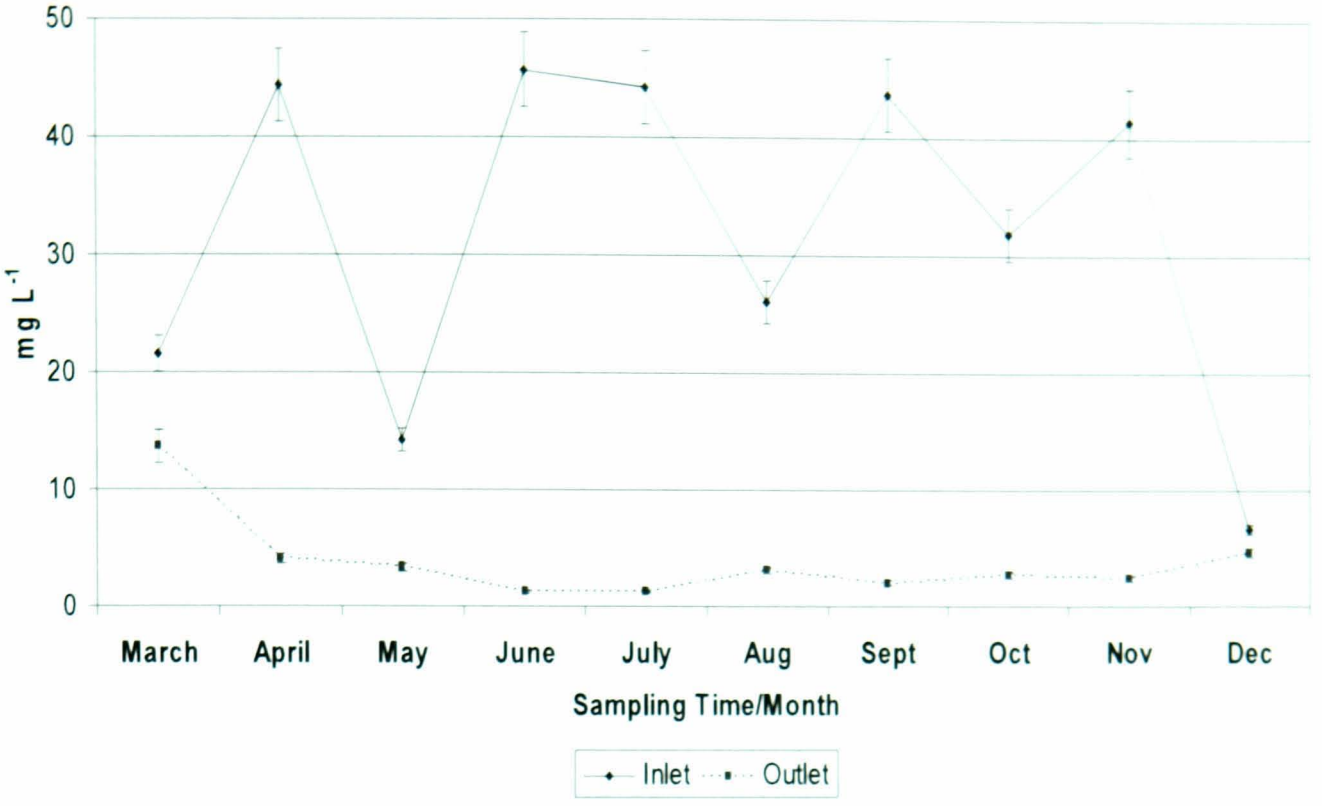

Figure 6.24: Mean total hydrolysed iron concentrations (mg L^{-1}) for samples collected in 2006 at Bowden Close site. Error bars denote standard error of the mean (where n=4).

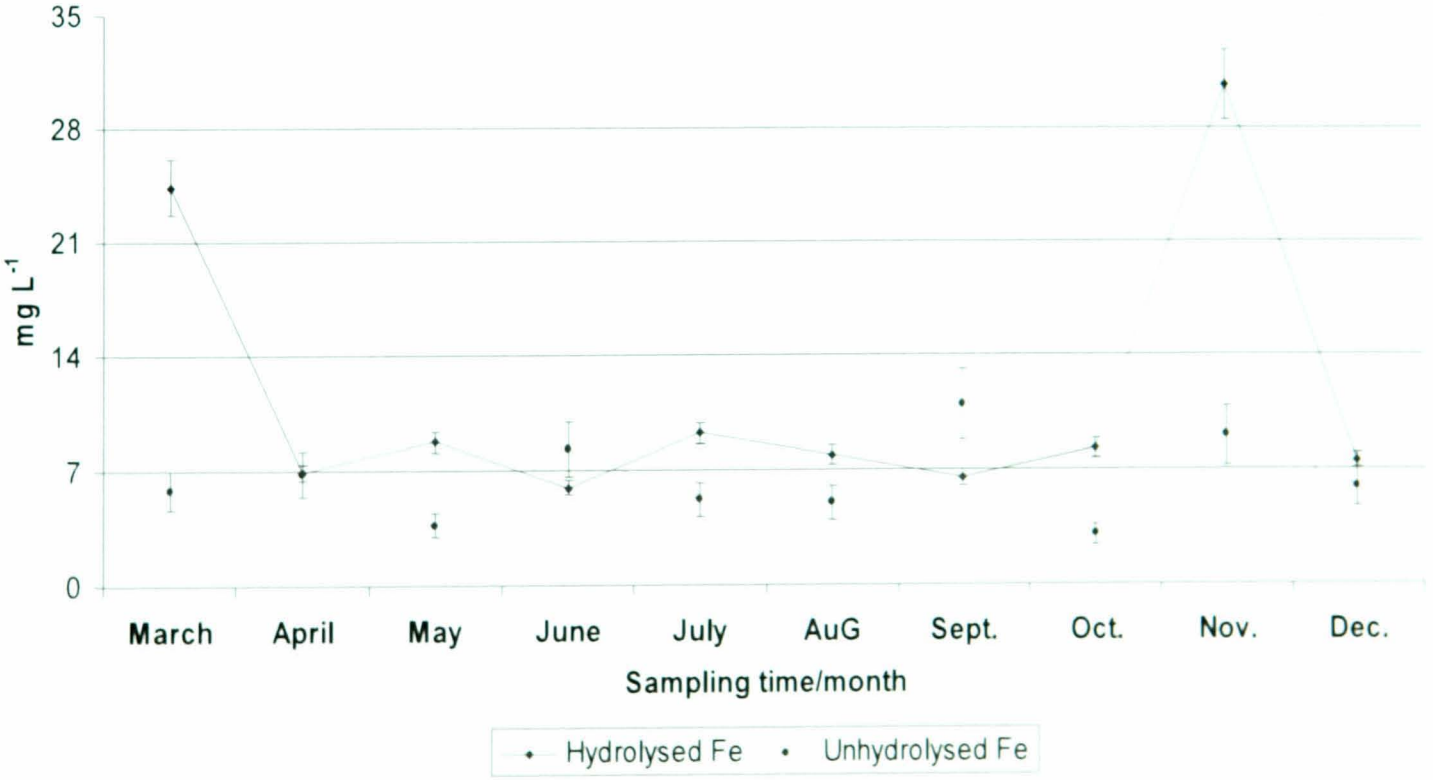

Figure 6.25: Mean total hydrolysed and unhydrolysed iron concentrations (mg L^{-1}) for samples collected between March-December 2006 at Bowden Close site. Error bars denote standard error of the mean (where n=4).

Summary of mean monthly unhydrolysed iron concentrations-figure 6.23 (most likely Fe (II)) as fully discussed in the analytical section in chapter 4. The results show that outlet concentrations are lower than the influent concentrations. The concentrations of both inlet and outlet appeared stable except for July and August. This observations indicate that outlet unhydrolysed iron concentration is lower than the influent. This is not surprising as one would expect reduction in concentration since some of the iron must have been precipitated during the remediation process. The higher concentrations observed for the months of July and August could be due to less rainfall during these months. Summary of hydrolysed iron concentrations presented in figure 6.24 shows the same trend as unhydrolysed iron but was more complex. These influent concentrations appeared to be less stable which could be attributed to the rate of hydrolysis in the water body. Hydrolysed iron concentration is likely to be Fe (III) as explained in chapter 4. Comparison of the mean total unhydrolysed and hydrolysed iron concentration (figure 6.25) shows a complex pattern of variation but in general, hydrolysed iron concentrations are higher than the unhydrolysed iron. This complex variation may be due to the rate of hydrolysis of Fe in the water system and this rate will be affected by a number of complex geochemical factors including but not limited to parameters such as *Eh*, pH and alkalinity.

6.3: Conclusions

Water quality parameters such as *Eh*, pH, temperature, conductivity and alkalinity indicate that water quality for the effluent is of better quality than the influent water. This shows the improvement in the water quality after the water has passed through the entire treatment processes. Moreover, the quality of water discharged into the receiving water course-Willington Burn has improved considerably with the pH of discharged water greater than 7 and showing net-alkalinity and also reduced iron.

Comparisons of various water quality parameters suggest that there is a correlation between water pH and measured iron concentrations with iron precipitation as iron oxyhydroxide at elevated pH.

In this study, it has been shown for the first time that iron can be measured and monitored by voltammetric technique with potential in-situ application. Considerable lower iron concentration of the effluent water demonstrates that the treatment regime is effective and efficient.

Seasonal variability in iron concentrations revealed that iron concentrations were seasonally highest in the summer and lowest in the winter. This is probably due to the dilution from the runoff water during the winter.

At the effluent, there was a significant decrease in iron concentration by up to 60%. This decrease can be attributed to the precipitation of iron during the treatment cycle and there has been evidence of iron sulphide and ochres on the water surface of the soil at the bottom of the pond.

The study clearly suggests that based on the proportion of hydrolysed and unhydrolysed iron, most of the iron in the water may exist in hydrolysed form as this has a higher concentration than the unhydrolysed iron.

The percentage of the temporal and seasonal concentration of dissolved and colloidal iron was found to vary seasonally and averaged 30% over the 14 months sampling period. This is observed across the sampling locations.

6.4: References

[1]. Younger, P.L. *Quarterly Journal of Engineering Geology*, **1995**, S101-S113.

[2]. Jarvis, A.P. & Younger, P.L. *Chemistry and Ecology*, **1997**, 13. 249-270.

[3]. Amos, P., Aplin, A.C., Bowden, L., Daugherty, A.J.. Elliot, A.. Jayaweera, A.. Johnson, D.B., Martin, A., Wood, R. & Younger, P.L. *Land Contamination Reclamation*, **2003**, 11, 127-135.

[3]. Younger, P.L. Coulton, R.L. & Froggatt, E.C. *Science of the Total Environment*, **2004**, 137-154.

[4]. Younger, P.L., Jayaweera, A., Elliot, A., Wood, R.. Amos, P.. Daugherty. A.J.. Martin, A., Bowden, L., Aplin, A.C. & Johnson. D.B. *Land Contamination and Reclamation*, **2005**, 12, 135.

[5]. Younger, P.L., Jayaweera, A. & Wood, A. Proceedings of the CL:AIRE Annual Project Conference, April **2004**, London.

[6]. Younger, P.L. Proceedings of CL: AIRE Annual Project Conference, April **2002**, London, 21pp.

[7]. Younger, P.L. Final report to Durham County Council and the County Durham Environmental Trust (CDENT). **2000**.

[8]. CL:AIRE Case Study Bulletin CSB4 (March **2006**). Coal Mine Sites for Targeted Remediation Research: The CoSTaR initiative.

[9]. Fabian, D., Aplin. A.C. & Younger. P.L. Proceedings of 9th International Mine Water Congress, 5-7 September **2005**, Ovendo, Spain. 383-387.

[10]. Fabian, D., Jarvis, A.J. & Younger. P.L. CL:AIRE Technology Demonstration Report (TDP5). April. **2006**.

[11]. CL:AIRE Case Study Bulletin CSB4 (March **2004**). Mine Water Treatment at Wheal Jane Tin Mine, Cornwall.

[12]. Mukhopadhyay, B., Bastias, L. & Mukhopadhyay. *Mine Water and the Environment*, **2007**, 26, 29-45.

[13]. Singer, P.C. & Strumm, W. *Applied Geochemistry*, **1970**. 167, 1121-1123.

[14]. Gray, N.F. *Environmental Geology*, **1996**, 27, 358-361.

[15]. Apello, C.A.J. and Postma, D. Geochemistry. Groundwater and Pollution. *Rotterdam: Balkema*; **1993**, 536pp.

[16]. Gandy, C.J., Smith, J.W.N. and Jarvis, A.P. *Science of the Total Environment*, **2007**, 373, 435-446.

[17]. Krauskopf, K.B. Introduction to Geochemistry, *McGraw-Hill*, **1979**, 617pp.

[18]. Brown, C.J., Walter, D.A. and Colabufo, S. *Long Island Geologists*, **1999**, 96pp.

[19]. Whitehead, P.G. and Prior, H. *Science of the Total Environment*, **2005**, 338, 15-21.

[20]. Hedin, R.S. *Mine Water Environment*, **2008**, 230, 41-49.

[21]. Whitehead, P.G., Cosby, B.J. and Prior, H. *Science of the Total Environment*, **2005**, 338, 125-135.

[22]. Neal, C., Jarvie, H.P., Whitton, B.A. and Gemmell, J. *Science of the Total Environment*, **2000**, 251, 153-172.

[23]. Crovata, C.A. *Mine Water Environment*, **2007**, 26, 128-149.

[24]. Younger, P.L. *Mine Water Environment*, **2000**, 2, 84-97.

Chapter 7

ACOMB SITE, HEXHAM, NORTHUMBERLAND

In this chapter, background site history and the net-alkaline mine-water problems and treatment regime at this site will be discussed briefly. In addition, on-site data together with the voltammetric results of iron concentrations will be presented before closing the chapter with some geochemical implications and significance of these results followed by some conclusions.

7.1: Site History, Background, Problems and Treatment Regime

The Acomb mine-water treatment system is owned by the Coal Authority and is located 1 mile NNW of Hexham in Northumberland County. Two coal seams were mined at this site during the 19^{th} and 20^{th} centuries. After its closure in 1952, polluted mine wastes from the site were discharged into a nearby stream-Red Burn- via an old pipe which is known to have been present prior to reclamation of the colliery area. The discharge which occurred approximately 100 m above the Red Burn intersection with the River Tyne caused severe surface water contamination which was highly visible in the village of Acomb.

Following this contamination, construction work was carried out in 2001 and mine-water was pumped from the drift top into an aeration tower. The mine-water from this site is with average pH of 6.6 and previous studies on the site (for examples, [1, 2] suggest that total iron concentration at this site is in the region of 25 to 40 mg L^{-1}. In addition, unpublished reports have reported high levels of other metals such as lead, copper, nickel and zinc which might be due to nearby local metal mines [3].

The treatment system at Acomb site is "hybrid" with hydrogen peroxide dosing upstream of the settlement lagoons and an aerobic reed-bed wetland. This peroxide dosing ensures that neutralisation of the mine-water is partially achieved, thus raising the water pH and leading to oxidation of Fe^{2+} to Fe^{3+} and the generation of iron oxyhydroxide precipitate. The peroxide acts as an oxidising agent in this process.

The Acomb passive treatment system consists of aeration, settlement lagoons and aeration wetlands to remove the iron from solution. The system works by dosing the aerated water with a small volume of hydrogen peroxide before passing into two irregular shaped lagoons which are parallel to each other. The lagoons are approximately 3 m deep with a total area of 750 m^2 and some peripheral planting to improve the aesthetics of the scheme. Effluents from the two lagoons then pass into two reed-beds in sequence, with a combined area of 1200 m^2, which are planted with a variety of reeds including *Typha latifolia*, *Phragmites australis* [3]. Figures 7.1 shows a schematic plan of the site whilst figure 7.2 shows one of the settlement lagoons.

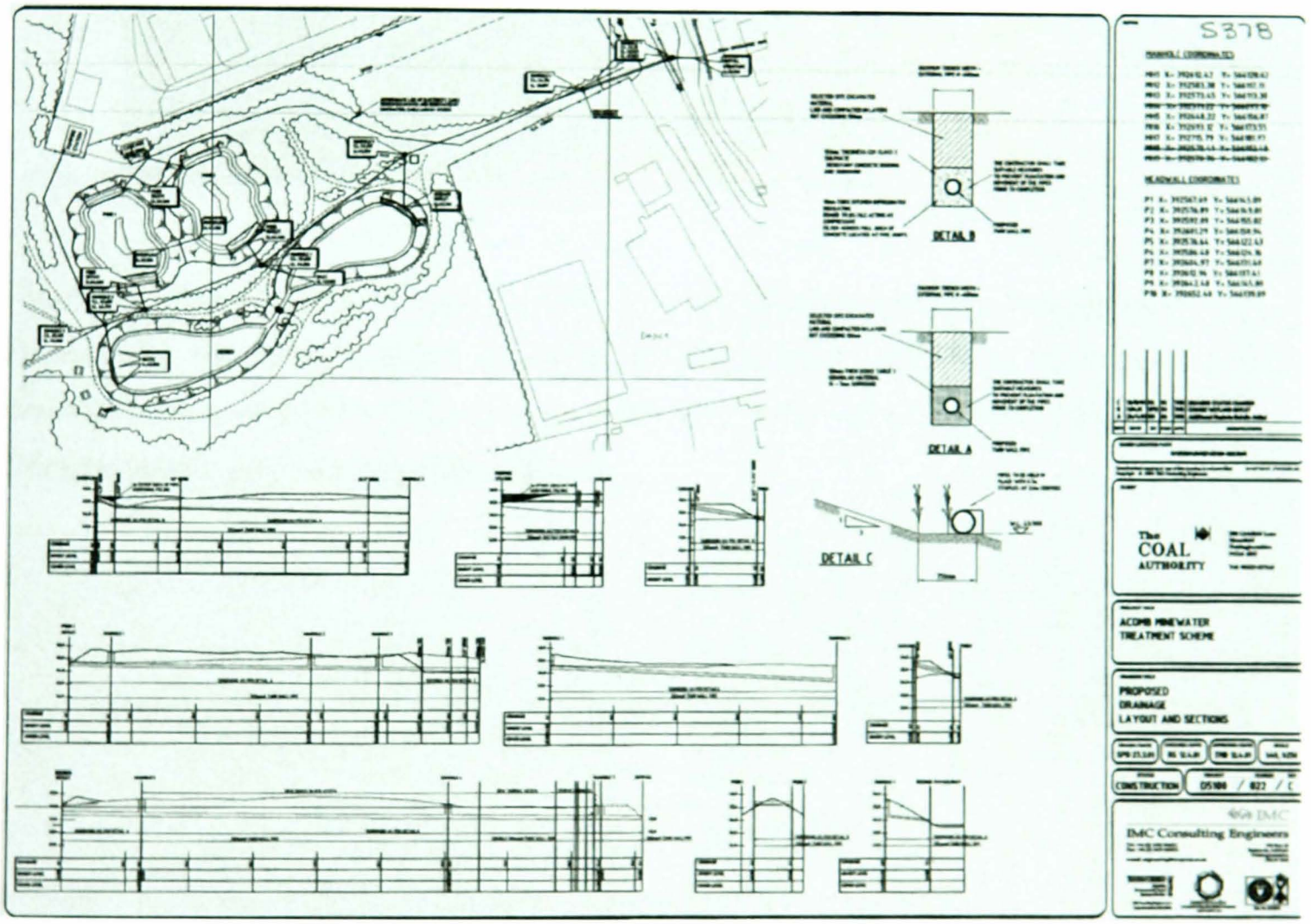

Figure 7.1: Schematic of the layout of the passive treatment system at Acomb site, Hexham, Northumberland-Courtesy of the HERO research Group at Newcastle University.

Figure 7.2: Photograph taken June 27, 2006 by Kola, showing a settlement lagoon at Acomb site receiving hydrogen peroxide pre-dosed mine-water from the mine drainage with some peripheral plants to improve the aesthetics of the scheme. Effluent from the lagoon goes to a polishing wetland.

7.2: Results and Discussion

Results from monthly monitoring of site water quality parameters are presented, together with the laboratory measured iron concentrations determined by the voltammetric method as fully described in chapter 4 and also the relationship and correlation between various parameters. The section closes with some concluding remarks.

7.2.1: On-site results

Knowledge of mine-water quality parameters is important as the geological setting of a mine-water discharge exerts a significant influence on the water quality. Summaries of the monthly water quality parameters taken from this site, together with their means are presented in tables 7.1 and 7.2 respectively. These water quality parameters include water temperature, pH, *Eh*, conductivity and alkalinity. Seasonal and temporal variability in water quality parameters collected from May to December, 2006 in this site are also presented in figures 7.3 to 7.7. This section will discuss the observed trends of these parameters.

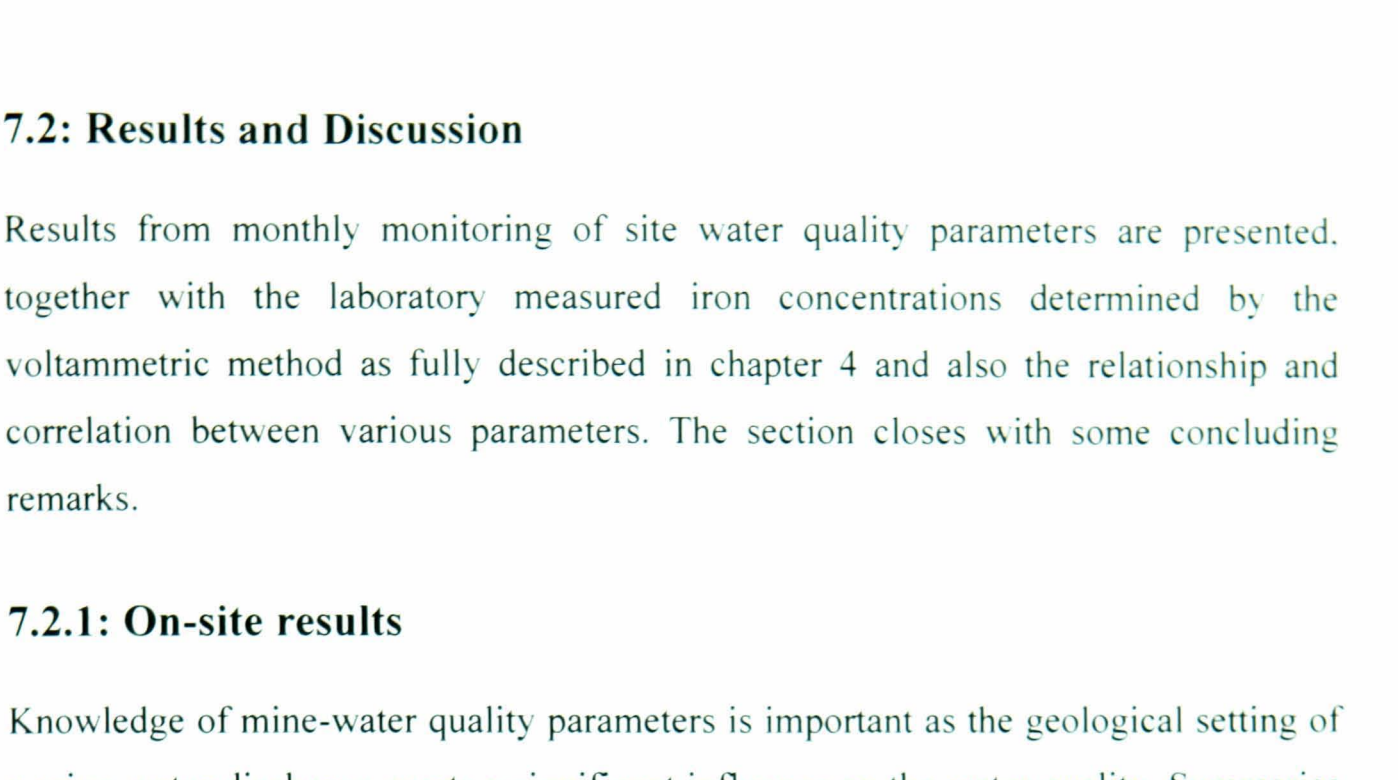

Figure 7.3: Showing temporal change in temperature at Acomb site over the sampling period (May-December, 2006). Error bars denote standard error of the mean.

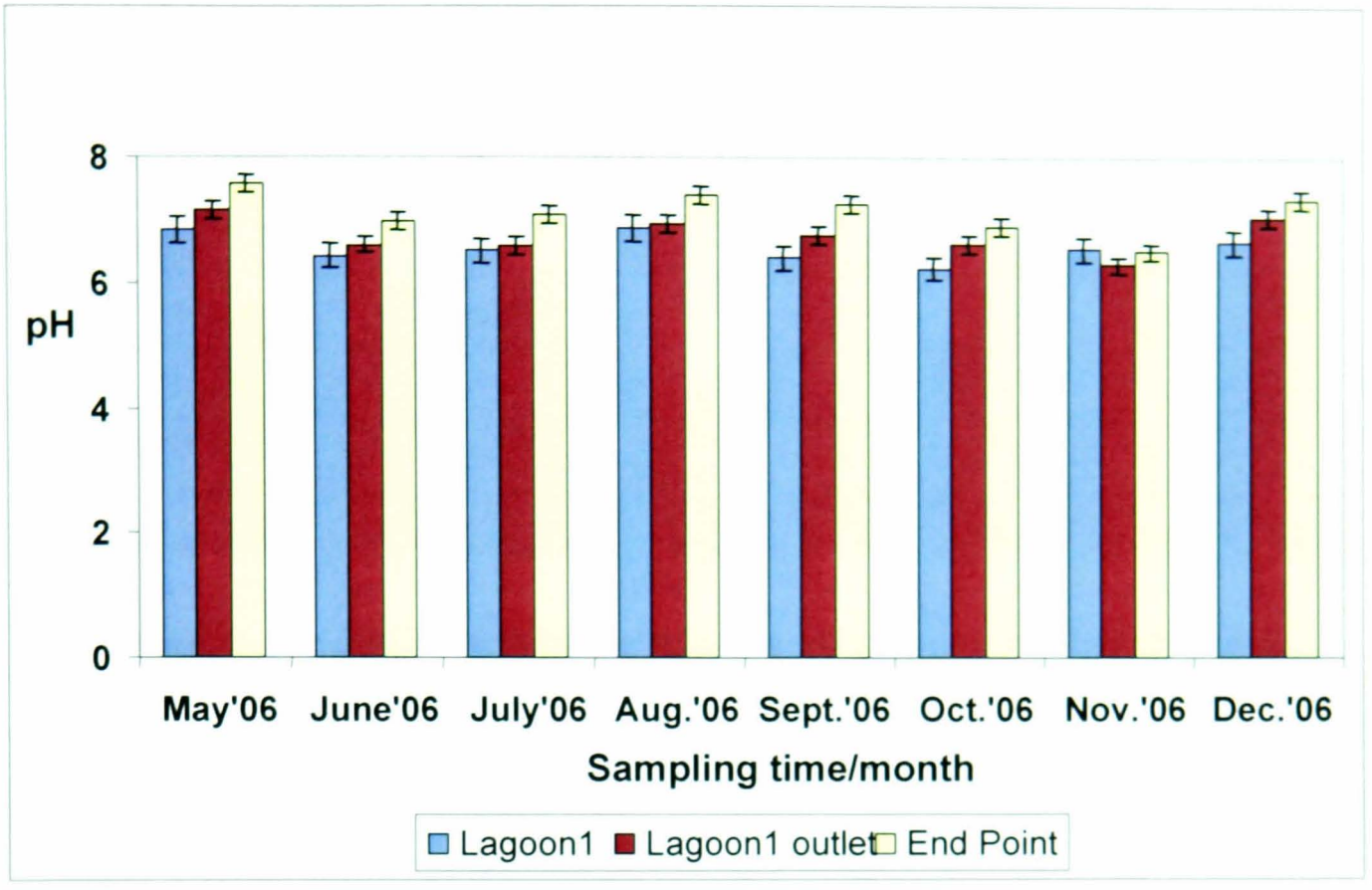

Figure 7.4: Showing temporal change in pH at Acomb site over the sampling period (May-December, 2006). Error bars denote standard error of the mean.

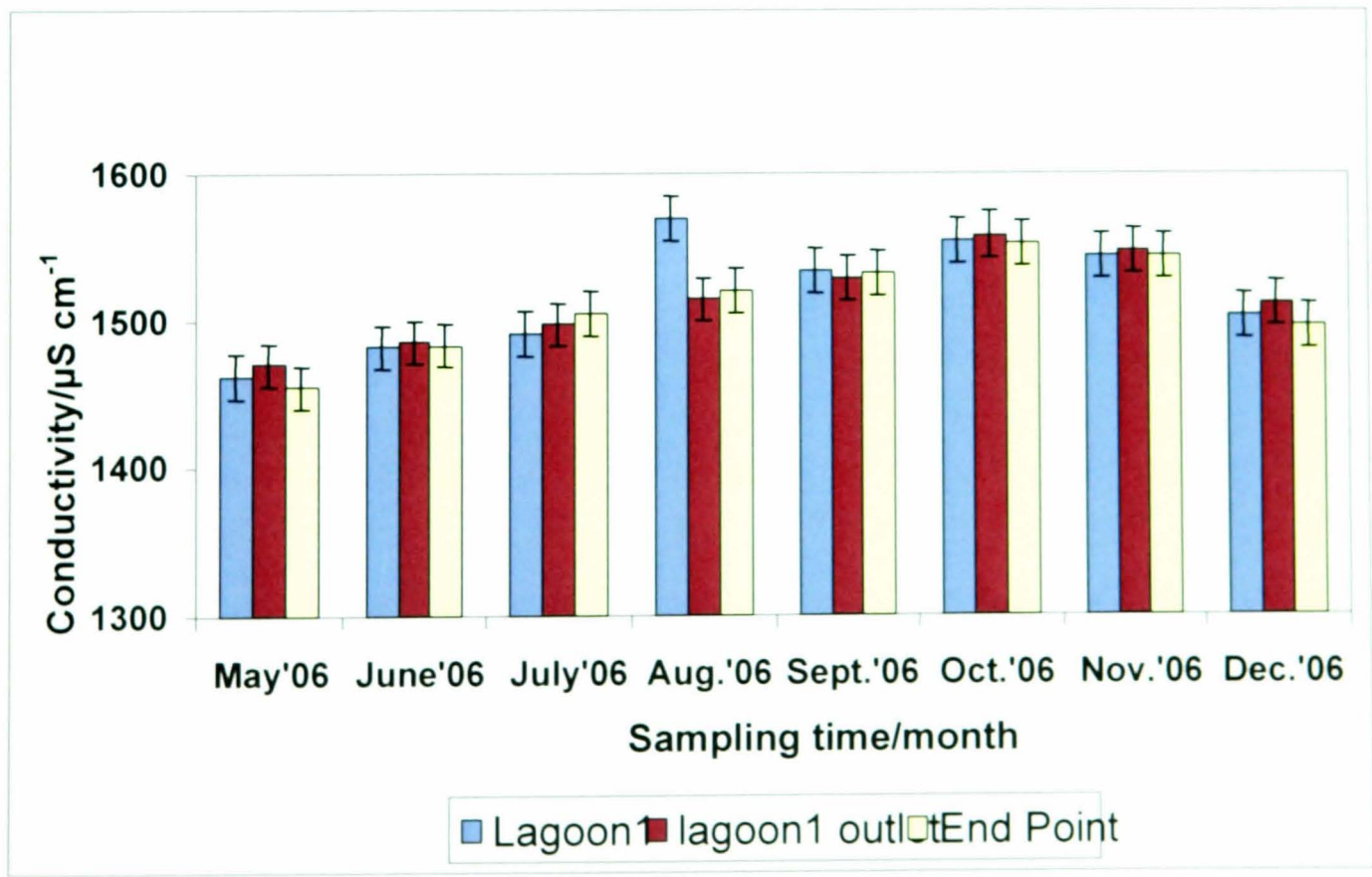

Figure 7.5: Showing temporal change in conductivity at Acomb site over the sampling period (May-December, 2006). Error bars denote standard error of the mean.

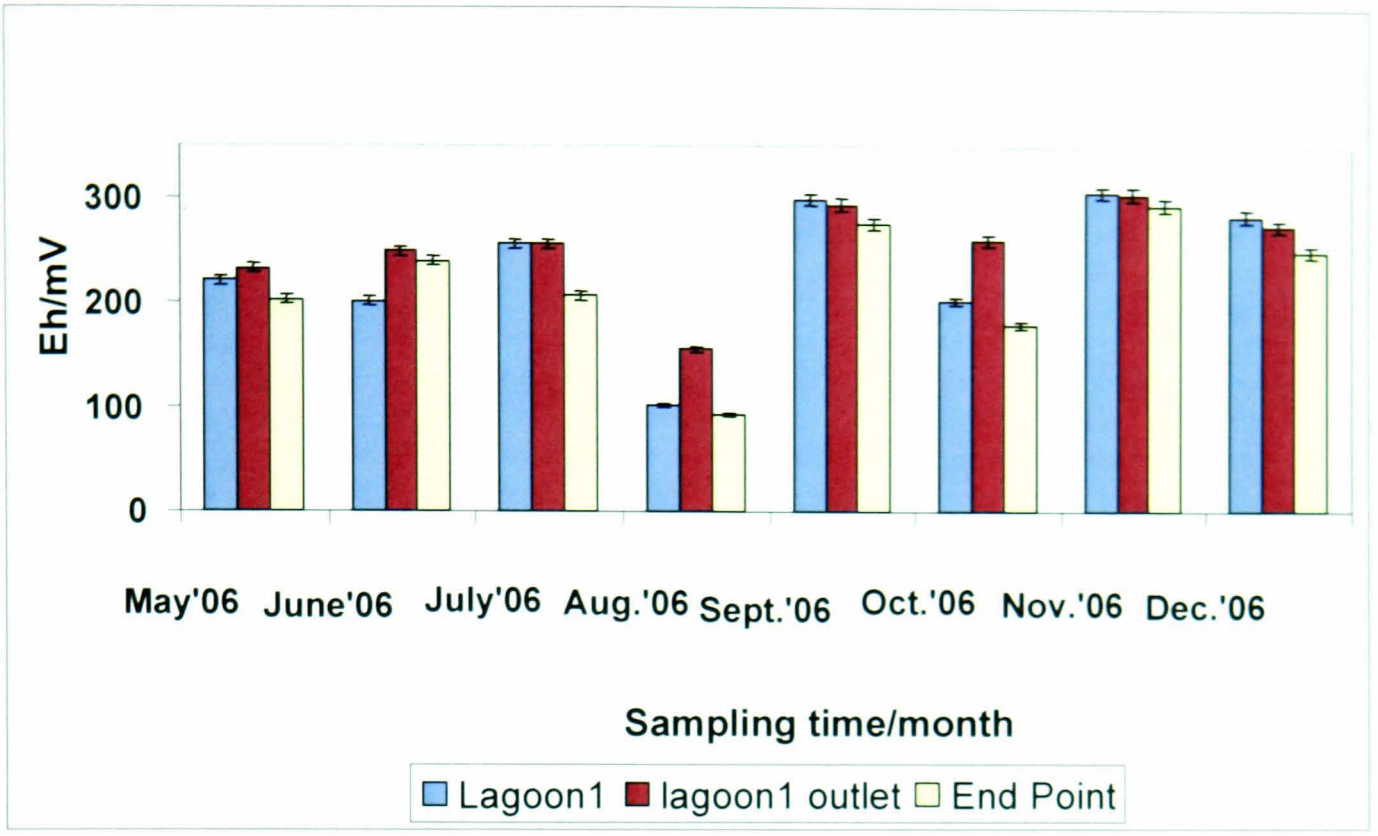

Figure 7.6: Graph showing temporal change in *Eh* at Acomb site over the sampling period (May-December, 2006). Error bars denote standard error of the mean.

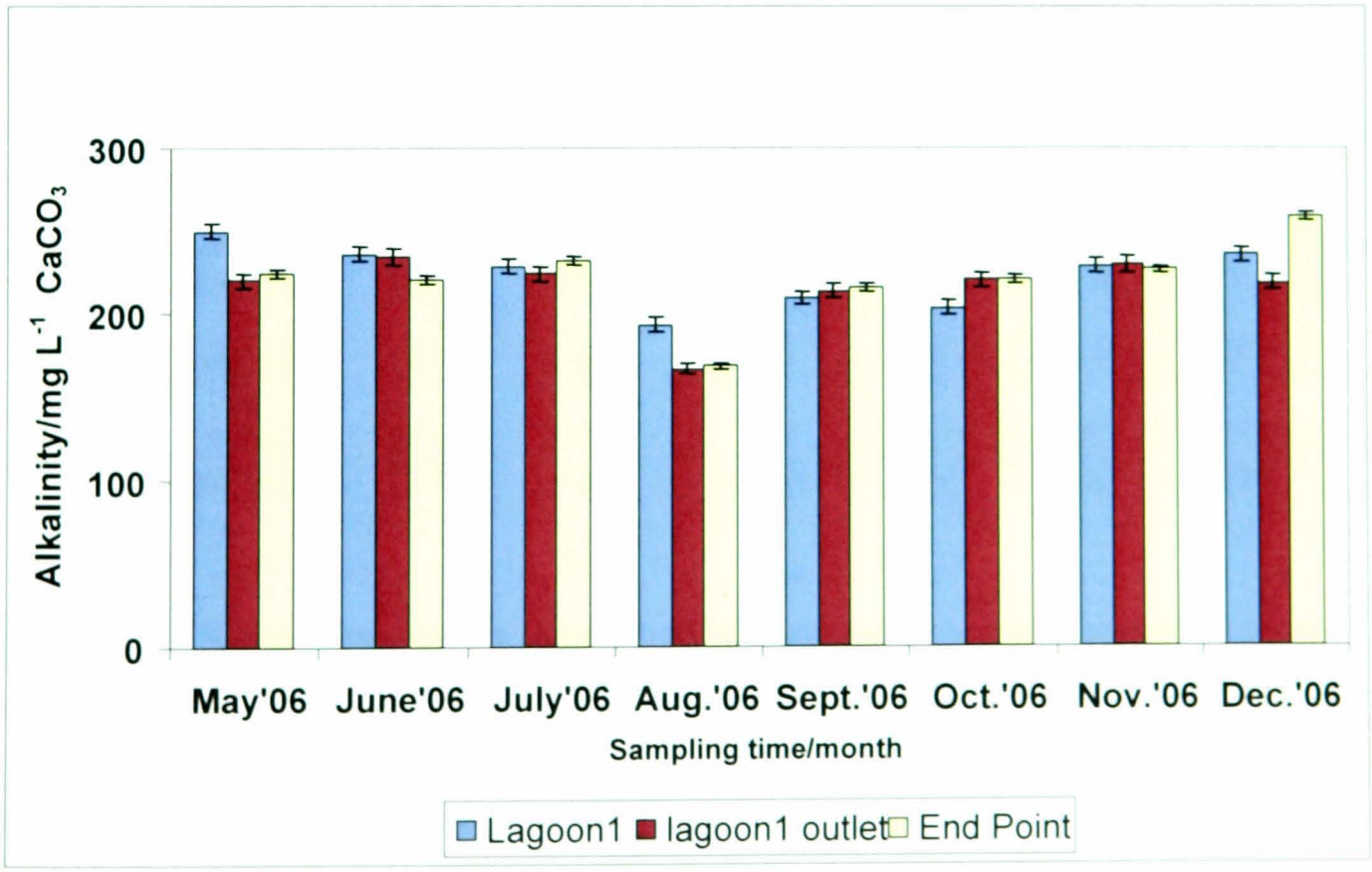

Figure 7.7: Showing temporal change in alkalinity at Acomb site over the sampling period (May-December, 2006). Error bars denote standard error of the mean.

Table 7.1: Water quality parameters determined at various sampling points at Acomb site from May-December, 2006.

Dates	Sample	pH	*K* (µS cm^{-1})	Alkalinity mg L^{-1} CaCO3)	*Eh*(mV)	*Tf*°C	[Dissolved Fe] mg L^{-1}	[Colloidal Fe] mg L^{-1}
	Lagoon1	6.83	1462	250	221	12.1	29.6	16.5
31-May'06	Lag.1 outlet	7.14	1470	220	233	12.7	8.62	3.41
	End Point	7.57	1455	224	203	12.9	7.28	6.11
	Lagoon1	6.43	1482	236	201	11.9	37.7	27.7
27-June'06	Lag.1 outlet	6.60	1485	234	249	11.7	6.01	0.29
	End Point	6.97	1483	220	240	11.6	4.49	3.06
	Lagoon1	6.51	1491	228	256	11.9	27.8	15.2
20-July'06	Lag.1 outlet	6.59	1497	224	256	13.3	4.19	0.68
	End Point	7.07	1505	232	207	13.7	6.72	5.66
	Lagoon1	6.87	1569	193	-102	12.4	33.5	24.7
30-Aug.'06	Lag.1 outlet	6.94	1514	166	156	13.8	4.90	0.00
	End Point	7.40	1520	168	93	12.8	6.76	4.96
	Lagoon1	6.4	1534	209	299	12.3	13.7	4.85
26-Sep.'06	Lag.1 outlet	6.77	1528	213	294	12.7	3.74	0.00
	End Point	7.27	1532	215	276	13.0	5.42	3.79
	Lagoon1	6.24	1554	203	202	12.0	18.2	13.9
31-Oct.'06	Lag.1 outlet	6.63	1558	220	261	11.4	4.22	0.00
	End Point	6.92	1552	220	179	11.5	2.42	1.29
14-Nov.'06	Lag.1 outlet	6.30	1547	229	305	11.1	3.72	0.00
	End Point	6.51	1543	226	294	10.5	4.19	2.49
	Lagoon1	6.65	1503	235	284	11.5	24.5	13.9
11-Dec.'06	Lag.1 outlet	7.06	1511	218	274	9.50	5.52	0.00
	End Point	7.34	1496	258	250	9.50	2.51	1.38

Table 7.2: Mean water quality parameters determined at various sampling points across the Acomb site from May-December 2006(where n=8).

Sample	pH	*K*(µS cm^{-1})	Alkalinity mg L^{-1} CaCO3)	*Eh*(mV)	*Tf*°C	[Dissolved Fe] mg L^{-1}	[Colloidal Fe] mg L^{-1}
Lagoon1	6.56	1517.38	222.75	208	11.9	26.2	16.3
Lag.1 outlet	6.75	1513.75	215.50	254	12.0	5.12	0.55
End Point	7.13	1510.75	220.38	218	11.9	4.97	3.59

Scrutiny of tables 7.1 and 7.2 show that the mine-water discharge entering the settlement lagoons is circumneutral with average pH in the region of 6.5. In addition. the tables revealed that water temperatures are higher in the summer months than in the winter. Similarly, dissolved iron concentrations are higher in the summer months than in the winter months. The circumneutral of the mine-water discharge at Acomb site can be attributed to the peroxide pre-dosing of the discharge before it enters the settlement lagoons. This ultimately increases the pH by reducing the water *Eh* leading to iron oxyhydroxide precipitation. Elevated water temperature and dissolved iron concentrations during the summer months could be attributed to increased sunlight and less rainfall respectively during the summer compared to the winter. Alkalinity for both influent and effluent samples is comparable because the influent mine-water is net-alkaline. The water temperature of both outlet mine-water from lagoon 1 and the final effluent are slightly higher than the influent water entering lagoon 1 (figure 7.3). Also, water temperatures in the summer months (July-September) are slightly higher compared to the winter. The reasons could be due to increased sunlight and less rainfall in the summer compared to the winter.

Although inlet and outlet water pH are net-alkaline and comparable, however, in general, outlet water pH is slightly higher than the inlet (figure 7.4). This elevated pH could be attributed to the fact that the influent water has passed through the treatment system which increased the overall water quality discharged into the local stream and hence the pH. Conductivity profiles for both inlet and outlet are quite similar and comparable (figure 7.5). This trend shows that probably the levels of dissolved ions. particularly sulphate dissolution are quite comparable in the inlet and effluents samples. Similarly, the *Eh* profile follows similar pattern as conductivity (figure 7.6). This observation is probably an indication that both influent and effluent samples are in more reduced environment. Figure 7.7 shows that alkalinity trend for both influent and effluent waters are quite similar. This observation is not surprising as both waters are net-alkaline and with no acidity.

7.2.2: Voltammetric results

This section presents the monthly measured iron concentrations at various sampling points across the site. As with all analyses in this research work, differential pulse voltammetry (DPV) was used to determine dissolved Fe. Shown in figures 7.8 to 7.10 are the mean of the total unhydrolysed (inlet vs. outlet), hydrolysed (inlet vs. outlet) and their comparison (unhydrolysed vs. hydrolysed) iron concentrations respectively over the sampling period of eight months. Trends in seasonal and temporal change in dissolved and colloidal iron concentrations at influent and effluent sampling points are revealed in figures 7.11 and 7.12 respectively while comparison of the mean of dissolved and colloidal iron concentrations at various sampling points are presented in figure 7.13. Figure 7.14 shows the percentage proportion of both dissolved and colloidal iron at various sampling points and percentage ratio of Fe(II) to Fe(III) are presented in figure 7.15.

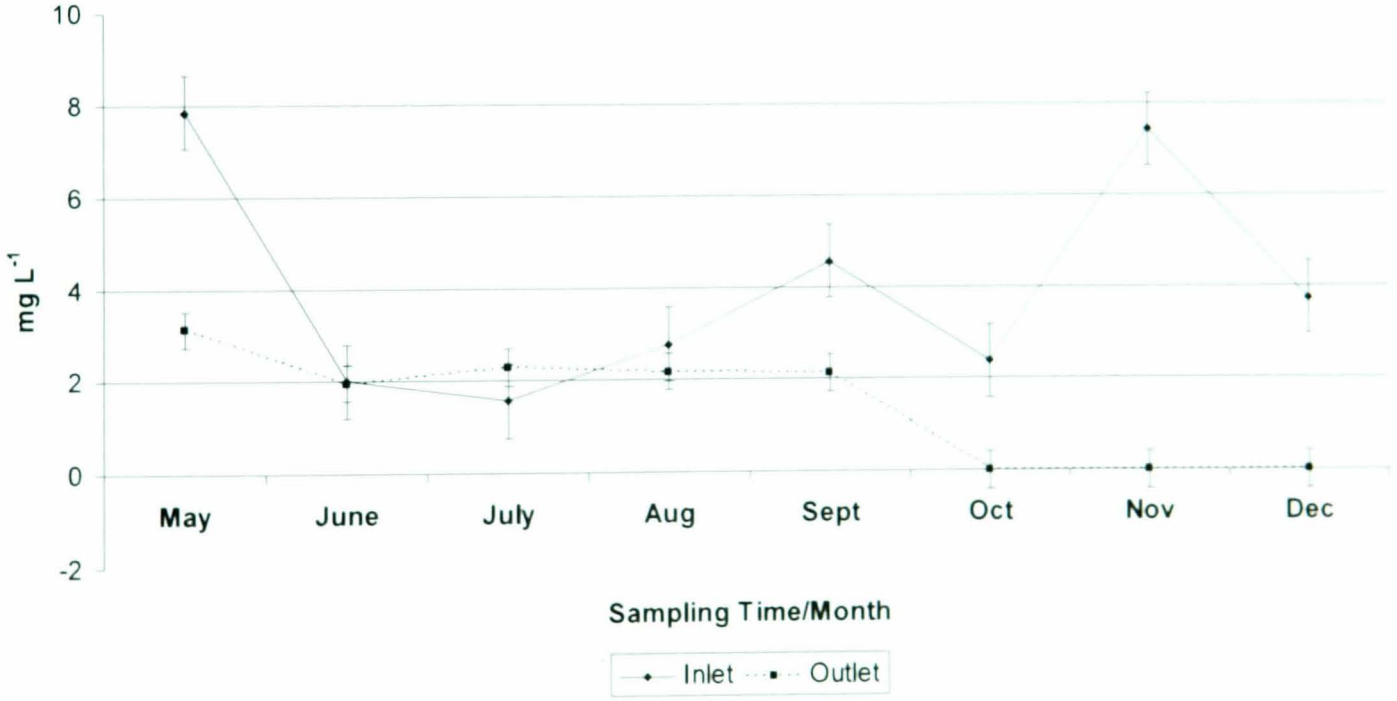

Figure 7.8: Mean total unhydrolysed iron concentrations (mg L^{-1}) for samples collected (May-December, 2006) at Acomb site. Error bars denote standard error of the mean.

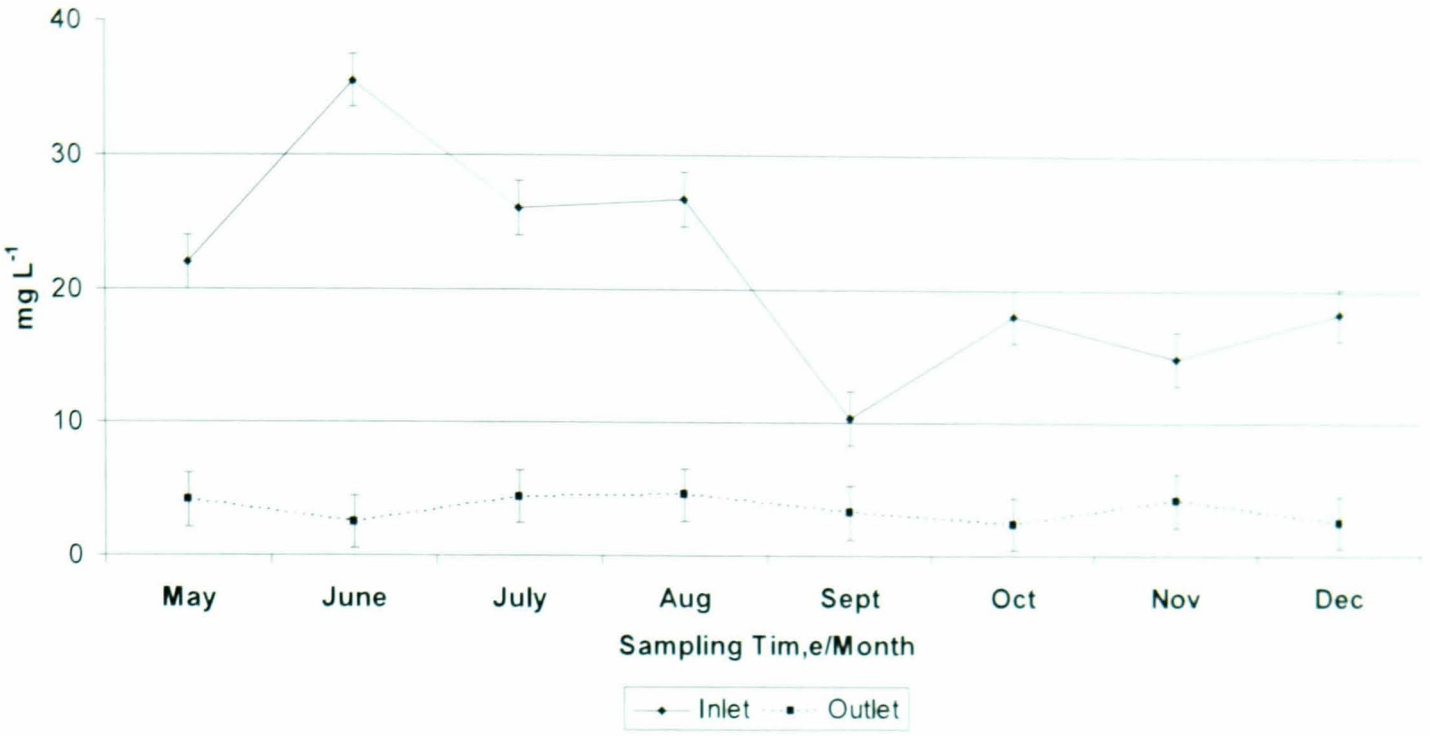

Figure 7.9: Mean total hydrolysed iron concentrations (mg L^{-1}) for samples collected (May-December, 2006) at Acomb site. Error bars denote standard error of the mean.

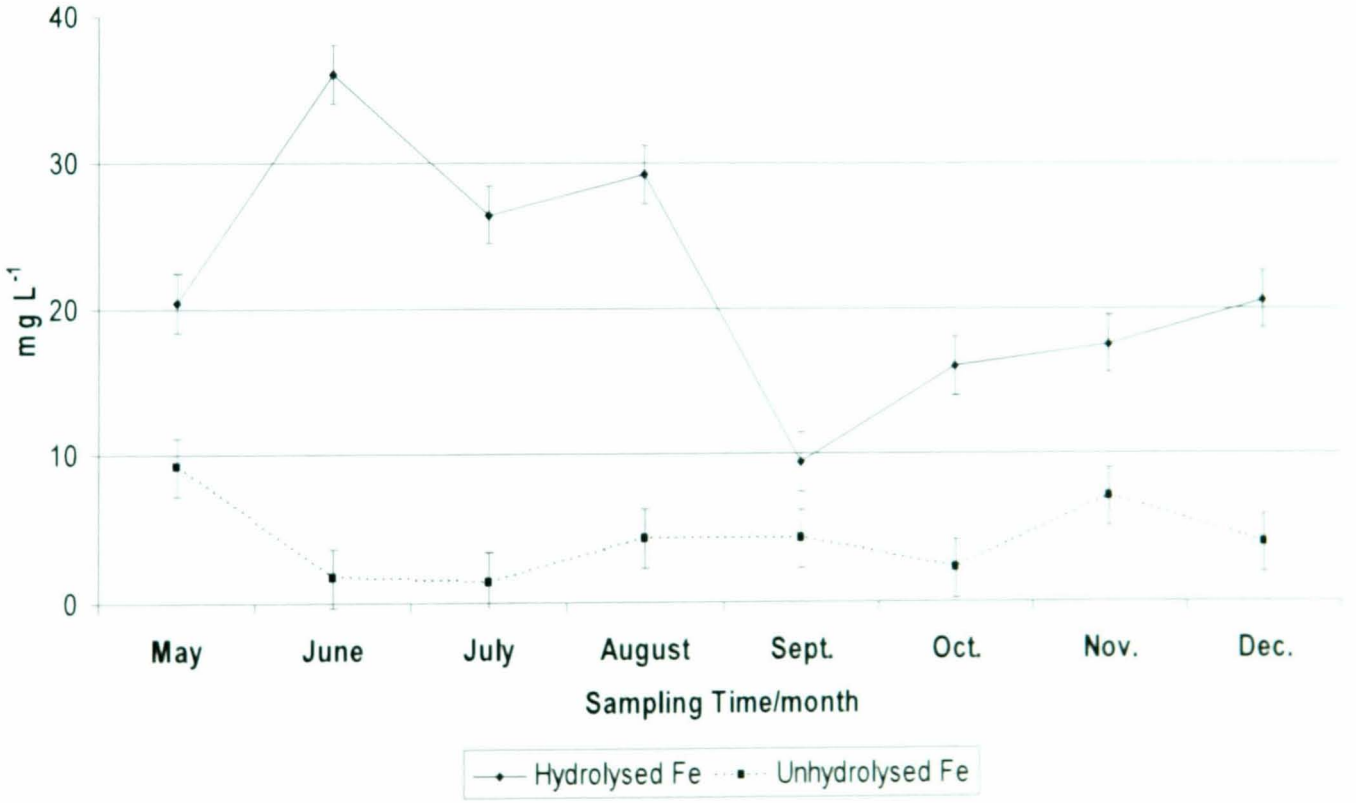

Figure 7.10: Mean total hydrolysed and unhydrolysed iron concentrations (mg L^{-1}) for samples collected (May-December, 2006) at Acomb site. Error bars denote standard error of the mean.

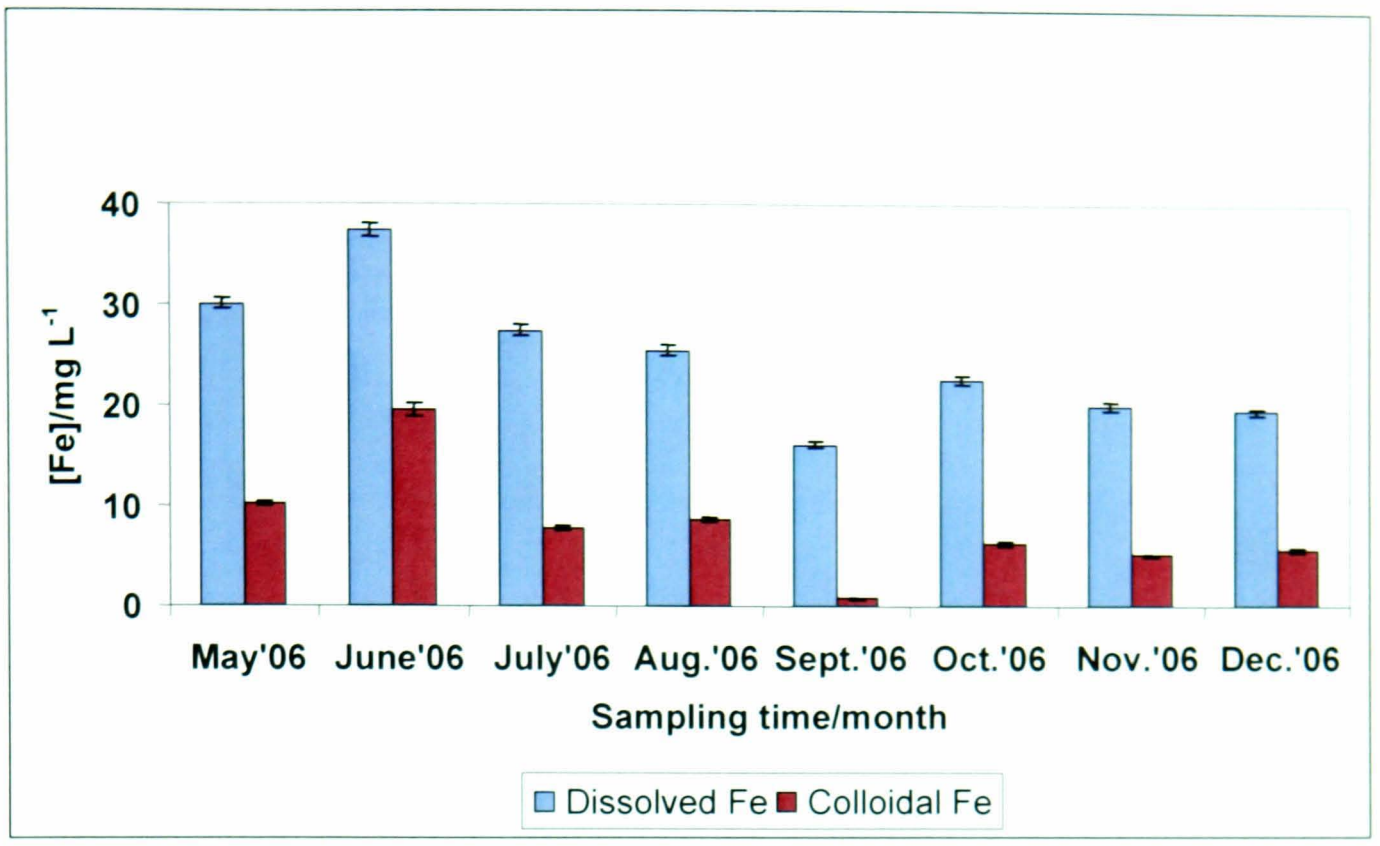

Figure 7.11: Comparison of measured proportion of dissolved and colloidal Fe at influent sampling point (May-December, 2006) at Acomb site. Error bars denote standard error of the mean.

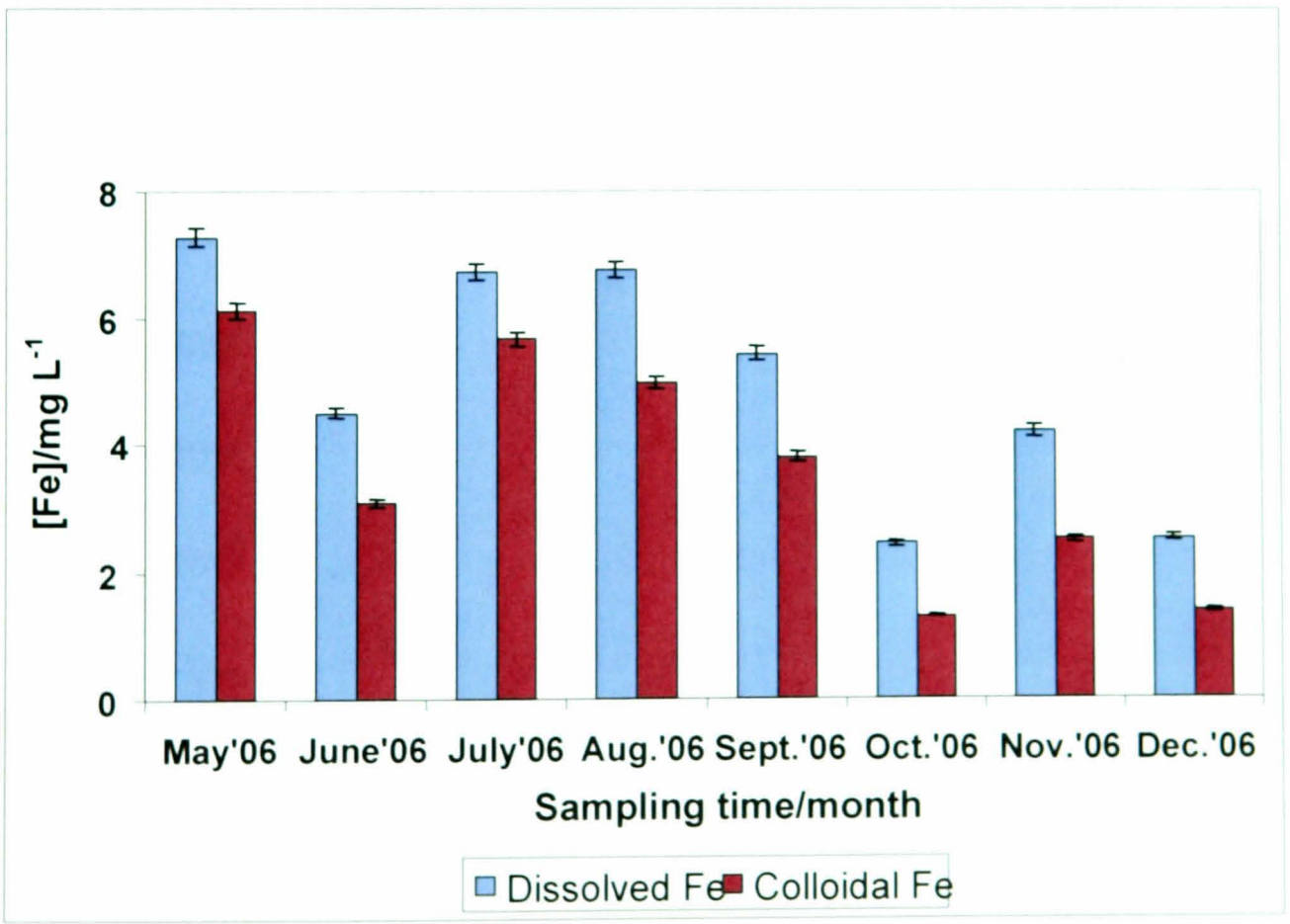

Figure 7.12: Comparison of measured proportion of dissolved and colloidal Fe at effluent sampling point (May-December, 2006) at Acomb site. Error bars denote standard error of the mean.

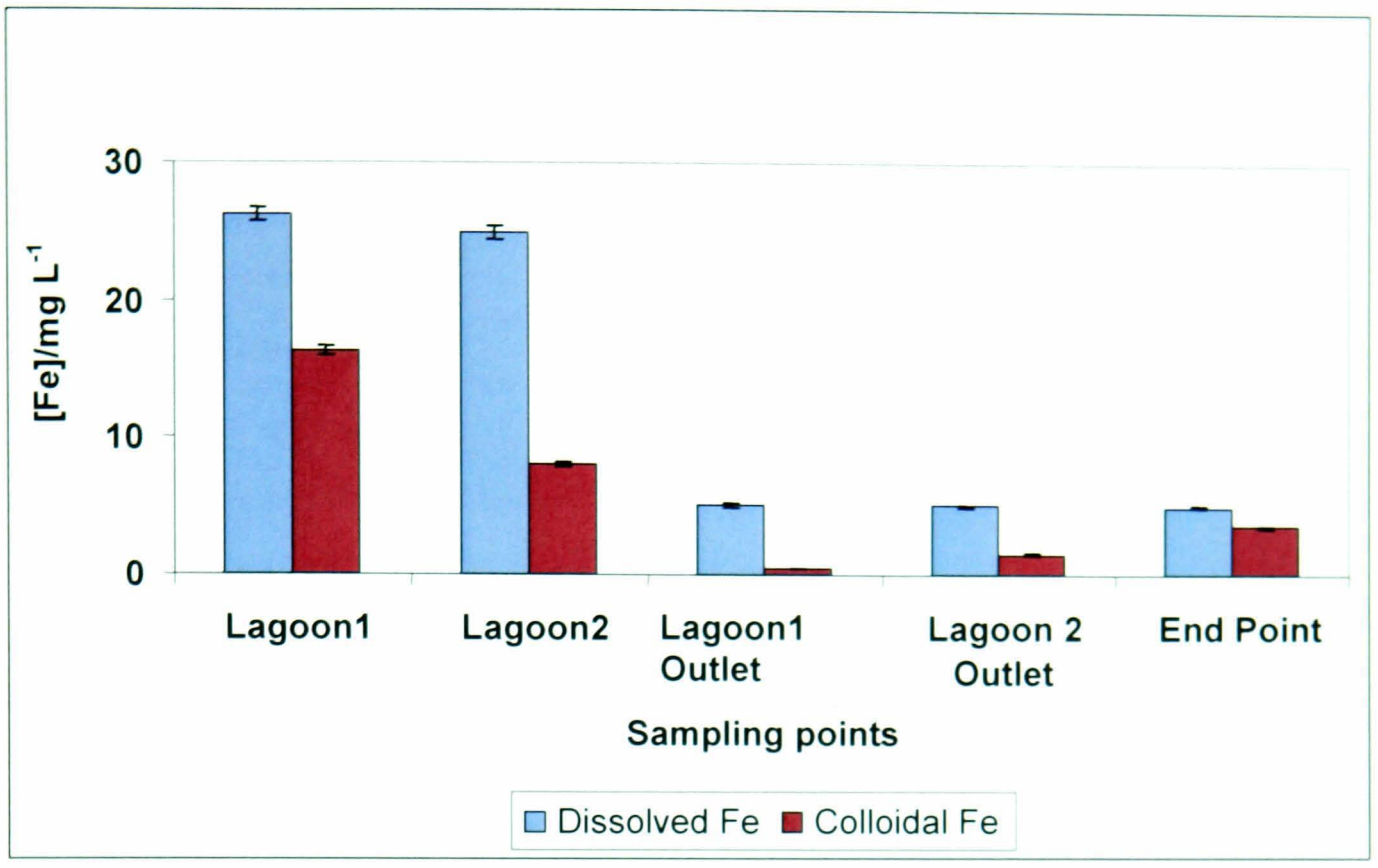

Figure 7.13: Comparison of average measured dissolved and colloidal Fe at various sampling points (May-December, 2006) at Acomb site. Error bars denote standard error of the mean.

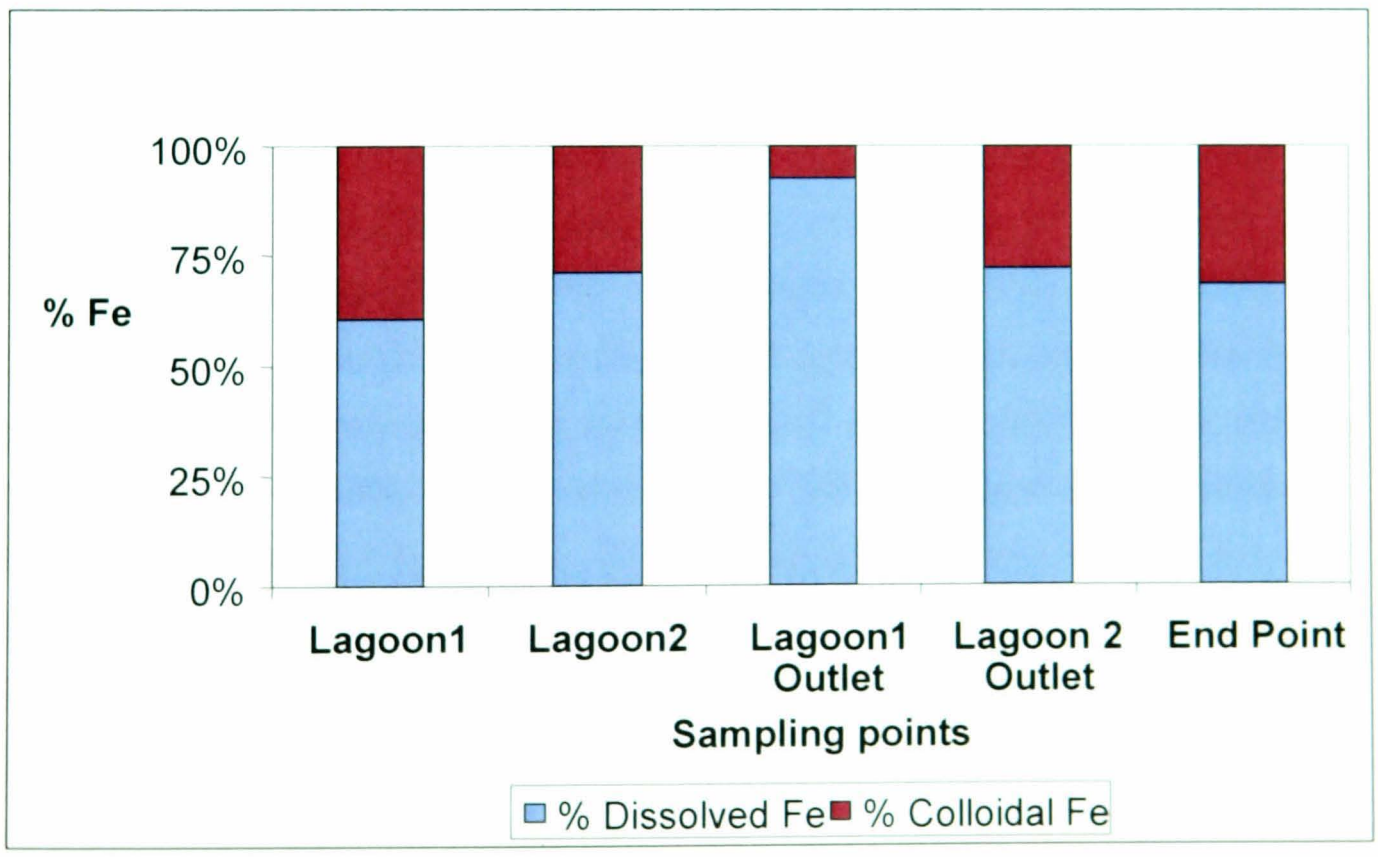

Figure 7.14: Comparison of percentage proportion of dissolved and colloidal Fe at various sampling points (May-December, 2006) at Acomb site.

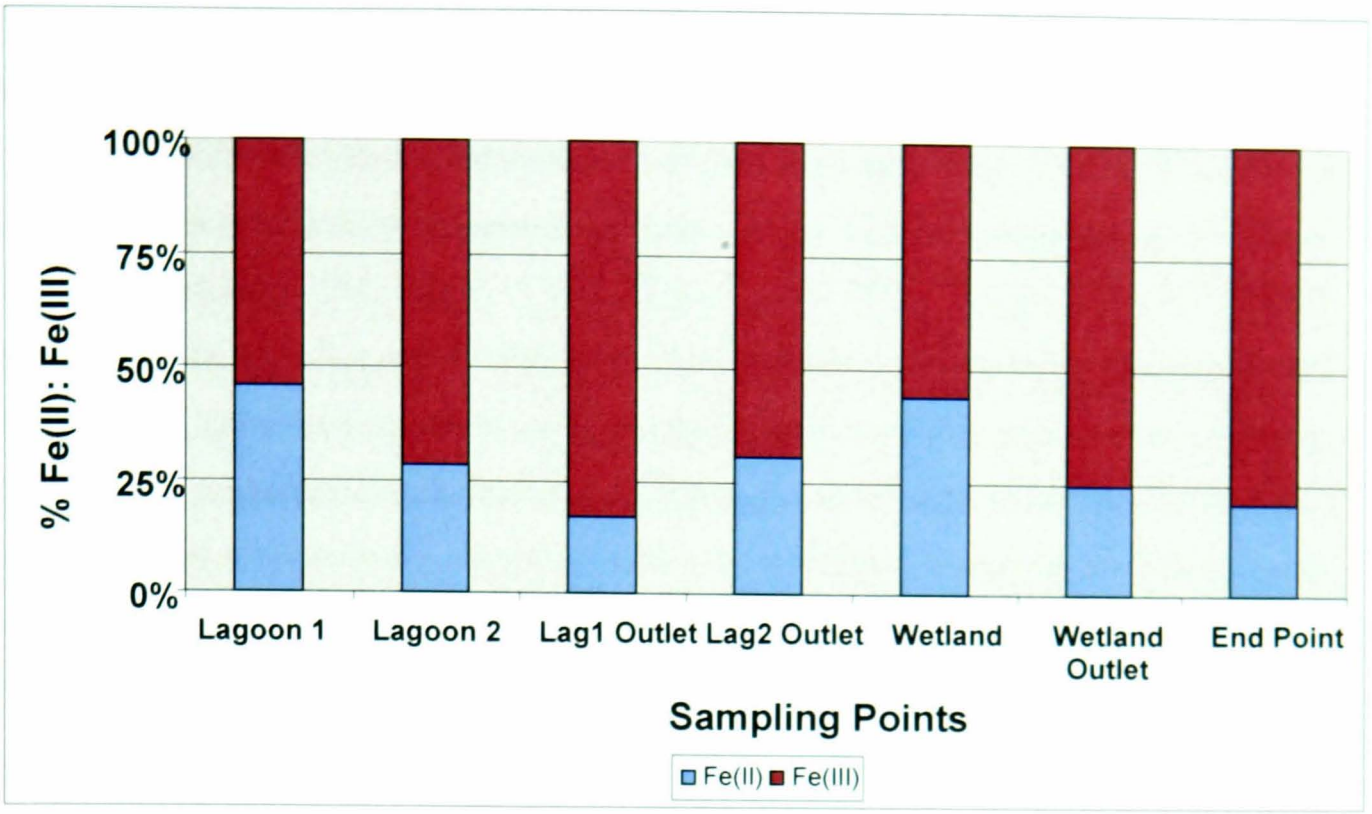

Figure 7.15: Comparison of the ratio of measured Fe (II) to Fe (III) at various sampling points (May-December, 2006) at Acomb site.

Mean concentrations of unhydrolysed iron for the influent which ranged from 2-8 mg L^{-1} was higher than the corresponding effluent which ranged from below detection limits to 3 mg L^{-1} except for July (figure 7.8). In fact, effluent concentrations are below the detection limits for the months of October- December. This trend is not surprising as one would expect reduction in the concentration of iron to reflect the effectiveness of the treatment regime. Mean concentrations of hydrolysed iron appeared stable for the effluent while influent varied widely from 12 to 35 mg L^{-1} (figure 7.9). This observation shows that influent concentrations are controlled by a wide range of geochemical factors including water pH and rainfall events among others while the effluent reflects consistency in the performance of the treatment regime. Comparison of hydrolysed and unhydrolysed iron concentrations revealed that there is more proportion of hydrolysed iron than unhydrolysed iron as shown in figure 7.10. Although, hydrolysis of iron would normally generate more acidity, however, at the Acomb site, probably the acidity is neutralised by the peroxide pre-dosing at this site. Hydrolysis of iron:

$$Fe^{3+} + 3H_2O \text{ ---------} \rightarrow Fe(OH)_3 + 3H^+$$

Since hydrolysed iron is essentially Fe(III), this means that Fe(III) is more abundant than the unhyrolysed iron.

Comparison of the proportion of dissolved iron to colloidal iron for the influent samples (figure 7.11) shows that in general, dissolved iron is higher than the colloidal iron. In addition, elevated concentrations of dissolved iron ranged from 28 to 38 mg L^{-1}, were observed during the summer months (May- August) compared to the winter months (September-December), which ranged from 18 to 22 mg L^{-1}. The effluent profile followed similar trends (figure 7.12), but at lower concentrations compared to the influent. These observations are consistent with the rainfall event which probably led to lower concentrations in the winter months due to dilution from the runoff water. The mean the total dissolved and colloidal iron at various sampling point across the site show progressive reduction in the concentrations of both dissolved and colloidal iron from the inlet to the end point (figure 7.13). This observation suggests that the treatment regime is effective and efficient in reducing iron concentration and probably some iron might have been precipitated as iron oxyhydroxides during the process as water passes through the wetland.

The average dissolved and colloidal irons ranged from 60 to 90% and from 10 to 40% respectively (figure 7.14). However, the proportion of colloidal iron at the end point is 30%. The data suggests that about 70% of the total effluent discharged into the stream is 70% dissolved, though at low concentration which is not deemed to be polluting though still higher than the EU recommended limits of 1 mg L^{-1}. Figure 7.15 showing comparison of the ratio of Fe(II) to Fe(III) shows that the ratio varied widely from different sampling points across the site. For example, the ratio was 1: 1 at the influent and about 1: 4 at the lagoon outlet, and then changed to 1: 1 within the polishing wetland and finally 1:3 at the end point. These observations suggest that the tracking of the ratio of Fe(II) to Fe(III) trends are complex.

7.2.3: Relationships between iron concentrations and the various measured parameters that controls iron geochemistry; *Eh*, pH and alkalinity

Relationships and correlations between various measured parameters together with explanations of the observed trends and geochemical significance and implications of these trends are presented in this section. Figure 7.16 shows the relationship between measured water alkalinity as a function of dissolved and colloidal iron concentrations over the sampling period May-December 2006. Seasonal and temporal variability in temperature as a function of dissolved and colloidal iron concentrations is presented in figure 7.17 while figure 7.18 shows the trend in redox potential (*Eh*) as a function of water pH. The plot of water pH against water alkalinity is shown in figure 7.19 while the mean total iron concentrations as a function of pH is presented in figure 7.20. Total iron concentrations as functions of water pH, *Eh* and alkalinity are presented in figures 7.21-7.23.

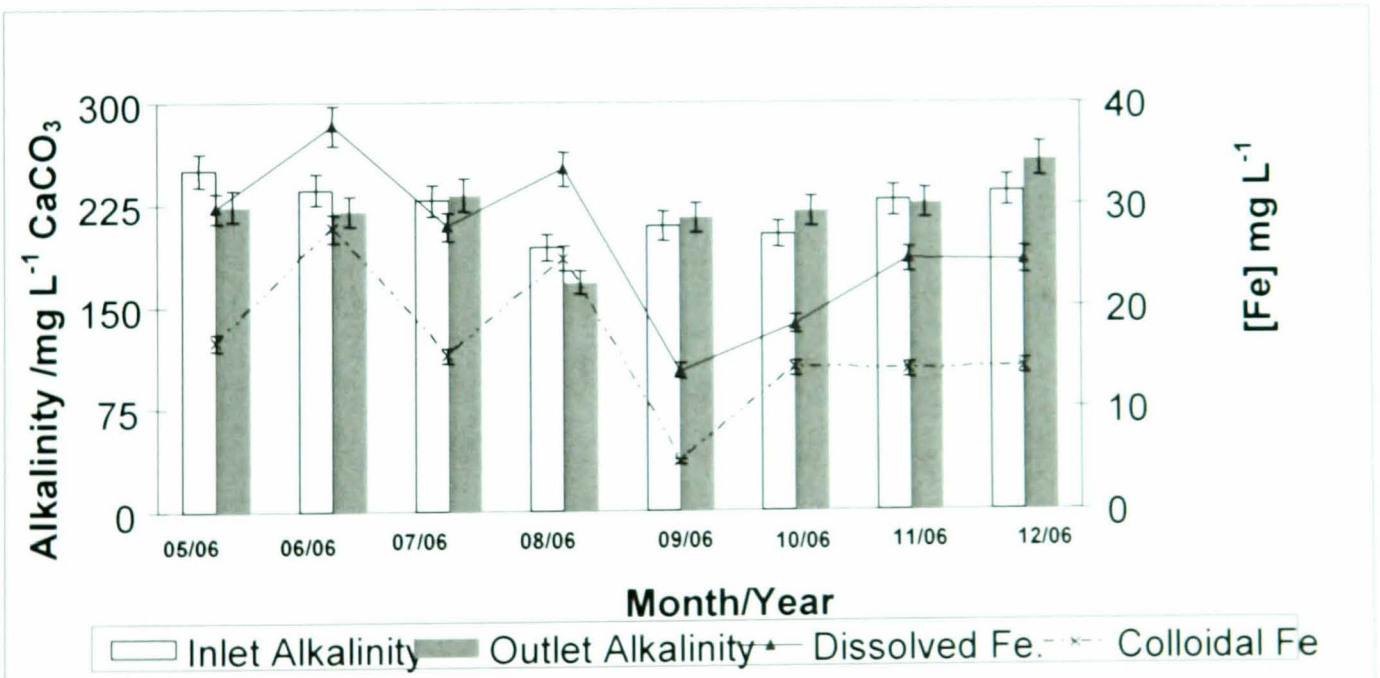

Figure 7.16: Showing seasonal and temporal profile of alkalinity, dissolved and colloidal Fe concentrations for samples taken May-December 2006 at Acomb treatment system site at Hexham, Northumberland.

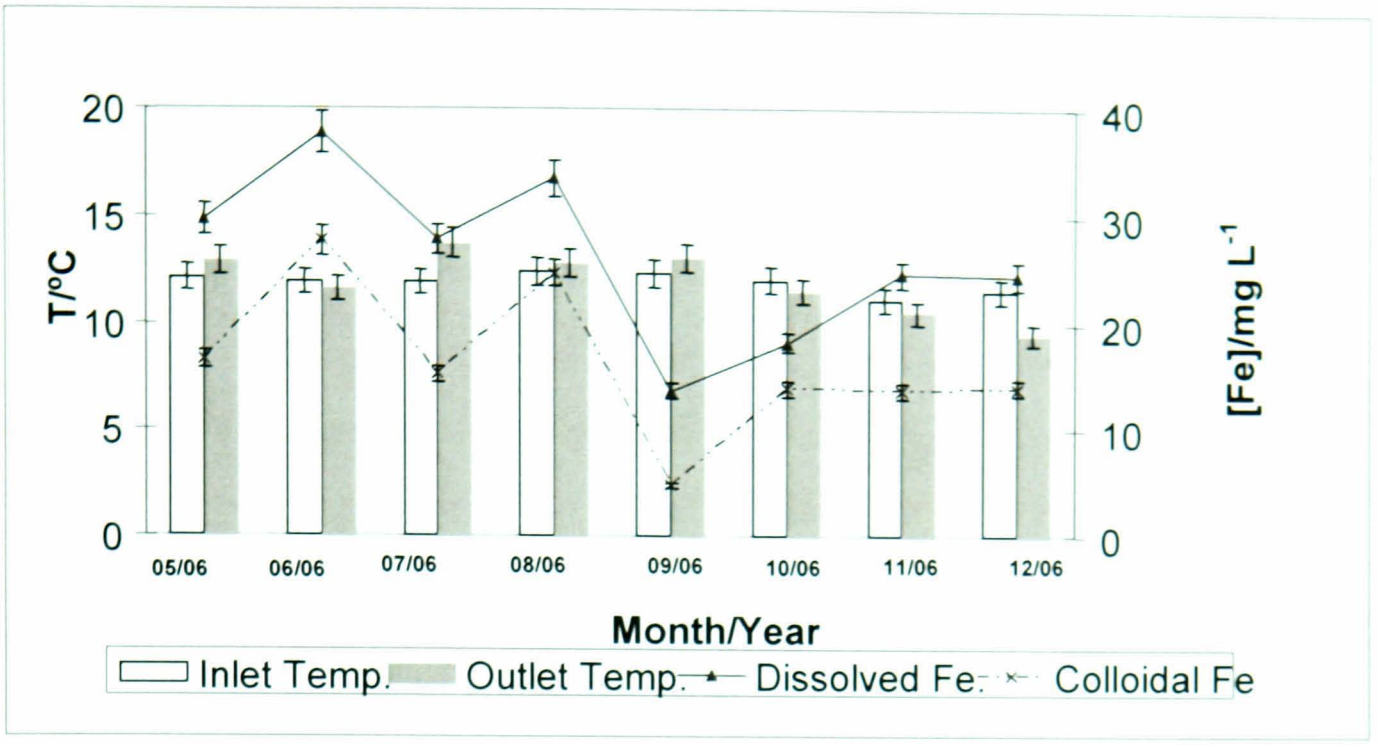

Figure 7.17: Graph showing seasonal and temporal profile of temperature as a function of dissolved and colloidal Fe concentrations for samples taken May-December 2006 at Acomb treatment system site in located at Hexham, Northumberland.

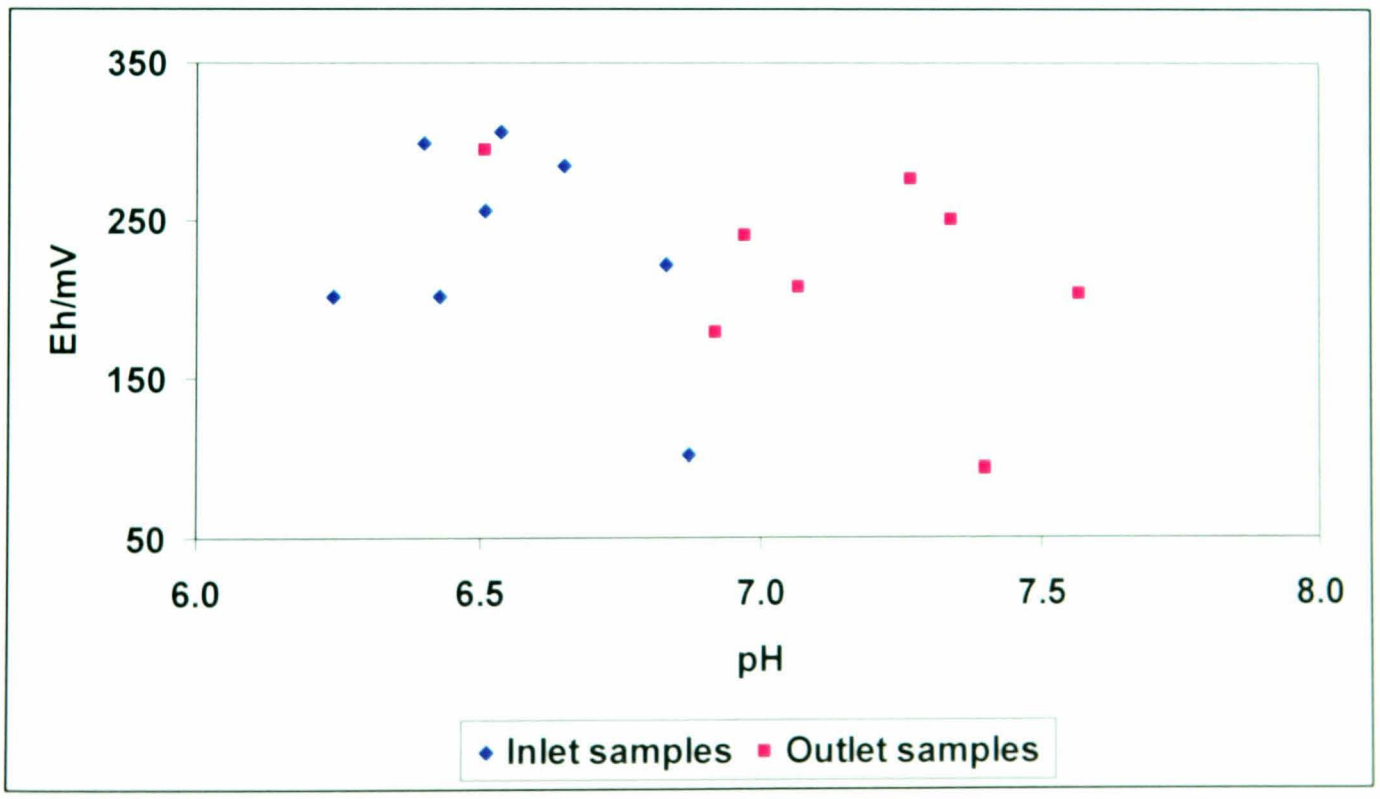

Figure 7.18: Measured *Eh* as a function of pH for inlet and outlet samples taken from May-December 2006 at Acomb treatment system site. The least square regression equation is: pH=-118.01* Eh + 1007.9 and R^2=0.14.

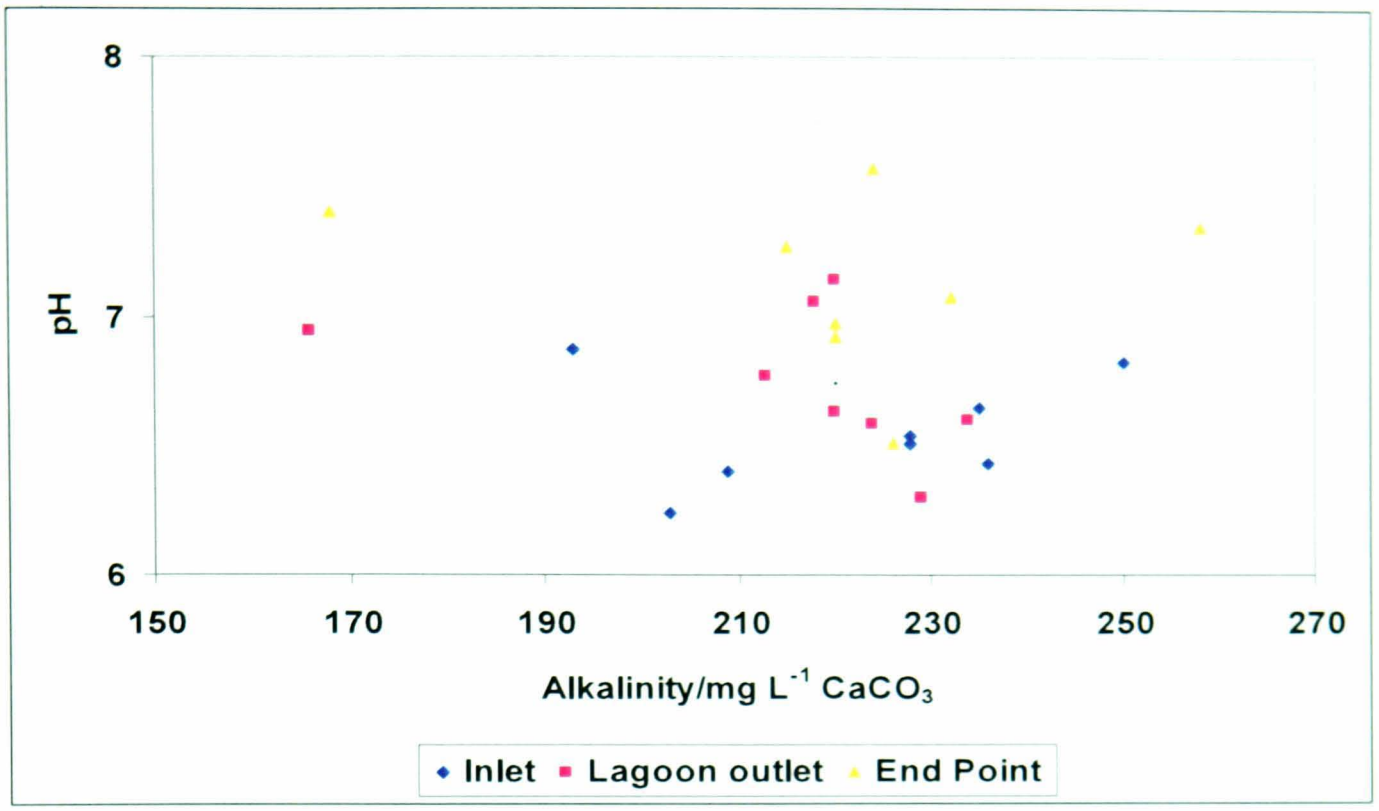

Figure 7.19: Showing the relationship between pH and alkalinity for samples taken from May-December 2006 at Acomb treatment system site.

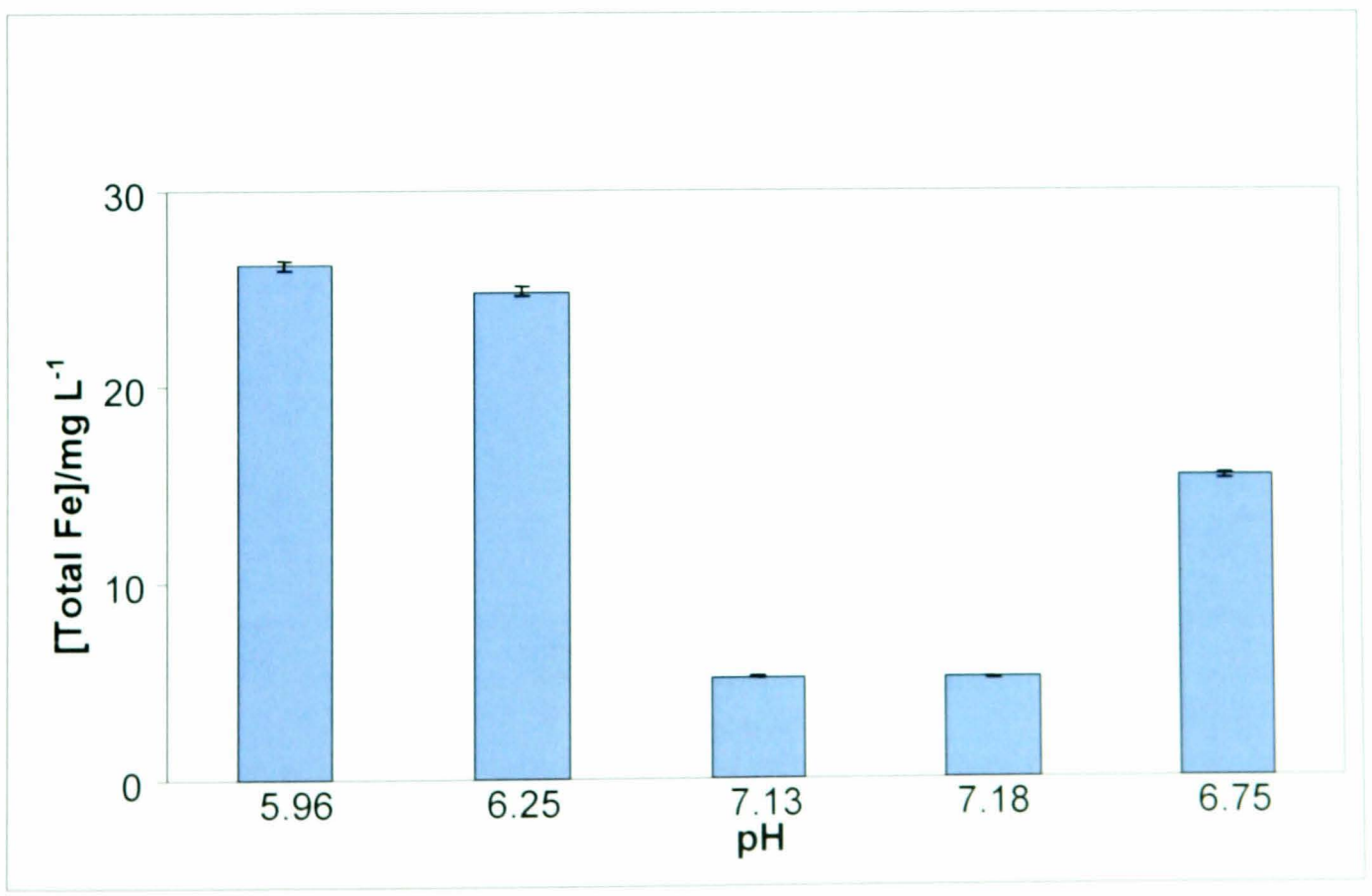

Figure 7.20: Mean total iron concentrations as a function of pH for samples taken May-December 2006 at Acomb treatment system site at Hexham, Northumberland.

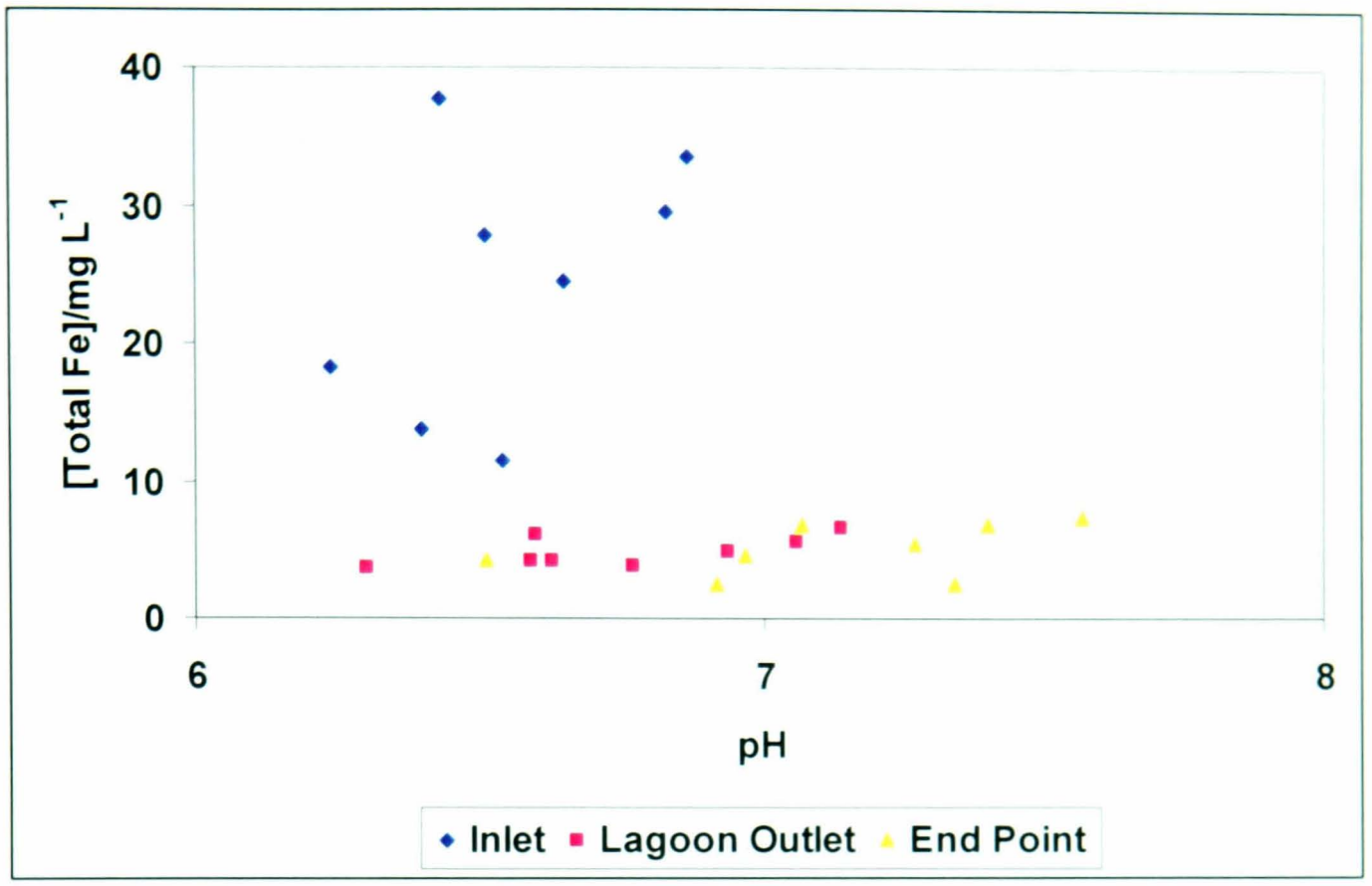

Figure 7.21: Total iron concentration as a function of pH for samples taken from May-December 2006 at Acomb treatment system site.

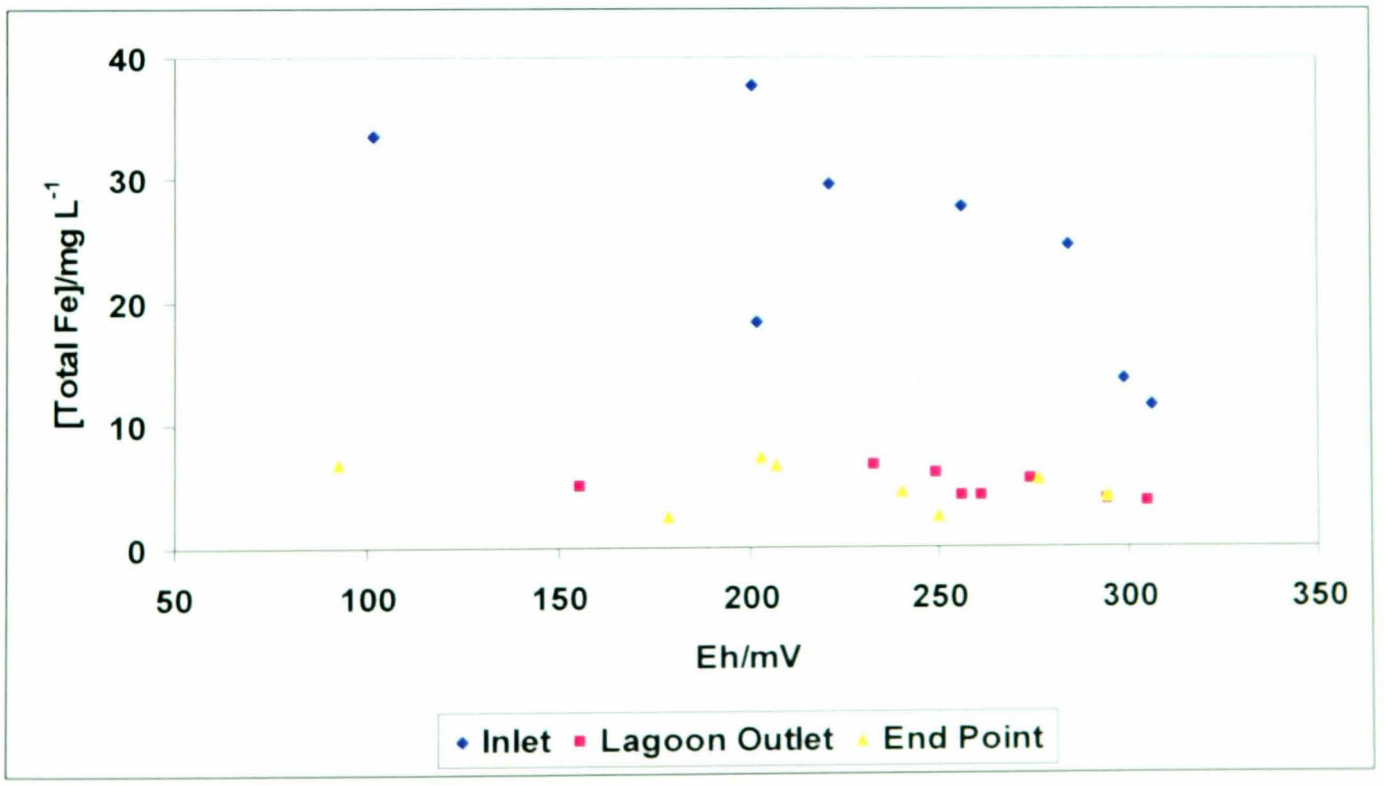

Figure 7.22: Total iron concentration as a function of redox potential (*Eh*) for samples taken from May-December 2006 at Acomb treatment system site.

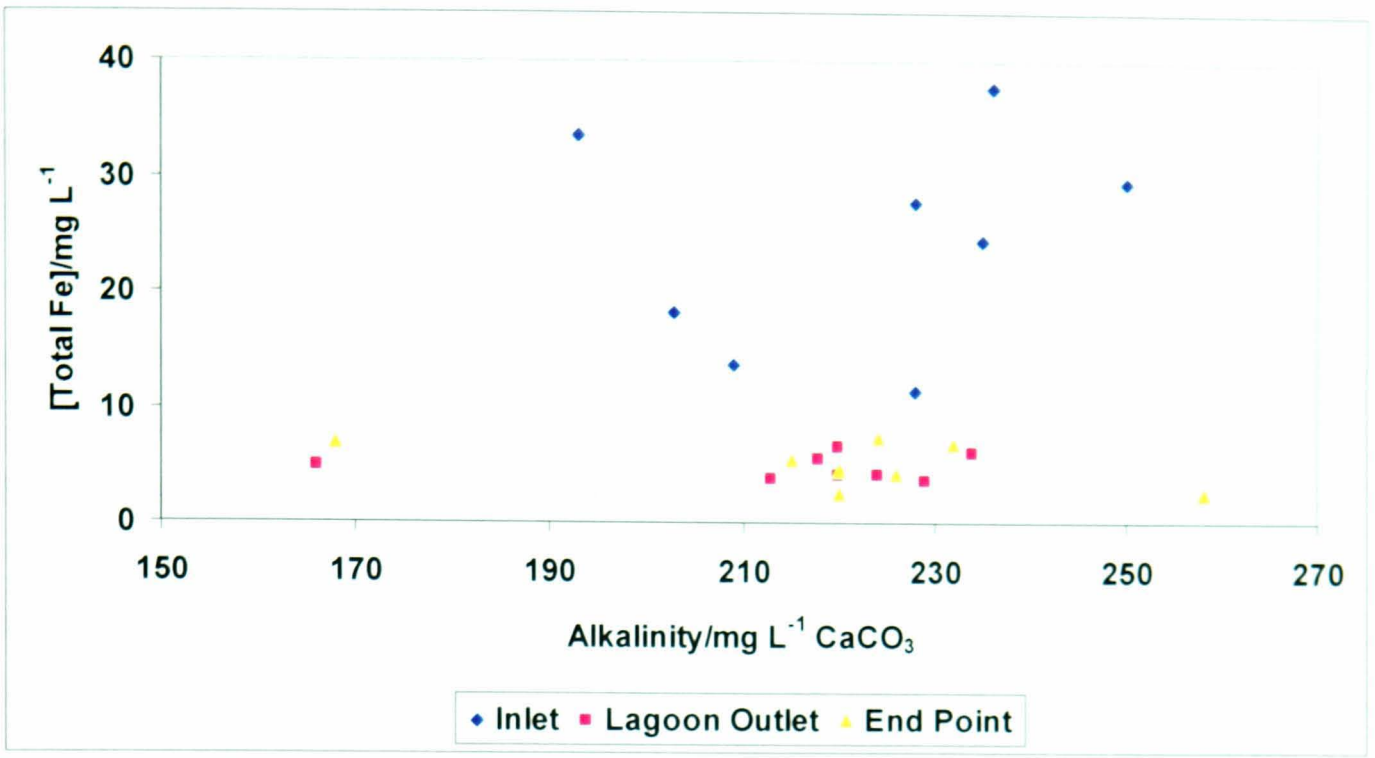

Figure 7.23: Total iron concentration as a function of alkalinity measured as mg L^{-1} of $CaCO_3$ for samples taken from May-December 2006 at Acomb treatment system site.

Relationship between alkalinity and the proportion of dissolved and colloidal iron showed a complex trends as both dissolved and colloidal iron appeared to increase with increasing alkalinity with few exceptions (figure 7.16). The trend for both dissolved and colloidal iron concentrations are comparable and similar. This irregular behaviour could be attributed to the fact that the influent sample is net-alkaline due to peroxide pre-doing treatment. The proportion of dissolved and colloidal iron concentrations increase with increasing water temperature except for September and October as shown in figure 7.17. This trend suggests that when the water body is warmer, more iron is dissolved in the water, thus, the elevated iron concentrations. However, we observed more complex and unexplainable trends in the relationship between temperature and pH for both influent and effluent samples. But in general, water temperature increases with increasing pH in both cases, with few exceptions. The graph of water *Eh* as a function of water pH shows no correlation for both inlet and outlet samples with (R^2= 0.14 and 0.21) respectively (figure 7.18). This observation is rather surprising as both Eh and pH are analogous in many ways [5].

In addition, the process of iron reduction in mine-water treatment systems is such that high pH is accompanied by low water *Eh* leading to reduction in iron concentrations [6]. The observed trends could however be attributed to the fact that determination of *Eh* in natural environments is quite complex [5] as some of the reactions that determine the *Eh* of a water body are slow and the measured potential may not represent the true equilibrium potential of the water [6, 7]. Previous works have shown that measured *Eh* values for oxygen-containing environments are generally lowered than the equilibrium value [7, 8, 9]. Similarly, pH-alkalinity profiles for inlet, lagoon outlet and endpoint samples show no correlation (figure 7.19). In most cases, outlet samples attained pH > 7 with increasing alkalinity. This indicates that acidity has been neutralised and the outlet water has become net alkaline. Furthermore, previous works [6, 7, 8, 9] show that alkalinity generation could be associated with sulphate removal due to microbial activities of the sulphate reducing bacterial (SRB), thus giving a rather complex and variable behaviours. As stated in the above paragraph, pH-alkalinity relationship is determined by complex biogeochemical processes of iron and sulphate reductions, coupled with pH elevation and $CaCO_3$ dissolution [5, 8]. In addition, water pH is determined by the combined effects of the carbon dioxide system, the boric acid system and various organic acids in the systems [5]. Measured mean total iron concentration as a function of pH (figure 7.20) shows that iron concentrations increases with reducing pH. This observation is not surprising as more iron will be precipitated out as iron oxyhydroxides at higher pH. However, total iron concentrations show rather poor correlation with pH for all datasets as shown in figure 7.21. This observed trend is rather surprising and this could only be attributed to the fact that reducing zones are associated with anoxic conditions where relatively large amounts of Fe(III) oxyhydroxides grain coatings are present [9, 10]. Generally, oxidation of iron takes place much more completely in alkaline medium than in acid [8, 9], thus, larger amounts of dissolved iron are commonly present in slightly acid water than in the faintly alkaline water [10, 11, 12].

It is apparent from figure 7.22 that whilst measured total iron concentrations with water *Eh* is poorly correlated (R^2=0.5) for the inlet water samples, there is no correlation between measured total iron concentrations and the water *Eh* for samples taken from both lagoon outlet (R^2=0.17) and endpoint (R^2=0.13) respectively.

The aforementioned similarity of the trend in *Eh* and total iron concentration profiles indicate that the controlling influence of *Eh* and pH is very significant in determining the iron chemistry. These complex influences include redox transformations associated with oxidation and reduction of iron and sulphur (genesis of alkalinity) and overall iron precipitation. Previous studies have reported high degree of variability in the extent to which RAPS treatment systems is remediated by wetland ecosystems [13, 14, 15]. Studies have shown that major remediative processes including iron geochemistry within the wetland systems are microbially driven [16, 17] and many dissolved trace elements including iron have been found to exhibit strong relationship with flow conditions [17], suggesting predominantly diffuse nature of these elements [18]. For example, it has been observed that sulphate-reducing zones are characterised with low concentrations of dissolved iron (through iron disulfide precipitation) [16] and both aerobic and anaerobic bacteria can proliferate around areas of high dissolved iron concentrations [15, 16]. Moreover, redox potentials (*Eh*) in natural environments are difficult to predict because some of the reactions that determine *Eh* are slow and the measurements may not give the true equilibrium potentials differences, this is particularly true for reactions involving oxygen-containing environment with rather complicated mechanism and which generally give *Eh* values lower than equilibrium values [17]. This limits of measured *Eh* values means that redox potential measurements in natural environments can only provide qualitative or semi-quantitative information [17]. Nevertheless, the general observation (with few exceptions) from total iron concentrations as a function of *Eh* is that elevated pH and reduced *Eh* environment lead to reduction in total iron concentrations.

The plots of total iron concentrations as a function of water alkalinity as mg L-1 of $CaCO_3$ shows no correlation for inlet, lagoon outlet and the endpoint samples respectively (figure 7.23). This observation is consistent with studies by Hedin [19], attributing water alkalinity to the rate of iron oxidation and hydrolysis. In general, as water flows through the wetland treatment system, water pH rose while concentrations of alkalinity and iron fell. The observed decrease in alkalinity is due to the neutralisation of acidity produced by iron oxidation and hydrolysis:

$$Fe^{2+} + 2HCO_3^- + 1/4O_2 \dashrightarrow FeOOH\,(s) + 3/2H_2O + 2CO_2.$$

Increased pH is a common feature of passive treatment systems such as the treatment system at Acomb site with net alkaline water which is attributed to exsolution of CO_2 as shown in the equation above [20, 21]. This implies that acidity has been neutralised and the effluent water has become net alkaline. Furthermore, oxidation of iron takes place much more completely in alkaline medium than in acid medium. Thus, larger amounts of dissolved iron are commonly present in slightly acidic waters than in the faintly alkaline waters [21]. Previous work by [6] shows that alkalinity generation could also be associated with removal of sulphate, that is, with microbial sulphate reduction, thus, giving a rather complex and variable behaviour.

7.3: Conclusions

The following conclusions could be drawn from the study of this site:

Onsite water quality parameters such as water temperature, pH, conductivity, *Eh* and alkalinity suggest that although, both values at influent and effluent are comparable and similar, however, the overall water quality at the effluent is better than the influent. This observation demonstrates the improvement in the effluent water quality after the treatment process.

Voltammetric data indicate that the proportion of hydrolysed iron accounts for up to 70% of the total abundant iron concentration while unhydrolysed proportion accounts for 30%. This observation is very significant in the treatment and remediation of mine-waters as this will shed more light into the iron redox chemistry particularly, in the ratio of Fe (II) to Fe (III). It is believed that this is the first time this observation has been made and reported in the study on CoSTaR sites.

Furthermore, there is change in the proportion of dissolved and colloidal iron in the influent waters and effluent waters respectively. For example, on the average, colloidal accounts for a fourth of the total influent iron concentrations and about one-tenth of the total effluent iron. This is very significant and important in the choice of remediation strategies for mine-water treatment.

Reduction in the concentration of iron from 28 mg L^{-1} for influent water to about 6 mg L^{-1} for effluent suggests that the treatment regime is effective and efficient.

Overall, the percentage of the proportion of the colloidal iron varied from the influent composition to the effluent. For example, the colloidal proportion is about 40% in the influent water and 30% in the effluent water. This observation is very significant in the treatment of polluted mine-water and it can determine the choice of remedial technology. For example, if iron exists in solid phase in the mine-water, this can be physically trapped and a simple wetland based technology can be used. However, where the situation is more complex, the choice could be between systems such as reducing and alkalinity producing system (RAPS) or permeable reactive barrier (PRB).The rate of iron removal is influenced by a number of factors but it is significantly influenced by the efficiency and effectiveness of the treatment regime particularly the wetland.

Data from determination of the ratio of Fe (II) to Fe (III) suggest that the ratio varies from influent water to the effluent waters. For example, the study shows that the ratio of Fe (II) to Fe (III) appeared to be 1: 1 whereas, it is 1:3 for the effluent. This observation of the variation in the ratio of both iron species at influent and effluent are very important in understanding the change in the iron speciation and redox processes.

It is important to point out that the pH of influent water in this site is net-alkaline and present a different challenge from the sites with net-acidity.

Overall, the Acomb remediation project has addressed the environmental issues related to iron concentration as summarised in this chapter with a comprehensive program of integrated and cost-effective remedial actions.

These studies have shown (for the first time) that voltammetric technique such as differential pulse voltammetric (DPV) is robust and offers alternative means of monitoring iron concentration in polluted mine-waters with potential for in-situ application.

7.4: References

[1]. Amos, P., Aplin, A.C., Bowden, L., Daugherty, A.J., Elliot, A., Jayaweera, A., Johnson, D.B., Martin, A., Wood, R. & Younger, P.L. *Land Contamination Reclamation*, **2004**, 11, 127-135.

[2]. Younger, P.L., Jayaweera, A., Elliot, A., Wood, R., Amos, P., Daugherty, A.J., Martin, A., Bowden, L., Aplin, A.C. & Johnson, D.B. *Land Contamination and Reclamation*, **2003**, 12, 135.

[3]. CL:AIRE Case Study Bulletin CSB4 (March **2006**). Coal Mine Sites for Targeted Remediation Research: The CoSTaR initiative.

[4]. Younger, P.L. *International Mine Water Association, Johannesburg*, **1998**

[5]. Younger, P.L., Jayaweera, A. & Wood, A. Proceedings of the CL: AIRE Annual Project Conference, April **2004**, London.

[6]. Younger, P.L. Proceedings of CL: AIRE Annual Project Conference, April **2002**, London, 21pp.

[7]. Younger, P.L. Final report to Durham County Council and the County Durham Environmental Trust (CDENT). **2000**.

[8]. CL:AIRE Case Study Bulletin CSB4 (March **2006**). Coal Mine Sites for Targeted Remediation Research: The CoSTaR initiative.

[9]. Fabian, D., Aplin, A.C. & Younger, P.L. Proceedings of 9th International Mine Water Congress, 5-7 September **2005**, Ovendo, Spain, 383-387.

[10]. Fabian, D., Jarvis, A.J. & Younger, P.L. CL: AIRE Technology Demonstration Report (TDP5), April, **2006**.

[11]. CL: AIRE Case Study Bulletin CSB4 (March **2004**). Mine Water Treatment at Wheal Jane Tin Mine, Cornwall.

[12]. Mukhopadhyay, B., Bastias, L. & Mukhopadhyay. *Mine Water and the Environment*, **2007**, 26, 29-45.

[13]. Singer, P.C. & Strumm, W. *Applied Geochemistry*, **1970**, 167, 1121-1123.

[14]. Gray, N.F. *Environmental Geology*, **1996**, 27, 358-361.

[15]. Apello, C.A.J. and Postma, D. Geochemistry, Groundwater and Pollution. *Rotterdam: Balkema*; **1993**, 536pp.

[16]. Gandy, C.J., Smith, J.W.N. and Jarvis, A.P. *Science of the Total Environment*, **2007**, 373, 435-446.

[17]. Krauskopf, K.B. Introduction to Geochemistry, *McGraw-Hill*, **1979**, 617pp.

[18]. Brown, C.J., Walter, D.A. and Colabufo, S. *Long Island Geologists*, **1999**, 96pp.

[19]. Whitehead, P.G. and Prior, H. *Science of the Total Environment*, **2005**, 338, 15-21.

[20]. Hedin, R.S. *Mine Water Environment*, **2008**, 230, 41-49.

[21]. Whitehead, P.G., Cosby, B.J. and Prior, H. *Science of the Total Environment*, **2005**, 338, 125-135.

Chapter 8

SHILBOTTLE SITE, NORTHUMBERLAND

This chapter focuses on the Shilbottle site, Northumberland. The first section of the chapter provides an overview of the site background and the problems of acidic, metalliferous leachate arising from this site. The chapter goes on to present water quality data and results determined at various sampling points across the site. These results are then discussed before drawing some conclusions in the closing section. The Shilbottle site contains some of the highest iron concentrations in the UK [2, 5, 6]; it differs from the other sites in this study because the waters consist of spoil-heap leachate.

8.1: Site History, Background, Problems and Treatment Regime

Shilbottle Colliery, formerly known as Grange Pit was one of the largest working mines in the UK during its 100 years lifetime from 1882 to 1982. Although, there are records of mining activity on this site from 1882, production increased significantly from 1914 when the site was taken over by the Cooperative Society. The mine site was closed and abandoned for nearly 50 years and no attempt at remediation was made until 2002. The site was acquired by Northumberland Council County after its closure in 1982.

The major source of the acidic and metalliferous leachate from this site is from the spoil heap and due to the presence of highly pyritic shale which is embedded in the seam (which was worked on during its operation), within the carboniferous limestone series (Dinatian). Although, waters from the flooded mine workings are buffered by the limestone which overlies the shale, the spoil does not contain any limestone and is therefore highly acidic. In fact, the leachate from this site is the most polluted spoil heap documented in the UK [6, 7]. The highly polluted leachate is acidic with a pH of 3 and contaminated by various metals particularly Fe, Mn, and Al [6]. This contamination led to severe pollution in the form of iron oxyhydroxides ('ochres'), aluminium hydrosulphate foams and localised patches of black manganese ('wad') of the local stream-Tyelaw Burn. The Tyelaw Burn is a tributary of the River Coquet which is a Site of Special Scientific Interest (SSSI) and renowned for its salmon

fishing. The River Coquet is also a drinking water resource and therefore its quality is constantly monitored.

Based on preliminary laboratory work carried out by Amos & Younger [1], a Permeable Reactive Barrier (PRB) was designed and constructed on the site. Although, there were a series of wetlands which predate the construction of the PRB by some years, however, the problem with this existing system was that it only received 40% of the water at the site and there was also no mechanism for alkalinity generation [4]. PRB was constructed in order to address these two key issues to ensure that the water discharged into the receiving water course-Tyelaw Burn is of good quality, that is, increased pH and considerable reduced iron concentration. PRB is essentially a trench filled with carefully selected porous media which have reactive properties appropriate to the attenuation of the contaminants of interest [6]. A cross-section illustrating the PRB concept is given below (figure 8.1).

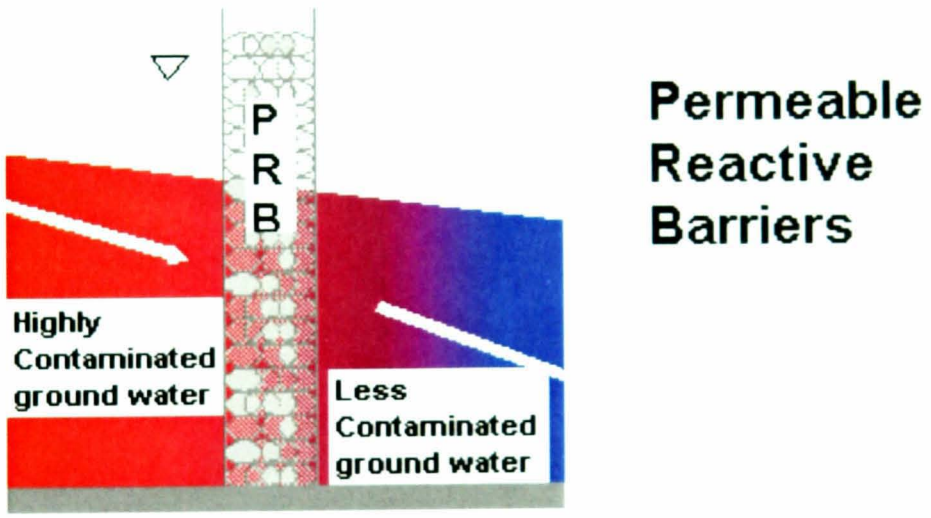

Figure 8.1: Schematic diagram showing a cross-section of a PRB at Shilbottle site-Courtesy of HERO research Group at Newcastle University.

The first of the processes in PRB is the dissolution of calcite (usually in the form of carboniferous limestone) which at pH < 5, is represented by the reaction [13]:

$$CaCO_3 + 2H^+ \longleftrightarrow Ca^{2+} + H_2O + CO_2 \qquad (1)$$

The consumption of protons (H^+) in equation 1 will results in an increase in pH. which gives rise to equation 2, which becomes dominant by generating bicarbonate alkalinity [2].

$$CaCO_3 + H_2CO_3 \leftarrow\text{---}\rightarrow Ca^{2+} + 2HCO_3^- \qquad (2)$$

Both reactions (1) and (2) occur more efficiently over time under anoxic conditions [2], because iron and aluminium in particular may form a hydroxide precipitate on the surface of the calcite, thus limiting the rate of these reactions under oxic environments. The second key treatment process in PRB systems is dissimilatory bacterial sulphate reduction (BSR), which can only proceed under anoxic conditions are illustrated by equations 3-5.

$$2CH_2O + SO_4^{2-} + 2H^+ \text{----------}\rightarrow 2CO_2 + H_2S + 2H_2O \qquad (3)$$

$$2CH_2O + SO_4^{2-} \text{------}\rightarrow H_2S + 2HCO_3^- \qquad (4)$$

$$M^{2+} + H_2S + 2HCO_3^- \text{----}\rightarrow MS + 2H_2O + 2CO_2 \qquad (5)$$

where CH_2O represents a source of carbon (carbohydrate) and M^{2+} represents a divalent metal ion. The final reaction in composed based systems takes place in the aerobic cells of lagoons and wetland designed to remove further iron, principally through hydrolysis and precipitation of ferric (Fe^{3+}) iron as represented by equation 6:

$$Fe^{3+} + 3H_2O \text{----}\rightarrow Fe(OH)_3\,(S) + 3H^+ \qquad (6)$$

At Shilbottle, the PRB is a compost-based system comprising of 50% limestone gravel, 25% green waste compost and 25% composted horse manure and straw thoroughly mixed together as substrates. The PRB is approximately 180 m long, 3 m deep and 2 m wide with a normal hydraulic retention time of 48 hours [4]. The schematic layout plan of the site is shown in figure 8.2 while figure 8.3 shows the layout of the permeable reactive barrier (PRB) and the settlement lagoons.

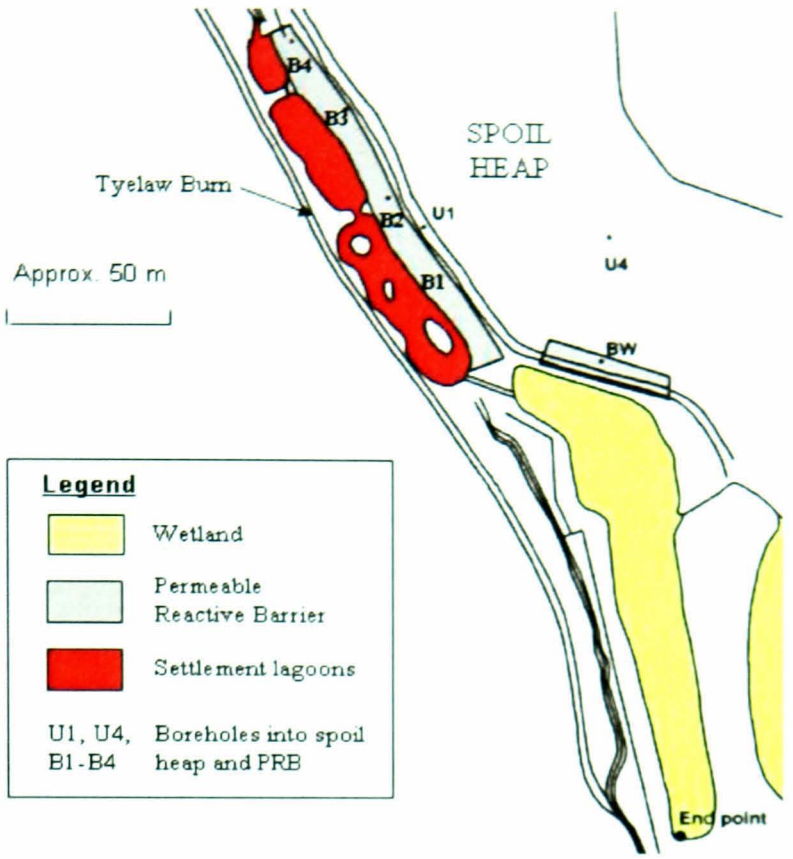

Figure 8.2: schematic layout of plan at Shilbottle site showing settlement lagoons and the underground purpose built boreholes-Courtesy of HERO research Group at Newcastle University.

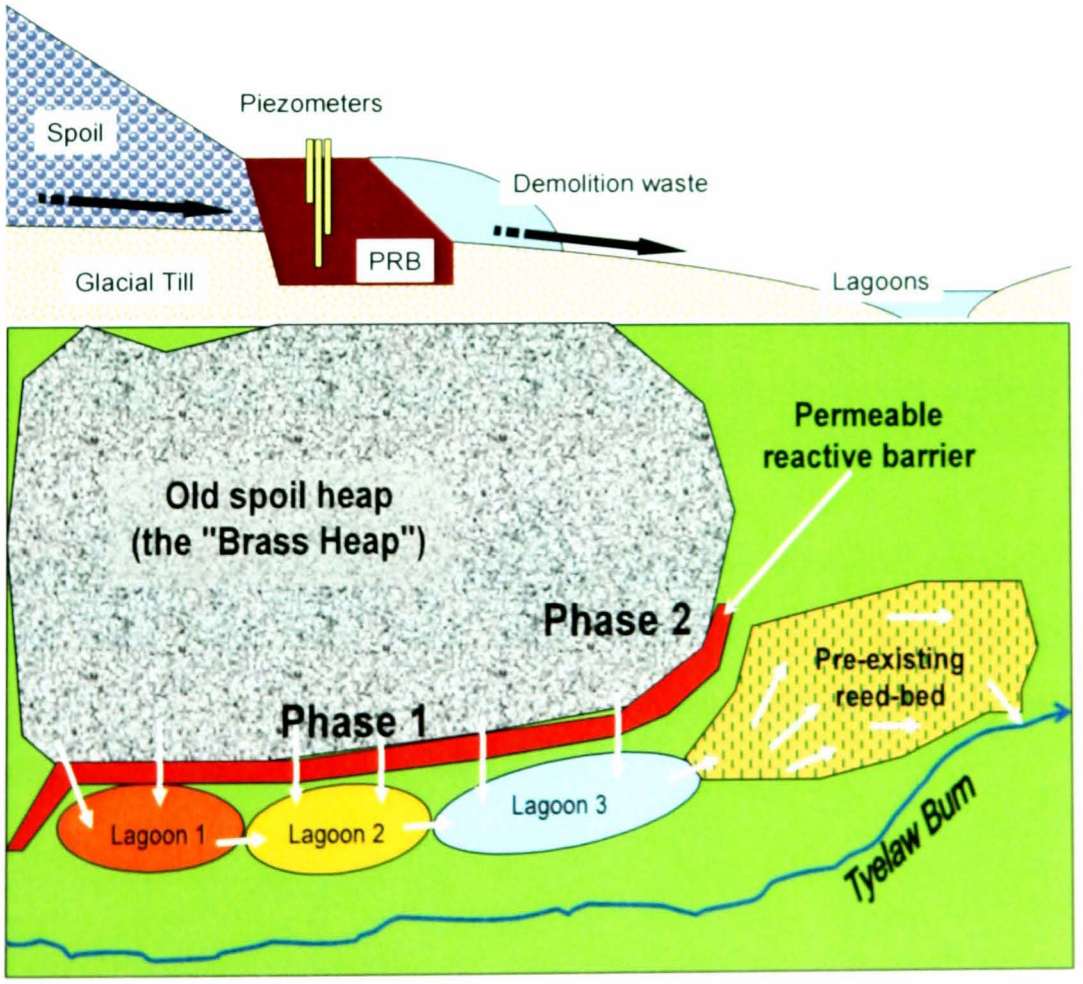

Figure 8.3: Schematic of the PRB at Shilbottle site showing settlement lagoons and wetland-Courtesy of HERO research Group at Newcastle University.

The treated leachate exits the barrier through a permeable phase, lined with brick rubble and into a series of three settlement ponds for polishing. From the third pond, the water enters a reedbed for a final polishing before entering the Tyelaw Burn. The mechanism for treatment of acid mine drainage (AMD) by PRBs is the reduction of sulphate to sulphide and the precipitation of metal sulphides via aerobic conditions and sulphate reducing bacteria [4]. The lagoons and wetland are aerobic treatment cells designed to remove further iron, principally through hydrolysis and precipitation of ferric ion. Figure 8.4 shows one of the settlement lagoons. The PRB at Shilbottle site is the UK's first large-scale permeable reactive barrier for mine spoil leachate remediation.

Figure 8.4: One of the three settlement lagoons showing orange colouration of acidic and polluted mine water (with ochre precipitate) that has passed through the PRB at Shilbottle site. This highly turbid orange water contains solid iron oxyhydroxide; the wetland effectively removed these solids.

8.2: Results and Discussion

Samples were collected at this site between April 2006 and April 2007. Samples were taken from all the sampling stations approximately monthly and analysed for all fields and laboratory parameters. The sampling method was designed in such a way that samples were collected from the underground (through boreholes) spoil heaps (main source of contamination), followed by samples within the permeable reactive barrier (PRB) and finally samples from PRB effluents-that is, from the three settlement lagoons, within the polishing wetland, the effluent and the receiving local stream-Tyelaw Burn where the final discharge flows. Samples were also taken from 30, 20 and 10 meters distance before the lagoons. This is to monitor the water quality before the lagoons and to compare this with the lagoons' water quality. In addition, it has been suggested that there might be contamination arising from the spoil heaps during rainfall because of the possible contribution of run-off waters.

8.2.1: On-site results

Understanding of the environmental controls (e.g., water temperature, pH, conductivity, *Eh* and alkalinity) that affect iron chemistry are crucial in the complex heterogeneous conditions such as the polluted mine-waters. Consequently, all these parameters have been measured at this site during sampling. Results of the water quality parameters collected from the 24 sampling points across this site are presented in this section. Figures 8.5 to 8.12 give graphical representations of some of these water quality parameters while tables 8.1 to 8.10 present the whole data from the entire sampling points across the site on an expanded scale and more detailed. Figures 8.5 & 8.6 reveal temporal and typical monthly pH profile at various sampling points across the site while the temporal change in *Eh* and alkalinity profiles of samples taken from the underground of the spoil heaps, underground samples within the permeable reactive barrier (PRB), surface water after the PRB and surface water at various sampling distances before the settlement lagoons are respectively presented in figures 8.7 to 8.12.

Table 8.1: Water quality parameters of water samples taken (quarterly) from the spoil heaps (underground waters-before the permeable reactive barrier (PRB), the main contamination source) at Shilbottle site May 2006-March 2007.

Dates	Sample	pH	K.(μS cm^{-1})	Alkalinity mg L^{-1} as CaCO3)	Eh/mV	T/°C	[Dissolved Fe] mg L^{-1}	[Colloidal Fe] mg L^{-1}	Comments
23-May'06	U3	4.01	6440	0	279	16.0	79.4	2.16	Underground water from spoil heaps
	U4	6.54	5800	920	142	12.7	3.89	2.68	Underground water from spoil heaps
	U5	6.74	5260	604	35	13.9	27.2	7.10	Underground water from spoil heaps
	U6	3.92	17100	0	258	13.1	918	472	Underground water from spoil heaps
	U7	4.56	4230	0	225	13.4	95.7	0.29	Underground water from spoil heaps
	U8	6.71	2730	330	150	13.5	14.6	4.17	Underground water from spoil heaps
	U1	4.15	2610	0	419	15.3	3.13	0.43	Underground water from ~2m of PRB
	BW1	3.06	5520	0	431	14.1	104	4.29	Underground water from spoil heaps
22-Aug.'06	U3	4.36	7050	0	256	15.1	44.5	9.10	Underground water from spoil heaps
	U4	6.35	5740	648	54	13.8	11.6	0.80	Underground water from spoil heaps
	U5	6.64	5440	460	-41	13.9	3.98	0.00	Underground water from spoil heaps
	U6	3.48	25600	0	311	16.3	120	627	Underground water from spoil heaps
	U7	4.44	4800	0	204	15.6	315	124	Underground water from spoil heaps
	U8	7.44	2790	650	124	19.9	7.06	0.39	Underground water from spoil heaps
	U1	4.06	5630	0	266	15.4	223	0.00	Underground water from ~2m of PRB
	BW1	3.77	5300	0	343	15.3	133	19.3	Underground water from spoil heaps
24-Nov.'06	U3	4.07	6990	0	390	11.7	4.41	1.48	Underground water from spoil heaps
	U4	6.31	5690	820	173	10.9	3.00	1.82	Underground water from spoil heaps
	U5	6.73	5420	480	29	12.0	37.2	2.34	Underground water from spoil heaps
	U6	3.76	3720	0	260	10.9	210	1570	Underground water from spoil heaps
	U7	3.54	4530	0	370	9.7	82.6	7.38	Underground water from spoil heaps
	U8	6.64	2710	0	224	8.1	29.2	4.02	Underground water from spoil heaps
	U1	4.06	3650	0	329	10.3	5.47	0.00	Underground water from ~2m of PRB
	BW1	3.36	6030	0	412	10.4	95.2	28.4	Underground water from spoil heaps

Table 8.1 (continued).

Dates	Sample	pH	*K*.(μS cm^{-1})	Alkalinity mg L^{-1} $CaCO_3$)	*Eh*/mV	*T*/°C	[Dissolved Fe] mg L^{-1}	[Colloidal Fe] mg L^{-1}	Comments
20-Mar.'07	U3	3.73	7160	0	319	10.5	84.2	33.8	Underground water from spoil heaps
	U4	6.37	5610	622	102	9.3	14.6	7.13	Underground water from spoil heaps
	U5	6.70	5630	422	-27	9.5	33	16.4	Underground water from spoil heaps
	U6	3.13	37000	0	327	10.5	571	339	Underground water from spoil heaps
	U7	4.20	6790	0	220	6.7	359	186	Underground water from spoil heaps
	U8	6.99	2680	296	178	8	10.1	2.3	Underground water from spoil heaps
	U1	4.01	3140	0	366	7.6	1.97	0.59	Underground water from ~2m of PRB
	BW1	2.79	7130	0	495	8.1	73.2	21.8	Underground water from spoil heaps

Table 8.2: Mean water quality parameters determined at various underground sampling points of the spoil heaps (before PRB) across the Shilbottle site from May 2006-March 2007(where n=4).

Sample	pH	*K*.(μS cm^{-1})	Alkalinity mg L^{-1} $CaCO_3$)	*Eh*/mV	*T*/°C	[Dissolved Fe] mg L^{-1}	[Colloidal Fe] mg L^{-1}	Comments
U3	4.04	6910	0.00	311	13.3	72.7	26.7	Underground water from spoil heaps
U4	6.39	5710	753	118	11.7	16.9	5.89	Underground water from spoil heaps
U5	6.70	5440	492	-1.00	12.3	28.6	9.73	Underground water from spoil heaps
U6	3.57	29200	0.00	289	12.7	814	492	Underground water from spoil heaps
U7	4.19	5090	0.00	255	11.4	233	102	Underground water from spoil heaps
U8	6.95	2730	319	169	12.4	16.2	4.62	Underground water from spoil heaps
U1	3.94	4260	0.00	354	11.7	82.7	10.0	Underground water from ~2m of PRB
BW1	3.25	5990	0.00	420	11.9	84.1	20.9	Underground water from spoil heaps

Table 8.3: Water quality parameters of water samples taken within the permeable reactive barrier (PRB)-underground waters taken from the boreholes at Shilbottle site April 2006-April 2007.

Dates	Sample	pH	*K*.(μS cm^{-1})	Alk.mg L^{-1} $CaCO_3$)	*Eh*/mV	*T*/°C	[Dissolved Fe]mg L^{-1}	[Colloidal Fe]mg/L	Comments
13-April'06	B1L	5.07	8790	30	113	7.7	686	293	Underground water within the PRB
	B2L	4.23	10700	0	208	9.2	419	16.8	Underground water within the PRB
23-May'06	B1 Upper	4.24	9160	0	169	14.2	609	1.52	Underground water within the PRB
	B1 Middle	4.27	9010	0	170	13.8	445	26.9	Underground water within the PRB
	B1L	4.58	9170	0	117	13.3	814	489	Underground water within the PRB
	B2 Upper	4.07	10200	0	196	13.6	421	48.1	Underground water within the PRB
	B2 Medium	4.09	10500	0	213	13	496	229	Underground water within the PRB
	B2L	4.07	10500	0	199	12.9	523	139	Underground water within the PRB
	B3	4.02	10700	0	261	14.7	356	114	Underground water within the PRB
	B4	3.71	9320	0	264	14.7	417	98.9	Underground water within the PRB
23-June'06	B1L	4.53	10300	2	79	15.9	811	496	Underground water within the PRB
	B2L	4.04	11300	0	209	13	423	78	Underground water within the PRB
17-July'06	B1L	4.73	10400	4	19	14.4	781	354	Underground water within the PRB
	B2L	4.06	11100	0	256	15	662	211	Underground water within the PRB
22-August'06	B1 Upper	4.51	10200	0	97	15.2	968	253	Underground water within the PRB
	B1 Middle	4.51	10200	0	98	15.9	448	42.3	Underground water within the PRB
	B1L	4.82	10000	5	61	15.3	976	605	Underground water within the PRB
	B2 Upper	4.26	11000	0	166	16	429	104	Underground water within the PRB
	B2 Medium	4.2	11000	0	257	15.1	571	219	Underground water within the PRB
	B2L	4.18	11100	0	211	15	538	85.5	Underground water within the PRB
	B3	4.39	11600	0	190	16.9	394	219	Underground water within the PRB
	B4	3.83	8540	0	316	16	335	47.5	Underground water within the PRB
21-Sept.'06	B1L	5.09	10300	70	-30	14.2	891	587	Underground water within the PRB
	B2L	4.1	10900	0	133	14.6	633	92.8	Underground water within the PRB
26-Oct.'06	B1L	4.85	9810	6	57	12.3	811	593	Underground water within the PRB
	B2L	4.31	10700	0	152	12.8	656	278	Underground water within the PRB

Table 8.3 (continued).

Dates	Sample	pH	*K*.(μS cm^{-1})	Alkalinity mg L^{-1} $CaCO_3$)	*Eh*/mV	*T*/°C	[Dissolved Fe] mg L^{-1}	[Colloidal Fe] mg L^{-1}	Comments
24-Nov.'06	B1 Upper	4.44	9230	0	132	8.9	918	221.5	Underground water within the PRB
	B1 Middle	4.47	9920	0	125	9.6	492	34.8	Underground water within the PRB
	B1L	4.7	10100	8	69	10.1	837	501	Underground water within the PRB
	B2 Upper	4.33	10500	0	202	9.2	565	67.8	Underground water within the PRB
	B2 Medium	4.25	10500	0	241	10.5	676	333	Underground water within the PRB
	B2L	4.33	10500	0	192	10.9	654	242	Underground water within the PRB
	B3	4.56	11100	0	0.8	10.9	456	208	Underground water within the PRB
	B4	3.44	9100	0	378	11.9	364	91.5	Underground water within the PRB
4-January'07	B1L	4.69	9700	8	2	8.6	734	332	Underground water within the PRB
	B2L	4.24	10300	0	265	9.4	488	132	Underground water within the PRB
8-Feb.'07	B1L	4.91	9300	20	68	7.6	251	134	Underground water within the PRB
	B2L	4.15	10300	0	205	8.6	158	99.7	Underground water within the PRB
20-March'07	B1 Upper	4.57	7250	0	142	6.7	369	185	Underground water within the PRB
	B1 Middle	4.51	8410	0	144	7.1	290	114	Underground water within the PRB
	B1L	4.84	8990	10	89	7.3	544	210	Underground water within the PRB
	B2 Upper	4.19	11500	0	200	7.7	296	128	Underground water within the PRB
	B2M	4.19	11500	0	194	8.2	187	82.9	Underground water within the PRB
	B2L	4.26	11500	0	220	7.9	313	114	Underground water within the PRB
	B3	4.3	11500	0	121	9.6	271	110	Underground water within the PRB
	B4	4.02	11900	0	268	10.8	186	85.9	Underground water within the PRB
17-April'07	B1L	4.42	10600	0	145	9.4	340	152	Underground water within the PRB
	B2L	4.01	12100	0	192	10.4	369	93.8	Underground water within the PRB

Table 8.4: Mean characteristics of water quality parameters determined at various underground boreholes within the PRB system at Shilbottle site, May 2006-March 2007(where n=4).

Sample	pH	*K.*(μS cm^{-1})	Alkalinity mg L^{-1} $CaCO_3$)	*Eh*/mV	*T*/°C	[Dissolved Fe] mg L^{-1}	[Colloidal Fe] mg L^{-1}	Comments
B1 Upper	4.44	8970	0.00	135	11.3	479	123	Underground water within the PRB
B1 Lower	4.44	9390	0.00	134	11.6	323	66.6	Underground water within the PRB
B1L	4.77	9790	13.6	65.8	11.3	713	411	Underground water within the PRB
B2 Upper	4.21	10800	0.00	191	11.6	327	95.9	Underground water within the PRB
B2 Medium	4.18	10900	0.00	226	11.7	344	158	Underground water within the PRB
B2L	4.17	10900	0.00	204	11.6	497	137	Underground water within the PRB
B3	4.32	11200	0.00	143	13.0	275	126	Underground water within the PRB
B4	3.75	9710	0.00	307	13.4	239	71.7	Underground water within the PRB

Table 8.5: Summary of water quality parameters of samples taken after passing through the permeable reactive barriers (PRB) at Shilbottle site April 2006-April 2007.

Dates	Sample	pH	*K*.(µS cm^{-1})	Alkalinity mg L^{-1} $CaCO_3$)	*Eh*/mV	*T*/°C	[Dissolved Fe] mg L^{-1}	[Colloidal Fe] mg L^{-1}	
13-April'06	Lagoon 1	3.46	7220	0	381	10.8	244	73.3	Settlement lagoon water after PRB
	Lagoon 2	3.46	7880	0	400	10.3	214	63.7	Settlement lagoon water after PRB
	Lagoon 3	3.36	7590	0	414	9.7	198	18.1	Settlement lagoon water after PRB
	End point	3.8	5860	0	476	8.6	6.73	0	Polishing wetland effluent sample
	LTBR	6.16	1450	83	240	9.3	1.37	1.14	From downstream of Tyelaw Burn
23-May'06	Lagoon 1	3.25	6180	0	405	17.1	188	39.9	Settlement lagoon water after PRB
	Lagoon 2	3.2	6820	0	466	17.5	149	0	Settlement lagoon water after PRB
	Lagoon 3	3.01	6830	0	523	14.6	209	15.9	Settlement lagoon water after PRB
	End point	3.81	3990	25	503	14.5	5.59	0	Polishing wetland effluent sample
	LTBR	6.67	1040	99	265	13.8	2.49	2.35	From downstream of Tyelaw Burn
23-June'06	Lagoon 1	3.1	7140	0	480	17.9	226	75.9	Settlement lagoon water after PRB
	Lagoon 2	3.02	8690	0	530	17.8	176	26.3	Settlement lagoon water after PRB
	Lagoon 3	2.97	8780	0	538	17.4	217	93.0	Settlement lagoon water after PRB
	End point	3.53	6950	0	467	15	9.03	0.24	Polishing wetland effluent sample
	LTBR	7.22	1070	143	140	13.4	0.67	0	From downstream of Tyelaw Burn
17-July'06	Lagoon 1	3.1	6810	0	424	23	214	40.1	Settlement lagoon water after PRB
	Lagoon 2	2.88	8840	0	487	26.1	217	133	Settlement lagoon water after PRB
	Lagoon 3	2.85	9330	0	545	24.8	210	87.2	Settlement lagoon water after PRB
	End point	3.33	7890	0	471	22.4	19.9	6.46	Polishing wetland effluent sample
	LTBR	7.26	1050	106	178	19.4	3.17	2.07	From downstream of Tyelaw Burn

Table 8.5 (continued).

Dates	Sample	pH	*K*.(µS cm^{-1})	Alkalinity mg L^{-1} $CaCO_3$)	*Eh*/mV	*T*/°C	[Dissolved Fe] mg L^{-1}	[Colloidal Fe] mg L^{-1}	Comments
22-August'06	Lagoon 1	3.22	6130	0	454	21.1	170	14.6	Settlement lagoon water after PRB
	Lagoon 2	3.57	2020	0	431	18.9	29.3	0	Settlement lagoon water after PRB
	Lagoon 3	3.92	1770	0	391	18.8	12.9	0	Settlement lagoon water after PRB
	End point	3.33	6830	0	487	18.6	31.0	11.5	Polishing wetland effluent sample
	LTBR	6.91	983	106	101	16.4	0.94	0.73	From downstream of Tyelaw Burn
21-Sept.'06	Lagoon 1	2.89	6990	0	464	20.2	182.6	30.3	Settlement lagoon water after PRB
	Lagoon 2	2.83	7940	0	550	19.8	137.2	31.3	Settlement lagoon water after PRB
	Lagoon 3	2.78	8100	0	576	18.6	182	47.4	Settlement lagoon water after PRB
	End point	2.99	6400	0	485	19	55.2	13.9	Polishing wetland effluent sample
	LTBR	6.9	951	110	225	16.3	0.86	0.86	From downstream of Tyelaw Burn
26-Oct.06	Lagoon 1	3.33	5390	0	432	11.6	115	0	Settlement lagoon water after PRB
	Lagoon 2	6.17	706	82	281	11.8	5.44	0	Settlement lagoon water after PRB
	Lagoon 3	6.57	759	76	117	11.7	3.04	0	Settlement lagoon water after PRB
	End point	6.23	797	22	56	11.4	5.80	0	Polishing wetland effluent sample
	LTBR	7.12	647	58	4	12	1.9	1.9	From downstream of Tyelaw Burn
24-Nov.'06	Lagoon 1	3.39	6900	0	395	4.6	211	42.5	Settlement lagoon water after PRB
	Lagoon 2	3.2	6730	0	407	4.7	185	23.9	Settlement lagoon water after PRB
	Lagoon 3	3.22	7100	0	446	4.2	191	6.54	Settlement lagoon water after PRB
	End point	3.74	4220	0	480	6.6	4.64	0	Polishing wetland effluent sample
	LTBR	6.63	838	167	145	7.5	0.87	0.87	From downstream of Tyelaw Burn

Table 8.5 (continued).

Dates	Sample	pH	*K*.(µS cm^{-1})	Alkalinity mg L^{-1} $CaCO_3$)	*Eh*/mV	*T*/°C	[Dissolved Fe] mg L^{-1}	[Colloidal Fe] mg L^{-1}	Comments
4-January'07	Lagoon 1	3.15	6950	0	408	6.8	219	94.8	Settlement lagoon water after PRB
	Lagoon 2	2.99	7550	0	433	5.8	212	70.1	Settlement lagoon water after PRB
	Lagoon 3	2.97	7520	0	444	5.8	216	80.5	Settlement lagoon water after PRB
	End	3.65	5560	0	440	5.4	1.85	1.44	Polishing wetland effluent sample
	LTBR	7.62	1030	162	81	9.3	0.35	0.35	From downstream of Tyelaw Burn
8-Feb.07	Lagoon 1	3.32	6660	0	392	3.4	149	71.4	Settlement lagoon water after PRB
	Lagoon 2	3.15	6660	0	380	1.4	109	47.1	Settlement lagoon water after PRB
	Lagoon 3	4.31	5490	0	263	2.4	126	80.6	Settlement lagoon water after PRB
	End point	3.95	4370	0	443	3	0.92	0.92	Polishing wetland effluent sample
	LTBR	6.54	1480	150	188	4.8	0	0	From downstream of Tyelaw Burn
20-March'07	Lagoon 1	3.32	7110	0	422	5.7	170	54.8	Settlement lagoon water after PRB
	Lagoon 2	3.09	7940	0	457	4.1	144	30.9	Settlement lagoon water after PRB
	Lagoon 3	3.05	8060	0	473	3.8	139	66.5	Settlement lagoon water after PRB
	End point	3.81	5910	0	475	5.6	2.46	1.17	Polishing wetland effluent sample
	LTBR	6.33	1480	80	261	5.5	0	0	From downstream of Tyelaw Burn
17-April'07	Lagoon 1	3.19	6910	0	404	12	164	54.3	Settlement lagoon water after PRB
	Lagoon 2	2.98	8170	0	466	12.4	147	54.5	Settlement lagoon water after PRB
	Lagoon 3	2.9	8030	0	496	11.5	145	58.8	Settlement lagoon water after PRB
	End point	3.75	6940	0	421	10.2	2.73	0.4	Polishing wetland effluent sample
	LTBR	6.14	1280	95	246	10.8	0	0	From downstream of Tyelaw Burn

Table 8.6: Mean water quality determined at various sampling points across the Shilbottle site (after passing through PRB) from April 2006-April 2007(where n=13).

Sample	pH	*K*.(µS cm^{-1})	Alkalinity mg L^{-1} $CaCO_3$)	*Eh*/mV	*T*/°C	[Dissolved Fe] mg L^{-1}	[Colloidal Fe] mg L^{-1}	
Lagoon 1	3.23	6670	0.00	422	12.9	191	52.8	Settlement lagoon water after PRB
Lagoon 2	3.38	6660	6.83	441	12.6	148	42.6	Settlement lagoon water after PRB
Lagoon 3	3.49	6610	6.33	436	11.9	159	46.9	Settlement lagoon water after PRB
End point	3.83	5480	3.92	434	11.7	11.5	2.77	Polishing wetland effluent sample
LTBR	6.79	1110	113	173	11.5	1.04	0.86	From downstream of Tyelaw Burn

Table 8.7: Monthly mean of pH, electrical Conductivity (*K*), Oxidation Reduction Potential (*Eh*), Temperature, Total Alkalinity, Total and Dissolved Fe respectively Polluted Mine water samples collected in 2006 from inlet (Lagoon 1) at Shilbottle (SB) site.

Lagoon1 Months	pH	*K* (µS cm^{1})	*Eh*/mV	*T*/°C	Alkalinity mg L^{-1} $CaCO_3$)	[Total Fe] mg L^{-1}	Dissolved Fe mg L^{-1}	Colloidal Fe mg L^{-1}	Comments
April	3.57	7220	381	10.8	0.0	317	244	73.3	Samples collected in the spring
May	3.33	6180	405	17.1	0.0	228	188	40.1	There was heavy rainfall this month
June	3.15	7140	480	17.9	0.0	302	226	76.1	Contamination from run off water from farmland
July	3.18	6810	424	23.0	0.0	253	213	40.0	Samples collected in the summer
Aug.	3.21	6130	454	21.1	0.0	185	170	14.6	Sample collected in the dry summer season
Sept.	2.92	6990	464	20.2	0.0	213	183	30.3	Samples collected in the Autumn
Oct.	3.36	5390	432	11.6	0.0	139	115	23.8	Samples collected in the winter
Nov.	3.53	6900	395	4.6	0.0	254	211	42.5	Samples collected in the winter
Dec.	3.21	6950	408	6.8	0.0	324	230	94.3	Contamination from run off water from farmland

All values are in mg L^{-1} except pH, electrical conductivity (*K*.: µS/cm), *Eh* (mV), temperature (°C) and total alkalinity (mg L^{-1} as CaCO3).

Standard error of the mean (standard deviation divided by the square root of n; n=3.

Table 8.8: Monthly mean of pH, electrical Conductivity (*K*.), Oxidation Reduction Potential (*Eh*), Temperature, Total Alkalinity, Total and Dissolved Fe respectively Polluted Mine water samples collected in 2006 from End point at Shilbottle (SB) site.

End point	pH	*K*	*Eh*/mV	*T*/°C	Alkalinity	[Total Fe]	Dissolved Fe	Colloidal Fe	Comments
Months		(μS cm^{-1})			mg L^{-1} as $CaCO_3$)	mg L^{-1}	mg L^{-1}	mg L^{-1}	
April	3.80	5860	476	9.3	0.0	6.73	6.73	0.00	Samples collected in the spring
May	3.83	3990	503	13.8	25.0	5.59	5.59	0.00	There was heavy rainfall this month
June	3.56	6950	467	13.4	0.0	9.27	9.03	0.24	Samples collected in the summer
July	3.37	7890	471	19.4	0.0	26.6	20.1	6.46	Samples collected in the summer
Aug.	3.34	6830	487	16.3	0.0	42.9	31.4	11.5	Sample collected in the dry summer season
Sept.	3.02	6400	485	16.4	0.0	69.1	55.2	13.9	Samples collected in the Autumn
Oct.	6.21	797	56	12.0	22.0	5.80	5.80	0.00	Samples collected in the winter
Nov.	3.74	4220	480	7.5	0.0	4.64	4.64	0.00	Samples collected in the winter
Dec.	3.72	5560	440	9.3	0.0	3.63	3.63	0.00	Samples collected in the winter

All values are in mg L^{-1} except pH, electrical conductivity (*K*.: μS/cm), *Eh* (mV), temperature (°C) and total alkalinity (mg L^{-1} as CaCO3). Standard error of the mean (standard deviation divided by the square root of n; n=3.

Table 8.9: Monthly water quality parameters of samples taken (August 2006-April 2007) upstream at various distance before the lagoons at Shibottle site.

Dates	Sample	pH	*K*.(μS cm^{-1})	Alkalinity mg L^{-1} $CaCO_3$)	*Eh*/mV	*T*/°C	[Dissolved Fe] mg L^{-1}	[Colloidal Fe] mg L^{-1}	Comments
22-Aug.'06	30m Away	5.68	8240	40	4	19.2	95.0	41.5	Surface water before lagoons
	20m Away	4.40	6260	0	248	14.3	186	96.4	Surface water before lagoons
	10m Away	3.27	6130	0	432	18.9	177	78.7	Surface water before lagoons
21-Sep.'06	30m Away	3.55	6990	0	464	20.2	92.3	58.2	Surface water before lagoons
	20m Away	4.14	7940	0	550	19.8	618	522	Surface water before lagoons
	10m Away	2.94	8100	0	576	18.6	218	80.6	Surface water before lagoons
26-Oct.'06	30m Away	5.65	5790	67	179	11.6	32.6	7.05	Surface water before lagoons
	20m Away	3.65	4530	0	369	11.8	65.9	30.7	Surface water before lagoons
	10m Away	3.45	5040	0	420	11.8	106	61.3	Surface water before lagoons
24-Nov.'06	30m Away	4.99	6420	19	208	5.1	53.1	39.4	Surface water before lagoons
	20m Away	4.27	6290	0	307	7.3	214	98.1	Surface water before lagoons
	10m Away	3.27	6560	0	385	4.6	234	135	Surface water before lagoons
4-Jan.'07	30m Away	5.64	6370	60	335	6.1	0.35	0.35	Surface water before lagoons
	20m Away	4.30	6290	0	246	9.9	315	113	Surface water before lagoons
	10m Away	3.28	6870	0	398	6.7	264	100	Surface water before lagoons
08-Feb.'07	30m Away	6.37	6310	45	314	2.1	0.57	0.19	Surface water before lagoons
	20m Away	4.02	6340	0	331	7.5	195	90.5	Surface water before lagoons
	10m Away	3.62	6480	0	378	4.8	154	47.9	Surface water before lagoons
20-March'07	30m Away	5.76	5960	40	286	5.8	0.00	0.00	Surface water before lagoons
	20m Away	4.30	6190	0	310	9.1	178	93.3	Surface water before lagoons
	10m Away	3.24	6990	0	421	6.2	169	73.6	Surface water before lagoons
17-April'07	30m Away	5.55	6420	44	246	9.3	6.12	3.23	Surface water before lagoons
	20m Away	3.99	6170	0	291	11.1	193	40.7	Surface water before lagoons
	10m Away	3.07	7740	0	424	13.4	185	72.5	Surface water before lagoons

Table 8.10: Mean water quality parameters of samples taken (August 2006-April 2007) upstream at various distance before the lagoons at Shibottle site (n=8).

Sample	pH	*K.*(μS cm^{-1})	Alkalinity mg L^{-1} $CaCO_3$)	*Eh*/mV	*T*/°C	[Dissolved Fe] mg L^{-1}	[Colloidal Fe] mg L^{-1}	Comments
30m Away	5.40	6560	39.4	255	9.9	36.3	17.8	Surface water before lagoons
20m Away	4.14	6250	0	332	11.4	187	97.5	Surface water before lagoons
10m Away	3.28	6740	0	429	10.6	159	66.0	Surface water before lagoons

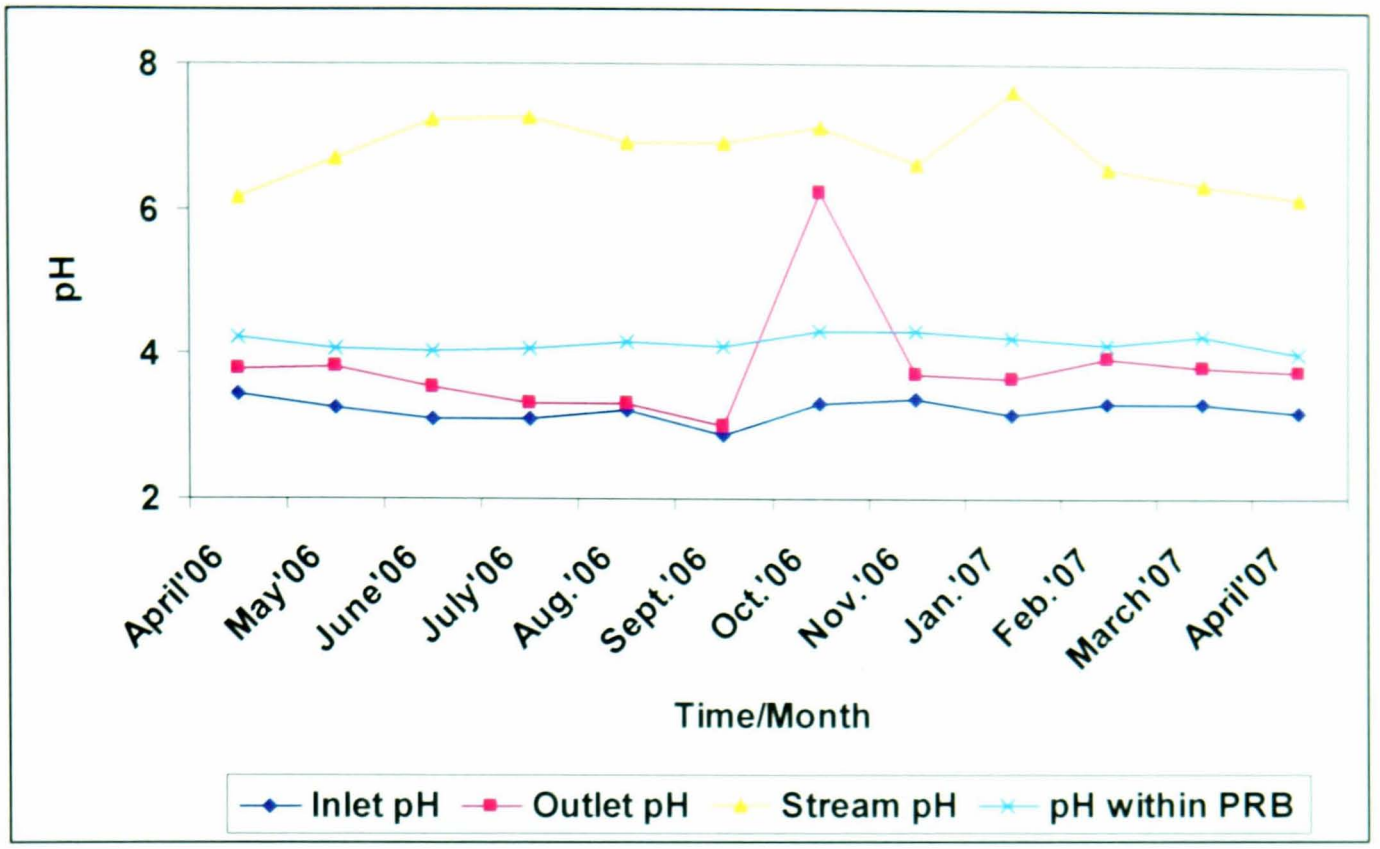

Figure 8.5: Graph showing temporal pH profiles of samples taken from inlet (underground spoil heaps waters), outlet, the stream (Tyelaw Burn) and within the PRB (underground waters) at Shilbottle treatment system site from April 2006-April 2007.

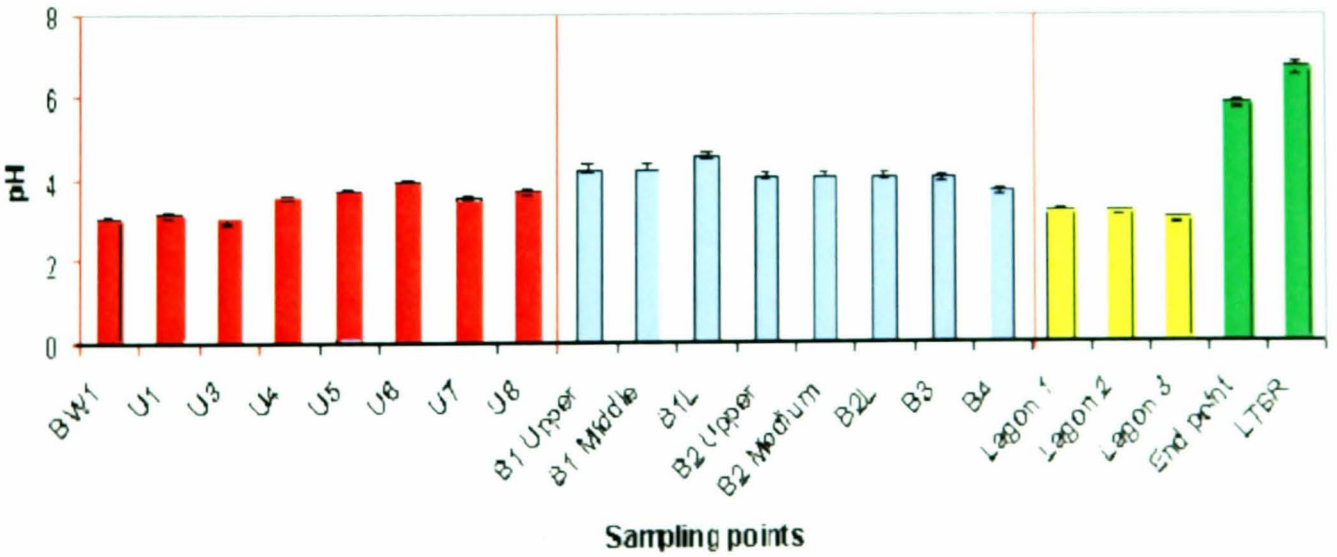

Figure 8.6: Typical monthly pH (May 2006) profile at various sampling points across the site. In red are underground samples from the spoil heaps, followed by the underground samples taken within the PRB, in yellow are samples taken from the three settlement lagoons and finally the end point and from the Tyelaw Burn stream.

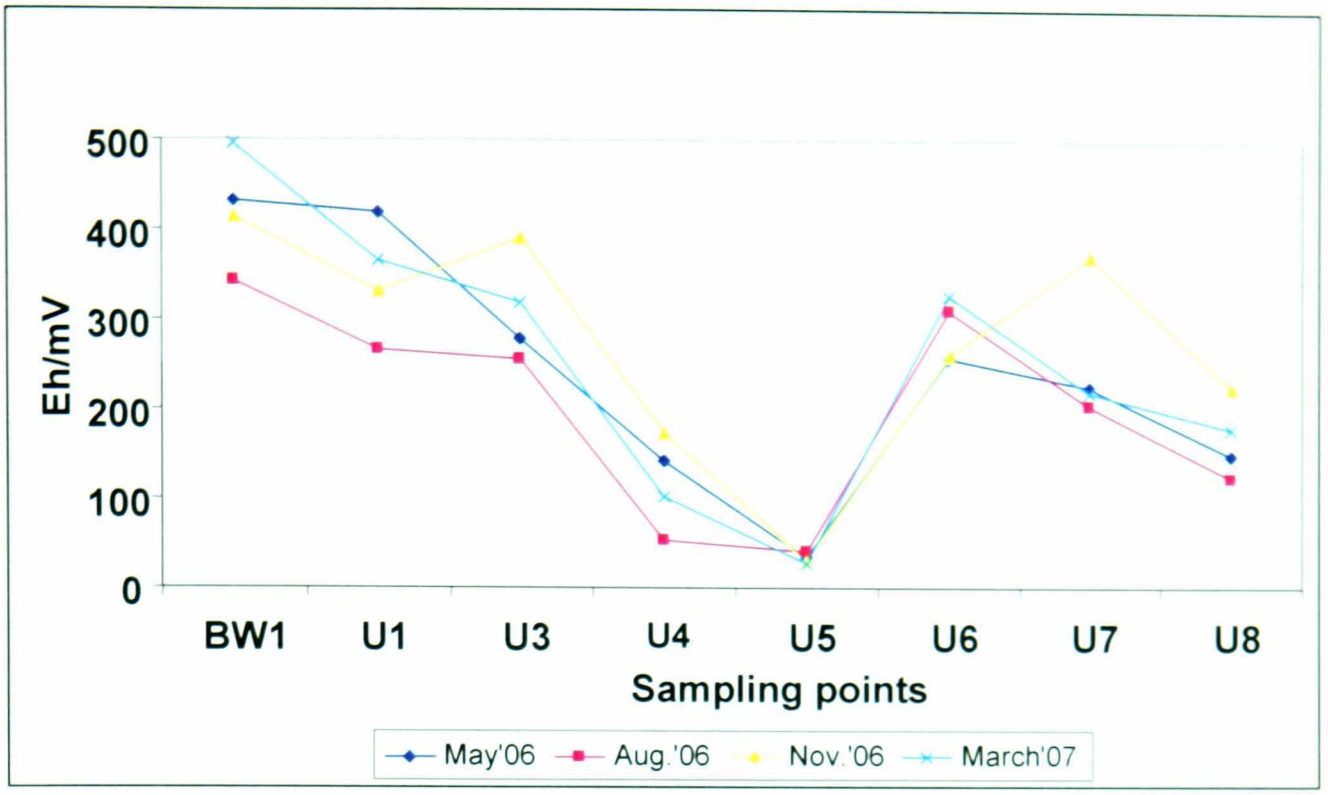

Figure 8.7: Graph showing the *Eh* profile at various sampling points from the underground samples taken quarterly from the spoil heaps samples taken at Shilbottle treatment system site, Northumberland.

Figure 8.8: Graph showing the temporal *Eh* profile of samples taken from inlet (underground spoil heaps waters), outlet, the stream (Tyelaw Burn) and within the PRB (underground waters) at Shilbottle treatment system site from April 2006-April.

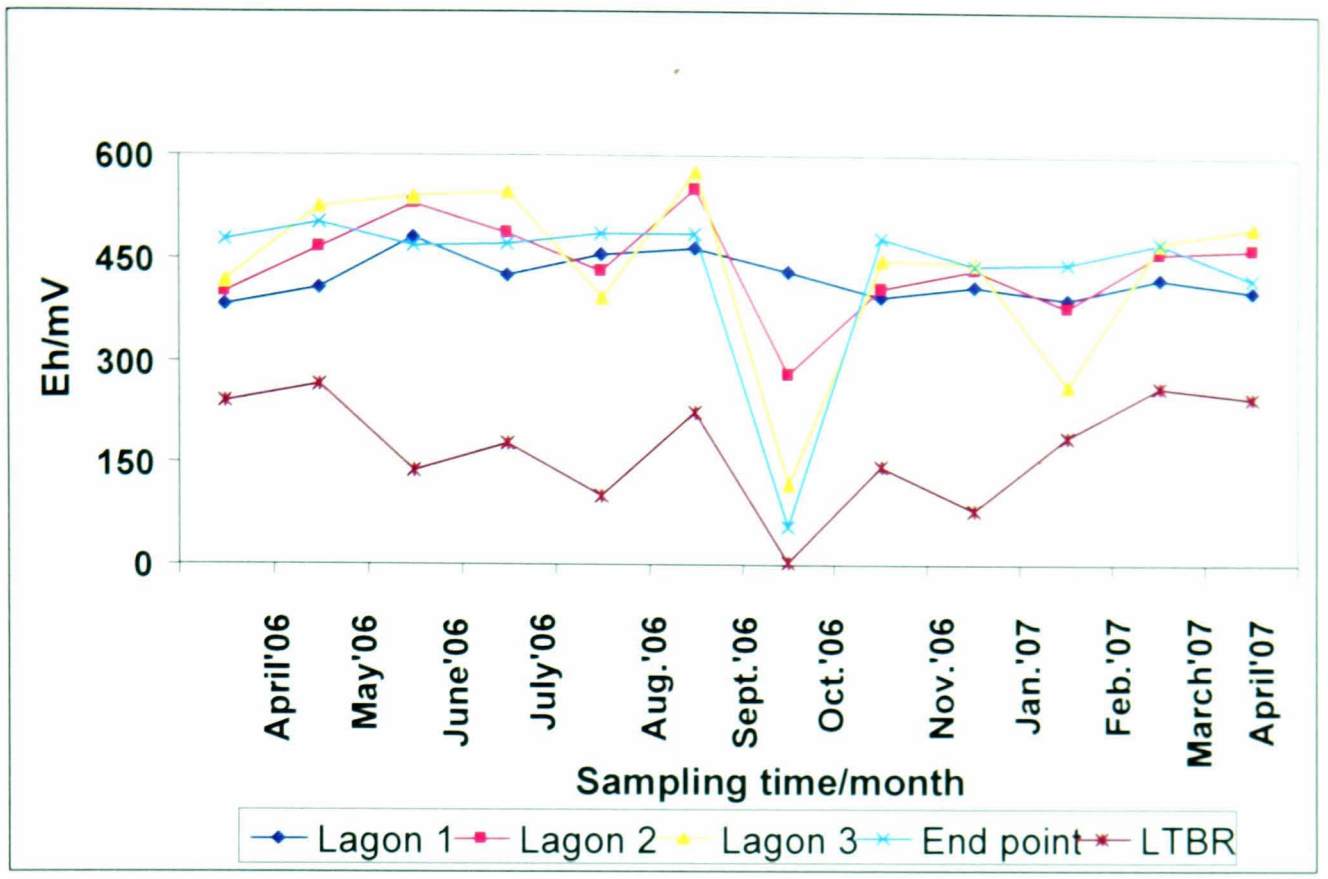

Figure 8.9: Plot showing the *Eh* profile at various sampling points from surface waters (April 2006-April 2007) that have passed through the reactive permeable barrier (PRB) at Shilbottle treatment system site, Northumberland.

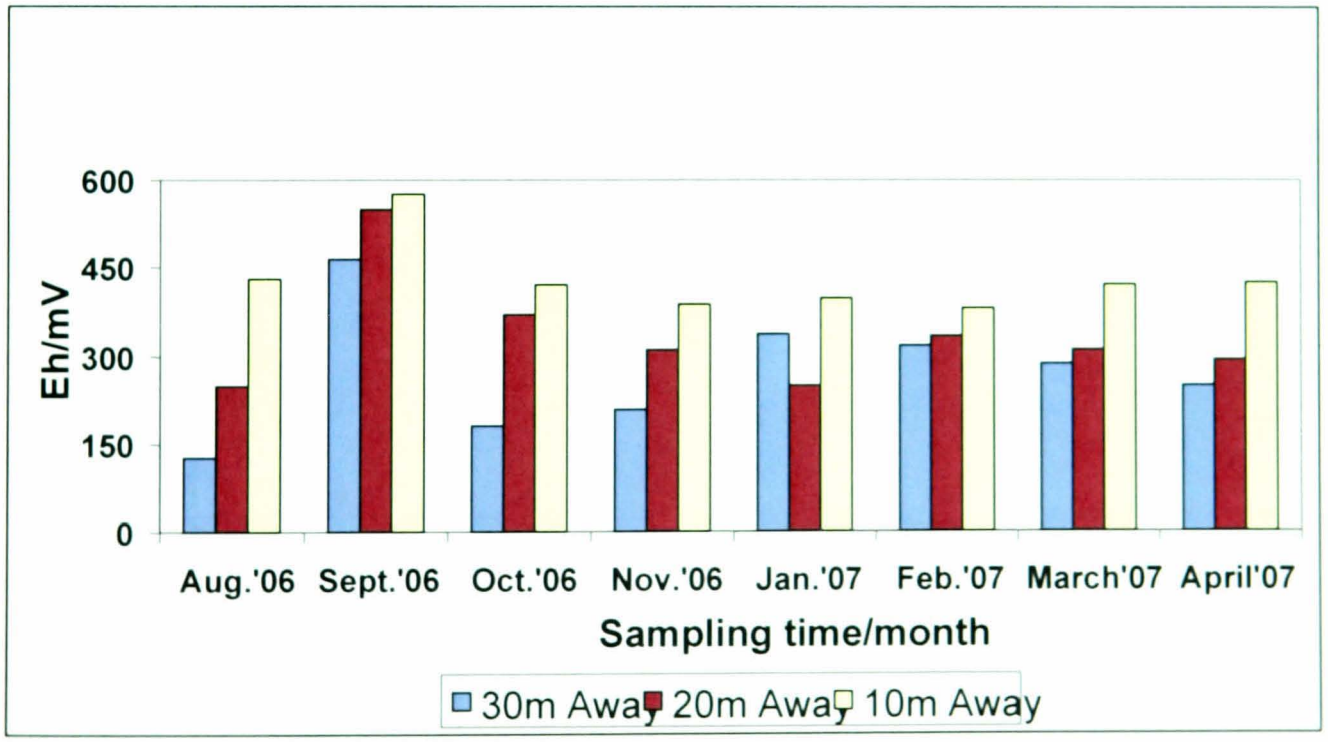

Figure 8.10: Graph showing the Eh profile (August 2006-April 2007) at various sampling distance points (30 m, 20 m & 10 m) respectively before the settlement lagoons at Shilbottle treatment system site, Northumberland.

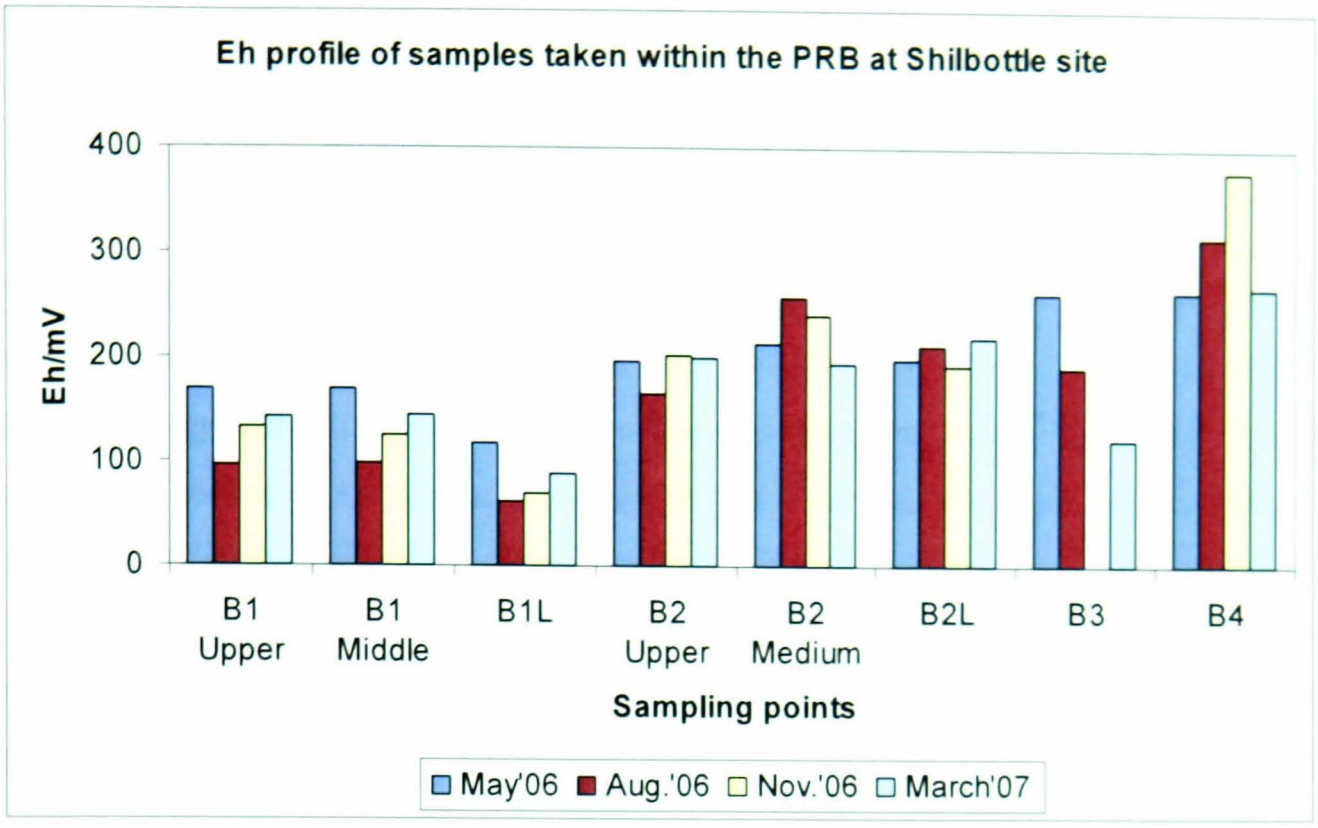

Figure 8.11: Showing the *Eh* profile at various sampling points from the underground samples taken quarterly within the reactive permeable barrier (PRB) at Shilbottle treatment system site at Northumberland.

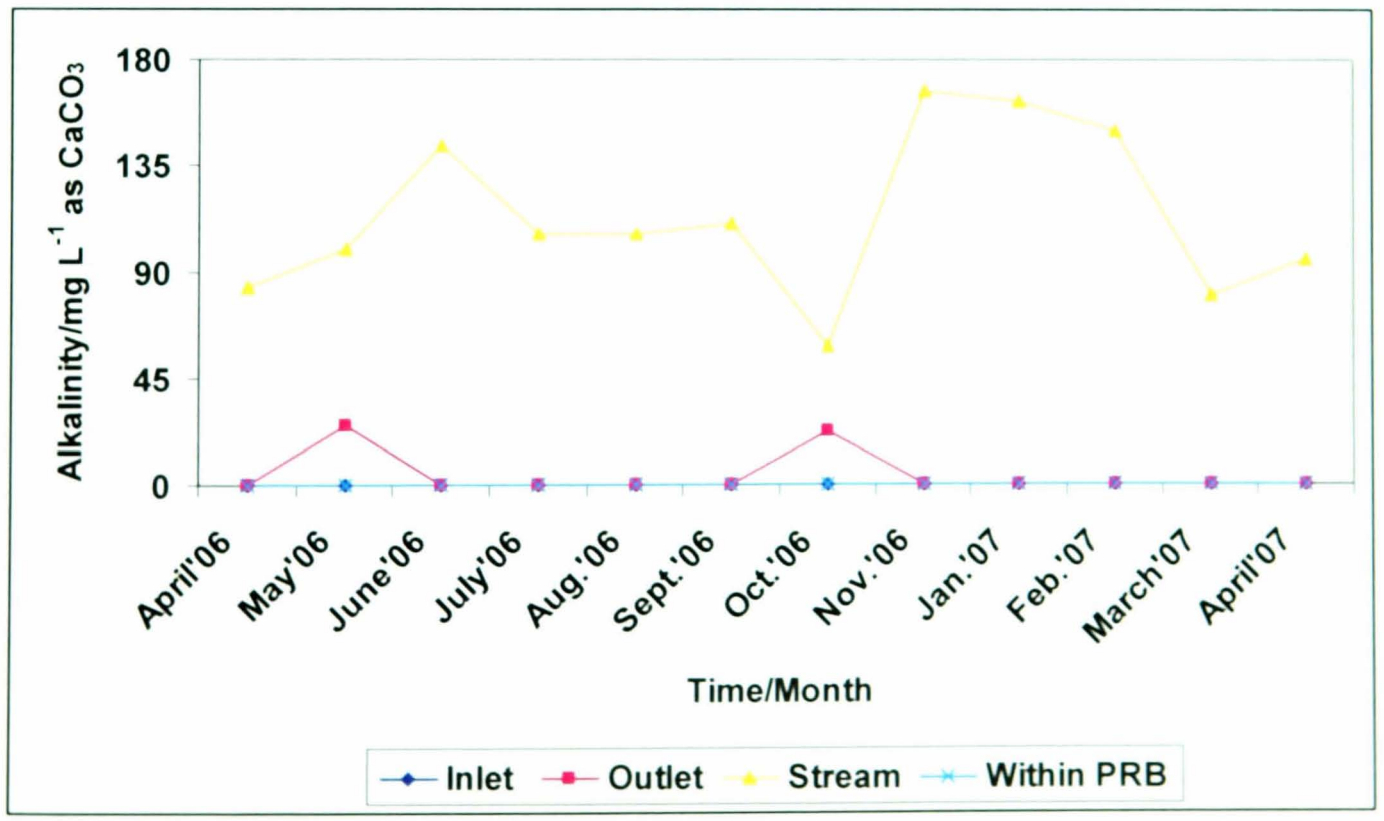

Figure 8.12: Graph showing temporal alkalinity trend of samples taken from inlet (underground spoil heaps waters), outlet, the stream (Tyelaw Burn) and within the PRB (underground waters) at Shilbottle treatment system site from April 2006-April.

It is clear from figures 8.5, 8.6 and tables 8.1 to 8.10 that the pH of the underground water samples from the spoil heaps (sampling points-BW1 and U1-U8-figure 8.5) are strongly acidic (pH 2-3) while samples from underground water samples within the permeable reactive barrier (PRB), although also acidic, however. they are higher than those from the spoil heaps and ranged between (pH 3-4). Although. samples taken from the settlement lagoons showed very acidic pH of 3 on the average, however, after passing through the polishing wetland system, the water from the effluent showed an elevated pH of about 7 on the average. The observed pH distributions are consistent with the sampling points. For example, the underground samples from the spoil heaps constitute the main pollution source and are highly acidic, the pH within the PRB will be largely dependent on the water residence time within the PRB before the pH is significantly elevated. Though, the system was designed for a resident time of about 48 hours, it is difficult to monitor how long the sampled waters have been in the PRB. However, the significant jump in water pH from about 2 for samples from the spoil heaps to 7 shows that PRB and the wetland systems have improved the water quality. Overall, as can be seen in figure 8.5, stream pH appeared stable and achieved pH> 7 in most cases, underground waters pH (inlet and PRB) also appeared stable; they are very acidic with pH ranging from 3-5. Endpoint water pH also appeared stable and the high pH of 6 in October is probably due to rainfall event, causing dilution and elevated pH. Underground waters are not affected by this run-off surface water dilution.

The *Eh* results (figure 8.7) for the underground samples taken from the spoil heaps shows that the water samples seem to be in reduced environment rather than being oxidised as observed in other samples taken from the surface. Comparison with the underground samples taken within the PRB (figure 8.11) and PRB effluents (fig. 8.9) lead to the suggestion that the *Eh* is lower which suggests a more reduced environment than samples from the spoil heaps. It is apparent from figure 8.8 that the *Eh* for the stream samples is consistently lower that other samples taken after the PRB. This trend suggests that *Eh* might be a function of water pH or it may suggest that there is a relationship between pH as lower pH waters tend to show high *Eh* value and vice versa. This indicates that more neutral waters cause precipitation of Fe(III). whereas more acidic waters have more dissolved Fe(III)-the presence of Fe(III) then result in higher *Eh*.

Similarly, the *Eh* for samples collected at various distances away from the settlement lagoons show similar behaviour (fig. 8.10), which is surprising. But the only plausible explanation is that may be during heavy rainfall, there is direct overflow or discharge of contamination from the spoil heaps to this place. This observation was particularly observed on site and in the month of September where the *Eh* value is the highest. Furthermore, as explained in the previous chapters, determination of redox potential (*Eh*) in nature is quite complicated as some of the reactions that determine redox potentials are slow [16] and it has been observed that redox potentials measured in oxygen-containing environments such as Shilbottle site are generally lower than equilibrium values [10, 16].

Trends in water alkalinity (figure 8.12) indicates that acidic water samples taken from various sampling locations have zero alkalinity but stream water samples shows high water alkalinity indicating that acidity has been neutralised as water passes through both the PRB treatment system and the polishing wetland. This observed trend is consistent with the fact that increased pH and net alkaline water is a common feature for passive treatment systems such as in this site [10, 11, 12].

8.2.2: Voltammetric results

Using differential pulse voltammetry (DPV), iron concentrations at various sampling points have been determined a selection of these results are shown in figures 8.13 to 8.20. Mean total concentrations of hydrolysed and unhydrolysed iron together with their comparison are plotted in the figures presented in 8.13, 8.14 and 8.15 respectively. Figure 8.16 presents the mean concentrations of dissolved and colloidal iron for samples taken at various distances away from the settlement lagoons, within the PRB and the effluent while mean percentage proportion of dissolved and colloidal iron for samples taken from the underground spoil heaps, within the PRB and after the PRB are presented in figures 8.17, 8.18 and 8.19 respectively. Comparison of the ratio of Fe (II) to Fe (III) for samples taken at various sampling points across the site, as determined by the ultramicroelectrodes technique is presented in figure 8.20.

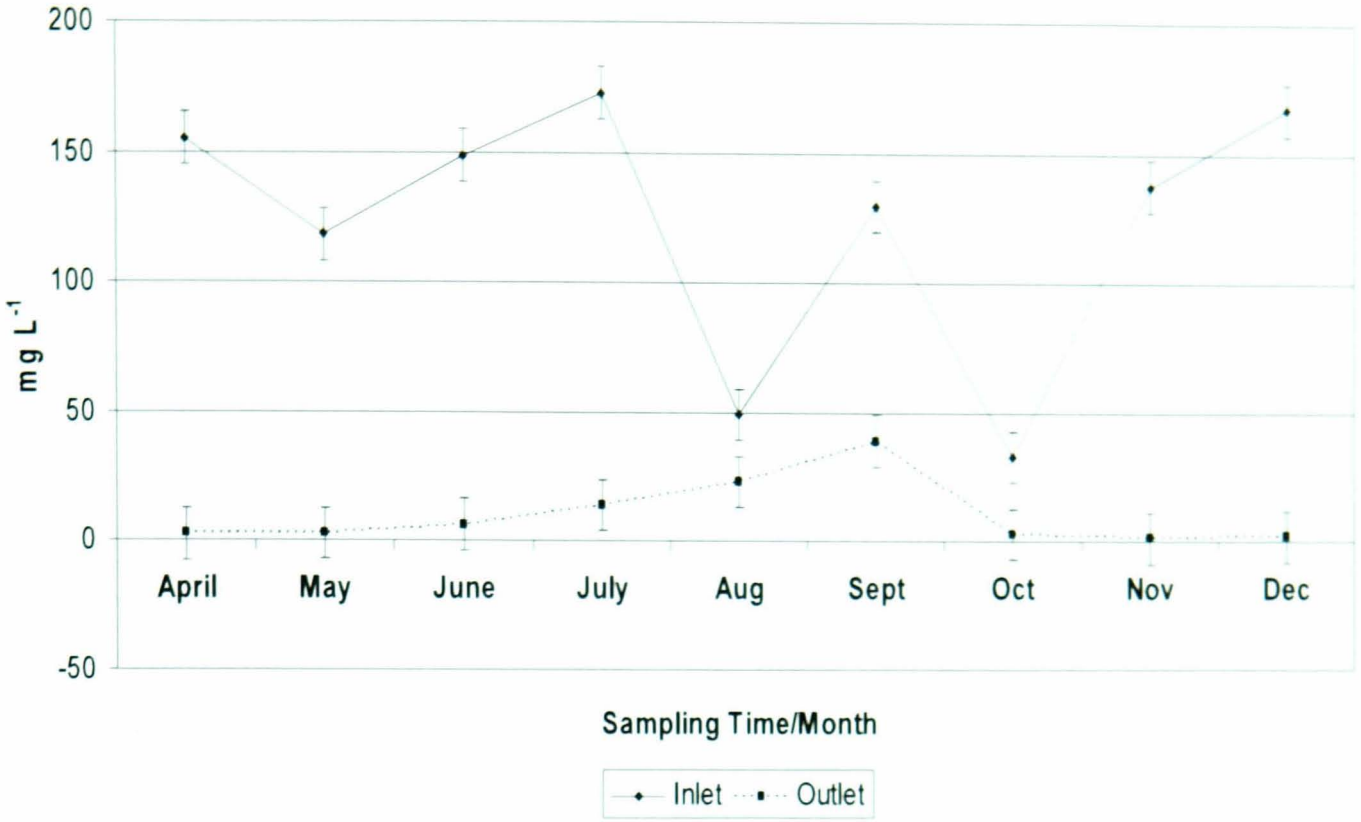

Figure 8.13: Mean total hydrolysed iron concentrations (mg L^{-1}) for samples collected (April-December, 2006) at Shilbottle treatment system site at Northumberland. Error bars denote standard error or the mean.

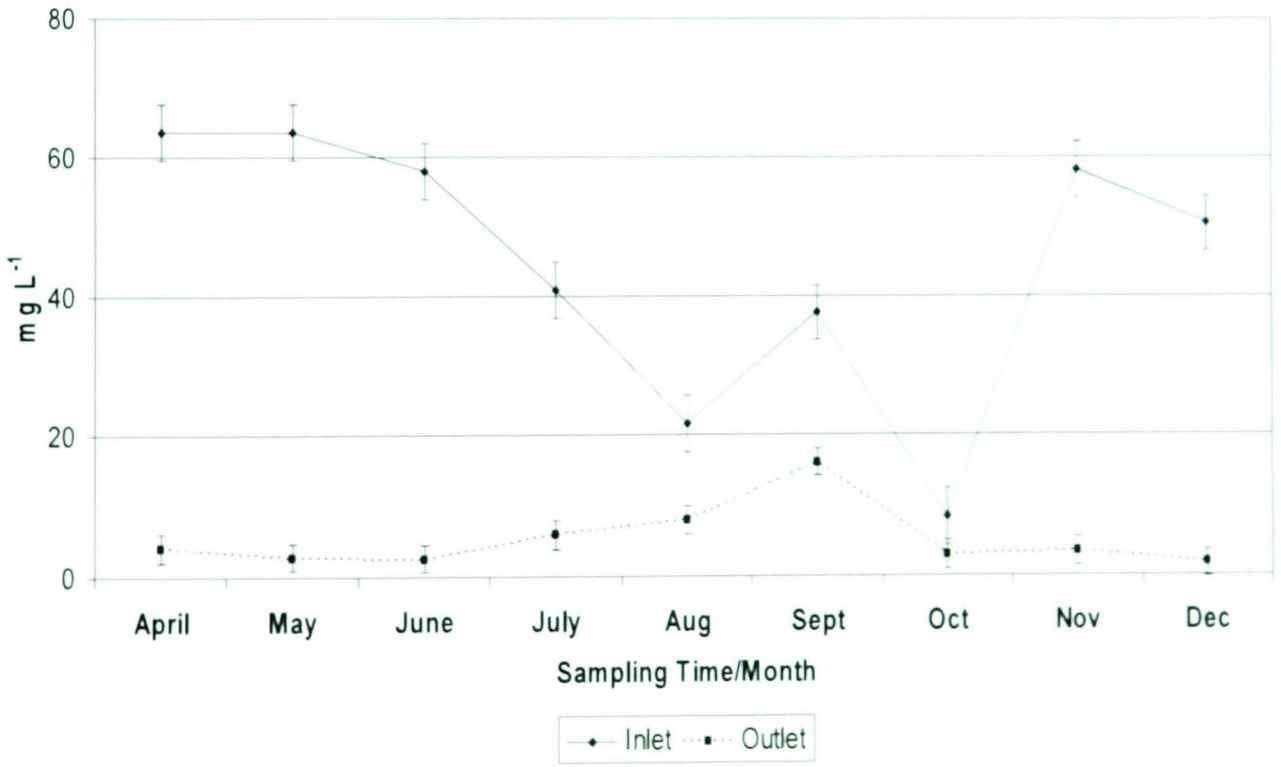

Figure 8.14: Mean total unhydrolysed iron concentrations (mg L^{-1}) for samples collected (April-December, 2006) at Shilbottle treatment system site at Northumberland. Error bars denote standard error or the mean.

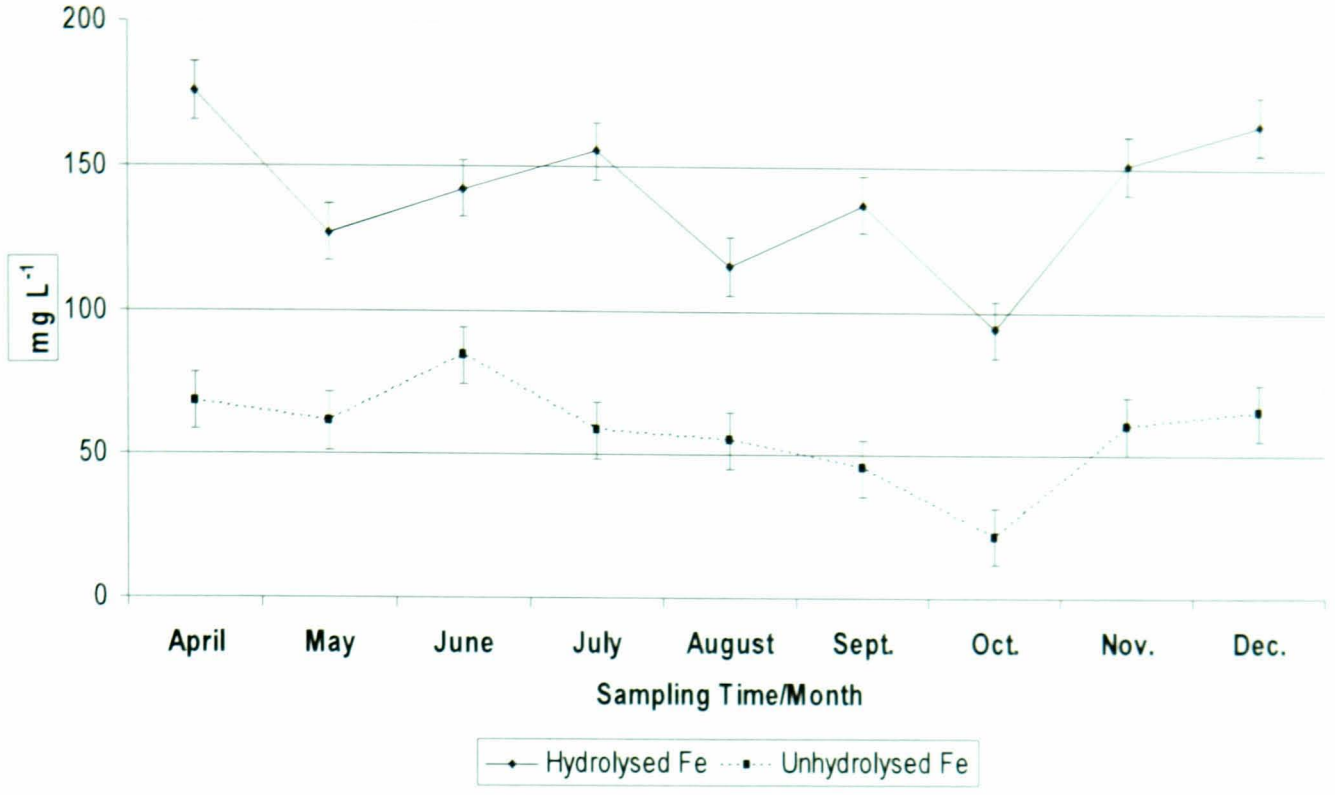

Figure 8.15: Mean total hydrolysed and unhydrolysed iron concentrations (mg L^{-1}) for samples collected (April-December, 2006) at Shilbottle treatment system site at Northumberland. Error bars denote standard error or the mean.

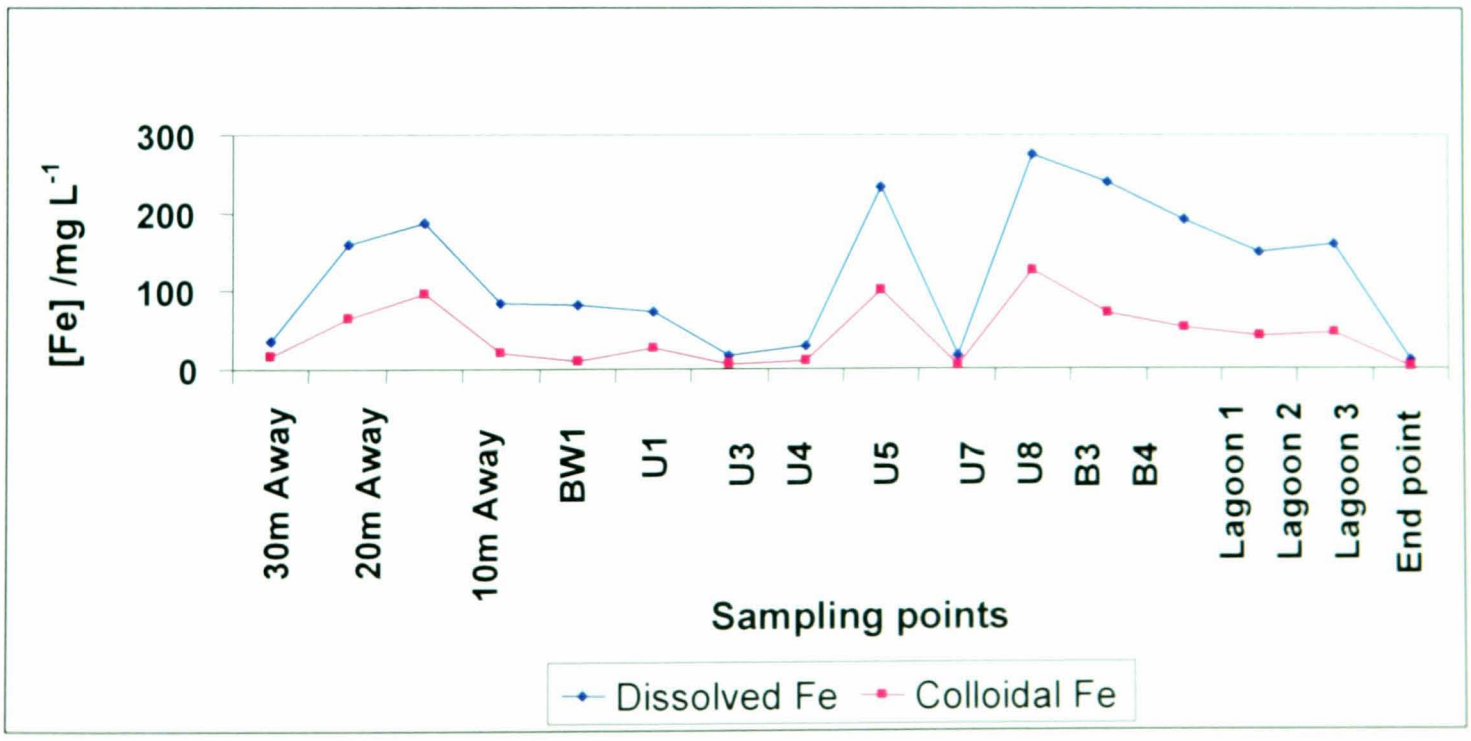

Figure 8.16: Showing mean concentrations of dissolved and colloidal iron for samples taken at various distances before the settlement lagoons, samples from the spoil heaps and samples from lagoons and the end point respectively.

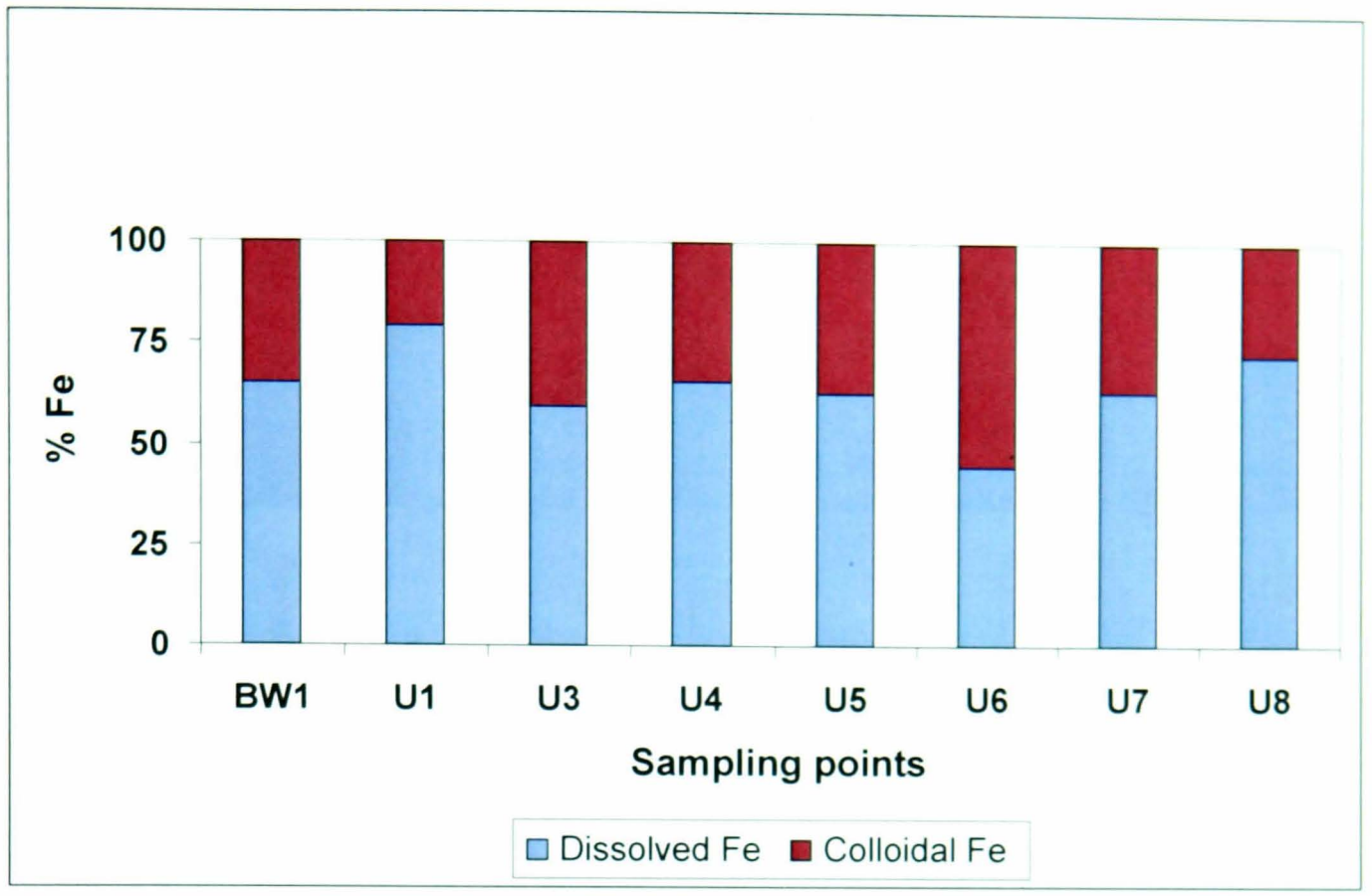

Figure 8.17: Mean percentage proportion of dissolved and colloidal iron in the underground samples from the spoil heaps at Shilbottle treatment system site, Northumberland.

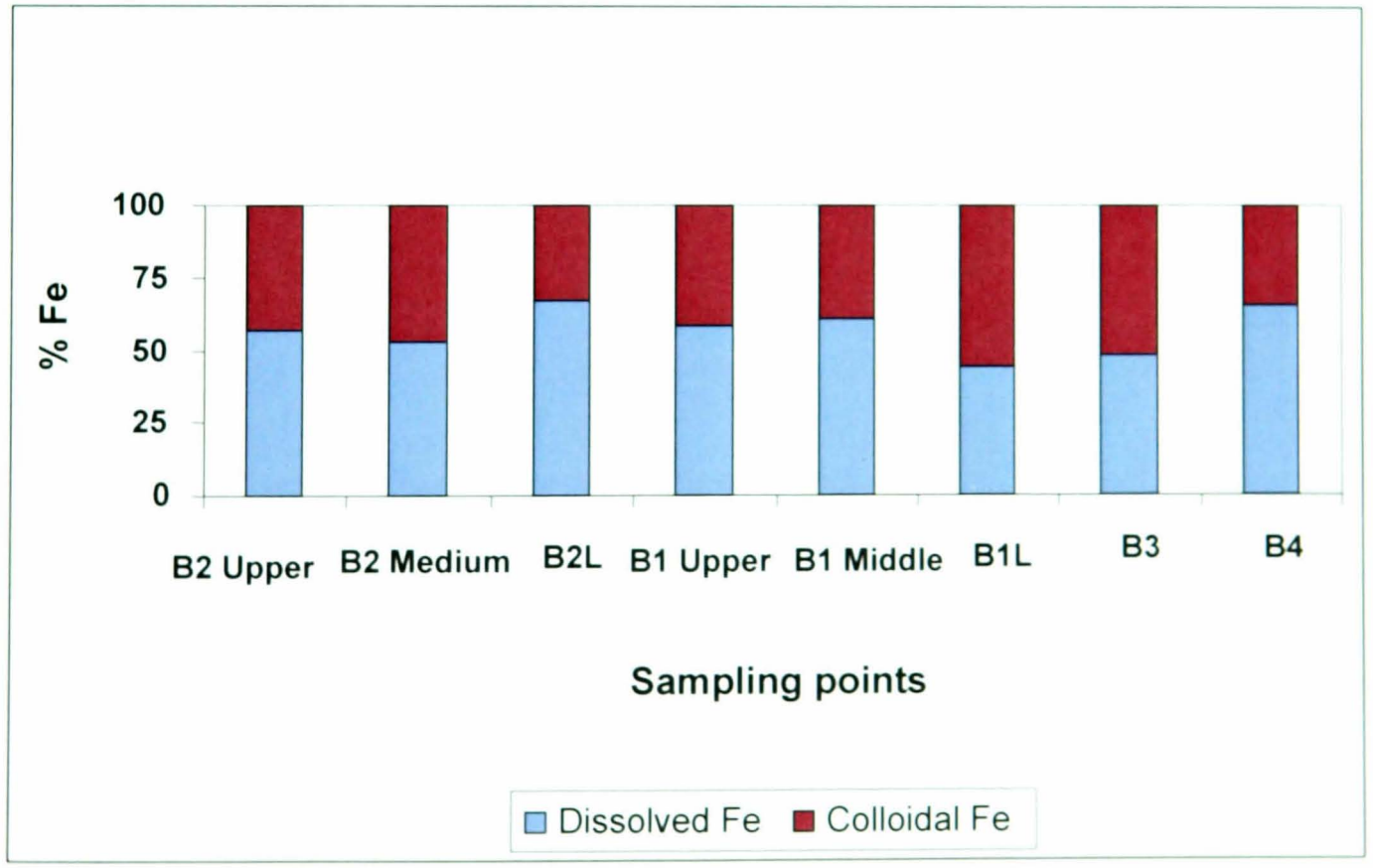

Figure 8.18: Mean percentage proportion of dissolved and colloidal iron in the underground samples taken from within the permeable reactive barrier (PRB) at Shilbottle treatment system site, Northumberland.

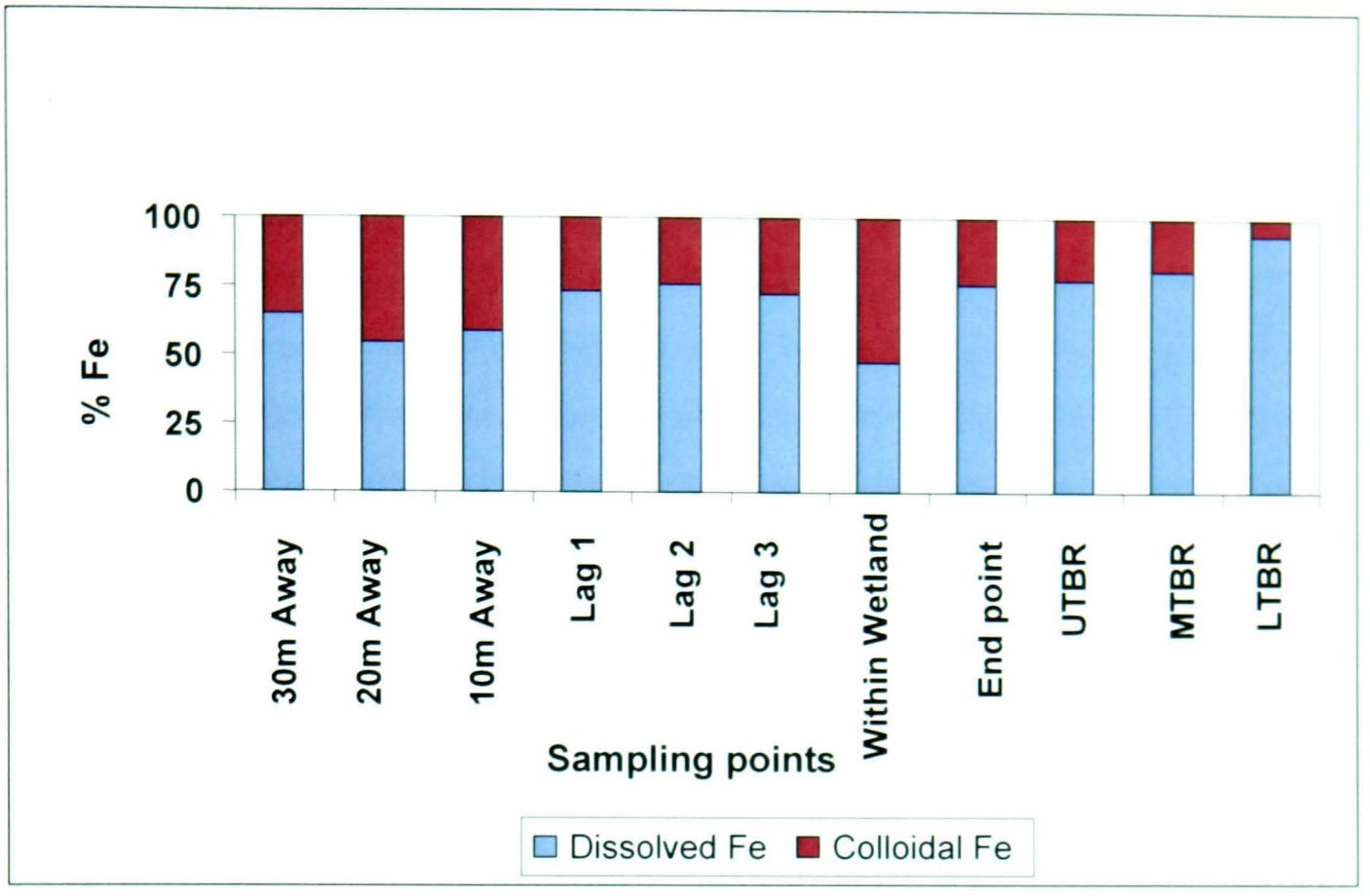

Figure 8.19: Mean percentage proportion of dissolved and colloidal iron in the surface samples taken from various distances away from the settlement lagoons, from the settlement lagoons, effluent and the Tyelaw Burn.

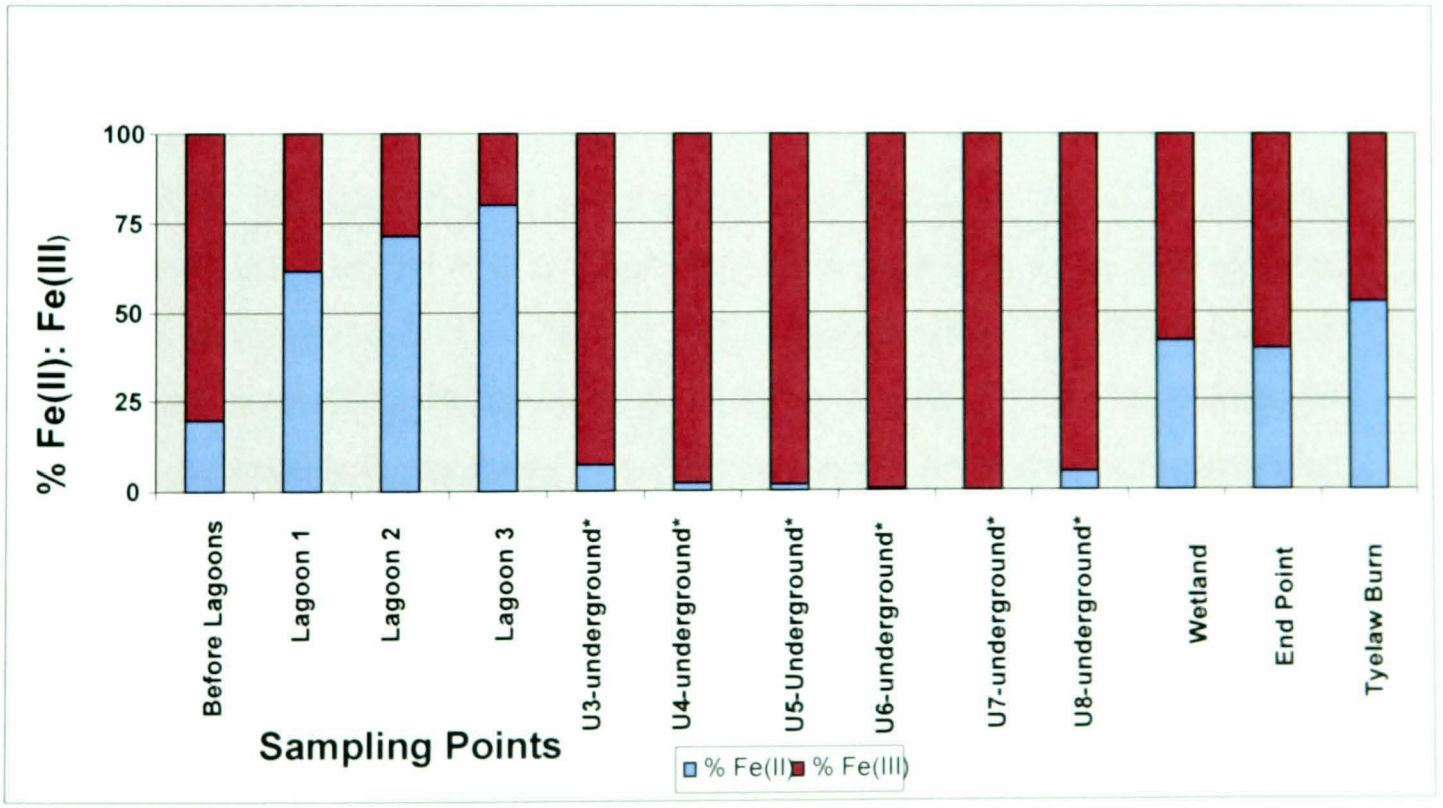

Figure 8.20: Comparison of the ratio of measured Fe(II) to Fe(III) using ultramicroelectrodes at various sampling points across Shilbottle treatment system site, Northumberland.

The results shown in figures 8.13 and 8.14 respectively suggest that effluent hydrolysed and unhydrolysed iron are consistently lower than the influent concentrations. This trend is not surprising as the solubility of iron would have significantly reduced due to elevated pH of the effluent sample and in addition, some iron would have precipitated as was visually observed in the highly turbid orange water which contains solid iron oxyhydroxides in the settlement lagoons and the wetland effectively removed these solids. In fact, effluent hydrolysed and unhydrolysed iron appeared stable and in very low concentrations where they are not below the detection limits. Comparison of measured concentrations of hydrolysed and unhydrolysed iron (figure 8.15) suggests that the proportion of unhydrolysed iron is smaller than that of the hydrolysed iron. This observed distribution is consistent with the fact that the bioavailability of iron is strongly dependent upon its chemical speciation due to variations in the solubility, mobility, sorption properties and precipitation mechanism for each oxidation state of iron [7]. In addition, extensive research on the chemistry of iron interaction with bacteria has shown that the biogeochemical cycling of iron in the mine-water environment is largely regulated by micro-scale changes in redox conditions [7]. The observed temporal and seasonal trends shown by both hydrolysed and unhydrolysed iron follow similar distribution pattern which is consistent with the rainfall events during the sampling period.

In figure 8.16, average dissolved and colloidal iron before the settlement lagoons, underground water samples from the spoil heaps and samples from the PRB effluent are shown. Samples taken from 30, 20 and 10 metres away from the settlement lagoons were to monitor whether water do overflow directly from the spoil heaps to this place, particularly during heavy rain event, as this has been observed before. The result suggests that this is indeed the case and iron concentrations reduce with distance from the settlement lagoons. Although, the proportion of colloidal iron follows the same trend as the dissolved iron, however, at much more lower concentrations and the effluent sample is evidently very low compared to the rest of the sampling points. Generally, underground water in the spoil heaps is of worse quality with higher concentration of iron than surface water in the lagoons. The deterioration in water quality of samples taken from distances before the lagoons could be attributed to the addition of contaminated underground base flow from the spoil heaps.

The proportion of dissolved to colloidal iron shows wide variation across the underground spoil heaps sampling points (figure 8.17). However, on average, the results reflect 60% of dissolved to 40% of colloidal iron. On comparison with samples taken from the PRB (figure 8.18), on average, a 50: 50 percentage proportion of dissolved and colloidal iron was observed. Similarly, although, the proportion remained widely varied in the samples taken after the PRB (figure 8.19), however, the overall percentage proportion is similar to the samples taken within the PRB. These complex observations indicate variations in the percentage proportion of iron concentrations between surface and underground water samples. These complex observations are consistent with the fact that the oxidative removal of iron from acidic waters occurs through its oxidation to ferric iron, followed by hydrolysis to a suspended solid-iron oxyhydroxides solid and precipitation of iron solid. Under alkaline conditions where the pH is maintained between 6 and 8, the hydrolysis is rapid and the limiting processes are oxidation and solids settling. Thus, the oxidation step is generally considered rate limiting for mine-water treatment systems [8] and has received a lot of attention by the acid mine drainage (AMD) researches across the world. Percentage ratio of Fe(II) to Fe(III) varied widely across the sampling locations (figure 8.20) reflecting similarities and differences of iron chemistry at each sampling location and across the site. For examples, samples taken before lagoons show ratio 4:1 (80%: 20%), samples from lagoons reflect a similar trend on average. However, a rather significant change was observed for samples taken from the underground spoil heaps which shows that the iron chemistry favours predominantly Fe(III) and most iron in the underground spoil heaps exist in +3 oxidation states. Furthermore, samples from the wetland, effluent and the stream (Tyelaw Burn) show 1: 1 relationship respectively. These observed trends could be attributed to the fact that mine-water reaction is dominated by abiotic processes above pH 5 [10 & 11]. Two abiotic processes have been identified [10]. The homogeneous reaction involving oxidation of dissolved Fe^{2+}, and a heterogeneous reaction involving Fe^{2+} sorbed onto ferric oxyhydroxides solids [11]. Both (that is, homogeneous and heterogeneous oxidations) mechanisms have been found to be first order with respect to Fe^{2+} and dissolved oxygen. The heterogeneous mechanism is also first order with respect to Fe(III) and pH [10]. Furthermore, the relative importance of the mechanisms varies with pH and concentrations of Fe(III). Thus, at high pH, such as those created in chemical treatment systems, the homogeneous reaction can dominates, but the amount of

Fe(III) available is limited by its initial formation via the loss of Fe(III) solids from the water through settling and precipitation.

8.2.3: Relationships between iron concentrations and the various measured parameters that controls iron geochemistry; *Eh*, pH and alkalinity

Establishing and understanding the relationships and correlations between various environmental parameters are fundamental to the understanding and plausible explanations of the observed spatial and seasonal trends in this site. Relationships between environmentally significant parameters are thus presented in this section. Figure 8.21 shows the relationships between the total dissolved iron and the water pH while the relationship between total colloidal iron against the pH is presented in figure 8.22. Relationship between the water temperature and pH of samples taken from the spoil heaps, within the PRB and the effluents are presented in figures 8.23 to 8.25. Shown in figure 8.26 is the overall relationship between the water temperature and the pH for all samples taken at various sampling points across the site while figure 8.27 shows water *Eh* as a function of pH across the site.

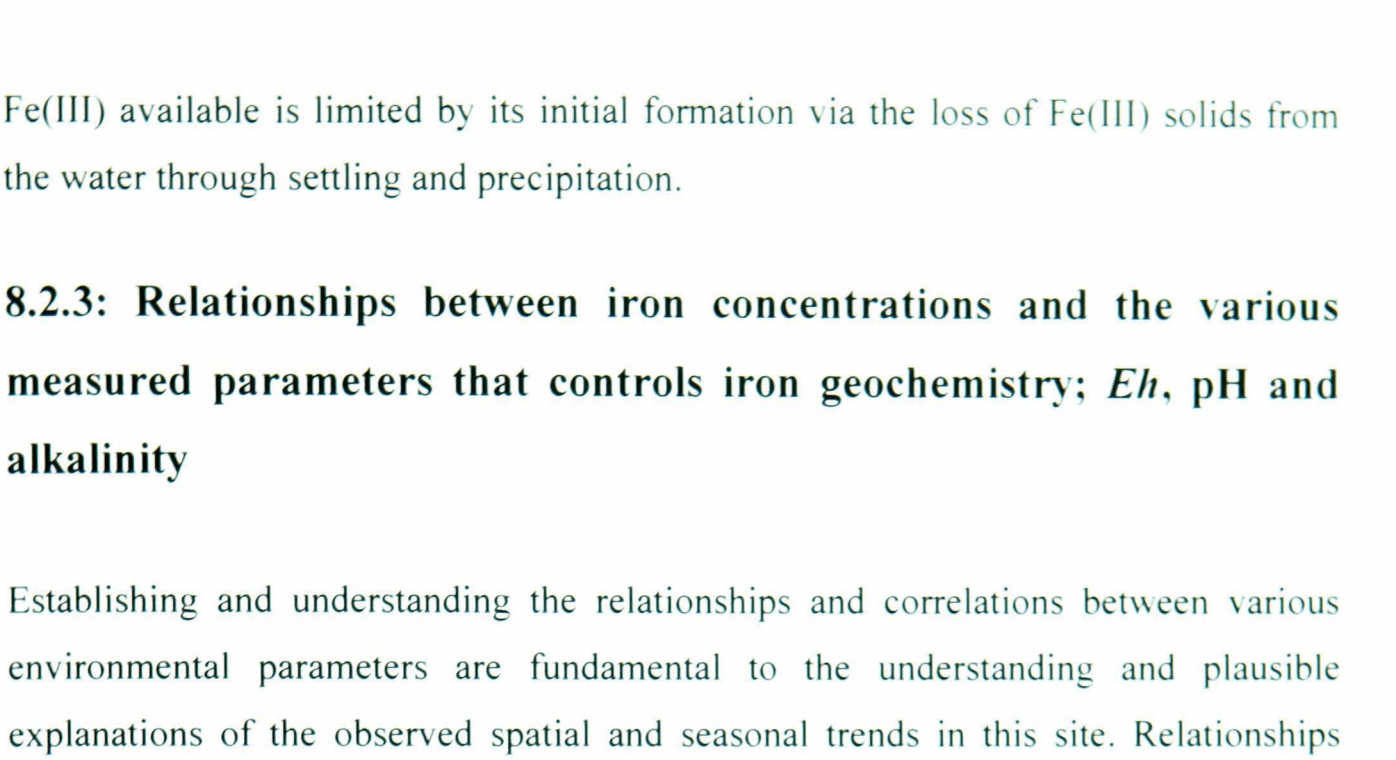

Figure 8.21: The relationship between the measured total dissolved iron concentrations and the pH across various sampling points at Shilbottle site.

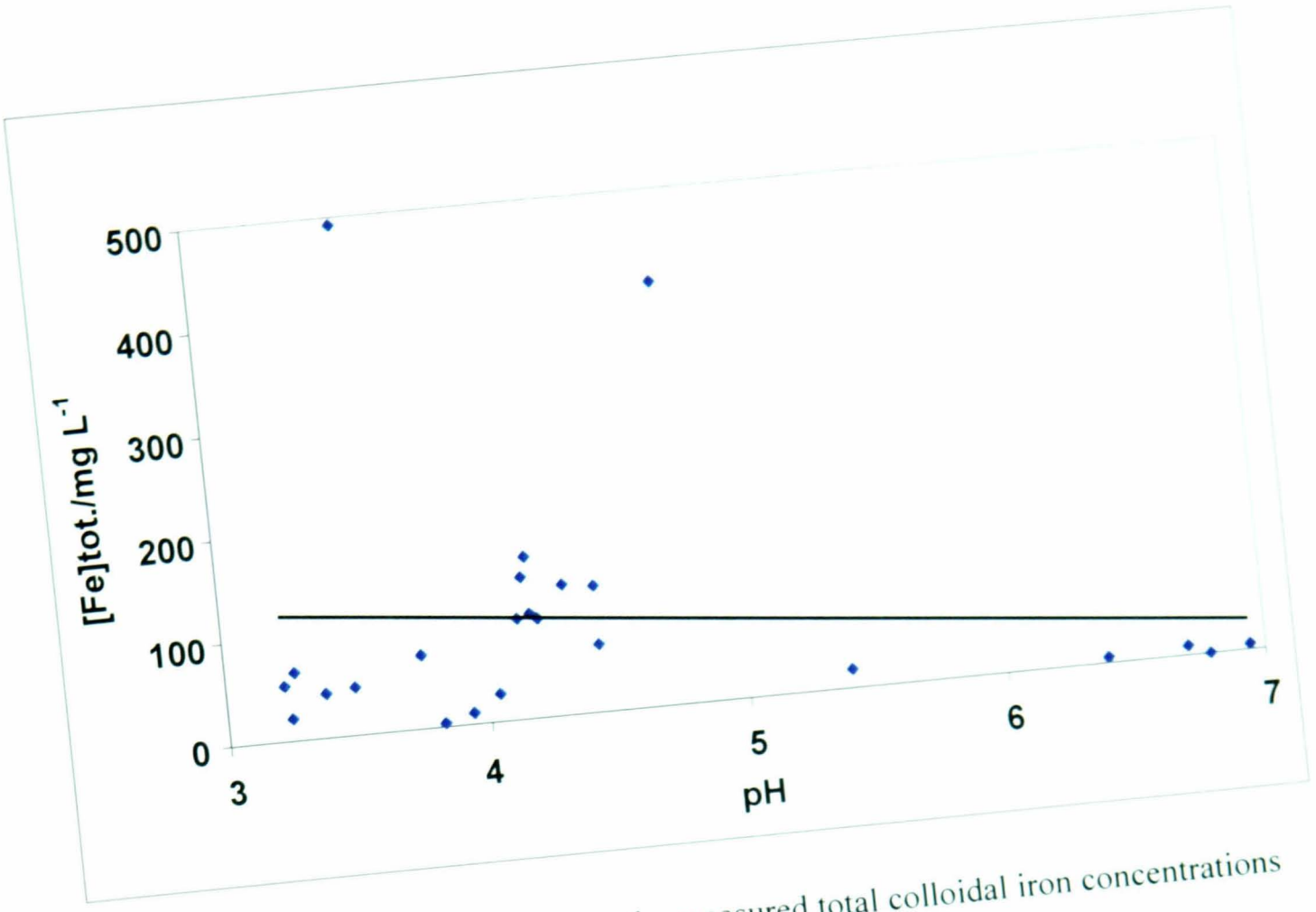

Figure 8.22: The relationship between the measured total colloidal iron concentrations and the pH across various sampling points at Shilbottle site.

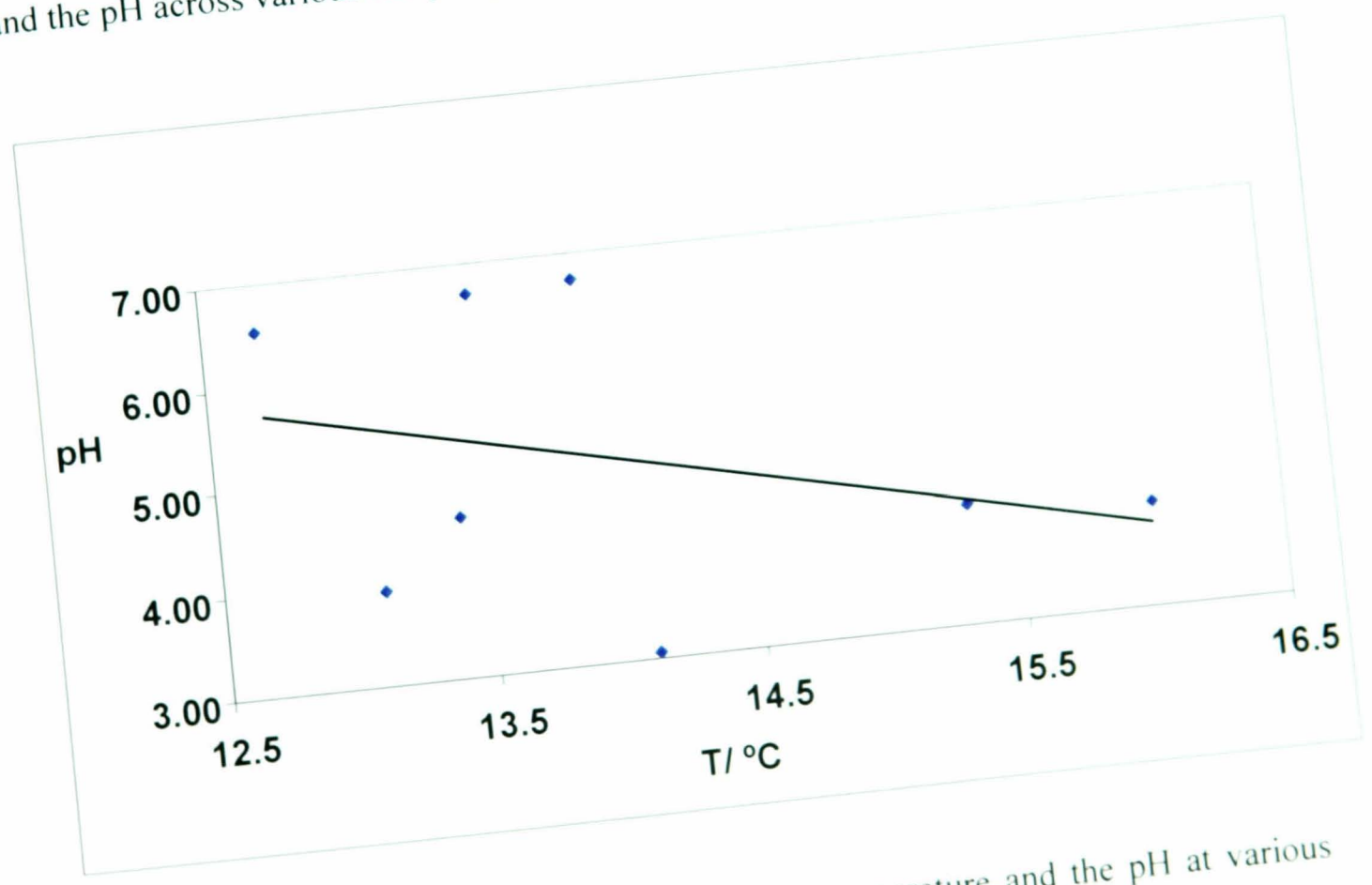

Figure 8.23: The relationship between the water temperature and the pH at various sampling points across for samples taken from the spoil heaps at Shilbottle site.

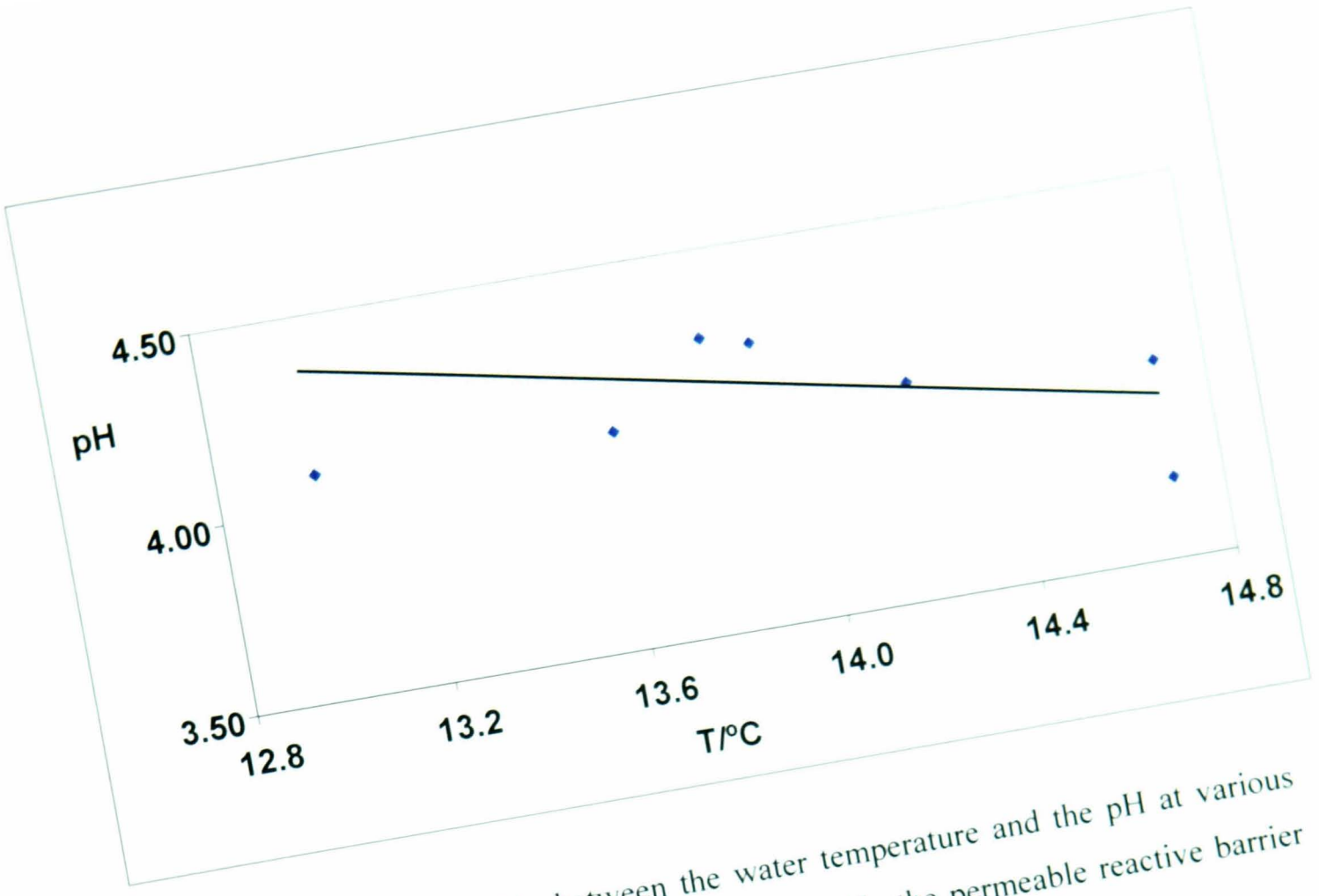

Figure 8.24: The relationship between the water temperature and the pH at various sampling points across for samples taken from within the permeable reactive barrier (PRB).

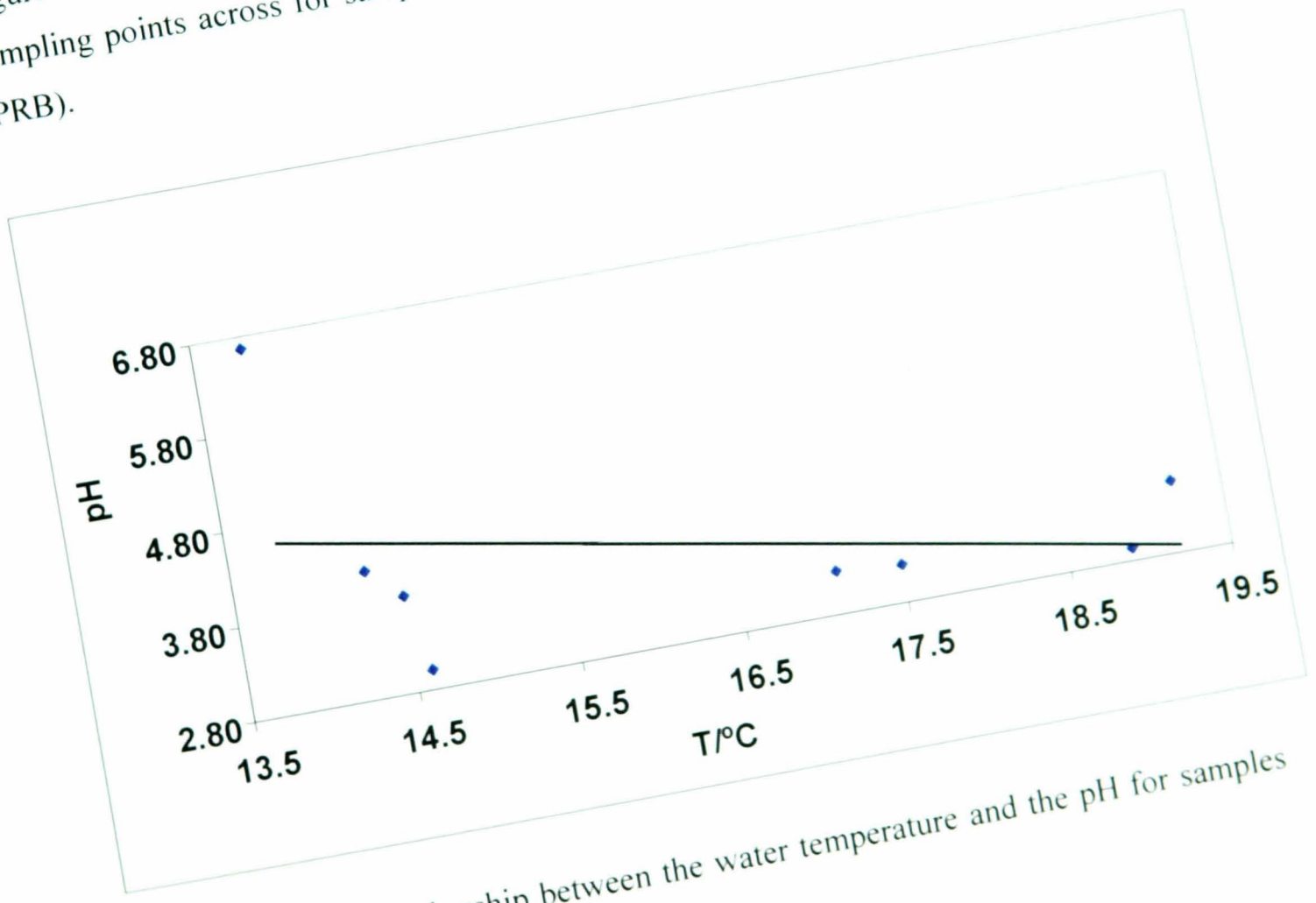

Figure 8.25: The relationship between the water temperature and the pH for samples taken from the effluent at Shilbottle site.

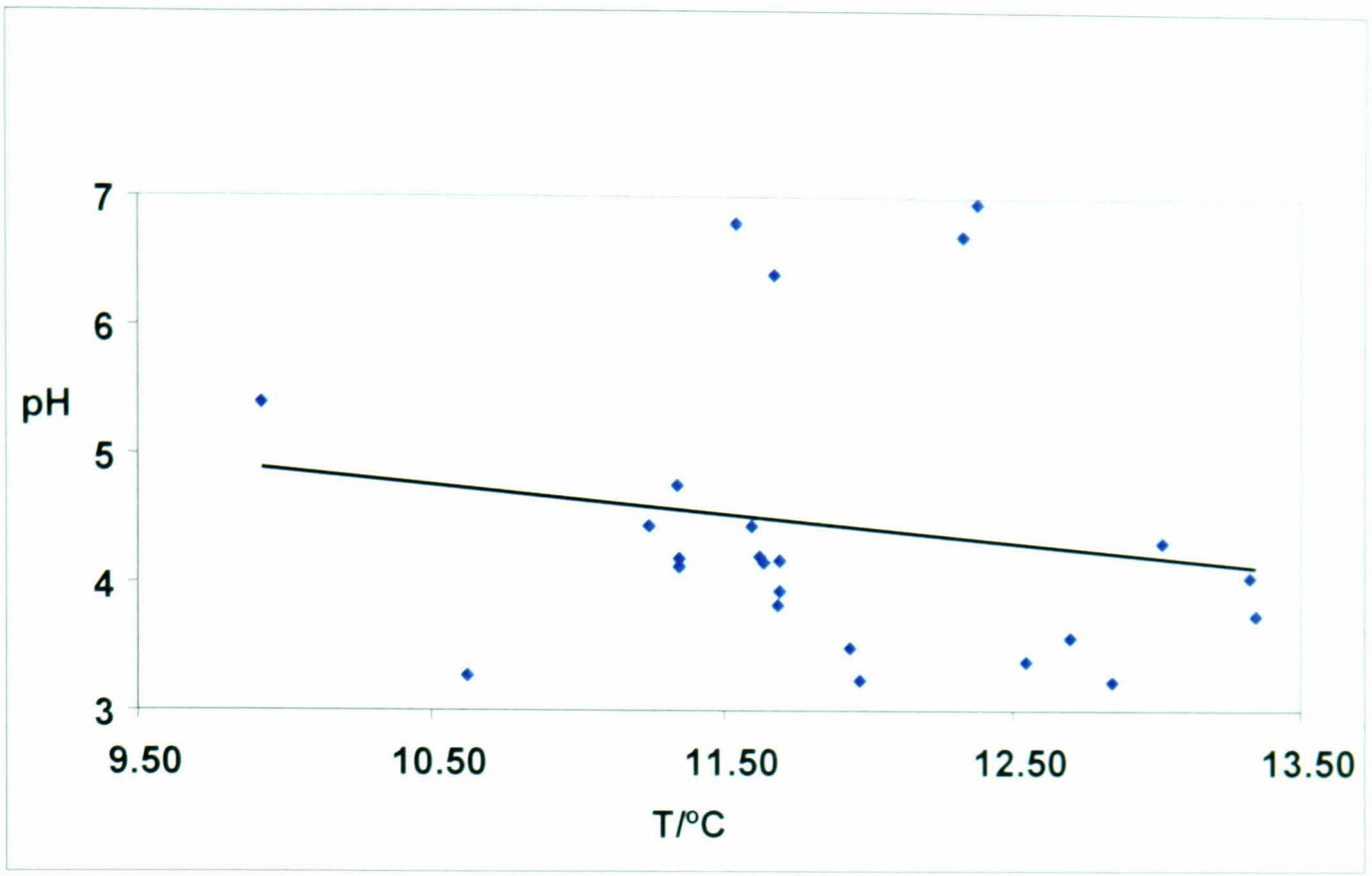

Figure 8.26: The relationship between the water temperature and the pH of samples taken at various sampling points across at Shilbottle site.

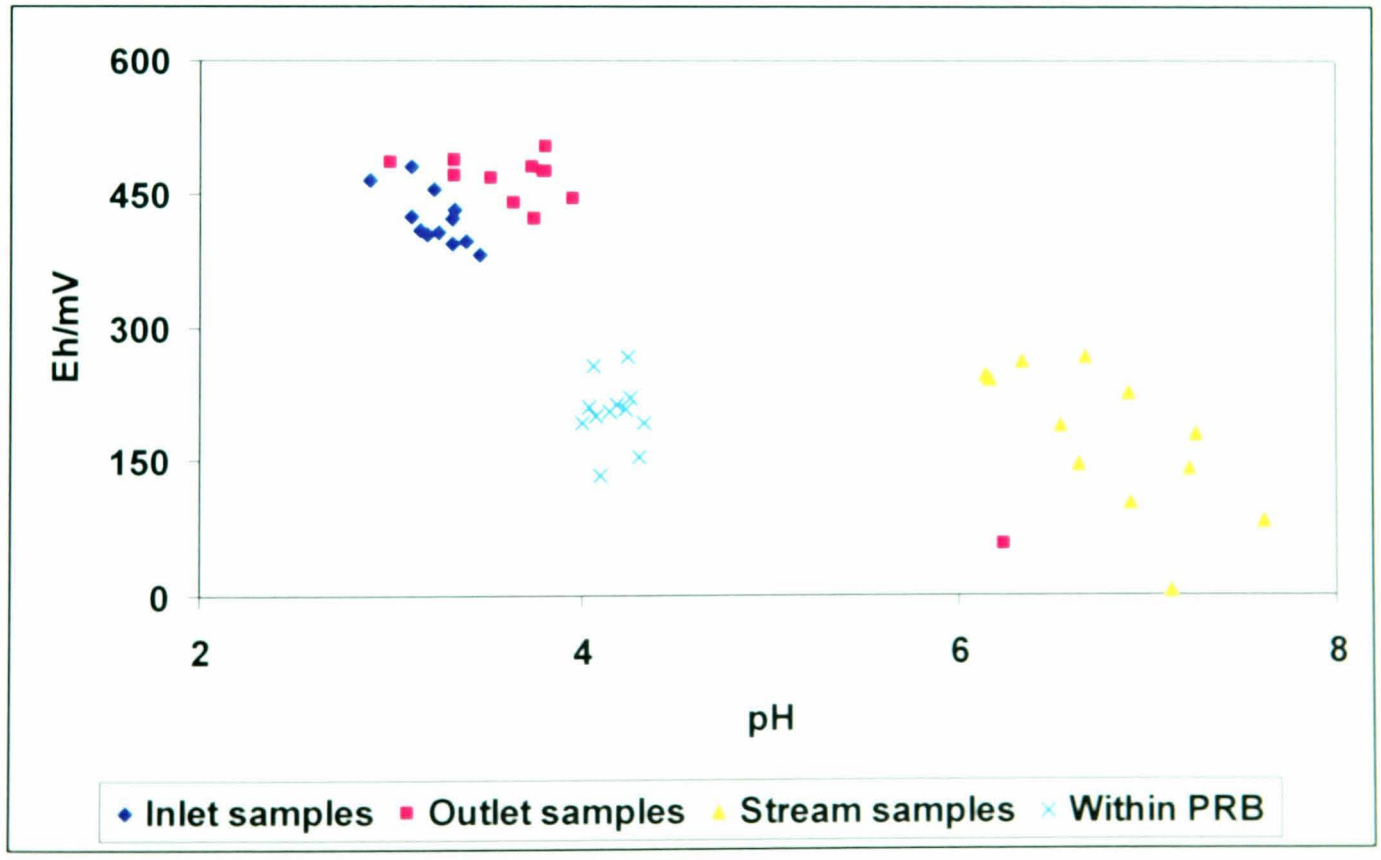

Figure 8.27: The relationship between the water Eh as a function pH for samples taken various sampling points across Shilbottle site. The least squares regression equation is (R^2=0.49, 0.89, 0.00 & 0.48) for inlet, outlet, within PRB and stream respectively.

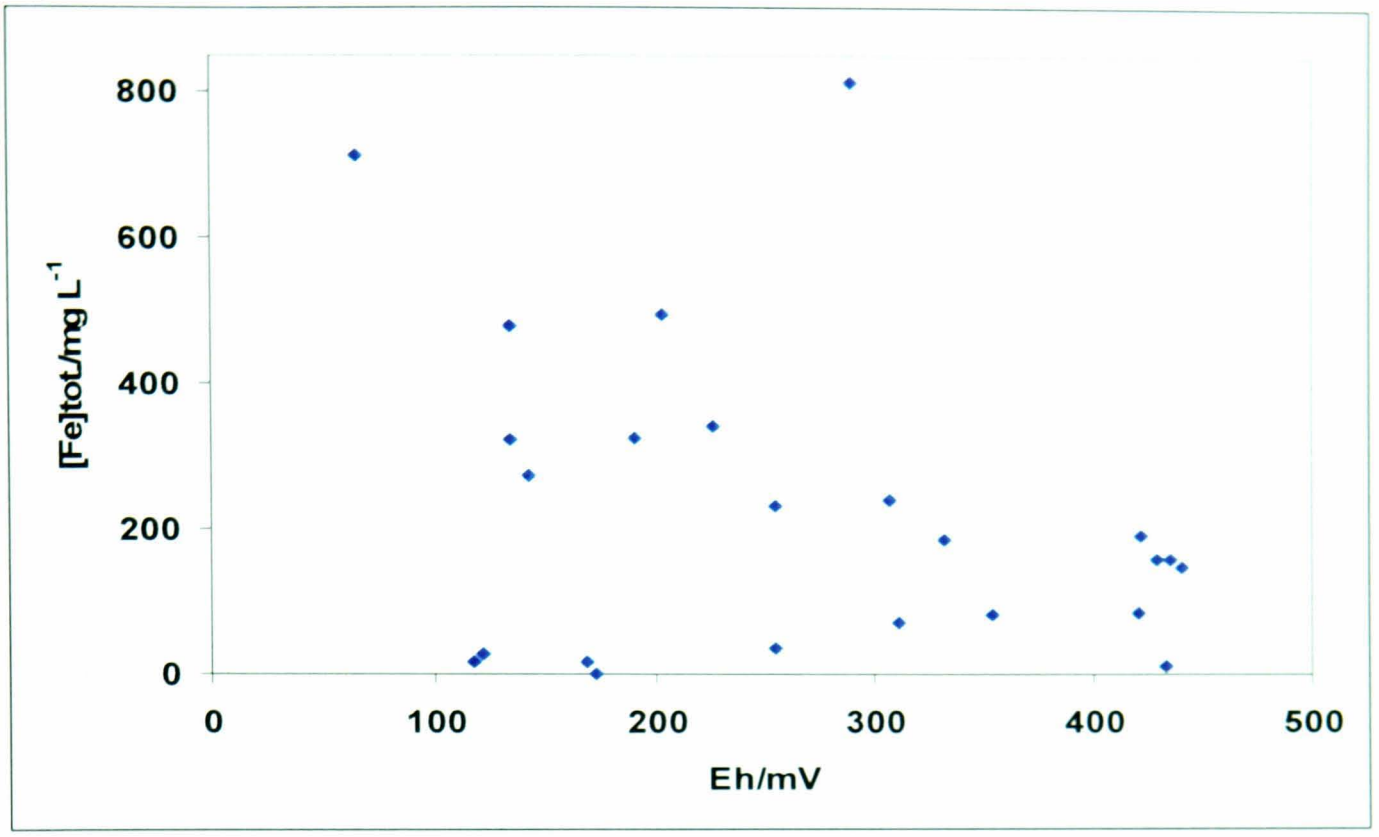

Figure 8.28: Measured total iron concentrations as function of *Eh* for samples taken various sampling points across Shilbottle site.

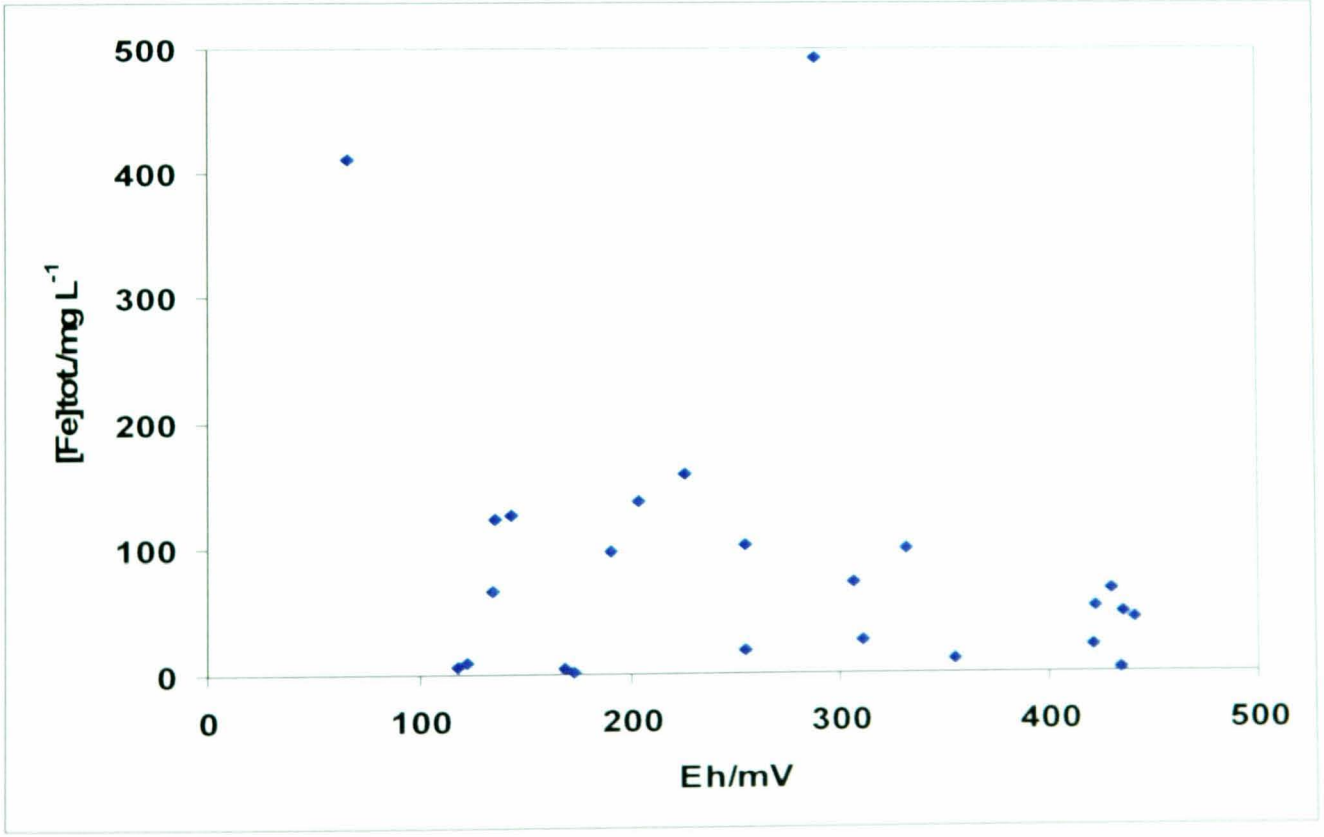

Figure 8.29: Measured total colloidal iron concentrations as a function of *Eh* for samples taken various sampling points across Shilbottle site.

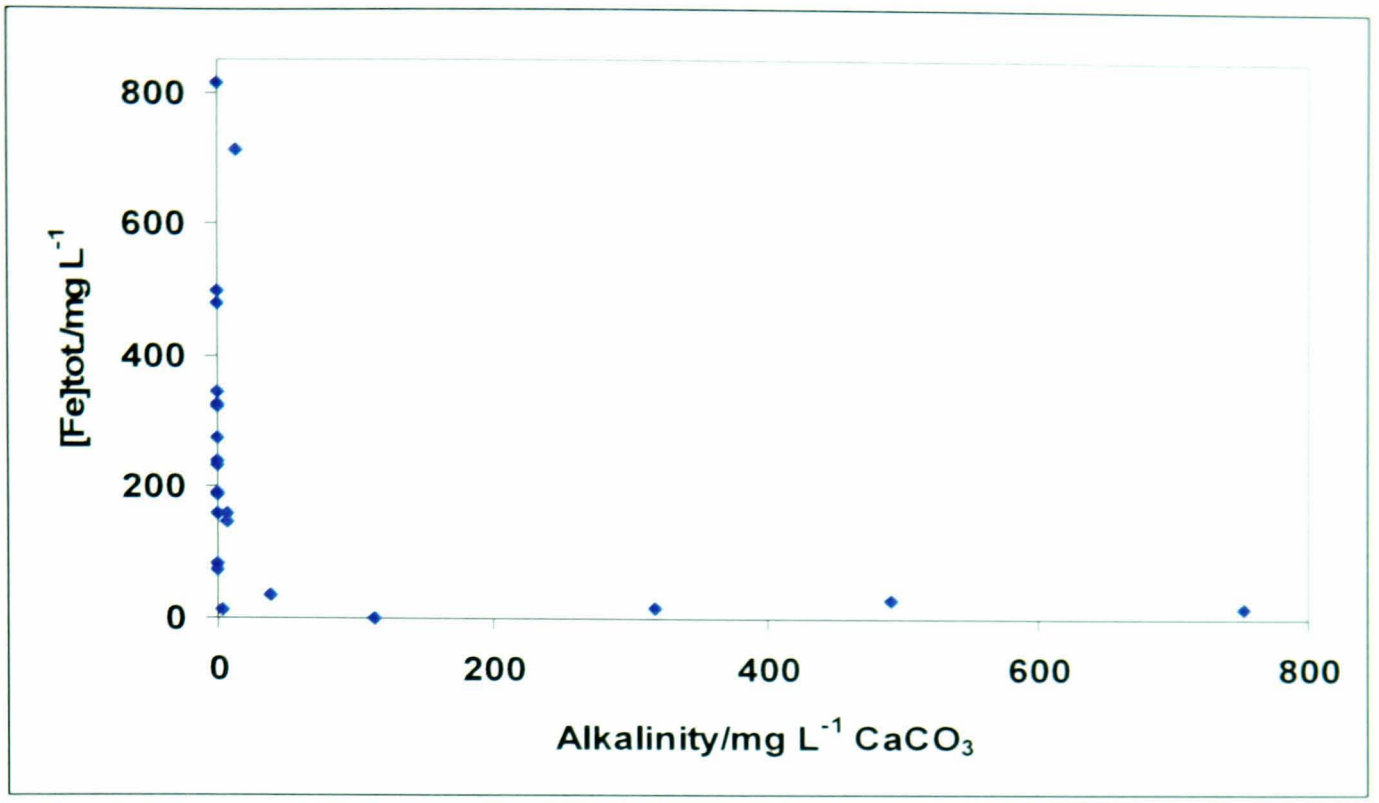

Figure 8.30: Measured total iron concentrations versus water alkalinity of samples taken various sampling points across Shilbottle site.

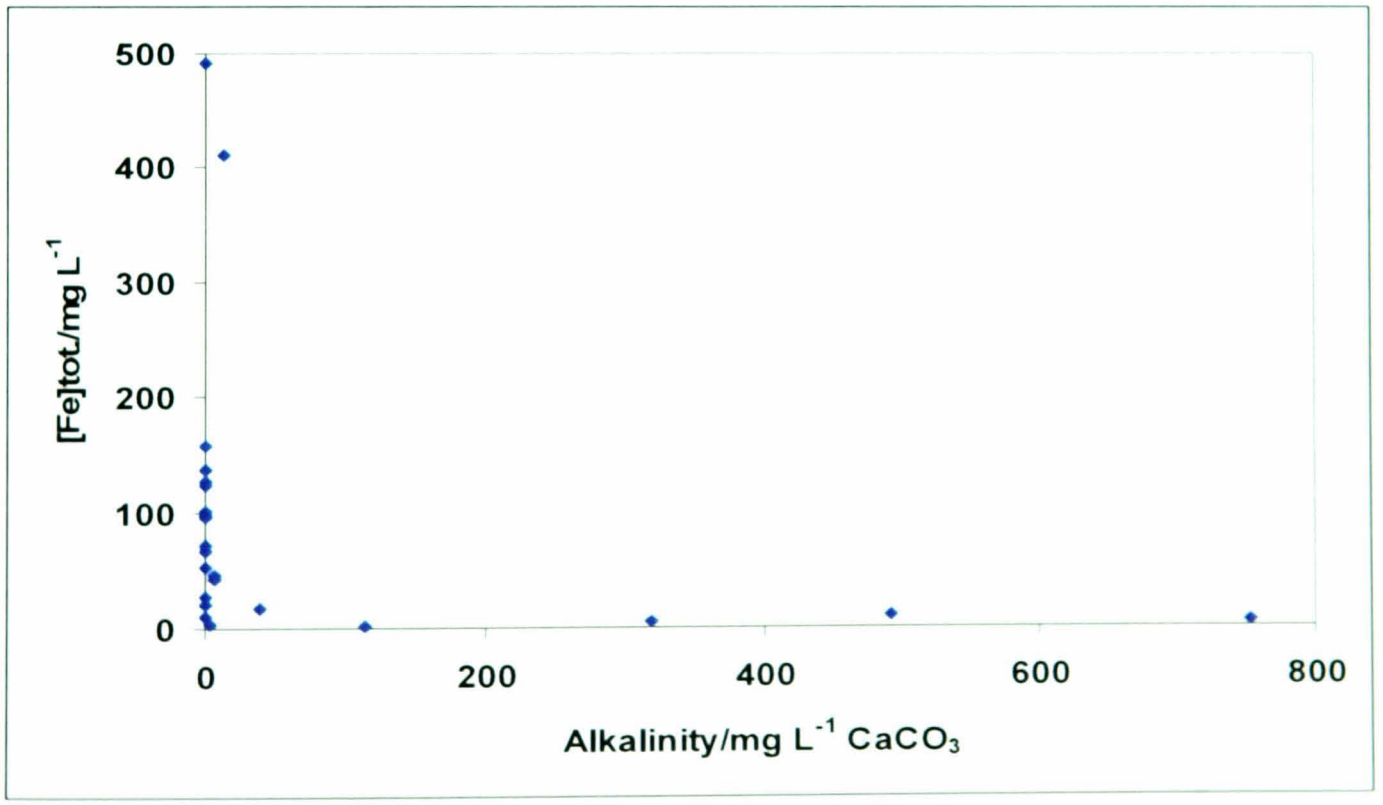

Figure 8.31: Measured total colloidal iron concentrations versus water alkalinity of samples taken various sampling points across Shilbottle site.

Relationships between the measured total iron concentrations and total colloidal concentrations as a function of water *Eh* and water alkalinity are presented in figures 8.28 to 8.31.

Figures 8.21 and 8.22 show typical results for the measured total dissolved and colloidal iron concentrations as a function of pH respectively. In general, there appeared to be a negative correlation between the measured total dissolved iron concentrations as a function of pH. The same trend was observed for the colloidal iron versus pH and the same pattern of variation of iron concentrations as observed in the total dissolved iron profile. The straight line fitted passing through the plot is a linear regression fitted to the data, demonstrating that though there is no correlation, the declining trend appears to correspond to gradual depletion of vestigial acidity with iron concentration. These trends show the precipitation of iron at high pH. The slight variations observed in these trends could be attributed to the fact that the solubility, mobility and environmental risk of many metal ions including iron that are released by sulphide weathering as the case in Shilbottle site, increases dramatically in the near-acid pH range of 5.6 [12]. Furthermore, acidic discharges are associated much more strongly with solute metal contamination, while circumneutral and alkaline mine- water discharges are associated with ochre formation due to low solubility of iron (III) oxyhydroxides minerals in this pH range [12].

Relationship between water temperature and water pH at different mine-water conditions are presented in figure 8.23, 8.24, 8.25 and 8.26 for samples taken from the underground spoil heaps, samples taken from within the PRB, samples taken from the PRB effluents and the whole samples taken across the site respectively. The results show mixed inverse relationship between pH and water temperature which is quite surprising. While there are no correlations between water pH and temperature for samples taken from the spoil heaps and the entire samples (R^2=0.19 & 0.02) respectively, there appear to be slight correlations, though weak for the PRB and the effluent samples (R^2=0.40 & 0.32) respectively. However, similar analyses of pH and temperature at common sampling locations have not been reported and it is presently unknown whether this is a common phenomenon or a unique result of the Shilbottle PRB system water chemistry. Furthermore, this inverse relationship between water temperature and both dissolved iron and pH is more than sufficient to offset the direct

relationship between temperature and reaction kinetics for iron oxidation. The effect of temperature variation on the settling rate of iron oxyhydroxides is not known. It is possible that lesser iron removal by some passive systems in winter is due to less efficient solids settling rates, and not slower ferrous iron oxidation. However, in general, water temperature will affect water viscosity, dissolution rate, diffusion rate and equilibrium constants of the metal present in the system [10]. In addition, biological activity (that is microbial activity) will also be affected by temperature. Consequently, variation in water temperature will affect the total water solute load and an increase in temperature increases the rate of dissolution [11].

The plot of measured water *Eh* as a function of pH for samples taken from underground inlet, within the PRB, the outlet and the stream shows a rather complex correlation between these two water quality parameters (figure 8.27). Whilst there is strong correlation (R^2=0.89) for the outlet samples, both underground inlet samples and the stream show weak relationships (R^2=0.49 & 0.48), there is no correlation (R^2=0.00) for samples taken within the PRB system. These complex observations could be attributed to the fact that high *Eh* and low pH in the influent samples are probably controlled by the degree of acidity (H^+) generated during the oxidation and dissolution of pyrite. Thus, we would expect to find a change from Fe^{2+} to Fe^{3+} or vice-versa depending on the shift in the pH or *Eh* of the environment. However, in general, Eh tends to increase with increasing pH (with few exceptions) which shows that influent samples are in oxidised environment whilst effluent samples are in reduced environment. Furthermore, as explained in chapters 6, 7 and 8, determination of redox potential (*Eh*) in nature is quite complicated as some of the reactions that determine redox potentials are slow [10] and it has been observed that redox potentials measured in oxygen-containing environments are generally lower than the equilibrium values [14, 15, 16].

There is no correlation between measured total and colloidal iron concentrations as a function of water *Eh* (R^2= 0.09 and 0.06) as shown in figures 8.28 and 8.29 respectively. Similarly, measured total and colloidal iron concentrations as a function of water alkalinity show no correlation (R^2= 0.14 and 0.07) as presented in figures 8.30 and 8.31 respectively. The aforementioned similarity of the trend in the measured total and colloidal iron concentrations as a function of water *Eh* and alkalinity indicate

that the controlling influence of *Eh* and pH is very significant in determining the iron chemistry. These complex influences include redox transformations associated with oxidation and reduction of iron and sulphur (genesis of alkalinity) and overall iron precipitation. Furthermore, previous studies [e.g., 16, 17, 18] have reported that major remediative processes including iron geochemistry in passive treatment systems like in Shilbottle site are microbially driven. For example, it has been reported that both aerobic and anaerobic bacteria can proliferate in and around areas of high dissolved iron concentration [14, 18] whilst sulphate-reducing bacteria zones are characterised with low concentrations of dissolved iron [7, 11]. Moreover, oxidation of iron takes place much more completely in alkaline medium than in acidic. Thus, larger amounts of dissolved iron are commonly present in slightly acidic waters than in faintly alkaline waters.

8.3: Conclusions

Monitoring changes in iron speciation in polluted mine-waters is difficult due to the complexity and heterogeneity of these systems. This study demonstrates for the first time the ability that voltammetric technique could be an invaluable for probing iron speciation in polluted mine waters with potential for in-situ application. Though, not yet tested on the filed scale, results in the laboratory are very encouraging.

Generally, samples from underground water in the spoil heaps was of the worse quality with higher concentration of iron than surface water in the lagoons and other sampling points across the site.

Downstream of Tyelaw Burn, there was a significant decrease in iron concentration by up to 85% with elevated pH. In most cases, effluents water attained pH > 7 with increasing alkalinity, which implies that acidity has been neutralised and the water has become net alkaline. This decrease can be attributed to increased alkalinity as the acidic water passes through the permeable reactive barrier (PRB) and decrease in iron concentration could be attributed to the precipitation of iron at high pH onto the streambed as the water passes through the lagoons and the polishing wetland.

Iron concentrations were seasonally highest in the summer and lowest in the winter/spring mostly due to the seasonal variation in surface runoff not in contaminant concentrations, which remained reasonably constant throughout the year.

The evidence of high degree of chemical variation in colloidal iron is used to support the hypothesis that water chemistry are not uniform across the site and that the chemistry of water within the underground spoil heaps therefore, may be considerably different from the chemistry of the surface water.

Evidence of a large spatial variation of the water chemistry suggests a rather complex systems and this observation alone has implications for the remediation strategies.

The voltammetric technique can potentially allow for direct monitoring of iron chemistry within the aquatic environment, in this work; the results have shown that voltammetric technique can be used to determine colloidal and dissolved iron in mine waters.

The study revealed for the first time the spatial distribution and temporal variability of iron concentrations across the site which are crucial for understanding and monitoring iron chemistry in polluted mine-water. In the underground spoil heaps, the iron content is dominated by ferric iron-Fe(III), the situation was reversed in the wetland and the effluent samples while ferrous iron dominates the iron chemistry for samples taken before the lagoons. This is the first time this has been shown and observed in this site.

UME results (figure 8.20) indicate that the low *Eh* at the surface is due to the drop in Fe(III) concentrations.

The concentrations of hydrolysed iron are consistently higher than the concentrations of unhydrolysed iron across the sampling locations. These trends show that the dissolved iron in this site must be predominantly hydrolysed iron because of the low solubility of the unhydrolysed iron, particularly at elevated pH.

8.4: References

[1]. Amos, P.W. & Younger, PL. *Water Research*, 37, 108-120, **2003**, 11. 127-135.

[2]. Jarvis, A.P., Moustafa, M., Orme, P.H.A & Younger, P.L. *Environmental Pollution*, **2006.** 143, 261-268.

[3]. Younger, P.L. *International Mine Water Association, Johannesburg*, **1998.**

[4]. Bowden, L., Jarvis, A.P., Orme, P.H.A. & Younger, P.L. *Unpublished Report. Newcastle University*, **2004.**

[5]. CL: AIRE Case Study Bulletin CSB4 (March **2006**). Coal Mine Sites for Targeted Remediation Research: The CoSTaR initiative.

[6]. CL: AIRE Case Study Bulletin (Autumn **2002**). Shilbottle Colliery Remediation Scheme: The UK's First Large-Scale Permeable Reactive Barrier for Mine Spoil Leachate Remediation.

[7]. Kendall, T.A & Hochella, M.F. *Geochimica et Cosmochimica Acta*, 67, 3537-3546, **2003**, 19.

[9]. Hedin R.S., Watzlaf, G.R. & Narin, R.W. *Environmental Quality*, 23, **1994**, 1338-1345.

[10]. Hedin, S.R. *Mine Water Environment*, **2008**, 230, 41-49.

[11]. Hustwit, CC., Ackman, T.E. & Erickson, P.E. *Water Environment Research*, 64. **1992**, 817-823.

[12]. Banwart, S.A. *Tsinghua Science and Technology*, **2000**, 310-313.

[13]. Younger, P.L., Banwart, S.A. & Hein, R.S. Mine Water: Hydrology, Pollution, Remediation. *Kluwer Academic Publishers, Dordrecht, the Netherlands*, **2002**. 442pp.

[14]. Hedin, R.S., Narin, R.W. and Kleinmann, R.L.P. Passive treatment of coal mine drainage. *US Bureau of Mines Information Circular No.9389*. **1994**, United States Department of Interior, 35pp.

[15]. Walton-Day, K. *Reviews in Economic Geology*, **1999**, 6A, 215-228.

[16]. Krauskopf, K.B. Introduction to Geochemistry, *McGraw-Hill*. **1979**, 617pp.

[17]. Boshoff, G.A. and Bone, B.D. *IAHS Publication 298*, **2005**. Wallingford, UK, 163pp.

[18]. Environment Agency, the State of the Environment of England and Wales: Fresh Waters, **1998**, the Stationery Office, London.

[19]. Younger, P.L., Jayaweera, A., Elliot, A., Wood, R., Amos, P., Daugherty, A.J., Martin, A., Bowden, L., Aplin, A.C. and Johnson, D.B. *Land Contamination and Reclamation*, **2003**, 11, 127-135.

[20]. PIRAMID Consortium, *European Commission 5th Framework RTD Project No.EVK1-CT-1999-000021*, **2003**, 166pp.

Chapter 9

WHITTLE SITE, NORTHUMBERLAND

In this chapter, background history, iron rich mine drainage problems and the remediation regime in operation at the Whittle site in Northumberland are presented. This is followed by on-site water quality parameters and voltammetric results. Seasonal trends and variability in water quality parameters; temperature, pH, *Eh*, conductivity and alkalinity and the various measured iron concentrations results are then discussed in detail and finally conclusions.

9.1: Site History, Background, Problems and Treatment Regime

Mining operations ceased at Whittle Colliery in March, 1997 after nearly a century of activity. Mine-water contamination began in Whittle site after the dewatering of the underground workings stopped following the cessation of mining operations. At the time, measurement of the groundwater rebound of the workings was found to be 5 cm day^{-1} [1]. This rising contaminated groundwater gave cause for concern, as any uncontrolled release into the local stream-Hazon Burn would result in a major pollution event for this water course. The Hazon Burn is a tributary of the River Coquet, which is one of the 27 river Sites of Special Scientific Interest (SSSI) in Britain [5]. So, any pollution event in the Burn would have an adverse effect on the River Coquet.

The passive treatment at Whittle site is a preventative scheme and therefore the water is prevented from reaching the surface naturally. This is done by pumping the water through a purpose-drilled borehole that stretches 70 m within the Colliery drift, with the water entering into an aeration cascade as part of the treatment scheme. The aeration is done to oxygenate the water with the aim of precipitating iron as iron oxyhydroxides. The aerated water then flows to two parallel settling ponds with an area of 800 m^2, where the ochre precipitation takes place. From the settlement lagoons, the water then enters into three surface-flow aerobic wetlands in succession. These wetlands each have an area of 3000 m^2 . Wetlands 1 and 3 are planted with *Typha Latifolia*, and wetland 2 is planted with *Phragmites* [5]. The purpose of the

planting was to distribute the flow of the water and polish the final discharge into the Hazon Burn. Figure 9.1 shows the layout of the site whilst figure 9.2 shows the two parallel settling ponds at Whittle site.

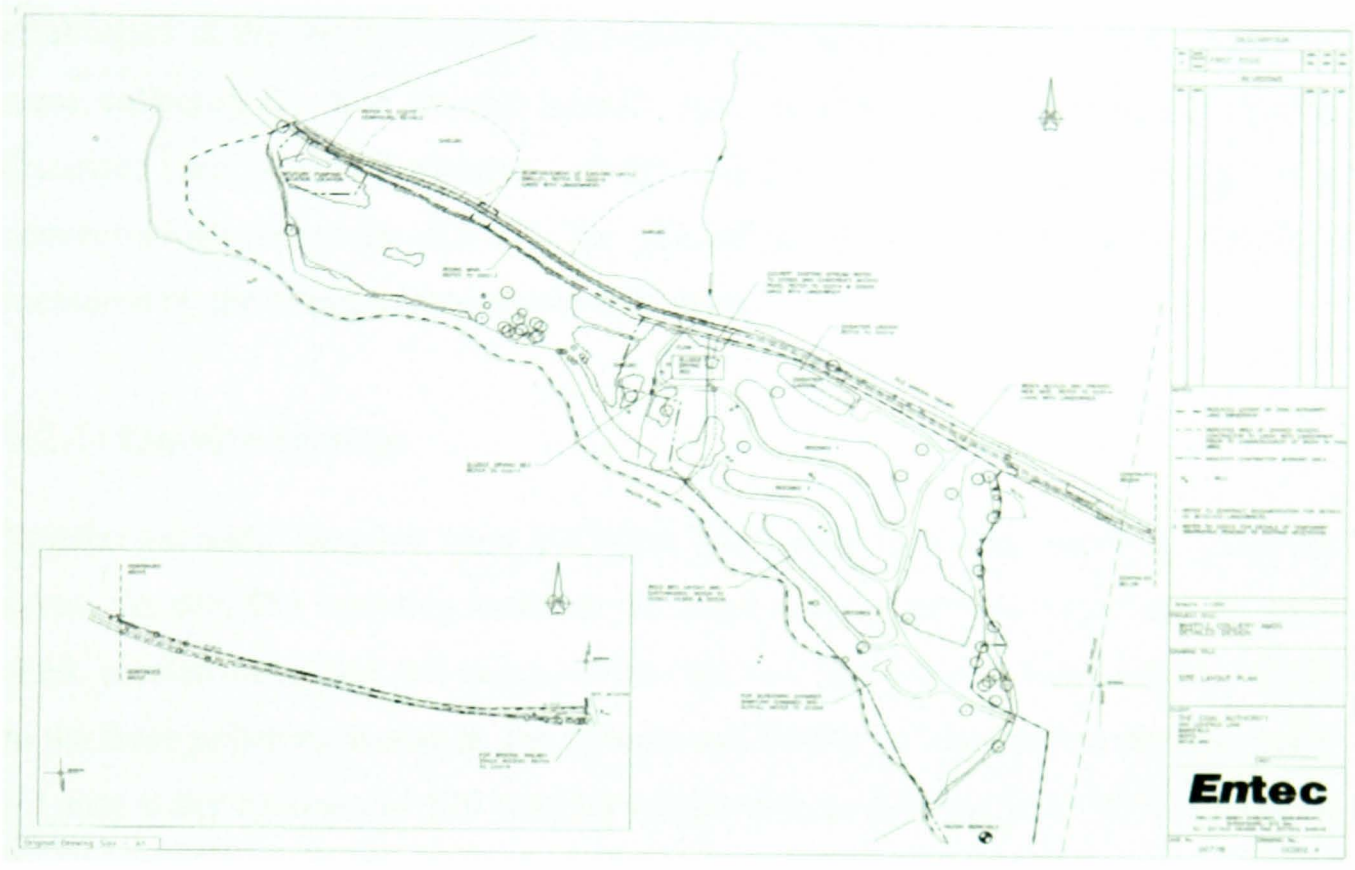

Figure 9.1: Schematic showing the layout plan of passive treatment regime at the Whittle site- Courtesy of HERO research Group at Newcastle University.

Figure 9.2: Photograph taken September 26, 2006 by Kola, showing two parallel settling ponds where ochre precipitation takes place after pumped water from the drift has been aerated through cascade.

9.2: Results and Discussion

Results of the monthly monitoring of water quality parameters such pH, *Eh*, temperature, alkalinity and conductivity collected from various sampling stations established at the Whittle site are presented and discussed in this section. Samples were collected for five months period, June-October, 2006. Also presented and discussed are the voltammetric results showing dissolved and colloidal iron concentrations across the site with the ratio of the proportion of Fe(II) to Fe(III) as measured by the ultramicroelectrodes technique.

9.2.1: On-site results

Regular monthly samples were collected from eight different sampling locations across the site. The sampling locations are: mine water coming directly from the mine shaft, aerated water that has cascaded into the two parallel settlement lagoons, inlets to the three polishing wetlands, the effluent and finally the stream-Hazon Burn. Table 9.1 lists water analyses of 120 samples collected from this site while table 9.2 shows the mean chemical characteristics of water at various sampling stations. Water temperature, pH, *Eh*, alkalinity and conductivity profiles are presented in figures 9.3 to 9.7.

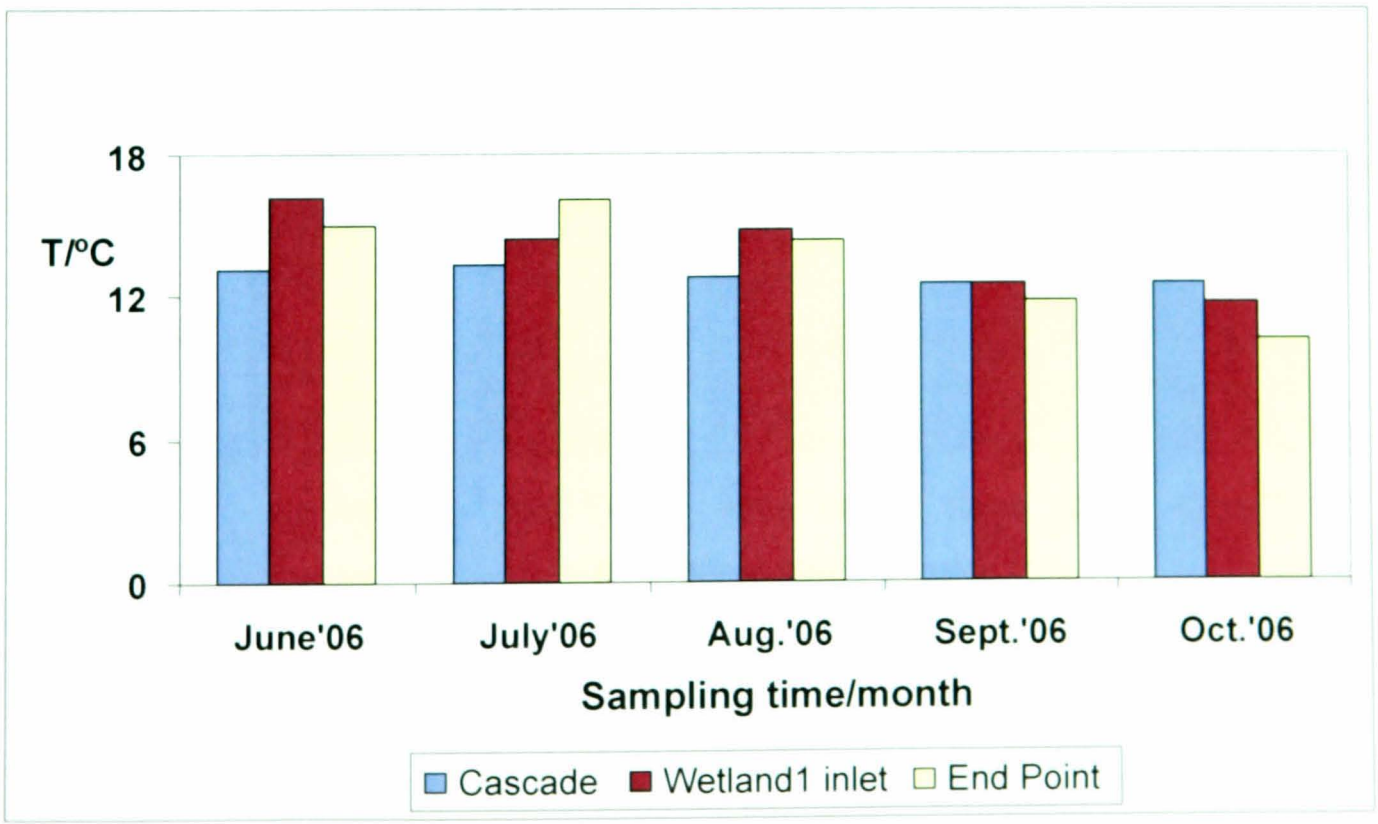

Figure 9.3: Graph showing water temperature profile at various sampling locations for the five months period, June-October, 2006 at Whittle treatment system site.

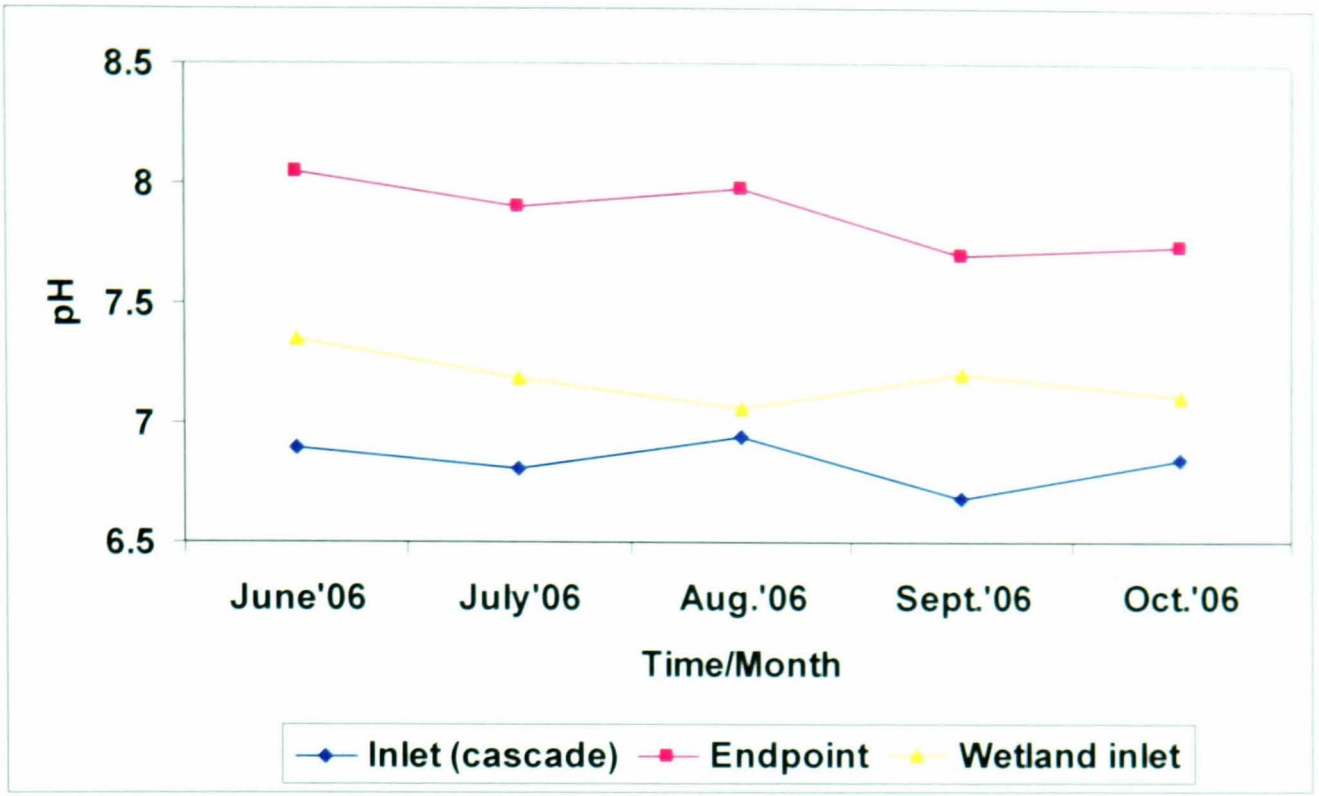

Figure 9.4: Plot showing water pH profile at various sampling locations for the five months period, June-October, 2006 at Whittle system treatment site.

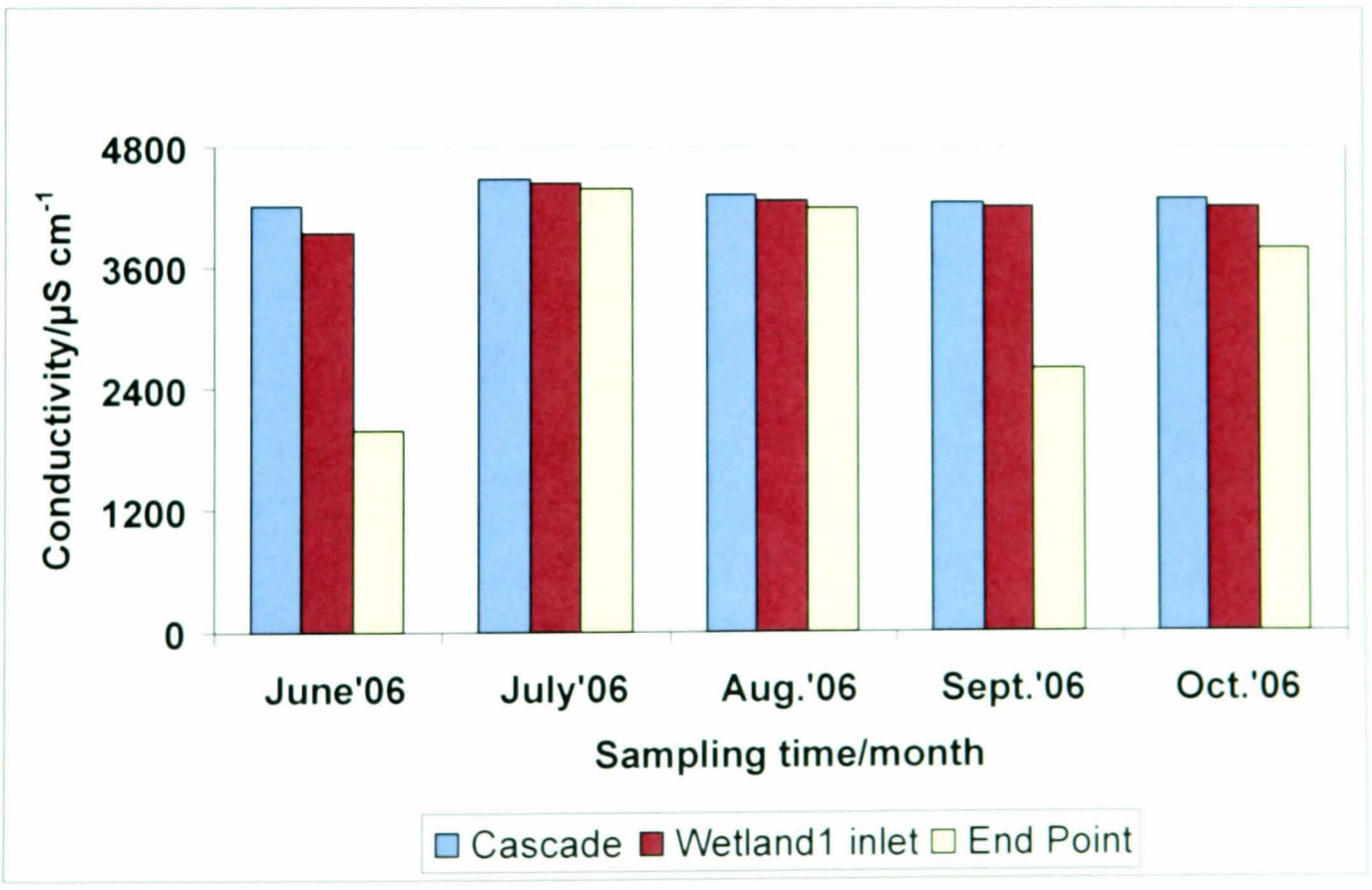

Figure 9.5: Showing water conductivity profile at various sampling locations for the five months period, June-October, 2006 at Whittle treatment system site.

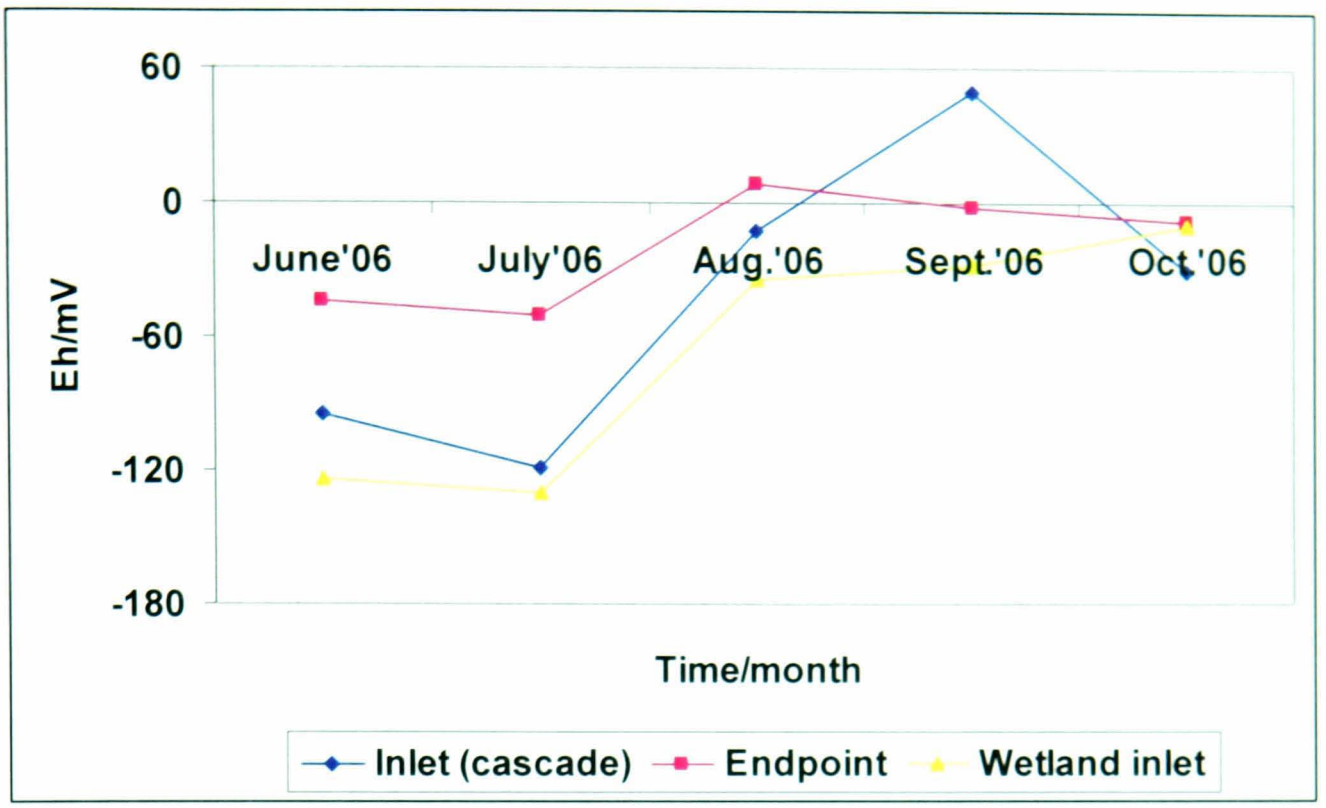

Figure 9.6: Showing temporal changes in water *Eh* over time at various sampling points across the Whittle treatment system site for samples taken June-October 2006.

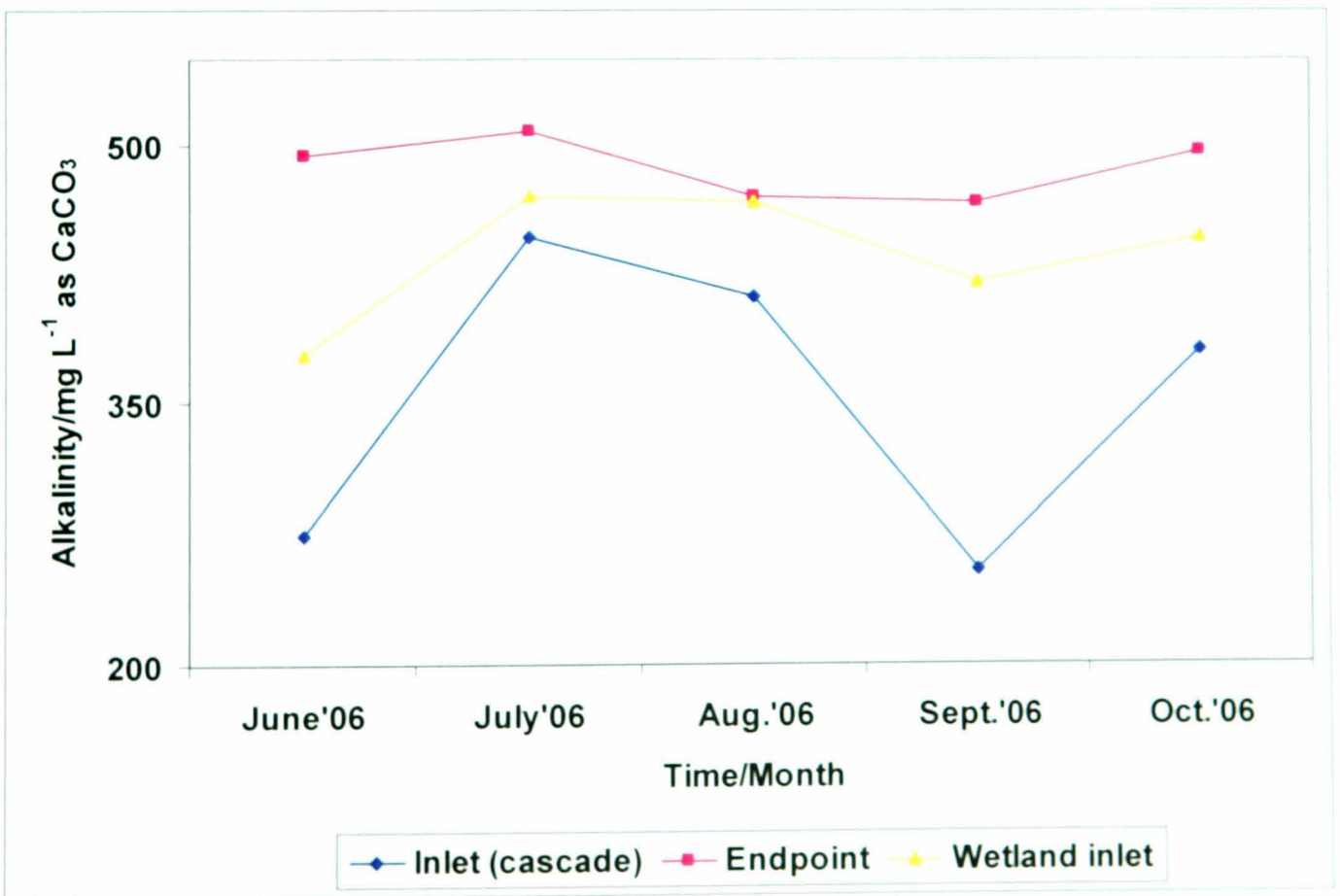

Figure 9.7: Showing temporal changes in water alkalinity over time at various sampling points across the Whittle treatment system site for samples taken June-October 2006.

Table 9.1: Water quality parameters determined at various locations at Whittle, Northumberland treatment system site from June-October 2006.

Dates	Sample	pH	*K*.(μS cm^{-1})	Alkalinity/mg L^{-1} $CaCO_3$	*Eh*(mV)	*T*/°C	[Dissolved Fe]/mg L^{-1}	[Colloidal Fe]/mg L^{-1}	Comments
23-June'06	Cascade	6.89	4209	494	-95	13.1	34.3	22.9	Mine water from mine shaft
	Wetland1 inlet	7.35	3949	378	-124	16.2	22.8	17.9	Aerated (i.e. oxygenated) water from cascade that has passed through the lagoons
	End Point	8.05	1983	274	-44	15.0	1.01	1.01	Effluent after 3 polishing wetlands
17-July'06	Cascade	6.81	4468	508	-119	13.3	23.5	9.33	Mine water from mine shaft
	Wetland1 inlet	7.18	4440	470	-130	14.4	22.8	13.1	Aerated (i.e. oxygenated) water from cascade that has passed through the lagoons
	End Point	7.90	4387	446	-50	16.1	1.07	1.07	Effluent after 3 polishing wetlands
23-Aug.'06	Cascade	6.94	4316	470	-13	12.8	26.9	15.5	Mine water from mine shaft
	Wetland1 inlet	7.06	4271	466	-35	14.8	20.3	13.1	Aerated (i.e. oxygenated) water from cascade that has passed through the lagoons
	End Point	7.98	4190	412	8	14.3	3.53	3.53	Effluent after 3 polishing wetlands
26-Sept.'06	Cascade	6.68	4242	466	50	12.5	36.2	24.5	Mine water from mine shaft
	Wetland1 inlet	7.20	4204	420	-28	12.5	24.6	15.5	Aerated (i.e. oxygenated) water from cascade that has passed through the lagoons
	End Point	7.70	2582	254	-2	11.8	3.19	3.19	Effluent after 3 polishing wetlands
27-Oct.'06	Cascade	6.85	4278	496	-30	12.5	29.9	23.5	Mine water from mine shaft
	Wetland1 inlet	7.11	4219	446	-11	11.7	24.4	17.4	Aerated (i.e. oxygenated) water from cascade that has passed through the lagoons
	End Point	7.74	3784	380	-8	10.1	2.53	2.53	Effluent after 3 polishing wetlands

Table 9.2: Mean water quality parameters determined at various sampling locations across the Whittle, Northumberland treatment system site from June-October. 2006 (where n=5).

			Alkalinity			[Dissolved Fe]	[Colloidal Fe]	Comments
Sample	**pH**	***K.*** **(µS cm^{-1})**	**mg L^{-1} as $CaCO_3$**	***Eh*****(mV)**	***T*****/°C**	**mg L^{-1}**	**mg L^{-1}**	
Cascade	6.83	4302.60	486.80	-41.40	12.84	30.1	19.1	Mine water from mine shaft
Wetland1 inlet	7.18	4216.60	436.00	-65.60	13.92	22.9	15.4	Aerated (i.e. oxygenated) water from cascade that has passed through the lagoons
End Point	7.87	3385.20	353.20	-19.20	13.46	2.27	2.27	Effluent after 3 polishing wetlands

The impressions given by tables 9.1 and 9.2 are that chemical characteristics of water vary between sampling location across the site. These observations are not surprising as the water quality parameters at each sampling station reflects the prevailing chemistry at such station which differs from location to location for a wide range of biogeochemical reasons. Water temperature generally ranged from 10 to 16 °C across the sampling points (figure 9.3). Scrutiny of figure 9.3 correctly implied that water temperature in the summer months (June-August) is slightly higher than in the winter months (September-October). As water flowed through the treatment system, the pH rose while concentrations of alkalinity and iron fell (figure 9.4 & table 9.1). The pH increased from 6.5 (influent sample) to 8 (effluent sample) and the effluent pH appeared stable. This shows that the water quality of the effluent sample has significantly improved. Increased pH is a common feature of passive systems with net alkaline water as in Whittle site and is attributed to exsolution of CO_2 [6, 7]. It has been found that discharges from mines have an average CO_2 partial pressure of $10^{-0.82}$ mm Hg which greatly exceeds the atmospheric CO_2 partial pressure ($\sim 10^{-3.5}$) mm Hg, causing CO_2 to exsolve [7]. Thus, generating OH^- as follows:

$$HCO_3^- \text{ ---------} \rightarrow CO_2(g) + OH^-$$

The exsolution decreases dissolved CO_2, and exchanges HCO_3^- for OH^-, which increases pH without affecting alkalinity. The decrease in alkalinity is due to neutralisation of acidity produced by iron oxidation and hydrolysis. The conductivity profile across the site revealed a more stable (4200 $\mu S\ cm^{-1}$) trend for samples taken from cascade and wetland 1 inlet whilst conductivity varied widely (2000-4000 $\mu S\ cm^{-1}$) for the effluent samples (figure 9.5). This trend probably shows that solute concentrations, particularly sulphate is stable in the influent samples but varied widely for the effluent samples. Although, sulphate and specific conductivity have traditionally been used as indicators for the degree of mine-water contamination in surface and ground water [8], this unusual trend particularly for the effluent sample is rather surprising and this could be attributed to the variability in the activities of the sulphate reducing bacteria (SRB) [9].

The *Eh* profile as shown in figure 9.6 indicates that the *Eh* for samples taken from the wetland inlet is consistently lower than the *Eh* values of samples taken from the inlet (cascade) and endpoint respectively. It was also observed that *Eh* of endpoint samples is higher than the inlet samples except for September.

This observation is quite surprising as one would expect the reverse trend to indicate the oxidising and reducing natures of the inlet and endpoint samples respectively [8]. The observed trends could be attributed to the cascading process in the inlet water samples at this site which is quite unique and different from the other studied sites. The Whittle treatment system was designed for the oxidative removal of iron and as mine-water from the underground mine-shafts cascades, this oxygenation may reduce the water *Eh*. Furthermore, as explained in the previous chapters, determination of redox potential (*Eh*) in nature is quite complicated as some of the reactions that determine redox potentials are slow [10] and it has been observed that redox potentials measured in oxygen-containing environments as in Whittle are generally lower than equilibrium values [9, 10].

Temporal trends in water alkalinity indicate that water alkalinity increases as it passes through the treatment system which shows that while influent water alkalinity varied widely from 254 to 446 mg L^{-1} of $CaCO_3$, both water alkalinity for the wetland inlet and endpoint samples appear stable over the sampling period (figure 9.7). This increased alkalinity of the endpoint water samples shows that the acidity of the influent samples has been neutralised as the water passes through the treatment system. In fact, water alkalinity appeared to follow the pH trends observed during the same period (figure 9.4). The sharp decrease in alkalinity observed in the inlet samples for the months of June and September (274 and 254 mg L^{-1} of $CaCO_3$ respectively) is quite surprising and this observation could be attributed to a number of factors including sulphate, rate of limestone dissolution and iron reduction leading to elevated pH. For example, [11, 12, 13] have shown that both aerobic and anaerobic bacteria can proliferate in and around areas of high dissolved iron concentrations and limestone dissolution can also be influenced by a number of factors including rainfall event and water residence time [6, 7, 8]. Detailed explanations of these factors have been provided in chapter 6 where similar trends were observed. However, in general, water alkalinity followed the expected trend of high alkalinity for endpoint which is consistent with the previous work carried out on this site [e.g., 1, 2].

9.2.2: Voltammetric results

In this section, voltammetric results are discussed. Voltammetric results presented here are based on the quantification of hydrolysed iron and unhydrolysed iron. Comparisons of the mean influent with outlet concentrations of hydrolysed and unhydrolysed iron are presented in figures 9.8 and 9.9 respectively. Figure 9.10 shows the comparison of mean hydrolysed and mean unhydrolysed iron over the sampling period June-October, 2006. Percentage proportion of total dissolved and colloidal iron are presented in figure 9.11. Typical temporal and seasonal variation in measured total dissolved iron concentrations as a function of winter and summer season are shown in figure 9.12 and the percentage ratio of Fe(II) and Fe(III), determined using ultramicroelectrodes is presented in figure 9.13.

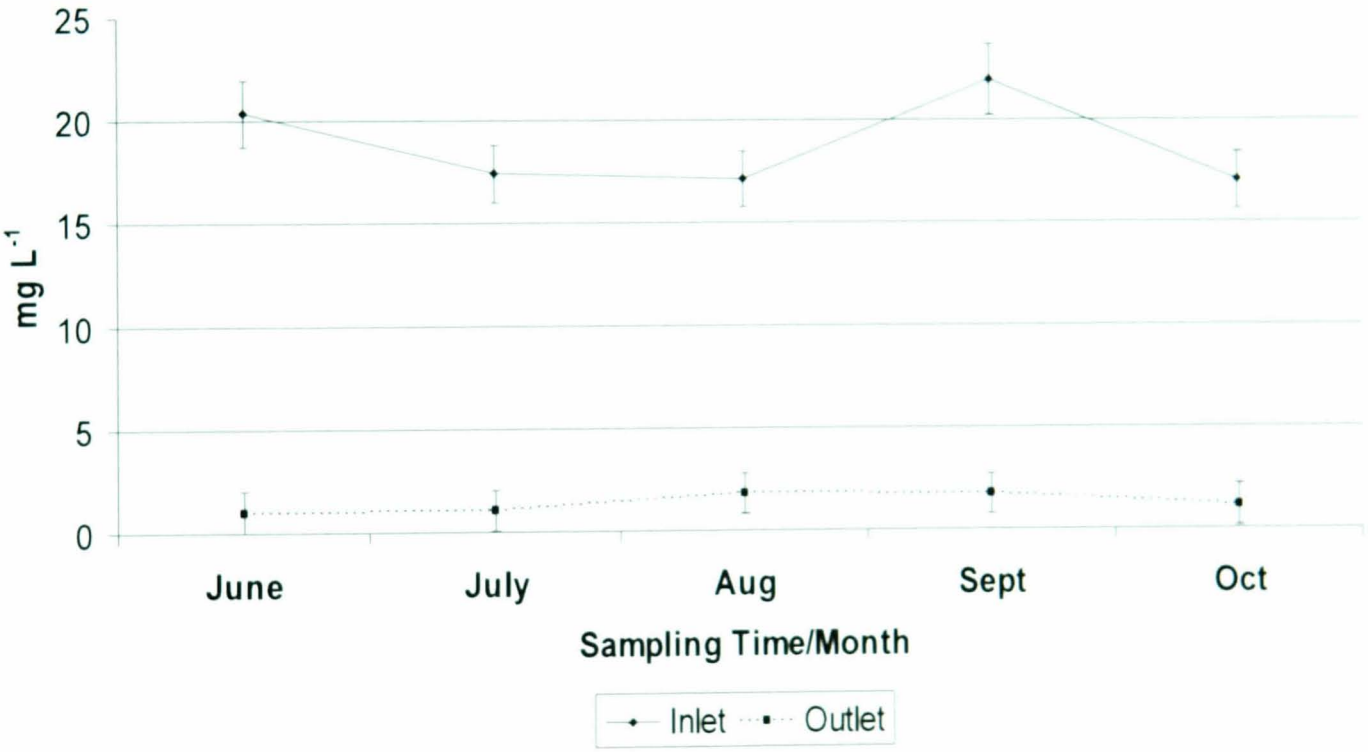

Figure 9.8: Mean total hydrolysed iron concentrations (mg L^{-1}) for samples collected June-October, 2006 at Whittle site. Error bars denote standard error of the mean.

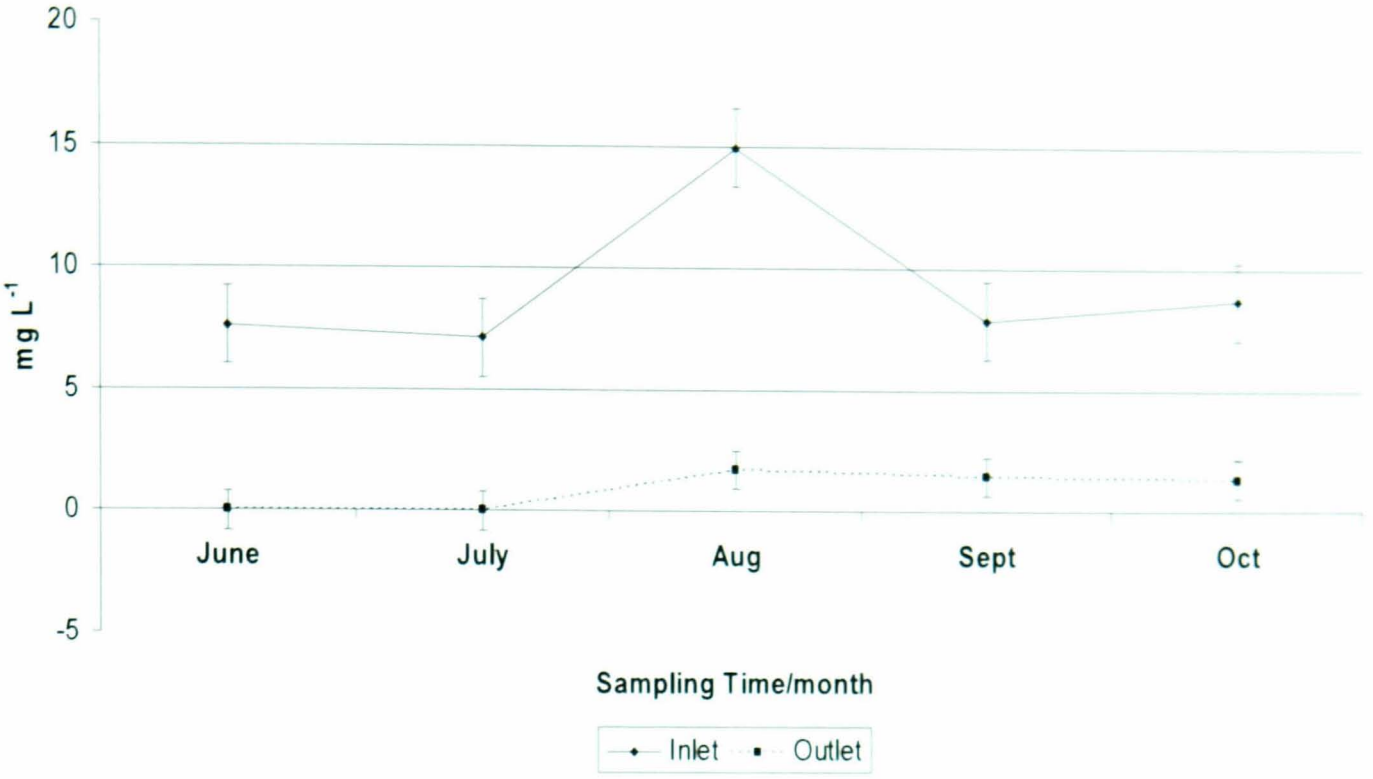

Figure 9.9: Mean total hydrolysed iron concentrations (mg L^{-1}) for samples collected June-October, 2006 at Whittle site. Error bars denote standard error of the mean.

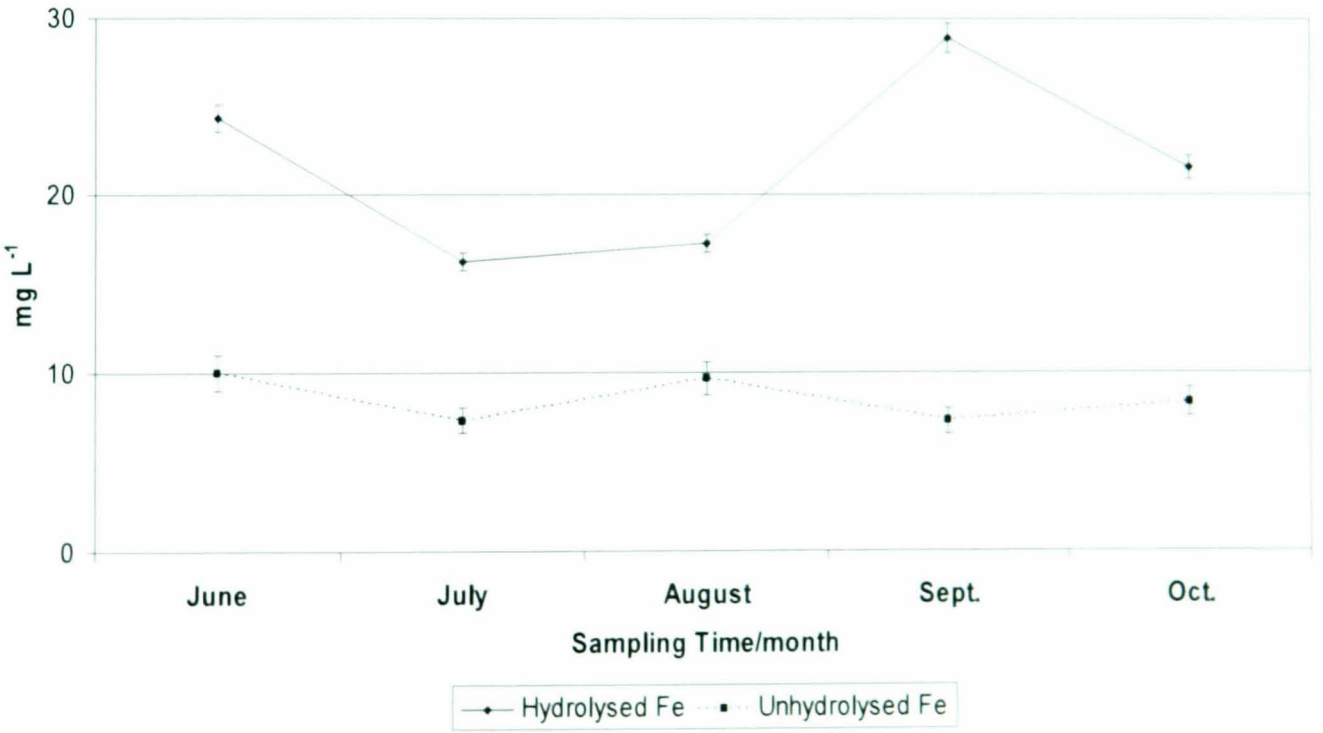

Figure 9.10: Mean total hydrolysed and unhydrolysed iron concentrations (mg L^{-1}) for samples collected June-October, 2006 at Whittle site. Error bars denote standard error of the mean.

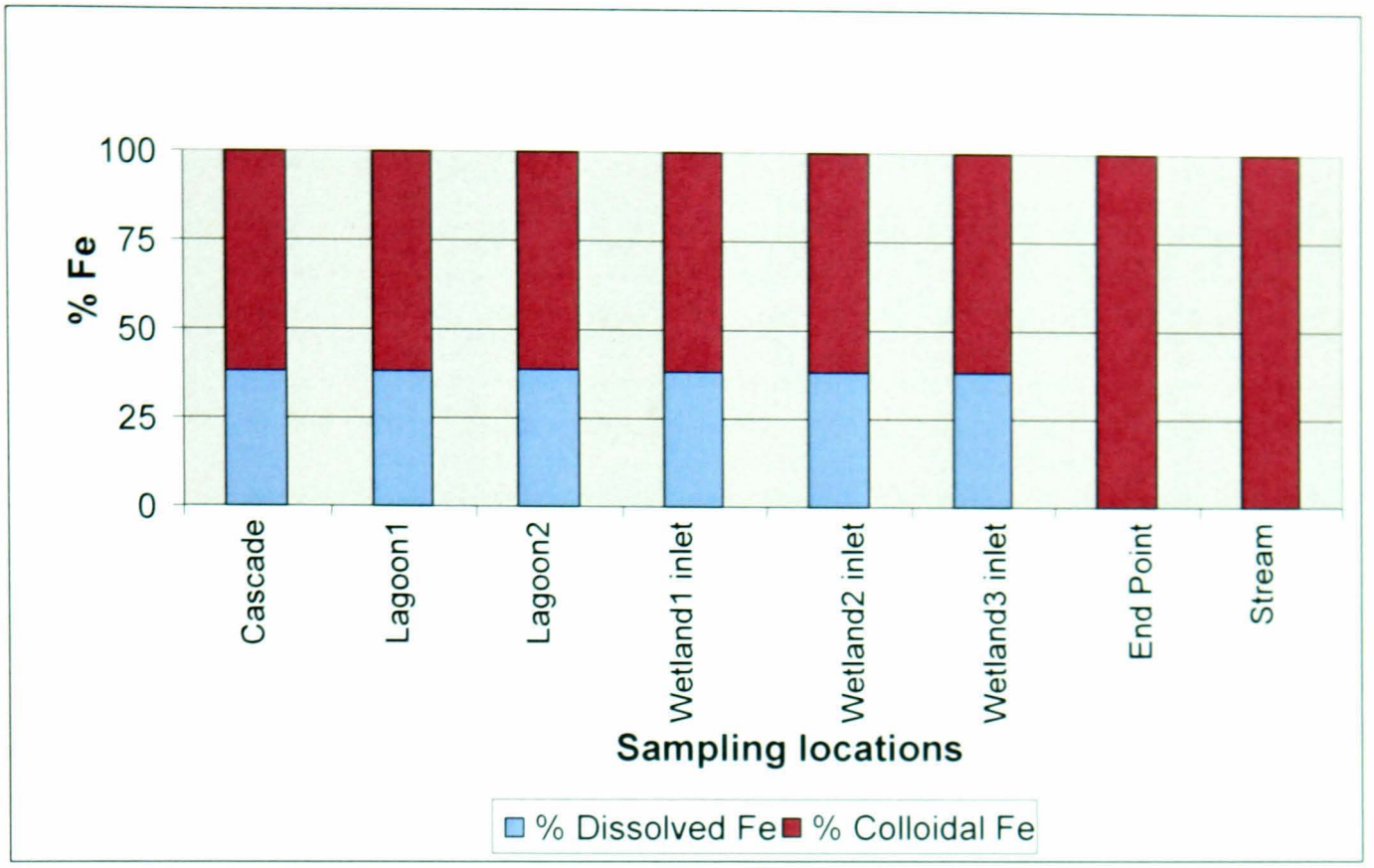

Figure 9.11: Showing percentage proportion of dissolved and colloidal iron at different sampling location across the Whittle site.

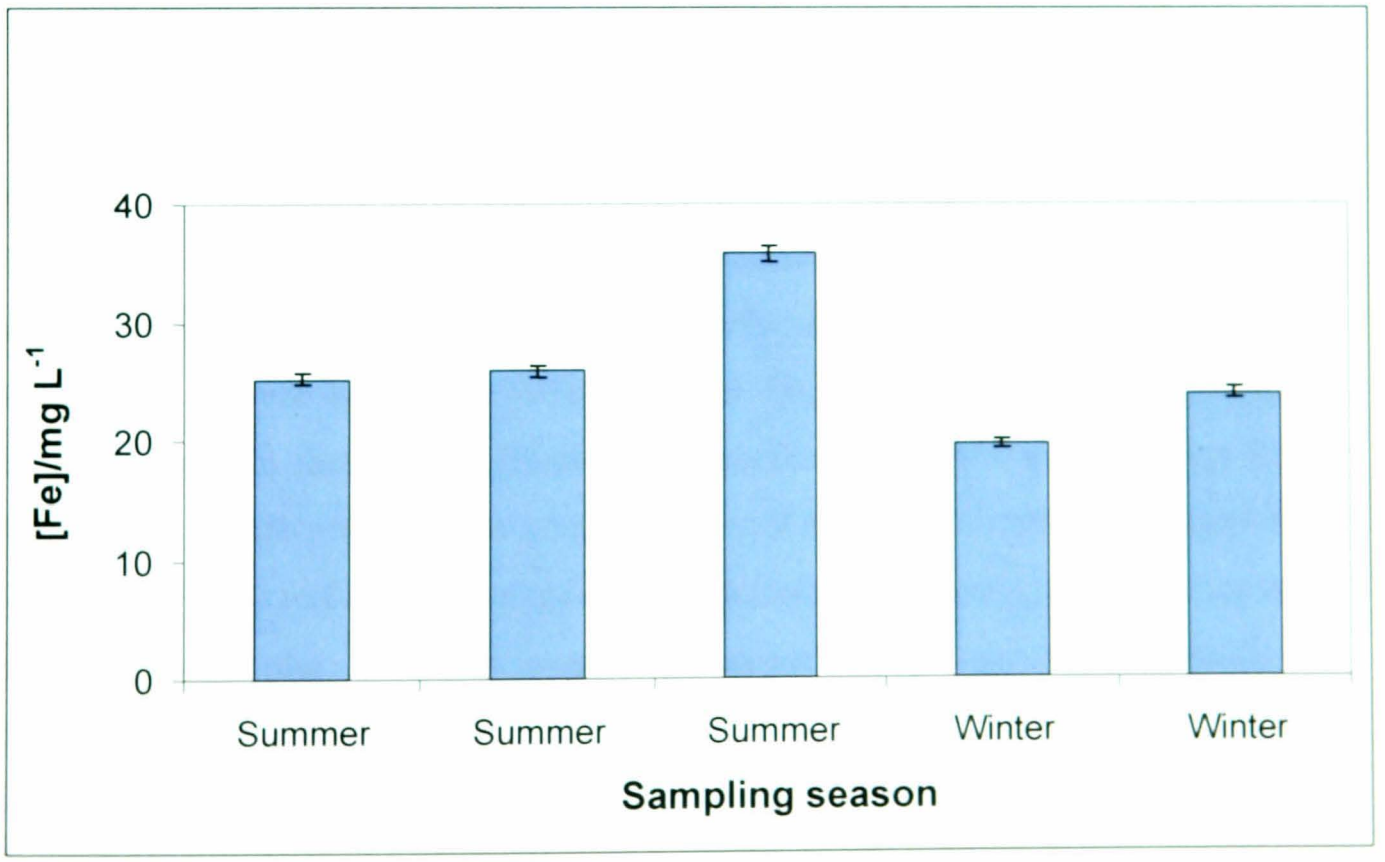

Figure 9.12: Showing typical seasonal concentrations of total dissolved iron for samples taken June-October, 2006 in lagoon 2 sampling point at Whittle site. Error bars denote standard error of the mean.

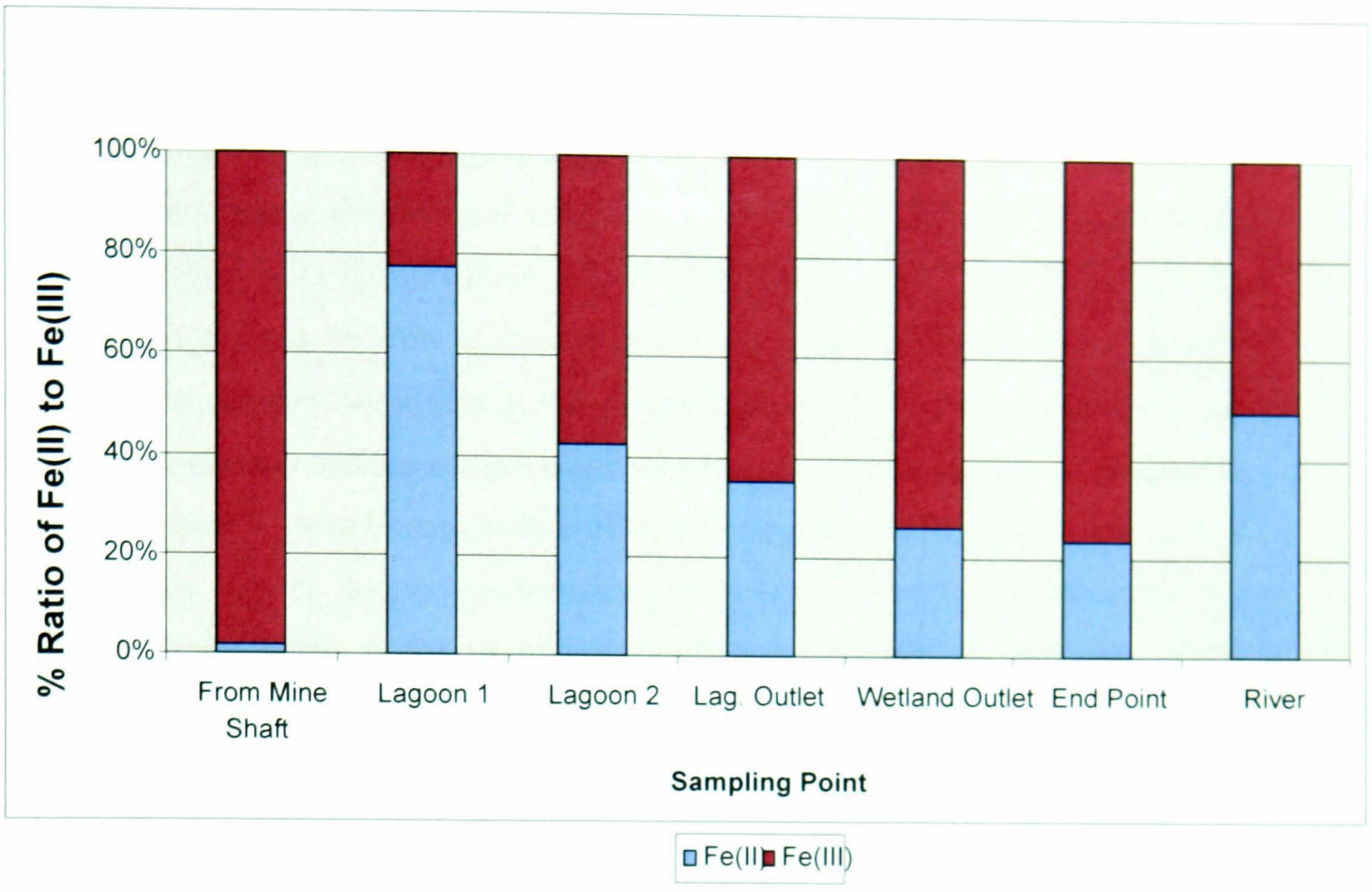

Figure 9.13: Showing percentage ratio of Fe(II) to Fe(III) at different sampling locations across the Whittle treatment system site as determined by ultramicroelectrodes.

Results of the mean monthly concentrations of hydrolysed iron clearly show that effluents concentrations are lower than the influent concentrations over the sampling period June-October, 2006 (figure 9.8). In addition, the effluent concentrations appeared stable over the same period whilst influent concentrations ranged from 18-22 mg L^{-1}. Unhydrolysed iron follows similar trend (figure 9.9) but with reduced concentrations. In fact, some effluent concentrations are below the detection limit. This significant decrease in iron concentrations of the effluent samples compared to the influent by up to 87% on average can be attributed to the precipitation of iron as it passes through the treatment systems. Comparison of the concentrations of hydrolysed and unhydrolysed iron shows that hydrolysed iron concentration is consistently higher than that of unhydrolysed iron (figure 9.10). It is apparent from figure 9.11 that the percentage proportions of dissolved and colloidal iron appeared stable at an average of 30% and 70% respectively across the site except in the effluent and the stream samples.

The 100% in colloidal iron proportion observed in the effluent and stream samples could be attributed to the fact that the dissolved iron concentrations are below the detection limit during this sampling period. The trend in this proportion reflects the iron chemistry across this site and the higher proportion of colloidal iron across the site is consistent with the treatment regime of physically trapping the iron through precipitation of iron as iron oxyhydroxides. Iron concentrations were seasonally highest in the summer and lowest in the winter (figure 9.12). This is mostly due to the seasonal variation in surface run-off water which is not at the same concentrations as the contaminants, which remained reasonably constant throughout the year. In addition, this may be due to the fact that generally, chemical reactions within the environment are slower in the winter compared to the summer and for every 10 °C decrease in water temperature, chemical reactions slow by 50% [9].

Percentage ratio of Fe(II) to Fe(III) varied widely across the site as shown in figure 9.13. The result suggests that water from the mine shaft is predominantly Fe(III) - 98%. Although, the percentage ratio shows an average of 50%: 50% for the aerated water in the settlement lagoons, however, the difference in the iron ratio between the two parallel lagoons is quite surprising. Since both received the same water, one would expect a similar iron ratio. This difference in behaviour can only be attributed to the rate of hydrolysis and precipitation of iron as iron oxyhydroxide. The rate of hydrolysis may be faster in one lagoon than the other, although, this is quite unusual.

9.2.3: Relationships between iron concentrations and the various measured parameters that controls iron geochemistry; *Eh*, pH and alkalinity

The purpose of this section is to establish whether there is any correlation or relationship between the measured geochemically significant water quality parameters (mainly pH, *Eh* and alkalinity) and electrochemically determined total iron concentrations that could help explain changes in equilibrium chemistry in the treatment system.

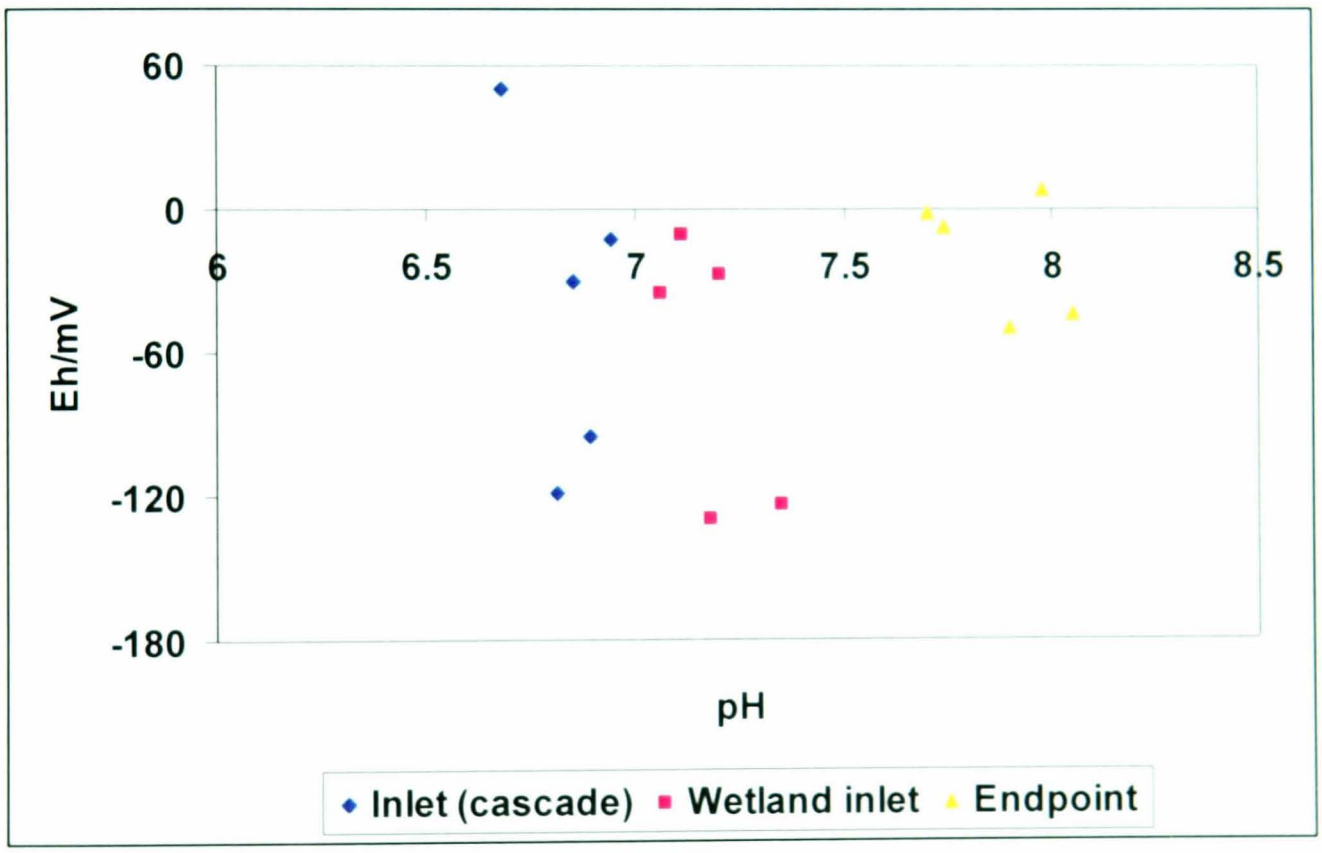

Figure 9.14: Measured *Eh* as a function of pH for inlet, wetland inlet and outlet samples taken from June-October 2006 at Whittle treatment system site. The least square regression (R^2= 0.20, 0.18 and 0.31 for inlet, wetland inlet and endpoint samples respectively).

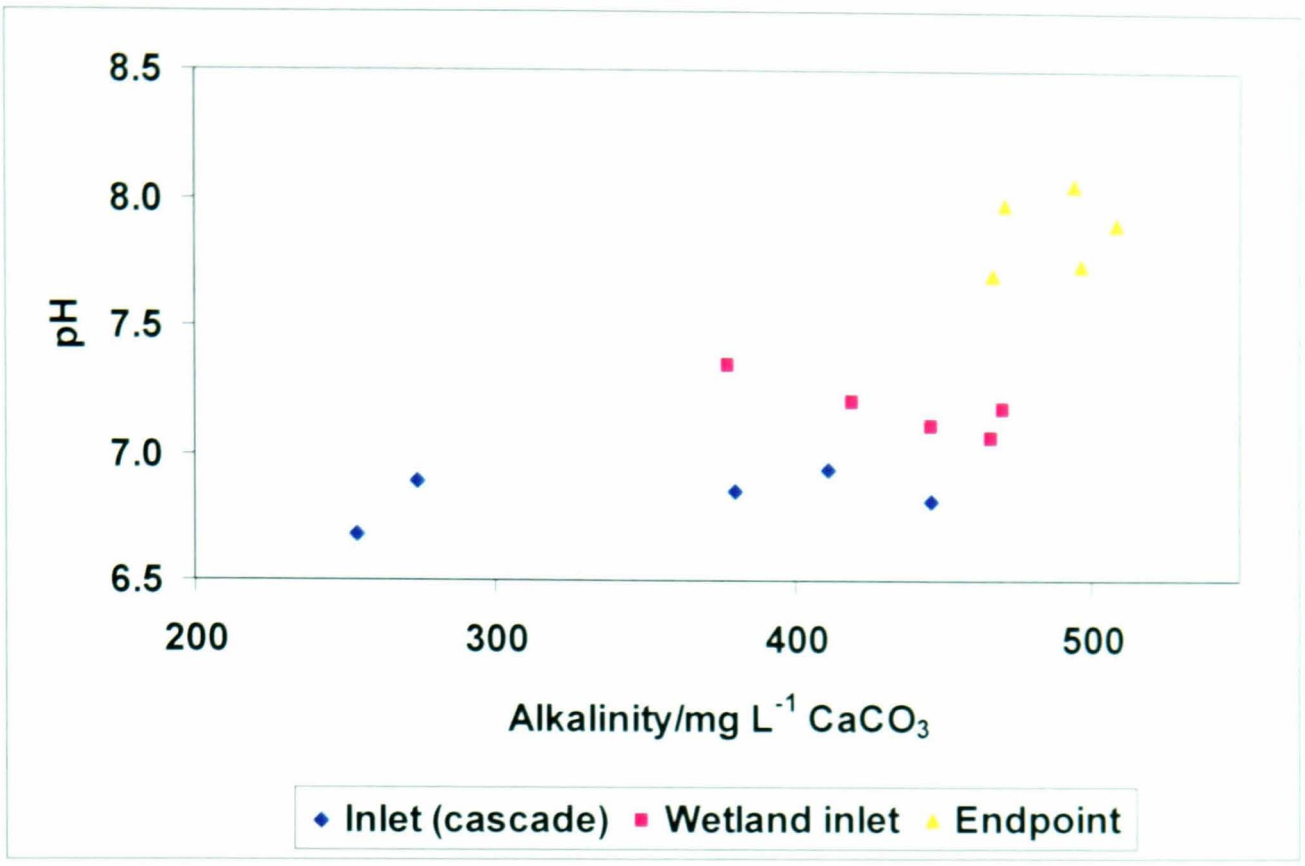

Figure 9.15: Measured pH as a function of alkalinity for inlet, wetland inlet and outlet samples taken from June-October 2006 at Whittle treatment system site.

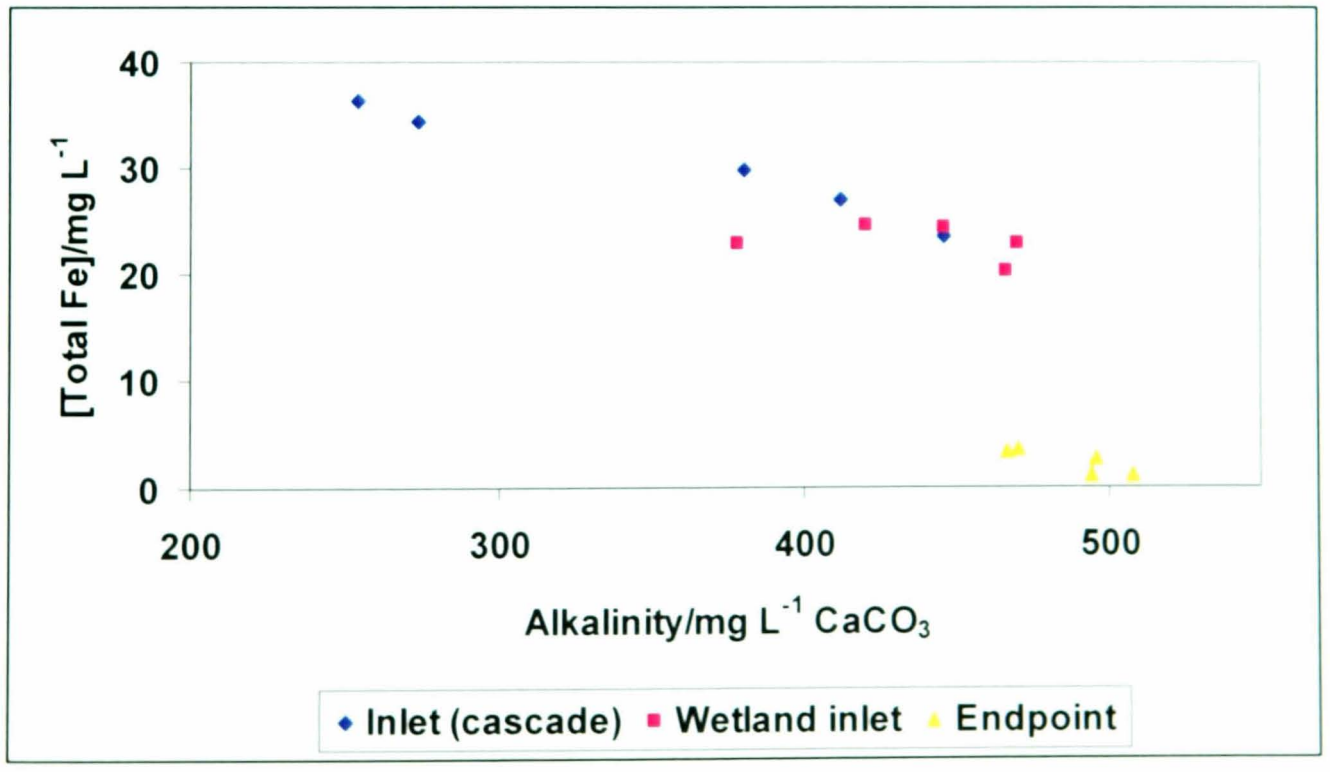

Figure 9.16: Measured total iron concentrations as a function of alkalinity for inlet, wetland inlet and outlet samples taken from June-October 2006 at Whittle treatment system site.

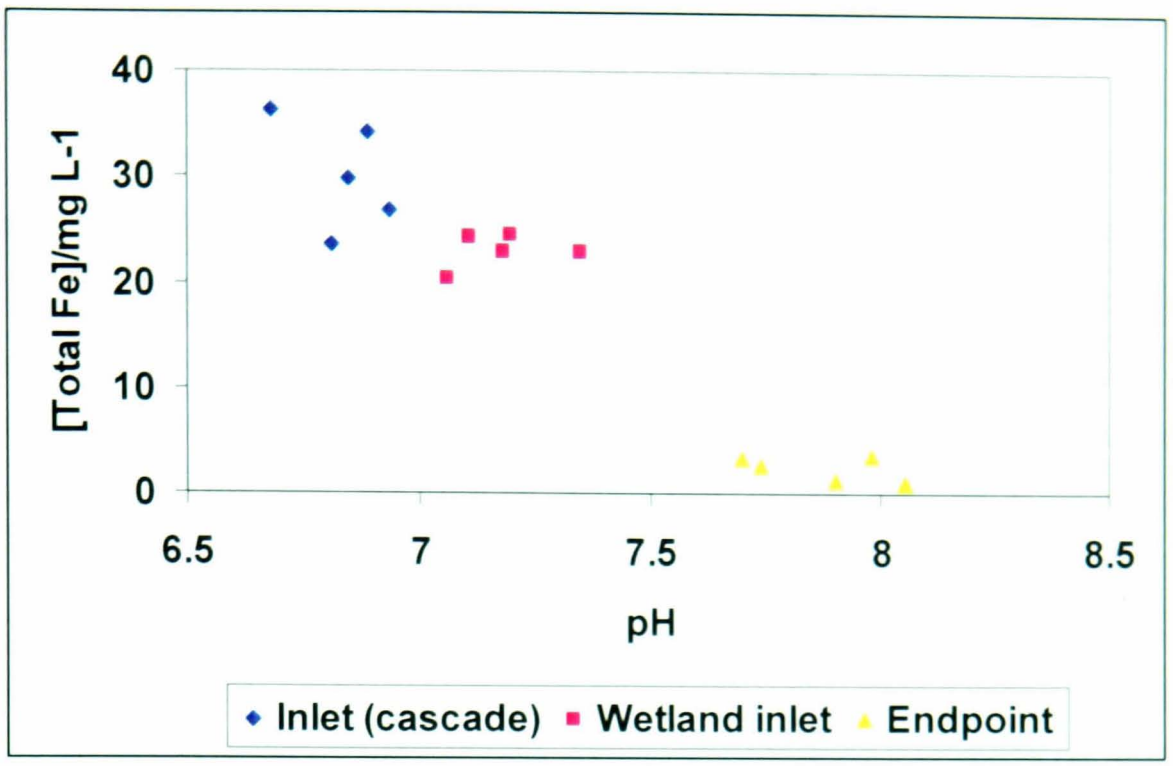

Figure 9.17: Measured total iron concentrations as a function of pH for inlet, wetland inlet and outlet samples taken from June-October 2006 at Whittle treatment system site.

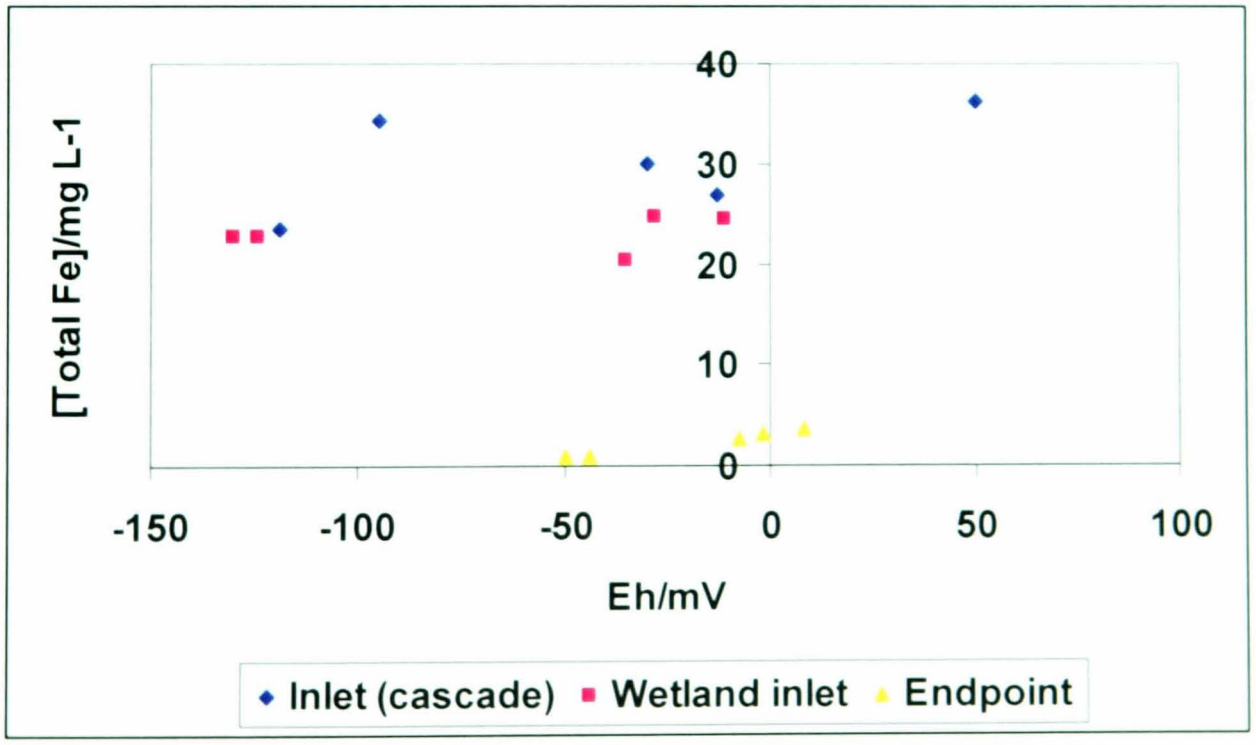

Figure 9.18: Measured total iron concentrations as a function of Eh for inlet, wetland inlet and outlet samples taken from June-October 2006 at Whittle treatment system site.

It is clear from figure 9.14 that there is no correlation between the measured water *Eh* and pH for the major sampling points indicated in the plot. This observed trend is quite surprising and this could be attributed to the complexity in the geochemistry of Eh measurements in the natural dynamic environment. For example, it has been reported that most oxidation reaction in nature (all reactions in oxygen-containing environments), *Eh* measurement is complex and generally give lower than equilibrium Eh values [9, 10, 11]. However, in general, *Eh* tends to increase with increasing pH (with few exceptions) which shows that influent samples are in oxidised environment whilst effluent samples are in reduced environment. This observation is consistent with the fact that high *Eh* and low pH in the influent samples are probably controlled by the degree of acidity (H^+) generated during the oxidation and dissolution of pyrite. *Eh*-pH of effluent samples is poorly correlated probably due to reduced acidity of the effluent samples. Thus, we would expect to find a change from Fe^{2+} to Fe^{3+} or vice-versa depending on the shift in the pH or Eh of the environment.

The pH-alkalinity trend presents a rather mixed observations, whilst there are no linear correlation between measured pH and alkalinity for inlet and endpoint samples (R^2=0.21 & 0.05) respectively, wetland samples shows very strong correlation (R^2=0.75)-figure 9.15. The lack of correlation in the inlet and endpoint samples is quite surprising as one would expect the outlet samples with elevated pH to show more correlation and this unexpected trend could only be attributed to the rather complex geochemistry occurring in natural environment as explained in the previous chapter. But generally, measured water alkalinity increases with increasing pH with few exceptions.

The graph of measured total iron concentrations as a function of alkalinity indicates that there is a strong relationship between the measured iron concentrations and water alkalinity (figure 9.16). The correlation is very strong for the inlet and endpoint samples (R^2 = 0.98 and 0.73) respectively whilst the intermediate water samples (wetland inlet) show no correlation (R^2=0.11). Lack of correlation observed in the wetland inlet water samples could be attributed to a number of factors including (but not limited to) the rate of dissolution of limestone/calcite that controls alkalinity and the rate of iron precipitation [6, 7, 9]. Reduced correlation observed in the endpoint

samples compared to the inlet samples is probably due to the fact that at elevated pH, the rate of iron precipitation becomes variables and depends on a number of geochemical parameters. This observation is consistent with study by Hedin [15]. attributing water alkalinity to the rate of iron oxidation and hydrolysis.

It is evident from figure 9.17 that in general, measured total iron concentrations decreases with increasing water pH and vice-versa. This observation is not surprising due to the fact that iron precipitation takes place at elevated pH. Thus, the reduced iron concentration observed as water pH increases is due to the precipitation and loss of iron. Furthermore, oxidation of iron takes place much more completely in alkaline medium than in acid medium. Thus, larger amounts of dissolved iron are commonly present in slightly acidic waters than in the faintly alkaline waters [14, 16].

Measured total iron concentrations as a function of redox potential (*Eh*) show a rather surprisingly complex trends as shown in figure 9.18. The plot shows that while there is no correlation for the inlet and wetland inlet samples (R2=0.29 and 0.04) respectively, endpoint samples show very strong correlation (R^2=0.98). This observed mixed correlation could be attributed to a number of reasons including difficulties in the measurement of *Eh* in a natural environment as described in chapter 6. Nevertheless, the general observation (with few exceptions) from total iron concentrations as a function of *Eh* is that elevated pH and reduced *Eh* environment lead to reduction in total iron concentrations.

9.3: Conclusions

The results presented here have implications in two important areas of biogeochemistry. Firstly in the understanding of the mechanism of iron speciation chemistry in mine waters. The second area is the potential application of the analytical techniques presented here, in in-situ monitoring of iron speciation and other redox active species that are of interest in integrating Fe cycles with the passive water treatment system.

This study demonstrates the use of voltammetric technique for quantifying dissolved, colloidal and the ratio of Fe(II) to Fe(III) which are very important in understanding and evaluating the spatial relationships among the key redox parameters and the development of framework for future assessment.

The findings in this study have several important implications (for example, understanding of iron speciation geochemistry) is important in the overall passive remediation technology of the polluted mine-water. In particular, for continual monitoring of iron chemistry within polluted mine waters. The technique is highly sensitive, stable, low cost and robust with low detection limit.

Though not shown in the results presented here, there is seasonal variation in iron concentrations which correlates well with the rainfall events which could be attributed to the dilution from the surface run-off.

Finally, assessing and monitoring the environmental impact of iron chemistry within the polluted mine water requires reliable analytical tools that can readily screen them with minimal sample handling; the analytical technique presented here demonstrates potential for solving real-life analytical problems.

9.4: References

[1]. Amos, P.W. & Younger, PL. *Water Research*, 37, **2003**, 11, 127-135.

[2]. Jarvis, A.P., Moustafa, M. & Younger, P.L. *Environmental Pollution*, **2006.** 143, 261-268.

[3]. Younger, P.L. *International Mine Water Association, Johannesburg*, **1998.**

[4]. Bowden, L., Jarvis, A.P., Orme, P.H.A. & Younger, P.L. *Unpublished Report, Newcastle University*, **2004.**

[5]. CL: AIRE Case Study Bulletin CSB4 (March **2006**). Coal Mine Sites for Targeted Remediation Research: The CoSTaR initiative.

[6]. Cravotta, C.A. *Mine Water Environment*, **2007**, 26, 128-149.

[7]. Younger, P.L., Banwart, S.A. & Hedin, R.S. **2002**, Kluwer, Dordrecht, p442.

[8]. Gray, N.F. *Environmental Geology*, **1996**, 27, 385-361.

[9]. Hedin, R.S. *Mine Water Environment*, **2008**, 230, 41-49.

[10]. Krauskopf, K.B. Introduction to Geochemistry, *McGraw-Hill*, **1979**, 617pp.

[11]. Anderson, R.F. and Schiff, S.L. *Canadian Journal of Fisheries and Aquatic Sciences*, **1987**, 44, 188-193.

[12]. Bannister, A.F. *Chartered Institute of Water and Environmental Management*, **1997**, London, 105-122.

[13]. Benner, S.G., Blowes, D.W. and Ptaceck, C.J. *Ground Water Monitoring and Restoration*, **1997**, 99-107.

[14]. Hamilton, Q.U.I., Lamb, H.M., Hallett, C. and Proctor, J.A. *Chartered Institute of Water and Environmental Management*, **1997**, London, 33-56.

[15]. Hedin, R.S., Nairn, R.W. and Kleinmann, R.L.P. Passive Treatment of Coal Mine Drainage, *U.S. Bureau of Mines I.C. 9389*, **1994**, 35pp.

[16]. Hard, B., Friendnich, S. and Babel, W. *Microbial Research*, **1997**. 152, 65-73.

[17]. Higgins, J., Hurd, S. and Weil, C. *Ecology Engineering*, **1999**. 4, 14-22

[18]. Higgins, J. *Environmental Science Health*, **2000**, A35. 1309-1334.

[19]. Mattes, A. Anaerobic/aerobic treatment system for removal of heavy metals constructed in Trial BC for Cominco Limited. Nature Works Remediation Corporation progress report for Environment Canada, **2002.**

[20]. Mattes, A., Gould, W. and Duncan, B. Multistage treatment system for removal of heavy metal contaminants. ESSA conference, Banff, Alberta, October, **2002**.

Chapter 10

IRON OXIDE NANOPARTICLES IN MINE WATERS: CHARACTERISATION STUDIES

Particle shape, size and composition are important properties that affect the chemical and physical properties of nanoparticles. To provide characterisation of these properties, a wide range of spectroscopic and microscopic measurements have been made on samples collected from the studied sites. This chapter presents results from the various methods used for the identification and characterisation of the solid phase iron oxide nanoparticles observed across the studied sites. A range of spectroscopic and microscopic techniques have been used for the characterisation of these solid phase iron oxides nanoparticles. Combined techniques have been used since they each provide different information about the particles which ultimately helped in the detailed characterisation of the iron oxides in the sample studied. The techniques used include atomic force microscopy (AFM), Fourier transform infrared spectroscopy (FT-IR), X-ray diffraction (XRD), scanning electron microscopy (SEM), Transmission electron microscopy (TEM) and energy dispersal X-ray (EDX).

10.1: Introduction

Iron is the second most abundant metal after aluminium and the fourth most abundant element in the earth's crust [1]. Iron occurs in a diversity of minerals including sulfides, oxides, hydroxides and complex hydroxide anions [1]. The major oxides of iron are haematite (Fe_2O_3), magnetite (Fe_3O_4), limonite (FeO(OH)). and siderite ($FeCO_3$) [2, 3]. In the past, colloidal ferric oxides and hydroxides have been the subject of a great deal of interest and several distinct phases have been characterised [2, 3, 4, 5]. Over the past decade, iron oxides have been recognised as being solid phases which exert a significant effect on the behaviour of a large number environmentally important species particularly the heavy metals and other toxic elements [20]. Iron oxides indirectly affect the environment by influencing the fate, mobility and decomposition of environmental pollutants [20]. It is now widely accepted that colloidal materials (size range from 1 nm-1 μm). including iron oxyhydroxides, plays a significant role in the transport and cycling of trace metals in

natural waters [1, 2, 3, 4, 5, 6]. For example, the adsorption of ions on iron oxides regulates the mobility of species in various parts of the ecosystem (biota, soils, rivers, lakes, oceans) and their transport between these parts [5]. Improved knowledge and understanding of the mineralogy of the precipitate from acid mine drainage (AMD) has recently open up the possibility of relating the occurrence of certain key minerals to generic factors such as pH and sulphate concentration in mine-water [11]. Mineral sequences may develop as a function of local changes conditions such as pH, sulphate and can serve to identify such variations in the field. For example, temporal changes and seasonal fluctuations of precipitation (leading to variations of water infiltration through and run off over mines and mine dumps), can also have noticeable effects on precipitate mineralogy [11]. In addition, organic compounds and iron are the most abundant colloidal components in natural waters and are considered as the major carrier phases for other chemical elements present [7]. Although, characterisation of iron oxides in fresh waters have been widely reported [1, 2, 3, 4], most of these were concerned with water and precipitate chemistry whereas, knowledge of the mineralogy of the ochreous precipitates formed in the mine-water and AMD is superficially understood. It is increasingly acknowledged that understanding of the morphology, composition and structure of iron colloids in mine-waters is essential in understanding their role in the environment [20]. A major cause for this lack of detailed information may have resulted from the complexity of the iron colloid structures; the poor crystallinity of many of these minerals in question which complicates their identification [11]. Although, schwertmannite is a component of acid mine drainage (AMD) precipitates, the first description of this iron oxyhydroxysulfate as a new mineral was published just a decade ago [12]. Recently, Alpers and Blowes [13] and Jambor and co-workers [15] published in-depth overviews of acid mine drainage, including information on the mineralogy of the associated precipitates.

This characterisation of ochreous and other Fe^{3+}-bearing precipitates will have a wide range of implications for the mine-water remediation. The physico-chemical properties of the colloids and information such as the morphology, structure, particle size and composition of the solid phase iron nanoparticles can provide more information about iron oxides nanoparticles in mine-water. For example, Fe(III) is easily hydrolysed at pH 6-8 and would be precipitated as the highly insoluble hydrous

$Fe(OH)_3$ which plays a significant role in the environmentally damaging phenomenon known as acid mine drainage (AMD). Thus, the nature of the solid phase resulting from hydrolytic precipitation from Fe(III) is of fundamental importance for understanding the environmental behaviour of this iron oxide and has been well studied and reviewed [4, 5, 7,8,9].

10.2: Sample descriptions

A total of 20 samples of powdered dry specimens of mine-water have been studied by spectroscopic and microscopic techniques for the characterisation of iron nanoparticles. These samples were collected from the five CoSTaR sites at Quaking Houses, Bowden Close, Acomb, Shilbottle and Whittle. The sampling locations were selected at different sites but on the basis that precipitates will be obtained from water filtration. Mine-water samples were collected and filtered using 0.45 μm size cellulose nitrate filter paper. Precipitates from these samples were then collected and then allowed to dry in open air. The dry powders were then crushed with mortar and pestle. FT-IR, XRD, SEM and TEM analyses were then carried out on these samples. Samples for AFM are prepared as fully described in chapter 3, section 3.8.2. In another experiment, few drops of mine water samples were placed on TEM copper grid and allowed to dry in open air, followed by SEM and TEM analyses. The latter experiment was carried out to compare results obtained from sample from powder and natural mine water and to see whether there is any change in the morphology of the powdered samples.

10.3: AFM results

AFM was used to study the morphology of iron oxides nanoparticles. In this section, representative and typical AFM images obtained for the four types of samples studied are presented. Four classes of samples were observed under AFM:

(a). samples that were acidified with 1% HCl.

(b). unacidified mine-water samples (natural mine-waters).

(c). acidified samples that were filtered using 0.45 μm filter paper.

(d). unacidified samples that were filtered using 0.45 μm filter paper.

Figure 10.1 below shows typical AFM images obtained for different class of mine-water samples under different treatment. All samples were analysed by dropping two drops of mine-water on mica and allowed to dry over night while preventing deposition of atmospheric particles and contaminants, followed by AFM analysis in the tapping mode.

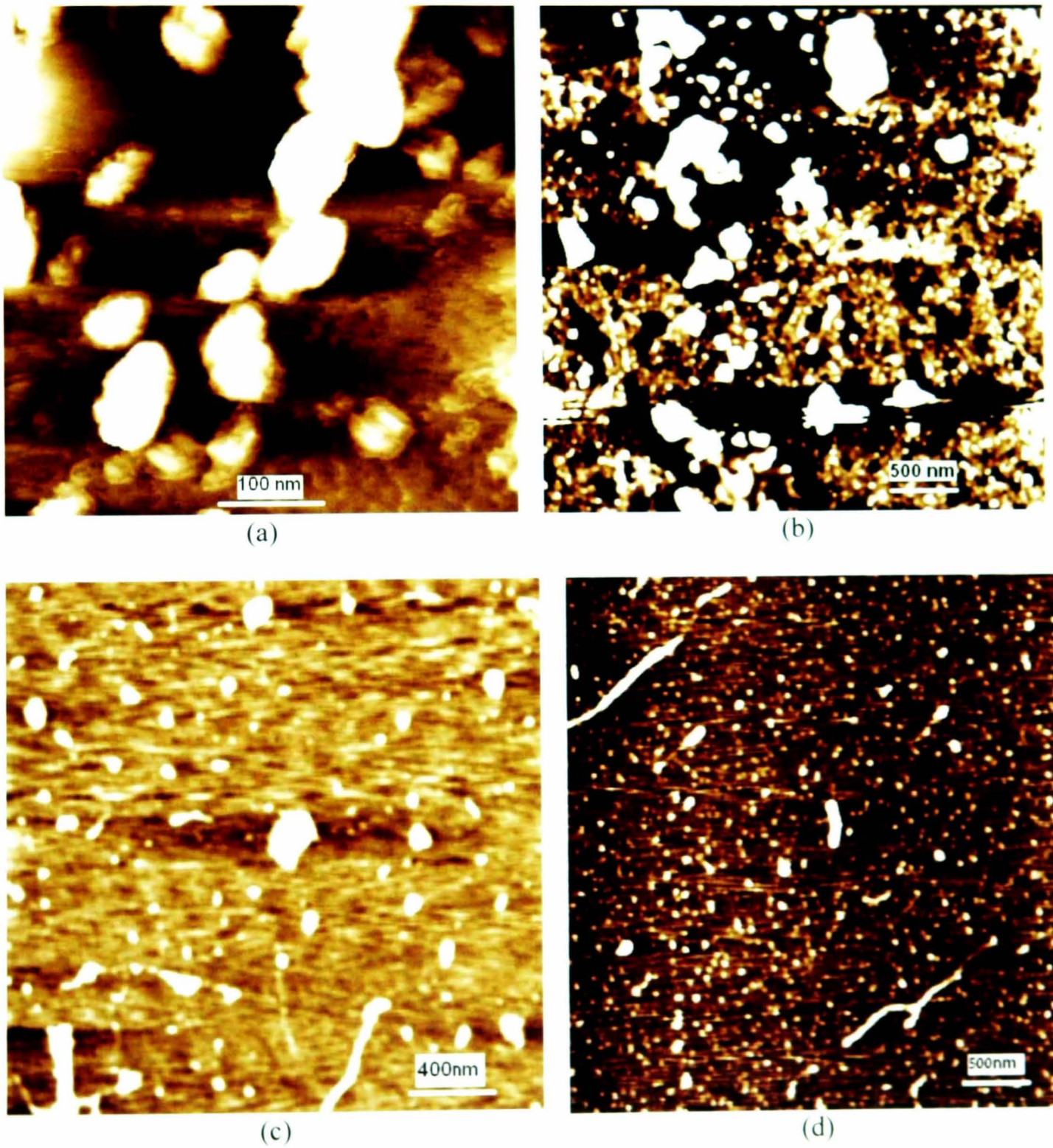

(a) (b)

(c) (d)

Figure 10.1: AFM images with background as mica of (a) unfiltered mine-water sample (natural mine-water), (b) filtered mine-water sample (c) acidified and

unfiltered mine-water sample and (d) acidified and filtered mine water sampled August 2007 from Shilbottle.

Representative AFM images of mine-water taken from Shilbottle site sampled August 2007 are presented in figure 10.1. Typical AFM (figure 10.1) images revealed that iron particles vary with the nature and treatment of mine-water. For examples, the AFM of natural (unfiltered and unacidified) mine-water shows particles rearrangement and aggregation (figure 10.1a), with individual particle size up to few hundreds nanometre while for the filtered samples (fig.10.1b), the particles show less tendency to aggregate. Furthermore, the AFM of acidified samples (fig.10.1c) with 1% HCl shows evenly distributed iron nanoparticles with small particle size while particle sizes are even smaller and more evenly and orderly arranged for the acidified and filtered samples as shown in figure 10.1d. In some samples (not included here), large colloid nanoparticles up to few micrometer in size was observed. This observation is not surprising and is in agreement with the fact that iron solid phases/colloids are quite complex and could be a complex mixtures of different physical, chemical and biological phases [20] which could be influenced by thermodynamic or environmental processes [21, 22]. In addition, AFM is more suited to measure smaller, fine nanoparticles than the large colloids nanoparticles which often exceed the maximum height measurable.

Although, not the aim of this study, previous characterization of freshwater natural aquatic colloids by AFM has shown that colloid nanoparticle structure and morphology is a function of pH [20] which was attributed to conformational changes due to aggregation and loss of small colloid particles prior to sorption on the mica and also on the greater repulsive charge interaction between the mica and the colloids with increasing pH [20]. AFM measures heights and has a typical resolution of below 1 nm, but does not determine chemical composition. The AFM images therefore do not demonstrate the presence of Fe in the nanoparticles, for this purpose, SEM and TEM techniques were used for further details and the results are presented in sections 10.6 and 10.7 respectively. In addition, at low pH, oxides will be protonated and positively charged, these will tend to avoid each other and not aggregate due to repulsion between charges, at higher pH, they may be neutral and will aggregate readily. Aggregation also depends on the ionic strength-that is salt content. Excess ions (of

any type) will "screen" the repulsive interactions between particles and favour aggregation.

10.4: FT-IR results

This chapter deals with the results obtained from the FT-IR analyses of the iron oxide nanoparticles from the studied sites. Typical IR spectra obtained from the analyses are presented in this section. Structural analysis of iron oxyhydroxides colloids by FTIR provides information on phase composition and bonding. FTIR analyses were done by placing a small quantity of ground powder on the crystal surface of the FTIR accessory (sample plate) and clamped in place and analysed in the wavelength range 4000-750 cm^{-1}, typically under the following conditions: resolution 2 cm^{-1}, background scan 16 times and scan time 2 min. Detailed experimental procedures is presented in chapter 3.

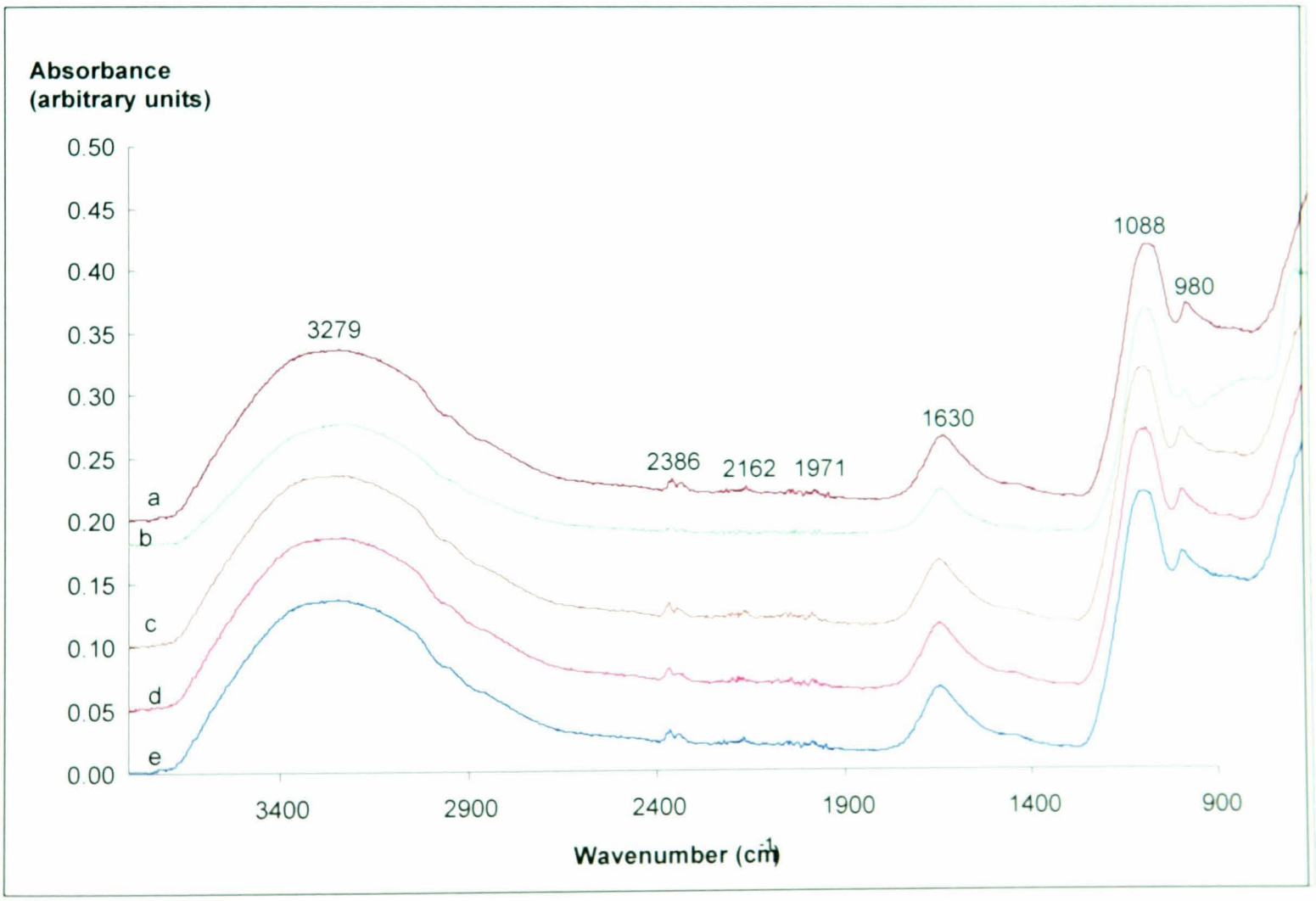

Figure 10.2: FTIR spectra of samples taken (August 2006) from different sites studied (a) sample from Shilbottle site (b) sample from Whittle site (c) sample from Bowden Close site (d) sample from Acomb site and (e) sample from Quaking Houses site. Spetra are vertically offset by 20,000.

Typical FTIR spectra of samples from various sites are presented in figure 10.2 above. It is apparent that the FTIR obtained from different site bear striking similarity with four distinct peaks of varying intensities in each spectrum. As can be seen, these four peaks appeared at 3279 cm^{-1}, 1630 cm^{-1}, 1088 cm^{-1} and 980 cm^{-1} respectively. Also three peaks of low intensity at 2386 cm^{-1}, 2162 cm^{-1} and 1971 cm^{-1} respectively were also observed. The intense, prominent and broad peaks at 3279 cm^{-1} is characteristic of bulk hydroxide (-OH) stretch. Peaks at 1630 cm^{-1} is due to the presence of organic materials (e.g., carbonyl) whilst the observed peaks at 1088 cm^{-1} is due to the Fe-O/Fe-OH vibrational modes. The peaks at 980 cm^{-1} is due to OH bending of (δ-OH)/(γ-OH). Less intense peaks between 2386 cm^{-1} and 1971 cm^{-1} are due to carbon dioxide (2386 cm^{-1}) and water (1971, 2162 cm^{-1}) in air respectively. The intense and broad band at 3279 cm^{-1} corresponds to hydroxyl stretching vibrations (bulk OH stretch) [23]. This band is a characteristic of FTIR of goethite, ferrihydrite or akaganeite iron oxide minerals [20, 23]. Although it has been observed that there is little distinction between the free surface and the bulk OH groups, however, free surface OH groups tend to have IR band in the region of 3600-3650 cm^{-1} [24] which was not observed in all the spectra analysed in this studies. For example, isolated OH stretching vibrations may be at 3600 cm^{-1} which is different from the bulk O-H, which is due to any OH involved in H-bonding. In an H-bond, some electron density from the oxygen atom is pulled away from the O-H sigma bond to the positive charge on the H-atom of the H-bond. This weakens the O-H bond and reduces the vibration frequency. In addition, it has been observed that hydroxyl stretching vibration band may also be decomposed to O-H stretches due to structural hydroxyls at ~3047 cm^{-1} with a shoulder at 2760 cm^{-1} as seen in goethite [23]. The broadness of the OH band could be attributed to a range of hydrogen bonding energies and this has been previously observed in the goethite bulk and isolated surface hydroxyls [25, 26, 27 and 28]. Moreover, the broad band may also be due to the presence of hydrogen -bonded surface hydroxyls which can also present at the surface [26, 29]. As with all FeOOH polymorphs, the absorption band at 1088 cm^{-1} arises from Fe-OH and Fe-O vibrations. Although, 36 possible Fe-O vibrations and 12 hydroxyl vibrations have been observed in goethite, only 12 Fe-O and five hydroxyl vibrations are infrared active [20]. The OH bending band at 980 cm^{-1} (δ-OH)/(γ-OH) is an important diagnostic band and also provides information about crystallinity [20].

It has been observed that the frequency of this vibration is dependent on both the position of the OH and on the resonance phenomena [37]. For example, it has been observed in goethite that decreasing crystallinity could cause the bands to broaden by decreasing the frequency of the OH bending and that of the OH stretch to increase [20]. Due to the incomplete information from the FTIR about the phase and nature of the iron particles, further characterisation methods were employed as reported below.

10.5: XRD results

Typical X-ray diffraction patterns of the iron oxide nanoparticles in the samples analyses are shown in figures 10.3-10.5. XRD provides three important diagnostic parameters, namely line (angle) position, width and intensity from which the nature of the oxides, its quantity (in a mixture), its unit cell parameters and, via the peak breadth, its crystallinity (crystal size and order) can be deduced. Because of the similarities and differences in the spectra, results have been grouped into three representing samples collected from Shilbottle site (figure 10.3), samples collected from Whittle site (figure 10.4) and samples collected from Quaking House, Acomb and Bowden Close sites (figure 10.5) respectively. The mean crystalline dimension was estimated using the Scherrer equation after correction for instrument broadening.

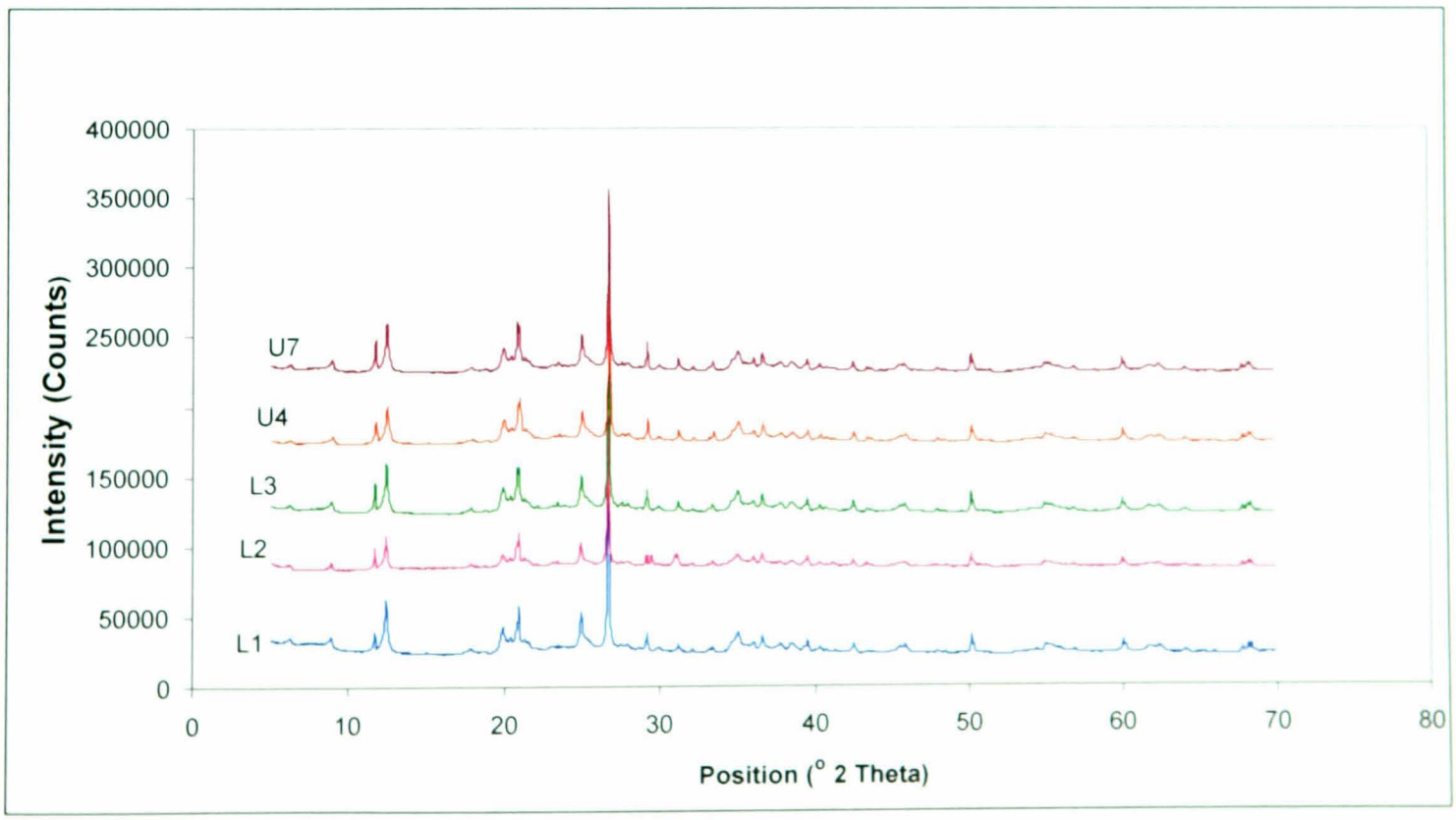

Figure 10.3: XRD spectra of sample taken (August 2006) at various sampling points across Shilbottle site-(U7) underground sample from the spoil heap, (U4) underground sample from the spoil heap, (L1)

sample from lagoon 1 (L2) sample from lagoon 2 and (L3) is sample from lagoon 3 respectively. Spetra are vertically offset by 20,000.

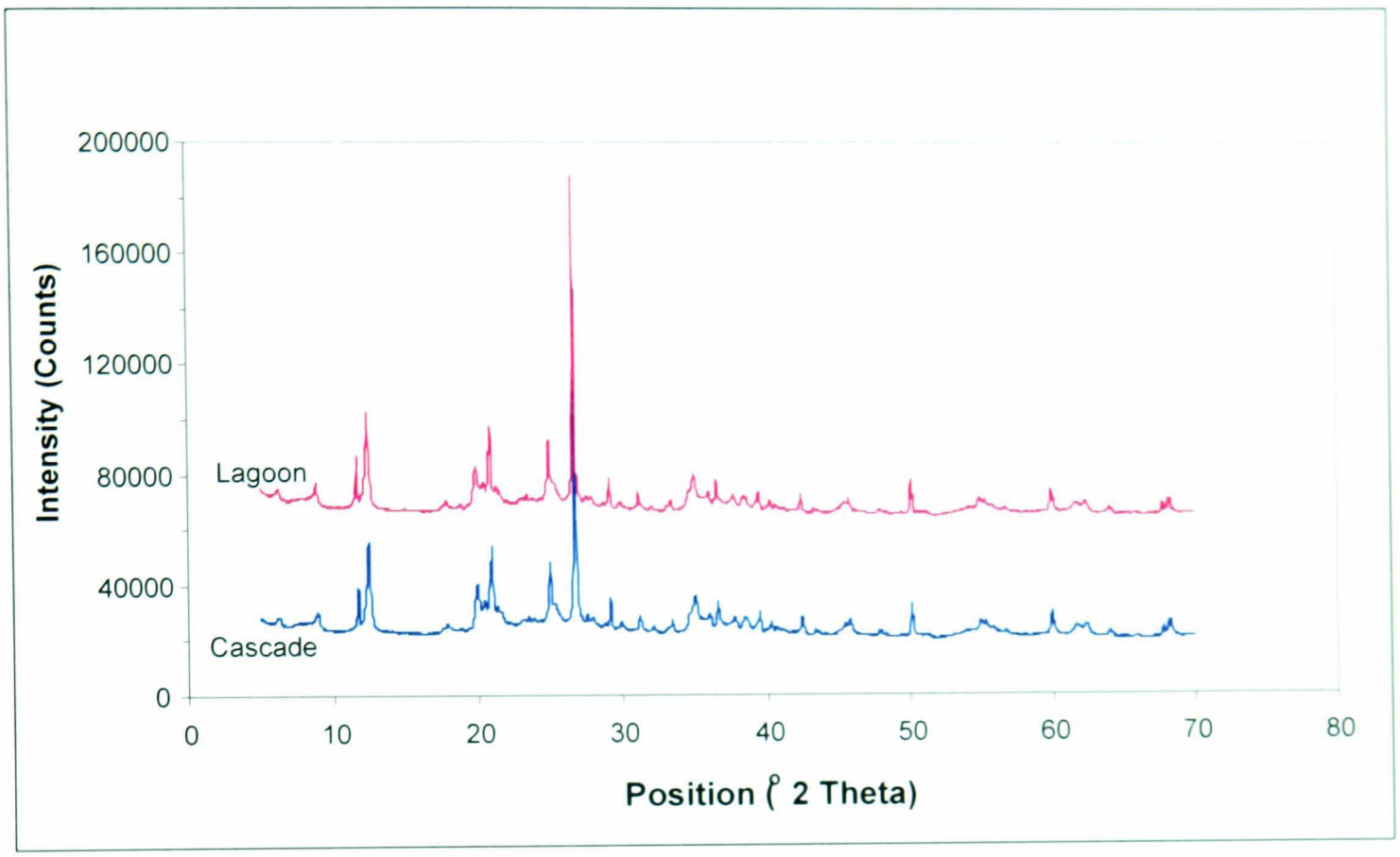

Figure 10.4: XRD spectra of samples taken (August 2006) from the Cascade and the settlement lagoon sampling points at Whittle site.

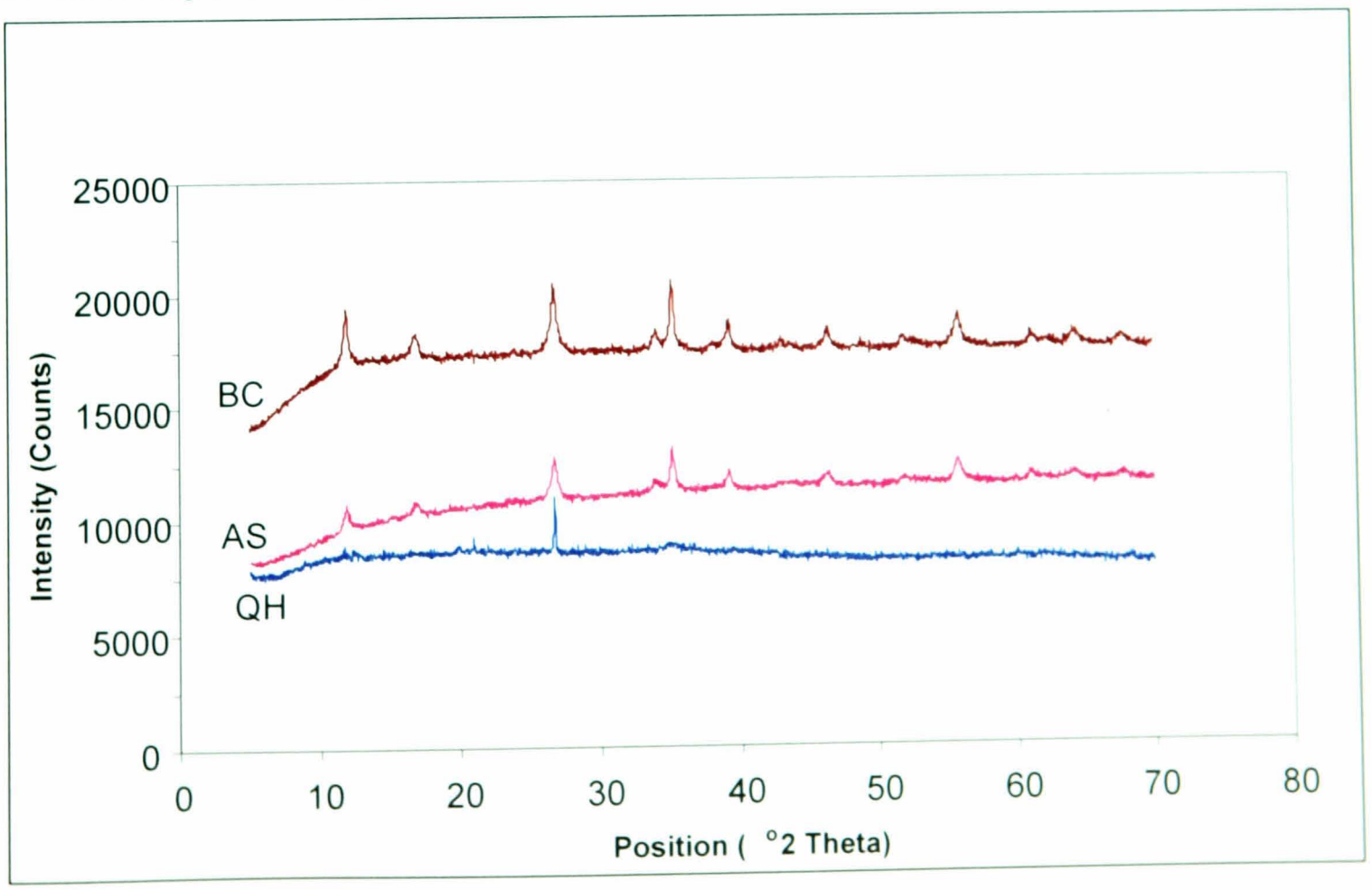

Figure 10.5: XRD spectra of samples taken (August 2006) from Quaking Houses. Acomb and Bowden Close sites respectively. The broad lines here usually clear evidence of smaller particles in the samples.

It was observed that all spectra give very similar XRD peaks (figures 10.3-10.5) but varying intensity. In general, the microstructure observed in all the different environmental batches was always very similar, showing low intensity peaks and high background XRD spectra were observed in all the samples analysed showing indirect evidence of poorly and non-crystalline iron oxide nanosized particles. The low intensity of the peaks in all the samples is due to the amorphous and poorly crystalline nature of iron oxide nanoparticles in the samples. The high background effect observed in all the samples analysed is typical for the analysis of iron containing minerals and is due to fluorescence caused by the Cu-based X-rays source. Generally, all the three metals of the first transition series before copper (Fe, Co and Ni), give high background due to Copper fluorescence and this effect is particularly significant for iron containing minerals [1].

Despite that all samples are poorly crystalline and amorphous, prominent peak at 27 degree 2θ, due to FeO.OH provided the strongest indication yet that the oxides are iron oxides nanoparticles. Additional peaks, although of low intensities at 12, 15, 20, and 34 degree 2θ respectively provided indirect evidence of the nature of the iron oxide nanoparticles which suggest ferrihydrite, goethite and schwertmannite. The peaks of the XRD spectra and the d-spacing of (1.49, 1.73, 2.51, and 4.45 Å) fit very well with those expected for a ferrihydrite mineral. However, due to the instability of ferrihydrite minerals, further spectroscopic analysis like TEM and EDX will be used to confirm this observation. For example, transformation of schwertmannite to goethite under moderately acidic environments has been reported [28]. Although, there have been difficulties in specific characterisation and identification of ferrihydrite because of the common designation of ferrihydrite as amorphous iron hydroxide, colloidal ferric hydroxide, $Fe(OH)_3$ etc [19]. Ferrihydrite is generally classified according to the number of X-ray diffraction lines that the material gives: typically, "2-line ferrihydrite" for material that exhibit little crystallinity and "6-line ferrihydrite" for best or highly crystalline material [20, 22]. However, close similarities between ferrihydrite structure and FeOOH-type minerals have been reported [22], specifically goethite and akaganeite, rather than hematitie [23].

10.6: High Resolution Scanning Electron Microscopy (HR-SEM) results

SEM was used to reveal further morphology details of the observed iron oxides nanoparticles in the studied samples and the results are presented in this section. For comparison purposes of the morphology of the surface, the same sample was analysed differently by using ground powder sample and by direct evaporation of few drops of the sample on the grid.

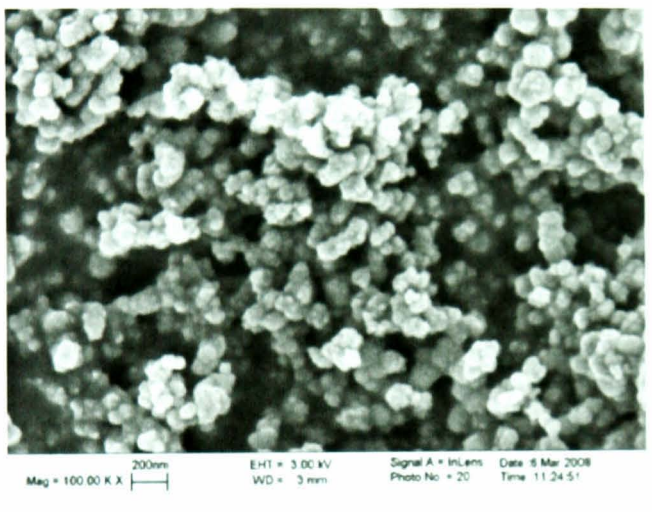

(a)

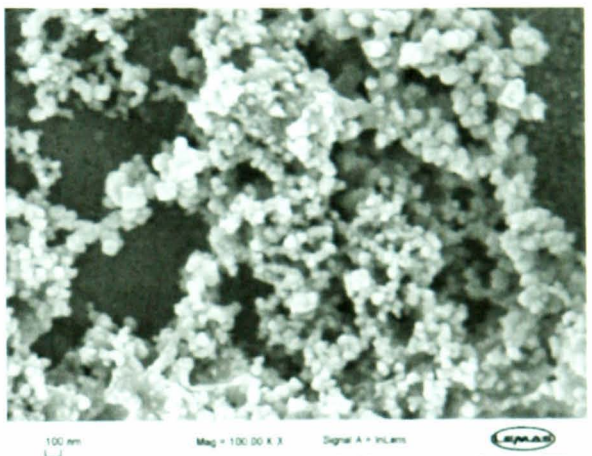

(b)

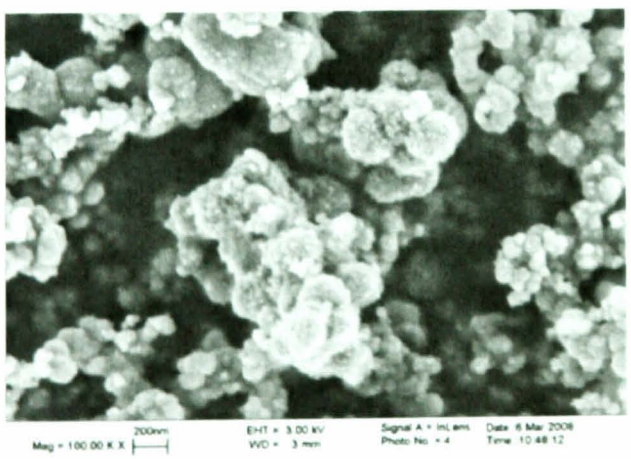

(c)

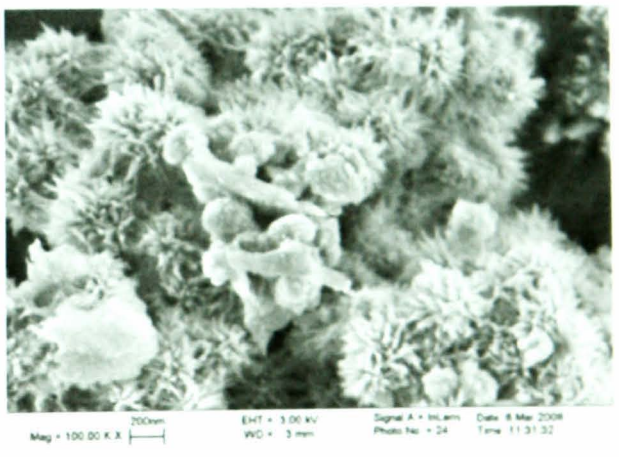

(d)

Figure 10.6: HR-SEM images of mine water samples from Shilbottle site showing different iron oxide nanoparticle morphologies and sizes; (a) sample analysed from powder (b) sample analysed by drying 2 drops of mine water on the SEM grid, (c) sample analysed from power and (d) sample analysed from powder.

Typical and representatives High Resolution Scanning Electron Microscope (HR-SEM) images of studied samples are presented in figure 10.6 above. SEM images reveal that the iron oxides nanoparticles vary in shapes, sizes and of different morphologies as can be seen in figure 10.6. The SEM images revealed the degree of iron oxide nanoparticles aggregation and single particle nature of the particles which shows varying and different particle sizes. The observed iron nanoparticles had diameters ranging from 50-100 nm. However, one significant observation in this study is that thin layers of oxides (probably iron or aluminium oxide), on the surface. protecting particles from the surface were observed in all the SEM images (figure 10.6b) of samples analysed by drying mine-water on the SEM grid rather than the powder. In addition, some iron oxide nanoparticles were observed on the surface of the film and some under the surface. It was thought that there is probably change in the surface and particle morphology by grinding the sample into powder and that the thin film layer on the surface are probably iron or aluminium oxides nanoparticles. This observation is consistent with a well known fact that iron oxides nanoparticles can form different morphologies in the powder form than those found in the bulk solution [31].

10.7: High Resolution Transmission Electron Microscopy (HR-TEM) results

The various morphologies and characterisation of structures and phase analyses of iron oxides nanoparticles observed in the sample remained inconclusive by all the techniques previously described above, the nature of iron oxides nanoparticles in the samples were eventually confirmed by the High Resolution Transmission Electron Microscopy (HR-TEM) and the results are presented in this section. The HR-TEM provides additional structural and morphological information of the different phases observed by the SEM. In general, HR-TEM revealed heterogeneous phase consisting of three distinct phases as shown in Figure 10.7(a-d). These identified phases consist of at least one fine structure, a poorly crystalline morphology and an amorphous phase. Figure 10.7a shows the HR-TEM of the observed three phases, while the HR-TEM of individual phase is shown in figure 10.7 (a-c).

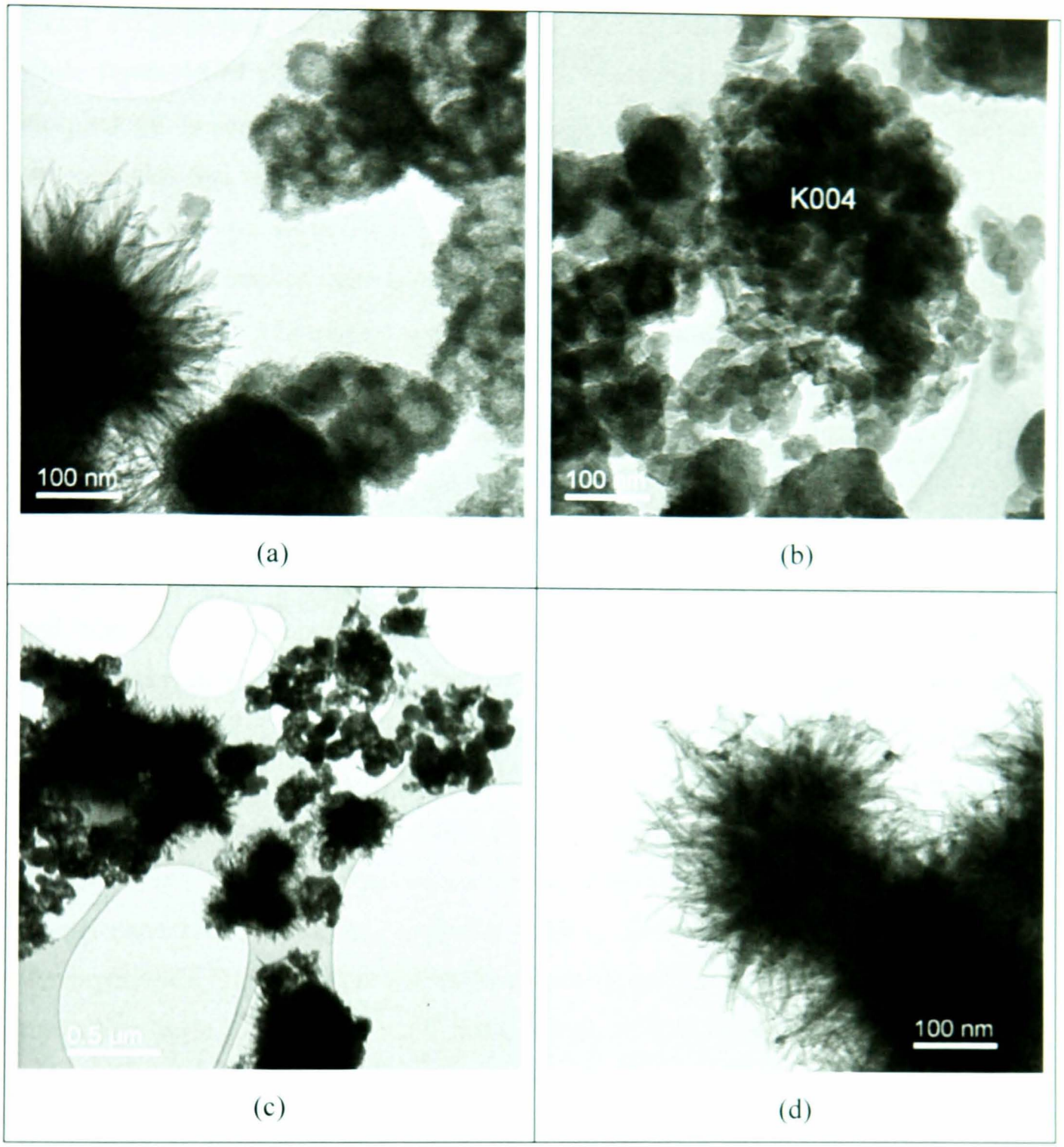

(a) (b)

(c) (d)

Figure 10.7: HR-TEM images of (a) the bright field region of the whole sample area (b) dark-field image of focussed area (c) dark-field image of focussed area (d) dark-field region of focussed area in the sample.

The microstructure characterisation of the samples was carried out and typical and representatives HR-TEM images of iron oxides nanoparticles observed in all the analysed samples are shown in the figure above. The HR-TEM of the bright field region of the whole sample revealed three iron oxide phases (figure 10.7a) and the dark-field imaging of one of the selected areas (figure 10.7b) shows particle to be spherical in shape and fairly uniform in size with a mean diameter of ~50 nm.

Figure 10.7c shows similar morphology but with particles appear to be in cluster while figure 10.7d shows a needle-like, poorly-ordered, pin-cushion and aggregate morphology. In general, figure 10.7(b & c) appear to be poorly crystalline iron oxides nanoparticles that are aggregated into approximately spherical 50-100 nm diameter particles, and these particles are further aggregated. Although, many iron oxides nanoparticles phases are thermodynamically competitive, however, the morphologies in figure 10.7 (b & c) images suggest a poorly crystalline ferrihydrite or iron oxides nanoparticles that are probably a mixture of Fe_2O_3 and Fe_3O_4 with a possible Fe_2O_3 surface as Fe_3O_4 nanoparticles tend to form into octahedral, or cube octahedral morphologies [32]. The observed phase in figure 10.7d is consistent with schwertmannite morphology [31, 32, 34]. This observation is consistent with the fact that the existence of schwertmannite has been well documented as a major component and most commonly found in acid mine drainage(AMD) streams [34, 36], in waters, the sediments of lakes receiving AMD [42, 43, 44] and in the substrates of wetlands receiving AMD [45]. Schwertmannite is commonly described as having the general formula $Fe_8O_8(OH)_{8-2x}(SO_4)_x.H_2O$ [45]. Whereas, schwertmannite is the most common direct precipitate from AMD [46] and forms in waters with pH values of between 3 and 4.5 and sulphate concentrations between 1000 and 30000 mg L^{-1}[47], at circumneutral pH values, a poorly-ordered ferric oxyhydroxides nano-phase (ferrihydrite-$Fe_2O_3.0.5H_2O$) becomes the dominant minerals formed, while jarosite (a crystalline ferric sulphate mineral), is the prevalent phase at pH<2 [48]. To confirm these observations, elemental mapping of selected areas followed by electron diffraction X-ray analyses was then carried out and the results are presented in the following sections respectively.

10.8: STEM results

After identifying three distinct morphologies of iron oxides nanoparticles as shown in the above section, to characterise and to answer the question of what these phases are, Scanning Transmission Electron Microscopy (STEM) was used for the elemental mapping of selected areas and the results are presented here. Each phase was mapped followed by elemental analysis using Energy Dispersive X-ray analysis (EDX) and the results presented in the subsequent section. Figure 8.1 shows the elemental mapping of each phase identified by TEM, representing a schwertmannite phase (fig. 10.8a), aluminium rich phase map is shown in figure 10.8b, the phase dominated by iron phase and the interface mapping of the schwertmannite and iron rich phase are presented in figure 10.8 (c & d) respectively.

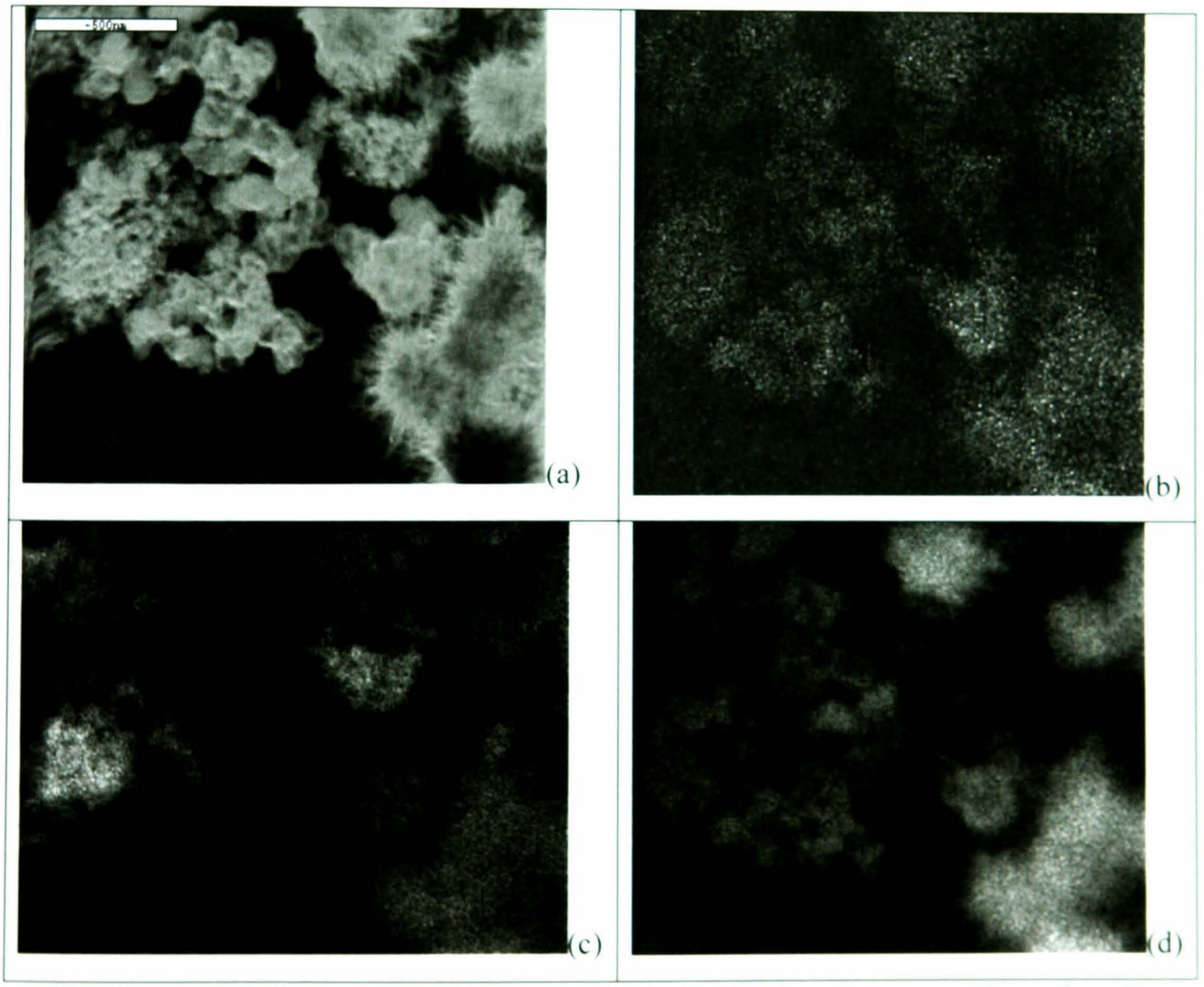

Figure 10.8: STEM images of (a) elemental mapping of the schwertmannite region (b) map of the Aluminium rich phase (c) map of the iron rich region (d) map of the Schwertmannite-Fe rich interface.

STEM results presented above are based on elemental mapping of selected areas and each phase identified by TEM has been mapped to identify various elements in each phase and their relative abundance. This helps to identify the structural composition and elemental distribution when the diffraction patterns of these mapped areas are analysed by EDX. The structures/images are described and defined by the abundance of the dominant elemental composition in the area mapped which gives other elements in addition. The EDX of these selected areas are presented in the following section.

10.9: Electron Diffraction X-ray Analysis (EDX) results

This chapter presents the diffraction pattern of the selected areas in the elemental mapping of each area identified by the TEM. The EDX spectra show the elemental composition in the selected areas mapped, their intensities and relative abundances. Figure 10.9 shows the three diffraction patterns representing a schwertmannite phase (figure 10.9a), the iron rich phase (ferrihydrite phase), (figure 10.9b) and the aluminium rich phase (figure 10.9c). In the spectrum, copper originates from the copper grid used for the analysis and this appears in all the spectra. The schwertmannite and the iron rich spectra borne very striking resemblance and similarity except that there is presence of elemental sulphur in the schwertmannite spectrum (figure 10.9a). The appearance of this sulphur peak is very significant to differentiate between the schwertmannite phase and the iron rich phase (ferrihydrite phase) and it is an important diagnostic tool the for schwertmannite phase.

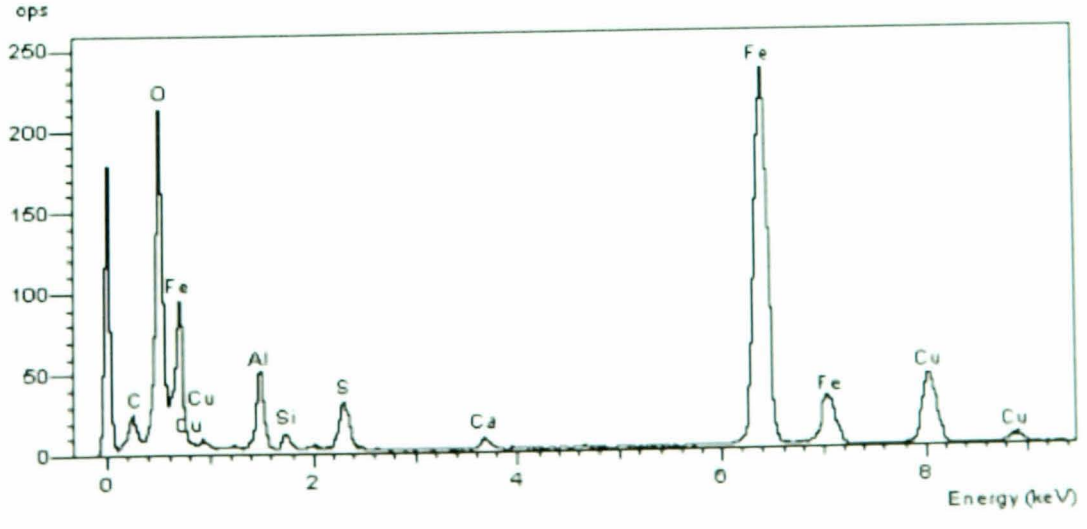

(a)

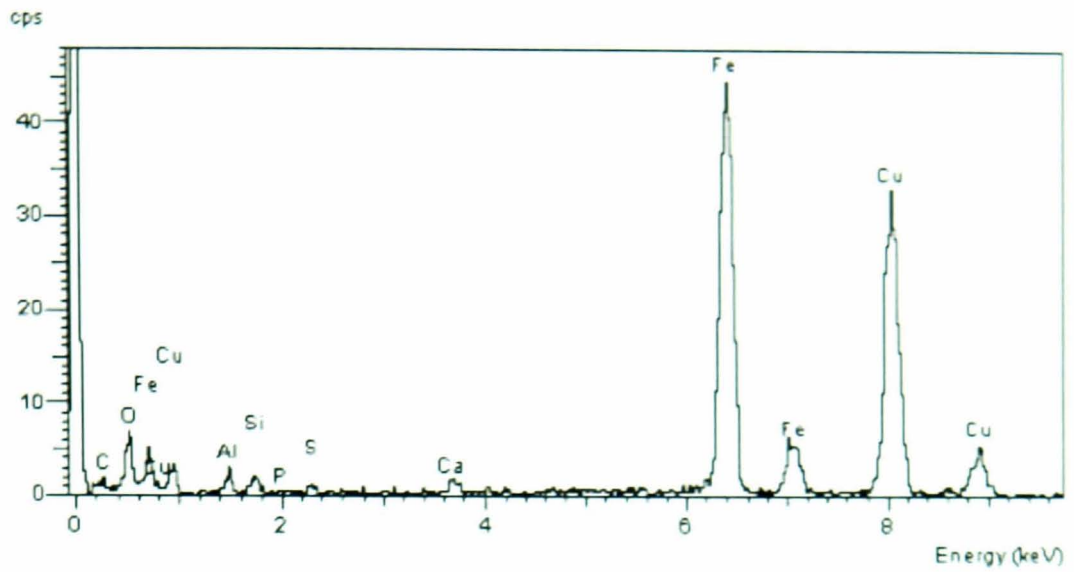

(b)

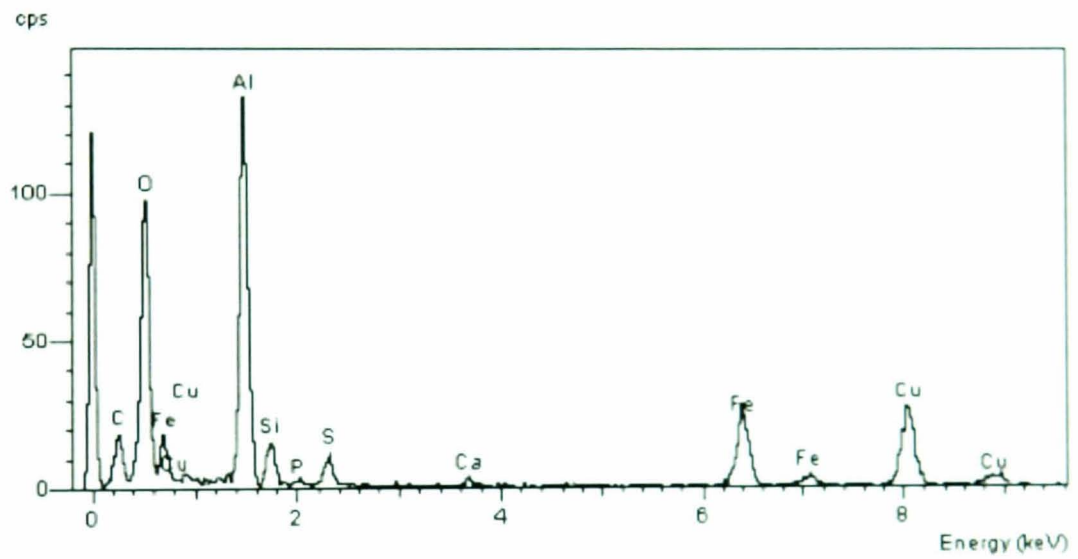

(c)

Figure 10.9: EDX spectra of (a) diffraction pattern from the schwertmannite phase (b) diffraction pattern from the iron rich phase (ferrihydrite phase) (c) diffraction pattern from the aluminium rich phase.

The observed diffraction patterns are very similar as shown in figure 10.9; the oxides nanoparticles appear to be nano-crystalline in nature. The diffraction pattern from the schwertmannite phase shows very intense iron peak and a sulphur peak which is absent in the iron rich phase (ferrihydrite phase). In addition, the main lattice spacing experimentally measured in the selected area diffraction pattern presented in figure 10.9 above (1.855, 2.96) correspond very well to the hkl values reported for polycrystalline ferrihydrite structure [40, 41, 42].

The nanocrystalline nature of the observed iron oxide nanoparticles in the samples studied is evident and has the lattice spacings consistent with Fe_2O_3. The appearance of phosphorous peak in figure 10.9 (b), though, very small, is a diagnostic element for ferrihydrite and it is associated with a ferrihydrite phase. The prominent and intensity of aluminium peak in figure 10.9(c) suggests that this is an aluminium rich nanoparticle phase observed by the TEM. It should be added that identification of ferrihydrite and schwertmannite is complicated because they occur in small particles close to or below 10 nm in size [45], so that physical parameters such as X-ray becomes smeared out [46]. However, recent identification and characterisation of these minerals have shown that they are "amorphous iron oxides" or "ferric hydroxide" [45]. Moreover, because of their small particle size and accordingly large surface area, these minerals can absorb significant amount of elements that are frequently released simultaneously with iron during the weathering of sulfides minerals [47, 48]. For example, the weathering of sulfides of complex compositions, such as the weathering of pyrite during mining activities, will result in the release of additional elements. Thus, the major element abundance and mineralogy of mine-waters depends strongly on chemical weathering, genetic environment and diagenic processes. In addition, previous characterisation of these minerals suggest that ferrihydrite formed in a mine-water drainage environment (as in this study), can transform under the influence of filamentous algae to goethite [40], with a gradual transformation of schwertmannite to goethite in a constructed wetland [41]. This shows that both minerals (ferrihydrite and schwertmannite) are perhaps unstable as they transform to a more stable goethite in the long run. Owing to a high surface area and increased surface reactivity, schwertmannite plays an important role in processes that control the environmental cycling of many trace contaminants [48, 49]. For example, several experimental studies have highlighted the significance of schwertmannite as a sink for arsenic [50, 51, 52, 53, 54, 55, 56, 57, 58], which is an important component frequently associated with mine-waters and acid mine drainage (AMD) [58].

10.10: Conclusions

AFM shows iron particles ranged from few nanometres to few micrometers; larger particles size at microscale for the colloidal iron phase and nanoscale size particles for the dissolved iron. This observation has important implications for understanding the mechanisms by which iron colloids might bind trace elements. Moreover, colloids have important effects on the fate, behaviour and transport in surface waters, groundwaters, bioavailability and toxicity of trace elements [22]. In general, AFM shows that there are both large and small particles present. Acidification reduces aggregation with the mean size of the nanoparticles of 100 nm.

FTIR suggest that the nature of iron oxides nanoparticles across all the studied site bear similarity as shown in fig.10.2 and the spectra revealed that it is likely to be poorly crystalline (as shown in the stretching OH and bending OH vibration bands in the spectra) form of iron oxides which could be either ferrihydrite or akaganeite, rather than crystalline form of iron oxide nanoparticles (goethite and hematite).

XRD analyses show that the iron oxides nanoparticles in all the analysed samples are poorly crystalline and some amorphous. The d-spacing strongly suggests that these iron oxides are likely to be largely poorly crystalline ferrihydrite or schwertmannite. These observations are very significant because precise knowledge of the solid products from mine-waters is an indispensable prerequisite for the comprehension of the stabilities of these oxides/colloid precipitates and their reactions and consequently for an assessment of the environmental impact that they may have. In addition, determination and characterisation of the mineralogy of mine-water precipitates can disclose the conditions under which the minerals were formed. Furthermore, precipitate mineralogy may have a dominant effect on the environmental impact of the entire mining wastes.

HR-SEM images revealed that the iron oxide nanoparticles have mixed phases of iron oxides with different morphology consisting of at least three distinct phases. In addition, one of the significant observations show that the analysis of these materials are better in powder form instead of liquid phase which forms a thin layer of film and

protecting the nanoparticles from the surface and thus resolution at high magnification.

The HR-TEM study revealed three distinct iron oxides nanoparticles phases with poorly crystalline, polycrystalline and amorphous whose morphologies consistent with ferrihydrite, schwertmannite and an aluminium-rich phase. The oxide nanoparticles had typical diameters of between 50-100 nm.

Elemental mapping followed by X-ray electron diffraction pattern analysis of the selected area on the iron nanoparticles revealed low concentrations of diffraction peaks, indicating that the iron nanoparticles are mostly polycrystalline or small crystallite size. EDX analysis and the experimentally determined lattice spacing brings to evidence that these iron oxides nanoparticles phases are a ferrihydrite phase, an iron rich phase and an aluminium rich phase. The diffraction patterns show the materials are polycrystalline with inter-atomic (d-spacing) of 1.855 and 2.96 Å which is similar to polycrystalline morphology of ferrihydrite and schwertmannite.

10.11: References

[1]. McCarthy, J.F. and Zachara, J.M. *Environmental Science Technology*, **1989**, 23, 496-502.

[2]. Buffle, J. & Leppard, G. *Environmental Science and Technology*, **1995a**, 29, 2169-2175.

[3]. Buffle, J. & Leppard, G. *Environmental Science and Technology*, **1995b**, 29, 2176-2184.

[4]. Gustafsson, O. and Gschwend, P.M. *Limnology Oceanography*, **1997**, 42, 519-528.

[5]. Lead, J.R., Davison, W., Hamilton-Taylor, J. and Buffle, J. *Aquatic Geochemistry*, **1997**, 3, 212-232.

[6]. Kersting, .A.B., Efurd, D.W., Finnegan, D.L., Rokop, D.J., Smith, D.K. and Thompson, J.L. *Nature*, **1999**, 397, 56-59.

[7]. Lyven, B., Hassellov, M., Turner, D.R., Haraldsson, C. & Andersson, K. *Geochimica et Cosmochimica Acta*, **2003**, 67, 3791-3802.

[8]. Chamritski, I. and Burns, G. *J. Physical Chemistry*, **2005**, 109, 4965-4968.

[9]. Guo, L., Huang, Q., Li, X. and Yang, S. *J.Chem.Chem.Phys.*, **2001**, 3, 1661-1665.

[10]. Schwertmann, U. and Cornell, R.M. Iron Oxides in the Laboratory. (Wiley VCH: Weinheim), 2000.

[11]. Murad, E. and Rojik, P. Australian New Zealand Soils Conference, 5-9, December, **2004**.

[12]. Bigham, J.M., Carlson, L. and Murad, E. *Mineralogy Magazine*. **1994**, 58, 641-648.

[13]. Alpers, C.N. and Blowes, D.W. ACS Symposium Series 550. American Chemical Society, Washington, DC, **1994**.

[14]. Alpers, N.N., Nordstrom, D.K. and Thompson, J.M. Eds CN Alpers and DW Blowes, **1994**, pp.324-344.

[15]. Jambor, J.L., Blowes, D.W., Ritchie, A.I.M. Mineralogical Association of Canada, Ottawa, **2003**.

[16]. Schwertmann, U. *Advances in Soil Science*, **1985**, 1, 171-200.

[17]. Schwertmann, U., Bigham, J.M. and Murad, E. *European Journal of Mineralogy*, **1995**, 7, 547-552.

[18]. Schwertmann, U. and Fitzpatrick, R.W. *Soil Science Society of America Journal*, **1977**, 41, 1013-1018.

[19]. Lambor, J.L. and Dutrizac, J.E. *Chem. Rev.*, **1998**, 98, 2549-2585.

[20]. Lead, J.R., Muirhead, D. and Gibson, C.T. *Environmental Science Technology*, **2005**, 39, 6930-6936.

[21]. Gustafsson, O. and Gschwend, P.M. *Limnology Oceanography*, **1997**, 42, 519-528.

[22]. Stumm, W. and Morgan, J.J. John Wiley and Sons, New York, **1996**.

[23]. Lead, J.R., Davidson, W., Hamilton-Taylor, J. and Buffle, J. *Aquatic Geochemistry*, **1997**, 3, 213-232.

[24]. Georgaki, I., Dudeney, A.W.L. and Monhemius, A.J. *Minerals Engineering*, **2004**, 17, 305-316.

[25]. Russell, J.D. *Clay Mineralogy*, **1979**, 14, 109-114.

[26]. Russell, J.D., Parfitt, R.L., Kloprogge, J.T and Duong, L. *Nature*. **1974**. 248. 220-221.

[27]. Rochester, C.H. and Thompson, S.A. *J.Coll. Interface Sci.*. **1979b**, 92. 508-516.

[28]. Morterra, C., Chiorino, A. and Borello, E. *J. Coll. Interface Sci.* **1984**. 10. 119-138.

[29]. Ishikawat, T., Cai, W.Y. and Kandori, T. *Langmuir*. **1993**, 9, 1125-2410.

[30]. Baltrusaitis, J. and Grassian, V.H. *J.Phys. Chem.*, **2005**, B109, 12227-12230.

[31]. Jean-Francois, B., Janos, S. and Andrew. R.F. *Geochimica*, **2006**. 70. 3613-3624.

[32]. Poulton, S.W. and Canfield, D.E. *Chemical Geology*. **2005**, 214, 209-221.

[33]. Poulton, S.W. and Raiswell, R. *Chemical Geology*, **2005**, 218, 203-221.

[34]. Nurmi, J.T., Tratynek, P.G., Sarathy, S., Baer, D.R., Amonette, J.E., Pecher. K., Wang, C., Linehan, J.C., Matson, D.W., Penn, R.L. and Driessen, M.D. *Environmental Science Technology*, **2005**, 39, 1221-1230.

[35]. Bilgin, A.A., Silverstein, J. and Hernandez. M. *Environmental Science Technology*, **2005**, 39. 7826-7832.

[36]. Benedetti, M.F., Ranville, J.F., Allard, T., Bednar. A.J. and Menguy, N. *Colloids and surfaces*, **2003**, 217. 1-9.

[37]. Campier. P. *Clay Mineralogy*, **1986**, 21. 191-200.

[38]. Bigham, J.M., Carlson, L. and Murad, E. *Mineralogical Magazine*, **1994**, 58, 641-648.

[39]. Bigham, J.M., Schwertmannite, U., Traina, S.J., Winland, R.L. and Wolf, M. *Geochemica et Cosmochimica Acta*, **1996a**, 60, 12, 2111-2121.

[40]. Bigham, J.M., Schwertmannite, U. and Pfab, G. *Applied Geochemistry*, **1996b**, 11, 845-849.

[41]. Carlson, L., Bigham, J.M., Schwertmannite, U., Kyek, A. and Wagner, F. *Environmental Science and Technology*, **2002**, 36, 1712-1719.

[42]. Childs, C.W., Inoue, K. and Mizota, C. Chemical Geology, 1998, 144, 81-86.

[43]. Cravotta, C.A., Brady, K.B.C., Rose, A.W. and Douds, J.B. *US Geological Survey, Water Research*, Investigation Report, **1999**, 313-324.

[44]. Gagliano, W.B., Brill, M.R., Bigham, J.M., Jones, F.S. and Traina, S.J. *Geochemica et Cosmoschimica Acta*, **2004**, 68, 2119-2128.

[45]. Murad, E., Schwertmannite, U., Bigham, J.M. and Carlson, L. *American Chemical Society*, **1992**, 204, 35.

[46]. Regenspurg, S., Brand, A. and Peiffer, S. *Geochemica et Cosmoschimica Acta*, **2004**, 68, 1185-1197.

[47]. Schwertmannite, U., Bigham, J.M. and Murad, E. *European Journal of Mineralogy*, **1995**, 7, 547-552.

[48]. Yu, J.Y., Heo, B., Choi, I.K., Cho, J.P. and Chang, H.W. *Geochemica et Cosmoschimica Acta*, **1999**, 63, 3407-3416.

[49]. Davidson, L.E. The formation and transformation of schwertmannite: Kinetics and the effects of toxic trace contaminants, PhD thesis, **2007**.

[50]. Dold, B. and Fontbote, L. *Chemical Geology*, **2002**, 189, 153-163.

[51]. Courtin-Nomade, A., Grosbois, C., Bril, H. and Roussel, C. *Applied Geochemistry*, **2005**, 20, 383-396.

[52]. Fukushi, K., Sato, T. and Yanase, N. *Goldschmidt Conference Abstract*, **2002**, A249.

[53]. Fukushi, K., Sato, T. and Yanase, N. *Environmental Science and Technology*, **2003a**, 37, 3581-3586.

[54]. Fukushi, K., Sasaki, M., Sato, T., Yanase, N., Amano, H.and Ikeda, H. *Applied Geochemistry*, **2003b**, 18, 1267-1278.

[55]. Fukushi, K., Sato, T., Yanase, N., Minato, J. and Yamada, H. *American Mineralogist*, **2004**, 89, 1728-1734.

[56]. Regenspurg, S. and Peiffer, S. *Applied Geochemistry*, **2005**, 20, 1226-1239.

[57]. Acero, P., Ayora, C., Torrento, C. and Nieto, J.M. *Geochemical et Cosmoschimica Acta*, **2006**, 70, 4130-4139.

[58]. Nordstrom, D.K. and Alpers, C.N. *Proceedings of the National Academy of Sciences of he United States of America*, **1999**, 96, 3455-3462.